CHEMICAL REVIEWS

pubs.acs.org/CR

Review

Low-Valent Transition Metalate Anions in Synthesis, Small Molecule Activation, and Catalysis

Vanessa R. Landaeta,* Thomas M. Horsley Downie, and Robert Wolf*

Cite This: *Chem. Rev.* 2024, 124, 1323−1463

Read Online

ACCESS | Metrics & More | Article Recommendations

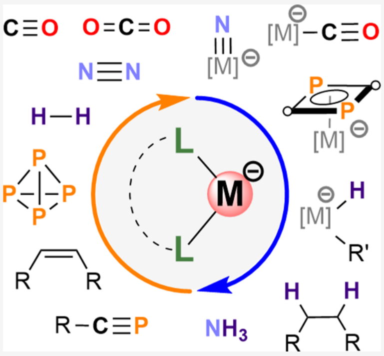

ABSTRACT: This review surveys the synthesis and reactivity of low-oxidation state metalate anions of the d-block elements, with an emphasis on contributions reported between 2006 and 2022. Although the field has a long and rich history, the chemistry of transition metalate anions has been greatly enhanced in the last 15 years by the application of advanced concepts in complex synthesis and ligand design. In recent years, the potential of highly reactive metalate complexes in the fields of small molecule activation and homogeneous catalysis has become increasingly evident. Consequently, exciting applications in small molecule activation have been developed, including in catalytic transformations. This article intends to guide the reader through the fascinating world of low-valent transition metalates. The first part of the review describes the synthesis and reactivity of d-block metalates stabilized by an assortment of ligand frameworks, including carbonyls, isocyanides, alkenes and polyarenes, phosphines and phosphorus heterocycles, amides, and redox-active nitrogen-based ligands. Thereby, the reader will be familiarized with the impact of different ligand types on the physical and chemical properties of metalates. In addition, ion-pairing interactions and metal−metal bonding may have a dramatic influence on metalate structures and reactivities. The complex ramifications of these effects are examined in a separate section. The second part of the review is devoted to the reactivity of the metalates toward small inorganic molecules such as H_2, N_2, CO, CO_2, P_4 and related species. It is shown that the use of highly electron-rich and reactive metalates in small molecule activation translates into impressive catalytic properties in the hydrogenation of organic molecules and the reduction of N_2, CO, and CO_2. The results discussed in this review illustrate that the potential of transition metalate anions is increasingly being tapped for challenging catalytic processes with relevance to organic synthesis and energy conversion. Therefore, it is hoped that this review will serve as a useful resource to inspire further developments in this dynamic research field.

CONTENTS

Received: February 27, 2023
Revised: October 9, 2023
Accepted: October 9, 2023
Published: February 14, 2024

https://doi.org/10.1021/acs.chemrev.3c00121
Chem. Rev. 2024, 124, 1323−1463

1. INTRODUCTION

This review article covers the chemistry of ionic complexes composed of s-block or organic cations and d-block metalate anions where the d-block metal atom is in an “uncommonly” low (sometimes even negative) oxidation state. Such metalates are highly electron-rich species, which may serve as powerful reagents in a variety of chemical transformations. Prime examples are the transition metal carbonylate anions, the first examples of which were described already a century ago.[1] In the second half of the last century, various other types of transition metalates stabilized by π-acids such as alkenes and arenes became available.[2−11] Early reports on the behavior in fundamental reactions such as transmetalation, ligand substitution, and oxidative addition strongly suggested that metalates often are highly reactive compounds, paving the way for applications in small molecule activation and homogeneous catalysis. As early as the 1970s, the oxidative addition of alkyl halides to anionic complexes such as $[Fe(CO)_4]^{2-}$ (**1**) or $[(\eta^5\text{-Cp})Fe(CO)_2]^-$ (**2**, Cp = C_5H_5) had been intensively investigated.[12−14] However, the structural diversity and synthetic versatility of transition metalate anions have begun to be fully appreciated only recently. Due to their highly reduced nature, low-valent metalates have the potential to activate inert element−element bonds (including those of fundamentally important inorganic molecules such as N_2, CO_2, and H_2) and to mediate catalytic reactions and multielectron transformations. Indeed, the interest in applications of metalate anions in bond activation, organic synthesis, stabilization of transient species, and homogeneous catalysis is growing rapidly. The purpose of this review is to summarize the most recent developments in this vibrant field in a comprehensive manner and to familiarize interested readers with current applications of low-oxidation state metalate anions in small molecule activation and catalysis.

Since we aim to focus on the chemistry of anionic transition metal complexes in “uncommonly” low (sometimes even negative) oxidation states, the concept of *metal oxidation state* deserves brief comment.[15] For the purpose of this review, we consider the oxidation state of any particular metal as “uncommonly low” when it is below the range of oxidation states in which most of its compounds are found.[16,17] In this case, the compounds discussed will be denoted as *low-valent* transition metalate anions. Naturally, this definition will depend on each element. For example, chromium complexes are frequently found in metal oxidation states of +III to +VI,[18] while metal +II and +III states are typical for iron and cobalt complexes.[19,20] Furthermore, while assigning oxidation numbers to metal atoms is straightforward for most transition metal compounds, the correct assignment may not be immediately obvious in cases where redox-active ligands are present. However, even if the formal oxidation state of the metal is debatable due to charge transfer to the ligands, the overall complex will still be in a highly reduced electronic state. For this reason, we will not apply the criterion of metal oxidation state in a very strict and exclusive manner, but it will be a useful guideline for selecting the appropriate material presented for this review. Complexes with redox-active ligands will be included when a low metal oxidation state is likely to be present. However, a treatment of transition metal complexes with redox-active ligands (e.g., bipyridines, diminopyridines, and diimines) and metal atoms in the more common oxidation states is beyond the scope of this review.

The chemistry of low-valent anionic transition metal compounds has been previously reviewed by other authors.[1−3,10,21] In 2006, a seminal review by J. E. Ellis, who has been a pioneer in the field for many decades, discussed the chemistry of s-, p-, and d-block compounds in negative oxidation states.[2] Furthermore, Ellis summarized the state of the art of the "Chatt reaction" as a method to synthesize arene metalates, but metalates with other ligand frameworks were not discussed.[3] C. G. Werncke recently dedicated a book chapter to the organometallic chemistry of main group as well as transition metal compounds with metal atoms in very low oxidation states, which gives a succinct overview of the field from its inception up to 2019.[10] Only a few reviews describe applications of metalates in small molecule activation and homogeneous catalysis. In 2018, Gómez-Suárez and Nolan reviewed the chemistry of anionic complexes of the late transition metals, including low-valent species as well as those in higher oxidation states, with particular emphasis on their catalytic performance.[21] Two recent accounts summarize the chemistry of very specific transition metalate complexes, i.e., dicarbonyl cyclopentadienyl ferrates and nacnac-stabilized rhenium(I) cyclopentadienyl anion.[11,14] The chemistry of linear 3d-metal(I) compounds has been summarized by Werncke and Gómez in a recent book chapter.[22] Metallocene anions are the subject of another recent review.[23] The chemistry of cobalt complexes and their application in C−H functionalization reactions, presumably involving low-valent intermediates, was reviewed in 2014.[24] A recent account describes the uses of cobalt-N-heterocyclic carbene (NHC) compounds, including low-valent Co(0) species, in homogeneously catalyzed reactions,[25] and another one accounts for the efforts to achieve hydrofunctionalization and cross-coupling reactions at low-valent chromium catalysts, mostly generated *in situ* from air-stable Cr(II) or Cr(III) salts.[18] A review article by Xu and co-workers discusses heterometallic complexes with Mg- or Zn-metalloligands.[26] Several reviews discuss dinitrogen fixation and functionalization, but the use of metalates is not a focal point of these articles.[27−32] Considering the varying scope of the previous reviews and the impressive growth of the field in the most recent years, a comprehensive treatment of the latest developments is highly desirable. This review therefore summarizes the chemistry of low oxidation state transition metalates in the period from 2006 to 2022. Recent selected literature from 2023 is also included. For work prior to 2006, readers are referred to the previously published reviews, though earlier reports will be included for context when appropriate.[1−3,10]

Upon inspection of the relevant literature, it becomes clear that most of the results in transition metalate chemistry have been achieved with first-row transition elements. While metalates are known for most of the 3d series, significant focus has been directed toward the study of the late first row metals iron, cobalt, and nickel. Since iron is the most earth-abundant transition metal, the use of iron complexes has gained considerable attention in catalysis.[19,20] Although the chemistry of the heavier second and third row metals is often distinct from their lighter first-row transition metal counterparts due to the primogenic effect,[33,34] many parallels are observed between group congeners in the chemistry of low-valent transition metalate anions. Examples for 4d- and 5d-transition metalates are therefore included throughout this review. A number of metalates are known for the lanthanides and actinides.[35−49] However, their chemistry is often distinct due to the more electropositive nature of these elements, and the more core-like character of the f orbitals, which gives rise to less directional, and more electrostatic, bonding. Due to the redox-active nature of the ligands, the oxidation state of the metal cations can be debatable in some cases. Therefore, we believe that the chemistry of the f-block metalates warrants a separate treatment, which is beyond the scope of this review.

The strong influence of ion-pairing effects on the stability and reactivity of metalates has become increasingly recognized in the last 15 years. Ion-pairing is observed in a wide range of metalates (especially highly charged ones) and can have dramatic effects on their structure and reactivity. To remain within the boundaries of this review, our treatment of ion-pairing effects will be limited to metalates that likely contain "low-oxidation state" metal atoms. Although interesting and important, a systematic treatment of ion-pairing in higher valent transition-metal species, e.g., imido[50] and nitrido complexes[51] and complexes with redox-active formazanate ligands,[52] is beyond the scope of this work.

Covalent bonds between p-block and d-block metal cations or two d-block metal cations can be used to stabilize highly reactive, nucleophilic species. Therefore, the utility of metal−metal interactions in stabilizing low-valent metalate anions will be discussed in this review as well. However, it is important to note that the chemistry of metal-based Lewis pairs in general is beyond the scope of this review.[53] This type of compound will only be considered here if they are formally anionic species, i.e., when s-block or organic counteranions are present. Specifically, the chemistry of nucleophilic gold(I) complexes having "auride character" and heterobimetallic transition-metal−zinc compounds has recently been covered by other reviews and thus will only be mentioned where appropriate for context.[26,54,55] Furthermore, heterometallic complexes featuring elements other than alkali or alkaline earth metals, such as tetrel atoms or heavier transition metals (4d, 5d), are not covered in this review even though such complexes may display transition metal atoms in formally negative oxidation states, e.g., Fe(−I), Co(−I), or Rh(−I).[56−61]

The review article is divided into four parts. Following the present section, section 2 summarizes the different methods for the preparation of metalates to familiarize readers with the synthetic protocols, the commonly used ligand types, and basic reactivity patterns. These highly reactive, electron-rich complexes require a suitable, stabilizing ligand framework, normally consisting of strong π-backbonding units. One of the most common ligand types is carbonyl. Numerous studies have proven that *inter alia* isocyanide, arene and alkene, phosphane, phosphite, carbene, alkyl and amido complex, and imine ligand frameworks also provide sufficient stabilization, allowing for comprehensive investigations of the reactivity and applications of low-valent transition metalate complexes. Accordingly, section 2 covers the chemistry of mononuclear transition metalate complexes according to ligand type. In addition, the importance of ion-pairing interactions and metal−metal bonding in the synthesis and reactivity of metalates is highlighted in a separate subsection. Section 3 summarizes the state-of-the-art in small molecule activation by metalate complexes, including catalytic transformations, focusing on the activation of dihydrogen, dinitrogen, carbon monoxide, carbon dioxide, white phosphorus, and other related molecules and model compounds. Section 4 presents a summary of the reviewed results and some perspectives for the future development of the field.

2. SYNTHESIS AND BASIC REACTIVITY PATTERNS OF D-BLOCK METALATES

Documented examples of carbonyl metalates date back to the early 1930s, when initial reports described the synthesis of $[Fe(CO)_4]^{2-}$ (**1**, Figure 1),[62] although its structure was not confirmed until the 1950s.[1] Since then, reported carbonyl metalates include almost every metal from groups 4−10 with varying charge and nuclearity. Additional examples, showcased in Figure 1, are $[V(CO)_6]^-$ (**3**) and $[Cr(CO)_5]^{2-}$ (**4**).[1,2] Isocyanide ligands can be used as tunable CO surrogates thanks to their R substituent. The first isocyano metalate, $[Co(CNXyl)_4]^-$ (**5**, Xyl = 2,6-$Me_2C_6H_3$; see Figure 1), was reported in 1989 by the Cooper group.[63,64] Furthermore, alkene and arene metalates constitute one of the most versatile groups of low-valent metalates.[2,3] Within this type of compound, selected examples are the arene titanate K[Ti(benzene)$_2$] (**6**), the manganate $[Li(dme)]_2[Mn(cod)_2]$ (**7**) (see Figure 1), and the nickelate $[Ni(C_2H_4)_3]^{2-}$ (**8**), which are homoleptic compounds with the metal in formally negative oxidation states.[7,65−68] By contrast, ferrate **2** (Figure 1) is heteroleptic and formally zerovalent.[12−14]

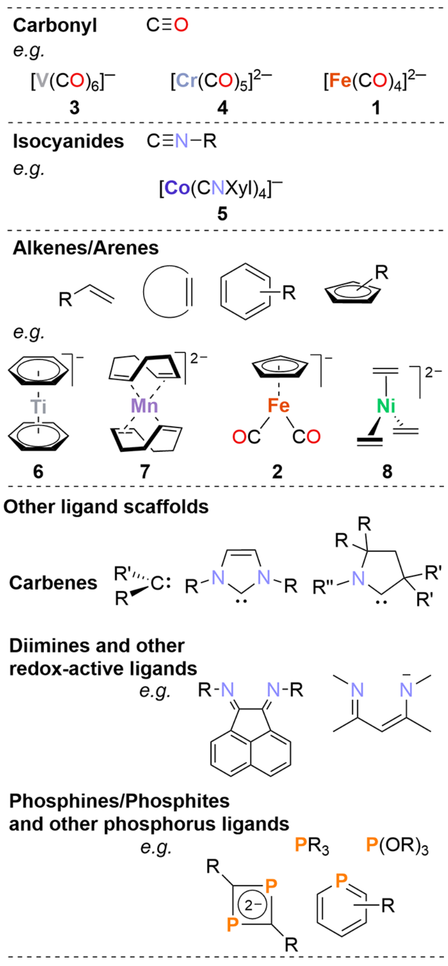

Figure 1. Ligands commonly used for stabilizing low-valent (uncommon) oxidation states in transition metal complexes.

2.1. Synthetic Routes

The methods for the synthesis of highly reduced d-block metalates can be summarized into the main types of reactions shown in Scheme 1 for selected early examples of such compounds.[7,8,65−67,69−71] Most metalate syntheses reported since 2007 generally follow one of these methods.[3] Jonas and co-workers pioneered the reductive cleavage of metallocenes with lithium in the presence of an olefin as a strategy to access highly reactive alkene metalates (Scheme 1, reaction type 1a).[7,8,65,71,72] Examples of complexes obtained using such strategy are $[Li_2(thf)_4\{Ni(\eta^2\text{-cod})(\eta^4\text{-cod})\}]$ (**9**) or the alkenemanganate **7**, shown in Scheme 1.[7,68] The use of other alkali metals (sodium, potassium, or their Hg amalgams) to reduce a transition metal salt or precursor is also a common synthetic route (see Scheme 1, reaction type 1b),[73] with examples including the reduction of a Co(II) precursor with sodium to afford $[(N_2)Co(PEt_2Ph)_3]^-$ (**10**), or the formation of bis(arene)titanates(−I), K[Ti(arene)$_2$] [arene = benzene (**6**, Figure 1, *vide supra*), toluene (**11**)] from their Ti(0) parent compounds.[66,67,69] Reducing agents such as KC_8[74−82] and cobaltocene (Cp_2Co)[83] can also be employed. The strategy used by Jonas is certainly a turning point in the synthesis of arene and alkene metalates.[9,68,84]

The reaction of alkali metal arene radical anions with transition metal (TM) salts is another powerful route to access highly reduced metalate complexes (Scheme 1c). This method was discovered in the early 1960s by J. Chatt as a route to hitherto unknown transition metal compounds and later expanded to enable the synthesis of a wide range of arene metalates.[85,86] To honor Chatt's groundbreaking work on the interaction of transition metal compounds with alkali metal arenides, Ellis recently proposed naming such methodology "the Chatt reaction".[3] Examples of metalates obtained by this pathway are two titanates analogous to the ones reported by Green and co-workers, **12** (arene = 1,1′-biphenyl) and **13** (arene = 4,4′-di*tert*-butyl-1,1′-biphenyl; Scheme 1, reaction type 1c),[66] and the first homoleptic polyarene cobaltate, bis(1,2,3,4-η^4-anthracene)cobaltate(−I) (**14**), usually regarded as a source of the "naked" atomic cobalt anion, Co^-.[67,70] Finally, new metalate compounds have been synthesized by displacement/exchange of labile alkene/arene ligands, in complexes such as $[Li_2(TMEDA)_2\{Fe(\eta^2\text{-}C_2H_4)_4\}]$ (**15**, TMEDA = 1,2-bis(dimethylamino)ethane Scheme 1, reaction type 2). This example by the Jonas group shows the synthesis of $[Fe(cod)_2]^{2-}$ (**16**) as two different lithium salts.[8] Thus, metalates can be accessed either by reduction of a high-valent compound or using precursors already featuring a low-valent metal center.[2,3]

The selected early examples of metalates shown in Scheme 1 share similar features. In most cases, they are synthesized via reduction of transition metal salts/precursors or metallocene compounds with alkali metals (e.g., lithium, sodium, potassium), and the metal centers are stabilized by π-acid ligands, capable of accepting the excess electron density on the metal atom through synergistic π-backbonding. Therefore, the presence of π-acceptor ligands, such as carbonyls, isocyanides (isolobal with the carbonyl ligand) and unsaturated hydrocarbons (arenes, alkenes), is common (see Figure 1).

Due to the lability of the hydrocarbon ligands, alkene and arene metalates are often referred to as "naked-metal atom" reagents, or storable sources of transition metal anions. Nonetheless, Ellis and co-workers have emphasized that the use of poly(arenemetalates) as sources of "naked" atomic metal

Scheme 1. General Methods for the Synthesis of (Highly Reduced) Anionic Complexes

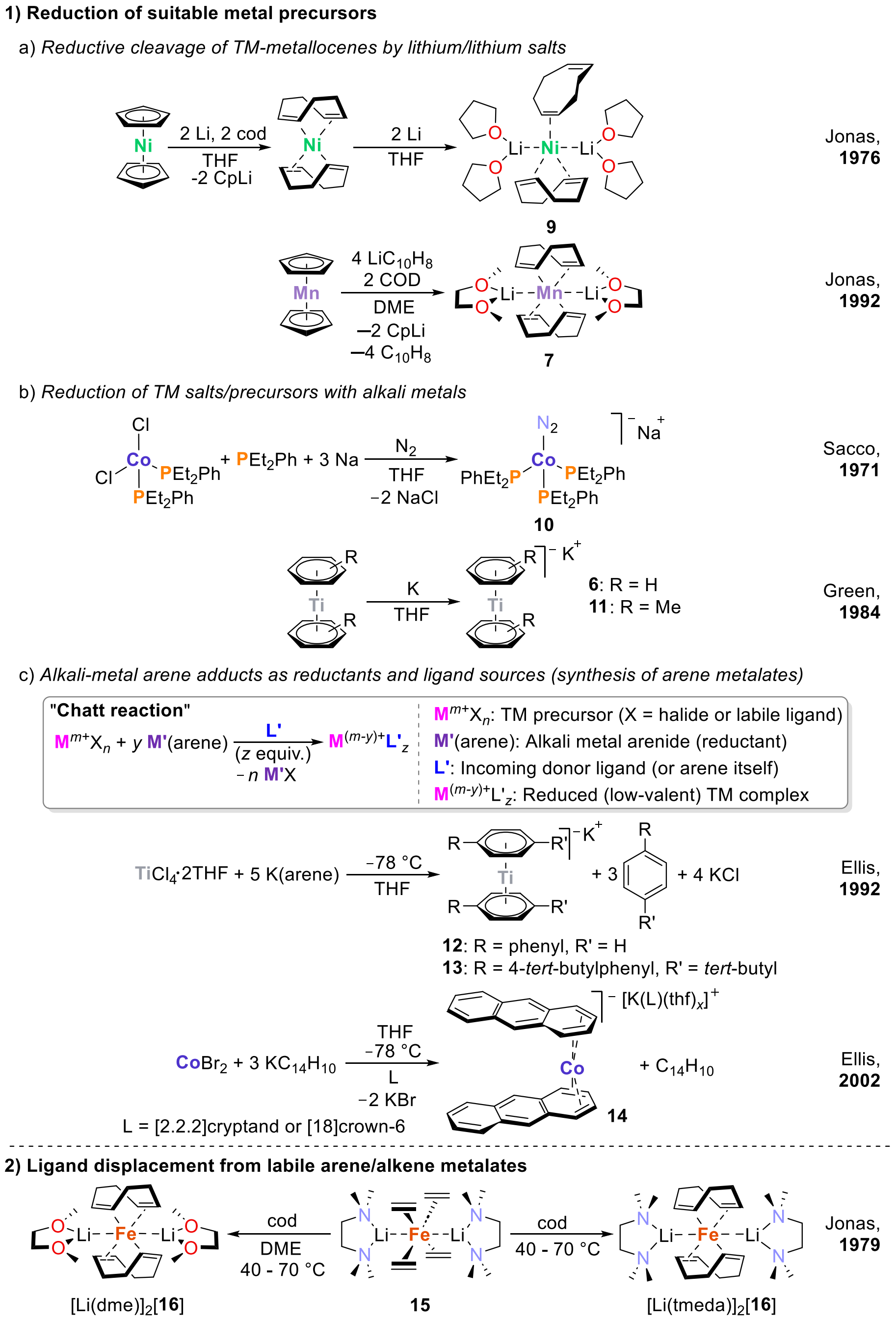

anions, due to their highly reduced nature, might be limited to the compatibility of the desired products with redox processes.[87] With a few exceptions, carbonyl-, isocyanide-, alkene-, and arene-metalates obey the 18-electron rule. Other metalates have been stabilized by carbenes, redox-active ligands, or phosphorus ligands (Figure 1), and examples of these will be discussed throughout the text.

In many cases, the successful isolation of a complex with the metal in a formally negative oxidation state has been enabled by a strong interaction with the countercation, generally obtained from the reducing agent. Consequently, a breadth of examples of carbonyl, alkene/arene or isocyanide metalates have been synthesized and crystallized as alkali metal salts, stabilized with coordinating solvents (e.g., THF or DME; see Scheme 1 for examples by Jonas and co-workers[7,8,65]), encapsulating agents ([18]crown-6, [2.2.2]cryptand), or by further exchange of the metal cations with organic cations [e.g., PPN^+ ($PPN^+ = [Ph_3PNPPh_3]^+$), NBu_4^+ or NMe_4^+].

2.2. Survey of Metalates Reported since 2006: The Crucial Influence of Ligands on Complex Structure and Reactivity

The following subsections describe the efforts made in the period from 2006−2022 to synthesize and understand the reactivity of low-valent anionic d-block metal complexes. The material is organized according to ligand type. The types of ligands capable of stabilizing d-block metalates have already been summarized in Figure 1. The chemistry of neutral or cationic species or complexes with metalloradical character goes beyond the scope of the present work and will not be included unless examples of these are related to low-valent anionic complexes.

2.2.1. Complexes Containing Carbonyl Ligands. The carbonyl ligand (CO) is among the most studied types of ligands in organometallic chemistry.[88] Upon coordination to a metal center, carbon monoxide behaves as a weak σ-donor and as a strong π-acceptor (strong π-acid). In fact, carbonyl ligands are very effective in stabilizing highly reduced metal centers and metals in uncommon oxidation states since they can accept the excess electron density through M−CO π-backbonding (Figure 2).[1,2,10]

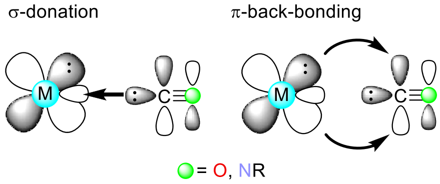

Figure 2. Bonding interactions in carbonyl or isocyanide transition metal complexes.

Consequently, homoleptic metal−carbonyl compounds featuring metal centers in formally negative oxidation states have been known for many decades.[1] To the best of our knowledge, the lowest formal oxidation state reported so far has been M(−IV), achieved in the series of homoleptic carbonyl metalates of the group 6 metals (Cr, Mo, W).[89]

Isocyanide ligands (C≡NR) are isolobal with CO but are weaker π-acids and stronger σ-donors than carbon monoxide.[90,91] While it has long been recognized that isocyanide ligands can be used as surrogates of carbonyl ligands, the former can undergo electronic and steric modulation in a way unavailable to CO.[90]

In many cases, the oxidation state of the metal atom in low-valent compounds featuring carbonyl or carbonyl-like ligands is ambiguous. For example, the description of the electronic structure of the NO ligand-ferrate compound $[Fe(CO)_3(NO)]^-$ (**17**) has been subject to considerable debate. Several groups have studied its spectroscopic characteristics, comparing its behavior to that of known $[Fe(CO)_4]^{2-}$ (**1**).[92,93] Despite being isoelectronic with complex **1**, which is widely accepted to be a Fe(−II) complex, there is no clear agreement on either the oxidation state of the Fe center or, consequently, on the charge/electronic description of the NO ligand in **17**. In their independent studies, the group of Plietker[93] and Gruden and Zlatar[92] concur that **17** cannot be described as a Fe(−II)/NO^+ species, and that, accordingly, it can be more accurately regarded as an Fe(0) species featuring a covalently bonded anionic (NO^-) ligand. The spectroscopic evidence (^{57}Fe Mössbauer, EXAFS and XES spectroscopy) and the theoretical calculations (DFT, TDDFT, and CASSCF) are not only in agreement[93] but consistent with the structural characterization (X-ray and FT-IR).[94,95] Based on their calculations, Plietker and co-workers suggested that in the ground-state the complex features an Fe(0) atom, and that the Fe−NO bond consists of two covalent π-bonds to an NO^- moiety.[93] Gruden and Zlatar performed a NOCV (natural orbitals for chemical valence) analysis on $[Fe(CO)_3]^{2-}$ and NO^+ fragments, finding large charge flow from the Fe center to the NO^+ ligand, which was held as additional evidence that the iron center cannot be in an Fe(−II) formal oxidation state.[92] Furthermore, a comparison of this analysis with that of the analogue **1** seems to confirm the disparate electronic configurations of the iron centers in each species.

The results by Plietker[93] and Gruden and Zlatar[92] contrast with a study by Bauer and co-workers.[96] The latter work investigated the bonding in **17** via a combined experimental and theoretical approach using valence-to-core X-ray emission spectroscopy (VtCXES), X-ray absorption near-edge structure spectroscopy (XANES), and high-energy-resolution fluorescence-detected XANES (HERFD-XANES) in combination with high-level quantum chemical calculations. The Fe(0) complex $Fe(CO)_5$ (**18**) was used as a model of a $3d^8$ metal, which would represent the proposal by Plietker.[93] According to the spectroscopic and theoretical results, the electronic structures of $[Fe(CO)_4]^{2-}$ (**1**) and $[Fe(CO)_3(NO)]^-$ (**17**) appear to be very similar, which would imply a formal Fe(−II) oxidation state in the nitrosyl compound **17**.[96] It should be noted though that complex **18** might not be an ideal reference point due to the simultaneous changes in oxidation state, coordination geometry, and coordination number in comparison with **1** and **17**. Thus, the electronic situation of $[Fe(CO)_3(NO)]^-$ (**17**) is still debatable. Nonetheless, the contrasting behavior in catalytic reactions exhibited by compounds **1** and **17** could well be the result of changes in the electronic characteristics of the metal center and the ligand. While **1** was inactive in most of the studied transformations, **17** showed activity in allylic substitutions, hydrosilylations, transesterifications, and carbene-transfer reactions.[97−101]

A series of $AFe(CO)_3^-$ (A = B, Ge, Sn, Pb, Sc, Y, La) anions and the nature of the formed A−Fe bonds were investigated by means of experimental and theoretical studies by Zhou, Li, and co-workers.[102−104] In all cases, the anionic compounds were generated experimentally in the gas phase and characterized by mass-selected infrared photodissociation spectroscopy. Quantum chemical calculations assisted in the identification and analysis of the electronic structure of the complexes. For instance, the $BFe(CO)_3^-$ (**19**) anion was found to have a cylindrical C_{3v} symmetric structure.[102] Geometry optimizations (DFT) indicated a very short equilibrium B−Fe bond distance of 1.63 Å, which is considerably shorter than the sum of the triple-bond covalent radii of iron and boron atoms (1.75 Å).[105] The latter observation suggests that the B−Fe bond order should be higher than three. Electronic structure and (quantum) chemical bonding analyses support the existence of a quadruple B≣Fe bonding interaction, composed of one electron-sharing σ bond, two Fe → B dative π bonds, and a weak B → Fe dative σ bonding interaction. DFT calculations predict a Fe−B stretching frequency of very low IR intensity for **19**, absorbing at 863 cm^{-1}, that could not be directly observed.[103] Similar studies on $AFe(CO)_3^-$ (A = Ge, Sn, Pb) indicated that the complexes exist in a $^2A_1$ doublet electronic ground state and present an A≡Fe triply bonded C_{3v} structure. The carbonyl ligands are all coordinated to the iron center. Bonding analyses indicated that the valence np atomic orbitals of the group 14 atoms and the hybridized 3d and 4p atomic orbital of the iron center are the main contributors to the triple bonding interactions.[103] Analogous to compound **19**, and contrasting with the heavier group 14 congeners, compounds $AFe(CO)_3^-$ (A = Sc, Y, La) were found to feature quadruple A−Fe metal−metal bonding interactions based on combined experimental and quantum chemical investigations.[104]

Similarly, the heteronuclear magnesium−iron carbonyl anionic complexes $MgFe(CO)_4^-$ (**20**) and $Mg_2Fe(CO)_4^-$ (**21**) were generated in the gas phase and their structures studied using a combination of mass-selected infrared photodissociation spectroscopy and quantum chemical calculations.[106] According to this study, the most stable structures of compounds **20** and **21** have a $^2A_1$ ground state and C_{3v} symmetry, presenting heteronuclear Mg−Fe or Mg−Mg−Fe bonds, respectively. Theoretical calculations indicate, however, that despite having some covalent character, the interactions between magnesium and iron have a significant electrostatic component. For both complexes, **20** and **21**, population analyses revealed that the negative charge is mainly located at the $Fe(CO)_4$ unit. In **20**, analysis of the bonding situation suggested the existence of a Mg−Fe σ-bond. In turn, in complex **21** the central Mg atom has a partial positive charge, and the terminal Mg atom is neutral, and the interaction was described as a σ-type electron-sharing bonding. The valence of the metal atoms was also analyzed, finding that in the σ-bonded complexes the atoms are formally in the Mg(I)−Fe(−II) oxidation states for **20**, whereas in **21** the covalent σ-bond is relatively weak, and involves Mg(0)−Mg(I)−Fe(−II) formal oxidation states.[106] This group extended their investigations to heteronuclear magnesium−iron carbonyl cationic complexes, $MgFe(CO)_n^+$ (n = 4−9) finding that for $n > 5$ the valence of the metal centers involved can formally be described as featuring Mg(II)−Fe(−I).[107]

By reaction of the radical anion salt of fullerene $[K([2.2.2]\text{-cryptand})][C_{60}^{\bullet -}]$ with $[Fe_3(CO)_{12}]$ (**22**), the Konarev group obtained the anionic iron-bridged fullerene C_{60} dimer $[K([2.2.2]\text{cryptand})]_2[Fe(CO)_2\text{-}\mu,\eta^2{:}\eta^2\text{-}C_{60}]_2\cdot 2.5C_6H_4Cl_2$ (**23**, see Figure 3).[108] Each iron atom coordinates to two C−C bonds of C_{60} hexagons in the two fullerene units, and to two carbonyl ligands. The coordination environment of the metal centers is completed by an Fe−Fe interaction (2.978(4) Å). In the solid state, the dianion presents two $[K([2.2.2]\text{cryptand})]^+$ cations interacting with carbonyl ligands. The combined experimental and DFT data indicated that the diamagnetic dimer **23** is in a singlet ground state and that the negative charges are localized both on the iron atoms and the fullerene cages. The reduced state of the metal centers is reflected by the shift of the IR stretching bands to lower frequencies (1880, 1902, 1920, and 1958 cm^{-1}) with respect to the parent cluster **22** (1909, 1991, and 2051 cm^{-1}). A similar anionic cobalt dimer $[nBu_4N][\{Co(Ph_3P)\}_2(\mu\text{-}Cl)(\mu,\eta^2{:}\eta^2\text{-}C_{60})_2]$ (**24**) was obtained by the same group.[109] The latter species, however, features phosphine ligands coordinated to the cobalt atoms instead of carbonyls and has a bridging chloride atom linking both metal centers.

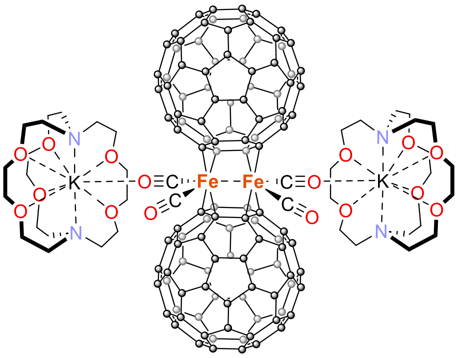

Figure 3. Representation of the molecular structure of **23**, according to X-ray crystallographic analysis.

Zhou and Frenking studied the species $ANi(CO)_3^-$ (**25**, A = Li, Na, K, Rb, Cs) using mass-selected infrared photodissociation spectroscopy in the gas phase, like with the previously discussed iron compounds $AFe(CO)_3^-$ (**19**).[102−104,110] In **25**, the alkali metal is covalently bound to the anionic nickel−carbonyl fragment, interacting with the metals and with the carbon atoms of the carbonyl ligands. The nickel center is in a nearly planar C_{3v} geometry, with the alkali metal located above this plane.[110]

In turn, the tricarbonyl nickelate $[Ni(CO)_3]^{2-}$ (**26**) was identified, and structurally characterized, as the anionic part of the carbonyl nickel salt $[A([18]\text{crown-6})]_2[Ni(CO)_3]\cdot 8NH_3$ (A = K, Rb).[111] $[Ni(CO)_3]^{2-}$ completes the series of known first-row carbonyl metalates. A previous attempt to obtain a similar compound via reduction of $Ni(CO)_4$ (**27**) with alkali metals had led only to the synthesis of two different nickelates: $[Ni_2(CO)_6]^{2-}$ (**28**) in pyridine or $H_2Ni_2(CO)_6$ [H_2(**28**)] in liquid ammonia.[112] The serendipitous discovery of anion **26** came after an attempt to functionalize germanium clusters with the Ni(0) compound $(PPh_3)_2Ni(CO)_2$ (**29**) in the presence of a crown ether and liquid ammonia. Single crystal X-ray structural analysis of the thermally unstable, air- and moisture sensitive crystalline material revealed that the nickel center is surrounded by the carbonyl ligands in an almost perfect trigonal planar geometry, with a D_{3h} point group symmetry (see Figure 4). The anion interacts with a crown ether-stabilized potassium cation and weakly with three ammonia molecules in the crystal lattice. Theoretical calculations supported X-ray diffraction results, thus ruling out the C_{3v} nonplanar structure previously predicted for **26** almost 40 years earlier.[111,113]

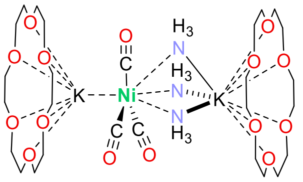

Figure 4. Representation of the structure of $[K([18]\text{crown-6})]_2[\mathbf{26}]\cdot 8NH_3$, according to X-ray crystallographic analysis.[111]

2.2.2. Cyanido Complexes.

Contrasting with the wide variety of highly reduced carbonyl metalates, cyanido compounds with metal centers in formally negative oxidation states have rarely been reported.[114] Exceptional examples of highly reduced complexes at group 8 and 9 transition metals are $[Fe(CN)_3]^{7-}$ (**30**), $[Fe(CN)_4]^{6-}$ (**31**), $[Ru(CN)_3]^{7-}$ (**32**), and $[M(CN)_3]^{6-}$ [M = Co (**33**), Rh (**34**), Ir (**35**)], which were reported by Jach and co-workers.[114−119] Unlike the cases summarized in Scheme 1, these cyanido complexes are synthesized by solid-state routes in which pelletized mixtures of the corresponding transition metal, an alkaline earth metal subnitride, graphite, and either nitride or cyanide salts (as a nitrogen source) react under argon at temperatures higher than 1020 K. The tricyanidometalates **30** and **32−35** were isolated as alkaline earth metal salts, $AE_{3.5}[M(CN)_3]$ (for M = Fe, Ru, AE = Sr, Ba) and $AE_3[M(CN)_3]$ (for M = Co, AE = Sr, Ba; for M = Rh, Ir, AE = Ba), respectively. Complex **30** also formed as the mixed salt $LiSr_3[Fe(CN)_3]$, whereas ferrate **31** was isolated as $(Sr_3N)_2[Fe(CN)_4]$. In all cases, the ligands exhibited elongated C−N bonds (1.20 to 1.28 Å) with respect to the classical cyanido ligand (1.15 Å, on average), and significantly

Scheme 2. Synthesis of Mixed Carbonyl/Isocyanide Mn-Metalates by the Group of Figueroa[123]

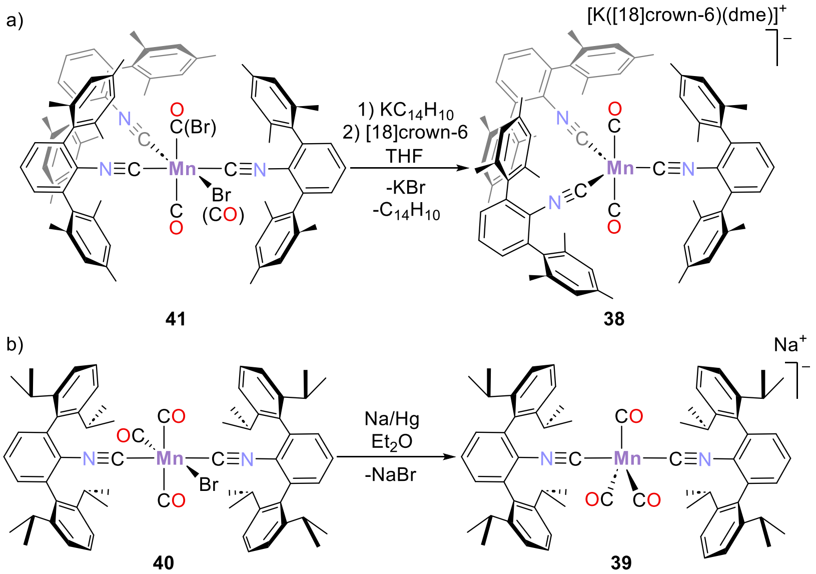

lower ν_{CN} stretching frequencies in IR, in the range 1490–1688 cm^{-1} (vs 2000–2100 cm^{-1} in classical CN^- ligands).[114,120] These values indicate strong π-backbonding interactions with the metal atoms. Physical characterization and quantum chemical calculations indicate that the reduced cyanidometalates are best described as $[M^{2-}(CN^{1.67-})_3]^{7-}$ (M = Fe, Ru) and $[M^{-}(CN^{1.67-})_3]^{6-}$ (M = Co, Rh, Ir) instead of the formal $[M^{4-}(CN^-)_3]^{7-}$ or $[M^{3-}(CN^-)_3]^{6-}$, respectively, with the transition metal centers in $d^{10}s^0$ configurations (18 valence electrons, VE). In turn, complex $[Fe(CN)_4]^{6-}$ (**31**) was also regarded as featuring an Fe(−II) center in a $d^{10}s^0$ configuration (18 VE). Given the similarities between the isoelectronic cyanido and carbonyl complexes, e.g., in the pair $[Fe(CN)_4]^{6-}$ (**31**) and $[Fe(CO)_4]^{2-}$ (**1**), or $[Co(CN)_3]^{6-}$ (**33**) and $[Co(CO)_3]^{3-}$ (**36**),[121,122] the authors anticipated that the isolation of further examples of highly reduced cyanido species analogous to known carbonyl metalates might be feasible.[114−119]

2.2.3. Isocyanide Complexes. *2.2.3.1. Manganese Isocyanide Complexes.* Figueroa and co-workers have contributed to the chemistry of 3d manganese,[123,124] iron,[125] and cobalt[126,127] metalates. In 2011, mixed carbonyl/isocyanide manganese monoanions were reported by this group.[123] Since isocyanides are both weaker π-acceptors and stronger σ-donors than CO, the synthesis of mixed carbonyl/isocyano complexes by substitution with isocyanides has been used as a strategy to increase the electron density, and therefore nucleophilicity, of carbonyl-containing complexes.[128] In an attempt to combine the steric and electronic tunability of isocyanide ligands with the reactivity pattern offered by the known $[Mn(CO)_5]^-$ (**37**), the group of Figueroa synthesized two examples of mixed complexes, namely $[Mn(CO)_2(CNAr^{Mes2})_3]^-$ (**38**) and $[Mn(CO)_3(CNAr^{Dipp2})_2]^-$ [**39**, synthesized from $BrMn(CO)_3(CNAr^{Dipp2})_2$ (**40**) see Scheme 2; Mes = 2,4,6-$Me_3C_6H_2$, Dipp = 2,6-$(i\text{Pr})_2C_6H_3$]. The synthesis of trigonal bipyramidal complex **38** proved challenging. Only after sequential treatment of the isomeric mixture of $BrMn(CO)_2(CNAr^{Mes2})_3$ (**41**) with potassium anthracenide ($KC_{14}H_{10}$) and [18]crown-6 was it possible to isolate and characterize complex **38** in a 20% yield. This compound is stable at −35 °C in the solid state but decomposes rapidly at room temperature in solution (over the course of 4 h in C_6D_6). Consequently, its reactivity could not be conveniently assessed. By contrast, with the more sterically demanding ligand $CNAr^{Dipp2}$, complex **39** is stable in C_6D_6 solution for days. IR stretching frequencies ν_{CO} and ν_{CN} for both complexes are listed on Table 1. The low-frequency ν_{CO} [**38**: 1841 cm^{-1}; **39**: 1896 and 1773 cm^{-1}] and ν_{CN} [**38**: 1891 cm^{-1} vs free $CNAr^{Mes2}$ = 2118 cm^{-1};[129] **39**: 1910 cm^{-1} vs free $CNAr^{Dipp2}$, C_6D_6 solution = 2118 cm^{-1}][130] stretches observed by FT-IR reflect the significant π-backdonation from the reduced manganese centers.

Furthermore, the reactivity of **39** differs notably from that of the related complex $[Mn(CNXyl)_5]^-$ (Xyl = 2,6-$Me_2C_6H_3$; **42**).[131] Cooper and co-workers found that **42** is thermally unstable and undergoes multiple insertion processes. The reaction of **42** with alkyl electrophiles led to an alkylation-induced coupling of two isocyanide ligands to form a structurally characterized 1,4-diazabutadien-2-yl complex of manganese.[132] Contrastingly, compound **39** reacted with HCl, MeI, or heavier main-group electrophiles such as $MeSiCl_3$ or $SnCl_2$ to afford the series of products *mer,trans*-$RMn(CO)_3(CNAr^{Dipp2})_2$ [R = H- (**43**), Me- (**44**), Cl_2MeSi- (**45**), ClSn- (**46**), Scheme 3], where the electrophile binds to the metal center. Remarkably, for the hydride and methyl derivatives **43** and **44**, the complexes behaved similarly to the carbonyl analogue $RMn(CO)_5$ (**47**), mimicking the chemistry of **47** while benefiting from the steric protection provided by the isocyanide ligand.[123]

Later, Figueroa and co-workers reported that the reaction of complex **39** with the triflate Mn(I) complex $[Mn(OTf)(CO)_3(CNAr^{Dipp2})_2]$ (**48**) affords the isolable Mn(0) monoradical $[Mn(CO)_3(CNAr^{Dipp2})_2]$ (**49**) in high yield (92%) via comproportionation. The same species is also accessible, albeit in a less convenient synthetic pathway, through oxidation of **39** with thallium triflate (TlOTf; 1.0 equiv), generating metallic thallium and NaOTf as byproducts.[124]

2.2.3.2. Isocyanide Ferrates. The groups of Ellis[133] and Figueroa[125] independently reported on the synthesis and reactivity of iron-isocyano metalates (Scheme 4). The dianionic complexes $[Fe(CNR)_4]^{2-}$ [CNR = CNXyl (**50**),

Table 1. ν_{CO} and ν_{CN} Stretching Frequencies (cm^{-1}) for Selected Metalates Bearing Carbonyl or Isocyanide Ligands

Complex	ν_{CO} (cm^{-1})	ν_{CN} (cm^{-1})	Ref
$[K([18]crown\text{-}6)(dme)][Mn(CO)_2(CNAr^{Mes2})_3]$	1841 (s, vb)[a]	1891	123
$Na[Mn(CO)_3(CNAr^{Dipp2})_2]$	1896, 1773	1910	123
$K_2[Fe(CNXyl)_4]$	-	1670	133
$Na_2[Fe(CNAr^{Mes})_4]$	-	1682	125
$Na[HFe(CNAr^{Mes2})_4]$	-	1994–1828	125
$K_2[Fe(CO)_2(CNAr^{Tripp2})_2]$	1878 (w), 1793 (m)	1599 (vw), 1562 (s)	74
$Fe(CO)_3(CNAr^{Tripp2})_2$	1940	2146 (vw), 2092 (vs)	74
$Fe(BF)(CO)_2(CNAr^{Tripp2})_2$	1980 (s), 1942 (vs)	2126 (vw sh), 2056 (s)	74
$Fe(N_2)(CO)_2(CNAr^{Tripp2})_2$	1953 (m), 1918 (s)	2122 (vw), 2075 (vs)	74
$[K(Et_2O)]_2[Fe(CNAr_3NC)_2]_2$	-	1982 (w) and 1961 (w)	75
$[K([18]crown\text{-}6)(dme)][Co\{1,2\text{-}(PMes)_2C_2B_{10}H_{10}\}(CNCy)_2]$	-	2029 and 1938	134
$[K([18]crown\text{-}6)(THF)_2][Co(CN\textit{t}Bu)_4]$	-	1778 (vs br)	87
$Na[Co(CNAr^{Mes2})_4]$	-	1903, 1821, and 1761	126
$[PPN][Co(CNAr^{Mes2})_4]$	-	1821	126
$(\eta^2\text{-}PPN)Co(CNAr^{Mes2})_3$	-	1952, 1860, and 1824	127
$Na[Co(CO)(CNAr^{Mes2})_3]$	1830	1904, 1864	135
$Na[Co(CO)_2(CNAr^{Mes2})_2]$	1852	1891	135
$Na[Co(CO)_3(CNAr^{Mes2})]$	1870 (vs), 1846 (s)	1932	135
$[(\mu\text{-}CNAr^{Mes2})_2\{CpCo\}_2]$	-	1834	136
$K[(\mu\text{-}CNAr^{Mes2})_2\{CpCo\}_2]$	-	1666	136
$K_2[(\mu\text{-}CNAr^{Mes2})_2\{CpCo\}_2]$	-	1511	136
$[\{K(Et_2O)\}_2\{Cp^*Co\equiv CNAr^{Tripp2}\}]$	-	1509	137
$[K(Et_2O)][Cp^*Co(H)(CNAr^{Tripp2})]$	-	1710	137
$[K(Et_2O)][Cp^*Co(SiMe_3)(CNAr^{Tripp2})]$	-	1707	137
$Ph_2B(\textit{t}BuIm)_2Fe(CO)_3$	1987, 1900	-	76
$[K([2.2.2]cryptand)][Ph_2B(\textit{t}BuIm)_2Fe(CO)_3]$	1926, 1836, 1800	-	76
$K_2[Ph_2B(\textit{t}BuIm)_2Fe(CO)_2]_2$	1838, 1742	-	76
$[PhB(MesIm)_3Fe(CO)_3][B(C_6F_5)_4]$	2100, 2040	-	77
$PhB(MesIm)_3Fe(CO)_2$	1956, 1886	-	77
$K[PhB(MesIm)_3Fe(CO)_2]$	1812, 1728	-	77
$K[Fe(PC_{carbene}P)(CO)_2]$	1826, 1767	-	80
$[Na([15]crown\text{-}5)][(^{Dipp}PDI)Fe(CO)_2]$	1935, 1863	-	138
$[(^{Dipp}nacnac)Ca(\mu\text{-}OC)_2Fe(\eta^5\text{-}Cp)(thf)_2]_2$	1823, 1780	-	139
$[(^{Dipp}nacnac)MgFe(\eta^5\text{-}Cp)(CO)_2(thf)]$	1926, 1857	-	140
$[(^{Dipp}nacnac)Mg\{(NTol)_2CFe(\eta^5\text{-}Cp)(CO)_2\}]$	2010, 1956	-	140
$[(P_3{}^B)Fe(CO)]$	1857	-	141
$[(P^{Ph}{}_3{}^{Si})Fe(CO)]$	1881	-	142
$[(P^{\textit{i}Pr}{}_3{}^{Si})Fe(CO)]$	1850	-	143
$[(P^{\textit{i}Pr}{}_3{}^{Si})Fe\{CONa(thf)_3\}]$	1717	-	143
$[Na([12]crown\text{-}4)_2][(P^{Ph}{}_3{}^{Si})Fe(CO)]$	1757	-	143

[a] $\nu_{CO} + \nu_{CN}$.

$CNAr^{Mes2}$ (**51**)] are the isocyanide analogues of the first known carbonylmetalate, $[Fe(CO)_4]^{2-}$ (**1**).[1,2,12]

Scheme 3. Reactivity of $Na[Mn(CO)_3(CNAr^{Dipp2})_2]$ (Na[**39**]) by Figueroa and Co-workers[123,124]

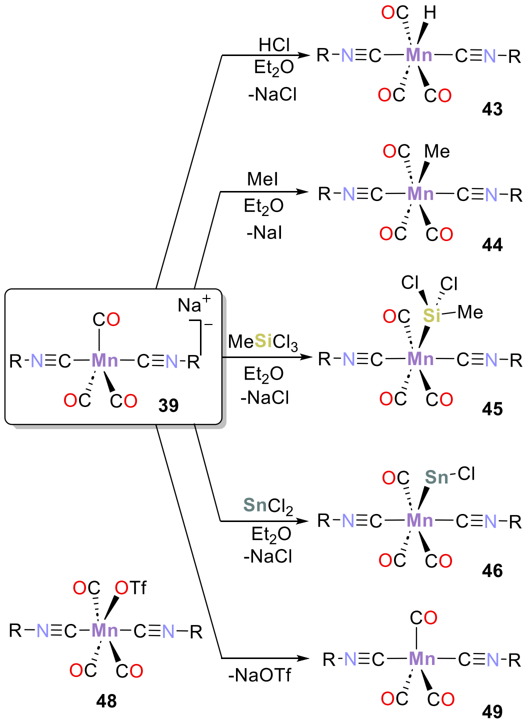

Scheme 4. Synthesis of the Iron-Isocyano Metalates $[Fe(CNR)_4]^{2-}$ (**50**, **51**) by the Groups of (a) Ellis[133] and (b) Figueroa[125]

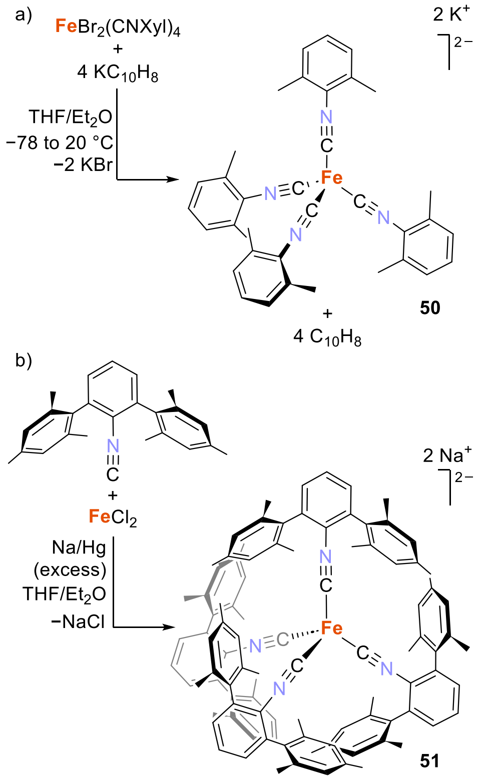

Despite being a successful strategy for the isolation of metalates, the direct treatment of the labile anthracene-Fe(−I) complex $[Fe(\eta^4\text{-}C_{14}H_{10})_2]^-$ (**52**, *vide infra*) with CNXyl did not afford homoleptic isocyanide-iron complexes.[144] Instead, compound **50** was obtained after reduction of iron(II) bromide by potassium naphthalenide at low temperatures, in the presence of CNXyl (4 equiv) (Scheme 4a).[133] The solid-state molecular structures of the Fe(II)-isocyanide complex $FeBr_2(CNXyl)_4$ (**53**), the zerovalent $Fe(CNXyl)_5$ (**54**), and a cocrystallized form containing **54** and the dinuclear $[Fe(CNXyl)_3]_2(\mu_2\text{-}CNXyl)_3$ (**55**) were later reported.[144] For metalate **50**, both the FT-IR stretching bands (ν_{CN} = 1670 cm^{-1}; see Table 1) and the C−N bond length (1.237(7) Å) indicate a strong metal-to-ligand backbonding, as a consequence of the electron-rich character of the Fe(−II) center.[133]

The reaction of **50** with Ph_3SnCl (2.0 equiv) furnishes the air-stable complex *trans*-$[Fe(CNXyl)_4(SnPh_3)_2]$ (**56**) (see Scheme 5). The CN*t*Bu analogue *trans*-$[Fe(CN\textit{t}Bu)_4(SnPh_3)_2]$ (**57**) was also isolated, via the proposed intermediate $[Fe(CN\textit{t}Bu)_4]^{2-}$ (**58**), which was not isolated due to thermal instability. The formation of complexes **56** and **57** contrasts with the behavior previously observed for carbonylmetalate **1**, for which similar reactions afford a series of compounds, among which is *cis*-$[Fe(CO)_4(SnPh_3)_2]$.[145] The *trans* arrangement instead observed in **56** and **57** was attributed to the poorer acceptor properties and higher steric hindrance of isocyanides compared to CO ligands.[91,133]

Scheme 5. Reactivity of $[Fe(CNR)_4]^{2-}$ [CNR = CNXyl (50), $CNAr^{Mes2}$ (51), CN*t*Bu (58)][125,133]

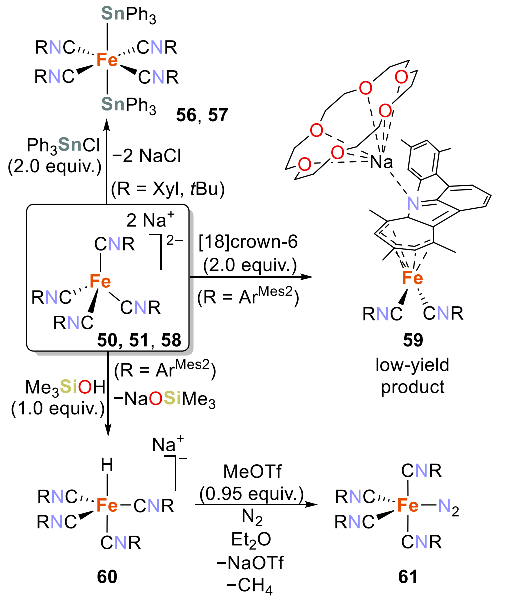

The bulkier iron-isocyano metalate **51**, reported by Figueroa and co-workers,[125] was obtained via reduction of $FeCl_2$ with sodium amalgam in the presence of the isocyano ligand $CNAr^{Mes2}$ (Scheme 4b). The complex formed as an unsolvated contact ion triple with the sodium cations, as confirmed via crystallographic characterization. Again, the FT-IR and ^{13}C NMR data obtained are consistent with significant metal-to-ligand backbonding, and the minimal structural differences observed are attributed to the steric constraint exerted by the bulkier isocyanide ligands. Attempts to disrupt the ion-pairing with [18]crown-6 resulted in decomposition of the ferrate Na_2[**51**] to the formally Fe(I)-1-azabenz[*b*]azulene product $[Na([18]crown\text{-}6)][(\eta^5\text{-}Me_6\text{-}1\text{-}azabenz[b]azulene)Fe(CNAr^{Mes2})_2]$ (**59**), seemingly obtained after an aza-Büchner ring expansion of an isocyanide $CNAr^{Mes2}$ ligand (Scheme 5).

Metalate **51** reacts with trimethylsilanol (Me_3SiOH) to yield the protonated product $Na[HFe(CNAr^{Mes2})_4]$ (Na[**60**], Scheme 5), in behavior similar to that of the tetracarbonyl analogue **1**.[125] Different reactivity was observed upon treating **51** with stronger Brønsted acids (3,5-dimethylbenzoic acid, pivalic acid, pyridinium chloride, or ethylammonium chloride) at low temperatures. These reactions yielded only complex mixtures of free ligand, unreacted material, and unidentified species. The authors attributed such behavior to the presumable formation of the doubly protonated product, $H_2Fe(CNAr^{Mes2})_4$, which would rapidly decompose under the studied conditions. This species could not be accessed from **60** and additional equivalents of Me_3SiOH, which would indicate that **60** displays only moderate Brønsted basicity. However, the characterization of complex Na[**60**], in particular its higher energy stretching bands in the FT-IR spectrum (ν_{CN} = 1994−1828 cm^{-1}; see Table 1), evidenced that the iron center in the complex remained highly reduced and would be expected to react with strong electrophiles.

Therefore, **60** was treated with MeOTf at low temperatures (Scheme 5), affording methane and the zerovalent product $Fe(N_2)(CNAr^{Mes2})_4$ (**61**), which could be regarded as a trapped form of the tetraisocyano complex $Fe(CNAr^{Mes2})_4$. The latter is analogous to the elusive $Fe(CO)_4$, which has been photochemically generated in matrix isolation experiments and characterized by infrared spectroscopy.[146−148] Complex **61**, however, decomposed completely in solution at room temperature in a relatively short time frame (4 h), through an intramolecular ligand C−H activation mechanism.[125] Such decomposition complicated the study of additional reactivity patterns for **61**. Nevertheless, this work highlighted the parallel in reactivity between carbonyl and isocyano metalate complexes.

The mixed isocyano/carbonyl metalates $K_2[Fe(CO)_2(CNAr^{Tripp2})_2]$ [**62**, Ar^{Tripp2} = 2,6-(2,4,6-$(iPr)_3C_6H_2)_2C_6H_3$] and $K_2[Fe(CO)_2(CNAr^{Dipp2})_2]$ [**63**, Ar^{Dipp2} = 2,6-(2,6-$(iPr)_2C_6H_3$)], analogous to **50**,[125] were also reported by the Figueroa group.[74,149] In a multistep synthetic protocol, pentacarbonyliron(0) is photolytically transformed, in the presence of the more sterically encumbered ligand $CNAr^{Tripp2}$ (2.2 equiv), to the iron(0) complex $Fe(CO)_3(CNAr^{Tripp2})_2$ (**64**), which is subsequently oxidized by molecular iodine (1.0 equiv) to afford $[Fe(I)_2(CO)_2(CNAr^{Tripp2})_2]$ (**65**). The latter complex reacted with KC_8 (4.5 equiv) to yield the formally Fe(−II) mixed isocyano/carbonyl complex **62** (Scheme 6).[74] Likewise, $[Fe(I)_2(CO)_2(CNAr^{Dipp2})_2]$ (**66**) was reduced with KC_8 (4.5 equiv) to obtain the analogue $K_2[Fe(CO)_2(CNAr^{Dipp2})_2]$ (**63**).[150]

Treatment of complex **62** with 2.8 equiv of $BF_3{\cdot}Et_2O$ (Scheme 7) afforded the unprecedented terminal fluoroborylene-iron complex, $Fe(BF)(CO)_2(CNAr^{Tripp2})_2$ (**67**). The same product was obtained at lower ratios of **62**:$BF_3{\cdot}Et_2O$ (1:1 and 1:2), although in lower yields/conversions and/or with the formation of the tetrafluoroborate ($[BF_4]^-$) ion as a byproduct. Based on such observations, the authors suggested that the transformation of complex **62** into **67** proceeds via an unobserved anionic irondifluoroboryl intermediate, presumably $[Fe(BF_2)(CO)_2(CNAr^{Tripp2})_2]^-$ (**68**), and that the loss of the second fluoride is promoted by the excess of BF_3. Compound **67** was the first crystallographically characterized terminal fluoroborylene complex. Its kinetic stability is sufficient to allow isolation at room temperature.[74] The structural and spectroscopic characterization of **67** indicates

Scheme 6. Synthesis of Mixed Carbonyl/Isocyano Fe(−II) Metalates by Figueroa and Co-workers[74,149,150]

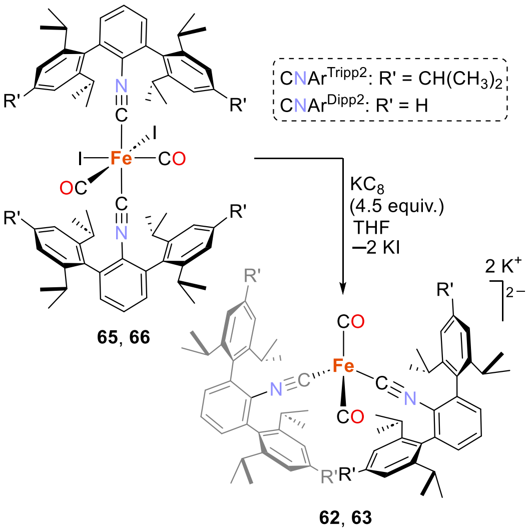

Scheme 7. Reactivity of the Mixed Complexes K$_2$[Fe(CO)$_2$(CNAr^{Tripp2})$_2$] (62) and K$_2$[Fe(CO)$_2$(CNAr^{Dipp2})$_2$] (63)[74,149,150]

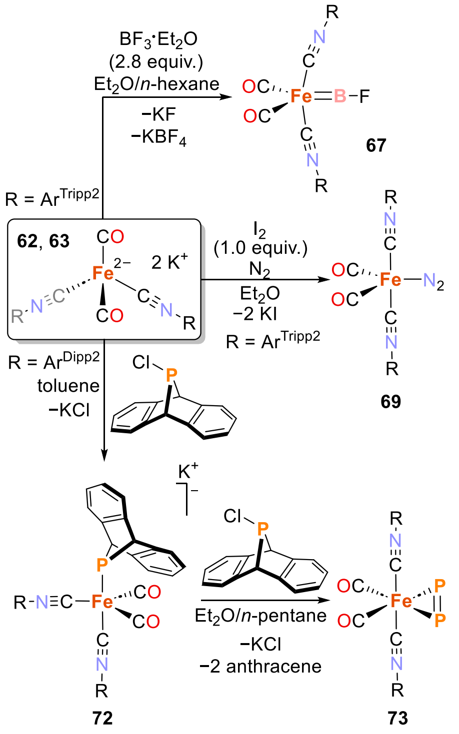

that the terminal fluoroborylene ligand displays characteristics of both a strong σ-donor and π-acceptor.

As with [Fe(CNXyl)$_4$]$^{2-}$ (**50**), ferrate **62** can be oxidized (with iodine) in the presence of N$_2$ to yield an analogue of **61**, namely Fe(N$_2$)(CO)$_2$(CNAr^{Tripp2})$_2$ (**69**, Scheme 7).[74,149] Compared with **61**, which exhibited poor thermal stability, **69** is more stable at room temperature in benzene, n-pentane, and Et$_2$O solution under an N$_2$ atmosphere. Such enhanced stability is a consequence of the greater steric protection of the bulkier isocyano ligands CNAr^{Tripp2} in combination with the additional electronic stabilization offered by the two CO ligands.[149] The authors found that the dinitrogen ligand has a low degree of activation, as reflected by the short N−N distance determined via X-ray diffraction (d_{NN} = 1.1059(41) Å) and by the high-energy FT-IR stretching band ($\nu_{N\equiv N}$ = 2194 cm^{-1}; see Table 2 below). This lack of activation was attributed to the presence of the strongly π-acidic CO and isocyanide ligands. Furthermore, it was found that the N$_2$ ligand was sufficiently labile to be displaced, opening the coordination sphere of **69** to engage in small molecule activation. The reactivity of **69** toward H−H or Si−H moieties contrasts with that of its analogue **61**. Oxidative addition of any of the studied substrates afforded the respective Fe(II) complexes HFeI(CO)$_2$(CNAr^{Tripp2})$_2$ (**70**, R = H, SiEt$_3$, or SiH$_2$Ph), with loss of N$_2$. In addition, the reaction of **69** with white phosphorus led to the cleavage of one edge of the P$_4$ tetrahedron, forming the butterfly-P$_4$ complex Fe(κ^2-P$_4$)(CO)$_2$(CNAr^{Tripp2})$_2$ (**71**).[151]

Table 2. Selected $\nu_{N\equiv N}$ Stretching Frequencies (cm^{-1}) for Dinitrogen-Bound Anionic Complexes

Complex	$\nu_{N\equiv N}$ (cm^{-1})	Ref
free N$_2$ (g)	2331	549
Fe(N$_2$)(CO)$_2$(CNAr^{Tripp2})$_2$	2194	149
[K([18]crown-6][(N$_2$)Fe(CAAC)$_2$]	1850	79
[(ICy)$_3$Co(N$_2$)]	1917	550
[K(ICy)$_2$Co(N$_2$)$_2$]	1807	550
K$_2$[(^{tBu}nacnac)Fe(NN)Fe(nacnac^{tBu})]	1589	551
K$_2$[(nacnac)Co(NN)Co(nacnac)]	1599	552
[(^{Ad}p^{Pym}DI)Fe(N$_2$)]	2050	393
[Na([18]crown-6)(thf)$_2$][(^{Ad}P^{Pym}DI)Fe(N$_2$)]	1935	393
(N$_2$)Co(SiMe$_3$)(CNAr^{Mes2})$_3$	2224	127
[(P$_3$^{B})Fe(N$_2$)]	2011	141
[Na([12]crown-4)$_2$][(P$_3$^{B})Fe(N$_2$)]	1905^a	141
[Na([12]crown-4)$_2$][K(DME)$_x$][(P$_3$^{B})Fe(N$_2$)]	1836	486
[(P^{Ph}$_3$^{Si})Fe(N$_2$)]	2041	142
[Na([12]crown-4)$_2$][(P^{Ph}$_3$^{Si})Fe(N$_2$)]	1967	142
[(P^{iPr}$_3$^{Si})Fe(N$_2$)]	2008	142
[Na([12]crown-4)$_2$][(P^{iPr}$_3$^{Si})Fe(N$_2$)]	1920	432
[(P$_3$^{B})Co(N$_2$)]	2089	528
[Na([12]crown-4)$_2$][(P$_3$^{B})Co(N$_2$)]	1978	553
[(N$_2$)FeAl{N[o-(NCH$_2$PiPr$_2$)C$_6$H$_4$]$_3$}]	2010	434
[(N$_2$)CoAl{N[o-(NCH$_2$PiPr$_2$)C$_6$H$_4$]$_3$}]	2081	434
[K([18]crown-6)]$^+$ [(N$_2$)FeAl{N[o-(NCH$_2$PiPr$_2$)C$_6$H$_4$]$_3$}]$^-$	1925	434
[K([2.2.2]cryptand)]$^+$ [(N$_2$)CoAl{N[o-(NCH$_2$PiPr$_2$)C$_6$H$_4$]$_3$}]$^-$	1995	434
[N(PPh$_3$)$_2$]$^+$ [(N$_2$)CoGa{N[o-(NCH$_2$PiPr$_2$)C$_6$H$_4$]$_3$}]$^-$	1999	527
[N(PPh$_3$)$_2$]$^+$ [(N$_2$)CoIn{N[o-(NCH$_2$PiPr$_2$)C$_6$H$_4$]$_3$}]$^-$	2021	527
[K([2.2.2]cryptand)]$^+$ [(N$_2$)CoV{N[o-(NCH$_2$PiPr$_2$)C$_6$H$_4$]$_3$}]$^-$	1971	496
[K([2.2.2]cryptand)]$^+$ [(N$_2$)CoCr{N[o-(NCH$_2$PiPr$_2$)C$_6$H$_4$]$_3$}]$^-$	1990	496
[K([2.2.2]cryptand)]$^+$ [(N$_2$)Co$_2${N[o-(NCH$_2$PiPr$_2$)C$_6$H$_4$]$_3$}]$^-$	1994	554

^{a}Average value.

Reaction between the nucleophilic complex K$_2$[Fe(CO)$_2$(CNAr^{Dipp2})$_2$] (**63**) and anthracendiyl-substituted chlorophosphine, ClP(anthr) (1 equiv; anthr = 9,10-anthracendiyl) afforded the anionic complex [Fe(P(anthr))(CO)$_2$(CNAr^{Dipp2})$_2$]$^-$ (**72**, Scheme 7, bottom).[150] Single crystal X-ray diffraction experiments revealed that the molecular structure features an intact anthracendiyl-substituted phosphanyl ligand. Although **72** is stable in solution for several

Scheme 8. Synthesis of Bidentate Isocyanide Iron Complexes by the Group of Wolf and Reiser[75]

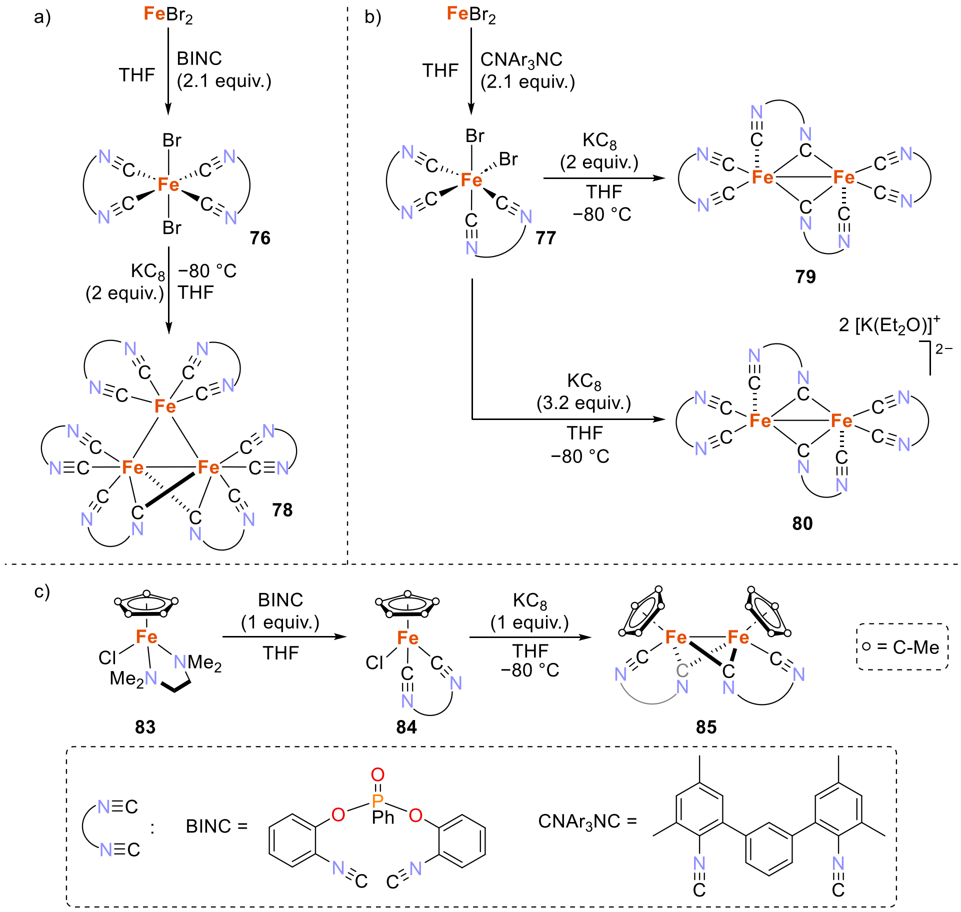

days at room temperature, it reacts quickly with additional ClP(anthr) (1 equiv) to yield complex $[(\eta^2\text{-}P_2)Fe(CO)_2(CNAr^{Dipp2})_2]$ (**73**), in which a side-on coordinated diphosphorus ligand has been formed. It was demonstrated that the susceptibility of ClP(anthr) to suffer C−P bond homolysis and its steric hindrance are essential in the formation of the diphosphorus ligand at the metal center: similar reactions between **72** and other electrophilic chlorophosphines, i.e., $ClPPh_2$ and $ClP(iPr)_2$, afforded only the phosphanylphosphine complexes $[Fe(\kappa^1\text{-}P(anthr)PR_2)(CO)_2(CNAr^{Dipp2})_2]$ (**74**, R = Ph, *i*Pr). It was proposed that the formation of **73** could go through an intermediate analogous to **74**, in which sequential anthracene extrusion leads to the formation of the diphosphorus scaffold. The average P−P bond distance for the diphosphorus ligand in **73** [d_{PP} = 1.988(1) Å] is longer than the experimentally determined distance for free P_2 [d_{PP} = 1.8934 Å], but still evidence of a strong interaction, with significant P−P multiple bond character. This is further corroborated by ^{31}P NMR analysis, DFT, and natural bond orbital (NBO) calculations. A comparison between the structural features of **73** and those of the η^2-alkyne complex $[(\eta^2\text{-BTMSA})Fe(CO)_2(CNAr^{Dipp2})_2]$ (**75**, BTMSA = bis-trimethylsilylacetylene) confirmed that both complexes are isostructural, suggesting a close electronic analogy. Nonetheless, these complexes exhibit disparate reactivity: while **73** reacts with diene nucleophiles (1,3-butadiene or 1,3-cyclohexadiene) to afford diphospha-Diels−Alder adducts, complex **75** failed to react with these substrates.[150]

Bidentate isocyanide ligands form chelates larger than those of typical N,N- or P,P-ligands due to the linear arrangement of the C≡N unit, which imposes rigidity to the structure of the complexes. Considering this, and the known ability of isocyanide ligands to stabilize low-valent iron centers,[74,125,133,149,150] Wolf, Reiser, and co-workers reported a series of mono- and polynuclear iron complexes featuring the bidentate ligands BINC (bis(2-isocyanophenyl)-phenylphosphonate) and CNAr$_3$NC (2,2′′-diisocyano-3,5,3′′,5′′-tetramethyl-1,1′:3′,1′′-terphenyl).[75] Although the reductions of isocyanide halide complexes led mainly to neutral complexes, we are including these results for context. Treating anhydrous $FeBr_2$ with either of the selected bidentate ligands (2.1 equiv; see Scheme 8a and b) afforded mononuclear compounds of general formula $[FeBr_2(diisocyanide)_2]$ [diisocyanide = BINC (**76**), CNAr$_3$NC (**77**)]. Reduction of **76** with KC_8 (2 equiv) resulted in the formation of $[Fe_3(BINC)_6]$ (**78**, see Scheme 8a), a structural analogue of the carbonyl-iron cluster $[Fe_3(CO)_{12}]$ (**22**). **78** possesses a triangular iron arrangement in which the shorter Fe−Fe bond (2.495(6) Å vs 2.682(6) and 2.685(6) Å) features two bridging isocyanide units. In solution, **78** has a fluxional behavior between the coordinated bridging and terminal isocyanide moieties. The difference in the stretching bands of the free ligand ($\nu_{C≡N}$ = 2126 cm^{-1}) with respect to the coordinated isocyanide in complex **76** ($\nu_{C≡N}$ = 2122 cm^{-1}) or **78** ($\nu_{C≡N}$ = 2035 cm^{-1}) evidenced the low-valent character of the metal centers in the latter. While the band in the Fe(II) complex **76** is essentially at the same frequency as in the free ligand, in the formally zerovalent **78** this is shifted to lower frequencies, thus indicating substantial metal-to-ligand back-bonding. This is additionally supported by the shortened Fe−C bond lengths (1.83(1) Å in **78** vs 1.87(4) Å in **76**, on average).

Analogous reduction of complex **77**, featuring the bulkier isocyanide CNAr$_3$NC, afforded either the dimeric complex [Fe(CNAr$_3$NC)$_2$]$_2$ (**79**) or the anionic dimer [K(Et$_2$O)]$_2$[Fe(CNAr$_3$NC)$_2$]$_2$ (**80**), depending on the stoichiometry of KC$_8$ used (2 or 3.2 equiv; Scheme 8b).

Both dimers possess a butterfly arrangement caused by the restrictions imposed by the bridging isocyanide ligands. Unlike its carbonyl analogue [Fe$_2$(CO)$_8$] (**81**), **79** is stable and isolable at room temperature. Such stability was attributed to the steric effect of the bulky isocyanide ligands. A contrast between the structural data of **80** and that of its carbonyl analogue [Fe$_2$(CO)$_8$]$^{2-}$ (**82**)[152−154] revealed that, in the latter, the Fe−Fe bond is significantly longer (2.804(1) Å) than in **80** ($d_{\text{Fe−Fe}}$ = 2.552(8) Å) due to the absence of bridging carbonyl ligands. Treatment of the Fe(II) precursor [Cp*FeCl(tmeda)] (**83**, Cp* = C$_5$Me$_5$, tmeda = tetramethylethylene-1,2-diamine) with the diisocyanide ligand BINC (Scheme 8c) led to the formation of the mononuclear complex [Cp*FeCl(BINC)] (**84**), which undergoes reduction by reaction with KC$_8$ (1 equiv) to form the dinuclear heteroleptic compound [Cp*Fe(BINC)]$_2$ (**85**). This crystallizes as the *cis*-isomer, with both Cp* groups coordinated above the Fe−Fe bond. However, in solution (THF-d_8), the NMR spectroscopic measurements revealed an equilibrium between the *cis* and *trans* isomers.[75]

2.2.3.3. Cobalt Isocyanides. The first examples of homoleptic isocyanide cobaltates were [K(dme)][Co(CNXyl)$_4$] (**5**), reported by Cooper and co-workers (*vide supra*, Figure 1),[63,64] and a closely related alkylisocyanocobaltate complex [K([18]crown-6)(thf)$_2$][Co(CN*t*Bu)$_4$] (**86**), reported by Ellis and Brennessel.[87] In 2010, Figueroa and co-workers described the synthesis and reactivity of bulky arylisocyanocobaltates, which have an extensive reaction chemistry.[126] The ion contact complex Na[Co(CNAr$^{\text{Mes2}}$)$_4$] (Na[**87**]), featuring a Co(−I) center, was synthesized by reduction of CoCl$_2$ with sodium amalgam, in the presence of the encumbering ligand CNAr$^{\text{Mes2}}$ (Scheme 9). The observed ion-pairing is similar to that previously discussed (*vide supra*) for the iron metalate **51**, reported by the same group.[125] Crystallographic characterization confirmed the ion contact, which was also observed in **5**. Addition of [Ph$_3$PNPPh$_3$]Cl {[PPN]Cl; PPN = [Ph$_3$PNPPh$_3$]$^+$) was found to disrupt the contact ion pair, and the ion-separated metalate [PPN][Co(CNAr$^{\text{Mes2}}$)$_4$] ([PPN][**87**]) was obtained. Stretching frequencies (FT-IR) for both the ion-paired and the ion-separated complexes are given in Table 1, with the number of bands reflecting the changes in pairing.

Reaction of Na[**87**] with FcOTf (1 equiv; Fc = ferrocenium) yields the neutral paramagnetic complex Co(CNAr$^{\text{Mes2}}$)$_4$ (**88**; Scheme 10a), contrasting with the behavior of the previously reported [K(dme)][Co(CNXyl)$_4$] (**5**), which dimerizes to Co$_2$(CNXyl)$_8$ after oxidation. Hence, the greater steric encumbrance of the isocyanide ligands CNAr$^{\text{Mes2}}$ stabilizes the monomeric neutral Co(0) species. The zerovalent tetraisocyanide complex **88** is a sterically encumbered analogue of the binary cobalt carbonyl complex Co(CO)$_4$. Addition of two equivalents of FcOTf to tetrahedral Na[**87**] in the presence of NaBAr$^{\text{F}}_4$ affords a diamagnetic square planar tetraisocyanocobalt(I) complex, [Co(CNAr$^{\text{Mes2}}$)$_4$]BAr$^{\text{F}}_4$ (**89**), while analogous reaction in THF as a donor solvent results in pyramidalization of the cobalt(I) species, yielding [Co(CNAr$^{\text{Mes2}}$)$_4$(thf)]OTf (**90**). Furthermore, it was observed that the Co(I) species **89** and **90** comproportionate with the cobaltate complex **87** to generate the neutral compound **88**. Therefore, the authors were able to identify a fully reversible one-electron modulation of the +I, 0, and −I formal oxidation states for the [Co(CNR)$_4$] fragment.[126]

Scheme 9. Synthesis of Sterically Encumbering Isocyanide Cobaltates[126]

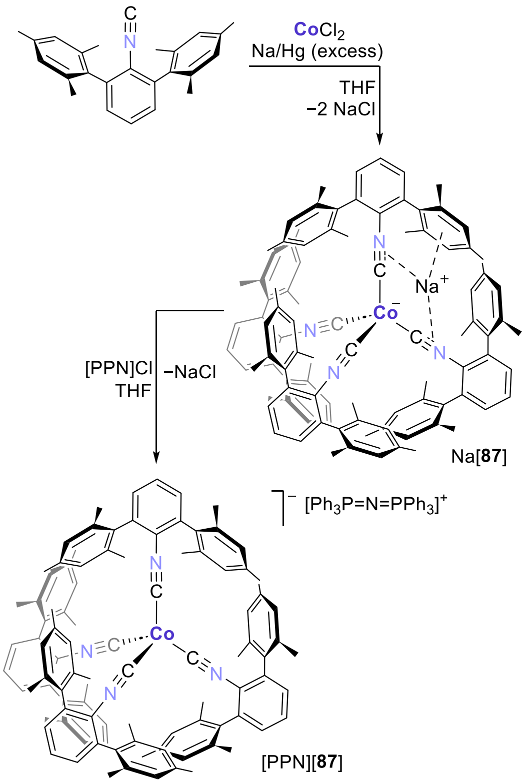

Moreover, Figueroa and co-workers isolated an unusual isocyano hydrido cobalt complex HCo(CNAr$^{\text{Mes2}}$)$_4$ (**91**) from Na[Co(CNAr$^{\text{Mes2}}$)$_4$] (Na[**87**]) and 3,5-dimethylbenzoic acid (1.05 equiv, Scheme 10a, right).[126,155] The hydride ligand gives rise to a strongly high-field shifted ^{1}H NMR resonance (δ = −13.1 ppm).[155] Compound **91** is the isocyano analogue of the carbonyl complex HCo(CO)$_4$ (**92**), known for its relevance in catalytic hydroformylation processes.[156,157] Hydride **91** reacts with H$_2$ (1 atm, r.t.) to afford the methylenimine derivative H$_2$C=NAr$^{\text{Mes2}}$ as the main product, along with small quantities of an η^6-arene iminoformyl species, [Co(κ^1-CC(H)NAr$^{\text{Mes2}}$)(CNAr$^{\text{Mes2}}$)$_3$] (**93**). The catalytic 1,1-hydrogenation of the isocyanide CNAr$^{\text{Mes2}}$ was achieved in good yields (76 ± 13%) using **91** as a catalyst, with a loading of 5 mol % (16 h, r.t.). It is worth noting that the authors carried out a full evaluation of the relative acidity of **91**, and its reactivity toward olefins and Brønsted acids, demonstrating its ability to undergo insertion chemistry and H atom transfer reactions.[135,155,158]

Prolonged stirring of [PPN][**87**] in *n*-hexane resulted in the dissociation of one isocyanide CNAr$^{\text{Mes2}}$ ligand, followed by precipitation of the zwitterionic tris(isocyano) complex (η^2-PPN)Co(CNAr$^{\text{Mes2}}$)$_3$ (**94**, Scheme 10b), which has been proposed as a highly reactive synthon for the coordinatively unsaturated monoanionic cobaltate [Co(CNAr$^{\text{Mes2}}$)$_3$]$^-$.[127] The

Scheme 10. (a) Oxidation of the Co(−I) Complex to Yield Co(0)/Co(I)-Isocyanide Compounds, and Synthesis of a Well-Defined Isocyano-Hydride-Cobalt Complex; (b) Formation of a Tris(isocyano)cobaltate and Its Subsequent Reactivity[126,127,155]

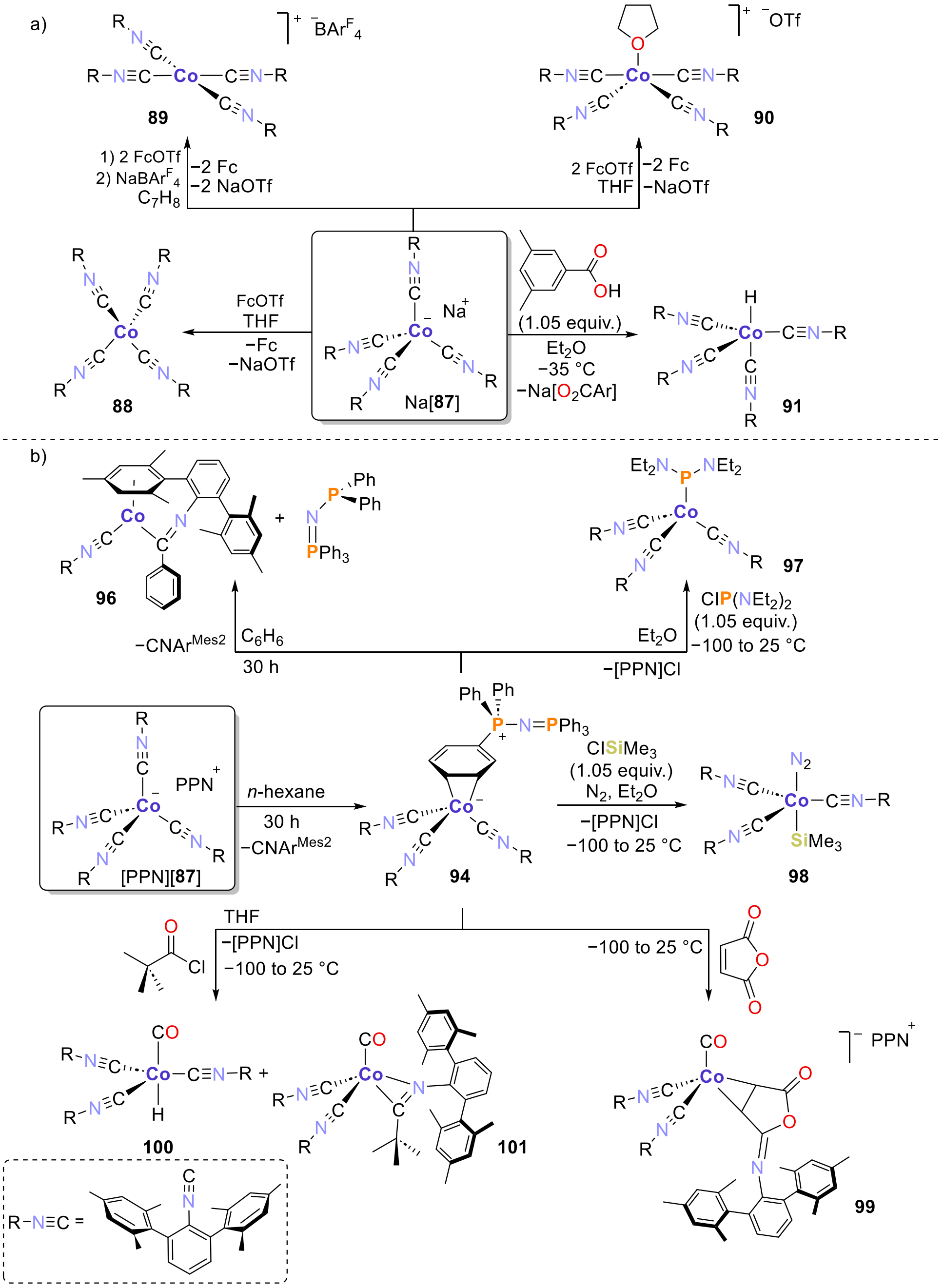

authors suggested that the dearomatization of the bound phenyl ring in **94**, as observed via X-ray diffraction analysis, evidenced a strong π-basic character on the $[Co(CNAr^{Mes2})_3]^-$ fragment. However, regardless of the strong π-back-donation toward the phenyl ring, in the solid state, the cobalt center in **94** remains a highly reduced one, as indicated by the shift on the FT-IR stretching bands of the isocyano moieties with respect to the free ligand [ν_{CN}(**94**) = 1952, 1860, and 1824 cm^{-1} (see Table 1) vs ν_{CN} (free $CNAr^{Mes2}$) = 2118 cm^{-1}].[129] It was also suggested that the ligation of the phenyl unit from the $[PPN]^+$ cation, usually noncoordinating, is essential for the (kinetic) stabilization of the coordinatively unsaturated, electron-rich fragment $[Co(CNAr^{Mes2})_3]^-$. Consequently, the isolation of analogues of the latter with different cations (alkali metal, alkaline-earth metal, tetra-alkylammonium or tetra-alkylphosphonium) was unsuccessful. The authors underlined the contrasting behavior between [PPN][**87**] and the tetracarbonyl compound $[PPN][Co(CO)_4]$ ([PPN][**95**]),[159] for which no CO-ligand displacement by the $[PPN]^+$ cation was reported. This disparate behavior highlights the utility of the isocyanide ligand analogues in the synthesis and stabilization of low-valent, low-coordinate transition metal complexes. The metalate **94** could then be proposed as an isocyano analogue of the tricarbonyl monoanionic compound $[Co(CO)_3]^-$, previously observed exclusively in the gas phase.[148]

Scheme 11. Synthesis of Mixed Ligand (Carbonyl/Isocyano) Cobaltates[135]

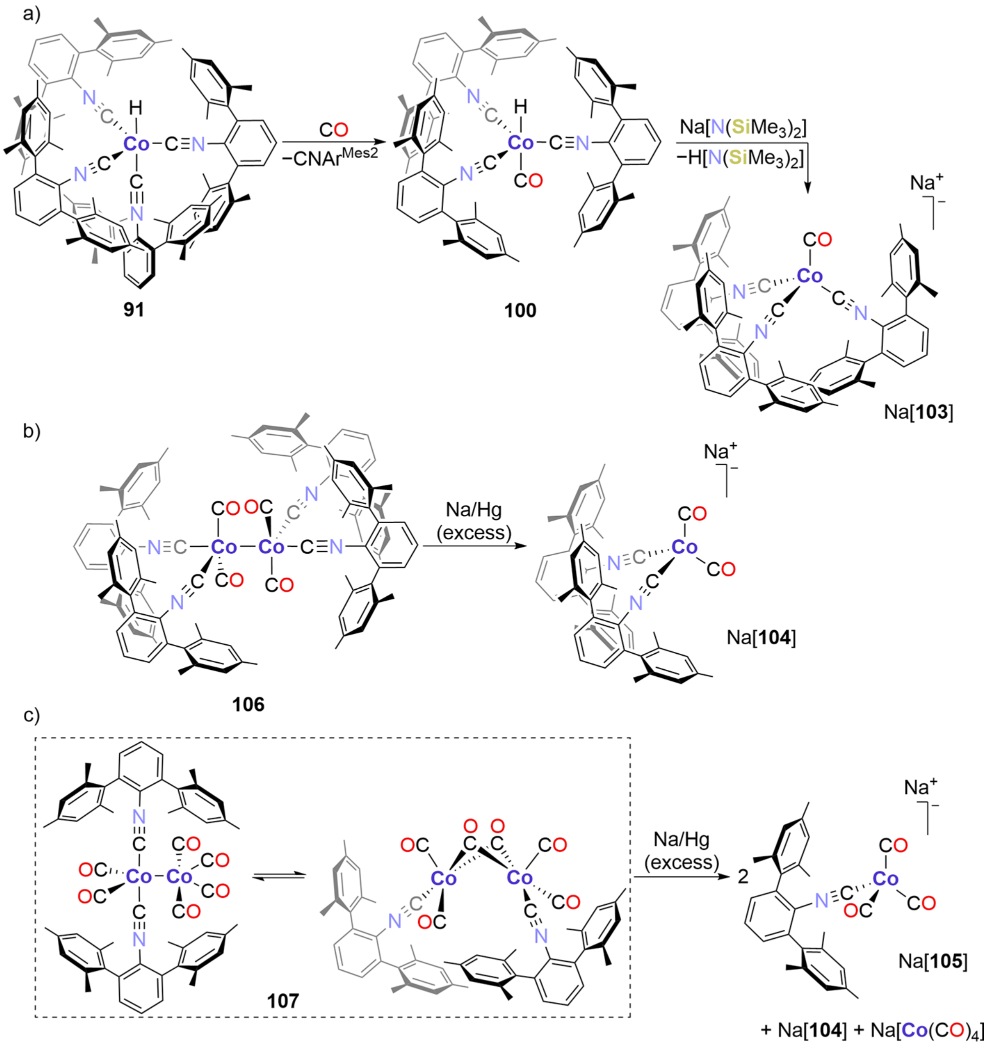

Despite the kinetic stability observed for **94**, the compound slowly decomposed, after 30 h in a solution of C_6H_6, to the η^6-arene, phenyl-substituted iminoacyl complex $\{[\eta^6\text{-Me-sAr}^{Mes}N{=}C(Ph)]Co(CNAr^{Mes2})\}$ (**96**). Experiments with the deuterium-labeled analogue $(\eta^2\text{-}[D_{30}]\text{-PPN})Co(CNAr^{Mes2})_3$ ($[D_{30}]$-**94**) afforded exclusively $\{[\eta^6\text{-Me-sAr}^{Mes}N{=}C(C_6D_5)]Co(CNAr^{Mes2})\}$ ($[D_5]$-**96**), thereby indicating that the iminoacyl Ph group came from the $[PPN]^+$ counterion, through P−C bond cleavage and formal transfer of a $[C_6H_5]^+$ moiety. The tris(isocyano)cobaltate **94** represented a highly reactive species toward electrophilic reagents (Scheme 10b). Treatment of **94** with bis(diethylamino)chlorophosphine ($ClP(NEt_2)_2$), or with trimethylsilyl chloride (Me_3SiCl) in the presence of N_2, yielded the complexes $(Et_2N)_2PCo(CNAr^{Mes2})_3$ (**97**) and $(N_2)Co(SiMe_3)(CNAr^{Mes2})_3$ (**98**), respectively. These results evidenced the nucleophilic character of metalate **94**, while, in the formation of **98**, remaining active for small molecule binding after the electrophilic functionalization. Additionally, metalate **94** acted as a nucleophile in multistep transformations of electrophilic organic carbonyls (Scheme 10b). The reaction of **94** with maleic anhydride forms the isomaleimide-containing complex $[PPN][(\eta^2\text{-}C,C\text{-}(IMAr^{Mes2})Co(CO)(CNAr^{Mes2})_2]$ [**99**; IMAr^{Mes2} = 5-(Ar^{Mes2}-imino)furanone], whereas analogous treatment with pivaloyl chloride [*t*BuC(O)Cl] afforded a 4:1 mixture of $HCo(CO)(CNAr^{Mes2})_3$ (**100**) and the iminoacyl complex $Co(CO)(\eta^2\text{-}C,N\text{-}(tBuC{=}NAr^{Mes2})(CNAr^{Mes2})_2$ (**101**). Mechanistic studies on the formation of **99** suggest a decarbonylation step of a bound acyl ligand generated after anhydride ring opening, and these observations would also explain the results obtained in the analogous reaction with *t*BuC(O)Cl. The inherent reactivity of the C−N bond in these isocyano ligands could be considered an impediment to further explore their interaction with other reagents.[127]

Interesting reactivity was also observed for the zerovalent tetraisocyanide complex $Co(CNAr^{Mes2})_4$ (**88**), which undergoes L-type ligand substitution or exhibits (metallo)radical behavior. Both types of reactivity were explored by Figueroa and co-workers.[160] Although further details on such reactivity go beyond the scope of this work, in general, ligand-exchange reactions displacing one CNAr^{Mes2} unit were observed upon interaction of **88** with two electron donors (triphenylphosphine, *tert*-butyl isocyanide, *tert*-butylethylene, acetylenes, maleic anhydride, and benzaldehyde), yielding a series of substituted products, $(L)Co(CNAr^{Mes2})_3$ (**102**). Despite the large steric profile of **88**, the complex undergoes associative ligand substitution reactions, as demonstrated through kinetic experiments. $HSnBu_3$ and $HCCl_3$ failed to react with **88** via a hydrogen- or chlorine-atom (X·) abstraction pathway, while other substrates (e.g., diphenyl disulfide, elemental sulfur, and

https://doi.org/10.1021/acs.chemrev.3c00121
Chem. Rev. 2024, 124, 1323−1463

Scheme 12. Synthesis of Heteroleptic $Cp^{R'}Co$(isocyanide) Complexes by the Group of Figueroa[136,137,162]

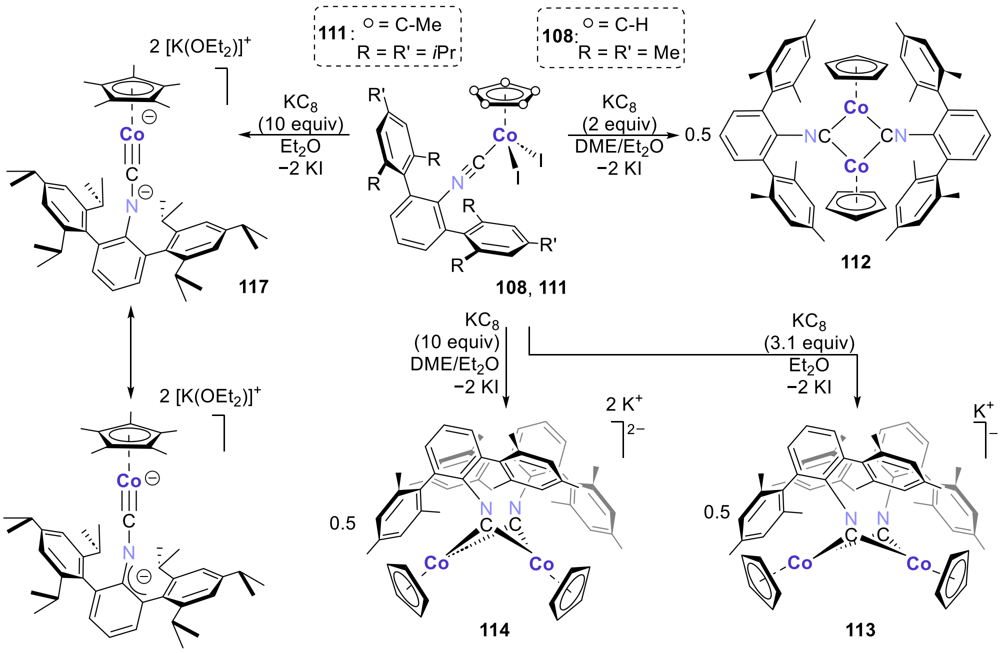

P_4) led to inner-sphere multielectron transformations, instead of one electron reactions, in every case.[160]

A series of mixed ligand (carbonyl/isocyano) analogues of $[Co(CNAr^{Mes2})_4]^-$ (**87**) and their derived hydrides were similarly described.[135] Initial attempts to synthesize the mixed ligand cobaltates from either of the tetraisocyano complexes, Na[**87**] or [PPN][**87**], or from the masked trisisocyano compound (η^2-PPN)$Co(CNAr^{Mes2})_3$ (**94**) by stoichiometric addition of CO (1, 2, or 3 equiv) resulted in a mixture of all monoanionic cobaltate complexes $[Co(CO)_{4-n}(CNAr^{Mes2})_n]^-$ [n = 3 (**103**), 2 (**104**), 1 (**105**)] and free isocyanide ligand ($CNAr^{Mes2}$),[126,127] which was attributed to a rapid redistribution process.

Independent synthetic routes were subsequently developed for compounds **103**−**105** and their corresponding hydrides (Scheme 11). $HCo(CNAr^{Mes2})_4$ (**91**) reacted with one equivalent of carbon monoxide to yield the hydride complex $HCo(CO)(CNAr^{Mes2})_3$ (**100**, Scheme 10b, *vide supra*) by ligand displacement. Compound **100** was subsequently deprotonated by $Na[N(SiMe_3)_2]$ to afford $Na[Co(CO)(CNAr^{Mes2})_3]$ (Na[**103**], Scheme 11a). The dicarbonyl compound **104** could not be similarly obtained from hydride **100**. An alternative synthesis, based on reductive cleavage of the reported dimer $Co_2(CO)_4(CNAr^{Mes2})_4$ (**106**) by sodium amalgam, afforded complex $Na[Co(CO)_2(CNAr^{Mes2})_2]$ (Na[**104**], see Scheme 11b).[135,161] Use of the dimer $Co_2(CO)_6(CNAr^{Mes2})_2$ (**107**) led to $Na[Co(CO)_3(CNAr^{Mes2})]$ (Na[**105**]). However, since dimer **107** exists in solution as a ∼1:1 mixture of the 1,1-$Co_2(CO)_6(CNAr^{Mes2})_2$ and 1,2-$Co_2(CO)_6(CNAr^{Mes2})_2$ isomers at room temperature, the reduction by sodium amalgam afforded a mixture of $Na[Co(CO)_4]$ (Na[**95**]), Na[**104**], and Na[**105**], in *ca.* 1:1:2 ratio according to NMR and IR spectroscopy (Scheme 11c).[135,161] After fractional crystallization, Na[**105**] was obtained (∼40% yield). X-ray crystallographic analysis of the sodium salts of **103**−**105** revealed that substantial ion-pairing interactions exist in the solid state between anions and cations. Similar to the case of Na[**87**], the ion-pairing interactions could be disrupted by addition of [PPN]Cl, generating the respective PPN salts [PPN][**103**], [PPN][**104**], and [PPN][**105**]. These three compounds give rise to low-energy ν_{CO} and ν_{CN} stretching bands (see Table 1) which reflect the highly reduced, π-basic character of the cobalt centers. The difference in the number of bands in each case evidences the changes in coordination environment and symmetry of the three mixed ligand cobaltates. The hydrides of complexes Na[**104**] and Na[**105**] were obtained by reaction with 3,5-dimethylbenzoic acid, as in the case of $HCo(CNAr^{Mes2})_4$ (**91**, Scheme 10a).[135,155] An assessment of the relative Brønsted acidity revealed a progressive increase in pK_α^{THF} values [in the range 40.7−28.6 for the different hydride complexes $HCo(CO)_{4-n}(CNAr^{Mes2})_n$, n = 1−4] as more isocyanide ligands were added to the Co center. This increase results from the inherently higher σ-donor/π-acid character of the isocyanide ligands. Therefore, this approach is a way to modulate the acidity of metal hydride complexes.

The Figueroa group also developed the chemistry of heteroleptic "$Cp^{R'}Co$(isocyanide)" complexes (R′ = H, Me) of different nuclearities, including anionic complexes.[136,137,162] Compounds $[Cp^{R'}Co(I)_2(CNAr^R)]$ [$Cp^{R'}$ = Cp, $CNAr^R$ = $CNAr^{Mes2}$ (**108**); $Cp^{R'}$ = Cp, $CNAr^R$ = $CNAr^{Dipp2}$ (**109**); $Cp^{R'}$ = Cp*, $CNAr^R$ = $CNAr^{Dipp2}$ (**110**); $Cp^{R'}$ = Cp, $CNAr^R$ = $CNAr^{Tripp2}$ (**111**)] served as starting materials for the synthesis of dinuclear or mononuclear complexes featuring either bridging isocyanide ligands or a terminal carbyne, respectively.[136,137] The dinuclear complexes $[(\mu\text{-}CNAr^{Mes2})_2\{CpCo\}_2]$ (**112**), $K[(\mu\text{-}CNAr^{Mes2})_2\{CpCo\}_2]$ (K[**113**]), and $K_2[(\mu\text{-}CNAr^{Mes2})_2\{CpCo\}_2]$ (K_2[**114**]) were obtained by reduction of **108** with increasing equivalents of KC_8 (see Scheme 12).[136] In the solid state, both anionic species, K[**113**] and K_2[**114**], form an ion pair with the potassium counterions and the arenes in the isocyanide ligand. The increasing electron density in the complexes as a function of the degree of reduction is reflected in the red shift for the ν_{CN} band of the bridging isocyanide ligands (ν_{CN}(**112**) = 1834 cm^{-1}, ν_{CN}(K-

[**113**]) = 1666 cm^{-1}, ν_{CN}(K_2[**114**]) = 1511 cm^{-1}; see Table 1), observed by FT-IR spectroscopy, demonstrating the successive increase in Co → (CN)π^* back-donation. The three dimers constitute the formal triad of d^8−d^8, d^8−d^9, d^9−d^9 complexes, analogous to the carbonyl species [(μ^2-CO)$_2$-[CpCo]$_2$]^n, for which the dianion has remained elusive to isolation.[163,164] In contrast, the dianionic isocyanide complex K_2[**114**] was isolated and characterized, despite isocyanide ligands being poorer π-acids than CO, thereby decreasing the reduction potentials of their complexes. This divergent behavior was ascribed to the ability of the CNAr^{Mes2} ligands to form CN π-bond and π-arene/alkali-metal-cation interactions, as observed in the anionic compounds K[**113**], K_2[**114**], and other isocyanocobaltates such as the homoleptic Na[Co(CNAr^{Mes2})$_4$] (Na[**87**]).[126] Unlike with Na[**87**], however, the π-arene/K^+ interactions in K_2[**114**] could not be conveniently disrupted with either sequestering agents ([18]crown-6 or dibenzo-[18]crown-6) or noncoordinating cations such as [PPN]$^+$, with reactions leading to intractable mixtures. Therefore, it was concluded that the structural stabilization of dimer K_2[**114**] critically depends on the tight ion pair formed with the K^+ counterion. Computational analysis of the bonding in the M_2(μ-CNAr^R)$_2$ core indicated that the predominant interaction is the π-backbonding with the bridging ligands instead of the formation of direct metal−metal bonds and that the former determines the geometric and electronic structures observed. Furthermore, the authors also synthesized the analogous d^8−d^9 and d^9−d^9 pairs [Co$_2${(μ-CNAr^{Mes})$_2$(η^6-Mes)Co}$_2$]^n (**115**, n = 0, 1+), in which one mesityl substituent on the isocyanide ligand coordinates to the cobalt center in an η^6-fashion, and the d^9−d^9 nickel dimer [(μ-CNAr^{Mes2})$_2${CpNi}$_2$] (**116**), isoelectronic with K_2[**114**]. For these complexes, the observed electronic and structural trends indicate that, as in the cobalt dimers, the π-backbonding interactions influence the electronic structure significantly more than metal−metal interactions.[136] Contrasting behavior was observed for the reduction of **109** or **110**, which afforded only neutral complexes: a dinuclear compound analogous to **112**−**114** or a mononuclear dinitrogen(isocyanide)cobalt adduct, respectively.[162]

Reduction of [Cp*Co(I)$_2$(CNAr^{Tripp2})] (**111**) by KC_8 yielded a low valent dianionic cobalt terminal carbyne (see Scheme 12, top left).[137] The product, [{K(Et$_2$O)}$_2${Cp*Co≡CNAr^{Tripp2}}] (**117**), shows a “pogo stick” structure additionally stabilized by contact ion pairing of the potassium counterions with the aryl (Tripp) substituents, the carbon atoms, and the nitrogen atoms of the ligand. FT-IR analysis revealed the presence of a significantly reduced C−N bond order through a substantial red-shift observed for the ν_{CN} band with respect to the free isocyano ligand [ν_{CN}(**117**) = 1509 cm^{-1} vs ν_{CN}(CNAr^{Tripp2}) = 2122 cm^{-1}] or reported Co(isocyano) complexes (see Table 1). This, along with the short Co−C bond length (d_{CoC}(**117**) = 1.670(3) Å), supports the formulation of the complex as a metal carbyne. However, the molecular structure of **117** also features a relatively long $C_{carbyne}$−N bond distance (d_{CN} (**117**) = 1.307(3) Å), a short distance between the nitrogen atom and the m-terphenyl-*ipso* carbon (d_{Ncipso} = 1.372(3) Å), and altered metric parameters in the central aromatic ring indicating dearomatization. These findings point toward a significant N → C π-donation opposite to the carbyne interaction, indicating the presence of a highly reduced (electron-rich) cobalt center. Therefore, the authors proposed a possible azabenzallyl resonance form as one of the contributors to the electronic structure of the dianionic complex **117** (Scheme 12, bottom left). DFT calculations on the simplified model complex [Cp*Co≡CNXyl]$^{2-}$ (**117′**, Xyl = 2,6-Me$_2$C$_6$H$_3$) indicate that the compound has a substantial atomic d-orbital character at the cobalt center, which suggests the presence of a metal−carbon multiple bond, like those in Fischer-type carbynes. The calculations support a bonding situation in which a low-valent cobalt center with highly filled d-orbitals binds to the ligand at the carbon atom, establishing a significant metal-to-carbon π-backdonation interaction.[137]

Insights into the electronic structure of **117** indicate nucleophilic character at cobalt. This was confirmed by treatment of **117** with HCCSiMe$_3$ and Me$_3$SiCl (Scheme 13), which afforded the two-legged piano stool complexes [K(Et$_2$O)][Cp*Co(H)(CNAr^{Tripp2})] (**118**) and [K(Et$_2$O)]-[Cp*Co(SiMe$_3$)(CNAr^{Tripp2})] (**119**). Both reactions illustrate cobalt-centered reactivity, with an electronic reorganization yielding the coordinated isocyano CNAr^{Tripp2} ligand and formal concomitant oxidation of the cobalt center to Co(I). The significant π-backbonding in these species was evidenced by their ν_{CN} stretching bands [ν_{CN}(**118**) = 1710 cm^{-1}; ν_{CN}(**119**) = 1707 cm^{-1}]. The observation that the metal center is the preferred site of electrophilic attack additionally supports the notion that the carbyne ligand is stabilized via an azabenzallyl resonance form. By contrast, the reaction of **117** with diphenylacetylene led to the formation of a new C−C bond after [2 + 2] cycloaddition to the Co≡C motif, with protonation of the α-carbon of the intermediate metallacycle, to finally form the vinyliminacyl complex [K(Et$_2$O)][**120**] (see Scheme 13, bottom). The authors proposed a possible mechanism to explain the formation of the vinyliminacyl product.[137]

Scheme 13. Reactivity of [{K(Et$_2$O)}$_2${Cp*Co≡CNAr^{Tripp2}}] (117) toward Protic Substrates and Silyl Electrophiles[137]

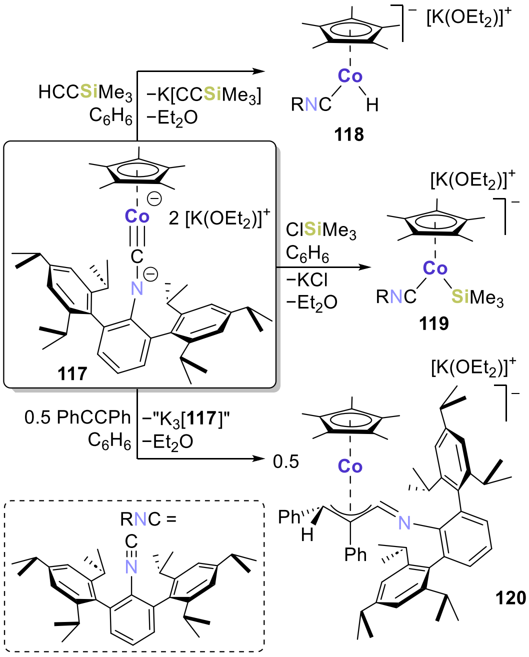

2.2.3.4. Isocyanide Complexes of the 4d and 5d Metals. Isocyanide metalates based on 4d or 5d metals have also been reported in the period from 2006−2022.[165−169] Ellis described the isolation of niobium and tantalum homoleptic isocyanidemetalate complexes, namely Cs[M(CNXyl)$_6$] [M = Nb (**121**), Ta (**122**), Xyl = 2,6-Me$_2$C$_6$H$_3$; Scheme 14].[165,170] The compounds Cs[M(CNXyl)$_6$] were obtained in two reaction steps which include, first, ligand exchange from the corresponding carbonyl metalate [Et$_4$N][M(CO)$_6$] [M = Nb (**123**), Ta (**124**)][171] while oxidizing with iodine, followed by subsequent reduction of the resulting [MI(CNXyl)$_6$] [M = Nb (**125**), Ta (**126**)] with CsC$_8$. These octahedral complexes, bearing formally d^6 M(−I) centers, were characterized by X-ray diffraction analysis, and ^{13}C{^{1}H} NMR spectroscopy for the tantalum species. In 2017, the Ellis group reported the tantalate complex K[Ta(CNDipp)$_6$] (**127**, Dipp = 2,6-*i*Pr$_2$C$_6$H$_3$) in two steps by a similar procedure starting from **124** (see Scheme 14).[167,172] Displacement of CO ligands by CNDipp under oxidative conditions (I$_2$) formed the precursor [TaI(CNDipp)$_6$] (**128**). **128** was then reduced by an excess of KC$_8$ to afford **127** in 70−80% yield. In this work, Ellis disclosed the discovery of appropriate oxidizing agents to access the until then elusive, isolable complex [Ta(CNDipp)$_6$] (**129**) from **127**. Oligomeric MoO$_3$, [Ta(CNDipp)$_7$][BF$_4$] (**130**) or [NEt$_3$H][BPh$_4$] cleanly oxidized metalate **127** to the desired homoleptic zerovalent tantalum species **129**. Later, Ellis and co-workers reported the crystal structure of the related complex [Ta(CNDipp)$_7$][Ta(CNDipp)$_6$] (**131**), obtained by reducing **128** with an excess CsC$_8$ (5.8 equiv).[166] In compound **131**, both the complex cation and anion are homoleptic, featuring the same transition metal and π-acceptor ligand. **131** undergoes comproportionation in solution to form the 17-electron complex **129**.

Scheme 14. Isocyanide Tantalate and Niobiate Complexes by the Ellis Group[165,167]

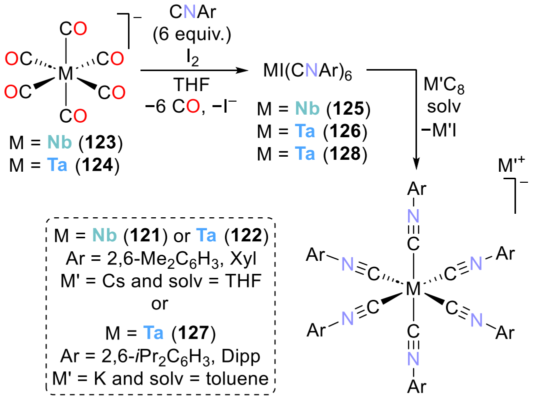

Figueroa reported that upon reduction of [ReBr(CO)$_3$(CNAr$^{\mathrm{Dipp2}}$)$_2$] (**132**), the isolation of the monomeric rhenium(−I) anion Na[Re(CO)$_3$(CNAr$^{\mathrm{Dipp2}}$)$_2$] (**133**, Ar$^{\mathrm{Dipp2}}$ = 2,6-(2,6-(*i*Pr)$_2$C$_6$H$_3$)$_2$C$_6$H$_3$) was achieved (Scheme 15a).[168] **133** contains an encumbering isocyanide scaffold well-suited to support the highly reduced rhenium atom, which is in a formally negative oxidation state. Later, Abraham and Figueroa described the convenient preparation of starting materials to access unprecedented low-valent rhenium and technetium anionic complexes (Scheme 15b).[169]

The compounds [MX(CO)(CNAr$^{\mathrm{DArF2}}$)$_4$] [M = Tc, X = Cl (**134**); M = Re, X = Br (**135**); Ar$^{\mathrm{DArF2}}$ = 2,6-(3,5-(CF$_3$)$_2$C$_6$H$_3$)$_2$-4-F-C$_6$H$_2$] can be reduced with Na/Hg to yield the respective Na[M(CO)(CNAr$^{\mathrm{DArF2}}$)$_4$] species [M = Tc (**136**), M = Re (**137**)], featuring formally M(−I) centers.

Scheme 15. Synthesis of Mixed Ligand Technetium and Rhenium Metalates Containing Formally M(−I) Metal Centers[168,169]

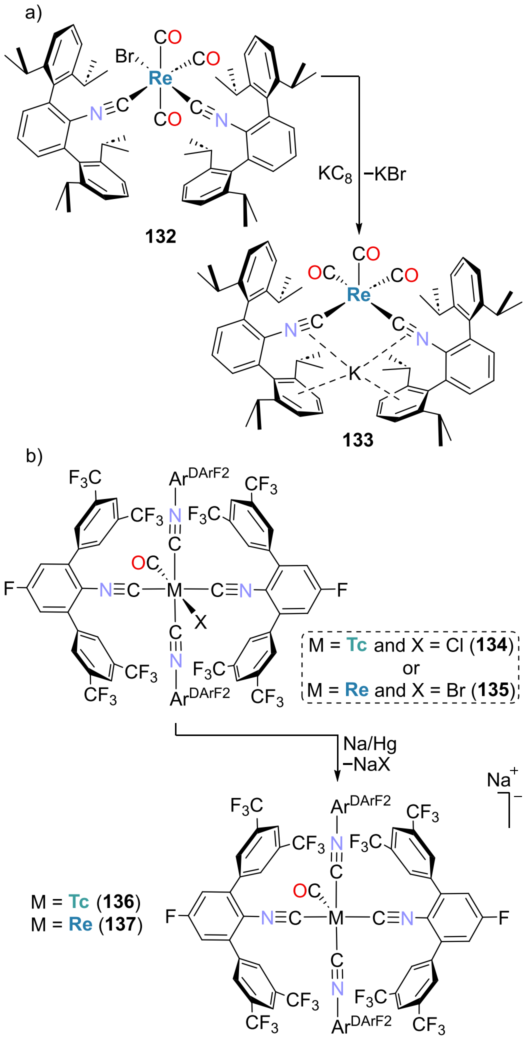

The encumbering fluorinated isocyanide ligand CNAr$^{\mathrm{DArF2}}$ has been key to stabilize the uncommonly low oxidation state by increasing the π-accepting properties, as well as to provide steric protection, thereby preventing dimerization. These anionic metalates are surprisingly robust and, for instance, the Re(−I) complex Na[Re(CO)(CNAr$^{\mathrm{DArF2}}$)$_4$] (**137**) readily reacted with electrophiles such as MeI, HCl, or F$_6$C$_5$C(O)Cl. The latter behavior mimicked that of the homoleptic carbonyl [Re(CO)$_5$]$^-$ (**138**). These mixed ligand Tc and Re [M(CO)(CNAr$^{\mathrm{DArF2}}$)$_4$]$^-$ complexes are heavier analogues of the manganese compounds [Mn(CO)$_2$(CNAr$^{\mathrm{Mes2}}$)$_3$]$^-$ (**38**) and [Mn(CO)$_3$(CNAr$^{\mathrm{Dipp2}}$)$_2$]$^-$ (**39**), described by the same group and depicted in Scheme 2 (*vide supra*).[123] This family of group 7 metal complexes [M(CO)$_x$(CNAr)$_y$]$^-$ has the coordination number $x + y = 5$ in common, but different carbonyl/isocyanide ratios, $x/y = 1/4$, 2/3, or 3/2 due to steric demand of the respective CNAr ligand and the relative size of the corresponding metal center (M = Mn, Tc, Re), resulting in disparate geometries.

Besides the series of [Re(CO)$_x$(CNAr)$_y$]$^-$ complexes by Figueroa and co-workers,[168,169] other rhenium metalates bearing carbonyl or isocyanide ligands with the metal atom in a formally negative oxidation state are rare. For instance,

Scheme 16. Synthesis of Dianionic and Radical Anionic Chini-type Triplatinum Clusters with Encumbering Isocyanide Ligands[176]

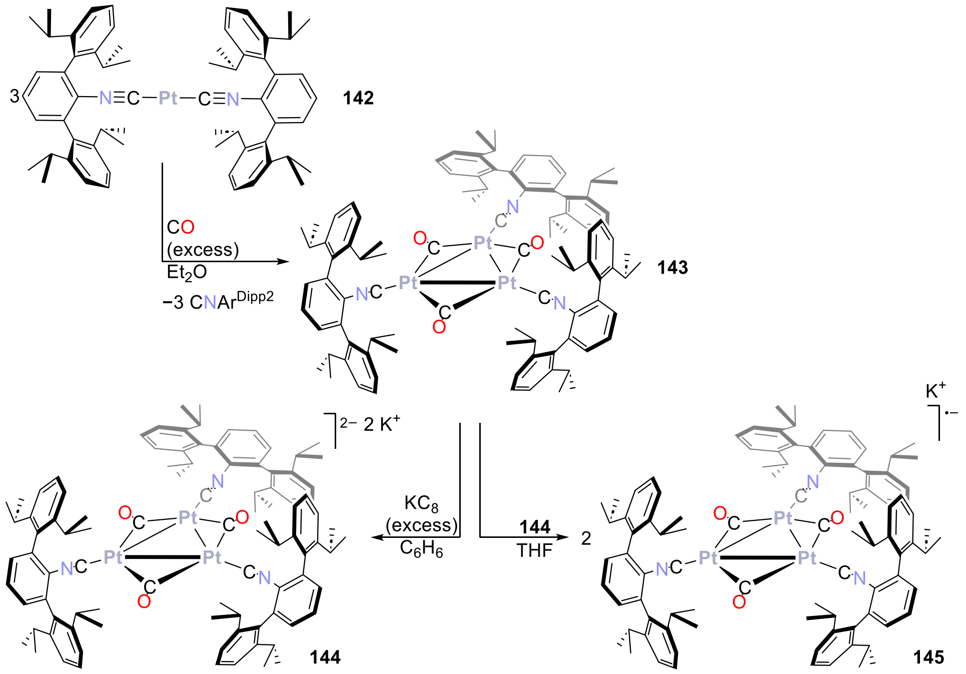

Kubiak and co-workers reported the $[Re(CO)_3(bpy)]^-$ anion (**139**), which is likely involved in the electrocatalytic reduction of CO_2 by $[Re(CO)_3(Cl)(bpy)]$ (**140**).[173,174] Nevertheless, a follow-up study revealed that the $[Re(CO)_3(bpy)]^-$ species is better described as $[Re^0(CO)_3(bpy^-)]$, rather than $[Re^-(CO)_3(bpy)]$, due to the presence of the redox-active α-diimine chelate.[175]

Figueroa and co-workers isolated mono- and dianionic triplatinum-isocyanide clusters related to the monomeric Chini cluster, $[Pt_3(CO)_6]^{2-}$ (**141**).[176] The encumbering *m*-terphenyl isocyanide ligands CNAr^{Dipp2} (Ar^{Dipp2} = 2,6-(2,6-(*i*Pr)$_2$C$_6$H$_3$)$_2$-C$_6$H$_3$) provide kinetic stability to the series $[Pt_3(\mu\text{-}CO)_3(CNAr^{Dipp2})_3]^{n-}$ (n = 0, 1, 2), allowing for its isolation and full characterization. The preparation of the heteroleptic trinuclear complexes is straightforward, starting with ligand exchange of $[Pt(CNAr^{Dipp2})_2]$ (**142**) under a CO atmosphere affording the neutral compound $[Pt_3(\mu\text{-}CO)_3(CNAr^{Dipp2})_3]$ (**143**, Scheme 16). **143** was reduced with KC$_8$ to yield the dianion $[Pt_3(\mu\text{-}CO)_3(CNAr^{Dipp2})_3]^{2-}$ (**144**), and comproportionation of **143** and **144** produces the radical monoanion $[Pt_3(\mu\text{-}CO)_3(CNAr^{Dipp2})_3]^{\cdot-}$ (**145**), as depicted in Scheme 16. The highly reduced cluster **145** reacted cleanly with various electrophiles, such as R$_3$ECl (R = Et and E = Si or R = Ph and E = Sn) or $[AuCl(PPh_3)]$ (**146**), giving rise to molecularly defined and isolable compounds. Interestingly, spectroscopic analysis (FT-IR, multinuclear NMR) and computational studies (DFT) suggest that the highest-occupied molecular orbitals (HOMO) of the charged clusters consist of a combined π*-framework of the CO and CN^{ArDipp2} ligands, which would imply that this set of isocyanide and carbonyl ligands exhibit redox noninnocent character.

Using the same bulky isocyanide ligands, Figueroa and co-workers very recently reported the isolation and reactivity studies of 16 valence-elctron rhodate and iridate anions, $[M(CNAr^{Dipp2})_3]^-$.[177]

Ruiz and co-workers have extensively studied the chemistry of mixed-ligand complexes of the group 6 metals, featuring multiple metal−metal bonds.[178] These complexes usually bear carbonyl, cyclopentadienyl, and phosphinidene ligands and, therefore, their chemistry is summarized in section 2.2.6.4 (*vide infra*).

2.2.4. Arene and Alkene (Hydrocarbon) Metalates.

Within the area of transition metal complexes in uncommonly low oxidation states, the chemistry of homoleptic alkene- and arene metalates has attracted considerable attention. Ellis and co-workers have made significant contributions to the chemistry of this type of metalate.[3] This group has synthesized numerous examples of low-valent arene and alkene complexes with different transition metals, including those of the 3d series and heavier congeners.[2,70,179,180] Many of these are nowadays considered key synthons in low-valent transition metal chemistry, and deemed storable sources of transition metal anions,[70,181] also known as "naked-metal atom" reagents.[2]

Due to the large number of metalates containing arene or alkene ligands, this subchapter is compartmentalized into sections according to the metal ion involved. Group 4 metalates (Ti, Zr, Hf) are discussed together due to their similar properties. Metalates of the 3d transition metals are then discussed sequentially, followed by an account of the smaller number of reported 4d and 5d metalates, which sometimes contrast with the 3d metalates.

2.2.4.1. Group 4 Metalates.

A striking example of the chemistry of alkene/arene transition metal anions is the synthesis of the triads of tris(anthracene)metalate(−II), $[M(C_{14}H_{10})_3]^{2-}$ [M = Ti (**147**), Zr (**148**), Hf (**149**)] and tris(naphthalene)metalate(−II), $[M(C_{10}H_8)_3]^{2-}$ [M = Ti (**150**), Zr (**151**), Hf (**152**)] complexes.[179,182] The synthetic protocol for the corresponding tris(polyarene)titanates(−II) [polyarene = anthracene (**147**), naphthalene (**150**)] is illustrated in Scheme 17.[182]

Scheme 17. Synthesis of Tris(polyarene)titanates(−II) [Polyarene = Anthracene (147), Naphthalene (150)] by Ellis and Co-workers[182]

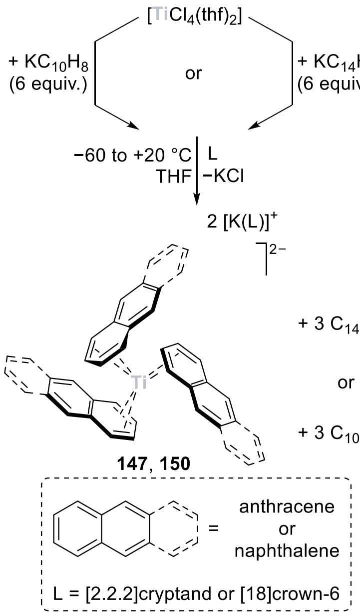

Although the characterization of these titanates in solution by NMR spectroscopy indicated that the three polyarene ligands are magnetically equivalent, the X-ray diffraction analysis showed that the structures observed in the solid state are more accurately formulated as $[Ti(\eta^4\text{-polyarene})_2(\eta^2\text{-polyarene})]^{2-}$. Thus, **147** and **150** are 16-electron homoleptic polyarene complexes with polyarene ligands of different hapticities. This reduced hapticity was attributed to the existence of strong intramolecular polyarene repulsions due to the short distance between the ligand and the Ti center, caused by a high degree of backbonding from the electron-rich metal to the ligand.

Brennessel and Ellis have reported the structural characterization of titanium[183] and vanadium[183,184] alkene or arene metalates. The Ti(−I) compound $\{[K([18]crown\text{-}6)][Ti(C_{16}H_{10})_2]\}_n$ (**153**, see Figure 5, left) was obtained by ligand exchange on the highly reactive titanate **150** with pyrene. The M(0) complexes $[M(C_{16}H_{10})_2]$ [M = V (**154**), Nb (**155**); see Figure 5 for the structure of the vanadium(0) complex] were obtained by reduction of the corresponding precursors $MCl_{4-n}(thf)_{2+n}$ (M = V: $n = 1$; M = Nb: $n = 0$) by alkali metal pyrene radical anion salts. These sandwich compounds bear pyrene ligands in an eclipsed conformation.[183]

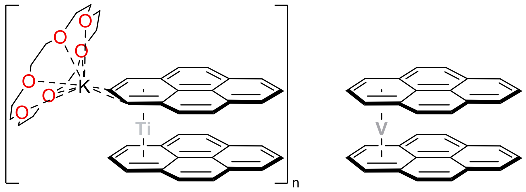

153 **154**

Figure 5. Homoleptic pyrene complexes of titanium and vanadium.[183]

Various other highly reduced naphthalene and anthracene complexes of Sc, Ti, Zr, and Hf supported by amide, anilide, triamidoamine, and triaryloxidemethyl ligands have been reported.[185−190] In these, the arene ligands are reduced to their dianionic form. Although these complexes are beyond the scope of the present review, because they feature metal atoms in the common oxidation states +III (for Sc) and +IV (for Ti, Zr, Hf), it is noteworthy that their reactivity with unsaturated substrates (e.g., with N_2, P_4, alkynes, and fluoroarenes) often resembles the behavior of low-valent metalate anions. We would like to refer to the original literature for further discussion.[189−193]

Arene complexes of titanium and vanadium supported by σ-/π-bonded pyrrolide-based ligands were developed by Gambarotta and co-workers.[194,195] The chemistry of these complexes is discussed in section 2.2.8.2 (*vide infra*).

2.2.4.2. Vanadium, Chromium, and Manganese.

The synthesis and structural characterization of a family of naphthalene- and anthracene-vanadates were reported.[184] Brennessel and Ellis described the reduction of the known compound bis(naphthalene)vanadium(0) (**156**)[196] by potassium naphthalenide (Scheme 18a), which affords brown solutions of a paramagnetic product too unstable for isolation or characterization, but able to act as an intermediate in the synthesis of well-defined vanadates. Given the subsequent reactivity observed, the identity of this intermediate was speculated to be $[V(\eta^4\text{-}C_{10}H_8)_2(thf)]^-$ (**157**), although the presence of the possible 18-electron vanadate $[V(\eta^6\text{-}C_{10}H_8)_2]^-$ (**158**) could not be ruled out.

Regardless, the *in situ* generated species reacted with a series of reagents: further reduction with potassium naphthalenide (1 equiv) in the presence of PMe_3 yielded the V(−II) complex $[K(thf)_2]_2[V(\eta^4\text{-}C_{10}H_8)(\eta^6\text{-}C_{10}H_8)]$ (**159**), whereas reaction with 1,2-bis(dimethylphosphino)ethane (dmpe, 1 equiv) returned $[V(\eta^4\text{-}C_{10}H_8)_2(dmpe)]^-$ (**160**, L = [18]crown-6 or [2.2.2]cryptand; Scheme 18a, top). Additionally, the intermediate species reacts with anthracene (2 equiv) at low temperatures to give complex $[V(\eta^4\text{-}C_{14}H_{10})_2(thf)]^-$ (**161**) (Scheme 18a, down). More efficient synthetic protocols for **159** and **161** consist of the direct reduction of $VCl_3(thf)_3$ with potassium naphthalenide (5 equiv, in the presence of PMe_3) or potassium anthracenide (5 equiv), respectively, in THF.

In addition, the anthracene vanadate **161** served as starting material for the synthesis of the phosphine adducts $[V(\eta^4\text{-}C_{14}H_{10})_2(PMe_3)]^-$ (**162**) and $[V(\eta^4\text{-}C_{14}H_{10})_2(dmpe)]^-$ (**163**) (Scheme 18a, bottom). Furthermore, in an attempt to synthesize a mixed arene-alkene anthracene-COD vanadate, $VCl_3(thf)_3$ was treated with sodium anthracenide (3 equiv) in the presence of 1,5-cyclooctadiene to afford crystals of the dimetallabis(anthracene) sandwich complex $\{[Na(thf)_3]\text{-}[V_2(C_{14}H_{10})_2]\}$ (**164**, Scheme 18b).[184]

In 2018, the Caulton group reported the dichromium sandwich complex $[Cr_2(naphthalene)_2]^-$ (**165**, as $[K([18]crown\text{-}6)]^+$ salt; see Scheme 19), obtained as a radical anion.[197] The sandwich compound is formed after reaction between the previously reported $Cr[N(SiMe_3)_2]_2(thf)_2$ (**166**)[198,199] and an equimolar amount of $[K([18]crown\text{-}6)][C_{10}H_8]$. The structure of the obtained species significantly differs from that of the long-known bis(naphthalene)chromium(0) complex $[Cr(\eta^6\text{-}C_{10}H_8)_2]$ (**167**), generated via reduction of $CrCl_3(thf)_3$ by lithium or sodium naphthalenide.[196,200,201]

Crystallographic characterization of **165** revealed the formation of a 1D coordination polymer with alternating units of the anion $[Cr_2(naphthalene)_2]^-$ and the cation $[K([18]crown\text{-}6)]^+$, forming an ion pair with two carbon

Scheme 18. Synthesis of Naphthalene and Anthracene Vanadates by the Group of Brennessel and Ellis[184]

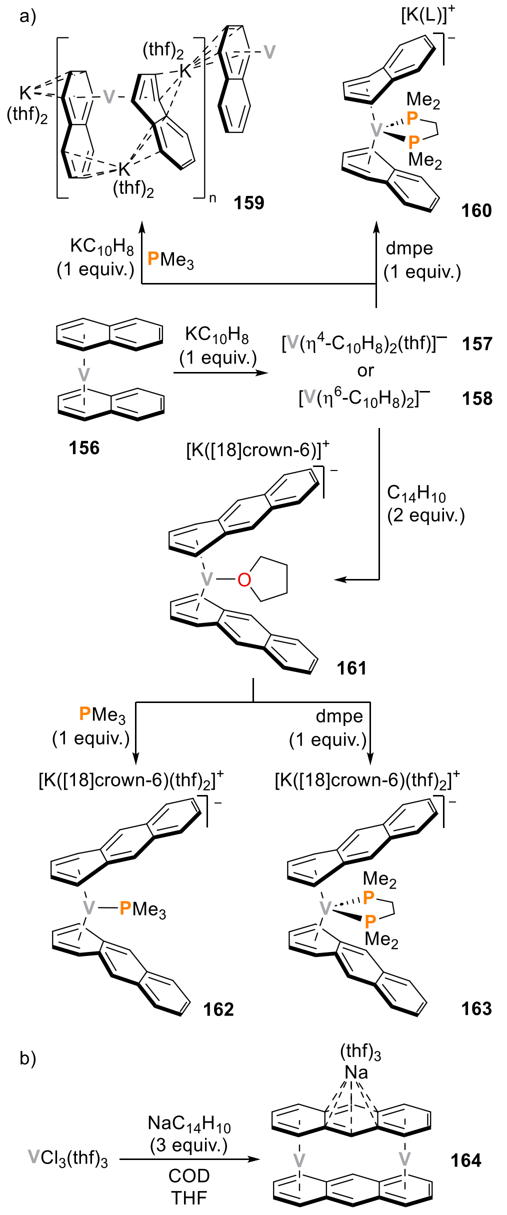

Scheme 19. Proposed Chemical Reaction for the Synthesis of the Bis(naphthalene)dichromium Sandwich Complex $[Cr_2(naphthalene)_2]^-$ (165)[197]

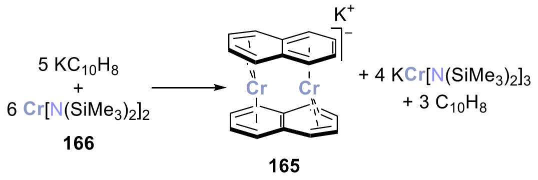

atoms in the naphthalene rings of different anionic scaffolds. Furthermore, each chromium center in the dinuclear sandwich is coordinated by both η^4 and η^6 naphthalene ligands. Based on the analysis of EPR spectra recorded at 298 and 77 K, it was proposed that the spin is strongly localized in the π-aromatic system, but there is also a significant contribution of the metal orbitals in the SOMO. Altogether, the analytical data indicate a certain degree of axial symmetry. Therefore, it was concluded that the two chromium centers in the sandwich compound do not form strong Cr–Cr interactions. The mass balance of the obtained material does not entirely account for the amounts used in the synthetic protocol and, consequently, two possible chemical reactions were proposed. The more feasible path is shown in Scheme 19, in which $[K([18]crown\text{-}6)][C_{10}H_8]$ acts as the reducing agent and displaces the amide ligands on chromium, which are sequestered by excess of the Lewis acidic chromium reagent. Consequently, the authors discussed the displacement of amide leaving groups for delivery of a metal center as a potentially generalizable method for the synthesis of low-valent compounds.[197]

Scheme 20. Synthesis of (Polyarene)(carbonyl) Complexes of Manganese, Affording Mono- and Bimetallic Compounds[83]

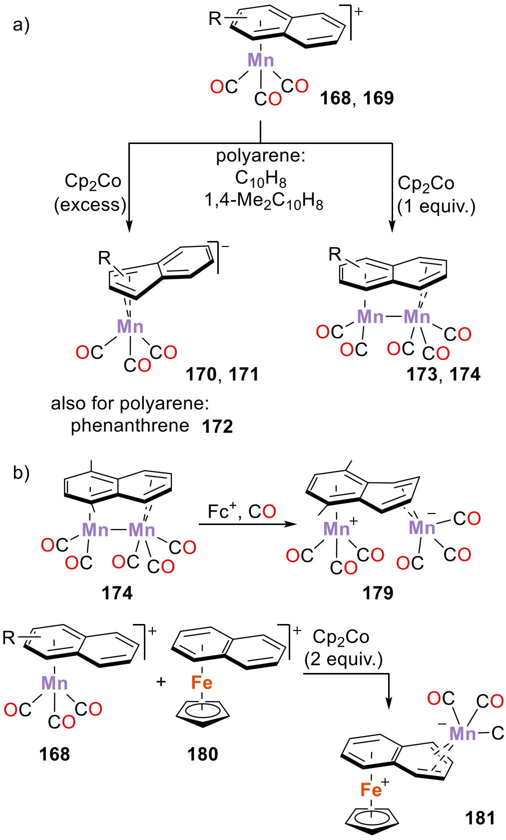

In 2005, (electro)chemical studies showed that the manganese complexes $[(\eta^6\text{-polyarene})Mn(CO)_3]^+$ [polyarene = naphthalene (**168**), 1,4-Me_2naphthalene (**169**)] undergo full and reversible two-electron reduction to afford $[(\eta^4\text{-polyarene})Mn(CO)_3]^-$ (**170**–**172**).[83] The series of complexes **170**–**172** was obtained for different polyarenes [naphthalene (**170**), 1,4-dimethylnaphthalene (**171**) and phenanthrene (**172**), see Scheme 20a for the synthesis of these examples) by reaction of the corresponding complexes **168** and **169** with an excess of cobaltocene (Cp_2Co). In contrast, the reaction between $[(\eta^6\text{-naphthalene})Mn(CO)_3]^+$ (**168**) or $[(\eta^6\text{-}1,4\text{-}Me_2naphthalene)Mn(CO)_3]^+$ (**169**) with only one equivalent of Cp_2Co afforded the bimetallic compounds $[(\eta^4,\eta^6\text{-}1,4\text{-}R_2naphthalene)Mn_2(CO)_5]$ [R = H (**173**) or Me (**174**)], which contain Mn–Mn bonds. For the acenaphthene and 1,2,3,6,7,8-hexahydropyrene analogues of **168** and **169**, different reaction temperatures afforded distinct products in the presence of an excess Cp_2Co: whereas at low temperatures the η^4-polyarene complex is obtained [polyarene = acenaphthene (**175**), hexahydropyrene (**176**)], the reduction at room temperature yields the corresponding bimetallic compounds with the polyarenes coordinated in the η^4,η^6-fashion (**177** and **178**). While complex $[(\eta^4,\eta^6\text{-1,4-Me}_2\text{naphthalene})Mn_2(CO)_5]$ (**174**) is relatively stable toward carbon monoxide (CO) at room temperature, in the presence of ferrocenium ions, a rapid oxidative activation occurs with rupture of the Mn−Mn bond, generating the zwitterionic *syn*-facial homonuclear product **179** (Scheme 20b). Furthermore, reduction of **168** in the presence of $[(\eta^6\text{-naphthalene})FeCp]^+$ (**180**) leads to the formation of the zwitterionic heteronuclear *anti*-facial η^4,η^6-naphthalene bimetallic compound **181** (Scheme 20b). It was proposed that the formation of both the homo- and the heteronuclear bimetallic compounds **179** and **181** is the result of facilitated displacement of the polyarene ligand in the cationic precursor by the nucleophilic fragments in the *in situ* generated reduced species, **170**−**172**.[83]

2.2.4.3. Iron. The synthesis of bis(1,2,3,4-η^4-anthracene)cobaltate(−I) (**14**) (see Scheme 1, above) and its iron analogue bis(1,2,3,4-η^4-anthracene)ferrate(−I), $[Fe(\eta^4\text{-}C_{14}H_{10})_2]^-$ (**52**), and the follow-up chemistry done with these as precursors, are two remarkable examples of the versatility of metalates.[70,181] The Fe(−I) compound **52** is a paramagnetic 17-valence-electron (VE) compound, unlike its Co(−I) analogue **14** which is diamagnetic, having 18 VE. The synthetic procedure used to obtain **52** is analogous to that of cobaltate **14** described in section 2.1, and consists of the reduction of iron(II) bromide by potassium anthracenide, as depicted in Scheme 21a. Single-crystal X-ray diffraction of **52** showed that its structure is also very similar to that of **14**.

Initial investigations of the reactivity of **52** (Scheme 21b) demonstrated the labile character of the coordinated polyarene ligands in ligand-substitution reactions. Complete ligand displacement was observed upon treatment of **52** with carbon monoxide or 1,3-butadiene, yielding the previously reported Fe(−I) complex, $[Fe_2(CO)_8]^{2-}$ (**82**),[152−154] and the first 17-electron homoleptic 1,3-butadiene complex, $[Fe(\eta^4\text{-}C_4H_6)_2]^-$ (**182**), respectively. Slightly different behavior was observed upon reaction with 1,5-cyclooctadiene, where only one anthracene ligand was substituted even when an excess of 1,5-cyclooctadiene was used, affording the heteroleptic complex $[Fe(\eta^4\text{-}C_{14}H_{10})(\eta^4\text{-cod})]^-$ (**183**). The naphthalene analogue of **183**, $[Fe(\eta^4\text{-}C_{10}H_8)(\eta^4\text{-cod})]^-$ (**184**) was later reported by the same group, and obtained by direct reduction of $FeBr_2$ with $KC_{10}H_8$ (3 equiv) in the presence of excess 1,5-cyclooctadiene in THF, at −78 °C.[202] Furthermore, the interaction of **52** with donor ligands stronger than cod resulted in oxidation to give Fe(0) complexes. For example, the reaction with $P(OMe)_3$ afforded the complex $[Fe(\eta^4\text{-}C_{14}H_{10})\{P(OMe)_3\}_3]$ (**185**) and the salt of anthracene radical anion, $[K([18]crown\text{-}6)(thf)_2][C_{14}H_{10}]$.[181]

The influence of the electron density of the Fe(−I) center was evidenced by the reaction of **52** with 2,2′-bipyridine (bpy), affording the homoleptic complex $[Fe(bpy)_3]^-$ (**186**),[203−206] which bears reduced bpy ligands.[207] The reduced nature of the bpy ligands in **186**, and similar species with the related chelating pyridines tpy (2,2′:6′,2″-terpyridine) and *t*bpy (4,4′-di-*tert*-butyl-2,2′-bipyridines), originally formulated as $[Fe^{-I}(bpy^0)_3]^{1-}$ or $[Fe^0(bpy^0)_3]^0$,[203−206] was confirmed through a combination of spectroscopic, crystallographic, electro-, and magnetochemical studies, EPR, and theoretical calculations.[208] As mentioned in section 2.2.3.2, an evaluation of the interaction between the anthraceneferrate **52** and CNXyl revealed that this compound was not a suitable precursor for the synthesis of isocyanoferrates due to oxidation of the Fe(−I) center to Fe(0) to form $Fe(CNXyl)_5$ (**54**), possibly via an intermediate Fe(0) polyarene-isocyano complex, $[Fe(\eta^4\text{-}C_{14}H_{10})(CNXyl)_3]$ (**187**), which was structurally characterized.[209]

Scheme 21. (a) Synthesis and (b) Initial Reactivity Screening of Bis(1,2,3,4-η^4-anthracene)ferrate(−I) (52) by the Group of Ellis[181]

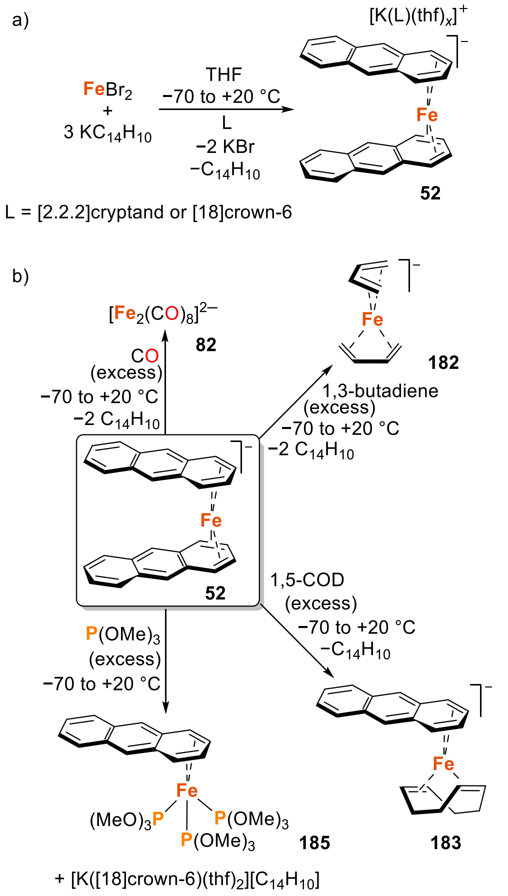

Wolf and co-workers also used the bis(anthracene)-metalates(−I) [M = Fe (**52**); Co (**14**)][70,181] as a platform to synthesize a variety of low-valent complexes. For example, a metal-mediated dimerization of phosphaalkynes was achieved at such complexes (Scheme 22, top).[210−212] The reaction of $[M(\eta^4\text{-}C_{14}H_{10})_2]^-$ with four equivalents of the corresponding phosphaalkyne results in the cyclodimerization of the phosphaalkyne and the formation of either the open-shell sandwich complex $[Fe(1,3\text{-}P_2C_2tBu_2)_2]^-$ (**188**)[211] or the 18-electron compound $[Co(1,3\text{-}P_2C_2R_2)_2]^-$ [R = *t*Bu (**189**), *t*Pent (**190**), Ad (**191**)].[210] The molecular structures of these compounds feature coplanar 1,3-diphosphacyclobutadiene rings in a staggered orientation (i.e., the two $P_2C_2R_2$ rings are rotated, with respect to one another, by 90°).[210−212] Reactivity of anions **188** and **189**−**191** is described in section 3.5 (*vide infra*).

By contrast, reaction of the metalate **52** with diphenylacetylene afforded the unusual hexaphenylbenzene complex $[K([18]crown\text{-}6)(thf)_2][Fe(\eta^6\text{-}C_6Ph_6)(\eta^2\text{-}C_2Ph_2)]$ (**192**),

Scheme 22. Divergent M(−I)-Mediated Phosphaalkyne (M = Fe, Co)[210−212] and Alkyne (M = Fe)[213] Cyclo-oligomerizations

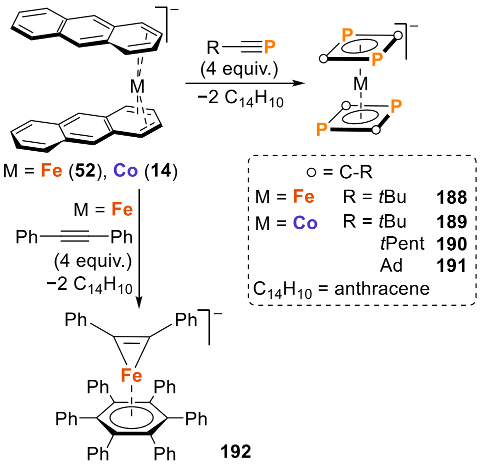

formed via alkyne cyclotrimerization (Scheme 22, down).[213] While phosphaalkynes are often invoked as analogues of alkynes, the reactivity of **52** toward both substrates showed marked differences in their cyclo-oligomerization reactions. DFT calculations performed on the simplified model complexes of the isomers $[\mathrm{Fe}(\eta^4\text{-}\mathrm{C_4Me_2H_2})_2]^-$ (**188C′**), $[\mathrm{Fe}(\eta^6\text{-}\mathrm{C_6Me_3H_3})(\eta^2\text{-}\mathrm{C_2MeH})]^-$ (**192′**), $[\mathrm{Fe}(\eta^4\text{-}\mathrm{P_2C_2Me_2})_2]^-$ (**188′**), and $[\mathrm{Fe}(\eta^6\text{-}\mathrm{P_3C_3Me_3})(\eta^2\text{-}\mathrm{PCMe})]^-$ (**192P′**), products of alkyne or phosphaalkyne cyclo-oligomerization, revealed that their relative stabilities are in accordance with the experimental results: the $\mathrm{Fe^{-I}}$-mediated cyclotrimerization is the favored reaction pathway for alkynes, whereas for phosphaalkynes the cyclodimerization is preferred. The divergent behavior of alkyne and phosphaalkyne cyclo-oligomerizations was correlated with the relative thermodynamic stabilities of the corresponding arene vs cyclobutadiene complexes and shown to be intimately dependent on the incorporation of phosphorus atoms into the ligand structures. Furthermore, the theoretical calculations and the characterization by physical methods (EPR, magnetic moment, X-ray diffraction) demonstrated that complex **192** is paramagnetic with one unpaired electron. The positive spin density is mainly localized on the Fe atom, indicative of a d^9 configuration. However, the electronic structure might differ from a formal $[(\mathrm{L^0})\mathrm{Fe^{-I}}(\mathrm{L^0})]$ since both of its ligands are potentially redox active.[213]

Scheme 23. Synthesis of Low-Valent Heteroleptic Cyclopentadienyl-alkene Metalates by the Group of Fürstner[214−216]

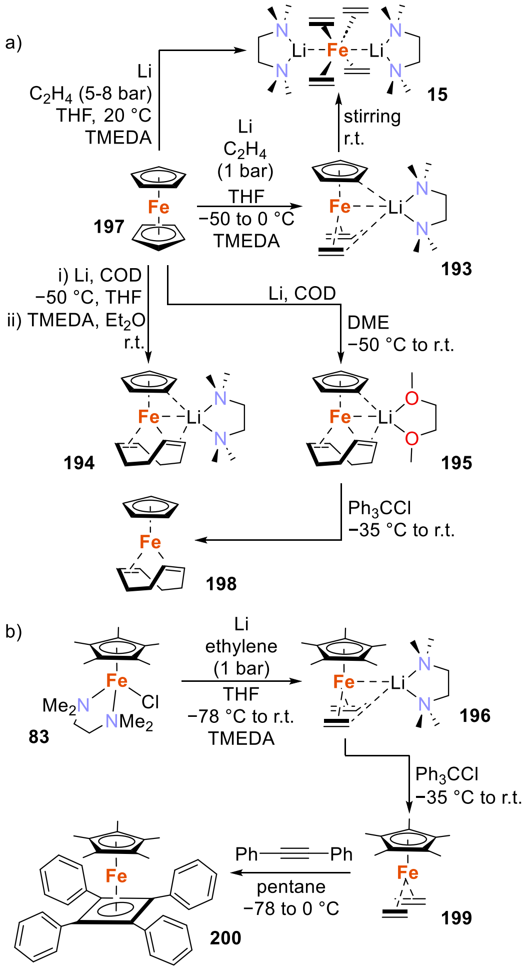

Inspired by the contributions of the Jonas group,[8,9,71,72] Fürstner and co-workers reported on the synthesis of the heteroleptic $\mathrm{Cp^RFe}$-alkene metalates $[\mathrm{Li(tmeda)}\{\mathrm{CpFe(C_2H_4)_2}\}]$ (**193**), $[\mathrm{Li(chelate)}\{\mathrm{CpFe(cod)}\}]$ [chelate = tmeda (**194**), dme (**195**)], and $[\mathrm{Li(tmeda)}\{\mathrm{Cp^*Fe(C_2H_4)_2}\}]$ (**196**), featuring zerovalent iron centers.[214−216] As shown in Scheme 1 (reaction type 1a), under reducing conditions, the Cp rings in metallocenes can be successively displaced. The group of Fürstner reported that performing a reductive cleavage on ferrocene (**197**) under an atmosphere of ethylene yields the heteroleptic Fe(0) half-sandwich complex **193** (Scheme 23a), which after prolonged stirring reacts further to form the homoleptic ferrate $[\mathrm{Li_2(TMEDA)_2}\{\mathrm{Fe}(\eta^2\text{-}\mathrm{C_2H_4})_4\}]$ (**15**). Performing the reaction in the presence of 1,5-cyclooctadiene (cod) instead of ethylene leads to the formation of the complexes $[\mathrm{Li(chelate)}\{\mathrm{CpFe(cod)}\}]$ (**194**, **195**). Furthermore, $[\mathrm{Li(dme)}\{\mathrm{CpFe(cod)}\}]$ (**195**) reacts with $\mathrm{Ph_3CCl}$ to afford the one-electron oxidation product $[\mathrm{CpFe(cod)}]$ (**198**). A similar synthetic approach, starting from precursor $[\mathrm{Cp^*FeCl(tmeda)}]$ (**83**), yields complex $[\mathrm{Li(tmeda)}\{\mathrm{Cp^*Fe(C_2H_4)_2}\}]$ (**196**) (Scheme 23b). Using these protocols (Scheme 23), various cyclopentadienyl-alkene metalates can be obtained in a multigram scale (up to 85 g, for **195**).[214−216] The authors also demonstrated the ability of these metalates to serve as intermediates in the formation of challenging scaffolds at transition metals. For instance, the Fe(I) complex $[\mathrm{Cp^*Fe(C_2H_4)_2}]$ (**199**), obtained via one-electron oxidation as for **198**, promotes the cyclodimerization of diphenylacetylene to yield the neutral cyclobutadiene iron(I) complex $[\mathrm{Cp^*Fe}(\eta^4\text{-}\mathrm{C_4Ph_4})]$ (**200**, Scheme 23b).[215]

In the search for further examples of heteroleptic ferrates, the Wolf group reported the complex $[\mathrm{K([18]crown\text{-}6)}\{\mathrm{Cp^*Fe}(\eta^4\text{-}\mathrm{C_{10}H_8})\}]$ (**201**, Cp* = $\mathrm{C_5Me_5}$, via reduction of "Cp*FeCl", prepared *in situ* from Cp*Li and $[\mathrm{FeCl_2(thf)_{1.5}}]$, with 2 equiv of potassium naphthalene, in the presence of 1 equiv of crown ether (Scheme 24a).[217−219] Unlike the naphthaleneferrate **184**, **201** is a diamagnetic 18-electron compound with a formally iron(0) center, obtained as a contact ion pair with the countercation $[\mathrm{K([18]crown\text{-}6)}]^+$. Furthermore, it is analogous to the species previously described by the Jonas group, $[\mathrm{Li(thf)_2}][\mathrm{CpFe}(\eta^4\text{-}$naphtha-

Scheme 24. (a) Synthesis and (b) Reactivity toward *tert*-Butylphosphaalkyne and Substituted Acetylenes of Complex $[K([18]crown\text{-}6)][Cp^*Fe(\eta^4\text{-}C_{10}H_8)]$ (201)[217,220,221]

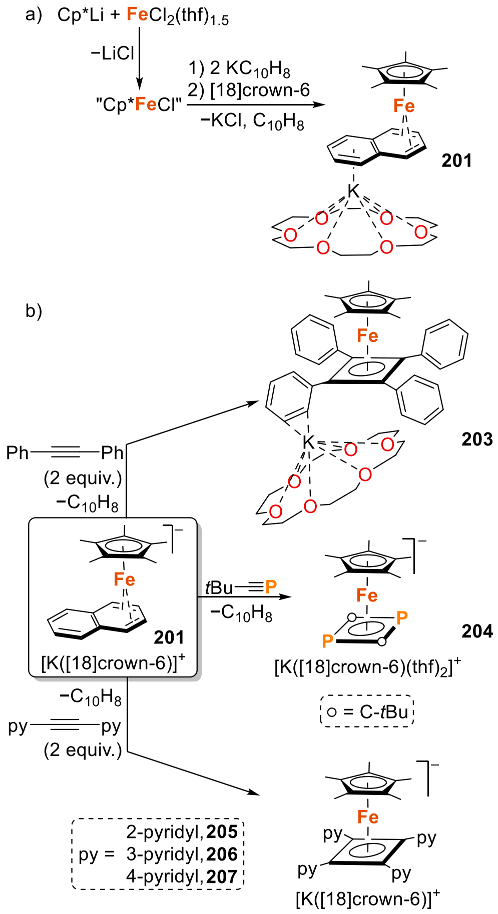

lene)] (**202**, Cp = C_5H_5).[9] The naphthalene precursor **201** behaves as an efficient Cp^*Fe^- synthon in its reaction with diphenylacetylene, mediating its cyclodimerization to form the anionic 18-electron cyclobutadiene iron(0) complex (**203**, Scheme 24b), analogous to the 17-electron Fe(I) compound **200** (Scheme 23b).[215] Also, when **201** is treated with *t*BuC≡P, a cyclodimerization of the phosphaalkyne occurs, affording the 1,3-diphosphabutadiene iron(0) sandwich compound **204** (Scheme 24b, top).[217] Follow-up studies demonstrated that the cyclodimerization of bis(pyridyl)-acetylene (pyridyl = 2-pyridyl, 3-pyridyl, 4-pyridyl) at **201** was also possible, generating potentially redox-active multi-topic substituted cyclobutadiene ligands with potential to form supramolecular assemblies.[220,221]

The complexes $[K([18]crown\text{-}6)\{Cp^*Fe(\eta^4\text{-}C_4py_4)\}]$ [py = 2-pyridyl (**205**), 3-pyridyl (**206**), 4-pyridyl (**207**)] present structural differences, as determined by X-ray diffraction; while the 2-pyridyl isomer **205** is monomeric with a contact ion pair,[220] the 3-pyridyl (**206**) and 4-pyridyl (**207**) analogues form coordination polymers with alternating cation−anion sequences.[221] The neutral complex $\{Cp^*Fe[\eta^4\text{-}C_4(2\text{-}py)_4]\}$ (**208**) was also obtained after oxidizing **205** with [CuBr(tht)] (1 equiv; tht = tetrahydrothiophene). Complexation of $ZnCl_2$ or $FeCl_2$ by **205** afforded 1:1 or 2:1 adducts $[K([18]crown\text{-}6)\{Cp^*Fe[C_4(2\text{-}py)_4]\}(ZnCl_2)]$ (**209**), $[K([18]crown\text{-}6)\{Cp^*Fe[C_4(2\text{-}py)_4]\}(FeCl_2)]$ (**210**), and $[K([18]crown\text{-}6)(thf)][Cp^*Fe[C_4(2\text{-}py)_4](ZnCl_2)_2]$ (**211**) in which the anionic complex acts as a bidentate chelate (see Figure 6).[221]

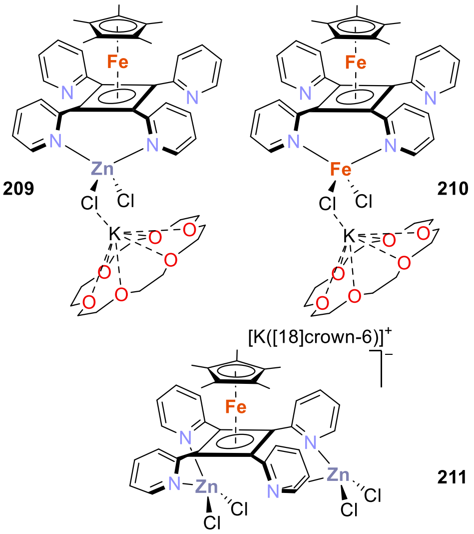

Figure 6. Iron(II) and zinc(II) adducts of complex $[K([18]crown\text{-}6)\{Cp^*Fe[\eta^4\text{-}C_4(2\text{-}py)_4]\}]$ (**205**).

$[K([18]crown\text{-}6)\{Cp^*Fe(\eta^4\text{-}C_{10}H_8)\}]$ (**201**) also acts as a two-electron reducing agent toward the imidazolium salt $[L^{Dipp}PCl_2]^+$ (**212**, L^{Dipp} = 1,3-bis(2,6-diisopropylphenyl)-imidazol-2-ylidene); see Scheme 25) to afford the diphosphorus cation $[L^{Dipp}{}_2P_2Cl_3]^+$ (**213**) and the related $[L^{Dipp}{}_2P_2Cl]^+$ (**214**).[222] Along with the mixture of the phosphorus cations, the oxidized cationic complex $[Cp^*Fe(\eta^6\text{-}naphthalene)]Cl$ (**215**) was identified. The relative ratio in which the phosphorus cations were obtained depended strongly on the reaction temperature and order of addition of the reagents. While **213** is the major product (>90% of the total P content) after 8 h when **201** is slowly added to a refluxing solution of [**212**]OTf in THF, with decreasing temperature (65 to −30 °C) the ratio shifts progressively in favor of **214**, which becomes the major product at −90 °C, in a ratio **213**:**214** = 1:8. Compound **213** is also efficiently synthesized by reduction of [**212**]OTf with sodium.[222]

Scheme 25. Reduction of the Imidazolium Salt $[L^{Dipp}PCl_2]OTf$ ([212]OTf) by $K([18]crown\text{-}6)][Cp^*Fe(\eta^4\text{-}C_{10}H_8)]$ (201)[222]

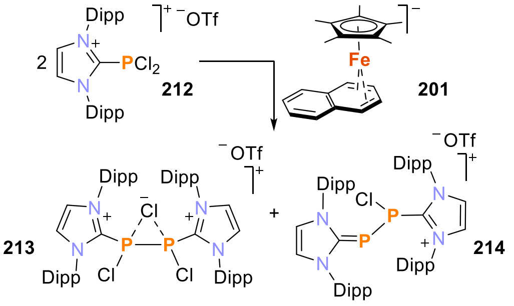

In many cases, it is difficult to provide a straightforward description of the electronic structure of transition metalates due to the redox noninnocence of their stabilizing ligands. To gain insight into the electronic structure of heteroleptic ferrates, Wolf and co-workers applied a combination of experimental analyses (NMR, UV−vis, ^{57}Fe Mössbauer spectroscopy, electron paramagnetic resonance (EPR) spectroscopy, magnetic susceptibility measurements and single-crystal X-ray crystallography) and theoretical calculations (DFT)[219] to investigate the behavior of the anionic complexes [K([18]crown-6)][Cp*Fe(η^4-polyarene)] [polyarene = naphthalene (**201**),[217−219] anthracene (**216**); Cp* = C_5Me_5],[219] and the neutral analogues [Cp*Fe(η^4-polyarene)] [polyarene = naphthalene (**217**) anthracene (**218**)]. Although compound **216** can be prepared via a procedure similar to that used for **201** (Scheme 24a) by using anthracene instead of naphthalene, this synthetic pathway is hampered by difficulties in the purification of the product. Consequently, an alternative protocol was devised, consisting of the exchange of the naphthalene ligand on **201** with anthracene (Scheme 26a). It was also observed that the reduction of "Cp*FeCl" with 2 equiv of potassium anthracenide in the absence of crown ether affords the neutral compound **218** (Scheme 26b). The naphthalene complex **217** cannot be similarly obtained and was synthesized via oxidation of the parent species **201** with AgOTf (Scheme 26a).

Scheme 26. Preparation of Low-Valent Naphthalene and Anthracene Iron Complexes by Wolf and Co-workers[219]

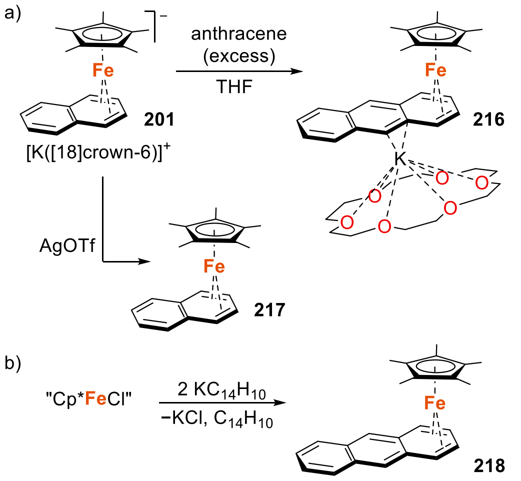

The redox properties of these complexes were studied through cyclic voltammetry and spectroelectrochemical analysis, revealing that the neutral complexes **217** and **218** can be both reversibly reduced to the monoanions [Cp*Fe(η^4-polyarene)]$^-$ (**201**, **216**) and reversibly oxidized to the cationic species [Cp*Fe(η^6-polyarene)]$^+$ (**217**$^+$, **218**$^+$). Density functional theory (DFT) calculations indicated reduced orbital charges and spin densities in the series of complexes [Cp*Fe(polyarene)]$^{-/0/+}$ (polyarene = naphthalene, anthracene). Altogether, the structural, spectroscopic and DFT studies showed that the *formal* oxidation state of the iron center in such species varies from Fe(0) to Fe(II). However, the spectroscopic oxidation state in all cases is close to Fe(II), with the sole exception of compound **217**, which possesses significant Fe(I) character. In any case, clearly, the naphthalene and anthracene motifs in these complexes behave predominantly as redox noninnocent ligands.[219]

In 2012, independent reports by Wolf and co-workers,[223] and by the group of Yoshizawa and Tatsumi,[224] described the synthesis of the homodinuclear compounds [Cp*Fe(μ−η^4:η^4-$C_{10}H_8$)FeCp*] (**219**, Cp* = C_5Me_5) and [Cp*Fe(μ−η^4:η^4-$C_{14}H_{10}$)FeCp*] (**220**). An analogue of complex **219** featuring the unsubstituted cyclopentadienyl ligand, [CpFe(μ−η^4:η^4-$C_{10}H_8$)FeCp] (**219′**), was previously described, but its characterization was not fully reported.[9] The procedure for the synthesis of [Cp*Fe(μ−η^4:η^4-polyarene)FeCp*] consists of a salt metathesis between [Cp*FeCl(tmeda)] (**83**) and the anionic Fe(0) complex **201** (Scheme 27a), in the case of **219**,[223] or of 1:1 reduction of [$FeCl_2(thf)_{1.5}$] by potassium anthracenide in the presence of stoichiometric equivalents of LiCp*, for **220** (Scheme 27b). Yoshizawa and Tatsumi obtained compound **219** via direct reduction of **83** with potassium naphthalenide (2 equiv; see Scheme 27a).[224] These complexes feature 17-electron, formally Fe(I) centers, and the structural characterization of **219** confirmed that two Cp*Fe moieties bind to the opposite faces of the naphthalene bridge. A similar *transoid* arrangement was found for the anthracene-bridged complex **220** (Scheme 27b). Despite being 17e$^-$ species and having one unpaired electron *per* metal center, the complexes are diamagnetic in the ground state, due to the strong magnetic coupling of both Fe(I) centers efficiently mediated by the polyarene bridge, as demonstrated via electrochemical, spectroscopic, and DFT investigations.[223,224] Other early reports described, contrastingly, paramagnetic [Cp*Fe(μ-polyarene)FeCp*] compounds (polyarene = dihydrophenanthrene, triphenylene, phenanthrene, pyrene) with weakly coupled iron centers.[225,226] For **219** and **220**, two well-separated one-electron oxidation steps were identified after studying their redox behavior by cyclic voltammetry and

Scheme 27. Synthesis of Low-Valent Redox-Active Polyarene-Bridged Homo- And Heterodinuclear Complexes[223,224,227]

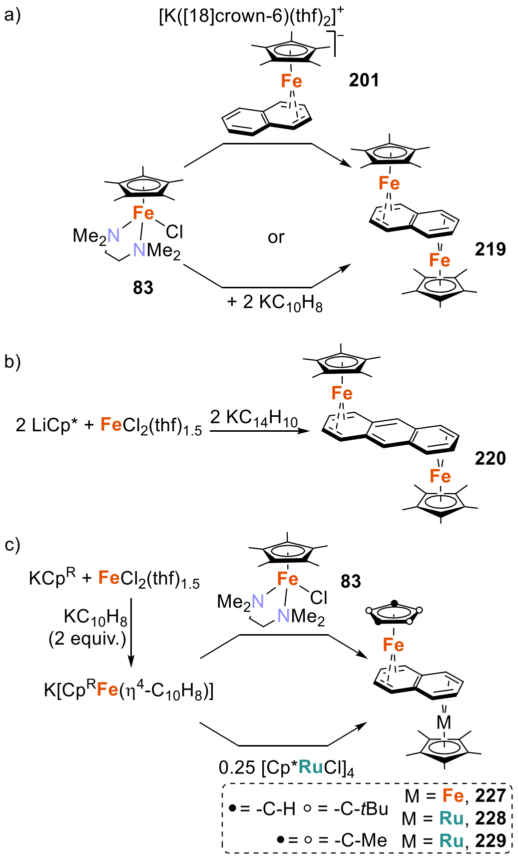

UV–vis spectroscopy. Reversible oxidations to the monocations [Cp*Fe(μ-polyarene)FeCp*]$^+$ [polyarene = naphthalene (**221**), anthracene (**222**)] and the dications [Cp*Fe(μ-polyarene)FeCp*]$^{2+}$ [polyarene = naphthalene (**223**), anthracene (**224**)] as well as reduction to the monoanions [Cp*Fe(μ-polyarene)FeCp*]$^-$ [polyarene = naphthalene (**225**), anthracene (**226**)] were observed.[223,224] Chemical oxidation with [Cp_2Fe]PF_6 allowed for the isolation of the mixed-valent Fe^I–Fe^{II} cationic compounds **221** and **222** as the $BAr^F{}_4{}^-$ salts. The molecular structure of **221** revealed that, upon oxidation, the naphthalene ligand changes its hapticity from η^4 in complex **219** to η^6 in the cationic compound. This hapticity change was assumed to account for the high thermodynamic stability of the mixed-valence species with respect to disproportionation.[224]

A slightly modified procedure was employed for the synthesis of dissymmetrical naphthalene-bridged complexes [Cp‴Fe(μ-$C_{10}H_8$)FeCp*] (**227**, Cp‴ = η^5-C_5H_2-1,2,4-*t*Bu_3, Cp* = η^5-C_5Me_5), [Cp‴Fe(μ-$C_{10}H_8$)RuCp*] (**228**) and the homoleptic heterodinuclear compound [Cp*Fe(μ-$C_{10}H_8$)-RuCp*] (**229**), as shown in Scheme 27c.[227] The main modification of this protocol is that "Cp^RFeCl" is initially generated *in situ* from [$FeCl_2(thf)_{1.5}$] and KCp^R (Cp^R = Cp‴, Cp*), then treated with potassium naphthalenide ($KC_{10}H_8$) to form the iron(0) species K[Cp^RFe($C_{10}H_8$)], onto which either [Cp*FeCl(tmeda)] (**83**, tmeda = tetramethylethylene-1,2-diamine) or [Cp*RuCl]$_4$ (**230**) are added to obtain the final dissymmetrical FeFe or FeRu complexes. **227**–**229** are structurally analogous to **219** and **220**: diamagnetic compounds with coordinating Cp^RM fragments on opposite faces of the bridging naphthalene ligand.

Cyclic voltammetry and UV–vis spectroelectrochemistry studies showed the feasibility of oxidizing complexes **227** and **228** to the monocations [Cp‴Fe(μ-$C_{10}H_8$)FeCp*]$^+$ (**231**) and [Cp‴Fe(μ-$C_{10}H_8$)RuCp*]$^+$ (**232**). These paramagnetic complexes are accessible as hexafluorophosphate salts after chemical oxidation with [Cp_2Fe]PF_6. Further oxidation to the corresponding dicationic species was observed via cyclic voltammetry, and proved reversible only for **232** and for the homoleptic [Cp*Fe(μ-$C_{10}H_8$)RuCp*]$^+$ (**233**). The structural and spectroscopic data are supported by the DFT calculations. Substituting the Cp* ligand by Cp‴ produces only modest perturbations of the electronic structures of the complexes, which do not seem to significantly change the compositions and shapes of their frontier orbitals. According to the DFT calculations, the redox behavior of complexes **227** and **228** seems to be significantly affected by the contributions from the Cp‴Fe motif and the naphthalene bridging ligand. By contrast, substitution of a Cp*Fe motif in complex **227** by a Cp*Ru scaffold in **228** seems to have little influence. Thus, the redox potentials of the complexes appear to respond more strongly to the changes on the Cp^R ligand than to the substitution of the Fe center by Ru.[227]

Scheme 28. Synthesis of an Fe(I) Organoferrate by Hu and Co-workers[230]

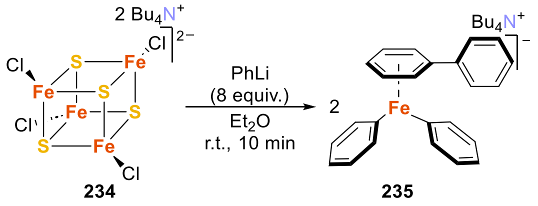

In the 1980s, an *in situ* generated catalytic system, composed by phenyl lithium and the iron–sulfur cluster [Bu_4N]$_2$-[$Fe_4S_4Cl_4$] (**234**) was developed for the hydrogenation of stilbenes and carbonyl compounds.[228,229] In an attempt to elucidate the nature of the catalytically active species, Hu and co-workers synthesized the unsupported Fe(I) organoferrate [Bu_4N][(η^6-biphenyl)Fe(Ph)$_2$] (**235**) by treating the cluster **234** with PhLi (8 equiv; Scheme 28).[230] Although the structure of **235** is very unusual, this complex was not a competent catalyst in the hydrogenation of olefins, nor did it react with H_2. Nonetheless, **235** reacts with 2-bromopyridine, *p*-bromoanisole, or 1-bromobutane to afford the corresponding C–C coupling products and free biphenyl in low yield.

2.2.4.4. Cobalt. The versatility of metalate complexes as sources of "naked-metal atom" reagents was further demonstrated through the synthesis of the ternary intermetalloid clusters [$Co@Sn_6Sb_6$]$^{3-}$ (**236**), [$Co_2@Sn_5Sb_7$]$^{3-}$ (**237**), and [$Ni_2@Sn_7Sb_5$]$^{3-}$ (**238**) (see Figure 7 for a representation of the structures of the cobalt clusters) by Dehnen and co-workers.[231] To obtain clusters **236**–**238**, the classic cobaltate [Co(η^4-cod)$_2$]$^-$ (**239**, as [K(thf)$_x$]$^+$ salt)[7] or the Ni(0) precursor [Ni(cod)$_2$] (**240**, cod = 1,5-cyclooctadiene),[4,5] in conjunction with [K([2.2.2]cryptand)]$_2$[Sn_2Sb_2] (**241**), served as starting materials. The cobalt-containing clusters cocrystallized in the salt [K([2.2.2]cryptand)]$_3$[(**236**)$_{0.83}$(**237**)$_{0.17}$]·2dmf·2toluene. Crystals allowed for an adequate characterization of the major component **236**, while for the minor component **237** the structure was not satisfactory. However, anion **237** was characterized in the salt [K([2.2.2]cryptand)]$_3$-[**237**], obtained after performing a similar reaction in a mixture of ethylenediamine (en) and DMF at 60 °C, and growing crystals from a filtered solution (in ethylenediamine) of the precipitated powder. The 12-vertex cluster **236** has a fused square-antiprism structure, and is asymmetrically occupied by a Co^- center, constituting a rare example of a compound in which the inner transition metal atom is not located at the center of the cluster.

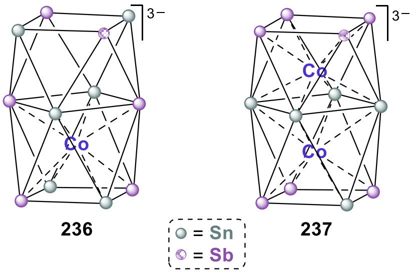

Figure 7. Representation of the structures of the anionic clusters [$Co@Sn_6Sb_6$]$^{3-}$ (**236**) in [K([2.2.2]cryptand)]$_3$[(**236**)$_{0.83}$(**237**)$_{0.17}$]·2dmf·2toluene and [$Co_2@Sn_5Sb_7$]$^{3-}$ (**237**) in [K([2.2.2]cryptand)]$_3$-[**237**], as determined by X-ray diffraction.[231]

Although certainly unusual, DFT calculations not only supported the molecular structure determined by X-ray diffraction but also revealed that other structures with the same stoichiometry are not feasible. The cobalt and nickel clusters **237** and **238** are isoelectronic and isostructural (a representation of the structure of **237** is shown in Figure 7), despite their different compositions. Calculated natural atomic charges for the three clusters support the presence of formal Co^- centers for **236** and **237**, and of the isoelectronic Ni(0) centers for **238**. Therefore, it was concluded that the three Sn/

Sb cages obtained are 56-valence-electron species (C_{4v}-type topology). The total valence electron count might then be the crucial factor controlling the types of structures obtained. Preliminary ^{119}Sn NMR studies in solution were also reported.[231]

Compound $[Co(\eta^4\text{-cod})_2]^-$ (**239**) was also used for the synthesis of the unusual Co_2Sn_2 heterobimetallic p-block/d-block element cluster $[Ar^{Dipp2}SnCo]_2$ [**242**, Ar^{Dipp2} = C_6H_3-2,6(C_6H_3-2,6-*i*$Pr_2)_2$; Scheme 29].[232] The cyclic rhomboidal Co_2Sn_2 core in **242** is obtained after reaction between cobaltate **239** and the tin compound $[Ar^{Dipp2}Sn(\mu\text{-Cl})]_2$ (**243**). **242** has strong metal−metal bonds between the tin and cobalt atoms, but also features a weaker tin−tin interaction, as evidenced in the molecular structure of the cluster. Furthermore, the cobalt atoms are η^6-coordinated by one of the flanking 2,6-diisopropylphenyl units in each terphenyl ligand, and a strong cobalt-arene interaction is indicated by the short cobalt−centroid distance (1.560(1) Å). This suggests strong d-π^* backbonding between the cobalt center and the coordinated arenes. DFT calculations support the existence of strong intermetallic bonds in the Co_2Sn_2 core and a weaker Sn−Sn interaction.

Scheme 29. Synthesis of the Cyclic Co_2Sn_2 (242) Cluster Using the Co^- Synthon $[Co(\eta^4\text{-cod})_2]^-$ (239)[232]

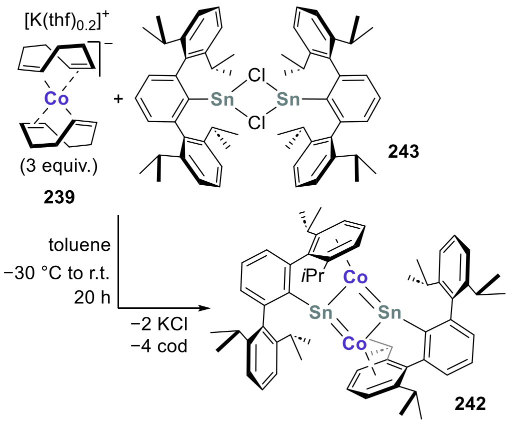

Whereas treatment of **242** with O_2 and CO yielded intractable mixtures, reaction with white phosphorus proved highly selective. Insertion of the P_4 tetrahedron into the Co_2Sn_2 core led to the formation of a *catena*-P_4 complex, $[Ar^{Dipp2}{}_2Sn_2Co_2P_4]$ (**244**, Ar^{Dipp2} = C_6H_3-2,6-{C_6H_3-2,6-*i*Pr_2}$_2$), which constitutes the first molecular cluster composed of phosphorus, cobalt and tin atoms. The molecular structure confirmed a functionalized P_4-chain, resulting from migration of a tin-bound terphenyl substituent to one P-atom.[232]

Among the polyarene complexes reported by Ellis,[70,181] naphthalene metalates of the late transition metals proved elusive until 2006.[233] The first naphthalenecobaltate(−I), $[Co(\eta^4\text{-}C_{10}H_8)(\eta^4\text{-cod})]^-$ (**245**, see Scheme 30), analogous to $[Fe(\eta^4\text{-}C_{14}H_{10})(\eta^4\text{-cod})]^-$ (**183**), was obtained by reduction of $CoBr_2$ by potassium naphthalenide[87,233] in the presence of a stoichiometric amount of 1,5-cod, in a procedure similar to that used for complexes $[M(\eta^4\text{-}C_{14}H_{10})_2]^-$ [M = Fe (**52**); Co (**14**)].[70,181]

Complex **245** is also accessible from cobaltocene, and the authors proposed that, according to their observations, both synthetic routes seem to have a common intermediate, presumably a homoleptic naphthalenecobaltate analogous to the anthracenecobaltate **14**. Such a species has proven difficult to isolate in pure form.[87] However, a mixture of yellow and red-black crystals suitable for X-ray diffraction was obtained after reaction of the known $[Co(C_2H_4)_4]^-$ complex (**246**, as the $[K([18]crown\text{-}6)]^+$ salt)[2,234,235] with naphthalene (3 equiv; THF, 20 °C). The yellow crystals were identified as the starting material **246**, while the red-black ones were characterized as the unusual "triple-salt" $[K([18]crown\text{-}6)]_3$-$[Co(\eta^4\text{-}C_{10}H_8)(C_2H_4)_2]_2[Co(\eta^4\text{-}C_{10}H_8)_2]$ (**247**), which provided structural evidence of the new metalate $[Co(\eta^4\text{-}C_{10}H_8)(C_2H_4)_2]^-$ and of the long sought-after homoleptic naphthalene metalate $[Co(\eta^4\text{-}C_{10}H_8)_2]^-$.[233]

Scheme 30. Synthesis of Naphthalenecobaltate(−I), $[Co(\eta^4\text{-}C_{10}H_8)(\eta^4\text{-cod})]^-$ (245)

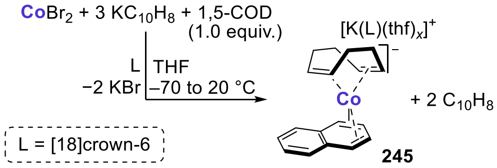

The reactivity of compounds **14** and **245** was examined by the same group (Scheme 31).[87] An early investigation of the reactivity of **14** was reported in 2002[70] and was later broadened to include a wider range of substrates.[87] Alternative and improved methods for the synthesis of classic cobaltates,[2,236−241] such as $[Co(\eta^4\text{-}C_4H_6)_2]^-$ (**248**), $[Co(PF_3)_4]^-$ (**249**), $[Co(PR_3)_4]^-$ [R = O*i*Pr (**250**) OMe (**251**)], or $[Co(bpy)_2]^-$ (**252**),[207,242] were developed, involving reactions of precursor **14** with 1,3-butadiene, PF_3, P(O*i*Pr)$_3$, or 2,2′-bipyridine, respectively. Crystallographic analyses were also performed for complexes **248**−**250**, and for the classic carbonyl compound $[Co(CO)_4]^-$ (**95**, characterized as the $[K([2.2.2]cryptand)]^+$ salt).[243] Additionally, **14** reacted with PMe_3, albeit with different results to those previously obtained with 1,2-bis(diphenylphosphino)ethane (dppe).[70] Instead of an analogue of the homoleptic compound $[Co(dppe)_2]^-$ (**253**),[70] the interaction of cobaltate **14** with PMe_3 yielded the known Co(0) species, $[Co(\eta^4\text{-}C_{14}H_{10})(PMe_3)_3]$ (**254**)[244] and the anthracene radical anion salt, $[K([18]crown\text{-}6)(thf)_2][C_{14}H_{10}]$. The authors proposed that complex **254** might be formed through an unidentified Co(−I) intermediate, which, due to its strongly reducing character, is oxidized to the Co(0) complex while reducing coordinated or free anthracene to $C_{14}H_{10}{}^-$. This behavior might parallel that observed by Klein and co-workers, who reported that another (trimethylphosphine)cobaltate, $[Co(PMe_3)_4]^-$ (**255**), prepared by reduction of $[Co(PMe_3)_4]$ (**256**) with alkali metals (Li, Na, K), acted as an extraordinarily strong reducing agent.[244,245]

The synthesis of a family of mixed arene/alkene cobaltates was also proposed, and the viability of the reactions using complexes **14** or **245** was compared (Scheme 31).[87] The heteroleptic complexes $[Co(\eta^4\text{-}C_{14}H_{10})(\eta^4\text{-cod})]^-$ (**257**), analogous to **245**, and $[Co(\eta^4\text{-}C_{14}H_{10})(C_2H_4)_2]^-$ (**258**) were obtained from **14** after treatment with an excess 1,5-cod or ethylene, respectively.[87] When the reduction of $CoBr_2$ to form **245** is attempted in the presence of an excess 1,5-cod, instead of the heteroleptic complex, the reaction affords the classic cobaltate $[Co(\eta^4\text{-cod})_2]^-$ (**239**),[7] which can also be obtained by direct reaction of **245** with 1,5-cod. Similarly, while **245** remains unchanged when treated with anthracene at room temperature, upon heating the reaction mixture to 60 °C,

Scheme 31. Reactivity of $[Co(\eta^4\text{-}C_{14}H_{10})_2]^-$ (14) and $[Co(\eta^4\text{-}C_{10}H_8)(\eta^4\text{-cod})]^-$ (245) in Contrast: Synthesis of a Family of Metalates from "Naked-Metal Atom" Cobaltates[87,247a]

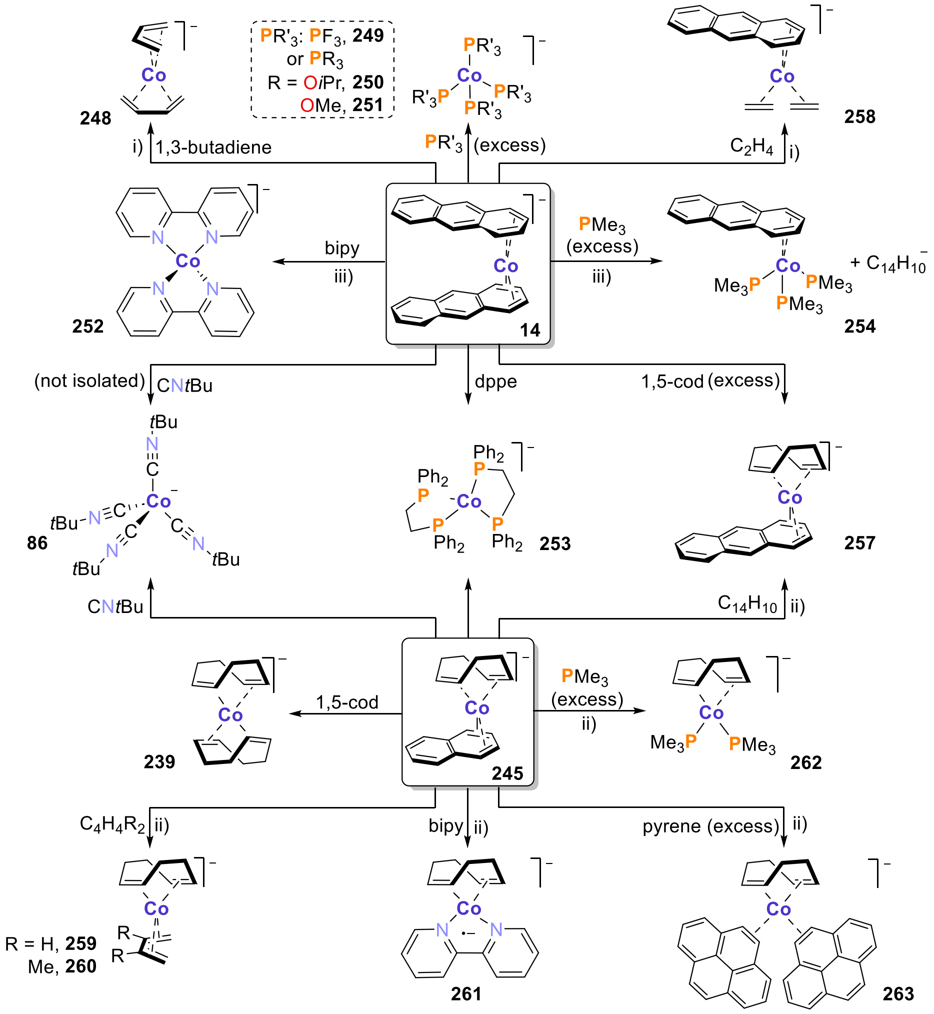

[a]Conditions: (i) Et_2O, 20 °C; (ii) THF, 20 °C; (iii) −78 to 20 °C.

anthracene displaces the naphthalene ligand in **245** to yield **257**. However, the synthesis of **257** using **14** as the starting material remains more efficient than the ligand exchange reaction at higher temperature. Displacement of the anthracene ligand from precursor **14** appears to be facile, explaining the formation of homoleptic complexes by ligand substitution. By contrast, the coordinated cod ligand on **245** appeared to be substantially less labile. As a result, a variety of mixed-ligand cyclooctadiene complexes are accessible by substitution of the naphthalene ligand of **245**, e.g., $[Co(\eta^4\text{-}C_4H_4R_2)(\eta^4\text{-cod})]^-$ [R = H (**259**), R = Me (**260**)] $[Co(bpy)(\eta^4\text{-cod})]^-$ (**261**),[246] and $[Co(\eta^4\text{-cod})(PMe_3)_2]^-$ (**262**). Detailed examination of the bond distances on the bpy scaffold on the solid-state structure of **261** revealed the presence of a coordinated bpy radical anion, $bpy^{\bullet-}$. Thus, **261** could be described as a Co(0) species, $[Co(bpy^{\bullet-})(\eta^4\text{-cod})]^-$.[87] Precursor **245** has also served as starting material for the synthesis of the bis(pyrene)metal complex $[Co(\eta^2\text{-pyrene})_2(\eta^4\text{-cod})]^-$ (**263**, as $[K([2.2.2]cryptand)]^+$ salt), which was structurally characterized.[247] Unlike the Ti(−I) or M(0) (M = V, Nb) sandwich complexes **153** or **154**,[183] **263** showcases pyrene ligands coordinated in η^2-fashion.[247]

Ellis and co-workers studied the formation of alkylisocyanometalates using precursors **14** and **245**.[87] While FT-IR spectroscopy of the interaction of **14** with CN*t*Bu suggested the possible formation of a homoleptic alkylisocyanometalate, the product could not be isolated (Scheme 31). However, its formation was corroborated by the isolation of the triphenyltin derivative, $(Ph_3Sn)Co(CNtBu)_4$ (**264**), similar to *trans*-$[Fe(CNtBu)_4(SnPh_3)_2]$ (**57**). In a similar vein, **245** reacted with CN*t*Bu (4 equiv) at −78 °C to afford the thermally unstable $[K([18]crown\text{-}6)(thf)_2][Co(CNtBu)_4]$ (**86**), the formulation of which was confirmed through structural characterization.

The cobaltates **14**, **239**, and **245** also served as starting materials for the synthesis of additional examples of homoleptic and heteroleptic alkene cobaltates.[248] The heteroleptic complexes $[K([18]crown\text{-}6)][Co(\eta^4\text{-cod})(\eta^2\text{-styrene})_2]$ (**265**) and $[K([18]crown\text{-}6)][Co(\eta^4\text{-dct})(\eta^4\text{-cod})]$ (**266**; dct = dibenzo[*a*,*e*]cyclooctatetraene, cod = 1,5-cyclooctadiene), and the homoleptic $[K(thf)_2][Co(\eta^4\text{-dct})_2]$ (**267**), were obtained by ligand exchange with the corresponding alkenes, using either complex **239** or **245** as a starting material (see Scheme 32a). The highly air-sensitive heteroleptic species **265** could be obtained from either **245** in the presence of a

Scheme 32. Synthesis of Heteroleptic and Homoleptic Alkene Cobaltates by Jacobi von Wangelin, Wolf, and Co-workers[248]

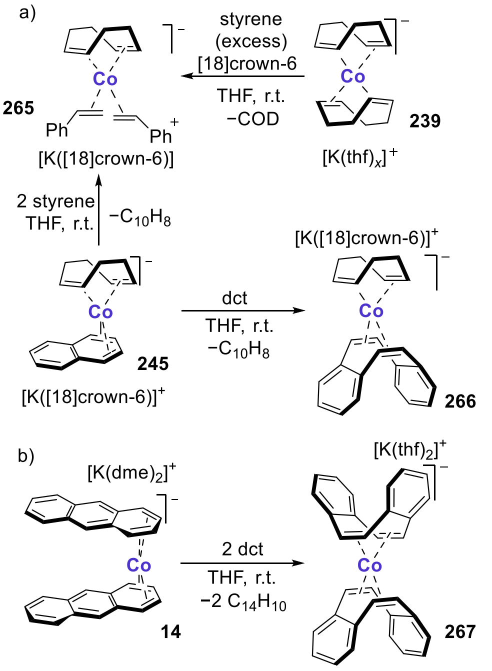

slight excess of styrene, or from **239** after reaction with a large excess of the olefin and in the presence of [18]crown-6. The latter procedure afforded **265** in a higher yield than the former. Similarly, addition of dct to **245** led to the formation of **266**, albeit not in pure form, being invariably contaminated with the bis(dibenzo[*a,e*]cyclooctatetraene) complex **267**. A more complex mixture of products was obtained by reaction of the bis(1,5-cyclooctadiene) cobaltate **239** with dct, furnishing again both **266** and **267**, as well as unreacted **239**. Such reactivity parallels behavior observed for **239** by Ellis and co-workers, in which attempted ligand exchange on Jonas' classic cobaltate led almost invariably to heteroleptic species or unreacted starting material, even in the presence of a large excess of ligand.[87]

The homoleptic complex **267** is obtained in pure form by reaction of **14** with dct (see Scheme 32b), albeit in low yield (19%). A significant improvement in the reaction yield (62%) was observed when styrene was added to **14** followed by the addition of dct. This observation might be indicative of a two-step substitution, in which an initially formed styrene complex analogous to **265** facilitates the formation of the homoleptic complex **267**. X-ray diffraction analysis of **267** revealed that the complex is obtained as a contact ion pair with the $[K(thf)_2]^+$ counterion.[248]

2.2.4.5. 4d and 5d Metalates.

As mentioned above, Ellis and co-workers described the triad of group 4 M(−II) complexes $[M(C_{14}H_{10})_3]^{2-}$ and $[M(C_{10}H_8)_3]^{2-}$, including the heavier tris(polyarene)zirconates(−II) [polyarene = anthracene (**148**), naphthalene (**151**)] and tris(polyarene)-hafnates(−II) [polyarene = anthracene (**149**), naphthalene (**152**)], as illustrated in Scheme 17 for the lighter titanate analogues (*vide supra*).[179,182] In a similar vein, the first isolable homoleptic butadienemetalates of 4d and 5d metals, $[M(\eta^4\text{-}C_4H_6)_3]^-$ [M = Nb (**268**), Ta (**269**)], were also reported by Ellis.[249] In previous work, the same group had succeeded in accessing the homoleptic arene tantalates $[Ta(\eta^4\text{-}C_{14}H_{10})_3]^-$ (**270**) and $[Ta(\eta^4\text{-}C_{10}H_8)_3]^-$ (**271**), with **271** serving as the starting material for the corresponding butadienemetalate $[Ta(\eta^4\text{-}C_4H_6)_3]^-$ (**269**, Scheme 33a).[180] Attempts to isolate and characterize the presumed homoleptic naphthaleneniobate(−I) $[Nb(\eta^4\text{-}C_{10}H_8)_3]^-$ failed. Nevertheless, the heteroleptic anion $[Nb(\eta^4\text{-}C_{10}H_8)_2(PMe_3)_2]^-$ (**272**) was obtained and used as a precursor to the niobium butadienemetalate $[Nb(\eta^4\text{-}C_4H_6)_3]^-$ (**268**, Scheme 33b). In species **272**, it is believed that the PMe_3 donors are key to strengthen the metal−naphthalene bond and, consequently, provide stability to the compound with respect to the hypothetical complexes $[Nb(\eta^4\text{-}C_{10}H_8)_3]^-$ and $[Nb(\eta^6\text{-}C_{10}H_8)_2]^-$, which have remained elusive. The isolation of the unprecedented homoleptic butadiene complexes $[M(\eta^4\text{-}C_4H_6)_3]^-$ [M = Nb (**268**), Ta (**269**)] could serve as an inspiration to attempt the synthesis of similar compounds with other 4d and 5d transition metals in formally negative oxidation states. The $[PPN]^+$ salt of the tris(naphthalene)tantalate(−I) **271** has been identified to undergo double *ortho*-metalation of two phenyl rings and hydrogenation of the third unit at tantalum to afford a tantalum bound 1,3-cyclohexadiene group.[250]

Scheme 33. Synthesis of Niobium and Tantalum Alkene or Arene Metalates by the Ellis Group[249]

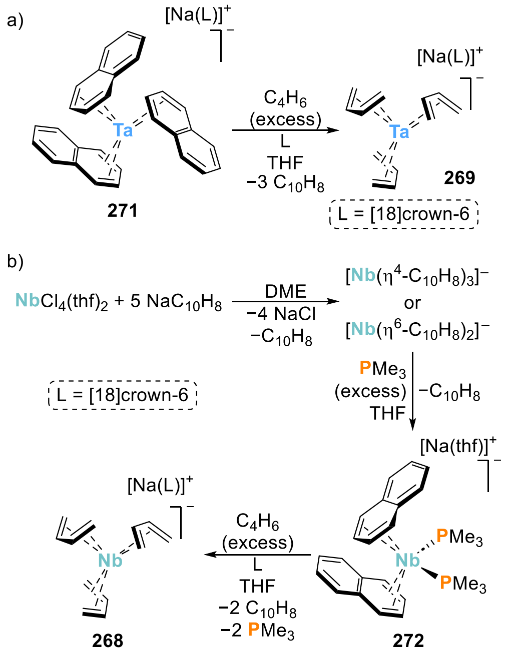

Girolami demonstrated that treatment of $HfCl_4$ (**273**), $[TaCl_2(OMe)_3]$ (**274**), or $[WCl_3(OMe)_3]$ (**275**) with ethyl lithium (LiEt) provides access to the anionic hafnium(II), tantalum(−I), and tungsten(−II) complexes $[Li(tmeda)]_2$-$[HfEt_4(C_2H_4)]$ (**276**), $[Li(tmeda)]_3[TaHEt(C_2H_4)_3]$ (**277**), and $[Li(tmeda)]_3[WH(C_2H_4)_4]$ (**278**), respectively (Scheme 34).[251] The lithium organyl LiEt acted both as a reductant and an ethylene source, formed by a β-hydrogen abstraction process, as demonstrated by labeling experiments. The ethylene ligands have a significant metallacyclopropane character in all these metalates. The hydride resonance in the tantalum complex is observed at δ 1.23 ppm, while in the tungsten species the hydridic signal is observed at δ −8.21 ppm. Variable temperature NMR measurements and spin

Scheme 34. Synthesis of Hafnium, Tantalum, and Tungsten (Ethylene)metalates by Girolami and Co-workers[251]

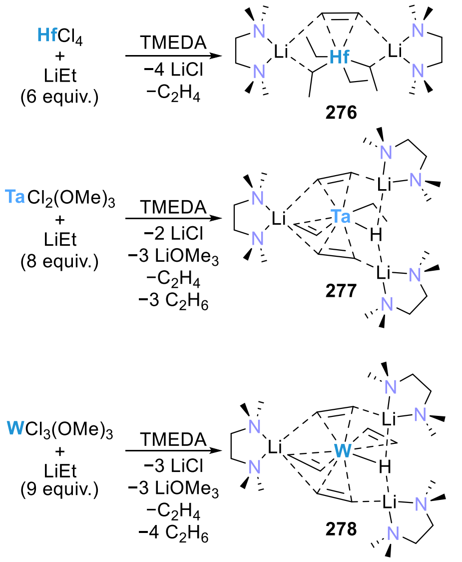

saturation transfer experiments indicate that exchange between the ethylene sites and the hydride environments for the tantalate and tungstate complexes does not take place on the NMR time scale. In the solid state, the anions **277** and **278** adopt distorted square-pyramidal geometries with the hydride group in the axial position and two of the ethylene ligands interacting with the lithium cations. The coordination environment of Hf in **276** is also distorted square-pyramidal, with the ethylene ligand in the axial position. The cations interact with the ethylene unit and with two of the ethyl groups in **276**.

2.2.5. Metallocene Anions.

Cyclopentadienyl ligands and their substituted derivatives have been well-studied in organometallic chemistry. However, as discussed so far, most cyclopentadienyl metalates are heteroleptic complexes, generally CpM(alkene/arene) compounds. Until the first decade of the new millenium, very few examples of homoleptic cyclopentadienyl metalate anions had been isolated.[23] This comes as a surprise since the electrochemical reduction of metallocenes to formally anionic species was documented decades ago.[252−259] This situation has completely changed over the last ten years, as numerous metallocene anions have become available. The remarkable development of the field has been comprehensively reviewed by Magnoux and Mills.[23] As a result, we will focus on the most recent developments. The excellent review article by Magnoux and Mills should be consulted for earlier work, such as the synthesis and reaction chemistry of the metallocenates $Na[Cp^*{}_2Mn]$ and $M[Cp_2Re]$ (M = Li, K).

In 2014, Bradley and co-workers described the first crystallographic characterization of a metallocene anion.[260] In a previous study,[261] the same group found that upon reduction of the Co(II)-indenyl complex $[Co(\eta^5\text{-}C_9H_5\text{-}1,3\text{-}(SiMe_3)_2)_2]$ (**279**) by sodium amalgam in the presence of excess vinyltrimethylsilane, instead of forming a product containing the bulky olefin, the neutral dimer $[Co_2(\eta^5{:}\eta^4\text{-}C_9H_5\text{-}1,3\text{-}(SiMe_3)_2)_2]$ (**280**, Scheme 35) was obtained. It was proposed that the formation of **280** could proceed through a formally 20-valence-electron bis(indenyl)cobaltate species and, therefore, the synthesis of such an intermediate was attempted.[260]

Scheme 35. Synthesis of the Bis(indenyl)cobaltate 281, an Intermediate in the Formation of Dimer 280[260]

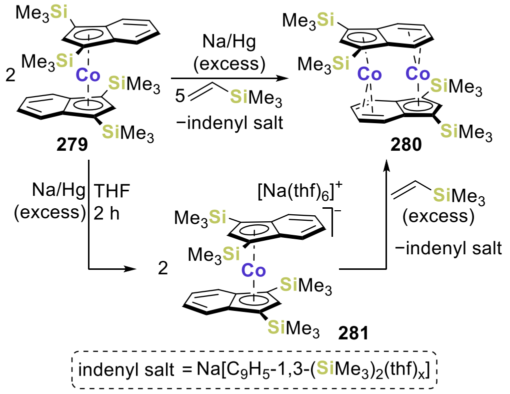

Initially, cyclic voltammetric studies in THF indicated that the Co(II) complex **279** presented reversible one electron processes for both the oxidation to cobaltocenium and reduction to cobaltate ions ($E_{1/2}$ = −0.850 and −1.800 V, respectively, vs Fc/Fc^+). Consequently, the 20 VE Co(I) anion $[Co(\eta^5\text{-}C_9H_5\text{-}1,3\text{-}(SiMe_3)_2)_2]^-$ (**281**, as the $[Na(thf)_6]^+$ salt; Scheme 35) was isolated after chemical reduction of **279** with sodium amalgam in THF, and its structure was confirmed by crystallographic analysis. A comparison of the metric parameters of **281** and **279** shows an elongation of the Co−C bond lengths [d_{CoC}(**279**) = 2.06−2.25 Å vs d_{CoC}(**281**) = 2.09−2.46 Å], but almost unchanged C−C bond distances in the anionic compound with respect to the neutral species, suggesting a metal-based reduction event. Reactivity studies toward σ and π donors, performed on **281**, as well as crossover experiments with a related indenide salt, revealed that the complex reacts by a reversible indenide ligand ejection. Mechanistically, **281** reacts via associative displacement of an indenide unit, both in the presence and in the absence of strong supporting donor ligands.[260]

The previously observed formation[261] of **280** was then proposed to proceed initially via associative displacement of indenide, probably through an unobserved ring slipped intermediate, which generates a 16 electron adduct $[Co(\eta^5\text{-}C_9H_5\text{-}1,3\text{-}(SiMe_3)_2)(L)]$ (L = vinyltrimethylsilane or aromatic amine). After substitution of the supporting donor ligand L by a benzo group and dimerization, **280** is formed. It was also proposed that the stabilization of the 20 VE cobaltate **281** is likely assisted by the bulkiness and less electron donating character of the silyl substituents.[260]

Other Cp-based metalates have been recently described.[262,263] As mentioned, the reduction of 3d metallocenes to their monoanions as transient species, from Cp_2V to Cp_2Ni, has been electrochemically achieved.[252−259] At extremely negative potentials and very low temperatures, some authors discussed the electrochemical reduction of ferrocene to its monoanion,[259,264] and that of cobaltocene and nickelocene to their corresponding dianions.[254,265] However, with the exception of the bis(indenyl)cobaltate **281**,[260] the products of metallocene reduction were not structurally characterized due to the highly reactive nature of the different anionic species. As recently as 2019, Malischewski reported the structural characterization of potassium salts of the decamethylmanganocene anion $[Cp^*{}_2Mn]^-$ (**282**; see Scheme 36a).[262] The synthesis and electronic structures of this anion were described more than four decades ago.[255,266] Following a

Scheme 36. Synthesis of Manganese-, Iron-, and Cobalt-Containing Metallocenates[262,263]

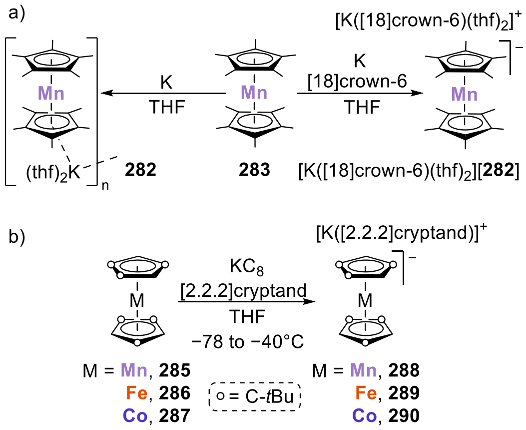

different synthetic protocol, [Cp*$_2$Mn] (**283**) was reduced by molten potassium (Scheme 36a) to afford the extremely air-sensitive anion **282**. In the absence of a sequestering agent, the product consists of polymeric chains with strong interactions between the potassium cation and the Cp* ligand of another molecule, as confirmed in the solid-state molecular structure. The presence of a sequestering agent ([18]crown-6; see Scheme 36a) disrupts such intermolecular interactions, as shown by the X-ray characterization of [K([18]crown-6)(thf)$_2$][Cp*$_2$Mn], which displays an ion-separated structure. For the ion-separated complex (18 VE), the M−C bond lengths compare well with those of the isoelectronic permethylated ferrocene, [Cp*$_2$Fe] (**284**) [d_{MnC}(**282**) = 2.048(8)−2.088(8) Å, vs d_{FeC}(**284**) = 2.045(3)−2.053(2) Å].[267]

Later, Chilton, Mills, and co-workers reported the preparation of an isostructural series of 3d metallocenates containing bulky Cp‴ ligands (Cp‴ = 1,2,4-tBu$_3$C$_5$H$_2$).[263,264] Reduction of [Cp‴$_2$M] [M = Mn (**285**), Fe (**286**), Co (**287**)] by KC$_8$ at low temperatures (−78 to −40 °C) yielded the anionic complexes [K([2.2.2]cryptand)][Cp‴$_2$M] [M = Mn (**288**), Fe (**289**), Co (**290**); Scheme 36b]. The compounds are highly sensitive (thermally and air-sensitive), decomposing rapidly above −30 °C. Despite their facile decomposition, a combination of physical and theoretical methods was used for the characterization of the reduced complexes. In the solid state, the Cp$_{\mathrm{centroid}}$−M−Cp$_{\mathrm{centroid}}$ angle for the manganese and cobalt compounds deviate from linearity by approximately 5° [angle(**288**) = 174.68(9)°, angle(**290**) = 175.96(5)°], while a much larger deviation was determined for the ferrocenate **289** [angle(**289**) = 169.38(11)°]. The derivatized cyclopentadienyl ligands play an important role in the kinetic and electronic stabilization of the metallocenates. Orbital analysis and Mössbauer spectroscopy indicate that the 19 VE Fe(I) ferrocenate exists in a high-spin S = 3/2 ground state, contrasting the low-spin S = 1/2 ground state observed in the formally isoelectronic cobaltocene compounds.

Recently, Hansen, Prokopchuk, and co-workers described the formation of a rare Mn(0) metalloradical anion and a mixed-valent Mn$^{-\mathrm{I}}$−Mn$^{\mathrm{I}}$ complex, obtained upon reduction of the aminoindenyl compound [Mn(CO)$_3$(Ind$^{\mathrm{Pyrr}}$)] (**291**, Ind$^{\mathrm{Pyrr}}$ = 1-(1H-inden-2-yl)pyrollidine).[268] The analogous unsubstituted complex [Mn(CO)$_3$(indenyl)] (**292**) undergoes two-electron reduction to form [Mn(CO)$_3$(indenyl)]$^{2-}$ (**293**). **292** and **293** react via comproportionation to afford [Mn(CO)$_3$(indenyl)]$^-$ (**294**).[269] Based on this precedent, the electrochemical behavior of **291** was investigated, and two clean cathodic redox processes were identified via cyclic voltammetry (CV).[268] Therefore, the chemical reduction of **291** with KC$_8$ was carried out in the presence of [2.2.2]-cryptand, yielding the Mn(0) complex [K([2.2.2]cryptand)]-[Mn(CO)$_3$(Ind$^{\mathrm{Pyrr}}$)] (**295**) and the Mn(−I) carbonylmetalate [Mn(CO)$_5$]$^-$ (**37**, see Scheme 37, top). The metalloradical character of **295** was confirmed by X-ray crystallography and EPR spectroscopic characterization, as well as by DFT calculations which indicate that the residual unpaired spin density is located mainly at the Mn center.

Scheme 37. Reduction of the Aminoindenyl Complex [Mn(CO)$_3$(Ind$^{\mathrm{Pyrr}}$)] (291) in the Presence of Different Sequestering Agents[268]

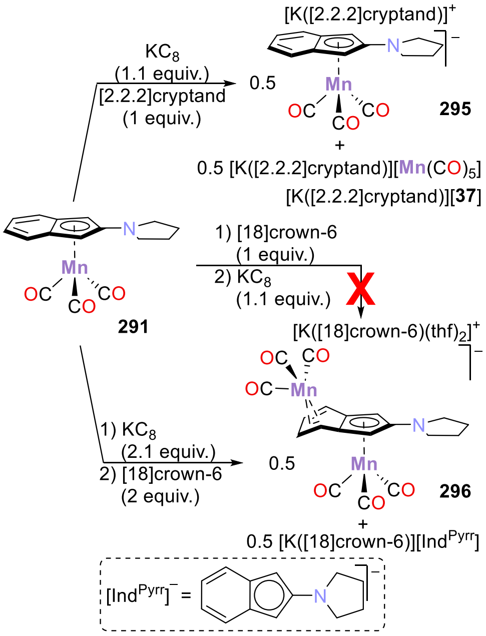

Contrasting with the behavior observed in the synthesis of **295**, the use of [18]-crown-6 as an encapsulating agent not only led to an entirely different product but also demonstrated an influence of the order of addition of the reagents.[268] The reaction of **291** with KC$_8$ (2.1 equiv), followed by addition of [18]crown-6, yielded the Mn(−I)/Mn(I) complex [K([18]-crown-6)(thf)$_2$][(OC)$_3$Mn(μ−η^4:η^5-Ind$^{\mathrm{Pyrr}}$)Mn(CO)$_3$] (**296**, Scheme 37, bottom) and the indenide anion salt [K([18]-crown-6)][Ind$^{\mathrm{Pyrr}}$]. In **296**, both metal centers are bound to a single indenyl motif, with the Mn(−I) coordinated to the six-membered ring in η^4 fashion. Given the disparate behavior observed with the two encapsulating agents, the influence of the order of addition of the reagents was investigated. When the reduction of **291** was carried out adding first the crown ether and then the reductant, only intractable mixtures of products were obtained and the mixed-valent compound **296** could not be identified. On the contrary, changing the order of addition of reductant and [2.2.2]cryptand did not alter the outcome of the synthesis of **295**. This study underlines the importance that pairing interactions have on the outcome of the reaction, and the potential differences that arise between the electrochemical and preparative studies.[268]

In 2019, Saito and co-workers reported the isolation and structural characterization of a related anionic stannaferrocene complex, $[Li(thf)_4][Fe\{3,4\text{-}Me_2\text{-}2,5\text{-}(SiMe_3)_2SnC_4\}_2]$ (**297**).[270] The stannaferrocene forms when $Fe(acac)_3$ (**298**) reacts with the dilithiostannole ligand precursor **299** (Scheme 38). The compound is obtained as a stable solid under ambient conditions, albeit in low yield (15%). The planarity of the two stannole ligands was confirmed by their metric parameters in the solid state (sums of internal bond angles = 539°, on average). A spectroscopic and theoretical examination of the electronic structure of **297** gave insights on the configuration of the iron center, suggesting three resonance structures: $[Fe^{III}(L^{2-})_2]^-$, $[Fe^{II}(L^{2-})(L^-)]^-$, and $[Fe^{I}(L^-)_2]^-$ (L = $3,4\text{-}Me_2\text{-}2,5\text{-}(SiMe_3)_2SnC_4$). The ^{119}Sn Mössbauer spectrum presented characteristic features (isomer shift, IS and quadrupole splitting, QS) associated with the presence of Sn(II) atoms in the stannole ligands. Furthermore, contrasting the ^{57}Fe Mössbauer spectrum of **297** with that of a known Fe(III) species such as ferrocenium tetrafluoroborate, suggested that the contribution of the Fe(III)-based resonance structure is negligible. A comparison with the spectrum of ferrocene and of known Fe(I) species revealed that the hyperfine parameters in these cases are in the range of those obtained for **297** and, therefore, do not give conclusive evidence on the electronic nature of the metal center (Fe^{II} vs Fe^{I}) in this compound. However, the data obtained from the Mössbauer spectra, along with scalar relativistic quantum-chemical calculations (including an analysis of Mulliken charges and spin populations) indicated that the stannole ligands should be monoanionic, while the Fe atom exists in a formal +I oxidation state with a $4s^1 3d^6$ electron configuration. This oxidation state was proposed to be the result of reduction of the iron center by the dilithiostannole proligand. Cyclic voltametric studies on **297** revealed, additionally, that this anionic stannaferrocene is significantly prone to oxidation, as expected for this type of reduced compound (quasi-reversible oxidation wave at $E_{1/2}$ = −1.50 V, and irreversible oxidation wave at E_{pc} = −0.64 V; vs Fc/Fc^+).[270]

Scheme 38. Synthesis of an Anionic Stannaferrocene[270]

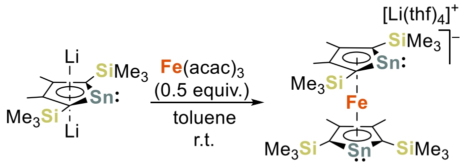

299 **297**

2.2.6. Metalates Containing Phosphorus Ligands.

Anionic complexes bearing phosphorus ligands, including

Scheme 39. Synthesis and Reactivity of Cp*Fe-2,4,6-Triphenylphosphinine Complexes by Müller, Wolf, and Co-workers[275,278]

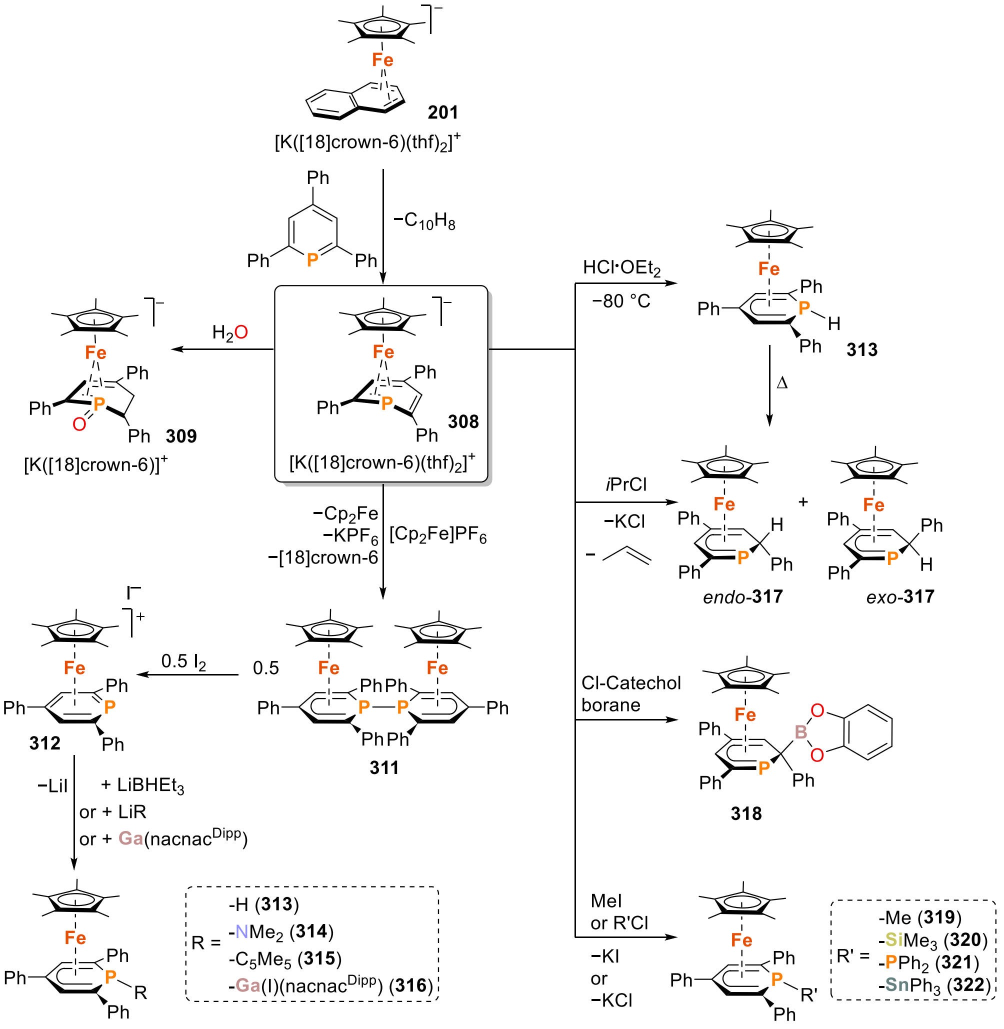

low-valent species, have long been known. Early examples of these include, among others, the previously discussed cobaltates $[(N_2)Co(PEt_2Ph)_3]^-$ (**10**) $[Co(PMe_3)_4]^-$ (**255**), or $[Co(dppe)_2]^-$ (**253**, dppe = 1,2-bis(diphenylphosphino)-ethane).[69,70,244,245] Additionally, the Le Floch group contributed significantly to this area, by using phosphinine ligands to stabilize reduced metal centers, forming species such as homoleptic complexes of the group 4, 8, and 9 metals $[M(tmbp)_3]^{2-}$ [M = Ti (**300**), Zr (**301**), Hf (**302**), Fe (**303**), Ru (**304**); tmbp = 4,4′,5,5′-tetramethyl-2,2′-biphosphinine] and $[M(tmbp)_2]^-$ [M = Co (**305**), Rh (**306**)], and the heteroleptic compound $[Mn(CO)_3(tmbp)]^-$ (**307**).[271−274] However, in these cases, the authors concluded that the negative oxidation states proposed for the metals are only *formal*, with the complexes featuring reduced forms of the biphosphinine ligand. Further examples of metalates with phosphorus ligands, reported in the period 2007−2023, are described in the following sections.

2.2.6.1. Iron. The metalate [K([18]crown-6){Cp*Fe(η^4-$C_{10}H_8$)}] (**201**) served as the starting material for the synthesis of Cp*Fe-phosphinine complexes.[275−277] Müller, Wolf, and co-workers reported on the synthesis of the first anionic iron complex with a π-coordinated phosphinine, [Cp*Fe(η^4-TPP)]$^-$ (**308**, as the $[K([18]crown\text{-}6)(thf)_2]^+$ salt; TPP = 2,4,6-triphenylphosphinine), obtained by exchange of the labile naphthalene ligand in **201** with the free phosphinine (Scheme 39).

As in the polyarene complexes [Cp*Fe(η^4-polyarene)]$^-$ (**201**, **216**),[219] DFT calculations support a d^6 electron configuration for the iron center, in a formally zerovalent oxidation state, and corroborate the crystallographically determined structure for **308**. Complex **308** undergoes hydrolysis to yield [K([18]crown-6)]{Cp*Fe(η^4-2,4,6-triphenyl-2,3-dihydrophosphinine-1-oxide)}] (**309**, Scheme 39). Oxygen atom transfer to the phosphorus atom with simultaneous hydrogenation of one carbon−carbon bond of the phosphinine ligand afforded the unusual phosphinine-oxide motif. Such behavior contrasts with the previously observed formation of a 1-hydrophosphinine-1-oxide ligand in the similar compound [CpFe(η^5-2,4,6-triphenyl-1-hydrophosphinine-1-oxide)] (**310**).[279]

Furthermore, reaction between complex **308** and $[Cp_2Fe]PF_6$ afforded the neutral dimer [Cp*Fe(η^5-2,4,6-triphenylphosphinine)]$_2$ (**311**), which was then further oxidized using I_2 (1 equiv), to yield the cationic iron(II) compound [Cp*Fe(η^6-2,4,6-triphenylphosphinine)]I (**312**, Scheme 39). Complex **312** can also be obtained by direct oxidation of **308** with I_2. Moreover, P-centered reactivity was identified for complex **312** through reaction with nucleophiles [$LiBHEt_3$, $LiNMe_2$, LiCp*, or Ga(^{Dipp}nacnac), see Scheme 39, bottom left], affording P-substituted η^5-phosphacyclohexadienyl complexes **313**−**316** [R = −H (**313**), $-NMe_2$ (**314**), −Cp* (**315**), and −GaI(^{Dipp}nacnac) (**316**)]. The structural characterization of complexes **308**, **309**, and **311**−**316** highlighted the flexibility of 2,4,6-triphenylphosphinine as a ligand, varying hapticity in accordance with the electronic requirements of the metal: the ligand acts as a $4e^-$ donor in the anionic complexes **308** and **309**, as a $5e^-$ donor in the neutral dimer **311** or the P-substituted compounds **313**−**316**, or as a $6e^-$ donor in **312**.[275]

A complementary protocol for the synthesis of other phosphacyclohexadienyl complexes, analogous to **313**−**316**, is based on the direct functionalization of the anionic complex **308**.[278] This route gives access to 1-phosphacyclohexadienyls (P-substituted products) and 2-substituted phosphacyclohexadienyls (substitution on an adjacent carbon atom), as shown in Scheme 39, right.

Kinetic and thermodynamic substitution isomers were identified following protonation of compound **308** with HCl·OEt_2. At −80 °C, the kinetic product, **313**, was observed after 1 h. At −30 °C, NMR spectroscopic evidence suggests the formation of a mixture of *endo*- and *exo*- conformers of the 2-hydrophosphacyclohexadienyl complex **317**, as the thermodynamic products (Scheme 39). In fact, at room temperature and in the presence of HCl·OEt_2 (10 mol %), **313** slowly converts to the *exo*-conformer of **317**, in an apparent acid-catalyzed rearrangement. A 65:35 mixture of *endo*-**317** and *exo*-**317** was cleanly obtained by direct reaction of **308** with isopropyl chloride (*i*PrCl) in THF at room temperature, without observation of **313**.

In a similar vein, the 2-substituted phosphacyclohexadienyl complex **318** is isolated from the reaction of the anionic phosphinine compound **308** with Cl-catecholborane. Monitoring the reaction at −100 °C provided evidence of formation of the P-substituted intermediate [Cp*Fe(1-Bcat-$PC_5Ph_3H_2$)] (**318**-P), which upon warming transforms into the isolable compound **318**. By contrast, direct reactions between **308** and the electrophiles MeI, Me_3SiCl, Ph_2PCl, or Ph_3SnCl afforded, respectively, the P-substituted analogues **319**−**322** [R = Me (**319**), $SiMe_3$ (**320**), PPh_2 (**321**), $SnPh_3$ (**322**)]. Thereby, it was proposed that an initial attack of the electrophile at the phosphorus atom occurs, yielding the P-substituted phosphacyclohexadienyl ligands, which, in some cases, rearrange to afford C-substituted compounds. This rearrangement was evident for the complexes *endo*-**317**, *exo*-**317**, and **318**. The synthesis of the P-substituted compounds **319**−**322** by direct reaction between the anionic complex **308** and electrophilic reagents (Scheme 39, bottom right) is thus a more convenient protocol than that shown in Scheme 39, bottom left, which involves a minimum of two synthetic steps.[278]

Similarly, **201** reacts with the analogous chelating phosphinine 2-(2′-pyridyl)-4,6-diphenylphosphinine (L) to afford the product of naphthalene ligand displacement, [K([18]crown-6)][Cp*Fe(*P*,*N*-L)] (**323**, Scheme 40).[276] However, unlike the case of the TPP derivative, **323** features a chelating σ-bonded P,N ligand, and the iron center adopts a trigonal planar geometry. The solid state ^{31}P CP MAS NMR spectrum featured a single resonance at δ_{iso} = 121.1 ppm, supporting the coordination mode identified in the solid-state structure. Nonetheless, the $^{31}P\{^1H\}$ NMR spectrum in solution showed two distinct resonances, a singlet at δ = 130.7 ppm and a broad resonance at −46.2 ppm, which were assigned to the σ-coordinated 2-(2′-pyridyl)-4,6-diphenylphosphinine and to the η^4-bonded phosphinine compound, **323**-π (Scheme 40), analogous to **308**.[275] DFT calculations support the assignment of the species observed in solution and indicate that the conversion between the isomeric forms **323**-π and **323**-σ proceeds through a barrier of 27.0 kcalmol^{-1}, consistent with an equilibrium at room temperature, illustrating coordinative flexibility of the ligand.

Addition of two equivalents of the pyridyl-phosphinine ligand L to compound **201** yielded the P−P coupled compound [K([18]crown-6)][Cp*Fe(η^5-L_2)] (**324**, Scheme 40), whose structure was confirmed by X-ray diffraction analysis. The molecular structure of **324** features a dimerized ligand L_2; one-half of this ligand coordinates to the iron center

Scheme 40. Synthesis of Anionic Iron Complexes Featuring Pyridyl-phosphinine Ligands[a]

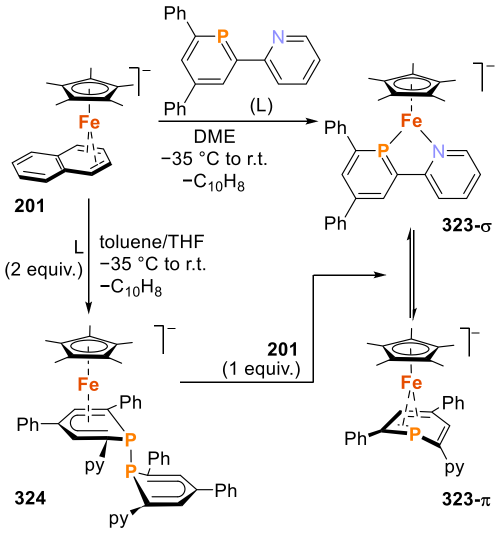

[a]All anions are stabilized by $[K([18]crown\text{-}6)]^+$ cations.

in an η^5-fashion. Addition of a second equivalent of **201** to **324** affords compound **323**. DFT calculations suggest that the transformation of **323-*π*** into **324** through an additional equivalent of ligand L is favorable by 23.5 kcalmol^{-1}, proceeding over a low energy barrier of 7.5 kcalmol^{-1}. It should be noted that the pyridyl-phosphinine ligand participates in reactions of **323-*π*** and **323-*σ*** with CO_2 (see section 3.3.2).[276]

2.2.6.2. Cobalt. In 2021, the Hunter group reported that the bidentate ligand *cis*-1,2-bis(diphenylphosphino)ethylene (dppv) provides access to a series of cobalt complexes in five sequential oxidation states.[280] The series $[Co(dppv)_2(CH_3CN)_x]_n$ (x = 0, 1, or 2; n = 1−, 0, 1+, 2+, 3+) constitutes a rare example of a redox series of complexes spanning the electron configurations d^6−d^{10} while featuring redox-innocent ligands. The Co(−I) complex was prepared by reduction of the Co(II) compound $[Co(dppv)_2]^{2+}$ (**325**) with potassium naphthalenide (3 equiv), followed by treatment with [18]crown-6, thereby providing $[K([18]crown\text{-}6)][Co(dppv)_2]$ (**326**). Complex **326** exhibits a *pseudo*-tetrahedral geometry and is essentially isostructural with the previously reported $[Co(dppe)_2]^-$ (**253**, Scheme 31, *vide supra*).[70] Moreover, a comparison of the metric parameters of the five complexes and the free ligand confirmed that the coordinated dppv motif remained almost unaltered through the range of different oxidation states (Co−P bond length, on average = 2.352 Å for Co^{3+} to 2.1165 Å for Co^-, C=C bond length = 1.319−1.334 Å, on average vs 1.334 Å in free dppv).[281] Therefore, the ligand does not undergo redox events in this series of complexes and behaves as redox-innocent. The structure of **326** and the rest of the neutral and cationic complexes in the series correspond to the idealized geometries, in accordance with the predictions of the crystal field theory for low-spin d^6−d^{10} metals.

Wolf and co-workers also investigated the classic bis(1,5-cyclooctadiene)cobaltate anion, $[Co(\eta^4\text{-cod})_2]^-$ (**239**), as a platform for the synthesis of cobaltates with different ligands.[134,232,282] For instance, **239** reacts with two equivalents of the 1,2-diphosphetane ligand **327**[283] to afford a homoleptic cobalt(III)-carborane-bridged bis(phosphanido) complex via successive oxidative addition of the P−P bonds to the Co(−I) center.[282] Regardless of the ratio of ligand to metal used (2:1 or 1:1), the product obtained is $[K(thf)_4][Co\{1,2\text{-}(PtBu_2)_2C_2B_{10}H_{10}\}_2]$ (**328**, Scheme 41, left). The behavior of electron-rich Co(−I) thereby resembles that of, for example, elemental lithium by promoting the reductive cleavage of the P−P bond in **327** and similar compounds.[284,285] According to the structural characterization and theoretical calculations (DFT), in compound **328** the Co(III) center ($3d^6$) resides in a distorted tetrahedral geometry, with Co−P single bonds. Measurements of the magnetic susceptibility revealed that complex **328** is diamagnetic in the range of 2 to 270 K in the solid state (SQUID measurements) and at 298 K in THF-d_8 solution. Theoretical calculations suggest that the diamagnetism of **328** is explained by a low-spin singlet ground state resulting from the strong *σ*-donor and moderate *π*-donor properties of the bis(phosphanido) ligand. Treatment of **239** with phenylene-1,2-diphosphetane or tetraphenyldiphosphane afforded only intractable mixtures containing paramagnetic species.

Scheme 41. Reactivity of a Low-Valent Cobaltate toward Orthocarborane-Substituted 1,2-Diphosphetanes[134,282]

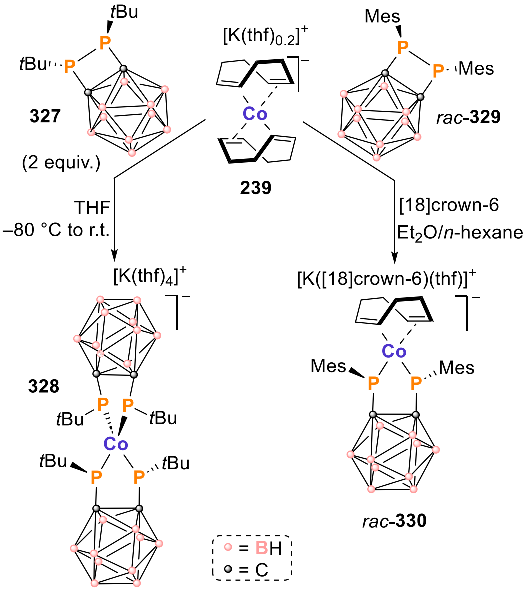

These results indicate that the carborane backbone is required to form the diamagnetic Co(III) product, providing electronic stabilization due to its electron-withdrawing properties and the attractive London dispersion forces observed in the solid state between the *t*Bu substituents on the P atoms. Furthermore, **328** did not react with tetraphenyldiphosphane.[282] Given the limited reaction profile observed for **328**, the authors anticipated that an increase in the bulk of the ligand used would allow for the synthesis of heteroleptic complexes that could maintain labile ligands or vacant coordination sites. Thus, the mesityl-substituted diphosphetane *rac*-**329** was treated with cobaltate **239** in the presence of [18]crown-6 (Scheme 41, right) to afford the heteroleptic compound $[K([18]crown\text{-}6)(thf)][Co\{1,2\text{-}(PMes)_2C_2B_{10}H_{10}\}(\eta^4\text{-cod})]$ (*rac*-**330**).[134] Similarly, reaction of the diphosphetane *rac*-**329** with the Ni(0) complex $[Ni(IMes)(\eta^2\text{-}H_2C{=}CHSiMe_3)_2]$ (**331**, IMes = 1,3-bis(2,4,6-trimethylphenyl)imidazolin-2-ylidene) affords the neutral nickel(II) complex $[Ni\{1,2\text{-}(PMes)_2C_2B_{10}H_{10}\}(IMes)]$ (*rac*-**332**).[282]

Complex *rac*-**330** provided a suitable platform to synthesize a variety of bis(phosphanido) complexes by exploitation of the labile η^4-cod ligand.[134] Treating *rac*-**330** with cyclohexyl isocyanide cleanly substitutes the cyclooctadiene ligand, yielding the bis(isocyanide) complex $[K([18]crown\text{-}6)(dme)][Co\{1,2\text{-}(PMes)_2C_2B_{10}H_{10}\}(Cy\text{-}N{\equiv}C)_2]$ (*rac*-**333**; see Scheme 42, top). The characterization of this bis(isocyanide) complex by multinuclear NMR and FT-IR spectroscopy, elemental analysis, and X-ray diffraction confirmed the substitution of the labile ligand, and indicated that the bis(phosphanido) ligand acts as a strong σ-donor, making the Co(I) center more electron-rich [ν_{CN}(**333**) = 2029 and 1938 cm^{-1} (see Table 1) vs ν_{CN} (free ligand) = 2136 cm^{-1}]. Furthermore, as previously observed with other low-valent cobaltate complexes (Scheme 22, *vide supra*),[210−212] *rac*-**330** mediated the dimerization of *tert*-butylphosphaalkyne to afford the diphosphacyclobutadiene complex $[K([18]crown\text{-}6)][Co(\eta^4\text{-}1,3\text{-}P_2C_2tBu_2)\{1,2\text{-}(PMes)_2C_2B_{10}H_{10}\}]$ (*rac*-**334**; Scheme 42, bottom). The structure was confirmed through a combination of multinuclear NMR spectroscopy, elemental analysis, and X-ray diffraction. Both *rac*-**333** and *rac*-**334** are 16 VE species. The reactivity of *rac*-**330** toward white phosphorus is discussed in section 3.4.3 (*vide infra*).

Scheme 42. Reactivity of $[K([18]crown\text{-}6)(thf)][Co\{1,2\text{-}(PMes)_2C_2B_{10}H_{10}\}(\eta^4\text{-}cod)]$ (*rac*-330) toward Cyclohexyl Isocyanide and *tert*-Butylphosphaalkyne[a]

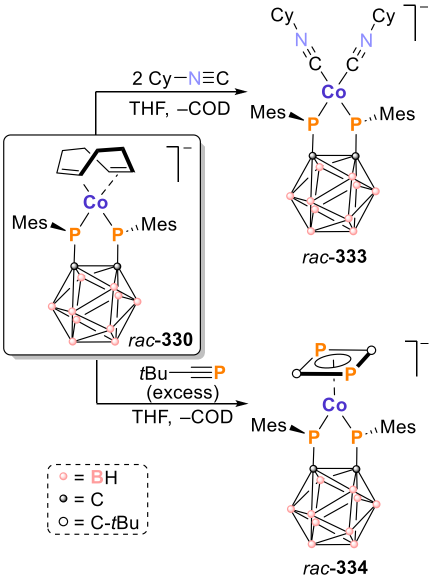

[a]Only the complex anions are shown, cations are omitted for clarity.

Rovis and co-workers described a Co(−I) complex featuring a perfluorinated Taddol-based phosphoramidite ligand.[286] An interesting 1:1 complex $[nBu_4NCo(CO)_3{\cdot}$**CKphos**] (**335**, see Figure 8) was isolated by reaction of the ligand **CKphos** with $[nBu_4N{\cdot}Co(CO)_3]$ (**336**).

The crystallographic analysis revealed that **CKphos** interacts with the metal center through two perfluorinated aryl rings and the phosphorus atom. The distorted tetrahedral geometry observed for the cobalt atom was attributed to the presence of rather strong Co−C_6F_5 interactions.[287−289] The Co−C_6F_5 bond distances and the distorted tetrahedral geometry at cobalt suggest that the two perfluoroaryls of **CKphos** act as Lewis acidic, Z-type ligands.

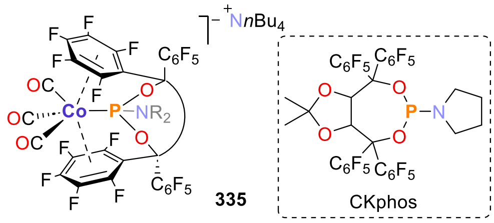

Figure 8. Representation of the structure of compound $[nBu_4NCo(CO)_3{\cdot}CKphos]$.[286]

2.2.6.3. *Anionic Palladium and Platinum-Phosphine Complexes.*

Anionic Pd^0 and Pd^{2+} species are crucial intermediates in Heck reactions and cross-couplings. Knowledge in this field was summarized by Amatore and Jutand in the year 2000.[290] More recently, Koszinowski investigated the phosphine-palladate complexes $[(PR_3)_2PdX]^-$ [X = Br (**337**), *n*Bu (**338**), Ph (**339**); PR_3 = tris[3,5-bis(trifluoromethyl)-phenyl]phosphine] by means of negative-ion mode electrospray-ionization mass spectrometry, electrical conductivity measurements, and NMR spectroscopy.[291,292] The species **337−339** were generated by treating the zerovalent compound $[(PR_3)_2Pd]$ (**340**) with LiBr or a Grignard reagent, RMgCl (R = *n*Bu or Ph). This transmetalation-like reaction is supported by the electron-poor ligand, which stabilizes the formal anionic state, since electron-richer palladium precursors $[L_2Pd]$ (L = phosphine) exhibit less tendency to form palladates. Species **337−339** react with selected aryl halides ArX′ (e.g., ethyl 4-iodobenzoate) to afford Pd^{2+} complexes of the type $[(PR_3)_2Pd(Ar)XX']^-$ [X = Br (**341**), *n*Bu (**342**), Ph (**343**)]. For X = *n*Bu or Ph, gas-phase fragmentation of **342** and **343** results in the reductive elimination of the ArX cross-coupling products. Mechanistically, these results suggest that the transmetalation step takes place before the oxidative addition, contrary to the classical concept for reactions proceeding exclusively via neutral and cationic Pd-intermediates. Other authors have also analyzed organometallic complexes and their reactions using ESI mass spectrometry, including "ate" compounds or intermediates.[293−295]

In 2008, Milstein described the preparation and characterization of the monometallic anionic Pt^0 complex Na[Pt(PCP)] [**344**, PCP = $2,6\text{-}(CH_2PtBu_2)_2\text{-}1\text{-}yl\text{-}C_6H_3$] as well as computational and reactivity studies.[296] The 16-electron zerovalent platinum species **344** was obtained by reducing any of the Pt^{2+} precursors [PtCl(PCP)] (**345**) or $[Pt(PCP)][BF_4]$ (**346**) with sodium (Scheme 43). Although the solid-state molecular structure of **344** could not be determined, likely because the compound is only moderately stable in solution, it was thoroughly characterized by multinuclear NMR spectroscopy (^1H, ^{13}C, ^{31}P, ^{195}Pt). The NMR data, together with DFT calculations, suggest a monomeric planar T-shaped geometry in solution, instead of a dimeric $[PCP{-}Pt{-}Pt{-}PCP]^{2-}$ arrangement. Theoretical analysis of **344** indicates that the negative charge is localized at the metal center instead of being delocalized over the Pt−C σ-bond and the π-conjugated system of the aryl scaffold. This electron-rich anionic Pt^0 complex is a Brønsted base. For example, protonation by water affords a Pt(II)-hydride complex, [PtH(PCP)] (**347**). In addition, **344** is an effective electron-transfer reagent, even being capable of activating one C−F bond from hexafluorobenzene at −35 °C, with reoxidation to Pt(II) in **348**.

Scheme 43. Synthesis of a Pincer-type Anionic Pt(0) Complex and Reactivity toward H_2O or C_6F_6[296]

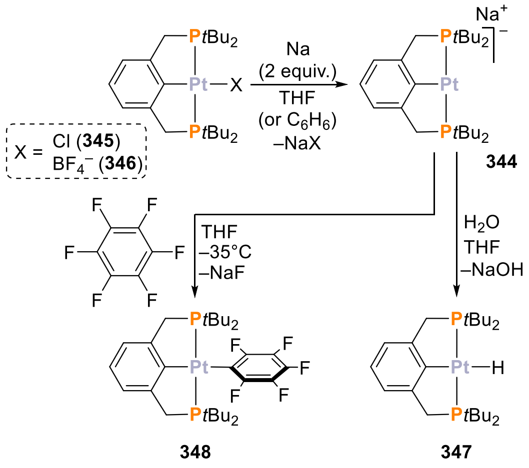

2.2.6.4. Molybdenum and Tungsten Complexes with Phosphinidene and Phosphinidene Oxide Ligands. Ruiz and co-workers have extensively investigated the chemistry of the anionic phosphinidene and phosphinidene oxide complexes illustrated in Figure 9.[297−310] A more extensive review of the chemistry of compounds **349** and **350** (and related compounds) was published by Ruiz in 2013, while the rich chemistry of the P_4 activation products $[M_2Cp_2(\mu\text{-}PCy_2)(CO)_2(\mu{-}\kappa^2{:}\kappa^2\text{-}P_2)]^-$ [M = Mo (**351**), W (**352**)] and their corresponding methylation products $[M_2Cp_2(\mu\text{-}PCy_2)(CO)_2(\mu{-}\kappa^2{:}\kappa^2\text{-}P_2Me)]$ [M = Mo (**353**), W (**354**)] was reviewed by Caporali, Wolf and co-workers in 2021.[151,178]

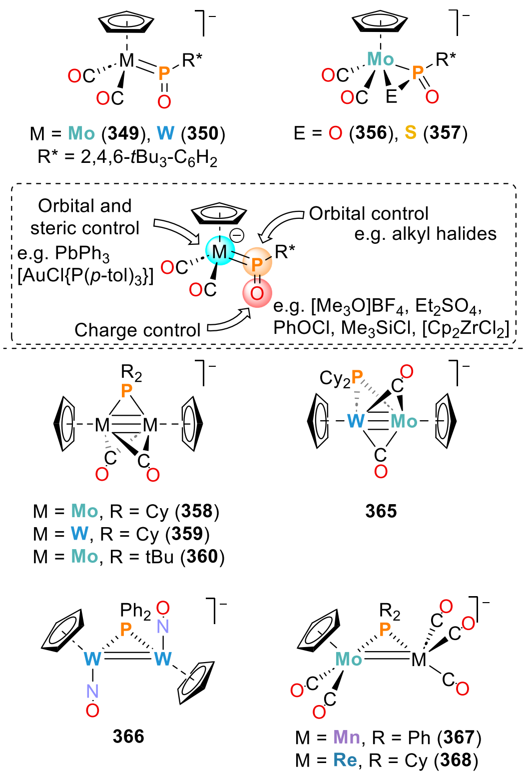

Figure 9. Mononuclear (top), homodinuclear, and heterodinuclear (bottom) anionic complexes featuring phosphinidene and phosphinidene oxide ligands.[297−310]

In 2004, Ruiz had described the anionic phosphinidene oxide complex (H-DBU)[MoCp{P(O)R*}$(CO)_2$] (**349**, DBU = 1,8-diazabicyclo [5.4.0] undec-7-ene; R* = 2,4,6-tBu$_3$-C_6H_2; Figure 9, top), which was obtained by deprotonation and controlled oxidation of the dimer $[Mo_2Cp_2(\mu\text{-}H)(\mu\text{-}PHR^*)(CO)_4]$ (**355**) with DBU and O_2.[297] In **349**, the carbene-like phosphinidene oxide ligand R−P═O is terminally bound to the Mo center, with the complex exhibiting interesting acid/base properties owing to the presence of three different nucleophilic sites: the O, P, and Mo atoms. The reactivity of compound **349** toward various electrophiles and oxidizing agents was thoroughly studied prior to the period covered by this contribution.[297,298] In 2010, the tungsten analogue (H-DBU)[WCp{P(O)R*}$(CO)_2$] (**350**) was reported, along with a complete theoretical description of the electronic structure of anion **349**, as a tool to rationalize its experimental chemical behavior toward different electrophiles.[299] An analysis of the relevant molecular orbitals and the topology of the electron density showed that the Mo−P bond has a strong π component and can thus be described as a double bond. The oxygen atom of the phosphinidene ligand bears the highest negative charge in the molybdate anion. This electronic situation is consistent with the observed transformations against neutral electrophiles (e.g., alkyl halides), which attack at the phosphorus atom. The authors referred to this phenomenon as orbital control reactivity (Figure 9). Positively charged electrophiles or strongly polarized species such as the Meerwein salt and diethyl sulfate preferably attack at the oxygen atom; this reactivity mode is called charge control. When using other bulky electrophiles such as AuCl{P(p-tol)$_3$}, addition of the electrophilic fragment to the group 6 metal instead of the phosphorus atom occurs due to steric reasons (Figure 9).[300]

Besides the incorporation of formal E^+ fragments to the O, P, and Mo atoms, Ruiz also reported the addition of a chalcogen atom (E) to the Mo−P double bond in the parent complex **349**, leading to the anionic dioxo- and thiooxophosphorane complexes $[MoCp(CO)_2\{\kappa E,\kappa P\text{-}EP(O)(2,4,6\text{-}t\mathrm{Bu}_3\text{-}C_6H_2)\}]^-$ [E = O (**356**), S (**357**)]. The thiooxophosphorane complex $[MoCp(CO)_2\{\kappa S,\kappa P\text{-}SP(O)(2,4,6\text{-}t\mathrm{Bu}_3\text{-}C_6H_2)\}]^-$ (**357**) exhibits a negative charge at the oxygen atom much higher than that at the sulfur atom, while its HOMO has a large contribution from a sulfur lone pair. As a result, the sulfur atom is attacked by an electrophile under the conditions of orbital control, while the oxygen atom favors the attachment of an incoming electrophile under the conditions of charge control (Figure 9).[301]

The reactivity of $[M_2(\eta^5\text{-}Cp)_2(\mu\text{-}PR_2)(\mu\text{-}CO)_2]^-$ [M = Mo (**358**), W (**359**), R = Cy; M = Mo, R = tBu (**360**); Figure 9) was extensively studied with a broad variety of electrophiles, including, for instance, the nitrosyl complex $[Re(\eta^5\text{-}C_5H_4Me)(CO)_2(NO)]^+$, Brønsted and carboxylic acids, $SnClPh_3$, $[AuCl(PR_3)]$ (R = iPr, p-tol), $PbClPh_3$, MeI, BnCl, $PClR'_2$ (R′ = tBu, Et, Cy), $PCl(O)(OPh)_2$, and P_4.[178,302−304] In 2017, the related lighter analogue $[Mo_2(\eta^5\text{-}Cp)_2(\mu\text{-}P t\mathrm{Bu}_2)(\mu\text{-}CO)_2]^-$ (**360**) was reported, which was used to obtain new unsaturated hydride and alkyl derivatives with very distinctive chemical properties due to the presence of the bulky $Pt\mathrm{Bu}_2^-$ ligand.[305] For example, complex $[Mo_2Cp_2(H)(\mu\text{-}Pt\mathrm{Bu}_2)(CO)_2]$ (**361**) bears a terminal hydride ligand both in solution and in the solid state, in marked contrast to the conventional bridging coordination seen in all related hydrides $[Mo_2Cp_2(\mu\text{-}H)(\mu\text{-}PR_2)(CO)_2]$ (**362**, R = Cy, Et, OEt, Ph).[178] Likewise, Scheme 44. Synthesis of Low-Valent Fe(I) and Fe(0) Complexes Featuring a (a) Bulky Bis(carbene)borate[76,315] and (b) Tris(carbene)borate Ligand[77]

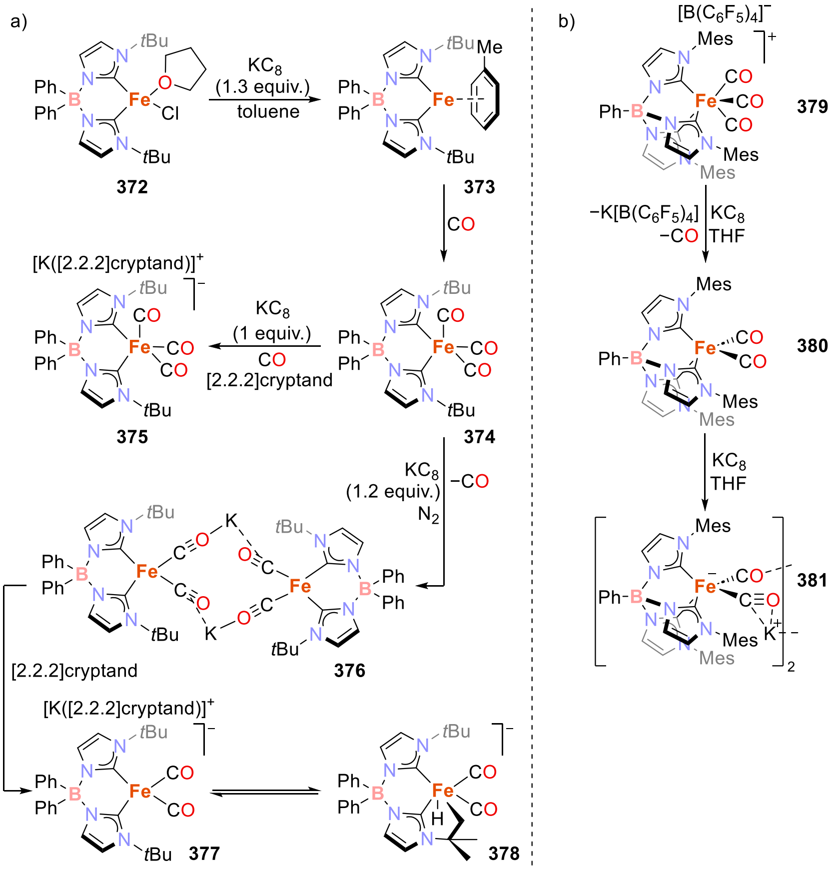

the agostic species $[Mo_2Cp_2(\mu{-}\kappa^1{:}\eta^2\text{-}CH_3)(\mu\text{-}PtBu_2)(\mu\text{-}CO)]$ (**363**) is more stable than that of the related PCy_2^- compound and can be thermally dehydrogenated to give the methylidyne derivative $[Mo_2Cp_2(\mu\text{-}CH)(\mu\text{-}PtBu_2)(\mu\text{-}CO)]$ (**364**).[305]

The heterobimetallic species $[MoW(\eta^5\text{-}Cp)_2(\mu\text{-}PCy_2)(\mu\text{-}CO)_2]^-$ (**365**, Figure 9) was recently incorporated into the family of anionic unsaturated group 6 complexes, with the aim of exploring the effects of the intermetallic multiple bond on the reactivity and properties of these anions.[306] Complex **365** shows an intermediate chemical behavior between that observed for the homonuclear analogues. The hydride and alkyl derivatives of **365** show clear heterobimetallic effects, in terms of the hydride formation preference (terminal at W) and faster dehydrogenation of the methyl ligand in comparison to the homonuclear $[Mo_2Cp_2(\mu{-}\kappa^1{:}\eta^2\text{-}CH_3)(\mu\text{-}PtBu_2)(\mu\text{-}CO)]$ (**363**).

In 2016, Ruiz published the first anionic nitrosyl complex $[W_2Cp_2(\mu\text{-}PPh_2)(NO)_2]^-$ (**366**, Figure 9) featuring a metal−metal double bond.[307] In this compound, the NO ligand is terminal and the bridging PPh_2^- scaffold was found to be crucial to stabilize both the W_2 anion and its derivatives against degradation. The reactivity of **366** toward Brønsted acids, $[AuCl\{P(p\text{-}tol)_3\}]$, and elemental sulfur was explored, revealing that compound **366** displays a considerable metal-based nucleophilicity. This feature makes **366** an attractive precursor for the preparation of several ditungsten nitrosyl derivatives and the subsequent study of nitric oxide activation.[311−314]

Furthermore, Ruiz and co-workers subsequently reported the complexes $[MoMCp(\mu\text{-}PR_2)(CO)_5]^-$ [M = Mn, R = Ph (**367**); M = Re, R = Cy (**368**); Figure 9], the first examples of organometallic anions with group 6−7 metals having M−M′ double bonds.[308] Reactions with selected electrophiles revealed high metal-based nucleophilic reactivity, accompanied by association of solvent molecules, to provide electron-precise species. Reaction of $[MoMnCp(\mu\text{-}PPh_2)(CO)_5]^-$ (**367**) with NH_4^+ afforded the hydride complex $[MoMnCp(\mu\text{-}H)(\mu\text{-}PPh_2)(CO)_5(NH_3)]$ (**369**).[309] Shortly after, the reactivity of the heavier congener $[MoReCp(\mu\text{-}PCy_2)(CO)_5]^-$ (**368**) toward simple donor ligands and *p*-block E−H reagents was reported.[310] Complex **368** binds L-type donors at the Re center to afford electron-precise anions of the type $[MoReCp(\mu\text{-}PCy_2)(CO)_5L]^-$ [**370**, L = CO, HSPh, HCC(*p*-tol)]. The incoming ligand L generally binds in a position *cis* to the PCy_2^- bridge. By contrast, $HPPh_2$ also coordinates at rhenium but occupies the less sterically demanding *trans*-position to the PCy_2^- bridge. Activation of the E−H bonds only proceeds upon protonation of the corresponding anion $[MoReCp(\mu\text{-}PCy_2)(CO)_5L]^-$ (**371**), followed by thermal or photochemical dehydrogenation and/or decarbonylation.

2.2.7. Carbene Metalates.

As mentioned in section 2.2.3.2, the tetraisocyano complex $Fe(N_2)(CNAr^{Mes2})_4$ (**61**), reported by Figueroa and co-workers, is a masked, nitrogen-trapped, analogue of the transient $Fe(CO)_4$ complex.[125] In the search for further examples of complexes analogous to the elusive $Fe(CO)_4$, Smith and co-workers reported the synthesis of a series of low-valent Fe(I) and Fe(0) complexes featuring a bulky bis(carbene)borate ligand.[76]

The diphenylbis(carbene)borate ligand $Ph_2B(tBuIm)_2^-$ reacts with the Fe(II) precursor $[FeCl_2(thf)_{1.5}]$ to the compound $Ph_2B(tBuIm)_2FeCl(thf)$ (**372**) (Scheme 44a). One-electron reduction of **372** in toluene affords $Ph_2B(tBuIm)_2Fe(\eta^6\text{-}C_7H_8)$ (**373**, Scheme 44a). EPR and Mössbauer spectroscopic analysis of **373** support its formulation as a low-spin ($S = 1/2$) Fe(I) complex. Furthermore, the $C_{carbene}$–Fe bond lengths (1.981(3) and 1.975(3) Å), as provided by X-ray diffraction, revealed a stronger interaction in **373** compared to **372** (2.085(2), 2.100(2) Å). The C−C distances in the toluene ligand (on average, 1.405 Å) indicate that aromaticity is maintained, and thus, a metal-based reduction has occurred. Upon exposure to a carbon monoxide atmosphere, **373** converts to the square-pyramidal Fe(I)-carbonyl compound $Ph_2B(tBuIm)_2Fe(CO)_3$ (**374**). A reversible one-electron reduction was observed for **374** by cyclic voltammetry (−1.92 V vs Fc/Fc^+). Chemical reduction of **374** with KC_8 (1 equiv) under a CO atmosphere in the presence of [2.2.2]cryptand afforded the diamagnetic compound $[K([2.2.2]cryptand)][Ph_2B(tBuIm)_2Fe(CO)_3]$ (**375**, Scheme 44a). A comparison of the FT-IR stretching frequencies for the carbonyl ligands in **374** vs **375** [ν_{CO}(**374**) = 1987, 1900 cm^{-1} vs ν_{CO}(**375**) = 1926, 1836, and 1800 cm^{-1}] suggests a higher degree of π-backbonding in the latter species. Together with the remaining spectroscopic data, including the Mössbauer spectra, this indicates an Fe(0) center in **375**. When the reduction by KC_8 is carried out under an N_2 atmosphere instead, a CO ligand is lost and $K_2[Ph_2B(tBuIm)_2Fe(CO)_2]_2$ (**376**) is formed (Scheme 44a). The shift of the stretching bands to lower frequencies for the CO ligands [ν_{CO}(**376**) = 1838 and 1742 cm^{-1}] suggests reduction of the metal center. Single-crystal X-ray diffraction analysis of **376** revealed a centrosymmetric dimer featuring distorted square-planar coordination environment of the iron centers. The monomeric $[Ph_2B(tBuIm)_2Fe(CO)_2]^-$ anions associate via interactions of the carbonyl ligands with the K^+ cations.[76] Addition of [2.2.2]cryptand to **376** breaks the dimer, affording the four-coordinate complex $[K([2.2.2]cryptand)][Ph_2B(tBuIm)_2Fe(CO)_2]$ (**377**).[315] Crystallographic analysis showed that compound **377** features a trigonal pyramidal iron center. The complex cocrystallized with the six-coordinate iron(II) hydride complex **378**. The latter species is the result of oxidative C−H activation of a *tert*-butyl substituent in the bis(carbene)borate ligand. As expected, FT-IR stretching frequencies [ν_{CO}(**377**) = 1846 and 1753 cm^{-1}] are only slightly higher than in the dimer **376**. These data indicate the presence of an Fe(0) center, while the FT-IR stretching frequencies of hydride **378** (ν_{CO} = 1930 and 1859 cm^{-1}) are significantly higher, in line with the Fe(II) oxidation state. Variable temperature IR spectroscopy revealed that complexes **377** and **378** are in equilibrium, with the Fe(II) species being predominant at lower temperatures. DFT calculations revealed that the coordinatively unsaturated complex **377** must undergo a triplet to singlet spin-state change before C−H activation occurs on the singlet surface.

Similar reactivity was observed with the analogous tris(carbene)borate scaffold $PhB(MesIm)_3^-$ (MesIm = 1-mesitylimidazol-2-ylidene).[77] Fe(I) and Fe(0)-tris(carbene)borate complexes were obtained by sequential reduction of the cationic Fe(II) complex $[PhB(MesIm)_3Fe(CO)_3][B(C_6F_5)_4]$ (**379**). An initial reduction affords the neutral iron(I) radical $PhB(MesIm)_3Fe(CO)_2$ (**380**, see Scheme 44b), while further reduction affords the anionic complex $K[PhB(MesIm)_3Fe(CO)_2]$ (**381**). Similar to compound **376**, compound **381** crystallized as a potassium-bridged dimer. The tris(carbene)borate ligand acts as a strong donor in both species obtained. The structural and spectroscopic data for compound **380** revealed that it adopts a low-spin ($S = 1/2$) configuration, as in the case of the Fe(I) complex **373**. The expected increase in electron density in **380** with respect to **379** was evidenced by the shorter Fe−CO distances observed in the X-ray data (d_{FeCO} = 1.771(5) and 1.791(5) Å vs average d_{FeCO}(**379**) = 1.821 Å) along with low carbonyl stretching frequencies in the FT-IR spectra [ν_{CO}(**379**) = 2100, 2040 cm^{-1} vs ν_{CO}(**380**) = 1956, 1886 cm^{-1}; see Table 1]. The π-backbonding interaction is even more pronounced in the anionic complex **381** [average d_{FeCO}(**381**) = 1.729(4) Å; ν_{CO}(**381**) = 1812, 1728 cm^{-1}; see Table 1].[77]

Smith and co-workers additionally described a related anionic bis(carbene)borate iron complex, featuring a dinitrogen ligand.[316] The ferrate compound is accessed by a two-step synthetic protocol which involves the alkylation of complex $Ph_2B(tBuIm)_2FeCl(thf)$ (**372**)[76] with $LiCH_2tBu$ (1 equiv) to obtain the tricoordinate compound $Ph_2B(tBuIm)_2Fe(CH_2tBu)$ (**382**), and subsequent reduction with KC_8 in the presence of [2.2.2]cryptand under a nitrogen atmosphere to afford $[K([2.2.2]cryptand)][Ph_2B(tBuIm)_2Fe(N_2)(CH_2tBu)]$ (**383**, Scheme 45). The four-coordinate complex **383** features a low frequency FT-IR band attributed to the coordinated dinitrogen ligand ($\nu_{N\equiv N}$ = 1897 cm^{-1}).

Scheme 45. Synthesis of an Anionic Iron Bis(carbene)borate Featuring a Dinitrogen Ligand, and Its Ligand Substitution Reaction[316]

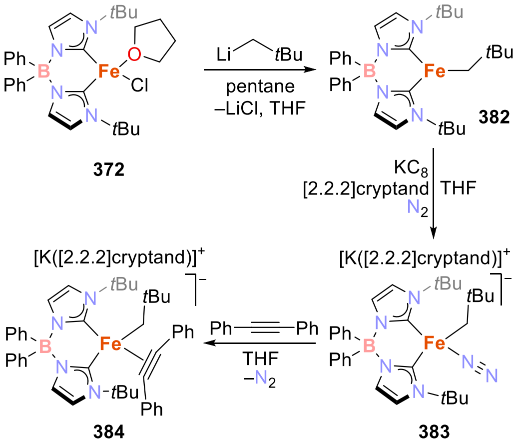

Treatment of **383** with diphenylacetylene substitutes the N_2 ligand to give $[K([2.2.2]cryptand)][Ph_2B(tBuIm)_2Fe(PhC\equiv CPh)(CH_2tBu)]$ (**384**). The strong backdonation from the iron center in **384** is evidenced by the elongation of the C−C bond distance (1.281(7) Å) in the coordinated alkyne ligand. Complex **383** catalyzes the isomerization of 1-hexene to 2-hexene. The authors proposed that the isomerization of the olefin substrate occurs by the allyl mechanism.[317,318] The combined experimental and computational study revealed that species with two different spin states (S = 3/2 and 1/2) are involved in the operating mechanism. This two-state (spin) reactivity provides resistance toward common catalyst poisons to the catalyst.

In 2014, Bertrand, Peters, and co-workers reported the synthesis of two-coordinate, formally Fe(0) and Co(0) complexes $[M(CAAC)_2]$ [M = Fe (**385**), Co (**386**); CAAC = cyclic (alkyl)(amino)carbene].[78] CAAC ligands are strong σ-donors and efficient π-acceptors, known to be redox-active.[319,320] Reaction of the corresponding M(II) salt precursor with the CAAC ligand **387** (2 equiv) followed by reduction with sodium amalgam (1 equiv), afforded the three-coordinate complexes [MCl(CAAC)$_2$] [M = Fe (**388**), Co (**389**)]. Complexes **388**/**389** reacted with NaBAr$^F_4$ (BAr$^F_4$ = tetrakis[3,5-bis(trifluoromethyl)phenyl]borate) as a chloride scavenger to obtain cationic species [M(CAAC)$_2$]BAr$^F_4$ [M = Fe (**390**), Co (**391**)], which were further reduced to yield the neutral, two-coordinate compounds **385** and **386** (Scheme 46 shows compound **385**). The cationic (**390**/**391**) and neutral (**385**/**386**) complexes have a moderately bent structure in all the cases, with angles ranging from 165.4 to 170.5°.[78]

Scheme 46. Reduction of a Low-Valent and Low-Coordinate Fe(0)-CAAC Complex to Form an Fe(−I)-Dinitrogen Complex[78,79]

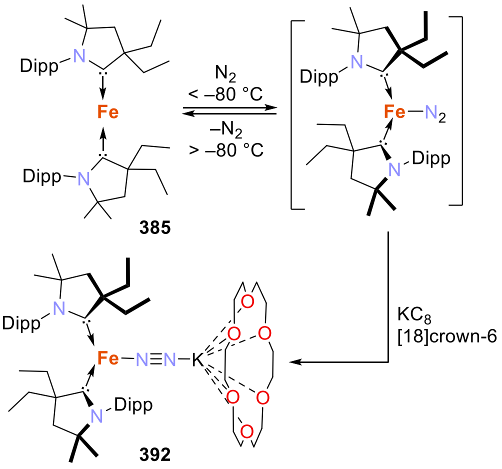

Later, Peters reported that the two-coordinate Fe(0) compound [Fe(CAAC)$_2$] (**385**) coordinates the dinitrogen molecule at low temperatures ($T < -80$ °C).[79] Evidence of coordination was obtained via variable temperature UV−vis spectroscopy since the absorption spectrum of **385** presents drastic, but reversible, changes below −80 °C. This behavior might be indicative of the formation of a three-coordinate dinitrogen complex, proposed to be [(N$_2$)Fe(CAAC)$_2$] (Scheme 46), though such a species was not isolated. Nonetheless, further reduction of **385** with KC$_8$ in the presence of [18]crown-6 afforded the formally Fe(−I) complex [K([18]crown-6){(N$_2$)Fe(CAAC)$_2$}] (**392**, Scheme 46). X-ray crystallographic data for this compound revealed that a further elongation of the C−N bonds in the coordinated carbene ligands has occurred upon formation of the Fe(−I) compound (on average: d_{CN}(**385**) = 1.37 Å vs d_{CN}(**392**) = 1.40 Å), reflecting the increased spin density at the metal center.[78,79] The stretching band (FT-IR, $\nu_{N\equiv N}$ = 1850 cm^{-1}; see Table 2) of the coordinated dinitrogen ligand in the metalate **392** suggests that this motif presents some degree of activation. Magnetic susceptibility and EPR measurements (1.9 μ_B in C_6D_6, $S = 1/2$ in the ground state) are consistent with a highly reduced, formally Fe(−I) center. The presence of an activated N$_2$ ligand served as a starting point to pursue functionalization studies (see section 3.2.3).[79]

In 2021, Krämer, Young, and co-workers reported the stabilization of iron centers in the range of formal oxidation states Fe(II), Fe(I), and Fe(−I) using a PC$_{carbene}$P pincer ligand scaffold.[80] In the search for a readily accessible iron pincer complex, this group synthesized an Fe(0) PC$_{carbene}$P pincer compound via dehydration of an isolated α-hydroxylalkyl hydrido complex and evaluated its reactivity toward a breadth of reagents and its redox behavior. The pincer complex [Fe(PC$_{carbene}$P)(CO)$_2$] (**393**, see Scheme 47) reacts with KC$_8$ in benzene to afford the formally Fe(−I) compound K[Fe(PC$_{carbene}$P)(CO)$_2$] (**394**).

Scheme 47. Synthesis of a Formal Fe(−I) PC$_{carbene}$P Pincer Complex and Its Reactivity toward Hydrogen Atom Transfer (HAT)[80]

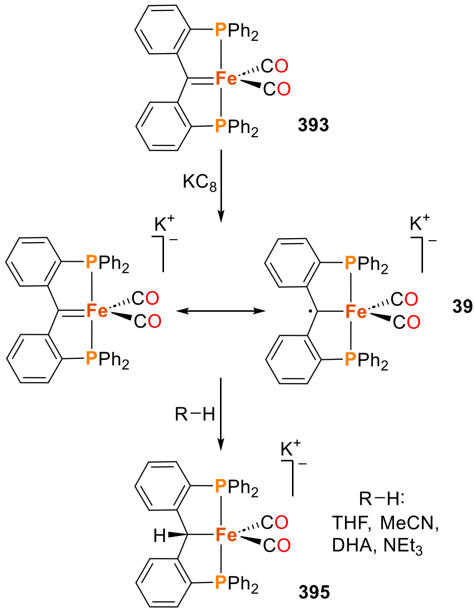

FT-IR analysis of **394** indicated the presence of a significantly reduced iron center, according to the stretching bands of the carbonyl ligands [ν_{CO}(**394**) = 1826 and 1767 cm^{-1} vs ν_{CO}(**393**) = 1961 and 1894 cm^{-1}], whereas the EPR spectrum suggested the formation of a carbon centered radical. Since **394** is an extremely reactive compound, it was not possible to further characterize it in solution. However, it was found that **394** abstracts hydrogen atoms from aliphatic sources (such as THF, MeCN, 9,10-dihydroanthracene, and NEt$_3$; see Scheme 47) to form a PC$_{alkyl}$P ferrate complex, [K([18]crown-6)][Fe(PC$_{alkyl}$P)(CO)$_2$] (**395**). Indirect confirmation of the structure of **394** was therefore achieved by characterization of the hydrogen atom transfer (HAT) product **395** via X-ray diffraction (Scheme 47). Furthermore, DFT calculations support the presence of a markedly reduced iron center with a significant carbene radical character. Calculated Fukui parameters also suggested the presence of an increased nucleophilic character on the carbene C atom, while the iron center was more electrophilic.

G. de Ruiter and co-workers described the synthesis of the anionic pincer monohydride iron complex Na[(PC$_{NHC}$P)Fe(H)(N$_2$)] (**396**, PC$_{NHC}$P = 2,10-(*t*Bu)$_2$-4,8-(P*i*Pr)$_2$C$_{11}$H$_4$N$_2$; Scheme 48) and its high catalytic activity in the isomerization of olefins.[321] The two-step synthesis of **396** comprises the reduction of the previously reported dichlorido complex [(PC$_{NHC}$P)Fe(Cl)$_2$] (**397**)[322] with KC$_8$ under a nitrogen atmosphere to afford the neutral complex [(PC$_{NHC}$P)Fe(N$_2$)$_2$] (**398**). The latter species then reacts with NaBHEt$_3$ to afford

Scheme 48. Synthesis of ferrate Complex Na[(PC$_{NHC}$P)Fe(H)(N$_2$)] (396)[321]

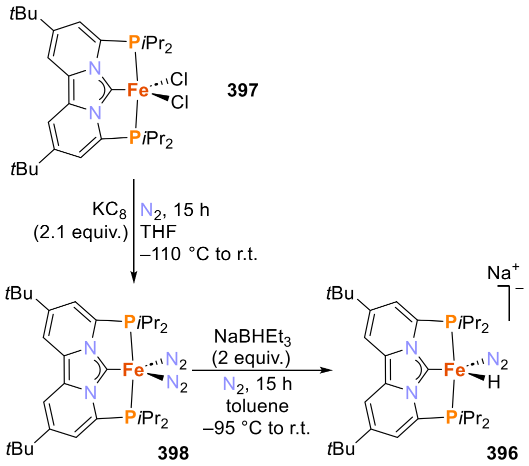

the monohydride compound **396**. ^{1}H NMR spectroscopic analysis confirmed the formation of the hydride ligand at the iron center (δ = −10.85 ppm (t), $^2J_{PH}$ = 55.1 Hz). Crystallographic characterization of **396** showed a dimer in which two sodium atoms link the two iron fragments by interactions with the dinitrogen ligands. These interactions, along with the presence of the electron-rich metal center, account for the slightly activated dinitrogen ligands evidenced by the N−N bond distances (1.155(6) Å). Complex **396** is a rare example of a well-defined anionic Fe(0) hydride species not supported by π-acidic carbonyl or isocyanide ligands. The striking catalytic activity observed in the isomerization of alkenes with complex **396** (TONs up to ≥160,000, TOFs up to 6,600 h^{-1}) contrasts with that of the known dihydride compound [(PC$_{NHC}$P)Fe(H)$_2$(N$_2$)] (**399**), described by the same group, which proved inactive despite effectively mediating other transformations.[321,323] Similar to the case of complex [K([2.2.2]cryptand)][Ph$_2$B(*t*BuIm)$_2$Fe(N$_2$)-(CH$_2$*t*Bu)] (**383**),[316] computational studies indicated that a two-state reactivity (from the low-spin singlet to the high-spin triplet) might be responsible for the catalytic performance. Catalyst **396**, however, operates via an alkyl-type mechanism.[317,318]

In 2020, independent reports by the groups of Deng, and Tejel and Ciriano described the synthesis of three-coordinate group 9 metalates featuring N-heterocyclic carbene ligands.[324,325] Reduction of [(IMes)Co(dvtms)] (**400**, IMes = 1,3-dimesitylimidazol-2-ylidene, dvtms = divinyltetramethyldisiloxane) or a mixture of [RhCl(cod)]$_2$ (**401**) and IPr (IPr = 1,3-bis(2′,6′-diisopropylphenyl)imidazol-2-ylidene) with KC$_8$ (in the presence of [18]crown-6, see Scheme 49, a and b, respectively), afforded, instead of the desired compound [K([18]crown-6)][(IMes)Co(dvtms)] or its rhodium analogue, the products of single C−N bond cleavage (dearylation) of an aryl substituent in the NHC ligands. These compounds were characterized as the Co(0) N-aryl imidazolate complex [K([18]crown-6)(μ-C$_3$H$_2$N$_2$Mes-κC^2,κN^3)Co(dvtms)] (**402**) and the Rh(I) species [K([18]crown-6)(THF)][(cod)$_2$Rh$_2$(μ-C$_3$H$_2$N$_2$(Dipp)-κC^2,κN^3)$_2$(μ-Dipp)$_2$K] (**403**). The authors proposed that the dearylation of the NHC ligands in **402** and **403** is possibly mediated by cobalt(−I) and rhodium(−I) metal centers, formed as intermediates in the reduction of the precursor complexes **400** or **401**/IPr. Such activation by the

Scheme 49. Anionic Cobalt and Rhodium Complexes Derived from NHC Ligands by Deng and Co-workers and Tejel, Ciriano, and Co-workers[324,325]

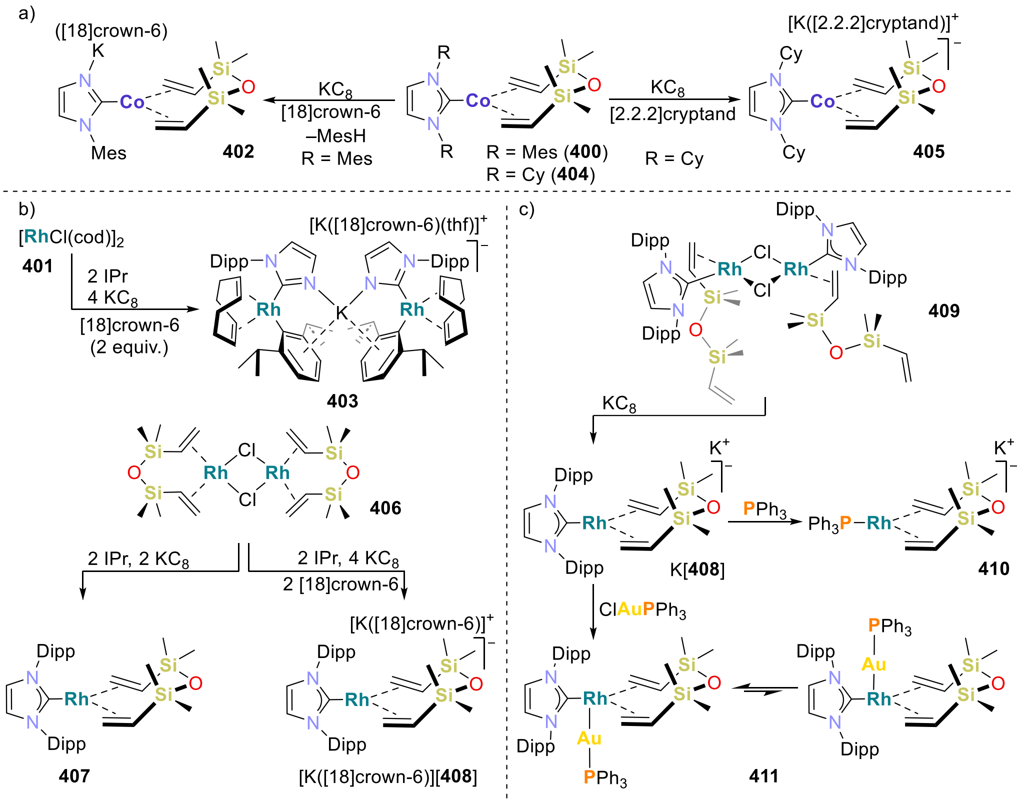

highly reduced metal center becomes more evident in the case of **403**, given that the aryl substituents remain coordinated to the Rh(I) centers.

It was proposed that a similar cobalt intermediate formed from the undetected Co(−I) compound $[(\mathrm{IMes})\mathrm{Co}(\mathrm{dvtms})]^-$, via intramolecular oxidative addition of the C−N bond, followed by homolytic cleavage of the Co−C(aryl) bond to generate the isolable Co(0) complex **402** and a mesityl radical. The formation of the latter was confirmed by detection of mesitylene by gas chromatography (GC). The observed mesitylene is the product of hydrogen atom abstraction from the solvent by the mesityl radical.

For a deeper study of the behavior of the highly reduced Co(−I) and Rh(−I) metal centers, further examples of the desired complexes were synthesized. Analogous treatment of [(ICy)Co(dvtms)] (**404**, ICy = 1,3-dicyclohexylimidazol-2-ylidene) with KC_8 in the presence of [2.2.2]cryptand yielded the formal Co(−I) complex [K([2.2.2]cryptand)][(ICy)Co(dvtms)] (**405**, Scheme 49a). Similarly, dimer $[\mathrm{RhCl}(\mathrm{dvtms})]_2$ (**406**) reacted with IPr and KC_8 to afford either the Rh(0) complex [(IPr)Rh(dvtms)] (**407**) or the formal Rh(−I) species [K([18]crown-6)][(IPr)Rh(dvtms)] ([K([18]crown-6)][**408**], see Scheme 49b), depending on the relative amount of reductant used. Neither **405** nor [K([18]crown-6)][**408**] undergoes C−N bond cleavage, even under heating conditions (50 or 70 °C for the cobalt or rhodium complexes, respectively). The authors proposed that, in the case of the cobalt complex, the formation of **405** responded both to the weaker π-accepting character of the ICy ligand and to the inability of the substituents on the NHC scaffold to form arene−metal interactions, thought to play an important role in the early activation (dearylation/intramolecular oxidative addition) of the C−N bond by the reduced metal center. Deng and co-workers also proposed that the lower electronegativity of cobalt in contrast to rhodium and the different π-accepting nature of the COD ligand versus that of the divinylsiloxane might explain the distinct behavior observed between compounds **405**/[K([18]crown-6)][**408**] and **402**/**403**. Altogether, the collective evidence supports M(−I) mediated C−N bond oxidative addition processes for the dearylation reactions observed.[324]

Tejel and Ciriano had previously reported the formal Rh(−I) compound K[Rh(IPr)(dvtms)] (K[**408**], Scheme 49c) by reduction of the Rh(I) dimer $[\mathrm{Rh}(\mu\text{-Cl})(\mathrm{IPr})(\mathrm{dvtms})]_2$ (**409**, IPr = 1,3-bis(2,6-diisopropylphenyl)-imidazolyl-2-ylidene).[325] The solid-state molecular structure of K[**408**] showed that the Rh center has a trigonal-planar geometry, where the metal is bound to the NHC ligand and both C═C bonds in dvtms. It is noteworthy that all the carbon atoms in the Rh coordination sphere are essentially in the molecular plane. This is a consequence of increased π-backdonation, as revealed by the elongation of the C═C bond distances compared to those of the uncoordinated C═C units in the dimer **409** (ca. 1.43 vs 1.30 Å). NMR spectroscopy also supports the increased π-backdonation evidenced in the solid state. Considering this, the Rh(−I) diene complex K[**408**] can alternatively be described as the corresponding Rh(I) metallacyclopropane resonance structure.

Complex K[**408**] undergoes NHC ligand exchange by PPh_3 forming $\mathrm{K}[\mathrm{Rh}(\mathrm{PPh}_3)(\mathrm{dvtms})]$ (**410**), while salt metathesis with $[\mathrm{AuCl}(\mathrm{PPh}_3)]$ (**146**) gave $[(\mathrm{IPr})(\mathrm{dvtms})\mathrm{RhAu}(\mathrm{PPh}_3)]$ (**411**, Scheme 49c). NMR spectroscopic data, along with NBO analysis, indicate a higher contribution of the $\mathrm{Rh}^{-\mathrm{I}}$-$\mathrm{Au}^{\mathrm{I}}$ resonance form than the Rh^0-Au^0 form to the ground state of **411**, which is therefore a rare example of a TM complex with two closed-shell d^{10} metals.

Kennedy reported the family of anionic nickel(0) complexes bearing bidentate NHC−pyridone ligands, and their use in hydroboration catalysis.[326] Reactions of $[\mathrm{Ni}(\mathrm{cod})_2]$ (**240**) with the corresponding ligand in a 1:2 ratio gave the series of complexes $[(\kappa^2\text{-}C,N\text{-}^{\mathrm{Ar}}\mathrm{NHCPyO})\mathrm{Ni}(\mathrm{cod})]^-$ [Ar = Mes (**412**), Dep (**413**), Dipp (**414**)] as the $[\mathrm{K}([18]\mathrm{crown}\text{-}6)]^+$ salts (see Scheme 50). The 1,5-cyclooctadiene ligand in **412**−**414** is labile, undergoing ligand displacement by MeCN to yield the tricoordinate 16-electron complexes $[(\kappa^2\text{-}C,N\text{-}^{\mathrm{Ar}}\mathrm{NHCPyO})\mathrm{Ni}(\eta^2\text{-MeCN})]^-$ [Ar = Mes (**415**), Dep (**416**), Dipp (**417**)] as the $[\mathrm{K}([18]\mathrm{crown}\text{-}6)]^+$ salts. In the solid state, the $[\mathrm{K}([18]\mathrm{crown}\text{-}6)]^+$ counterions in **412**, **413**, and **415** form a contact ion pair with the O atom of the pyridonyl unit, thereby preventing bridging coordination modes and multimetallic aggregation. The MeCN ligand in **415** has an elongated C−N bond (1.235(2) Å), reflecting the significant backbonding from the electron-rich nickel center. The series of $(\kappa^2\text{-}C,N)\mathrm{Ni}^0$ complexes were evaluated as catalysts for hydroboration reactions (see section 3.1.6).

Scheme 50. Synthesis of Anionic Ni(0) Complexes Featuring Bidentate NHC−Pyridone Ligands[326]

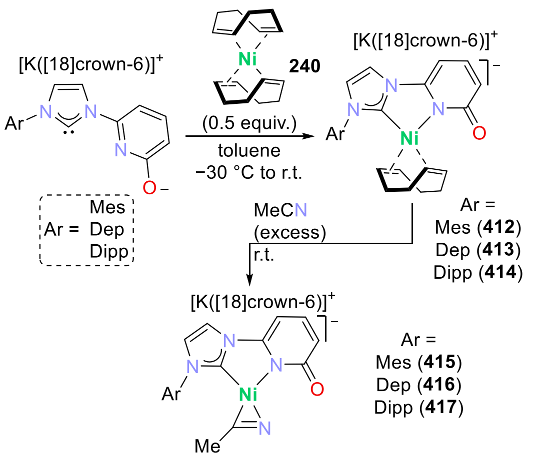

2.2.8. Alkyl, Amido, and Imido Complexes.

2.2.8.1. Monodentate Alkyl, Silyl(aryl)amido, and Imido Complexes. The Sc^{2+} complexes $[\mathrm{K}(\mathrm{L})][\mathrm{Sc}\{\mathrm{N}(\mathrm{SiMe}_3)_2\}_3]$ (**418**, L = [2.2.2]cryptand; **419**, L = [18]crown-6) and $[\mathrm{Cs}([18]\mathrm{crown}\text{-}6)][\mathrm{Sc}\{\mathrm{N}(\mathrm{SiMe}_3)_2\}_3]$ (**420**) were synthesized by Evans and co-workers, upon reduction of $[\mathrm{Sc}\{\mathrm{N}(\mathrm{SiMe}_3)_2\}_3]$ (**421**) with elemental K and Cs (Scheme 51).[327,328] These

Scheme 51. Synthesis of Mononuclear Scandate(II) Bis(silyl)amide Complexes[327,328]

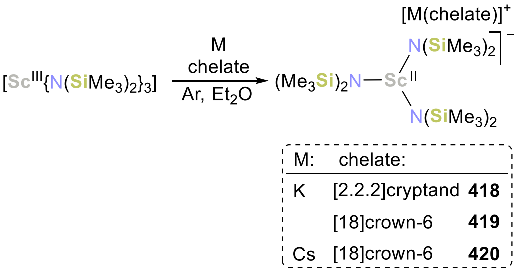

compounds are the first crystallographically characterized Sc^{2+} complexes. The presence of Sc^{2+} ions was also confirmed by their eight-line EPR spectra arising from the $I = 7/2$ ^{45}Sc nucleus. It is interesting to note that the complexes do not readily react with N_2 even though reduction of **421** under dinitrogen affords the crystallographically characterized complex $\{K([2.2.2]cryptand)\}_2\{[\{(Me_3Si)_2N\}_3Sc]_2[\mu{-}\eta^1{:}\eta^1{-}N_2]\}$ (**422**) with rare end-on $(N{=}N)^{2-}$ ligands.[327] The reactivity of $[K([18]crown{-}6)][Sc\{N(SiMe_3)_2\}_3]$ (**419**) with CO_2 is discussed in section 3.3.2.

The first example of a linear two-coordinate iron(I) complex, $[K([2.2.2]cryptand)][Fe\{C(SiMe_3)_3\}_2]_2$ (**423**) was reported by Long and co-workers in 2013.[329,330] The possibility of accessing the reduced complex **423** was identified upon studying the electrochemical behavior (CV) of the Fe(II) precursor, $[Fe\{C(SiMe_3)_3\}_2]_2$ (**424**), for which a reversible reduction event ($E_{1/2} = -1.82$ V, vs Fc/Fc^+) was observed. Based on these data, the chemical reduction of **424** with KC_8 in the presence of [2.2.2]cryptand was carried out, yielding [K([2.2.2]cryptand)][**423**]. Crystallographic analysis showed that anion **423** exhibits almost perfect linearity [C−Fe−C angle: 179.2(2)°].[329] Compound **423** exists in a triplet spin ground state ($S = 3/2$). Due to its high symmetry, it features a large magnetic anisotropy with a high barrier for magnetic relaxation ($U_{eff} = 226(4)$ cm^{-1}) even in the absence of an applied magnetic field and a magnetic blocking temperature of 4.5 K. Information on the magnetization dynamics of both **423** and **424** was obtained through Mössbauer spectroscopic studies, which agreed well with the corresponding calculated hyperfine parameters.[330]

As mentioned in section 2.2.4.2, silylamido complexes such as $Cr[N(SiMe_3)_2]_2(thf)_2$ (**166**) can be used for the synthesis of metalate complexes, e.g., $[Cr_2(naphthalene)_2]^-$ (**165**).[197] However, a series of low-valent and low-coordinate anionic M(I)-(aryl)silylamido or M(I)-bisilylamido species (M = Cr−Ni) have also been described.[331−339] These are generally obtained by reduction of the corresponding two-coordinate M(II) precursors with KC_8 or alkali metals,[340,341] in most cases in the presence of crown ethers or cryptands.[331−338]

In 2013, Power described the formation of a tetranuclear chromium-silyl(aryl)amido $[Cr\{N(SiMe_2CH_2)Dipp\}_2Cr]_2(thf)$ (**425**) complex, obtained in an attempt to synthesize a two-coordinate Cr-silyl(aryl)amido species. The ligand failed to stabilize the low-coordinate species by undergoing C−H activation at a methyl substituent of the $-SiMe_3$ group, leading to the tetra-nuclear chromium compound **425** (see Figure 10).[340]

Later, in 2014, Tilley and co-workers reported on the synthesis of a series of chromium compounds in the formal oxidation states +I, +II, and +III, stabilized by the bulkier silyl(aryl)amido ligand $(Si\textit{i}Pr_3)(Dipp)N^-$ (Dipp = 2,6-diisopropylphenyl).[331] The mononuclear Cr(II) compound $[Cr\{N(Dipp)Si\textit{i}Pr_3\}_2]$ (**426**) was obtained by a salt metathesis of $CrCl_2$ with 2 equiv of $K[N(Dipp)Si\textit{i}Pr_3\}_2]$ in THF. Cyclic voltammetry performed on **426** revealed a reversible Cr(I/II) couple ($E_{1/2} = -2.04$ V, vs Fc/Fc^+) and, therefore, its chemical reduction with 1.1 equiv of KC_8 was attempted, affording $[K(dme)_4][Cr\{N(Dipp)Si\textit{i}Pr_3\}_2]$ (K[**427**], Scheme 52a). K-[**427**] reacts with tetrabutylammonium bromide to afford the Bu_4N^+ salt $[Bu_4N]$[**427**]. The solution magnetic moments of both salts (Evans method, 5.2 and 5.7 μ_B, respectively) are consistent with the metal centers in a high-spin d^5 configuration.

Oxidation of **426** by I_2 yielded the cationic Cr(III) compound $[(I)Cr\{N(Dipp)Si\textit{i}Pr_3\}_2]$ (**428**), which could be further functionalized.[331] Likewise, the same group reduced the Ni(II) precursor $[Ni\{N(SiMe_3)Dipp\}_2]$ (**429**)[342] with KC_8 (1.1 equiv) to access the anionic complex $K[Ni\{N(SiMe_3)Dipp\}_2]$ (K[**430**]) in toluene at −30 °C (Scheme 52b).[336] As with the chromium analogues,[331] the ligand scaffold proved useful to stabilize three different formal oxidation states at the nickel center, Ni(I/II/III). Fully reversible Ni(I/II) ($E_{1/2} = -1.28$ V, vs Fc/Fc^+) and Ni(II/III) ($E_{1/2} = +0.18$ V, vs Fc/Fc^+) redox couples were identified in the cyclic voltammogram of **429**. X-ray crystallographic characterization of K[**430**] revealed an almost perfectly linear N−Ni−N geometry (178.05(9)°) and that the potassium counterion is coordinated by two aryl rings in η^6-fashion. Subsequent exchange of the potassium cation by tetrabutylammonium (NBu_4^+) afforded the ion-separated analogue $[NBu_4]$[**430**]. According to the analysis of the calculated molecular orbitals in the latter, a considerable nucleophilic character was expected for $[NBu_4]$[**430**] due to the double occupation of its antibonding (dz^2-derived) orbital. As a result, reaction of K[**430**] with methyl iodide at low temperatures (−78 °C to r.t.) yields the product of two-electron oxidative addition, the T-shaped Ni(III) compound $[(Me)Ni\{N(SiMe_3)Dipp\}_2]$ (**431**). Attempts to access a Ni(III) species by oxidation of the Ni(II) complex **429** (e.g., with Ag(I) reagents) led to intractable mixtures or no reaction. The formal oxidation states proposed for the anionic Ni(I) complex and for the Ni(III) oxidative addition product are supported by DFT calculations and EPR spectroscopic analysis.[336]

Additional examples of (aryl)(silyl)amido complexes $[K([18]crown{-}6)][M\{N(Dipp)SiMe_3\}_2]$ [M = Fe (**432**/**433**), Co (**434**), Ni (**435**)][335] or $[KM\{N(Dipp)SiR_3\}_2]$ [M = Cr, R = *i*Pr (**436**); M = Mn (**437**), Fe (**438**), Co (**439**, toluene solvate), R = Me][334] have been reported by different groups. Power, Long, and co-workers obtained **432**−**435** by reduction of the corresponding M(II) precursors [M = Fe (**440**), Co (**441**), Ni (**429**)][340,342−344] in the presence of [18]crown-6.[335] Compound **432** was obtained as a diethyl ether-cation adduct ($[K([18]crown{-}6)(Et_2O)_2]^+$, **432**, Scheme 52c, right), which undergoes loss of Et_2O upon storage at ambient pressure and temperature, under vacuum or after dissolution in noncoordinating solvents (pentane, toluene) to generate the $[K([18]crown{-}6)]^+$ salt **433**. The cobalt and nickel compounds **434** and **435** are perfectly linear, while the iron(I) complexes **432** and **433** have a slightly bent structure in the solid state [N−M−N angles: 171.99(6) (**432**) and 172.67(7)° (**433**)].[335]

Similar complexes **436**−**438** were obtained by Werncke and co-workers (Scheme 52d). The characterization by single-crystal X-ray diffraction revealed that these species are

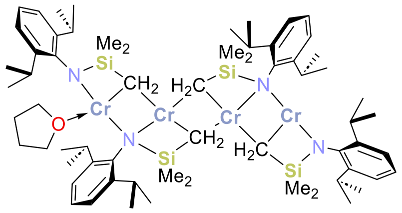

425

Figure 10. Representation of the structure of the tetranuclear compound $[Cr\{N(SiMe_2CH_2)Dipp\}_2Cr]_2(thf)$ (**425**).[340]

Scheme 52. Synthesis of Low-Valent M(I)-(Aryl)silylamido Complexes of the 3d Metals from Chromium to Nickel[331−335]

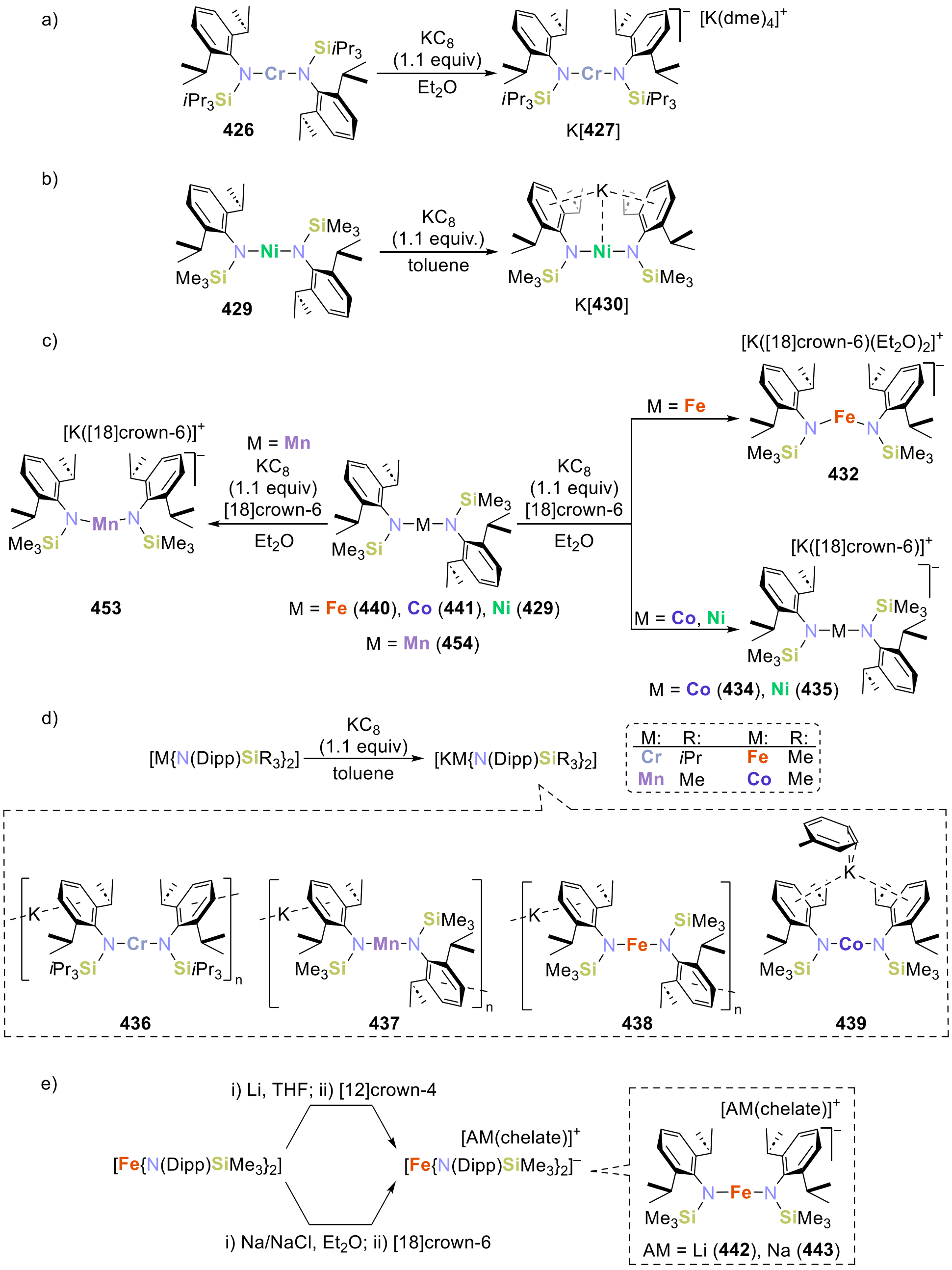

associated by contact ion pairing in the solid state, which results in the formation of 1D-coordination polymers with a zigzag arrangement for **437** and **438**, while the polymer **436** is more linear.[334] By contrast, the cobalt compound **439** (Scheme 52d) does not form an aggregate in the solid state. Instead, the potassium cation is sandwiched by aryl rings and additionally η^2-coordinated by a toluene molecule.[334] The molecular structures are slightly bent [N−M−N angles 177.44(10)° (**436**), 165.56(6)° (**437**), 170.59(5)° (**438**), 178.43(8)° (**439**)], with a greater deviation from linearity for the manganese and iron compounds, **437** and **438**, than for cobalt. NMR studies revealed the presence of an ion-pairing between potassium and the complex anion, which depends on the nature of the solvent: while in weakly/noncoordinating solvents (e.g., toluene-d_8) the ion-pairing seems to persist in solution, ion-separated species appear to be formed in polar coordinating solvents such as THF-d_8. These findings are corroborated by the crystallographic characterization of the monomeric adducts **436**·3THF, **438**·Et_2O, **438**·2DMAP (DMAP = *p*-dimethylaminopyridine), which are structurally similar to compound **439**. In these, polymer formation is prevented by the coordination of additional donor molecules, although the potassium cation remains in the “coordination pocket” formed by two aryl rings of the amido ligands. Furthermore, the addition of a crown ether prior to reduction of the M(II) precursor with lithium or sodium affords ion-separated compounds [AM(chelate)][Fe{N(Dipp)$SiMe_3$}$_2$] [AM = alkali metal = Li, chelate = [12]crown-4 (**442**); AM = Na, chelate = [18]crown-6 (**443**)] (Scheme 52e). In the absence of crown ether, only decomposition or the formation of oxidized products was observed. These observations suggest that the coordination of lithium or sodium cations strongly influences the stability of these bis(amido)metalates(I).[334]

Anionic silylamido complexes of general formula [K(chelate)][M{N(SiMe$_3$)$_2$}$_2$] [M = Cr (**444**), Mn (**445**, dimeric), Fe (**446**), Co (**447**), Ni (**448**); chelate = [18]crown-6 or [2.2.2]cryptand] (see Scheme 53) were described by the team of Bontemps, Sabo-Etienne, and Werncke.[332,333,338] Compounds **444**, **446**, and **447** were prepared by reduction of M(II)-silylamido-Lewis base adducts [M{N(SiMe$_3$)$_2$}$_2$(L)$_n$] [M = Cr (**449**), L = thf, *n* = 2; Fe (**450**), L = PCy$_3$ or thf, *n* = 1; Co (**451**), L = thf, *n* = 1] in the presence of a crown ether or cryptand (Scheme 53a). In the solid state, the molecules reside on crystallographic inversion centers. As a result, perfectly linear structures are found within an eclipsed conformation of the substituents on the silylamido ligands.

Scheme 53. Synthesis of M(I)-Silylamido (M = Cr, Mn$_2$, Fe, Co, Ni) Complexes[332,333,338]

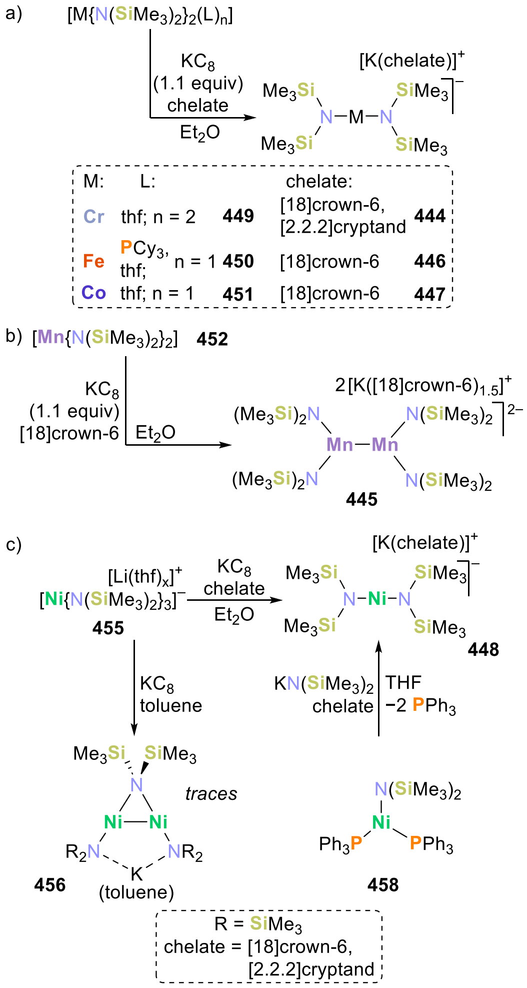

For the manganese species, an analogous reduction procedure on [Mn{N(SiMe$_3$)$_2$}$_2$] (**452**) failed to give access to the expected monomeric Mn(I) complex, affording the dianionic dimer [K([18]crown-6)$_{1.5}$]$_2$[Mn{N(SiMe$_3$)$_2$}$_2$]$_2$ (**445**), featuring a Mn−Mn bond instead (Scheme 53b). Stabilization of a low-coordinate Mn(I) complex was attempted by using the more encumbering (aryl)silylamido ligand (SiMe$_3$)(Dipp)N$^-$. Gratifyingly, the two-coordinate complex [K([18]crown-6)][Mn{N(Dipp)SiMe$_3$}$_2$] (**453**) was accessible after reduction of the Mn(II) precursor [Mn{N(Dipp)(SiMe$_3$)}$_2$] (**454**) with KC$_8$ in the presence of [18]crown-6 (see Scheme 52c, left, above). Crystallographic analysis revealed that the orientation of the substituents on the nitrogen atoms changes from *trans* in the neutral complex **454** to *cis* in the reduced compound **453**, with one isopropyl group of each ligand pointing toward the phenyl ring of the opposing ligand. Complex **453** features a bent structure (N−M−N angle 167.12(14)°).[332]

The nickel complex [K(chelate)][Ni{N(SiMe$_3$)$_2$}$_2$] (**448**, Scheme 53c, chelate = [2.2.2]cryptand, or [18]crown-6) proved more difficult to access than its analogues **444**−**447** with Cr, Mn, Fe, and Co.[338] Initial attempts to reduce the Ni(II) precursor Li(thf)$_x$[Ni{N(SiMe$_3$)$_2$}$_3$] (**455**) with KC$_8$ in toluene afforded only traces of the crystalline dimer [K(toluene)][Ni$_2${N(SiMe$_3$)$_2$}$_3$] (**456**, Scheme 53c, down left). By contrast, reducing **455** with KC$_8$ in the presence of a sequestering/chelating agent in Et$_2$O afforded the desired compound **448** (Scheme 53c). However, despite giving access to **448**, it was difficult to control the ratio of the reactants due to the tendency of **455** to disproportionate in nonpolar solvents, the sensitivity of the Ni-containing intermediates, and difficulties in determining the THF contents of the precursor, which varies because of decoordination. Therefore, the product was usually obtained with various contaminants, which included the tris(disilyl)amido complex [K([18]crown-6)][Ni{N(SiMe$_3$)$_2$}$_3$] (**457**). This problem was not solved by using a different sequestering agent ([2.2.2]cryptand). An alternative approach yielded a reliable method for the synthesis of pure **448** in good yields. Displacing the phosphine ligands in the adduct [Ni{N(SiMe$_3$)$_2$}(PPh$_3$)$_2$] (**458**) with K{N(SiMe$_3$)$_2$} affords **448** as pure [K([18]crown-6)]$^+$ and [K([2.2.2]cryptand)]$^+$ salts in good yields (Scheme 53c). Analysis of the spectroscopic and magnetic properties indicated that the open-shell complex was best described as an *S* = 1/2 system. NMR and EPR spectroscopic data of **448** suggested the presence of different conformations in solutions, which may result from distortion of linearity or the suppression of rotation of the silylamido ligands along the main axis. This dynamic behavior of the complexes is likely caused by ion-pairing interactions.

Moreover, the linear or quasilinear N−M−N arrangement of the M(I)-disilylamido complexes results in interesting magnetic properties such as a large magnetic anisotropy and slow relaxation of the magnetization. For example, [K(chelate)][Fe{N(SiMe$_3$)$_2$}$_2$] (**446**) exhibits large magnetic moments at ambient temperature μ_{eff} = 5.12 and 5.14 μ_B in solution, which are close to the free ion value (d^7, 5.19 μ_B).[333] These data suggested a large magnetic contribution from unquenched orbital angular momentum. In line with this hypothesis, variable-frequency, variable-temperature magnetic susceptibility measurements revealed effective barriers to magnetic relaxation of U_{eff} = 43 and 64 cm^{-1}, and relaxation times of $\tau_0 = 4.9 \times 10^{-6}$ and 8.9×10^{-6} s for compound **446** when chelated by [18]crown-6 or [2.2.2]cryptand, respectively.

An attempted alternative synthesis of **444**−**447** was later described,[345] consisting of the reduction of a series of trigonal halido bis(silylamido) M(II) metalates, from manganese to cobalt, by KC$_8$. However, attempts to reduce the [NBu$_4$]$^+$ salts of the complexes led only to partial formation of the linear metal(I) silylamides, while degradation of the metal complex and decomposition of the [NBu$_4$]$^+$ cations was also observed.

By contrast, reduction of $[\mathrm{K([18]crown\text{-}6)}][\mathrm{M^{II}Br\{N(SiMe_3)_2\}_2}]$ (**459**, M = Fe, Co) afforded the expected $[\mathrm{M\{N(SiMe_3)_2\}_2}]^-$ products, albeit in low yield. Similar results were obtained from the trigonal halido (aryl)silylamido metalates(II) $[\mathrm{M^{II}Br\{N(Dipp)SiMe_3\}_2}]^-$.[345] Therefore, the reduction of the M(II) bis(silylamido) or bis(aryl)silylamido precursors remains the most efficient reaction pathway for the synthesis of the M(I) anionic compounds known to date.

It is worth mentioning that bipyridine adducts of anionic M(I) silylamido complexes of the formula $[\mathrm{K([18]crown\text{-}6)}][\mathrm{M\{N(SiMe_3)_2\}_2(bipy)}]$ [M = Cr (**460**), Mn (**461**), Fe (**462**), Co (**463**)] are also accessible. These complexes were prepared by addition of 2,2′-bipyridine to the anionic M(I) silylamides **446** and **447**, or additionally with *in situ* reduction of the neutral homoleptic M(II) precursors **449** and **452** by $\mathrm{KC_8}$ (Scheme 54).[346] Complexes **460**−**463**, along with the zinc analogue $[\mathrm{K([18]crown\text{-}6)}][\mathrm{Zn\{N(SiMe_3)_2\}_2(bipy)}]$ (**464**), could also be accessed by direct reduction of the neutral heteroleptic M(II) precursors $\mathrm{M\{N(SiMe_3)_2\}_2(bipy)}$ [M = Cr (**465**), Mn (**466**), Fe (**467**), Co (**468**), Zn (**469**)]. However, it should be noted that X-ray diffraction analyses of **460**−**463** and further physical measurements (UV−vis spectra, magnetic susceptibility, and electrochemical measurements) suggest the presence of metal centers in the +II oxidation state and 2,2′-bipyridine radical anions in each case as observed for other anionic bipyridine complexes (*vide infra*), and these compounds are therefore not discussed in greater detail.[2,85,200−203,268,344−349]

Scheme 54. Synthesis of Anionic Heteroleptic Bipyridine-silylamido Complexes of the 3d Metals[346]

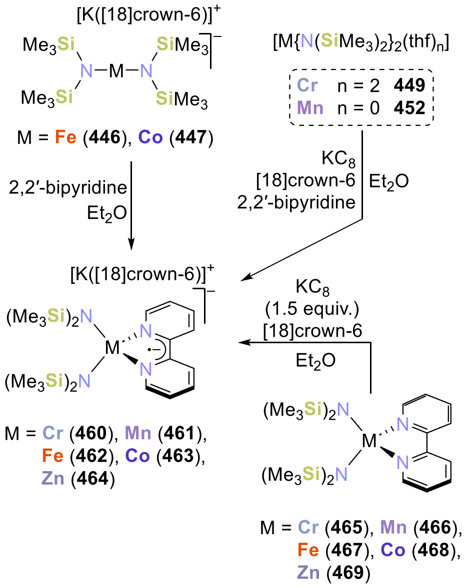

Reactivity studies evaluated the behavior of the silyl(aryl)-amido complexes $[\mathrm{KM\{N(Dipp)SiMe_3\}_2}]$ [M = Mn (**437**), Fe (**438**), Co (**439**)] and of the hexamethyldisilazanide complexes $[\mathrm{K([18]crown\text{-}6)}][\mathrm{M\{N(SiMe_3)_2\}_2}]$ [M = Cr (**444**), Mn (**445**), Fe (**446**), Co (**447**)] toward alkynes (Scheme 55).[334,353] For instance, [18]crown-6 adducts $[\mathrm{K([18]crown\text{-}6)}][\mathrm{M\{N(Dipp)SiMe_3\}_2}]$ of **437** and **438** form adducts of the type $[\mathrm{M\{N(Dipp)SiMe_3\}_2(\eta^2\text{-}RC{\equiv}CR)}]^-$ (**470**, M = Mn, R = Ph, Et; **471**, R = Ph) with diphenylacetylene and 3-hexyne (Scheme 55a, right).[334,353] The molecular structures of these complexes feature side-on coordinated alkyne ligands. The alkyne ligands in **470** are labile.[353] Analogous reactivity was observed for **444**−**447** (Scheme 55b), affording compounds of general formula $[\mathrm{K([18]crown\text{-}6)}][\mathrm{M\{N(SiMe_3)_2\}_2(\eta^2\text{-}RC{\equiv}CR)}]$ [M = Cr (**472**), Mn (**473**), Fe (**474**), Co (**475**)], although some combinations of metal and alkyne resulted in deviating reactivity and products (*vide infra*). The authors concluded that, for this series (Scheme 55b), the chromium and manganese derivatives bind the alkyne ligand more strongly and more covalently and, consequently, the C≡C bond is more activated in those complexes, in contrast to the iron and cobalt analogues.[353]

The chromium compounds shown on Scheme 55b (left) illustrate the different reactivity observed for the hexamethyldisilazanide complexes of the studied early transition metals.[353] The side-on coordinated alkyne complex **472** is formed by reaction of **444** and bis(trimethylsilyl)acetylene (btmsa). By contrast, the reaction of **444** with diphenylacetylene afforded the alkyne-bridged compound $[\mathrm{K[18]crown\text{-}6}][\mathrm{Cr_2\{N(SiMe_3)_2\}_2\{\mu\text{-}N(SiMe_3)_2\}(\mu\text{-}1\kappa C^1{,}2\kappa C^2{-}PhCCPh)}]$ (**476**). The formation of **476** was attributed to partial oxidation of the metal atoms, with concomitant 2-fold reduction of the alkyne as a result of strong metal-to-alkyne ligand back-bonding.[353]

Treating **445** with btmsa similarly yielded $[\mathrm{K[18]crown\text{-}6}][\mathrm{Mn_2\{N(SiMe_3)_2\}_2\{\mu\text{-}N(SiMe_3)_2\}(\mu{-}\eta^2\text{-}Me_3SiCCSiMe_3)}]$ (**477**), which features a reduced alkyne ligand and an oxidized metal framework, whereas analogous treatment with diphenylacetylene afforded the side-on complex **473**. The latter species, however, reacts with additional equivalents of **445**, via a series of C≡C activation processes, to generate first the dinuclear compound $[\mathrm{K([18]crown\text{-}6]_2[Mn\{N(SiMe_3)_2\}_2(\mu{-}\kappa^1{:}\kappa^1\text{-}PhCCPh)}]$ (**478**), and then, in the presence of further substrate, the heteroleptic complex $[\mathrm{K([18]crown\text{-}6)}][\mathrm{Mn(\eta^6\text{-}C_6Ph_6)(\eta^2\text{-}C_2Ph_2)}]$ (**479**) accompanied by formation of $[\mathrm{Mn\{N(SiMe_3)_2\}_3}]^-$ (**480**) as a byproduct (see Scheme 55b, right down). The alkyne thereby undergoes coordination, 2e-reduction, and cyclotrimerization during the transformation of complex **473** into **479**. These processes involve a disproportionation of **445** as well as ligand exchange and metal-mediated substrate trimerization. Unambiguous determination of the oxidation state in **479** was inhibited by a lack of pure analytical samples. The elongated C−C bond of the alkyne [1.346(7) Å] according to X-ray diffraction data led the authors to suggest that **479** could be described as a manganese(I) metallacyclopropene compound. However, its depiction as a formally manganese(−I) alkyne complex was also discussed, which would account for redox disproportionation leading to the formation of the manganese triamide **480**.[353]

Analogously, the more encumbering neutral (contact ion pair) compounds $[\mathrm{KM\{N(Dipp)SiMe_3\}_2}]$ also engage in metal-mediated trimerizations of diphenylacetylene, probably as the result of redox disproportionation of the corresponding metal complex. For the manganese complex **437**, the characterization of the unusual species **481** and **482** (Scheme 55a, left) was achieved. Such species are probably intermediates en route to the cyclotrimerization of PhC≡CPh.[334] In the case of the iron complex **438**, the trimerization afforded the previously reported anion $[\mathrm{Fe(\eta^6\text{-}C_6Ph_6)(\eta^2\text{-}C_2Ph_2)}]^-$ (**192**, *vide supra*), analogous to **479**.[213]

For the bis(silylamide) complex $[\mathrm{Co\{N(SiMe_3)_2\}_2}]^-$ (**447**) and the more sterically encumbered precursor **439**, a weak and

Scheme 55. Reactivity of (a) M(I)-Bis(silylamide) (as [K([18]crown-6)]$^+$ Salts) and (b) Neutral and Ion-Separated M(I)-Silylamido Complexes by the Group of Werncke[334,353]

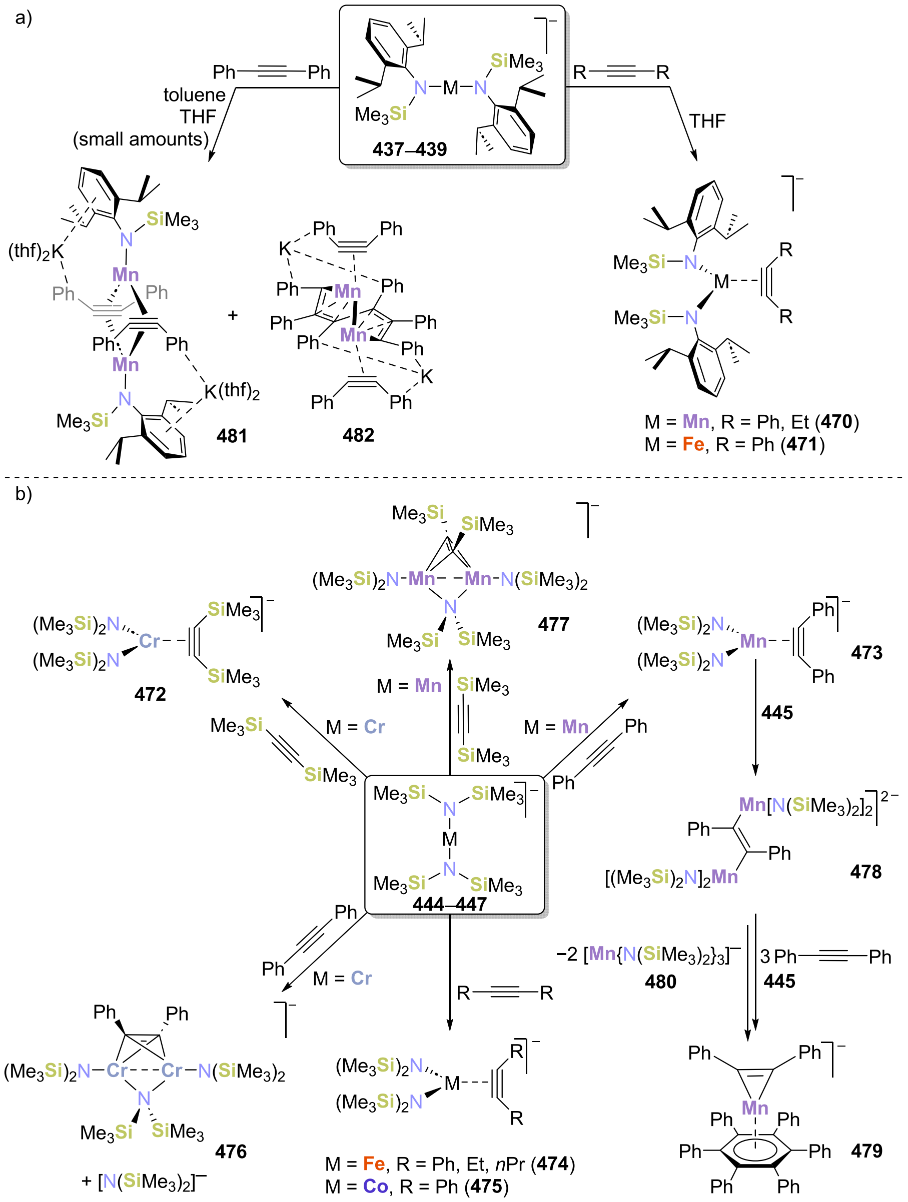

reversible coordination of the alkyne motif to the metal center, attributed to the anionic nature of the precursors,[334,353] was identified for all the substrates (RC≡CR with R = Ph, SiMe$_3$, Et, and *n*Pr). Despite such weak coordination, the reaction product between **447** and diphenylacetylene, [K([18]crown-6)][Co{N(SiMe$_3$)$_2$}$_2$(η^2-PhC≡CPh)] (**475**) was isolated and crystallographically characterized. Computational analysis of the hexamethyldisilazanide/alkyne compounds [K([18]crown-6)][M{N(SiMe$_3$)$_2$}$_2$(η^2-RC≡CR)] supports the structural observations indicating a partial reduction of the alkyne ligands by the metal centers. Consequently, the compounds were described as metal(II) complexes with covalently bound alkyne ligands bearing some radical character (formal 1e$^-$ reduction of the alkyne ligands).[353]

Further reactivity studies showed that the quasilinear complexes [M{N(SiMe$_3$)$_2$}$_2$]$^-$ [M = Fe (**446**), Co (**447**)] behave as reductants toward ketones, aldehydes, and imines, generating the corresponding M(II) stabilized radical anions.[354] Examples of the latter are the anionic ketyl complexes [K(chelate)][M(bp){N(SiMe$_3$)$_2$}$_2$] [M = Fe (**483**), Co (**484**); bp = benzophenone, chelate = [18]crown-6 or [2.2.2]cryptand], which were evaluated in terms of their ability to engage in radical-like reactivity, specifically in hydrogen atom abstraction. Whereas the iron(II) complex **483** did not react with the H atom donor 1,4-cyclohexadiene (1,4-CHD), **484** promoted its dehydrogenation to benzene.

Furthermore, the reaction of **484** with an excess/of 1,4-CHD formed not only benzene (see Scheme 56) but also a bis(1,3-cyclohexadiene)cobaltate(−I) complex, [Co(η^4-1,3-C$_6$H$_8$)$_2$]$^-$ (**485**), and the tris(silylamido)cobalt(II) complex [Co{N(SiMe$_3$)$_2$}$_3$]$^-$ (**486**).[354] The structure of **485** is analogous to the bis(butadiene)cobaltate **248** and to the bis(anthracene)cobaltate **14** (*vide supra*).[87] Moreover, the authors proved that the ketyl ligand in **484** is not required to obtain **485** since it was also independently synthesized by reactions of **447** (3 equiv) with either 1,3- or 1,4-CHD (see

Scheme 56. Formation of a Bis(1,3-cyclohexadiene)cobaltate(−I) Complex by Two Different Reaction Pathways, Described by the Group of Werncke[354]

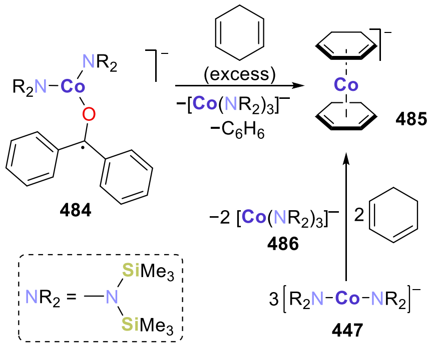

Scheme 56). The reaction also produces the Co(II) complex **486**, thereby representing a disproportionation of the Co(I) complex **447** into Co(II) and Co(−I). Together, the independent synthesis of **485** from **447** and the reactivity observed with the ketyl radical complex **484** indicated that the role of the latter involved promotion of the H atom abstraction process.[354]

In 2015, Tilley and co-workers demonstrated the potential of a low-valent and low-coordinate heteroleptic carbene/silyl(aryl)amido Fe(I) complex as a precatalyst in the trimerization of alkynes.[337] The neutral compound [Fe{N(Dipp)(SiMe$_3$)}(IPr)] (**487**, IPr = 1,3-bis(2,6-diisopropylphenyl)imidazolin-2-ylidene, Dipp = 2,6-diisopropylphenyl) was obtained via a one-pot reaction, by protonating *in situ* generated [Fe{N(Dipp)SiMe$_3$}$_2$] (**440**),[343] adding the carbene ligand and finally reducing the formed species with KC$_8$ (Scheme 57). Further reduction of neutral

Scheme 57. Synthesis of a Heteroleptic Carbene/Silyl(aryl)amido Iron(I) Complex and Its Reduction to Afford the Fe(0) Complex 488[337]

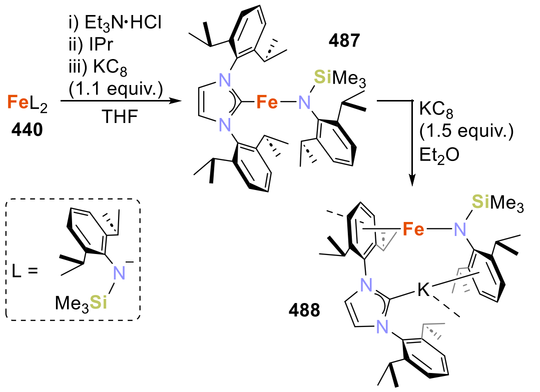

487 with KC$_8$ yielded a rearranged product, K[(η^6-IPr)Fe{N(Dipp)(SiMe$_3$)}] (**488**). Here, the carbene ligand coordinates to the metal atom as a π-bonded arene ligand, with the C$_{\text{carbene}}$-atom interacting with the potassium cation. ^{57}Fe Mössbauer spectroscopic analysis confirmed that **487** is an Fe(I) compound and that the reduction occurs at the metal center, making product **488** an Fe(0) species. Additionally, **487** was found to catalyze the cyclotrimerization of both internal and terminal alkynes at catalyst loadings of 2−5 mol % under mild conditions to afford substituted arenes.[337]

2.2.8.2. Amido Ligands with Pendant Donors. Gambarotta reported low-valent titanium and vanadium complexes featuring σ-/π-bonded pyrrolide-based ligands.[194,195] A tripyrrolide ligand served as platform for the synthesis of a mixed-valent anionic titanium complex.[194] Treatment of [TiCl{2,5-[(C$_4$H$_3$N)CPh$_2$]$_2$[C$_4$H$_2$N(Me)]}] (**489**) with potassium in toluene, followed by recrystallization from DME, afforded complex [K(dme)$_2$][{2,5-[(C$_4$H$_3$N)CPh$_2$]$_2$[C$_4$H$_2$N(Me)]}Ti(μ,η^6:η^6-C$_7$H$_8$)Ti[{2,5-[(C$_4$H$_3$N)CPh$_2$]$_2$[C$_4$H$_2$N(Me)]}]·toluene (**490**, Scheme 58a) which has an inverse

Scheme 58. Synthesis of Anionic Titanium or Vanadium Complexes Featuring σ-/π-Bonded Pyrrolide-Based Ligands[194,195]

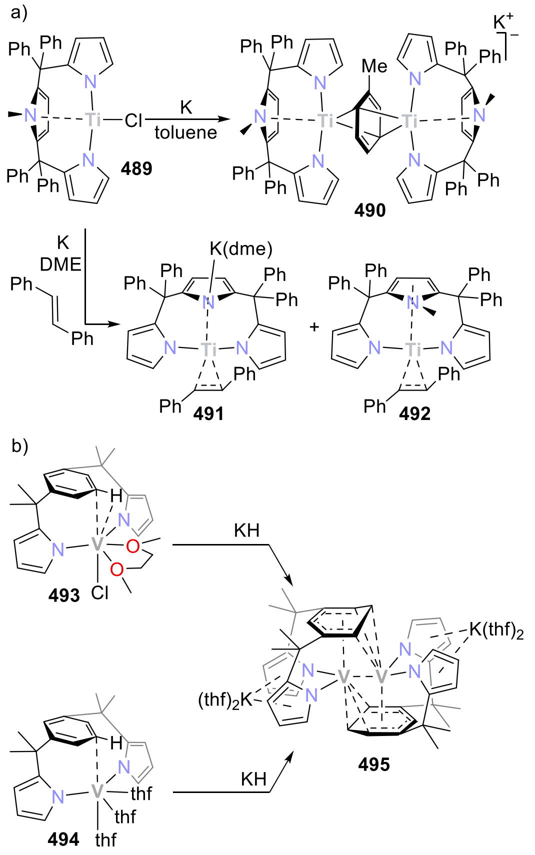

sandwich-type structure. The dianionic polydentate ligand framework in **490** has three pyrrole rings, one of which is π-coordinated to each titanium center. The metric parameters in the crystal structure point toward the presence of a mixed valent complex. Furthermore, the bridging toluene ligand is significantly distorted, suggesting increased metal-to-ligand backbonding. In turn, the magnetic moment (μ_{eff} = 1.73 μ_B) indicates that the species has one unpaired electron. These findings were corroborated by DFT calculations and **490** was proposed to be a formally Ti(I)/Ti(II) complex. By reducing **489** with potassium in the presence of *trans*-stilbene, a mixture of two diamagnetic complexes was obtained after crystallization, [K(dme)][Ti{2,5-[(C$_4$H$_3$N)CPh$_2$]$_2$[C$_4$H$_2$N]}(η^2-*trans*-PhHC=CHPh)] (**491**) and [Ti{2,5-[(C$_4$H$_3$N)CPh$_2$]$_2$-[C$_4$H$_2$N(Me)]}(η^2-*trans*-PhHC=CHPh)] (**492**, Scheme 58). The tripyrrrolide ligand has lost the methyl substituent in **491**, through an unknown mechanism, thereby becoming trianionic. The elongated C−C bond distance (1.443(6) Å) of the coordinated *trans*-stilbene ligand reflects the increased electron density and metal-to-ligand backbonding in **491**. According to the authors, **491** can be considered either a Ti(II)- or a Ti(IV)-species. Later, the same group achieved the reduction of N_2 to nitride at tripyrrolide Ti(III) neutral complexes.[355]

A related dipyrrolidephenyl ligand scaffold supported the V(III) or V(II) complexes $[(dme)VCl\{1,3\text{-}[(C_4H_3N)CMe_2]_2\text{-}(C_6H_4)\}]$ (**493**) or $[(thf)_3V\{1,3\text{-}[(C_4H_3N)CMe_2]_2(C_6H_4)\}]$ (**494**), respectively.[195] Compounds **493** and **494** reacted with the appropriate amount of KH to the low-valent anionic dinuclear V(I) complex $[\{(thf)_2K\}V\{1,3\text{-}[(C_4H_3N)CMe_2]_2\text{-}(C_6H_4)\}]_2$ (**495**, Scheme 58b). The vanadium atoms in **495** are connected through bridging interactions with the central phenyl ring of the ligand framework, and a weak V−V bond. The two phenyl rings are significantly distorted, indicating strong covalent bonding between each vanadium atom and the ring π-system. Theoretical calculations indicated that, despite these interactions, the central phenyl ring has a net charge of almost zero, and therefore, the distortion does not affect the formal oxidation state of the metal centers. Consequently, the authors concluded that, in **495**, the metal atoms are formally in the d^4 V(I) configuration. A striking contrast in behavior was observed between complex **494** and the analogous vanadium species with the tripyrrolide ligand: whereas **494** is inert toward N_2 coordination, the related neutral tripyrrolide-vanadium complex mediated nitrogen fixation and cleavage.[356]

Recently, Fortier and co-workers reported that the reduction of the dimeric titanium compound $[Cl_2Ti(\mu\text{-}NIm^{Dipp})]_2$ (**496**) (NIm^{Dipp} = $[1,3\text{-bis(Dipp)imidazolin-2-iminato}]^-$) by 4 or 6 equiv of KC_8 generates the dinuclear compounds $[(\mu\text{-}N\text{-}\eta^6\text{-}Im^{Dipp})Ti]_2$ (**497**) and $\{[(Et_2O)_2K](\mu\text{-}N\text{-}\mu\text{-}\eta^6\text{:}\eta^6\text{-}Im^{Dipp})Ti\}_2$ (**498**), respectively (Scheme 59).[357] X-ray structural analyses suggested that the η^6-bound Dipp groups in both compounds had undergone two-electron reduction, lending formal oxidation state assignments of Ti(III)/Ti(III) for neutral **497** and Ti(II)/Ti(II) for anionic **498**. However, reactivity of these species with small organic molecules revealed reducing capabilities beyond their formal oxidation states.

Scheme 59. Synthesis and Reducing Capabilities of the Dinuclear Anionic Complex $\{[(Et_2O)_2K](\mu\text{-}N\text{-}\mu\text{-}\eta^6\text{:}\eta^6\text{-}Im^{Dipp})Ti\}_2$ (498)

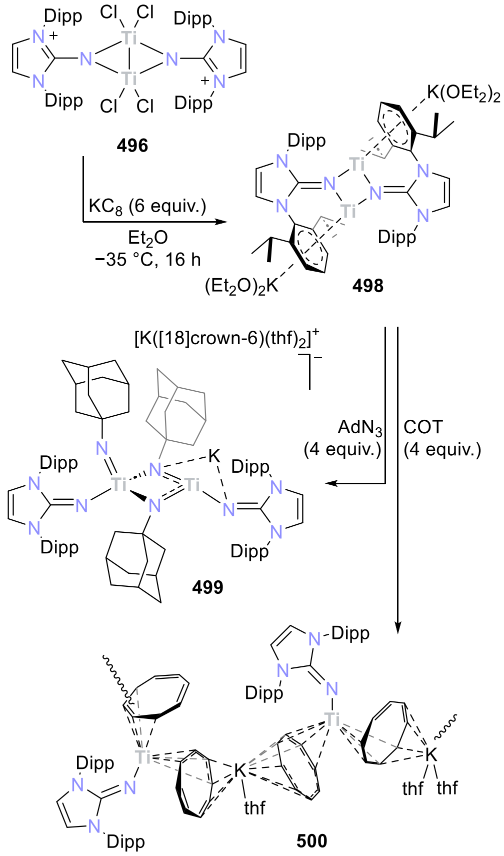

The reaction of **498** with 4 equiv of AdN_3, followed by addition of [18]crown-6, allowed isolation of the tris(imido) complex $[K([18]crown\text{-}6)(thf)_2]\{[(Im^{Dipp}N)Ti(NAd)](\mu\text{-}NAd)_2K[Ti(NIm^{Dipp})]\}$ (**499**), consistent with the 6-electron reduction of 3 equiv of AdN_3 with loss of N_2. Additionally, reaction of **498** with 4 equiv of cyclooctatriene (COT) yielded a polymeric species of repeat unit $[(Im^{Dipp}N)(\eta^4\text{-}COT)\text{-}Ti(\mu\text{-}\eta^4\text{:}\eta^6\text{-}COT)K(thf)(\mu\text{-}\eta^5\text{:}\eta^4\text{-}COT)Ti(NIm^{Dipp})\text{-}(\mu\text{-}\eta^4\text{:}\eta^4\text{-}COT)K(thf)_2]_n$ (**500**). Inspection of the C−C bonds in the coordinated COT rings of the solid-state structure revealed either localized -ene dianionic character or charge delocalization consistent with an overall 8-electron oxidation of **498**. Thus, the authors proposed that, despite the formal assignment of its metal centers as Ti(II), compound **498** acts as a masked anionic Ti(0)/Ti(0) species. Related experiments implicated the neutral compound **497** as a similarly masked Ti(I)/Ti(I) species.

It is worth mentioning that Khusniyarov, Meyer, Mindiola, and co-workers have isolated highly reduced, dinuclear dipyrrolide pyridine Fe complexes with the ligand $^{tBu}pyrr_2py^{2-}$ ($^{tBu}pyrr_2py^{2-}$ = 2,6-bis((3,5-di*tert*-butyl)pyrrol-2-yl)pyridine), which feature nonlinearly bridged dinitrogen ligands.[358] Dianionic and even tetraanionic species with $Fe(\mu_2\text{-}\eta^1\text{:}\eta^1\text{-}N_2)$ Fe cores were isolated. Spectroscopic and quantum-chemical studies suggest that these compounds contain high-spin Fe(II) centers, even in the case of the tetraanionic species, and reduced ligand scaffolds or dinitrogen units. The chemistry of these species is, therefore, out of the scope of this review.

Lichtenberg, Grützmacher, and co-workers described the synthesis and redox properties of a low-valent anionic $[Fe_4N_4]^-$ heterocubane cluster stabilized by an imido-olefin ligand.[359] Upon reaction between complex $[Fe(NCy_2)_2]$ (**501**) and the H_2Ntrop ligand (trop = 5H-dibenzo[*a*,*d*]cyclohepten-5-yl) at room temperature in toluene, the neutral heterocubane $[Fe_4(Ntrop)_4]$ (**502**) assembles (Scheme 60). Cluster **502** can be reduced by reaction with either Cp^*_2Co or a sodium amalgam to afford $[Cp^*_2Co][Fe_4(Ntrop)_4]$ (**503**) or [Na-

Scheme 60. Formation of Iron/Nitrogen Heterocubane Clusters by Lichtenberg, Grützmacher, and Co-workers[359]

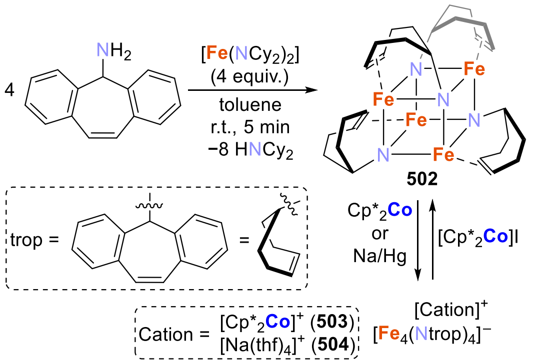

$(thf)_4][Fe_4(Ntrop)_4]$ (**504**), respectively (Scheme 60). Reaction of the anionic $[Fe_4N_4]^-$ cluster with $[Cp^*_2Co]I$ yielded compound **502** again. Cluster **502** has a heterocubane structure in which each iron atom coordinates an olefin of one trop unit in the deprotonated ligand $Ntrop^{2-}$, and the general structural parameters are maintained upon reduction. The neutral cluster **502** possesses a 56-valence-electron Fe_4 unit.

Cyclic voltammetry of **502** (THF, 23 °C) revealed four redox events between −1.72 and −3.59 V (vs Fc/Fc^+) that were assigned to four consecutive formal Fe^{II}/Fe^{I} redox couples and indicate that $[Fe_4N_4]^n$ exists in five different oxidation states (n = 0, 1−, 2−, 3−, 4−). Therefore, the cluster **502** can store up to four electrons. Analysis of the electronic structure of the reduced species revealed that, in the ground state, the unpaired electron is localized predominantly at one iron center and fluctuates with increasing temperatures. Due to the chemical reversibility of the $[Fe_4(Ntrop)_4]/[Fe_4(Ntrop)_4]^-$ couple, the authors evaluated the use of this system as an electron-transfer catalyst for C−C bond couplings.

In 2008, Tejel and de Bruin discovered an exceptional redox asymmetric dinuclear $Rh^{-I}–Rh^{I}$ complex bearing a doubly deprotonated bis(2-picolyl)amine (bpa) scaffold and two norbornadiene (nbd) ligands.[360] The two-electron mixed-valence $Rh^{-I}–Rh^{I}$ complex $[\{Rh(nbd)\}_2(\mu\text{-bpa-2H})]$ (**505**) was obtained by deprotonation of the homovalent $Rh^{I}–Rh^{I}$ compound $[\{Rh(nbd)\}_2(\mu\text{-bpa-1H})]Cl$ (**506**) or by reaction of the dimer $[Rh(nbd)(\mu\text{-OMe})]_2$ (**507**) with bis(2-picolyl)-amine (Scheme 61a). After double deprotonation of bpa, an electronic reorganization takes place, formally reducing Rh(I) to Rh(−I) and oxidizing bpa-2H to the neutral imine $PyCH_2N{=}CHPy$ (Py = pyridine). Species **505** can be seen as a rhodate(−I) anion for which the counterion is the second rhodium atom, formally a Rh(I) center. Indeed, the distinct nature of the two Rh centers was confirmed both in the solid state and in solution. In the molecular structure of **505**, the Rh(−I) atom is in an almost tetrahedral geometry while the Rh(I) center is, typically, square planar. The bridging $PyCH_2N{=}CHPy$ moiety binds to Rh(I) as a σ-imine through the central N donor and to Rh(−I) as η^2-imine, rather than forming a rhoda-aza-cyclopropane.[361] In solution, the nbd bound to Rh(I) is almost static whereas the nbd fragment bound to the tetrahedral Rh(−I) is dynamic, as observed by ^1H NMR spectroscopy. Moreover, EXSY revealed that a 1,3-prototropic shift of one of the methylene protons to the CH$=$N group takes place, suggesting that electrons are pumped from one metal to the other via the ligand, exchanging their formal oxidation state. The authors did not rule out the possibility of having a singlet diradical structure with a monoanionic ligand and $Rh^{0}–Rh^{I}$ centers, as an alternative electronic description for **505**.[360]

Later, the same authors further examined this chemistry by using cod (cod = 1,5-cyclooctadiene) instead of nbd and extending the study to iridium.[364] By mixing $[M(cod)(bpa)]^+$ [M = Rh (**508**), Ir (**509**)] and $[M(cod)(bpa\text{-}2H)]^-$ [M = Rh (**510**), Ir (**511**)], the related complexes $[\{M(cod)\}_2(\mu\text{-bpa-2H})]$ [M = Rh (**512**), Ir (**513**)] were obtained. As with **505**, the related complex **512** can be described as a mixed-valent $Rh^{-I}–Rh^{I}$ species, exhibiting both very similar spectroscopic and structural features. Interestingly, in the case of iridium, the reaction mixture $[Ir(cod)(bpa)]^+$ (**509**) plus $[Ir(cod)(bpa\text{-}2H)]^-$ (**511**) affords the $Ir^{-I}–Ir^{I}$ analogue $[\{Ir(cod)\}_2(\mu\text{-bpa-2H})]$ (**513**) in solution and one equivalent of free bpa, which further reacts with the dinuclear complex via reprotonation and electronic rearrangement to yield the neutral amido mononuclear compound $[Ir(cod)(bpa\text{-}H)]$ (**514**, Scheme 61b).

Scheme 61. Synthesis of a Family of Mixed-Valent (bpa) $M^{-I}–M^{I}$ (M = Rh, Ir; bpa = Bis(2-picolyl)amine) Complexes[360,362−364]

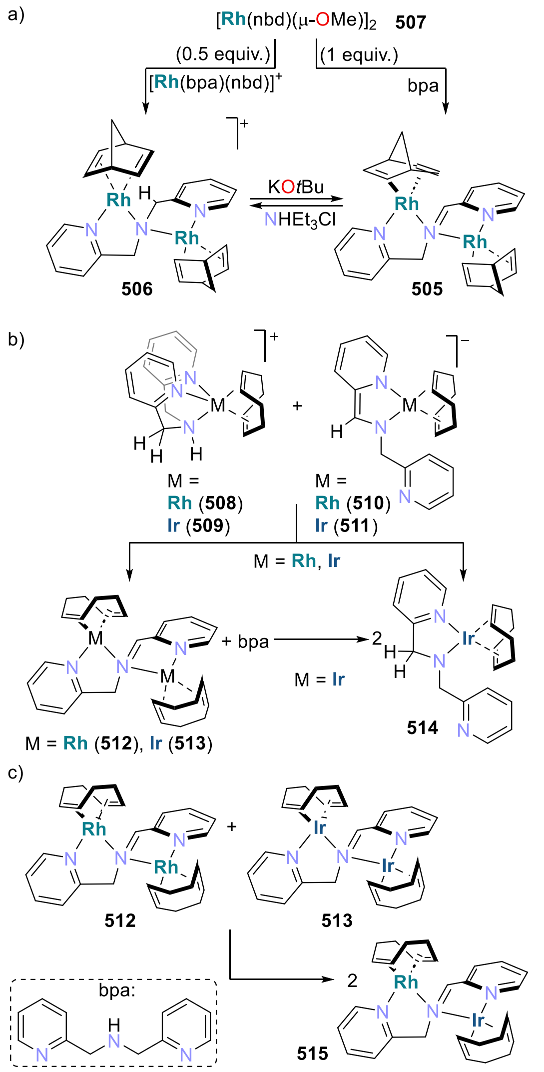

The preparation of the related Rh-amido complex [Rh(cod)(bpa-H)] was unsuccessful and led instead to the mixed-valence species **512** and free bpa. The thermodynamic differences in $[\{M(cod)\}_2(\mu\text{-bpa-2H})]$ [M = Rh (**512**), Ir (**513**)] were explained in terms of the lower stability of the M(−I) oxidation state for iridium as compared to rhodium. This was further evidenced by the fact that the heterodinuclear Rh(−I)−Ir(I) compound $[Rh(cod)(\mu\text{-bpa-2H})Ir(cod)]$ (**515**) can be readily isolated upon metal exchange between **512** and **513**. In **515**, the Rh(−I) center is located in the tetrahedral compartment of the μ-bpa-2H ligand and the Ir(I) atom lies in the square planar compartment (Scheme 61c).

This family of anionic amido-olefin complexes reacts with molecular oxygen resulting in the monooxygenation of the bpa-2H scaffold instead of the diolefins, as would be anticipated.[360,362−364] Another example of mixed-valence Rh species was reported by Goswami and McGrady in 2010 with an azopyridine ligand. This presumed Rh(−I)−Rh(III) complex exhibits a significant rhoda-aza-cyclopropane character; thus, the formal oxidation states appear in fact to lie in between Rh^{I}−Rh^{III} and Rh^{III}−Rh^{III}.[365]

2.2.9. Metalates Featuring β-Diketiminato Ligands.

Bill, Hoffman, Holland, and co-workers reported β-diketiminate-supported iron(I) complexes of relevance to biochemistry.[366,367] Reduction of the iron(II) hydride $[(^{tBu}nacnac)Fe(\mu\text{-}H)]_2$ [**516**, ^{tBu}nacnac = $CH[C(tBu)N(2,6\text{-}iPr_2C_6H_3)]_2$] by a slight excess of KC_8 yielded the dimeric iron(I) hydride $K_2[(^{tBu}nacnac)FeH]_2$ (**517**, see Scheme 62a).[366] Furthermore, sequestration of the potassium cation was effected by chelating agents such as [18]crown-6 and [2.2.2]cryptand to give the monomeric, three-coordinate ion-separated complexes $[K(chelate)][(^{tBu}nacnac)FeH]$ [chelate = [18]crown-6 (**518**), [2.2.2]cryptand (**519**)].

Scheme 62. Synthesis of (a) the Fe(I) Hydride Complex $K_2[(^{tBu}nacnac)FeH]_2$ (517) and (b) the Fe(I) Sulfide Complexes $[AM]_2[\{(^{Me3}nacnac)Fe\}_2(\mu\text{-}S)]$ (521, 522)[366,367]

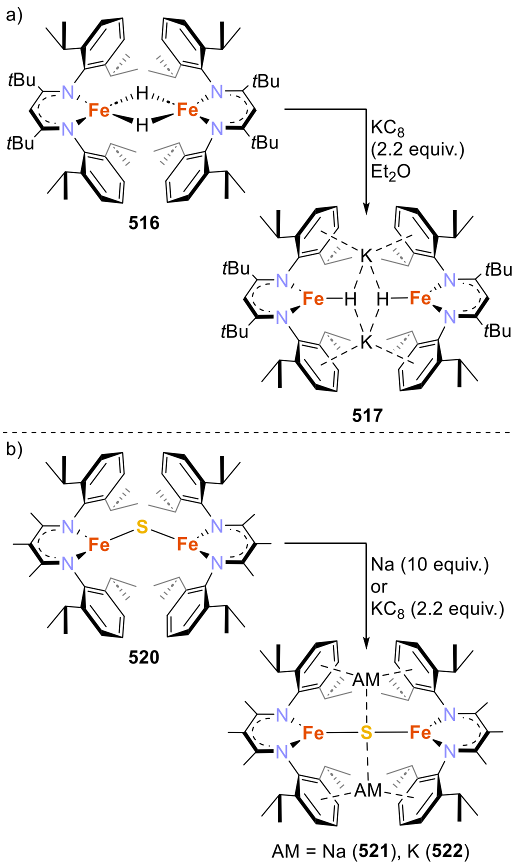

Magnetic measurements, Mössbauer spectroscopy, and DFT calculations of **517**−**519** were consistent with high-spin $S = 3/2$ iron(I) centers in each case. Calculations suggested that π-backbonding into the β-diketiminate assists the ligand in supporting the very electron-rich metal center. The solid-state structures of **518** and **519** each showed a terminal Fe−H moiety, and ENDOR analysis revealed a near-axial anisotropic coupling tensor (**T**) expected for a terminal hydride ligand for **518**. Similar to this hydride example, reduction of the sulfide-bridged diiron(II) complex $[\{(^{Me3}nacnac)Fe\}_2(\mu\text{-}S)]$ [**520**, ^{Me3}nacnac = $MeC[C(Me)N(2,6\text{-}iPr_2C_6H_3)]_2$] by KC_8 or Na afforded the corresponding diiron(I) metalate $[AM]_2[\{(^{Me3}nacnac)Fe\}_2(\mu\text{-}S)]$ [AM = Na (**521**), K (**522**)] (Scheme 62b).[367] The assignment of the Fe(I) oxidation states was supported by crystallography, Mössbauer spectroscopy, magnetic susceptibility measurements, and DFT calculations. The stability of the low-valent iron complex was attributed to steric protection of the Fe−S−Fe core, and favorable interactions of this anionic core with the cations. Unusual linear μ-sulfido bridges were observed in the crystal structures of **521** and **522**, possibly due to geometric restraints from the π-interactions between the cations and aryl groups. The alkali metal cations underwent exchange in solution, with ^1H NMR spectroscopic monitoring of a solution of **521** and **522** revealing the formation of a third species, assigned as the mixed-cation complex.

Arnold and co-workers have extensively studied the synthesis and reactivity of rhenium metalates featuring β-diketiminato ligands.[11,368−372] The anionic Re(I) complex $Na[(\eta^5\text{-}Cp)Re(nacnac)]$ (Na[**523**]; nacnac = *N,N′*-bis(2,6-di*iso*propylphenyl)-3,5-dimethyl-β-diketiminate) displays a rich chemistry which includes, among other reactions, N_2 coordination and trapping and bond formation, as well as serving as a precursor to other metal complexes, including heterometallic compounds. The variety of reactions mediated by **523** is based on its ability to act as a base, nucleophile, or reductant.

The chemistry of this reactive Re(I) β-diketiminate cyclopentadienide and related species was comprehensively reviewed.[11] Therefore, we will only highlight some of the key transformations exerted by either **523** or some of its derivatives. Na[**523**] was obtained by reduction of the oxo rhenium(V) cation $[ORe(\eta^5\text{-}Cp)(nacnac)]^+$ (**524**) with sodium.[368] Protonation of metalate Na[**523**] with $[Et_3NH][BPh_4]$ afforded the terminal hydride $[(\eta^5\text{-}Cp)ReH(nacnac)]$ (**525**, see Scheme 63), whereas its oxidation with AgOTf afforded a rare neutral open-shell Re(II) complex $[(\eta^5\text{-}Cp)Re(nacnac)]$ (**526**).[368] The unsaturated Re(II)-d^5 complex **526** activated H_2, providing a different route to access the terminal hydride **525**, by formal H atom transfer (Scheme 63).[369] In addition, **526** activates P_4 at room temperature to yield a Re(V) species, $[(\eta^5\text{-}Cp)Re(\eta^3\text{-}cyclo\text{-}P_3)(nacnac)]$ (**527**). The reducing character of Na[**523**] was demonstrated with a variety of substrates. For example, Na[**523**] reacted with $ZnCl_2$ to afford the tetranuclear compound $[(\eta^5\text{-}Cp)Re(nacnac)Zn]_2$ (**528**) and **526**.[368] The molecular structure of **528** exhibits a nearly linear Re(I)−Zn(I)−Zn(I)−Re(I) arrangement (173.563(16)°) with a Zn_2^{2+} core flanked by datively bound anionic $[(\eta^5\text{-}Cp)Re(nacnac)]^-$ fragments on each side (Scheme 63). Moreover, by treating Na[**523**] with Me_3SiCl under a nitrogen atmosphere at −78 °C, the Re(III) complex $[(\eta^5\text{-}Cp)Re(nacnac)(N{=}NSiMe_3)]$ (**529**) was obtained (Scheme 63).[371] The structure of **529** features a silyldiazenide ligand, the product of N_2 functionalization at the rhenium metalate Na[**523**]. The authors demonstrated that the N_2 trapping reactivity is highly dependent on ion pairing interactions since a similar silylation using the ion-separated complex $[Na(benzo[12]crown\text{-}4)_2]$[**523**] afforded only small amounts of product. A related outcome was obtained from Na[**523**] and $[MCl(cod)]_2$ [M = Rh (**401**), Ir (**530**)] under a nitrogen atmosphere.[370] The products are heterobimetallic complexes $[(\eta^5\text{-}Cp)Re(\mu\text{-}nacnac)(\mu\text{-}N_2)M(\eta^4\text{-}cod)]$ [M = Rh (**531**), Ir (**532**)] featuring a bridging diazenido ligand end-on coordinated to the rhenium center and the group 9 atom (Scheme 63). The N≡N stretching vibrations [$\nu_{N\equiv N}$(**531**) = 1767 cm^{-1} and $\nu_{N\equiv N}$(**532**) = 1740 cm^{-1}] indicate that the N_2

Scheme 63. Reactivity of the Re(I) Metalate Na[(η^5-Cp)Re(nacnac)] (Na[523])

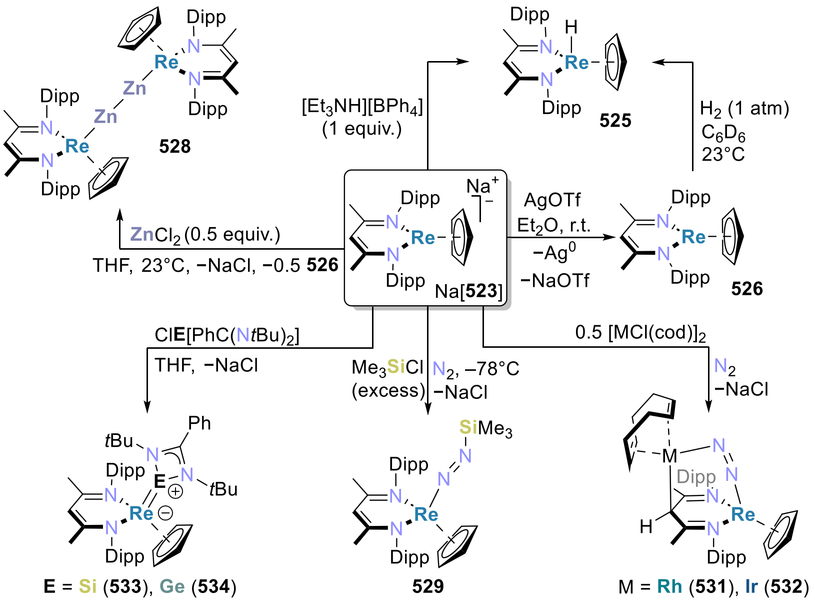

Scheme 64. Synthesis of Anionic Fe-$^{\text{Dipp}}$BIAN Complexes by the Wolf Group[378]

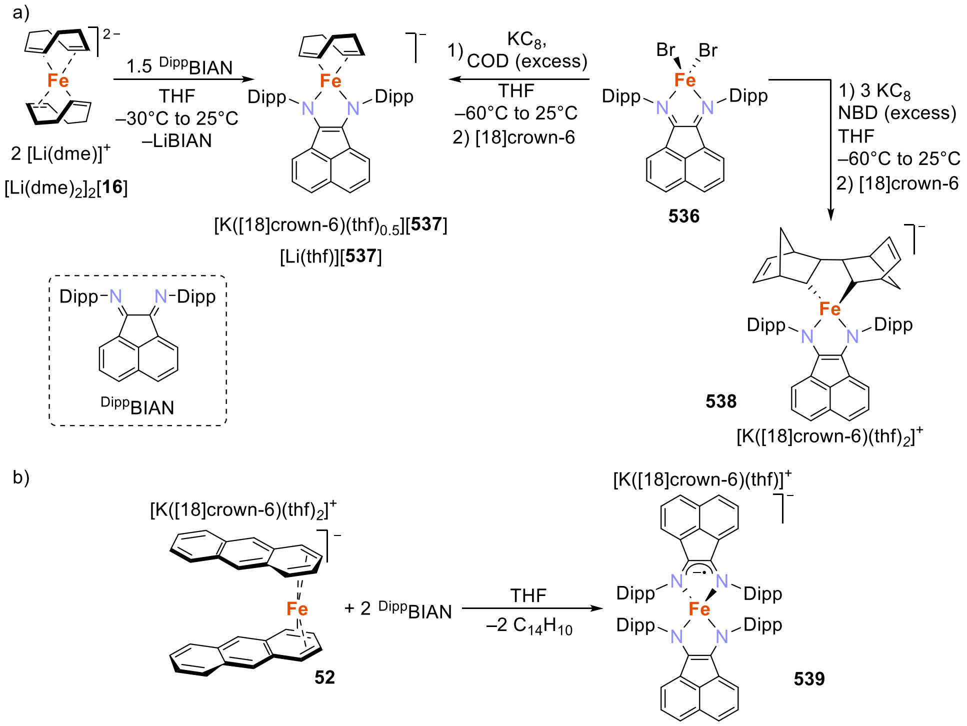

ligand is significantly activated, allowing for its subsequent functionalization. In turn, rhenium metallotetrylenes [(η^5-Cp)Re(E[PhC(N*t*Bu)$_2$])(nacnac)] [E = Si (533), Ge (534), Sn (535); Scheme 63 shows the Si and Ge derivatives] were obtained by salt metathesis between Na[523] and amidinate-supported tetrylenes, ClE[PhC(N*t*Bu)$_2$].[372] For the silicon and germanium analogues, the reaction yielded complexes with short Re−E multiple bonds, as a result of π-interactions with the tetrel atoms. By contrast, the tin derivative has a Re−Sn single bond formed by σ-donation to the Re atom, in a σ-metallotetrylene arrangement, and retains its electron lone pair.

2.2.10. Redox-Active Diimine Scaffolds.

Diimine ligands are redox-active *N,N′*-donors with a N═C−C═N backbone. This class of ligands includes various diimine scaffolds, e.g., bis(imino-acenaphthene) (BIAN), *o*-benzoquinonediimine (1,2-phenylenediamine dianion), 2,2′-bipyridine, 1,4-diazabutadiene, and imino-pyridine.[373] The chemistry of BIAN ligands and their use in metal-catalyzed reactions have been recently reviewed.[374] The interest in this type of ligands, particularly in combination with low-valent iron, is reflected by a large number of contributions.[375−383] Nonetheless, although there have been numerous contributions to the field in recent years, only selected examples have resulted in the formation of anionic complexes.

2.2.10.1. α-Diimine Ligands. Wolf and co-workers described the synthesis and characterization of anionic BIAN-iron complexes, which were used as precatalysts in hydroboration reactions.[378] Reduction of the [(^{Dipp}BIAN)-FeBr$_2$] (**536**, ^{Dipp}BIAN = 1,2-bis(2,6-diisopropylphenylimino)-acenaphthene) precursor by stoichiometric KC$_8$ in the presence of cod afforded [K([18]crown-6)(thf)$_{0.5}$]-[(^{Dipp}BIAN)Fe(η^4-cod)] ([K([18]crown-6)(thf)$_{0.5}$][**537**], see Scheme 64a). A similar complex [Li(thf)(^{Dipp}BIAN)Fe(η^4-cod)] (Li[**537**]) is also accessible by ligand exchange from the formally Fe(−II) homoleptic complex [Li(dme)$_2$]$_2$[Fe(cod)$_2$] ([Li(dme)$_2$]$_2$[**16**], Scheme 64a), albeit in lower yield. The mechanism of the latter reaction, which involves an oxidation of the Fe complex [Li(dme)$_2$]$_2$[**16**] by one electron, is not well-understood. An analysis of the X-ray structural data for Li[**537**] suggests the presence of a dianionic ^{Dipp}BIAN^{2-} ligand as indicated by the metric data of the ^{Dipp}BIAN moiety. Elongated C−N [1.385(4) Å] and shortened C−C [1.388(5) Å] bond lengths are observed in comparison with the free ^{Dipp}BIAN molecule and its alkali metal salts (cf. C−N 1.39 Å and C−C 1.40 Å, respectively, for Na$_2$[^{Dipp}BIAN]).[373,384] The proposed presence of a doubly negatively charged ^{Dipp}BIAN^{2-} ligand implies an oxidation state of +I with a d^7 configuration for the Fe atom. Attempts to synthesize a 2,5-norbonadiene (NBD) analogue of **537** by the same reduction pathway from **536** were unsuccessful. Instead, the isolated compound [K([18]crown-6)(thf)$_2$][(^{Dipp}BIAN)Fe(C$_{14}$H$_{16}$)] (**538**, C$_{14}$H$_{16}$ = 2,2′-bi(bicyclo[2.2.1]heptane-5,5′-diene-3,3′-diyl) contains a bis(norbornenediyl) ligand derived from the C−C coupling of two nobornadiene molecules (Scheme 64a, bottom right). Additionally, the bis(anthracene)ferrate(−I) complex **52** reacted with DippBIAN to give only the homoleptic compound [K([18]crown-6)(thf)$_2$][Fe(^{Dipp}BIAN)$_2$]^{Dipp}BIAN the homoleptic compound [K([18]crown-6)(thf)][Fe-(^{Dipp}BIAN)$_2$] (**539**) regardless of the metal-to-ligand ratio used (Scheme 64b). All the complexes were structurally characterized, and their physical and electronic properties were analyzed by spectroscopic methods (NMR, EPR, ^{57}Fe Mössbauer, UV−vis), magnetic susceptibility measurements, and theoretical calculations (DFT, CASSCF). These data provided evidence to conclude that complex salts of **537** have a low-spin ground state, while complex **538** features an intermediate-spin Fe(III) center, and complex **539** is an Fe(II) species in a quartet ground state. Complexes **537**−**539** were evaluated as precatalysts in hydroboration reactions; these results are discussed in section 3.1.6.[378]

Heteroleptic cobaltate complexes, bearing α-diimine and alkene/arene ligands, were also described.[385−389] Using the Co$^-$ source [K(thf)][Co(η^4-cod)$_2$] (**239**), Wolf and co-workers synthesized the [K(OEt$_2$){Co(^{Ar}BIAN)(η^4-1,5-cod)}] [^{Ar}BIAN: ^{Dipp}BIAN = 1,2-bis(2,6-diisopropyl-phenylimino)acenaphthene (**540**), ^{Mes}BIAN = 1,2-bis(2,4,6-dimethylphenylimino)acenaphthene (**541**); 1,5-cod = 1,5-cyclooctadiene][385,386] and [K([18]crown-6)(thf)$_{1.5}$][Co-(PHDI)(η^4-1,5-cod)] [**542**, PHDI = bis(2,6-diisopropyl-phenyl)phenanthrene-9,10-diimine)][387] (see Scheme 65), which are closely related to **537** discussed earlier. Again, X-ray diffraction analysis suggested the presence of BIAN^{2-} ligands in **540** and **541** [av. C−N 1.381 Å (**540**), 1.374 Å (**541**); C−C 1.383(3) Å (**540**), 1.377(5) Å (**541**)]

Scheme 65. Synthesis of α-Diimine Cobaltates by the Wolf Group[385−387]

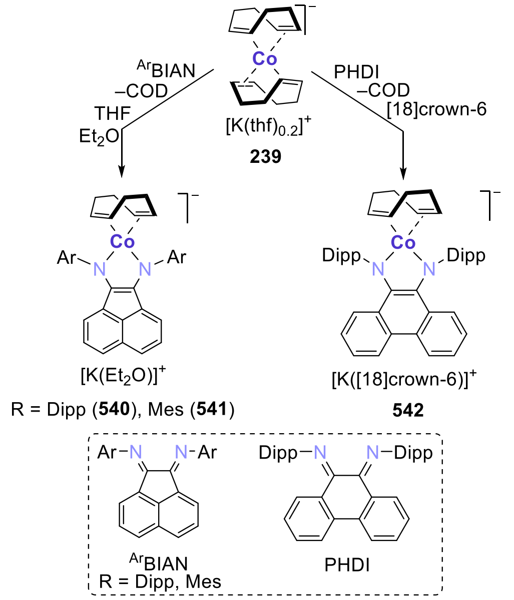

The related phenanthrene-9,10-diimine complex **542** was not crystallographically characterized, though the ^{1}H and ^{13}C NMR data compared well with those of the ^{Dipp}BIAN complex **540**.[387] This observation contrasts with those for the previously reported complex [Ni(^{Dipp}BIAN)(η^4-1,5-cod)] (**543**), which is isoelectronic with **537** and **540**.[390] Nonetheless, the structural data indicate the presence of a BIAN$^-$ ligand. The presence of a more reduced BIAN^{2-} ligand in **537** and **540** may be attributed to the lower effective nuclear charge of iron and cobalt in comparison with nickel.[385] Catalytic applications of complexes **540** and **541** are described in section 3.1.

Reactivity studies of the diimine cobaltates **540** and **541** revealed that the BIAN ligand mostly serves as a spectator ligand, whereas the cyclooctadiene ligand is readily displaced by other molecules.[385,391] For instance, the reaction of [K(thf){Co(^{Mes}BIAN)(η^4-1,5-cod)}] (**541**) and 1,2-bis-(diphenylphosphino)-*ortho*carborane (**544**) affords a 13-vertex *closo*-cobaltacarborane cluster compound **545** (Scheme 66). The product is a result of substitution of the 1,5-cod ligand and

Scheme 66. Synthesis of the Anionic 13-Vertex Closo-cobaltacarborane Cluster 545 from the (BIAN)cobaltate 541[391]

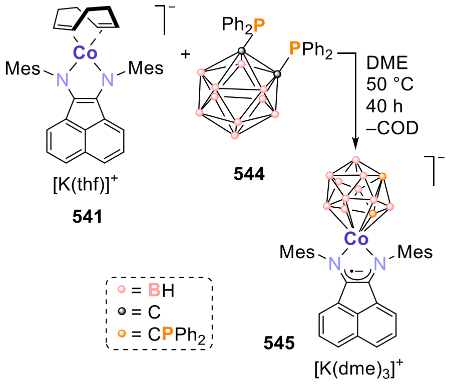

Scheme 67. Reduction of Complexes [LFe(CO)$_2$] (L = PDI, P$^{\text{Pym}}$DI, P$^{\text{Pz}}$DI; top) and [($^{\text{Ad}}$P$^{\text{Pym}}$DI)Fe(N$_2$)] (bottom)[138,392,393,404]

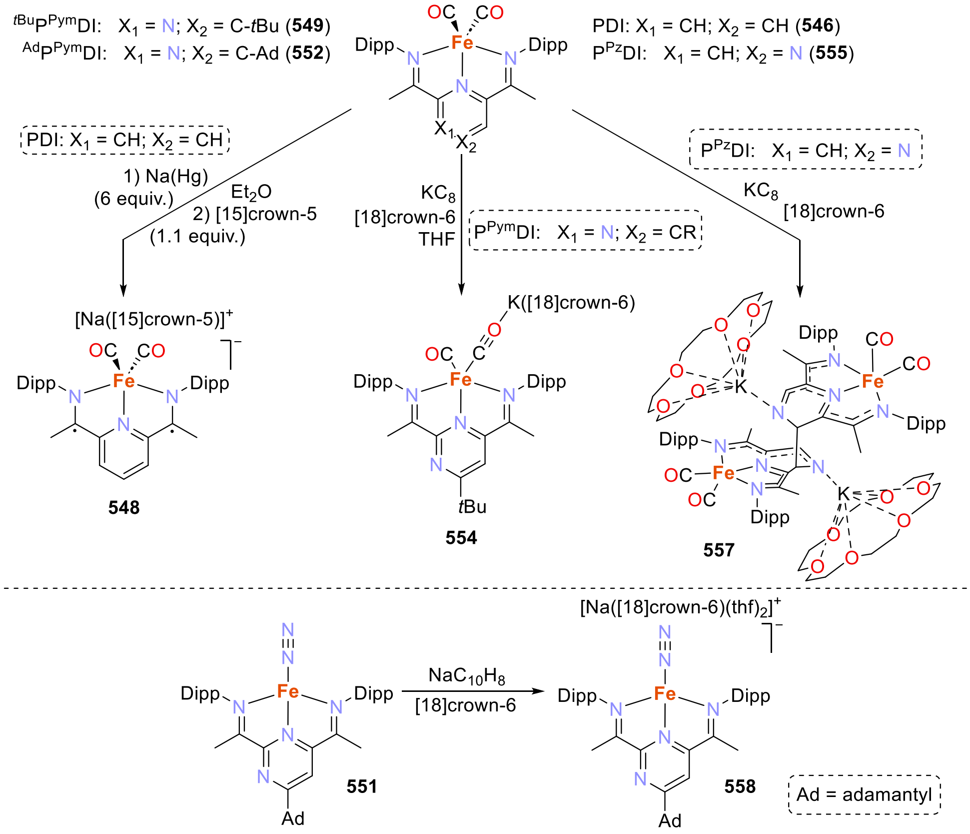

subsequent polyhedral expansion of the carborane framework. In the solid-state molecular structure, the 13-vertex cobaltacarborane cluster anion forms as a contact ion pair with the [K(dme)$_3$]$^+$ counterion. Shorter C−N (av. 1.332(2) Å) and C−C distances (1.420(2) Å) in the BIAN ligand framework with respect to **540** and **541** indicate the presence of a monoanionic BIAN$^-$ ligand in **545**. This notion is supported by DFT molecular orbital analysis of the complex. DFT calculations, the crystallization of intermediates and spectroscopic observations (specifically ^{31}P{^{1}H} NMR reaction monitoring and ESI-MS studies), enabled the authors to propose a mechanism for the formation of **545**. An initial electron transfer from **541** to **544** is followed by coordination of the resulting dianion **544**$^{2-}$ to the cobalt center. Oxidation and isomerization of the resulting complex gives **545**.[391]

2.2.10.2. Pyridine-diimine Ligands. Chirik and Roşca independently reported anionic iron complexes with pyridine-diimines (PDIs) and closely related pyrimidine and pyrazinediimines.[138,392,393] Cyclic voltammetry of the previously reported [($^{\text{Dipp}}$PDI)Fe(CO)$_2$] (**546**)[394] showed reversible one-electron oxidation and reduction events.[138] The accessibility of these products was later confirmed by the preparation of the cationic compound [($^{\text{Dipp}}$PDI)Fe(CO)$_2$]-[BAr$^{\text{F}}_4$] (**547**), obtained by oxidation of **546** with [Cp$_2$Fe]-[BAr$^{\text{F}}_4$], and of the anionic complex [Na([15]crown-5)]-[($^{\text{Dipp}}$PDI)Fe(CO)$_2$] (**548**, Scheme 67), synthesized by reduction of **546** with 0.5% Na(Hg) in the presence of [15]crown-5 (1.2 equiv, Scheme 67). Complex **548** is highly air-sensitive and prone to thermal decomposition. FT-IR spectroscopy showed two carbonyl stretching bands (ν_{CO} = 1935 and 1863 cm^{-1}) at lower wavenumbers in comparison with **546** (ν_{CO} = 1974 and 1914 cm^{-1}). These data are consistent with the expected increase in electron density at the reduced iron center. DFT calculations indicated that the anionic complex **548** features a strongly reduced, diradical dianionic bis(imino)pyridine ligand[395] and is thus best described as a low-spin Fe(I) complex with a high degree of covalency.[138]

By synthesizing carbonyl complexes analogous to **546** featuring either the pyrimidine- [$^{\text{R}}$P$^{\text{Pym}}$DI: R = *tert*-butyl (*t*Bu), adamantyl (Ad)] or pyrazine-based (P$^{\text{Pz}}$DI) ligands, Roşca and co-workers demonstrated that the redox potentials of such complexes reflect the differences in π-acidity of the central heterocycle of the ligand.[393] Compound [($^{t\text{Bu}}$P$^{\text{Pym}}$DI)-Fe(CO)$_2$] (**549**) was obtained from the free $^{t\text{Bu}}$P$^{\text{Pym}}$DI ligand and Fe(bda)(CO)$_3$ (**550**, bda = benzylideneacetone), whereas displacement of the dinitrogen ligand in [($^{\text{Ad}}$P$^{\text{Pym}}$DI)Fe(N$_2$)] (**551**) by carbon monoxide generates the adamantyl-substituted compound [($^{\text{Ad}}$P$^{\text{Pym}}$DI)Fe(CO)$_2$] (**552**). Similar to the previous report on **546** (*vide supra*),[138] **549** can also be chemically oxidized with [Cp$_2$Fe][BAr$^{\text{F}}_4$], yielding [($^{t\text{Bu}}$P$^{\text{Pym}}$DI)Fe(CO)$_2$][BAr$^{\text{F}}_4$] (**553**). Likewise, reduction of **549** with KC$_8$ in the presence of [18]crown-6 affords [K([18]crown-6)][($^{t\text{Bu}}$P$^{\text{Pym}}$DI)Fe(CO)$_2$] (**554**) (see Scheme 67, top).[393] Magnetic susceptibility measurements performed in solution with the Evans NMR method indicate that a one-electron reduction process has occurred (doublet state, $S = 1/2$, μ_{eff} = 1.7 μB). Similar synthetic protocols were used in an attempt to obtain the oxidized and reduced derivatives of the P$^{\text{Pz}}$DI complex [(P$^{\text{Pz}}$DI)Fe(CO)$_2$] (**555**). However, whereas a metal-centered oxidation led to [(P$^{\text{Pz}}$DI)Fe(CO)$_2$][BAr$^{\text{F}}_4$] (**556**),[392] the reduction of **555** with KC$_8$ in the presence of

[18]crown-6 afforded a ligand-based radical which dimerizes to form a dinuclear compound, **557**, with an additional C−C bond (see Scheme 67). In fact, the one-electron reduction of the three complexes $[\mathrm{LFe(CO)_2}]$ (**546**, **549**, and **555**, L = PDI, ${}^{\mathrm{R}}\mathrm{P}^{\mathrm{Pym}}\mathrm{DI}$, and $\mathrm{P}^{\mathrm{Pz}}\mathrm{DI}$, respectively) is ligand-based in each case, irrespective of the nature of the heterocyclic support. By contrast, one-electron oxidation is a metal-centered process, affording a metalloradical.[138,393] Contrasting behavior was observed for the reduction of the dicarbonyl complex $[({}^{\mathrm{Ad}}\mathrm{P}^{\mathrm{Pym}}\mathrm{DI})\mathrm{Fe(CO)_2}]$ (**552**) and that of the related dinitrogen complex $[({}^{\mathrm{Ad}}\mathrm{P}^{\mathrm{Pym}}\mathrm{DI})\mathrm{Fe(N_2)}]$ (**551**). While in both cases the one-electron reduction is ligand-based, for **552** a doubly reduced ligand state is preferred, initiating a metal-to-ligand electron transfer, which results in an Fe(I) center which is antiferromagnetically coupled with a ${}^{\mathrm{Ad}}\mathrm{P}^{\mathrm{Pym}}\mathrm{DI}^{2-}$ diradical. Reduction of **551** affords the anionic complex $[\mathrm{Na([18]crown\text{-}6)(thf)_2}][({}^{\mathrm{Ad}}\mathrm{P}^{\mathrm{Pym}}\mathrm{DI})\mathrm{Fe(N_2)}]$ (**558**, Scheme 67, bottom), in which the ${}^{\mathrm{Ad}}\mathrm{P}^{\mathrm{Pym}}\mathrm{DI}$ ligand stores three electrons, while the metal center appears to attain an Fe(II) oxidation state. This example illustrates the striking redox non-innocent behavior of the ${}^{\mathrm{Ad}}\mathrm{P}^{\mathrm{Pym}}\mathrm{DI}$ ligand.[393]

Chirik and co-workers reported additional examples of anionic manganese, iron, or cobalt complexes featuring PDI ligands.[138,396−402] The complexes $[({}^{\mathrm{Dipp}}\mathrm{PDI})\mathrm{Mn(CO)_2}]^-$ (**559**), $[({}^{\mathrm{Dipp}}\mathrm{PDI})\mathrm{Co(N_2)}]^-$ (**560**), and $[({}^{i\mathrm{Pr}}\mathrm{APDI})\mathrm{Co(N_2)}]^-$ (**561**) were synthesized by reduction of the appropriate neutral precursors with either sodium amalgam or sodium naphthalenide.[397−399] According to an analysis of the metric parameters, **559**−**561** feature dianionic PDI ligands (Figure 11). The electronic structures of **559**−**561** differ from that in $[({}^{\mathrm{Dipp}}\mathrm{PDI})\mathrm{Fe(CO)_2}]^-$ (**548**),[138] in which the ligand was reduced to the diradical dianionic form.[395] Further examples of anionic complexes are the alkyl- and aryl-substituted compounds $[({}^{\mathrm{Dipp}}\mathrm{PDI})\mathrm{Fe(N_2)(CH_2CMe_3)}]^-$ (**562**), $[({}^{\mathrm{Dipp}}\mathrm{PDI})\mathrm{Fe(N_2)}(p\text{-}\mathrm{C_6H_4\text{-}R})]^-$ [R = H (**563**), Me (**564**)], which feature ferrous metal centers and doubly reduced PDI scaffolds.[400,401] **562**−**564** are reminiscent of the previously reported bis(imino)pyridine iron methyl complex, $[\mathrm{Li(thf)_4}][({}^{\mathrm{Dipp}}\mathrm{PDI})\mathrm{FeMe}]$ (**565**) by Gambarotta and co-workers.[403]

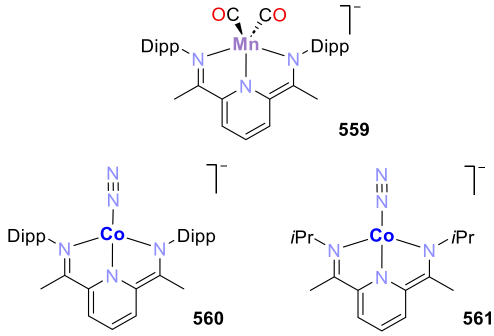

Figure 11. Anionic manganese or cobalt complexes featuring reduced PDI ligands.[397−399]

Gambarotta and Budzelaar investigated the reduction of PDI-iron dinitrogen complexes.[405] The reaction of the Fe(II) complex $[({}^{\mathrm{Dipp}}\mathrm{PDI})\mathrm{FeCl_2}]$ (**566**) with 3 equiv of NaH formed the ion-paired species $[\mathrm{Na(thf)}({}^{\mathrm{Dipp}}\mathrm{PDI\text{-}H})\mathrm{Fe(N_2)}]$ ([Na(thf)][**567**]), in which one methyl group from the PDI backbone is deprotonated (Scheme 68a). Increasing the relative amount of reductant led to mixtures of products. By reaction between **566** and either sodium or sodium hydride, a species equivalent to [Na(thf)][**567**] with different pairing interactions ($[\mathrm{Na(OEt_2)_3}]$[**567**]) was obtained along with the more reduced product $[({}^{\mathrm{Dipp}}\mathrm{PDI})\mathrm{Fe}(\mu\text{-}\mathrm{N_2})\mathrm{Na\{Na(thf)_2\}}]$ (**568**), in which the ligand remained neutral (Scheme 68a). Further increasing the amount of NaH to 2 equiv yielded another mixture of products, consisting of the neutral deprotonated compound $[({}^{\mathrm{Dipp}}\mathrm{PDI\text{-}H})\mathrm{Fe(N_2)}]$ (**569**), proposed to be the precursor of **567**, and the dinuclear $[\{({}^{\mathrm{Dipp}}\mathrm{PDI})\mathrm{Fe}(\mu\text{-}\mathrm{N_2})\}_2\mathrm{Na\{Na(thf)_2\}_2}]$ (**570**, Scheme 68a). Complexes **567**−**570** were characterized by X-ray crystallography, IR spectroscopy, elemental analysis, and the determination of their magnetic moments in solution. More detailed spectroscopic characterization is required to further substantiate their structural and bonding characteristics.

Scheme 68. Reduction of (PDI)Fe-Dinitrogen Complexes by Gambarotta and Chirik[402,405]

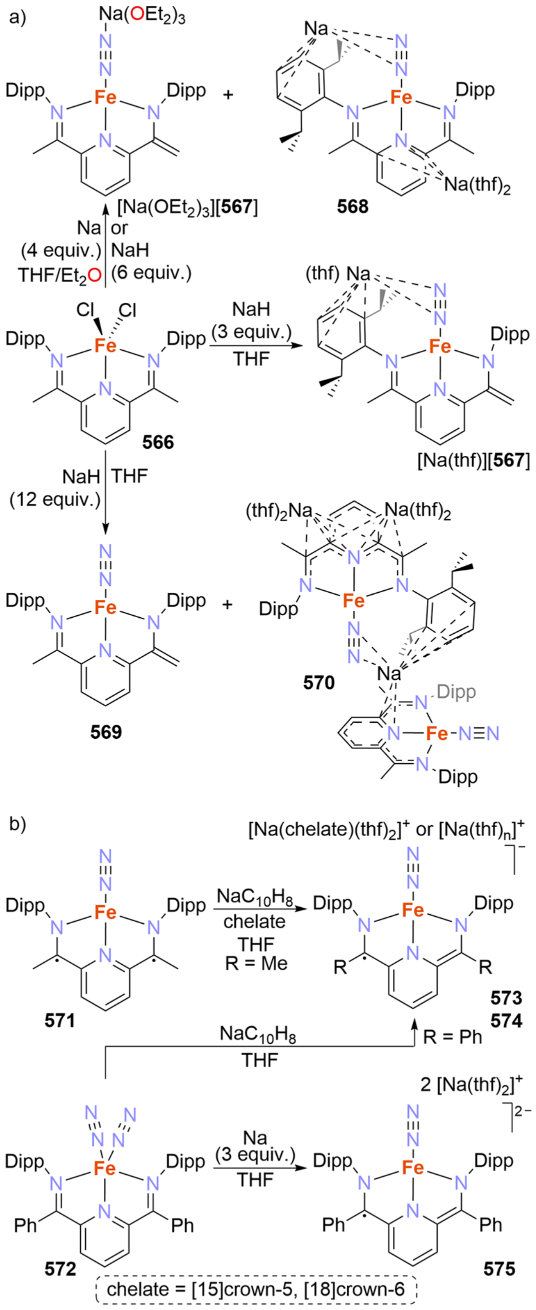

Scheme 69. Synthesis of Low-Valent (a) trop$_2$dad- and (b) trop$_2$dae-Iron Complexes by the Group of Grützmacher and Lichtenberg[381−383]

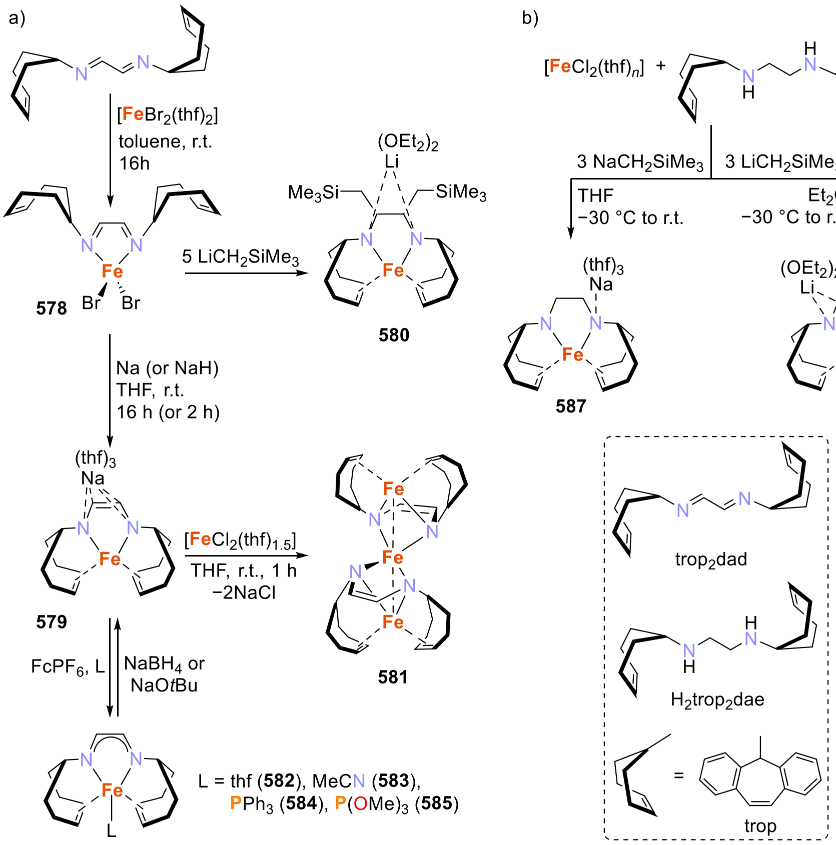

Complexes **567−570** feature only slightly activated dinitrogen ligands according to the stretching vibrations ($\nu_{\text{N}\equiv\text{N}}$ = 1868−2159 cm^{-1}), with the most weakened N≡N motifs present in the complexes with the highest degree of reduction, i.e., **568** (1899 cm^{-1}) and **570** (1868 cm^{-1}). Complex **568** was regarded as featuring an iron center in the negative divalent state. In general, it was concluded that the reduction processes affected *mainly* the metal center, and only to some extent the ligand scaffold.

Indeed, the Chirik group found evidence of the reduction of the PDI scaffold at iron-dinitrogen complexes up to a trianionic state.[402] To avoid ion pairing interactions like those reported by Gambarotta and Budzelaar,[405] the reduction reactions were carried out in the presence of sequestering agents ([15]crown-5 or [18]crown-6). Reduction of neutral compound [($^{\text{Dipp}}$PDI)Fe(N$_2$)] (**571**) and the phenyl-substituted analogue [($^{\text{Dipp}}$BPDI)Fe(N$_2$)$_2$] (**572**, BPDI = 2,6-(2,6-*i*Pr$_2$−C$_6$H$_3$N=CPh)$_2$C$_5$H$_3$N) by sodium naphthalenide afforded the salts [Na(chelate)(thf)$_2$][($^{\text{Dipp}}$PDI)Fe(N$_2$)] (**573**, chelate = [15]crown-5, [18]crown-6) and [Na(thf)$_n$]-[($^{\text{Dipp}}$BPDI)Fe(N$_2$)] (**574**, Scheme 68b). In both cases, the reduction events were ligand-based, and the electronic configuration of **573** and **574** was described as featuring intermediate spin ferrous centers, i.e., [(PDI^{3-})Fe$^{\text{II}}$N$_2$]$^-$. The phenyl-substituted compound **574** underwent further reduction, yielding the dianionic complex [Na(thf)$_2$]$_2$[($^{\text{Dipp}}$BPDI)-Fe(N$_2$)] (**575**, Scheme 68b). In this case, reduction is a metal-based process. The ligand framework in **575** remains in the trianionic state, while the intermediate-spin ferrous center was reduced to a low-spin Fe(I). Thus, three ligand-based electron transfer events occur upon reduction in the series of complexes, before the metal atom engages in redox chemistry.

2.2.10.3. Bipyridine Ligands. Bipyridine ligands are well-known to be particularly susceptible to redox activity in metal complexes. In his 2006 review, Ellis comments on the exclusion of various anionic bipyridine complexes of the form [M(bpy)$_3$]$^{n-}$ from the discussion, where metal centers had originally been assigned negative oxidation states.[2] These assessments were rendered erroneous by subsequent characterization that identified dianionic bipyridine ligands as responsible for the anionic character of the complexes.[271] In more recent years, experimental and computational investigations into the electronic structures of anionic bipyridine complexes have been reported,[347,348] notably by Wieghardt and co-workers.[349−352] For instance, in 2015, the Wieghardt group used a combination of X-ray crystallographic data, UV−vis spectroscopy, magnetochemistry, and broken-symmetry density functional theory to study the electronic structures of all the redox states of the bis- and tris-substituted 2,2′-bipyridine-nickel complexes, including anionic species.[352] [Ni(bpy)$_2$] (**576**) was also prepared according to modified literature methods and its crystal structure determined for comparison.[406,407] Cyclic voltammetry of the neutral complex [Ni(bpy)$_2$] (**576**) proved that its reduction to the monoanionic species [Ni(bpy)$_2$]$^-$ (**576**$^-$), and even to the dianionic [Ni(bpy)$_2$]$^{2-}$ (**576**$^{2-}$), was possible. The structures of the reduced anionic species were optimized using DFT. After analysis of the experimental and theoretical data, it was concluded that the reductions are ligand-centered, and therefore, the nickel atom in none of these complexes is in the Ni(0) oxidation state or lower. The anionic species $[\mathrm{Ni(bpy)_2}]^-$ features two identical π-radical anions and can be more accurately described as $[\mathrm{Ni^I(bpy^{\bullet-})_2}]^-$, i.e., a Ni(I) ($d^9$) complex with three unpaired electrons which are antiferromagnetically coupled with the ligand radicals. As a result, an $S = 1/2$ ground state is observed. Likewise, the tris(bipyridine) complex $[\mathrm{Ni(bpy)_3}]^-$ (**577**$^-$) was formulated as $[\mathrm{Ni^{II}(bpy^{\bullet-})_3}]^-$.[352]

Like in the previous example, detailed analyses of the contributions of Wieghardt and co-workers generally led to the conclusion that reduction events tend to occur at the bipyridine ligands.[349−352] Thus, the complexes feature metal centers retaining common oxidation states ($\mathrm{Fe^{II}}$, $\mathrm{Zn^{II}}$, $\mathrm{Cr^{III}}$, $\mathrm{V^{II}}$, etc.).[349−351] A similar phenomenon had been observed within the series of "anionic" iron-substituted bpy complexes $[\mathrm{Fe(^Rbpy)_3}]^-$ (**186**, *vide supra*),[203−206] and with the cobalt compound $[\mathrm{Co(bpy^{\bullet-})}(\eta^4\text{-cod})]^-$ (**261**).[87] Other examples[349−351] will not be subject to discussion in this present review due to its focus on metalates featuring low-valent metal centers.

2.2.10.4. Diazadiene Ligands. Grützmacher and Lichtenberg have developed iron systems featuring diolefin-diazadiene ligands such as $\mathrm{trop_2dad}$ (trop = 5*H*-dibenzo-[*a*,*d*]cyclohepten-5-yl, dad = diazadiene) and its saturated analogue $\mathrm{trop_2dae}$ (dae = $\mathrm{N{-}CH_2{-}CH_2{-}N}$; Scheme 69).[381−383] Reaction of the $\mathrm{trop_2dad}$ ligand with a suitable Fe(II) precursor, $[\mathrm{FeBr_2(thf)_2}]$ (Scheme 69a), affords the mononuclear Fe(II) compound $[\mathrm{FeBr_2(trop_2dad)}]$ (**578**), which can be reduced by sodium or sodium hydride to yield the ferrate(I) complex $[\mathrm{Na(thf)_3\{Fe(trop_2dad)\}}]$ (**579**).[381] Likewise, attempts to generate metal alkyl complexes by reaction of **578** with $\mathrm{LiCH_2SiMe_3}$ resulted in nucleophilic attack on the imine moieties with reduction of the metal center, yielding the low spin Fe(I) complex **580**.[382]

The crystallographic characterization of **579** indicates that the ligand is present as a diazadiene dianion $(\mathrm{trop_2dad})^{2-}$, featuring a short C−C bond distance (1.368(3) Å) and two elongated C−N bonds (N−C 1.384(3) and 1.375(3) Å),[408] and shows the formation of a contact ion pair with the cation $\mathrm{Na(thf)_3}^+$. Compound **579** was used as a building block, in a 2:1 ratio with $[\mathrm{FeCl_2(thf)_{1.5}}]$, to form the trinuclear iron cluster $[\mathrm{Fe_3(trop_2dad)_2}]$ (**581**, Scheme 69a). X-ray diffraction analysis performed on single crystals of **581** showed that the three iron centers are in an almost perfect linear arrangement through metal−metal bonds (Fe−Fe 2.6340(8)−2.6410(8) Å). ^{57}Fe Mössbauer spectroscopy and magnetic susceptibility measurements along with the X-ray crystallographic data suggest that the terminal Fe atoms are in a low spin Fe(I) state, while the central metal atom of the $\mathrm{Fe_3}$ chain appears to be in a high-spin Fe(II) state.[381] Oxidation of **579** with ferrocenium hexafluorophosphate ($\mathrm{FcPF_6}$; Scheme 69a, bottom) in the presence of a donor ligand L afforded the five-coordinate species $[\mathrm{Fe(trop_2dad)(L)}]$ [L = thf (**582**), MeCN (**583**), $\mathrm{PPh_3}$ (**584**), $\mathrm{P(OMe)_3}$ (**585**)]. Conversely, reaction of compounds **582**−**585** with the mild reducing agents $\mathrm{NaBH_4}$ or NaO*t*Bu regenerates compound **579**, illustrating the chemical reversibility of the oxidation reaction (Scheme 69a).[382] By comparing the X-ray structural data of **582**−**585** with that of **578**, bearing a neutral $\mathrm{trop_2dad}$ ligand, and that of the parent compound **579**, featuring a dianionic (fully reduced) $(\mathrm{trop_2dad})^{2-}$ moiety,[381] it was concluded that all of the complexes **582**−**585** contain monoanionic radical $(\mathrm{trop_2dad})^{\bullet-}$ ligands. The electronic structures of these compounds are thus best described as open shell singlets with the metal center in a low spin Fe(I) oxidation state which is antiferromagnetically coupled to the monoanionic ligand radical. This is corroborated by DFT calculations, ^{57}Fe Mössbauer spectroscopy, and magnetic susceptibility measurements. Therefore, the oxidation of **579** is a ligand-centered process, where one electron is removed from the redox-active ligand.

The chemically noninnocent ligand $\mathrm{trop_2dae}$ is the hydrogenation product of $\mathrm{trop_2dad}$.[409] Coordination studies show that $\mathrm{trop_2dae}$ is also able to stabilize low-valent Fe complexes. Ferrates $[\mathrm{M(solv)}_n\{\mathrm{Fe(trop_2dae)}\}]$ [M = Li, solv = $\mathrm{Et_2O}$, $n = 2$ (**586**); M = Na, solv = thf, $n = 3$ (**587**); Scheme 69b] were synthesized from $[\mathrm{FeCl_2(thf)}_n]$ and $\mathrm{trop_2dae}$ in the presence of $\mathrm{MCH_2SiMe_3}$, which acts both as a base and as a reductant. Subtle structural differences were observed in the molecular structures of the lithium and the sodium salt. Both complexes present a distorted planar coordination geometry about the iron center; whereas in **587**, the sodium cation is asymmetrically coordinated to the $\mathrm{trop_2dae}$ unit, in **586**, the lithium cation coordinates both nitrogen atoms. ^{57}Fe Mössbauer spectroscopy revealed a higher electron density in the Fe s orbitals for **587**, which is in line with $\mathrm{Li^+}$ acting as a stronger Lewis acid.

A series of (α-diimine)(polyarene)cobalt complexes with the ligand *N*,*N*′-bis(2,6-diisopropylphenyl)butane-2,3-diimine ($^{\mathrm{Dipp2}}$dmdad) was described by Yang and co-workers in 2015.[389] This series included neutral complexes $[(^{\mathrm{Dipp2}}\mathrm{dmdad})\mathrm{Co}(\eta^4\text{-anthracene})]$ (**588**), $[(^{\mathrm{Dipp2}}\mathrm{dmdad})\mathrm{Co}(\mu{-}\eta^4{:}\eta^4\text{-naphthalene})\mathrm{Co}(^{\mathrm{Dipp2}}\mathrm{dmdad})]$ (**589**), and $[(^{\mathrm{Dipp2}}\mathrm{dmdad})\mathrm{Co}(\mu{-}\eta^4{:}\eta^4\text{-phenanthrene})\mathrm{Co}(^{\mathrm{Dipp2}}\mathrm{dmdad})]$ (**590**) and the anionic species $[\{\mathrm{Na_2(Et_2O)_2}\}\{(^{\mathrm{Dipp2}}\mathrm{dmdad})\mathrm{Co}(\mu{-}\eta^3{:}\eta^3\text{-pyrene})\mathrm{Co}(^{\mathrm{Dipp2}}\mathrm{dmdad})\}]$ (**591**) and $[\{\mathrm{Na_2(Et_2O)_3}\}\{(^{\mathrm{Dipp2}}\mathrm{dmdad})\mathrm{Co}(\eta^3\text{-pyrene})\}]$ (**592**). All of those compounds have three potential redox-active sites: the metal center, the α-diimine ligand, and the polyarene moiety.

The dinuclear complexes **589** and **590** bear some analogy to anthracene- and naphthalene-bridged bis(cyclopentadienyliron) compounds previously described by the groups of Wolf and Tatsumi (see Scheme 27).[223,224] The salts **591** and **592** were obtained by treating the dimeric precursor $[(^{\mathrm{Dipp2}}\mathrm{dmdadCo})_2]$ (**593**) first with pyrene (in 1:1 or 1:2 stoichiometric ratio, see Scheme 70) and subsequently with

Scheme 70. Heteroleptic (α-Diimine)(polyarene)cobalt Complexes Described by Yang and Co-workers[389]

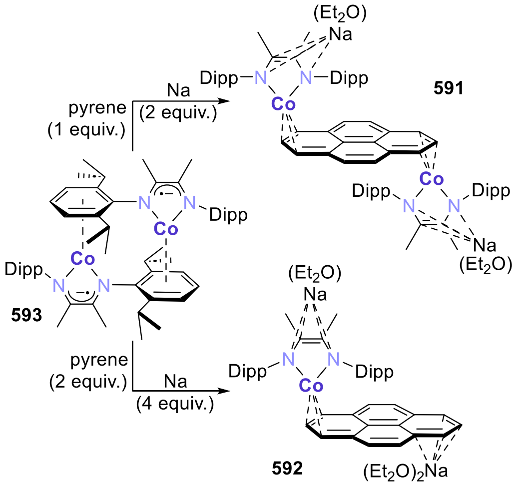

Scheme 71. Ruthenium Complexes Featuring (a) the trop Family of Diazadiene Ligands and (b) the Diazadiene-dct Ligands[409−417]

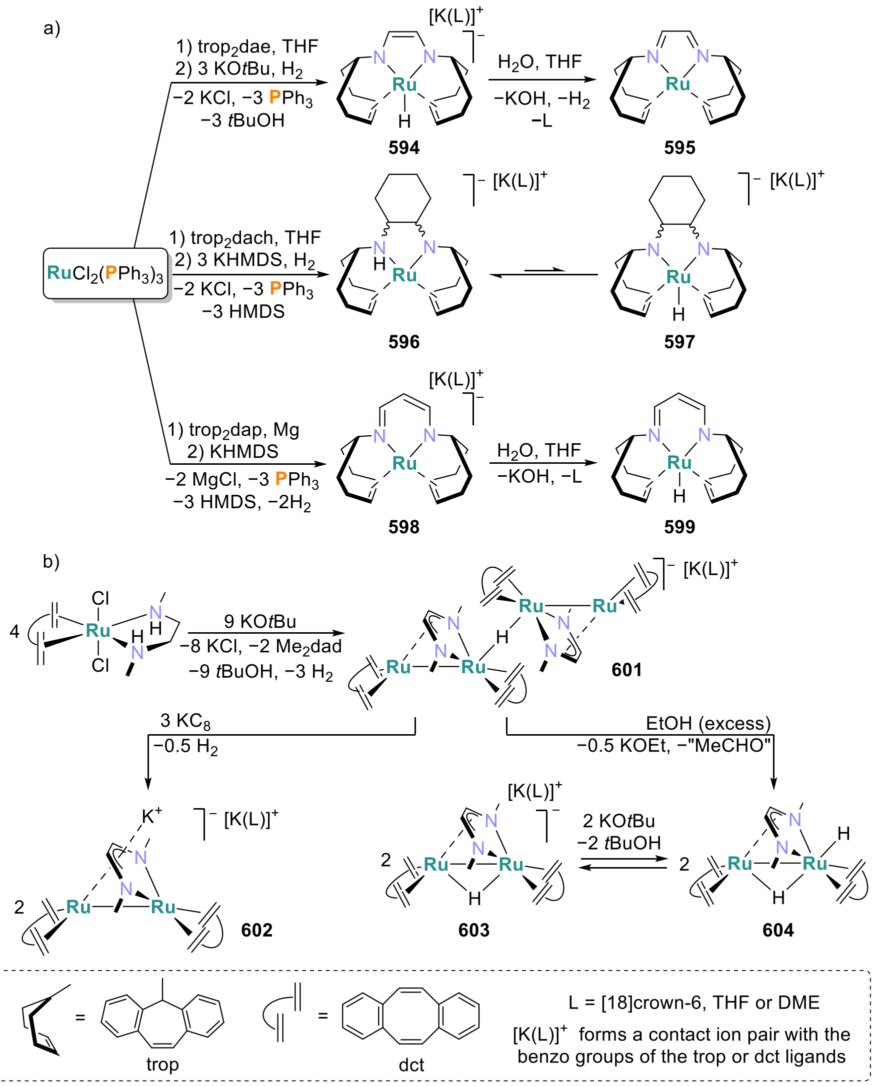

metallic sodium. X-ray diffraction studies, EPR spectroscopy, magnetic susceptibility measurements, and DFT calculations indicate the presence of a closed-shell dianionic $(^{Dipp2}dmdad)^{2-}$ ligand. Therefore, the sodium-mediated reduction is ligand (α-diimine, polyarene, or both)-based. In **592**, the pyrene ligand has also undergone reduction to some extent, as evidenced by the crystallographically determined C−C bond lengths and DFT calculations. Consequently, this mononuclear species features an antiferromagnetically coupled monoradical form of the pyrene ligand. Thus, the experimental data indicate that the cobalt center is in the formal Co(I) oxidation state, with a neutral pyrene ligand in **591** and a monoanionic one in **592**.[389]

The Grützmacher group has described 4d or 5d metalates featuring diamine and diazadiene ligands.[409−417] Grützmacher and Trincado demonstrated the versatility of several Ru-diazadiene-olefin complexes in hydrogenation reactions of organic substrates, as well as dehydrogenation reactions of light alcohols or formic acid.[409−417] For these Ru compounds, the ligand architecture plays a crucial role during the hydrogenative or dehydrogenative transformations in which they are involved, and it is supposed to be both redox and chemically non-innocent. The coordination environment is well-suited to stabilize the Ru center in low oxidation states, including anionic species (Scheme 71). An early example of this chemistry is the anionic hydride complex $[K(dme)_2][RuH(trop_2dad)]$ (**594**, Scheme 71a), which can be formally described as any of the three resonance forms $[Ru^{2+}(trop_2dad^{2-})]$, $[Ru^{+}(trop_2dad^{\bullet-})]$, or $[Ru^{0}(trop_2dad)]$ due to the noninnocence of the diazadiene ligand scaffold (the hydride ligand and potassium atom have been omitted for clarity).[409] Reaction of **594** with water generated the neutral diimino compound $[Ru(trop_2dad)]$ (**595**), with elimination of KOH and H_2.

Although the form $[Ru^{0}H(trop_2dad)]^{-}$ was initially considered as an adequate description of **594**, it was later proved, by means of multinuclear NMR spectroscopy, X-ray crystallographic data, and computational studies that the structure of this complex is consistent with a Ru^{2+} ion bearing a 1,2-enediamide chelate, i.e., the resonance form $[Ru^{2+}(trop_2dad^{2-})]$ has a greater contribution to the ground-state of **594**.[410−412] Changes in the ligand backbone were shown to dramatically influence both the reactivity in the hydrogenation/dehydrogenation reactions and the formal description of the electronic nature of complexes themselves. For instance, if the 1,2-diaminoethene unit that connects the trop groups in trop$_2$dad is replaced by the saturated 1,2-cyclohexane bridge, trop$_2$dach, a four-coordinate ruthenate complex can be obtained under reaction conditions like those used for **594**. The species [K([18]crown-6)(thf)][Ru(trop$_2$dach-H)] (**596**, Scheme 71a) was characterized as a zerovalent ruthenium center bearing a singly deprotonated trop$_2$dach ligand. In solution, this amido-amino-ruthenium complex undergoes intramolecular metal−ligand N−H addition/elimination leading to a transient diamido-ruthenium-hydride species [RuH(trop$_2$dach-2H)]$^-$ (**597**), as supported by NMR and DFT analysis.[413]

This phenomenon might be of mechanistic relevance in the methanol/water dehydrogenation mediated by **594**. If the backbone length in trop$_2$dad is increased by one ═CH− fragment, forming a *β*-diketiminate-type chelate trop$_2$ipa (ipa = iminopropenamide), the four-coordinate salt K[Ru(trop$_2$ipa)] (**598**) can be isolated under reaction conditions similar to those for **594**. In **598**, a formally monoanionic *β*-diketiminate ligand is coordinated to a Ru^0 center, which readily reacts with water to yield the Ru(II)-hydride complex **599** with elimination of KOH (Scheme 71a). Ruthenate **598** and its parental zerovalent complex [Ru(trop$_2$dap)] (**600**, dap = 1,3-diaminopropane), bearing a fully saturated ligand backbone, were used as catalysts in dehydrogenation and hydrogenation reactions of several organic substrates. Ruthenate **598** promotes the dehydrogenative coupling (DHC) reaction between benzyl alcohol and water in basic media to afford the corresponding carboxylic acid salt with release of molecular hydrogen.[414] In connection with the conversion of aqueous basic methanol or formaldehyde solutions into H$_2$ and carbonate catalyzed by **595**,[415] the Grützmacher group developed a modular version of such a zerovalent complex by separating the two dad and olefin motifs while maintaining the same coordination environment around the metal center. With this idea, trop$_2$dad was conceptualized as a Me$_2$dad fragment and a dct scaffold (Me$_2$dad = 1,4-dimethyl-diazabuta-1,3-diene; dct = dibenzo[*a*,*e*]cyclooctatetraene). Under reaction conditions like those used to obtain **594**, the modular diazadiene-olefin approach led to the tetrameric anionic complex K[Ru$_4$(μ-H)(Me$_2$dad)$_2$(dct)$_4$] (**601**, Scheme 71b) instead of the hypothetical K[RuH(Me$_2$dad)(dct)].[416] The tetramer can be reductively cleaved to the dianionic dimer K$_2$[Ru$_2$(Me$_2$dad)(dct)$_2$] (**602**) or reductively protonated and then deprotonated to the anionic bridging hydride K[Ru$_2$(μ-H)(Me$_2$dad)(dct)$_2$] (**603**, see Scheme 71b). The anionic dimers **602** and **603** and the tetramer **601** are in principle related by proton and electron transfer processes, mimicking the behavior of hydrogenases. In fact, the neutral dihydride [Ru$_2$H(μ-H)(Me$_2$dad)(dct)$_2$] (**604**), regarded as the thermodynamic sink within the [Ru$_2$(Me$_2$dad)(dct)$_2$] family, converts H$_2$ to protons and electrons (Rauchfuss test for hydrogenase activity), and catalyzes the selective hydrogenation of vitamins K$_2$ and K$_3$ to their corresponding hydroquinones without affecting the C═C double bonds. Moreover, **604** catalyzes the reduction of nitrous oxide (N$_2$O) with light alcohols as hydrogen source, forming molecular nitrogen and carboxylates.[417] The combination of the noninnocent Me$_2$dad ligand with the four electron π-donor and π*-acceptor dct scaffold has been essential to stabilize low-valent ruthenium centers and to achieve the observed hydrogenase- or alcohol dehydrogenase-like catalytic activity.

2.3. Stabilization of Low-Valent Metalates by Ion-Pairing and Element−Element Bonding

2.3.1. Ion-Pairing in Low-Oxidation State Organyl Complexes.

The countercation is an essential feature of every metalate compound. In many cases, the cation is an alkali metal such as Li$^+$, Na$^+$, or K$^+$, which is sequestered by crown ether or cryptand molecules to prevent ion-pairing and facilitate crystallization of the resulting ion-separated compound. Ion-pairing interactions can occur in the absence of a cation sequestering agent. While studies by Fürstner,[216] Hevia,[418−420] Mountford,[139,140,421,422] Crimmin,[423−426] Wolf,[427] Peters,[141−143,428−432] and Lu,[81,433−437] among other contributions, illustrate that ion-pairing is a frequent phenomenon, only a handful of the investigations explicitly address the influence of such interactions on their reactivity. However, from these investigations it has become clear that the countercation may have profound influence on the reaction patterns, stoichiometric or catalytic, of metalates. Indeed, modification of the countercations might provide an opportunity for developing finely tuned systems.[438] Evidence of counterions assisting in catalytic reactions has already been reported,[439−441] and whenever the anion/cation pair is metal based, these systems can be formally considered as (hetero)-bimetallic.[442,443]

This section collects the most relevant examples demonstrating the importance of ion-pairing effects in transition metalate chemistry. However, it should be noted that the role of the countercation is always worth considering. As such, further examples of countercation effects can be found in the preceding section 2.2.

While studying iron-catalyzed cross-coupling reactions, Fürstner and co-workers found that iron salts FeX$_n$ [X = Cl, acac (acac = acetylacetonate); n = 2, 3] are reduced by Grignard reagents bearing alkyl groups susceptible to *β*-hydride elimination to afford clusters of the formal composition [Fe(MgX)$_2$]$_n$ (**605**).[216,444−448] The authors proposed that, in the reduction leading to the heterometallic species **605**, the resulting iron center is in a formally −II oxidation state, reaching a d^{10} electron configuration. According to the authors, this type of compound might be sufficiently nucleophilic to promote cross-coupling reactions. Furthermore, the group also reported that the catalytic behavior of clusters **605** can be mimicked by using the known lithium ferrates [Li$_2$(TMEDA)$_2$-{Fe(η^2-C$_2$H$_4$)$_4$}] (**15**), [Li(dme)]$_2$[Fe(cod)$_2$] ([Li(dme)]$_2$[**16**]),[8] [Li(tmeda){CpFe(C$_2$H$_4$)$_2$}] (**193**), [Li(dme)-{CpFe(cod)}] (**194**), or [Li(tmeda){CpFe(C$_2$H$_4$)$_2$}] (**196**, see Scheme 23, above), with the Fe(−II) ferrate **15** being the most efficient precursor.[214−216,449] Based on several mechanistic studies, it was proposed that both for the *in situ* generated clusters **605** and the aforementioned electron-rich lithium ferrates **15**, [Li(dme)]$_2$[**16**], and **193**−**196**, a structural resemblance might be anticipated: the short intermetallic Fe−Li interactions influence the reactivity patterns of the iron species involved in the studied catalytic cross-coupling reactions.[216]

The effect of the intermetallic bonds was demonstrated by investigating ligand exchange reactions of the coordinated olefins (ethylene or 1,5-cod) in ferrates **193** and **194** by, for instance, 1,3-butadiene.[450] The substitution of the olefin ligands proved difficult for the studied lithium ferrates **193** and **194**, even under forcing conditions. Therefore, to facilitate the ligand exchange, the authors performed a transmetalation reaction of the lithium cation on these compounds by the less electropositive zinc cation (see Scheme 72). It was proposed that a reduction in the ionic character of the interaction would cause a decrease in the metal-to-ligand back-donation (ferrate → coordinated olefin), thus reducing their bond strength, and facilitating ligand exchange. The heterotrimetallic compound Zn[CpFe(C_2H_4)$_2$]$_2$ (**606**) was formed by the reaction of **193** with $ZnCl_2$. Its solid-state structure confirms the transmetalation, and the intermetallic contacts between the metal centers. Ligand-exchange of ethylene by an excess of 1,3-butadiene was achieved with **606**, although a reaction temperature of 60 °C to facilitate complete substitution was required to obtain the butadiene complex Zn[CpFe(1,3-C_4H_6)]$_2$ (**607**). Treatment of the butadiene complex with lithium in the presence of TMEDA afforded the desired, and otherwise inaccessible, lithium(butadiene)ferrate, [Li(tmeda)-{CpFe(1,3-butadiene)}] (**608**) with concomitant deposition of metallic zinc. Similar treatment of **194** afforded the analogous compound Zn[CpFe(cod)]$_2$ (**609**). The authors anticipated that the heterometallic complexes might be of interest as precatalysts in a variety of transformations, through reactivity of the intermetallic contacts.[450]

Scheme 72. Facilitating Ligand-Exchange of Ethylene by 1,3-Butadiene by Transmetalation to Form Zinc-Ferrates[450]

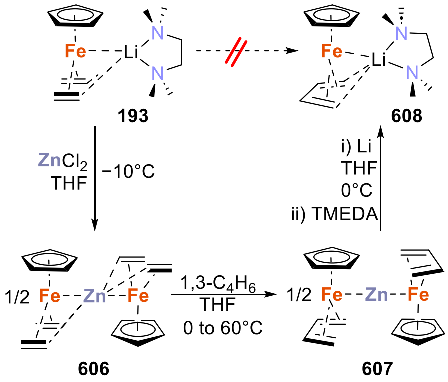

Nonetheless, despite various complexes having been identified and proposed as reaction intermediates, the exact role that the highly reduced iron species play in catalysis is not entirely clear. Other researchers have, therefore, revisited the evidence[438,451,452] and contributed to this area.[449,453,454] For instance, in 2011, Wolf and co-workers studied the catalytic cross-coupling of alkyl electrophiles with aryl Grignard reagents mediated by a series of metalate and other low-valent iron complexes.[449] The studied catalysts included the Fe(−II) compound [Li_2(TMEDA)$_2${Fe(η^2-C_2H_4)$_4$}] (**15**), the "iron Grignard" compound [Cp(dppe)FeMgBr(thf)$_2$] (**610**, dppe = 1,2-bis(diphenylphosphino)ethane)[455] and other organoiron complexes with formal oxidation states ranging from Fe(−I) to Fe(III). While compound **15** remained the most active precursor, the labile (anthracene)ferrates(−I) [Fe(η^4-$C_{14}H_{10}$)$_2$]$^-$ (**52**) and [Fe(η^4-$C_{14}H_{10}$)(η^4-cod)]$^-$ (**183**) were similarly competent, and the "iron Grignard reagent" **610** hardly showed any catalytic activity under the studied conditions. Therefore, the presence of metal−metal bonds did not enhance the catalytic behavior in this case, and the authors remained doubtful about whether the putative intermetallic iron Grignard compounds were the true catalysts in iron-catalyzed cross-couplings. Furthermore, it was concluded that, whereas the oxidation state of the iron center had little influence on the catalytic performance, a labile coordination environment was crucial for high catalytic activity.[449]

In 2015, Bedford reviewed the available mechanistic data for iron catalyzed cross-coupling reactions and concluded that scant evidence exists to support the participation of highly reduced (subzero-valent) iron species in the catalytic cycle.[451] It was argued that while Fe(−I) and Fe(−II) complexes, such as **15**, can function as precatalysts, this has no bearing on the oxidation state of the active species.[451] Bedford and co-workers instead proposed that the species accounting for the catalytic activity in iron-catalyzed cross-coupling reactions are homoleptic three-coordinate Fe(II)-"ate" complexes, of the type [FeR_3]$^-$ [R = mesityl[347] (**611**, as the [Mg_2Br_3(thf)$_6$]$^+$ salt) benzyl (**612**, as the [Mg_2Cl_2(OTf)(thf)$_3$]$^+$ salt); see Scheme 73]. Complexes **611** and **612** are observed under catalytically relevant conditions, and obtained by reaction of $FeCl_n$ (n = 2, 3) with Grignard reagents (in the presence of an excess of tetramethylethylene-1,2-diamine, TMEDA, for complex **611**). Although neutral [FeR_2(TMEDA)] [R = Mes (**613**), Bn (**614**)] complexes were also observed in these investigations, the authors demonstrated that the anionic **611** and **612** complexes undergo cross-coupling with electrophiles significantly faster than **613**/**614**. For coupling reactions of smaller aryl Grignard reagents, the formation of zerovalent nanoparticles was observed, whereas EPR spectra of the catalytic reaction mixture suggest the presence of low-valent Fe(I) species. Consequently, the formation of catalytically relevant species with oxidation states below Fe(II) cannot be completely excluded for reactions with smaller R substituents.[453] Neidig and co-workers identified a compound related to **611** and **612** under catalytically relevant conditions, the Fe(II)-"ate" compound [Mg(NMP)$_6$][$FeMe_3$]$_2$ (**615**, NMP = *N*-methylpyrrolidone), as the major species in a system catalyzed by Fe(acac)$_3$ (**298**) and MeMgBr, using NMP as a cosolvent. **615** is highly active and selective in the production of cross-coupled products.[454] Furthermore, this group also isolated and characterized the small anionic cluster [MgCl-(thf)$_5$][Fe_8Me_{12}] (**616**), obtained from $FeCl_3$ and MeMgBr in THF.[456] This compound is only slightly active in cross-coupling reactions by direct reaction with the electrophile, but in the presence of additional MeMgBr promotes the coupling reaction rapidly and selectively.

Scheme 73. σ-Organyl Ferrates Relevant in Cross-Coupling Reactions Catalyzed by Iron Precursors, Reported by Bedford and Co-workers[453]

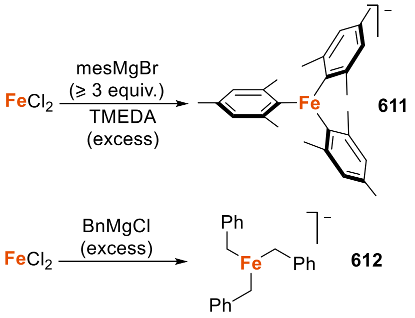

In this context, Koszinowski and co-workers also investigated the chemistry of organoferrate complexes,[457−459] demonstrating that cluster **616** can also be accessed by

Scheme 74. Lithium (cod)Nickelates and Polyheterometallic Organonickelates by Hevia and Co-workers[418,419]

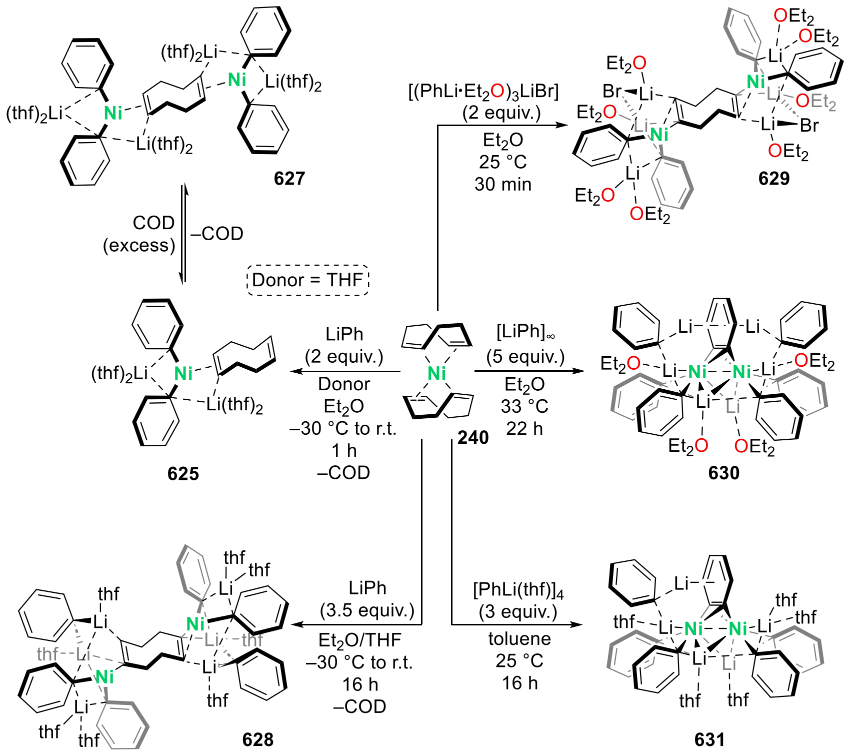

treating $Fe(acac)_3$ (**298**) with MeMgX (4 equiv; X = Cl, Br) in THF solution, and studied its reactivity through electrospray ionization (ESI)−mass spectrometry. The authors reported an average oxidation state of 1.4 for the iron centers in **616**. In the presence of TMEDA, the signal for **616** practically disappears. Similar heteroleptic organoferrate clusters $Me_{12-n}Fe_8Ar_n^-$ (n = 1−5, Ar = Ph, Tol), with identical average oxidation states to **616**, were prepared. The spectrometric identification of **616** corroborates the previous results by Neidig and co-workers[454] and further supports the possible involvement of this type of cluster ion in iron-catalyzed cross-coupling reactions.[458]

Further ESI−mass spectrometry investigations in solution, using a variety of iron salts ($Fe(acac)_3$, $FeCl_3$, $FeCl_2$, $Fe(OAc)_2$) and Grignard reagents RMgX (R = Me, Et, Bu, Hex, Oct, Dec, Me_3SiCH_2, Bn, Ph, Mes, 3,5-$(CF_3)_2$-C_6H_3; X = Cl, Br), led to the spectrometric identification of different mono- or polynuclear organoferrates with metal centers mainly in the +II or +III oxidation states.[459] For R = Ph, only small amounts of cluster $[Ph_7Fe_4]^-$ (**617**), featuring iron centers in an average oxidation state of 1.5, were identified.[457] In the presence of TMEDA, the alkylferrates displayed enhanced stability, and it was possible to identify the transient low-valent complex $[Bu_2Fe^I]^-$ (**618**), although most of the species still corresponded to organoferrates in the+II or +III oxidation states. In view of the observation of species **618**, the authors proposed that the formation of the Fe(III) alkylferrates might involve an oxidative addition to the low-valent Fe(I) intermediate.

Low-valent organoferrates were also observed upon treating $[FeCl_2(dppbz)_2]$ (**619**, dppbz = 1,2-bis(diphenylphosphino)-benzene) with EtMgCl. In this case, minor amounts of Fe(−I) and Fe(0) ferrates were identified.[459] In turn, treatment of **619** with PhMgCl (4 equiv) allowed identification of species in the −I, 0, and +I oxidation states, including dinuclear $[Ph_3Fe_2(dppbz)]^-$ (**620**) and mononuclear $[Fe(dppbz)]^-$ (**621**), $[PhFe(dppbz)]^-$ (**622**), and $[Ph_2Fe(dppbz)]^-$ (**623**). The dinuclear species $[Ph_2Fe_2(dppbz)]^-$ (**624**), having an average oxidation state of 0.5, was also observed.[457] The observation of the various low-oxidation Fe complexes was attributed to the additional stabilization provided by the bidentate phosphine ligand dppbz, which lowers the electron density of the ferrate species through π-backbonding and coordinative saturation of the iron center. Since most of the identified Fe(III) species underwent reductive elimination processes, the authors proposed that these could be considered as likely intermediates in iron-catalyzed cross-coupling reactions.[459]

Hevia and co-workers have reported several investigations on the chemistry of organonickelate complexes and their implications in catalytic cross-coupling reactions.[418−420,460,461] Monitoring of an NMR scale reaction between equimolar amounts of $[Ni(cod)_2]$ (**240**) and PhLi revealed only half of the nickel complex reacted. This suggested the formation of a 1:2 Ni:PhLi species, subsequently identified as $[Li_2(thf)_4Ph_2Ni(cod)]$ (**625**). By changing the concentration of the reaction, it was possible to identify a minor species with 1:1 ratio of Ni and PhLi $[Li(thf)_2PhNi(cod)]$ (**626**). This ion-paired species is in equilibrium with an ion-separated one, which in turn dissociates one or both the coordinated cod olefin units to afford compound **625** and partially regenerates complex **240**. Preparative reactions between **240** and PhLi resulted in three lithium (cod)nickelates, which were preferentially isolated depending on the ratio between the reactants and the crystallization conditions.[418] Treatment of **240** with PhLi in a 1:2 ratio in the presence of a donor afforded the corresponding lithium nickelates $[Li_2(donor)_xPh_2Ni(cod)]$ [**625**, donor: THF (x = 4), TMEDA (x = 2), PMDETA (x = 2); Scheme 74, left, shows only the THF derivative], as previously observed on an NMR scale. The complexes are extremely air- and moisture-sensitive.

Characterization through X-ray diffraction showed a trigonal planar environment for the Ni center. The C═C bond distances reflect the different coordination environment of the cyclooctadiene ligand: the coordinated C═C bond is significantly elongated (d_{CC} = 1.446(2)−1.452(2) Å) with respect to the uncoordinated C═C bond (d_{CC} = 1.321(5)−1.327(2) Å). The elongation of the coordinated C═C bond is attributed to the higher electron density on the Ni(0) center and, therefore, increase in backbonding to the C═C moiety. Compound **625** suffers a slow and reversible loss of half an equivalent of COD in solution to yield the bridged hexanuclear complexes [$Li_4(donor)_{4x}Ph_4Ni_2$(cod)] [**627**, donor: THF (*x* = 2), TMEDA (*x* = 1); Scheme 74, top left, shows only the THF adduct]. The shift toward nickelate **625** in the presence of excess COD is accompanied by formation of the nickel precursor **240**. Also, increasing the Ni:PhLi ratio (mimicking catalytic cross-coupling conditions) led to the isolation of a bridged octanuclear 3:1 lithium nickelate from the reaction mixture, namely [$Li_6(thf)_8Ph_6Ni_2$(cod)] (**628**, Scheme 74, bottom left). NMR monitoring of such reactions revealed, however, that the trinuclear compound **625** was the main component of the reaction mixture.

Further investigations helped to shed some light on the role that the lithium nickelates play on the Ni-catalyzed cross-coupling of aryl ethers. Catalytic, stoichiometric, and kinetic experiments of aryl ether cross-coupling reactions were performed. In a model reaction of cross-coupling of PhLi and 2-methoxynaphthalene, catalyzed by [$Ni(cod)_2$] (**240**, 5 mol %), solvent and donor effects were observed for the series of lithium nickelates. For instance, when THF was the solvent of choice, the reaction returned only products of *ortho*-lithiation of the aryl ether, instead of the cross-coupled compound.[418]

Likewise, by using a solvated PhLi aggregate, [PhLi(donor)]$_n$, in combination with **240**, the immediate formation of the trinuclear lithium nickelate **625** was observed.[418] Upon addition of the substrate 2-methoxynaphthalene to the mixture, it was possible to identify the cross-coupling and homocoupling products. Furthermore, the hexanuclear and octanuclear complexes **627** and **628** proved competent to promote the cross-coupling reactions at equal catalyst loadings. These observations, along with additional spectroscopic and experimental evidence, led to the conclusion that heterometallic Ni(0)-"ate" complexes play an important and cooperative role in the activation of the aryl ether substrate and, therefore, in the catalytic cycle. Both the nucleophilic Ni center and the Lewis acidic lithium cations seem to be involved in such activation of the substrate. Two mechanistic proposals were asserted based on the combined data. Starting from complex **240**, the addition of [PhLi(donor)]$_n$ can afford any of the observed 1:1 (**626**) or 1:2 nickelate species **625**. The latter seems to be favored, however, since the 1:1 nickelate was not routinely observed. Nonetheless, knowing that these two nickelates are related by equilibrium in the presence of [PhLi(donor)]$_n$, both were considered to be involved in the mechanism. Therefore, the authors proposed both an anionic and a dianionic reaction pathway. In the anionic pathway, complex **240** and [PhLi(donor)]$_n$ form compound **626**, which in turn coordinates the substrate, oxidatively adds the aryl−OMe bond with elimination of LiOMe, followed by reductive elimination of the cross-coupling product and regeneration of complex **240**. In the dianionic pathway, nickelate species **625** forms rapidly in the early stages of the reaction, and directly coordinates the substrate to engage in the additional steps of the catalytic reaction.

In further investigations,[419] Campos and Hevia revisited the structure of the homoleptic lithium nickelate "$Li_3NiPh_3(solv)_3$", reported by Taube and co-workers over four decades ago.[462−464] Based exclusively on its ^{13}C NMR spectroscopic characterization, this species was thought to adopt an extremely rare hexagonal planar coordination environment around the Ni atom which would be composed of three Li^+ cations and three phenyl ligands. The two initial synthetic routes proposed by Taube were reexamined. One of these involves the displacement of a COD ligand in [$Ni(cod)_2$] (**240**) by PhLi, which, as described above, affords three different lithium nickelates **625**−**628**, depending on the stoichiometric ratio between the reactants and on the crystallization conditions.[418] Similarly, treating precursor **240** with [$(PhLi\cdot Et_2O)_3LiBr$] (prepared from PhBr and *t*BuLi)[465] afforded [$Li_2(Et_2O)_4(LiBr)Ph_2Ni]_2$(cod) (**629**, Scheme 74, top right), which contains cocomplexed LiBr.

None of these experiments suggested the presence of a planar complex. While treatment of the Ni(0) precursor with donor-free PhLi (5 equiv) led to the formation of a deep red solution, as previously described by Taube, NMR spectroscopic characterization of this solution did not match the previous reports.[462−464] The choice of solvent influences the type of product obtained. If the reaction is carried out in THF, the major product will correspond to the nickelate **627**. By using Et_2O (Scheme 74, middle right), it was possible to isolate a crystalline solid in low yields, which corresponded to [$\{Li_3(Et_2O)_2Ph_3Ni\}_2(\mu,\eta^2:\eta^2\text{-}C_6H_4)$] (**630**), containing a benzyne ligand bridging the Ni centers. Additionally, treating **240** with 3 equiv of the THF adduct [$PhLi(thf)]_4$ in toluene afforded the related bridging benzyne complex [$\{Li_3(thf)_2Ph_3Ni\}(\mu,\eta^2:\eta^2\text{-}C_6H_4)\{Li_2(thf)_3Ph_2Ni\}$] (**631**, Scheme 74, bottom right). **629**−**631** were characterized via X-ray diffraction and NMR spectroscopy. DFT calculations were also carried out on the electronic structure of **630**, indicating that this is best described (lowest-energy state) as a closed-shell singlet, which agrees well with the crystal structure and the diamagnetic behavior observed. Additionally, the calculations confirmed that there is no metal−metal bond, which explains the long Ni−Ni distance (d_{NiNi} = 2.7117(8) Å) observed in the crystal structure. The phenyl carbanions in **630** act as strong σ-donors, increasing the electron density of the metal centers. NBO analysis suggested that the backdonation from a Ni d orbital to a π* orbital of the bridging C_6H_4 unit is, therefore, particularly strong. The latter corresponds then to an *in situ* generated, π-accepting and formally reduced $C_6H_4^{2-}$ motif, which alleviates the extremely high electron density at the nickel centers. Altogether, the results from these investigations confirm that the initially proposed species "$Li_3NiPh_3(solv)_3$" is in fact consistent with the dinickel structure **630**.

Attempts to replicate the observed chemistry with PhNa led to different results, suggesting a countercation effect.[419] Depending on the Ni:PhNa ratio, either the sodium nickelate [$Na_2(solv)_3Ph_2Ni(cod)]_2$ (**632**, 2:1 ratio) or [$Na_3(solv)_3Ph_2(C_8H_{11})Ni(cod)]_2$ (**633**, 3−5 equiv of NaPh) was obtained (Figure 12). Although the sodium nickelates do not feature the benzyne dianion ligand observed in **630**, the authors suggested that a lithium-containing analogue of **632** might be involved in the formation of **630**. Complexes **627** and **630** were evaluated as catalyst precursors in Csp^2−Csp^3 Kumada coupling,

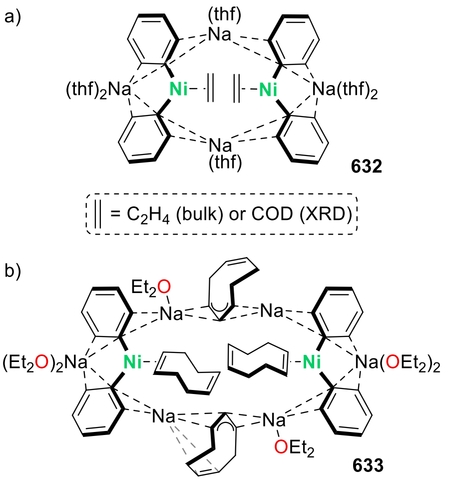

Figure 12. Sodium organonickelates by the group of Campos, Hevia, and co-workers.[419]

Scheme 75. Synthesis of Tri-lithium Nickelates Derived from Aryl-acetylides[420]

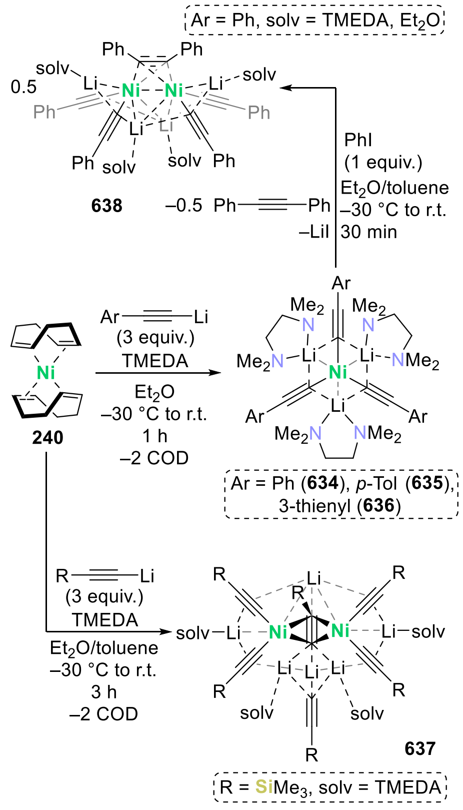

Buchwald−Hartwig coupling, and cross-coupling of aryl ethers (for **630**).[419] For the Kumada coupling, the nickelates performed better than precursor **240**, which might indicate that similar Ni-"ate" species might be involved in this type of catalytic transformation.

Later, Hevia and co-workers reported the formation of planar Ni(0) complexes supported by organolithium ligands.[420] Reactions of [Ni(cod)$_2$] (**240**) with lithium arylacetylides in the presence of TMEDA (slight excess) yielded a family of homoleptic lithium nickelates of general formula [$Li_3(TMEDA)_3Ni(C{\equiv}C{-}Ar)_3$] [Ar = Ph (**634**), *p*-Tol (**635**), 3-thienyl (**636**); see Scheme 75). As with the lithium nickelates illustrated in Scheme 74,[418,419] the solvent choice is critical for the synthesis of the complexes. In the absence of additional donors, neither THF nor Et_2O allowed for the spectroscopic characterization or isolation of the nickelates, and the presence of a sequestering agent (crown ether) led only to decomposition.

Stabilization of the cation by solvation with TMEDA as a donor was, therefore, deemed crucial, allowing for the reaction to be carried out in Et_2O. The nature of the acetylide ligand also influenced the type of compound formed as, for instance, the use of the more electron-rich $Me_3Si{-}C{\equiv}CLi$ led to the formation of the polynuclear cluster [$Li_6(TMEDA)_{3.5}Ni_2(C{\equiv}C{-}SiMe_3)_6]_2$ (**637**, Scheme 75, bottom) instead of an analogue of **634**−**636**. X-ray diffraction analysis of **634** (Ar = Ph) suggested that the nickel center in the complex is located in a planar coordination environment, surrounded by three lithium cations and three acetylide ligands in an alternating fashion. The C−Ni−Li angles (59.9°, on average) indicate a hexagonal planar geometry around nickel, whereas the Ni−Li distances (average d_{NiLi} = 2.50 Å) and the Li−C distances (average d_{NiLi} = 2.37 Å), along with a Hirshfeld surface analysis, show close Ni−Li and Li−C contacts.

A theoretical analysis of the bonding situation (Quantum Theory of Atoms in Molecules, QTAIM) indicated that bond critical points exist for all Ni−C bonds, but not for the Ni−Li interactions, indicating the absence of covalent Ni−Li bonds.[420] In fact, the noncovalent interaction index (NCI) revealed that the latter are repulsive in nature. By contrast, the Li−C contacts are attractive, and several H···C bond contacts between the methyl groups of the TMEDA donor and carbon atoms of the acetylide ligands, were identified. These were assigned as London dispersion (van der Waals) interactions, known to assist in the stabilization of compounds and to ease in their isolation.[466] Such observations would explain the difficulties in isolating the nickelates by using THF or Et_2O as solvents in the absence of TMEDA.

An analysis of the charge distribution in the complex also suggested that the acetylide ligands are negatively charged and that the overall charge transfer occurs from the Ni atom toward the ligands due to substantial metal-to-ligand backbonding. The transition metal would then formally be a neutral Ni(0) center. The lithium cations are then electrostatically attracted to the acetylide units. Altogether, the bonding analysis indicated that, instead of hexagonal planar organonickel complexes, the geometry of **634** corresponds to trigonal planar Ni(0) species stabilized by dispersion interactions between the Li-TMEDA motifs and the acetylide ligands. Compound **634** failed to react with phosphine ligands (PCy_3 or PEt_3) but reacted with iodobenzene (1 equiv) to afford the hexanuclear cluster **638** (Scheme 75, top), diphenylacetylene, and lithium iodide. The molecular structure of **638** features a side-on coordinated diphenylacetylene ligand, with the metal centers adopting a *pseudo*-trigonal planar environment composed of the bridging alkyne ligand and two terminal phenylacetylide ligands. Attempts to react **638** with additional iodobenzene, or with $PhC{\equiv}CLi$ to regenerate **634**, were unsuccessful. The authors concluded that, since **634** cannot be regenerated, the system is not suitable to perform catalytic Sonogashira-type cross-coupling reactions.

2.3.2. Transition-Metal Magnesium Compounds and Related Heavier Alkaline Earth Metal Complexes.

In comparison with the wealth of alkali metal (lithium, sodium, and potassium) metalates, alkaline earth (AE) metal salts of low-oxidation transition metalate anions, are relatively scarce. These heterobimetallic species can be formed either by interaction between reduced transition metal precursors and suitable magnesium species or from TM salts in common oxidation states and Grignard reagents or Mg(I) compounds, taking advantage of their reducing character.[467−469] As previously mentioned, a recent review by Xu and co-workers comprehensively discusses Mg- or Zn-heterometallic complexes.[26] Considering this, we will herein highlight the contributions including the chemistry of low-valent transition metals, also known as magnesium metalates, and related heavier analogues.

A handful of magnesium-transition-metal compounds (sometimes termed ‘inorganic Grignard reagents’) were reported by the groups of Felkin, Green, and Jonas prior to the period covered by this review.[455,470,471] The first examples of these, [Cp(dppe)FeMgBr(thf)$_2$] (**610**) and [Cp$_2$MoHMg(C$_6$H$_{11}$)(μ-Br)$_2$Mg(Et$_2$O)]$_2$ (**639**), were synthesized almost 50 years ago (Figure 13).[455,470] The magnesium cobaltates [CpCo(C$_2$H$_4$)PhMgBr(tmeda)] (**640**) and [CpCo(η^3-C$_3$H$_5$)MgBr(thf)$_2$] (**641**) were described by Jonas and co-workers in 1986 (Figure 13).[471]

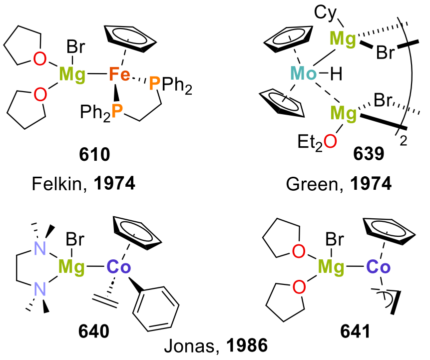

Figure 13. ‘Inorganic Grignard reagents’ by Felkin, Green, and Jonas.[455,470,471]

Similar to these early examples, Jones and co-workers reported a two-coordinate complex featuring an unsupported manganese−magnesium bond and reactivity of an ‘inorganic Grignard reagent’.[472] Reduction of the manganese(II) halide complex [L*Mn(thf)(μ-Br)]$_2$ (**642**) bearing the silyl amido ligand L*, −N(Ar*)(Si*i*Pr$_3$) (Ar* = 2,6-{CHPh$_2$}$_2$-4-*i*Pr−C$_6$H$_2$), with the magnesium(I) dimer [(^{Mes}nacnac)Mg]$_2$ (**643**, ^{Mes}nacnac = [(^{Mes}NCMe)$_2$CH]$^-$) in 1:2 ratio afforded [L*MnMg(^{Mes}nacnac)] (**644**, Scheme 76). According to X-ray crystallographic analysis, in **644**, the two-coordinate Mn(0) center is in a bent arrangement (N−Mn−Mg = 160.85(9)°). The Mn−Mg bond length (2.8244(13) Å) is within the sum of the covalent radii of Mg and high-spin Mn (3.02 Å). Magnetochemical studies suggested that **644** has a S = 5/2 ground state, corresponding to the expected high-spin Mn(0) center in 4s^{2}3d^5 configuration. Theoretical calculations performed on a simplified model in which the isopropyl groups have been truncated to methyl groups, **644′**, support the proposed occupation of the five, nonbonding Mn 3d orbitals by a single electron each, and indicate that the Mn−Mg bond has an effective bond order (EBO) of 0.97, essentially originating from the 4s and 3s orbitals on both Mn and Mg centers. Given the small differences in electronegativity of both metals (1.55 for Mn vs 1.31 for Mg, according to the Pauling scale), the Mn−Mg bond was expected to have a covalent character, and to be formed of Mn(0) and Mg(II) atoms. The ‘inorganic Grignard reagent’ behavior of **644** was demonstrated via transfer of the “L*Mn” fragment. For instance, **644** reacts with the Mn(II) dimer [L′Mn(thf)(μ-Br)]$_2$ (**645**, L′ = −N(Ar′)(SiMe$_3$) (Ar′ = 2,6-{CHPh$_2$}$_2$-4-Me-C$_6$H$_2$), less sterically hindered than its analogue **642**, affording the unsymmetrically substituted manganese(I) compound [L*MnMnL′] (**646**). Similarly, **644** reacted with a chromium(II) complex, forming a bis(amido)manganese mixed valent (Mn(II)−Cr(0)) species believed to result from an internal redox process on a Mn−Cr bonded intermediate, analogous to **646**.

Scheme 76. Synthesis of a Two-Coordinate Mn(0)−Mg(II) Complex by Jones and Co-workers[472]

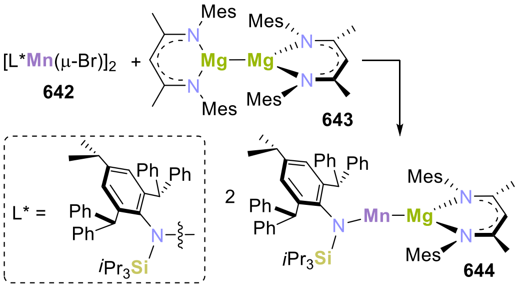

Kaltsoyannis and Mountford have systematically investigated the reactivity of transition metal compounds with a variety of alkaline earth precursors.[139,140,421,422] In 2011, this group reported on the reaction between the known ferrate K[(η^5-Cp)Fe(CO)$_2$] (K[**2**]) and alkaline earth metal precursors stabilized by β-diketiminate ligands. Reaction of K[**2**] with [(^{Dipp}nacnac)CaI(thf)$_2$]$_2$ [**647**, ^{Dipp}nacnac = HC{C(Me)N-(2,6-C$_6$H$_3$*i*Pr$_2$)}$_2$; see Scheme 77a] yielded a dimeric species, [(^{Dipp}nacnac)Ca(μ-OC)$_2$Fe(η^5-Cp)(thf)$_2$]$_2$ (**648**),[14,139] as observed in the solid state. **648** featured Fe−CO···Ca isocarbonyl interactions (see Table 1 for ν_{CO} stretching frequencies) and no apparent Ca−Fe bond. Furthermore, the synthesis of a Ca/Fe heterometallic species [Ca(thf)$_3${(μ-OC)Fe(η^5-Cp)(CO)}$_2$]$_2$ (**649**, Scheme 77b), and the Yb/Fe analogue [Yb(thf)$_3${(μ-OC)Fe(η^5-Cp)(CO)}$_2$]$_2$ (**650**) was reported, which were formed by reductive cleavage of the dimeric precursor [(η^5-Cp)Fe(CO)$_2$]$_2$ (**651**) with calcium or ytterbium amalgam (Ca/Hg or Yb/Hg). The molecular structure of **649** is composed of a centrosymmetric dimer formed via an isocarbonyl linkage to calcium and shows two unsupported calcium-transition metal bonds (d_{CaFe} = 3.0185(6) Å). The ytterbium analogue is isostructural to **649**. By contrast, attempting an analogous reaction between **651** and magnesium amalgam, followed by crystallization from THF, formed [(thf)$_4$Mg(μ-OC)$_2$Fe$_2$(η^5-Cp)$_2$(CO)$_2$] (**652**), in which no direct metal−metal bond exists (Scheme 77b). The six-coordinate Mg^{2+} center is connected to the coordination sphere of each iron center only through an isocarbonyl linkage. The natures of the electronic structures of **649** and its ytterbium analogue **650** were studied using theoretical calculations (DFT, molecular orbital, energy decomposition, and atoms-in molecules analyses), and the M−Fe interactions were found to be predominantly electrostatic. Moreover, these analyses explained the formation of **652**. The stabilization energy for the coordination of THF to Mg^{2+} is more favorable than the energy required for the Mg−Fe interaction, leading to

Scheme 77. Interaction of Ferrates with Alkaline Earth Metal Species to Obtain Heterometallic Fe-AE (and Lantanide) Complexes[139,140,421]

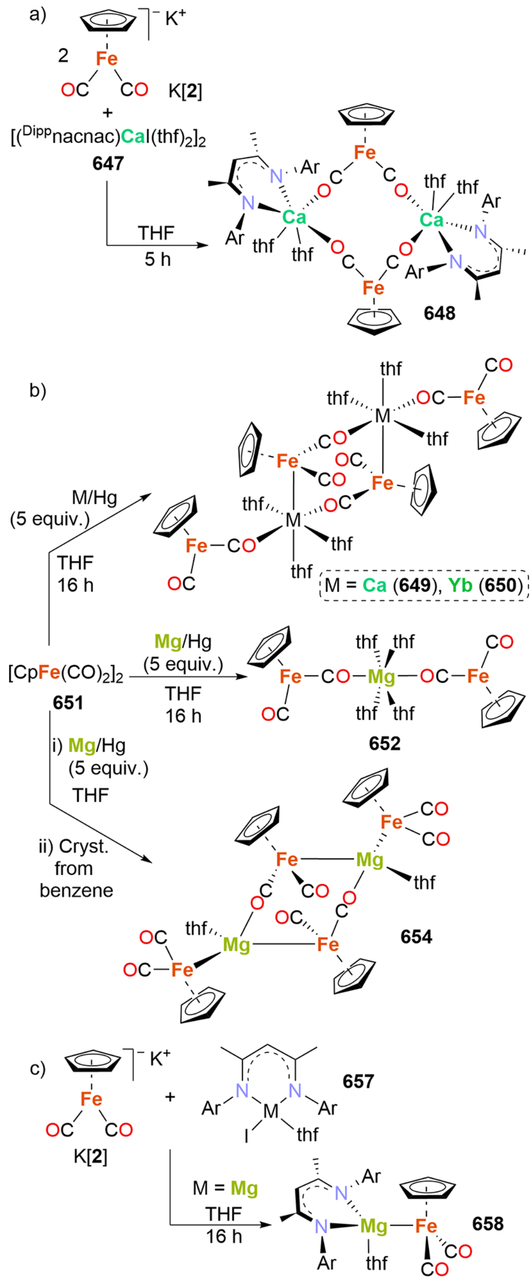

the formation of the isocarbonyl linkage. Reaction of either **649** or its Yb-analogue **650** with MeI yielded $[(\eta^5\text{-Cp})\text{Fe}(\text{Me})(\text{CO})_2]$ (**653**), consistent with the complexes being sources of anion **2**.[139] Subsequent studies revealed that, while compound $[(\text{thf})_4\text{Mg}(\mu\text{-OC})_2\text{Fe}_2(\eta^5\text{-Cp})_2(\text{CO})_2]$ (**652**, crystallized from THF) lacks metal−metal bonds, performing the same reductive cleavage, but crystallizing the product from benzene, yields the centrosymmetric dimeric complex $[(\text{thf})\text{Mg}\{\text{Fe}(\eta^5\text{-Cp})(\text{CO})_2\}_2]_2$ (**654**, Scheme 77b), featuring two Mg−Fe bonds.[139,421] The two Mg−Fe distances in **654** (2.6112(5) and 2.5629(5) Å) are comparable to that for $[\text{Cp}(\text{dppe})\text{FeMgBr}(\text{thf})_2]$ (**610**, 2.593(7) Å).[455] The strontium derivative "$\text{Sr}[\text{Fe}_2(\eta^5\text{-Cp})_2(\text{CO})_2]_2$"(**655**) was also reported, although without structural authentication due to its high sensitivity.[421] Additionally, the authors found that treating complex **652** with hexamethylphosphoramide (HMPA, 4 equiv) yielded the separated ion pair $[\text{Mg}(\text{HMPA})_4][(\eta^5\text{-Cp})\text{Fe}(\text{CO})_2]_2$ (**656**), whose structure was confirmed via X-ray diffraction.

Similar to the formation of $[(^{\text{Dipp}}\text{nacnac})\text{Ca}(\mu\text{-OC})_2\text{Fe}(\eta^5\text{-Cp})(\text{thf})_2]_2$ (**648**), treatment of K[**2**] with $[(^{\text{Dipp}}\text{nacnac})\text{MgI}(\text{thf})]$ (**657**) affords $[(^{\text{Dipp}}\text{nacnac})\text{MgFe}(\eta^5\text{-Cp})(\text{CO})_2(\text{thf})]$ (**658**, Scheme 77c).[140] X-ray diffraction analysis revealed the presence of unsupported Mg−Fe bonds (d_{MgFe} = 2.6326(4) Å), which are shorter than the sum of the covalent radii of the metals (Σ = 2.73(10) Å), and comparable to those in complexes **610** and **654**, described earlier.

The higher stretching frequencies of the carbonyl ligands in complex **658** (ν_{CO}(**658**) = 1926, 1857 cm^{-1}; see Table 1) compared to K[**2**] (ν_{CO} = *ca.* 1865, 1788 cm^{-1}) reflect the changes in electron density at the transition metal upon formation of the metal−metal bond. As with compound **649**, **658** reacted with MeI to afford **653** and regenerated **657**, after addition across the Mg−Fe bond. Similarly, di(*p*-tolyl)-carbodiimide (TolNCNTol) inserts into the Mg−Fe bond, affording $[(^{\text{Dipp}}\text{nacnac})\text{Mg}\{(\text{TolN})_2\text{CFe}(\eta^5\text{-Cp})(\text{CO})_2\}]$ (**659**). Although complex **659** was not crystallographically characterized, its structure was authenticated by DFT computations along with spectroscopic and analytical data of the isolated product. The increase in stretching frequencies in **659** (ν_{CO}(**659**) = 2010, 1956 cm^{-1}), with respect to those in **658**, indicates significant charge transfer from the transition metal center to the $(\text{TolN})_2\text{C}$ unit. Changes in the Mulliken charge for both complexes are consistent with the observations in infrared spectroscopy since the Fe center in **659** (−0.040) is substantially less negative than in the parent compound **658** (−0.164).[140]

Complementary results on the interaction between alkaline earth metal cations and lanthanide cations with the cobaltate anion $[\text{Co}(\text{CO})_3(\text{PR}_3)]^-$ (**660**, R = Cy) were reported in 2015.[421] A series of products $[\text{Mg}\{\text{Co}(\text{CO})_3(\text{PCy}_3)\}_2(\text{thf})]_2$ (**661**), $[\text{Ca}\{\text{Co}(\text{CO})_3(\text{PCy}_3)\}_2(\text{thf})_2]_\infty$ (**662**), $[\text{Sr}\{\text{Co}(\text{CO})_3(\text{PCy}_3)\}_2(\text{thf})_3]_\infty$ (**663**), and $[\text{Ba}\{\text{Co}(\text{CO})_3(\text{PCy}_3)\}_2(\text{thf})_6\}]$ (**664**) was generated by treatment of $[\text{Co}(\text{CO})_3(\text{PCy}_3)]_2$ (**665**) with amalgams of alkaline earth metals (AE = Mg, Ca, Sr, Ba). Representations of the structures of **661**−**663** are shown in Figure 14a. Of these, complex **661** features two Co−Mg bonds as in **654**, **662** presents only one Co−Ca bond per transition metal center, **663** has a long Co−Sr distance and bears one side-on bound CO ligand, while **664** lacks any metal−metal interaction. Based on the experimental evidence and a systematic theoretical analysis of the bonding situation in these complexes, the authors suggested that, going down the group of the alkaline earth metals, the AE−TM linkage becomes weaker.

In fact, theoretical calculations revealed that the AE−Co bonding becomes progressively more ionic going down the group. Nonetheless, by comparing the behavior of the series of complexes derived from cobaltate **660** with the previous results from ferrate **2** or with carbonylcobaltate $[\text{Co}(\text{CO})_4]^-$ (**95**), it was concluded that **660** forms inherently stronger AE−TM bonds than the other metalates studied. The HOMO in **660** is less stabilized (by 0.39 eV) than in **95**, accounting for the increased nucleophilicity of the former. In summary, although the AE−TM interactions are essentially ionic in general, their strength is favored by a larger charge/size ratio (stronger for Mg−TM bonds, weaker for Sr−TM bonds). However, as observed for complexes **652**, **654**, and **656**, Lewis bases (e.g.,

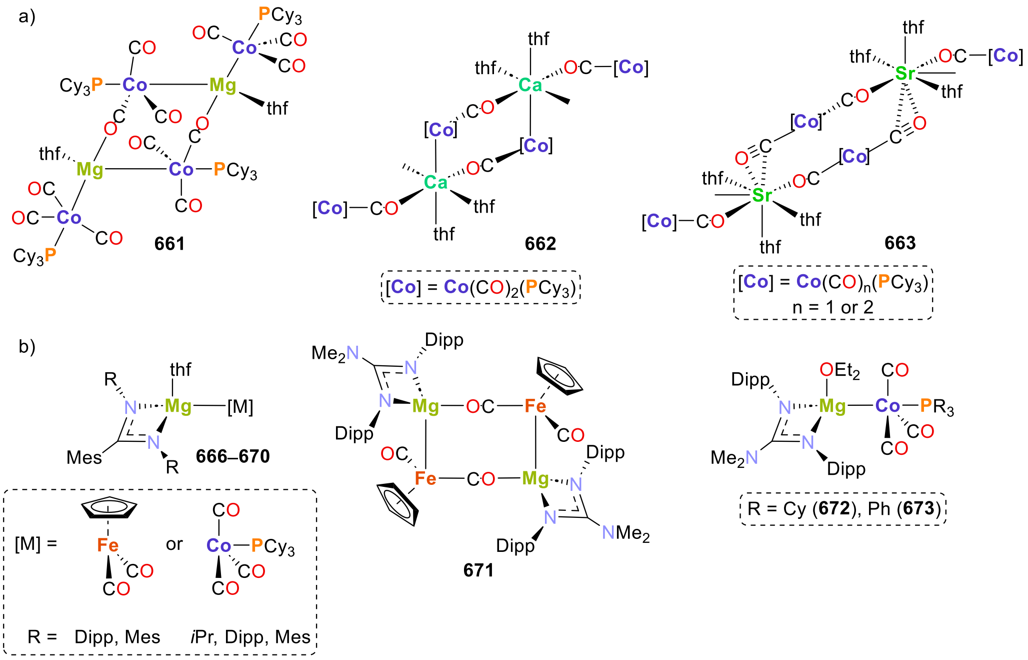

Figure 14. Representation of the structures of (a) Co-AE heterobimetallic complexes and (b) Fe or Co complexes featuring amidinate- or guanidinate-magnesium metalloligands by Mountford and co-workers.[421,422]

THF, (μ-OC)TM η^1-isocarbonyl groups) compete with the formation of the metal−metal bonds, even to the extent of forming ion-separated species.[421]

Similar studies were carried out using amidinate or guanidinate magnesium complexes, which were treated with the potassium salts of the transition metal anions $[(\eta^5\text{-Cp})\text{Fe}(\text{CO})_2]^-$ (**2**) and $[\text{Co}(\text{CO})_3(\text{PR}_3)]^-$ (**660**, R = Cy or Ph).[422] Reactions with the amidinate magnesium compounds afforded the heterobimetallic complexes $[\{\text{MesC}(\text{NR})_2\}(\text{thf})\text{Mg}\{\text{Fe}(\eta^5\text{-Cp})(\text{CO})_2\}]$ [R = Dipp (**666**), Mes (**667**); Figure 14b) and $[\{\text{MesC}(\text{NR})_2\}(\text{thf})\text{Mg}\{\text{Co}(\text{CO})_3(\text{PCy}_3)\}]$ [R = *i*Pr (**668**), Dipp (**669**), Mes (**670**); Figure 14b). Single crystal X-ray diffraction studies of **668** and **669** confirmed the presence of Mg−Co bonds in the solid state (d_{MgCo} = 2.525 Å, on average).

Analogous reactions with the guanidinate derivatives yielded the series of complexes $[\{\text{Me}_2\text{NC}(\text{Ndipp})_2\}\text{Mg}\{\text{Fe}(\eta^5\text{-Cp})(\text{CO})_2\}]_2$ (**671**) and $\{\text{Me}_2\text{NC}(\text{Ndipp})_2\}\text{Mg}\{\text{Co}(\text{CO})_3(\text{PR}_3)\}$ [R = Cy (**672**), Ph (**673**)], shown in Figure 14b (middle and right). The molecular structure of **671** features two Mg−Fe bonds (2.5279(4) Å) and isocarbonyl linkages, and its dimeric solid-state structure is maintained in solution, according to diffusion NMR spectroscopic measurements. The cobalt complexes consist of discrete Mg−Co bonds without forming isocarbonyl bonds, based solely on infrared spectroscopic data, since no structural authentication was available.[422]

Crimmin and co-workers reported the unsolvated analogue of complex **658**, $[(^{\text{Dipp}}\text{nacnac})\text{MgFe}(\eta^5\text{-Cp})(\text{CO})_2]$ (**674**), which was obtained via an improved protocol consisting of the reduction of dimer **651** with $[(^{\text{Dipp}}\text{nacnac})\text{Mg}]_2$ (**675**, Ar = Dipp; 1 equiv) in hydrocarbon solvents, therefore allowing for the exclusion of coordinating solvents such as THF.[423] The solid state molecular structure of **674** presents a shorter Mg−Fe distance (d_{MgFe} = 2.5190(7) Å) than the solvated analogue **658** (d_{MgFe}(**658**) = 2.6326(4) Å),[140] and significantly shorter than in the parent compound **675** (d_{MgMg} = 2.8457(8) Å).[467] Theoretical calculations (NBO analysis) confirmed the polar nature of the Fe−Mg bond, with negative and positive charges located on the Fe (−0.41) and Mg (+1.66) centers, respectively. The nucleophilic character of **674** was demonstrated through reactivity with fluoroarenes.

By reaction of compound **674** with the aromatic substrates in a 2:1 ratio (Scheme 78), aromatic substitution of a series of electron-deficient fluorinated aromatic compounds was achieved. Although the efficiency of the substitution was evidently dependent on the nature of the fluoroaromatic compound (perfluorobenzene and perfluorotoluene gave only small amounts of product), the reaction yielded the fluoroaryl-substituted complexes $[(\eta^5\text{-Cp})\text{Fe}(\text{CO})_2(\text{C}_6\text{F}_4\text{R})]$ (R = F (**676**), CF_3 (**677**), 2-py (**678**); Scheme 78). Structural authentication was reported for the 2-pyridyl derivative, **678**. Furthermore, a trimetallic reaction side product **679** was also characterized, which provided insight into the unusual **674**:fluoroarene = 2:1 stoichiometry. Single crystal X-ray diffraction revealed a triangular complex consisting of two

Scheme 78. Reactivity of $[(^{\text{Dipp}}\text{nacnac})\text{MgFe}(\eta^5\text{-Cp})(\text{CO})_2]$ (674) with Fluoroarenes, By the Group of Crimmin[423]

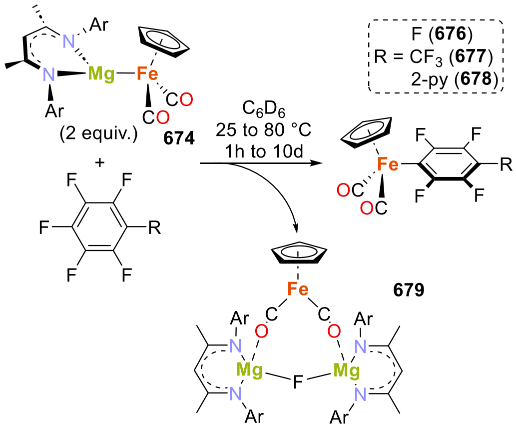

Mg(nacnac) units bridged by a fluoride anion, which are further connected to the (η^5-Cp)Fe(CO)$_2$ moiety via isocarbonyl linkages. It was proposed that this side product originates from a molecular magnesium fluoride formed as a transient intermediate, which reacts with an additional equivalent of starting material **674**. Further insights into the mechanism of nucleophilic aromatic substitution were gained from theoretical calculations. Two mechanistic pathways were considered, a concerted S$_N$Ar mechanism and a stepwise S$_N$Ar pathway with a low energy Meisenheimer intermediate. The analysis of the calculated reaction barriers suggests that a stepwise S$_N$Ar route is likely in operation and could be competitive with a concerted process identified for apolar M–M bonds. The charge separation between the two metals and polarization of the Mg–Fe bond in **674** were proposed as crucial factors favoring the S$_N$Ar mechanism leading to products **676–678**. The importance of charge separation to achieve a regioselective C–F functionalization was further demonstrated by the reaction of ferrate Na[(η^5-Cp)Fe(CO)$_2$] (Na[**2**]) with 2-(pentafluorophenyl)pyridine. This reaction affords the same reaction product, **678**, as observed when **674** is used as a reagent.[14,423]

A magnesium–iron complex analogous to **674** and related to **658**,[140,423] [(L)MgFe(η^5-Cp)(CO)$_2$] [**680**, L = CH$_2${PPh$_2$N(SiMe)$_3$}$_2$], featuring a phosphinimine based ligand, was prepared similarly from the corresponding magnesium iodide complex and Na[(η^5-Cp)Fe(CO)$_2$] (Na[**2**]).[473] Predominantly ionic bonding between the magnesium and iron centers was inferred from the stretching frequencies of the carbonyl ligands (ν_{CO} = 1924, 1860 cm^{-1}), and corroborated by DFT calculations.

Crimmin and co-workers additionally reported the Rh–Mg complex [(^{Dipp}nacnac)Mg(μ-H)$_2$Rh(η^5-Cp*)(SiEt$_3$)] (**681**), which was described as a complex of a cationic magnesium fragment coordinated by a rhodate anion (NPA charge at Rh = −0.99).[474]

Wolf and co-workers synthesized magnesium cobaltates related to **674** in an attempt to determine the influence of the countercation on the stability and reactivity of alkene metalate complexes.[427] As described, complexes bearing magnesium-transition metal bonds had long been known, but most of these were carbonyl complexes. The strong d–π* back-donation in such complexes weakens the metal–metal interaction. With the use of the bis(cyclooctadiene) complex K[Co(cod)$_2$] (K[**239**]), it was possible to synthesize highly reactive magnesium cobaltates and study their reactivity. A strong influence of the Mg^{2+} cation on the structure and their reactivity pattern was observed in the resulting complexes. Magnesium cobaltates [(^{Ar}nacnac)MgCo(η^4-cod)$_2$] [^{Ar}nacnac = [CH(ArNCMe)$_2$]$^-$; Ar = Mes (**682**), Dep (**683**), Dipp (**684**)] were synthesized via salt metathesis of [(^{Ar}nacnac)-MgI(OEt$_2$)] [Ar = Mes (**685**), Dep (**686**), Dipp (**687**)] with the potassium cobaltate K[**239**] (see Scheme 79). In the solid state, these complexes form contact ion pairs, as confirmed through X-ray diffraction analysis, with the formal oxidation state of the cobalt center unchanged, Co(−I).[427]

DFT calculations performed on **683** (population analyses, analyses of intrinsic bond orbitals, and atoms-in-molecules analyses) provided further insights on the nature of the interaction between both metal centers. NBO analysis shows no Lewis or non-Lewis shared orbitals between the magnesium and cobalt atoms. The Wiberg bond index for the Mg–Co bond is 0.027, and the atoms in molecules analysis reveal no bond critical point between the Mg and Co centers. Therefore, the combined theoretical analysis of the bonding in **683** indicated that the magnesium–cobalt interaction is highly electrostatic, and consistent with a cobalt atom more negatively charged than the magnesium atom. NMR scale studies on the interaction of the magnesium cobaltates toward donor/nondonor solvents showed that the contact ion pair structure is maintained in solution in nondonor solvents such as toluene, while the ion pair separates in donor solvents such as THF. The solvent-separated ion pair [(^{Dep}nacnac)Mg(thf)$_3$][Co(η^4-cod)$_2$] (**683**·thf) was obtained by crystallization from THF/*n*-hexane, and its molecular structure was determined via single-crystal X-ray diffraction. The formation of **683**·thf is reversible (Scheme 80), as demonstrated after drying **683**·thf *in vacuo* and redissolving it in C$_6$D$_6$. Furthermore, the ion-pairing has a direct influence on the reactivity and selectivity of the magnesium cobaltates toward phosphaalkynes. Upon reaction of **683** with *tert*-butylphosphaalkyne, *t*BuC≡P, in THF or toluene, different products are accessible, illustrating the influence of the ion-pairing on the reactivity of the magnesium cobaltates. While in THF the reaction with *t*BuC≡P afforded the previously reported homoleptic bis(1,3-diphosphacyclobutadiene)cobaltate,[210,475] [Co(P$_2$C$_2$*t*Bu$_2$)$_2$]$^-$ (**189**, as a [(^{Dep}nacnac)Mg(thf)$_3$]$^+$ salt), in toluene the heteroleptic sandwich complex [(^{Dep}nacnac)MgCo(P$_2$C$_2$*t*Bu$_2$)(η^4-cod)] (**688**) was obtained (Scheme 80). Since this heteroleptic complex bears a labile cod ligand, further functionalization was

Scheme 79. Synthesis of Magnesium Cobaltates by Wolf and Co-workers[427]

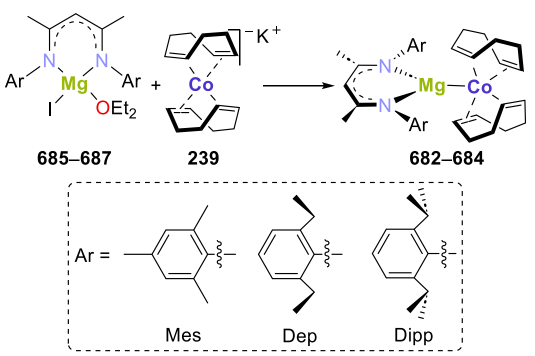

Scheme 80. Reversible Ion-Pairing in a Molecular Magnesium Cobaltate Complex and Subsequent Reactivity of Both Species toward Phosphaalkynes

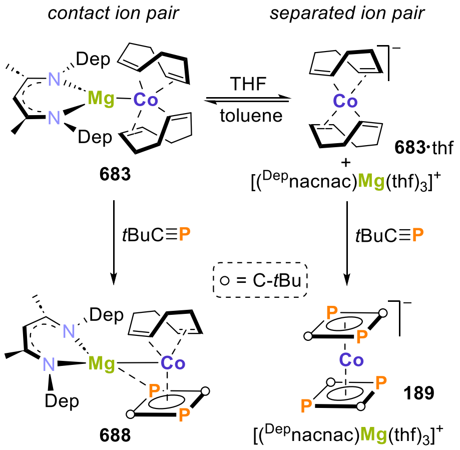

achieved by reaction with white phosphorus (P_4) (section 3.4.3).[427]

Moreover, the heterobimetallic complex $[(Cp^*NiP_2C_2tBu_2)\text{-}Co(\eta^4\text{-cod})]$ (**689**) was obtained after **688** reacted with Cp*Ni(acac) (see Scheme 81a). This complex results from the insertion of the "Cp*Ni" fragment into the diphosphacyclobutadiene ring.[427] A similar insertion had previously been observed by reaction of the homoleptic 1,3-diphosphacyclobutadiene complex **189** with $[Ni_2Cp_3]BF_4$ (Scheme 81b). This reaction initially affords an intermediate that proved too thermally unstable to allow for its isolation. This intermediate rapidly transforms into compound **690**, in which the Ni center is σ-coordinated by one of the P-atoms of a diphosphacyclobutadiene rings in **189**. Intermediate **690** slowly transforms into the 1,4-diphospha-2-nickelacyclopentadiene complex **691**, via insertion of the $[CpNi]^+$ fragment into a P−C bond of anion **189**. Furthermore, **691** rearranges to the thermodynamically more stable 1,3-isomer **692** upon heating.[476]

Scheme 81. Synthesis of Diphospha-nickelacyclopentadiene Species from 1,3-Diphosphacyclobutadiene Species from 1,3-Diphosphacyclobutadiene-Cobaltate Complexes[427,476]

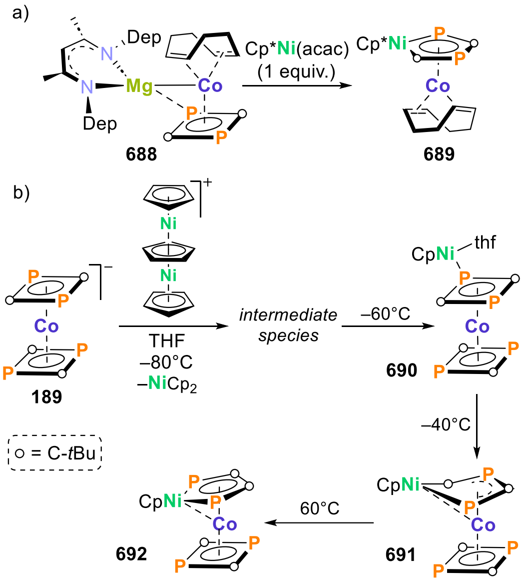

$[(^{Dep}nacnac)MgCo(P_2C_2tBu_2)(\eta^4\text{-cod})]$ (**688**) also served as a starting material for the preparation of bimetallic tetrel(II) cobaltate complexes, namely $[Ar^{Dipp2}TtCo(P_2C_2tBu_2)(\eta^4\text{-cod})]$ [Tt = Ge (**693**), Sn (**694**), Pb (**695**); $Ar^{Dipp2} = C_6H_3\text{-}2,6\{C_6H_3\text{-}2,6\text{-}iPr_2\}_2$; Scheme 82], and the homoleptic tin(II) complex $Sn[Co(P_2C_2tBu_2)(\eta^4\text{-cod})]_2$ (**696**).[477] Complexes **693**−**695** were cleanly obtained by reaction of the magnesium cobaltate **688** with terphenyl tetrel halides, $[Ar^{Dipp2}Tt(\mu\text{-}X)]_2$ (**697**, Tt = Ge, X = Cl; Sn, Pb, X = Br), either at −80 °C for the germanium derivative or at room temperature for the tin and lead compounds. X-ray crystallographic characterization of **693**−**695** revealed that the tetrel atoms are in *pseudo*-two coordinate environments ligated by the terphenyl-substituent and one of the P atoms of the diphosphacyclobutadiene ligand, and that no covalent metal−metal bonds are apparent between the tetrel atoms and the cobalt atom. Tt−Co distances are longer than the sum of their covalent radii (d_{GeCo} = 2.8434(6) Å, d_{SnCo} = 2.9534(5) Å, d_{PbCo} = 3.0318(6) Å, vs Σr_{GeCo} = 2.70 Å, Σr_{SnCo} = 2.89 Å, Σr_{PbCo} = 2.96 Å). These observations agree well with the quantum chemical calculations performed (DFT and atoms-in-molecules analyses). Likewise, reaction between **688** and $Sn(acac)_2$ afforded the homoleptic complex **696** (Scheme 82). $^{31}P\{^1H\}$ NMR spectroscopic studies of the reaction of **688** with $Pb(acac)_2$ indicated the formation of the analogous lead(II) complex $Pb[Co(P_2C_2tBu_2)(\eta^4\text{-cod})]_2$ (**698**). However, all attempts to isolate **698** were unsuccessful, due to its thermal instability, which resulted in the deposition of a black precipitate, assumed to be metallic Pb. The crystallographic characterization of **696** showed that, similar to the structures of **693**−**695**, the cobalt centers interact only weakly with the tin atom. The reactivity of complexes **693**−**696** toward white phosphorus was evaluated (see section 3.4.3).[477]

Scheme 82. Synthesis of Tetrel Cobaltates from the Magnesium Cobaltate $[(^{Dep}nacnac)MgCo(P_2C_2tBu_2)(\eta^4\text{-cod})]$ (688)[477]

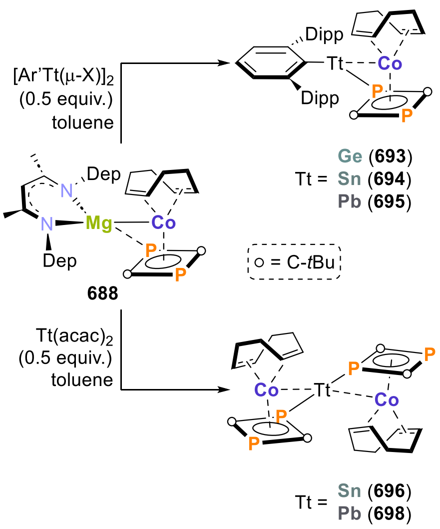

The chemistry of heterometallic magnesium−nickel hydride compounds has also been investigated.[478,479] Zhao, Maron, and Xu reported a dihydride-bridged heterotrimetallic complex bearing a tridentate β-diketiminato ligand with a pendant phosphine group.[478] Treating $[Ni(cod)_2]$ (**240**) with the magnesium-alkyl complexes [(NNP)MgR] [R = *n*Bu (**699**), Cy (**700**), *t*Bu (**701**); NNP = $[CH_3C(2,6\text{-}iPr_2C_6H_3N)CHC(CH_3)(NCH_2CH_2PPh_2)]$ in a 1:2 molar ratio afforded, in all cases, the trinuclear Mg−Ni−Mg complex **702** (see Scheme 83a) with elimination of the corresponding alkene and formation of two bridging hydride ligands. The NNP ligand in **699**−**701** adopts a different coordination mode upon reaction with the Ni(0) precursor, with the pendant phosphine arm dissociating from the magnesium atom and binding the nickel center in **702**, as verified by crystallographic characterization. Structural motifs similar to that in **702** were previously observed by this group at nickel or palladium, using a zinc-based reagent bearing the same NNP tridentate ligand.[480] The bridging hydride ligands in **702** result from nickel induced β-H elimination from the alkyl groups in the magnesium reagents. This was confirmed by treating a benzyl analogue of **699**−**701** with complex **240**. No reaction was observed, even when conducted at 60 °C, due to the lack of β-hydrogen atoms in the benzyl group. Additional information on the formation of cluster **702** was gained from the reaction of complex **700** with **240** in a 1:1 molar ratio, allowing for the formation of the

Scheme 83. Synthesis of (a) Hydride Bridged Heterobi- And Trimetallic Mg−Ni Complexes and (b) a Heterotrimetallic Nickelaspiropentane Featuring Magnesium-Based Metalloligands[478,479]

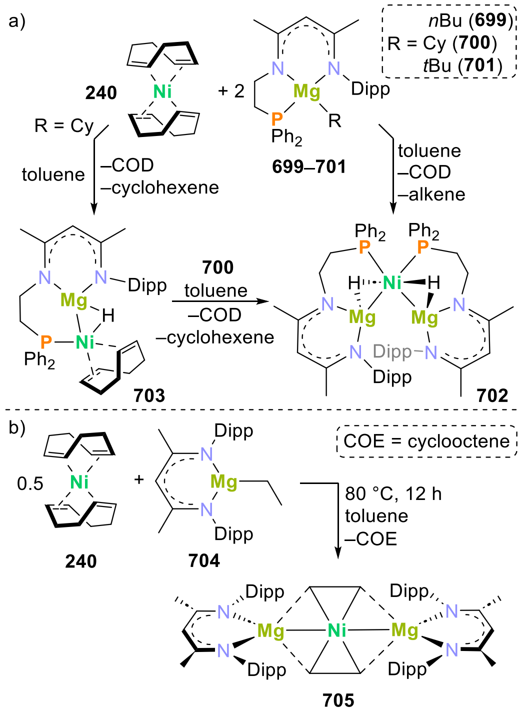

hydride-bridged heterobimetallic compound **703** (see Scheme 83a) with elimination of cyclohexene.

Crystallographic analysis of complex **703** confirmed that the nickel center retains a cyclooctadiene ligand and is coordinated by the pendant phosphine group of the NNP ligand. Further addition of one equivalent of **700** to **703** led to elimination of cyclohexene and cyclooctadiene and resulted in the heterotrinuclear cluster **702**. The calculated mechanism of formation of **702** supports the experimental observation of species **703** and its additional transformation leading to **702**, which occurs initially via coordination of the magnesium reagent to the nickel precursor, and later by alkyl transfer from the magnesium to the nickel center. NBO analysis suggests that the Ni−H−Mg motifs in this compound are best described as three-center two-electron bonds. Additionally, the reactivity of **702** toward isocyanides, carbodiimides and alkynes was studied. While isocyanides reversibly coordinate to the nickel center and induce rearrangement of one bridging hydride, the hydride moiety of **702** undergoes insertion of carbodiimides to give amidinate ligands coordinated to magnesium, or dehydrogenation of phenyl acetylene to give alkynyl ligands bridging the magnesium and nickel centers.[478]

Later, Maron, Xu, and co-workers reported a dimagnesium nickelate, a heterotrimetallic planar nickelaspiropentane complex, stabilized by magnesium-based metalloligands.[479] The reaction of **240** with the β-diketiminato magnesium monoalkyl compound ($^{\mathrm{Dipp}}$nacnac)MgEt (**704**, $^{\mathrm{Dipp}}$nacnac = $[\mathrm{CH(ArNCMe)_2}]^-$; Ar = Dipp) in a 1:2 ratio afforded the heterotrimetallic complex $[\{(^{\mathrm{Dipp}}\mathrm{nacnac})\mathrm{Mg}\}_2\mathrm{Ni}(\mathrm{C_2H_4})_2]$ (**705**, see Scheme 83b). The formation of **705** contrasted with that of complex **702**: whereas β-H elimination from the alkyl groups in **699**−**701** generated a thermally stable hydride-bridged complex, in the reaction leading to **705**, β-hydrogen elimination from the ethyl group at the magnesium metalloligand should generate a transient hydride species responsible for the hydrogenation of the cyclooctadiene ligands to cyclooctene at the nickel(0) center. The same process also generates the ethylene ligands coordinated to the transition metal in **705**. The rare metalla-*bis*-cyclopropane structure was determined by X-ray diffraction analysis, revealing a strictly linear Mg−Ni−Mg moiety (bond angle = 180°) and a planar hexagonal coordination geometry around nickel (sum of angles = 360°). Furthermore, the C−C bond length of the ethylene ligands indicates the presence of a single bond ($d_{\mathrm{C-C}}$ = 1.494(7) Å). DFT calculations indicate an absence of π-interactions between the carbon atoms, supporting single bond character for the ligands at the nickel center. NMR spectroscopy provided further evidence of the pronounced sp^3 character on the $\mathrm{C_2H_4}$ motif in solution. Altogether, the authors concluded that **705** is best described as a nickelaspiropentane species, instead of a π-bound ethylene complex. The coordination sphere of the complex is completed by σ Ni−C bonds and by weak Mg−C contacts, proposed to be agostic interactions, between the magnesium metalloligands and the ethylene units. Additionally, DFT and NBO analyses indicated that the (nacnac)Mg unit acts as a Z-type ligand to the Ni complex. The nickel center in **705** was proposed to be in the oxidation state +II. This assignment was supported by X-ray photoelectron spectroscopy (XPS) performed on the complex. Furthermore, the authors studied the activation of dihydrogen and the hydrogenation of unsaturated substrates by **705** (see section 3.1).[479]

In 2019, Crimmin reported the complex $[\mathrm{PdH_3}\{\mathrm{Mg}(^{\mathrm{Ar}}\mathrm{nacnac})\}_3]$ (**706**, $^{\mathrm{Ar}}$nacnac = $[\mathrm{CH(ArNCMe)_2}]^-$; Ar = Dipp; Scheme 84a), which exhibits a remarkable hexagonal planar arrangement around the central zerovalent transition metal.[424] The species **706** can be seen as a palladate(0) fragment $[\mathrm{PdH_3}]^{3-}$ and three magnesium-nacnac cations $[\mathrm{Mg}(^{\mathrm{Ar}}\mathrm{nacnac})]^+$. DFT calculations suggest that the Pd−Mg interactions in **706** are significantly ionic, with the magnesium atoms bearing a substantial positive charge, while the negative charge is located mainly on the hydrides, but also to some extent on the palladium atom. In the presence of selected alkyl phosphines $\mathrm{PR_3}$ (R = *t*Bu, Cy), **706** was found to be in a ligand exchange equilibrium with a T-shaped palladium phosphine dihydride $[\mathrm{Pd(PR_3)(H)_2}\{\mathrm{Mg}(^{\mathrm{Ar}}\mathrm{nacnac})\}_2]$ ($\mathrm{PR_3}$ = *t*Bu (**707**), Cy (**708**); Scheme 84a). The platinum complex $[\mathrm{Pt(PR_3)(H)_2}\{\mathrm{Mg}(^{\mathrm{Ar}}\mathrm{nacnac})\}_2]$ (**709**) shares similar features in terms of structure and reactivity. By contrast, the lighter analogue $[\mathrm{NiH_3}\{\mathrm{Mg}(^{\mathrm{Ar}}\mathrm{nacnac})\}_3]$ (**710**) adds $\mathrm{PR_3}$ (R = *t*Bu, Cy) without dissociation of $\mathrm{Mg}(^{\mathrm{Ar}}\mathrm{nacnac})$ ligands and preserving the original hexagonal arrangement of the hydrides and magnesium donors, thereby forming a compound with nearly ideal hexagonal pyramidal geometry (**710**·$\mathrm{PR_3}$, Scheme 84a). Calculated Wiberg bond indexes (WBIs) suggest more covalent Pd−Mg and Mg−H interactions in **708** than in **706**. Moreover, QTAIM calculations on **708** revealed bond-critical points between the magnesium and hydrogen atoms, but not between the palladium and magnesium centers, as opposed to what is observed for the hexagonal planar precursor **706**.

Shortly thereafter, the Crimmin group expanded on their study of the gap between the hexagonal planar $\mathrm{MH_3E_3}$ (D_{3h}) or trigonal planar $\mathrm{M(E{-}H)_3}$ (C_{3h}) bond situations for a low-valent group 10 transition metal atom interacting with three E−H donors (M = Pd or Pt, E = $\mathrm{Zn}\{^{\mathrm{Ar}}\mathrm{nacnac}\}$ or

Scheme 84. Hexagonal Planar Complexes of Low-Valent Group 10 Metals-M(nacnac) Complexes (M = Mg, Zn)[424,425]

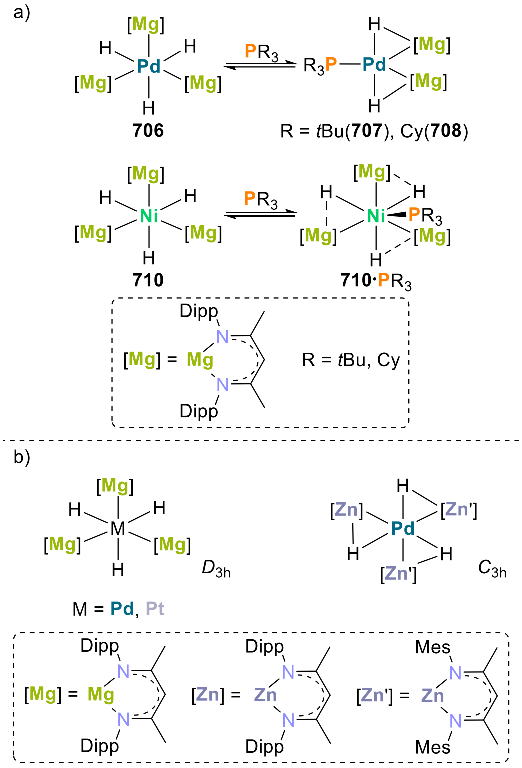

Scheme 85. Synthesis of the Nickel−Magnesium Cluster $[(\eta^5\text{-Cp})\text{Ni}[(i\text{Pr}_3\text{P})\text{Ni}]_4\text{H}_6(\mu_4\text{-MgCp})]$ (716)[481]

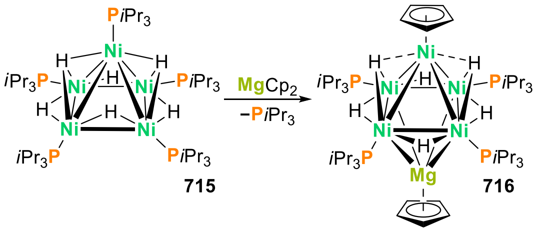

Mg{^{Ar}nacnac}).[425] X-ray and neutron diffraction studies in combination with computational studies revealed that the zinc-based donors tend to form C_{3h} geometries, while the magnesium analogues prefer to adopt a D_{3h} symmetry (Scheme 84b). The evidence from this work indicates that the hexagonal planar bonding extreme is favored in systems with large ionic contributions to the M−Mg interaction, implying a formal description of the system as a metalate(0) fragment $[MH_3]^{3-}$ with three $[Mg(^{Ar}nacnac)]^+$ cations. The deformation from the trigonal planar to the hexagonal planar configuration was found to have a low energy penalty at the expense of the M−E bond, as evidenced by the corresponding Walsh diagram. Furthermore, it is noteworthy that **706** reversibly reacts with molecular hydrogen to form the tetrahydride species $[PdH_4\{Mg(^{Ar}nacnac)\}_2]$ (**711**, ^{Ar}nacnac = $[CH(ArNCMe)_2]^-$; Ar = Dipp) and the dimer $[(^{Ar}nacnac)Mg(\mu\text{-}H)]_2$ (**712**).[426] In contrast, the heavier analogues $[PtH_4\{Mg(^{Ar}nacnac)\}_2]$ (**713**) and related $[PtH_4\{Zn(^{Ar}nacnac)\}_2]$ (**714**) feature $[M^{II}H_4]^{4-}$ fragments interacting with two cationic Mg or Zn moieties and, therefore, cannot be described as low-valent metalates.

Magnesium metalates based on metal aggregates have also been described. By treating the nickel cluster $[(i\text{Pr}_3\text{P})\text{Ni}]_5\text{H}_6$ (**715**) with $MgCp_2$, the nickel−magnesium compound $[(\eta^5\text{-Cp})\text{Ni}[(i\text{Pr}_3\text{P})\text{Ni}]_4\text{H}_6(\mu_4\text{-MgCp})]$ (**716**, Scheme 85) was obtained.[481] This compound formed by formal Cp^- transfer with release of a phosphine ligand from **715**, as observed upon reaction with either $MgCp_2$ or TlCp. However, the anionic cluster fragment obtained was found to interact differently with both metal cations: while the thallium cation is covalently bonded to the nickel cluster, forming $[(\eta^5\text{-Cp})\text{Ni}[(i\text{Pr}_3\text{P})\text{Ni}]_4\text{H}_4(\mu_4\text{-Tl})]$ (**717**) with release of H_2, the magnesium analogue stabilizes via ionic interactions. This disparate behavior was attributed to the presence of the harder Mg^{2+} cation in **716**, instead of the soft Tl^+ cation in **717**.

2.3.3. Metalates Stabilized by Lewis-Acidic Group 13 Metallatranes and Related Complexes.

A different tuning effect can be created by rational ligand design, using frameworks that accommodate the stereoelectronic requirements of the metal to support complexes which can react with a variety of substrates. The groups of Peters[141,143,428−430] and Lu[81,433−437] have extensively investigated the use of Group 13 metallatrane ligands, their coordination to base metals, and the reactivity of the resulting molecular species toward small molecules.[27]

2.3.3.1. Tris(phosphino)borane Complexes.

In 2011, Peters and co-workers reported that the ligand tris[2-(diisopropylphosphino)phenyl]borane (P_3^B)[482−484] stabilizes low-valent iron centers to afford anionic dinitrogen iron metallaboratrane complexes.[141,485] A comproportionation reaction between $FeBr_2$ and iron powder in the presence of the P_3^B ligand affords the complex $[(P_3^B)FeBr]$ (**718**). Reduction of **718** with sodium naphthalenide yields different, but related, products depending on the stoichiometry of reductant used. Treatment with a slight excess of $NaC_{10}H_8$ yields the neutral dinitrogen compound $[(P_3^B)Fe(N_2)]$ (**719**, Scheme 86), whereas reaction with 2.5 equiv of the reductant leads to the anionic complex $[(P_3^B)Fe(N_2)]^-$ (**720**; isolated as the Na^+ and $[Na([12]crown\text{-}4)_2]^+$ salts, Scheme 86 center right). **720** can also be generated *in situ* by reaction of the Fe(I) complex **718** with an excess of sodium amalgam under a nitrogen atmosphere.[428]

Exposure of **719** to vacuum resulted in spectroscopic changes indicative of a labile N_2-ligand. This was corroborated by reaction of **719** with carbon monoxide, which afforded the carbonyl compound $[(P_3^B)Fe(CO)]$ (**721**; ν_{CO} in Table 1).[141] Furthermore, treatment of **719** with *p*-methoxyphenyl azide yielded the diamagnetic imido complex $[(P_3^B)Fe{\equiv}N{-}Ar]$ (**722**, Ar = *p*-methoxyphenyl; Scheme 86, top right). Complex $[Na([12]crown\text{-}4)_2][\mathbf{720}]$ can be further reduced with KC_8 in DME to afford the dianionic complex $[Na([12]crown\text{-}4)_2][K(DME)_x][(P_3^B)Fe(N_2)]$ (**723**).[486] Compound **723** is diamagnetic in the ground state according to ^{57}Fe Mössbauer spectroscopy. Peters and co-workers generated this species *in situ* from **720** for use in nitrogen fixation studies (see section 3.2.6).

Crystallographic studies revealed that the complexes feature a trigonal bipyramidal structure, where the Lewis acidic borane unit of the ligand P_3^B occupies the apical position and may interact strongly with the Lewis basic Fe atom. A comparison of the crystallographic data for these complexes revealed that changes in the basicity of the metal center cause an adjustment in the Fe−B distance. Therefore, the P_3^B ligand acts as a

Scheme 86. Synthesis and Reactivity of Low-Valent Iron Compounds Derived from Tris(phosphino)borane (P_3^B) Ligand[141,428,429]

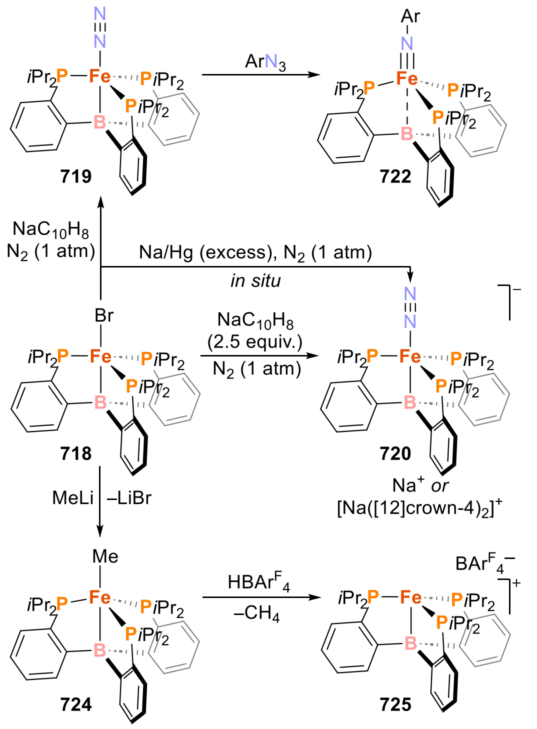

flexible scaffold that stabilizes different electronic environments. While in the highly reduced complex **720** a short Fe–B distance (d_{FeB} = 2.311(2) Å) indicates a strong iron–boron contact, a longer Fe–B distance (d_{FeB} = 2.608 Å) in the Fe(II) compound **722** (Fe≡N–Ar) suggests only a weak Fe–B interaction. The elongation of the Fe–B distance also has consequences on the geometry around the metal center, which shifts from a trigonal-bipyramidal in **720** to a pseudotetrahedral configuration in **722**.[141] Furthermore, **718** reacted with methyl lithium to form the Fe(I) complex $[(P_3^B)FeMe]$ (**724**). This can be protonated with $HBAr^F_4$ to generate the coordinatively unsaturated cationic complex $[(P_3^B)Fe]BAr^F_4$ (**725**, Scheme 86, bottom). The Fe–B distance in **725** is rather short (d_{FeB} = 2.217(2) Å), with the iron center residing in a distorted trigonal pyramidal geometry.[429] The overall conclusion from this work was that the ability to shuttle between different electronic configurations and molecular geometries makes these compounds particularly suitable for the activation and functionalization of small molecules, and the various contributions of the Peters group in this area are discussed in section 3.2 (*vide infra*).[27]

The neutral complex $[(P_3^B)Fe(N_2)]$ (**719**) served as a platform to synthesize a triad of highly reduced iron-nitrosyl complexes and study their electronic nature.[487,488] The series of complexes $[(P_3^B)Fe(NO)]^n$ [n = +1 (**726**), 0 (**727**), − 1 (**728**); see Scheme 87] are rare examples of isolable reduced nitrosyl compounds. The neutral dinitrogen complex **719** reacts with nitrosonium hexafluorophosphate ($[NO]PF_6$), which acts both as an oxidant and a nitrosyl source. Salt anion metathesis afforded compound $[(P_3^B)Fe(NO)]BAr^F_4$ (**726**). Reduction of **726** with cobaltocene yielded the neutral $[(P_3^B)Fe(NO)]$ (**727**), which was further reduced to yield the anionic $[Na([12]crown\text{-}4)_2][(P_3^B)Fe(NO)]$ (**728**). In the

Scheme 87. Synthesis of the Triad of Iron-Nitrosyl Complexes $[(P_3^B)Fe(NO)]^n$ (n = +1, 0, −1)[487,488]

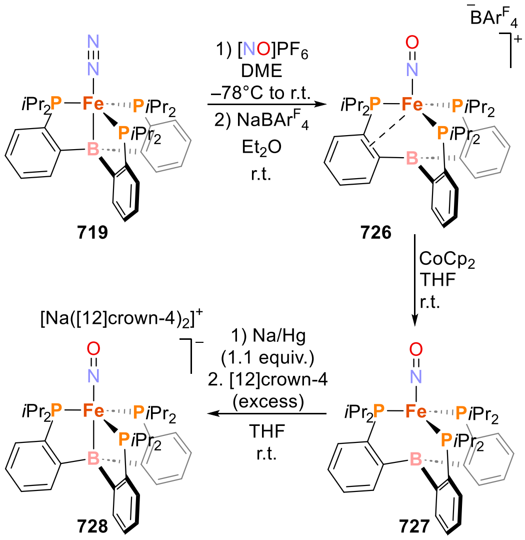

Feltham–Enemark notation,[489] these species are described as $\{FeNO\}^{8-10}$. The crystal structures of **726**–**728** ($\{FeNO\}^{8-10}$) revealed a high linearity in the Fe–N–O angle for all the complexes (**726**: 175.8(3)°, **727**: 176.18(6)° **728**: 179.05(12)°).

The structure and electronic nature of the series of iron-nitrosyl complexes was interrogated by experimental and computational methods. The complexes feature an NO^+ ligand and strong Fe–NO π-backbonding interactions. Hence, the compounds are significantly covalent, which could explain the remarkable stability observed across the three redox states, in contrast with observations for other nitrosyl complexes. The Fe-NO motifs exhibit closed-shell electronic structures thanks to the Fe–B interactions in the complexes. Compound **726** was described as an Fe(0)-NO^+ species, which features a low spin $\{FeNO\}^8$ configuration. Two very strong metal-to-ligand π-backbonding interactions are established with the NO^+ ligand.

The crystal structure of this complex revealed a unique metal-olefin π-bond between the iron center and a C═C bond in one of the aromatic benzene rings in the P_3^B ligand. The reduction leading to **727** was found to be metal-based according to EPR, which would indicate the presence of an Fe(−I)-NO^+ compound with a low spin $\{FeNO\}^9$ configuration in the ground state. Upon reduction of **726** to **727**, the Fe–NO bond becomes weaker due to reduction in the covalency of the two Fe–NO π-bonds. The weakening of this interaction was predicted by DFT calculations and is partly caused by the existence of spin polarization effects in the $\{FeNO\}^9$ configuration. In turn, compound **728** is diamagnetic in a closed-shell ground state. Analysis of the molecular orbitals of the complex revealed a completed^{10} shell for the iron center, indicating that the second reduction is also centered on the metal and leads to a low spin $\{FeNO\}^{10}$ configuration with a formally Fe(−II) center. The electron density of the highly reduced metal center, however, is accepted by the Fe–B interaction, which strengthens significantly due to the formation of an Fe–B σ single bond. Therefore, the iron center acts as a Lewis base and donates to the boron center. This interaction was described as a true reverse dative Fe → B bond, which resulted in the crucial stabilization of the highly reduced species. Consequently, compound **728** features an Fe(−II) ion ligated to a NO$^+$ motif through Fe−NO π-bonds and significantly stabilized by an Fe−B bond. In summary, despite the low formal oxidation states achieved at the iron centers, the nitrosyl ligands maintain the NO$^+$ redox state. These results highlight the role of the flexible P_3^B ligand scaffold in the stabilization of highly reduced metal centers, which in this case acts as an electron reservoir by storing two electrons on site. A similar theoretical analysis comparing $[(P_3^B)Fe(N_2)]^-$ (**720**) to the isoelectronic compound **727** revealed that the dinitrogen ligand in the former is less effective at stabilizing the Fe(−I) center than the NO$^+$ ligand in **727**. These observations agree well with the relative π-accepting abilities of both ligands and explain the formation of an Fe−B σ bond already in the d^9 state in **720**. The authors suggested that these observations additionally support their hypothesis that Fe−B bonding is critical to achieve effective small molecule activation, including N$_2$ fixation.[487,488]

2.3.3.2. Tris(phosphino)silyl Complexes. Peters and coworkers also developed the related tetradentate tris(phosphino)silyl ligands $[Si(o\text{-}C_6H_4PR_2)_3]^-$ $[P^R{}_3^{Si}$, R = Ph (**729**), *i*Pr (**730**)] and demonstrated their versatility in the stabilization of dinitrogen and monocarbonyl iron complexes in different formal oxidation states.[142,143,431,432] Reduction of the chlorido-complexes $[(P^R{}_3^{Si})FeCl]$ [R = Ph (**731**), *i*Pr (**732**)] with either sodium amalgam or sodium naphthalenide under a nitrogen atmosphere yielded the dinitrogen adducts $[(P^R{}_3^{Si})Fe(N_2)]$ [R = Ph (**733**), *i*Pr (**734**); Scheme 88]. In both cases, measurements of the magnetic moment indicated the presence of an Fe(I) center [$S = 1/2$; μ_{eff}(**733**) = 1.8 μB, μ_{eff}(**734**) = 2.2 μB)]. The presence of terminally coordinated N$_2$ molecules was revealed via X-ray diffraction analysis. In **733**, the short N≡N bond distance [d_{N2}(**733**) = 1.106(3) Å] is consistent with the high-energy N≡N stretching vibrations [$\nu_{N\equiv N}$(**733**) = 2041 cm^{-1}], which indicate that the dinitrogen ligand is only weakly activated.[142] As a result, the dinitrogen ligand in these complexes is labile, being easily removed under vacuum or displaced by carbon monoxide to generate the carbonyl compound $[(P^R{}_3^{Si})Fe(CO)]$ ([R = Ph (**735**), *i*Pr (**736**)]; see Scheme 88, Table 1 shows the CO stretching frequencies).[143]

Scheme 88. Synthesis of Dinitrogen- and Carbonyl-Iron Complexes Featuring Tetradentate Silylphosphino Ligands[142,143]

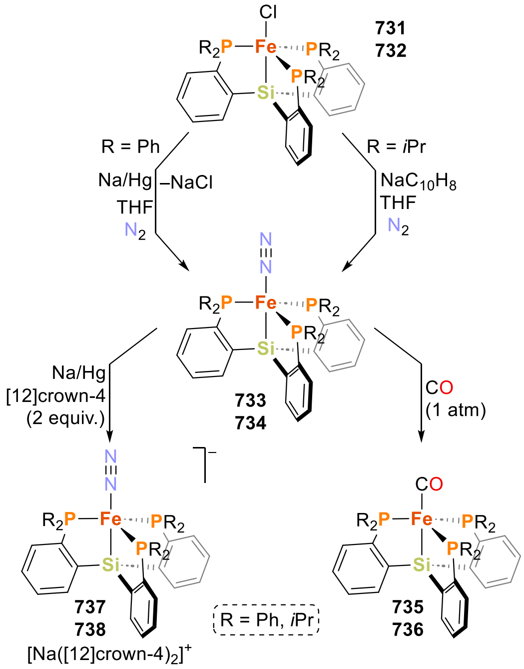

Further reduction of **733** affords the diamagnetic anionic complex $[Na([12]crown\text{-}4)_2][(P^{Ph}{}_3^{Si})Fe(N_2)]$ (**737**), formally an Fe(0) species. The analogous $[(P^{iPr}{}_3^{Si})Fe(N_2)]^-$ (**738**) was similarly obtained.[432] By contrast to the neutral **733**, the dinitrogen ligand is less labile in this highly reduced compound due to the stronger backbonding of the more electron-rich metal center, evidenced by the stretching vibration observed by FT-IR spectroscopy ($\nu_{N\equiv N}$ = 1967 cm^{-1}, see Table 2). Similar to the synthesis of precursor **731**, divalent or trivalent cobalt, nickel and iridium compounds bearing the tetradentate ligands $[Si(o\text{-}C_6H_4PR_2)_3]^-$ were obtained by the same group.[431] Furthermore, analogous reduction of the cobalt precursors by sodium amalgam afforded the dinitrogen adducts $[(P^R{}_3^{Si})Co(N_2)]$ [R = Ph (**739**), *i*Pr (**740**)].[431] However, no further reduction to afford anionic complexes, similar to **737**, was reported.

Scheme 89. Synthesis and Reactivity of $[(P^{iPr}{}_3^{Si})Fe\{CONa(thf)_3\}]$ (741)[143]

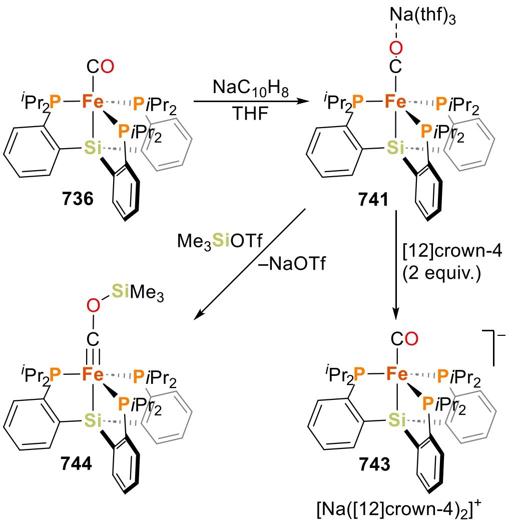

The redox chemistry of the carbonyl complex $[(P^{iPr}{}_3^{Si})Fe(CO)]$ (**736**) was investigated by cyclic voltammetry, which revealed two reversible one-electron redox couples.[143] These data are consistent with the electrochemical generation of the [Fe-CO]$^+$ (−0.68 V) and the [Fe-CO]$^-$ (−1.9 V vs Fc/Fc$^+$) species. Consequently, the chemical reduction of **736** was carried out, affording the diamagnetic ion-paired species $[(P^{iPr}{}_3^{Si})Fe\{CONa(thf)_3\}]$ (**741**, Scheme 89). The lower energy CO stretching vibrations in **741** (ν_{CO} = 1717 cm^{-1}, Table 1) with respect to the neutral **736** (ν_{CO} = 1850 cm^{-1}, Table 1) reflect the higher electron density and therefore increased backdonation in the former, more reduced species. Oxidation of **736** with $H(OEt_2)_2[B(3,5\text{-}(CF_3)_2\text{-}C_6H_3)_4]$ yielded the cationic Fe(II) species $[(P^{iPr}{}_3^{Si})Fe(CO)]BAr^F{}_4$ (**742**). Moreover, addition of [12]crown-4 (2 equiv) to **741** afforded the ion-separated complex [Na([12]crown-4)$_2$]-

$[(\mathrm{P}^{i\mathrm{Pr}}{}_{3}{}^{\mathrm{Si}})\mathrm{Fe(CO)}]$ (**743**, Scheme 89; ν_{CO} = 1757 cm^{-1}, Table 1).

X-ray diffraction analysis on the related neutral, reduced, and oxidized species revealed little geometric change about the iron center corresponding to changes in its formal oxidation state. By treating the reduced species **741** with trimethylsilyl trifluoromethanesulfonate ($\mathrm{Me_3SiOTf}$), functionalization of the terminal CO ligand occurs, affording the well-defined iron carbyne species $[(\mathrm{P}^{i\mathrm{Pr}}{}_{3}{}^{\mathrm{Si}})\mathrm{Fe{\equiv}C\text{-}OSiMe_3}]$ (**744**, Scheme 89). The crystallographic data show that the Fe−C bond in **744** is significantly shorter than the one in **736** or **741** [d_{FeC}(**736**) = 1.769(2) Å or d_{FeC}(**741**) = 1.732(3) Å vs d_{FeC}(**744**) = 1.671(2) Å], and that the C−O bond is consequently elongated [d_{CO}(**736**) = 1.169(2) Å or d_{CO}(**741**) = 1.188(3) Å vs d_{CO}(**744**) = 1.278(3) Å], suggesting carbynic character in **744**. DFT calculations along with comparative Mössbauer data for all the complexes enabled further insights into their electronic structure, providing evidence for the multiple bond character of the Fe−C bond. An initial analysis of the oxidation state of the metal center in **744** indicated the presence of an Fe(IV) (d^4) center, ligated by an anionic silylphosphino ligand and a $[\mathrm{COSiMe_3}]^{3-}$ carbyne. However, in analogy to complex **741**, the authors considered a scenario in which the carbyne ligand is regarded as a closed-shell cation $[\mathrm{COSiMe_3}]^{+}$, suggesting a "Fischer-type" carbyne character with inverted polarization, where the metal center back-donates electron density to the carbon atom. In this case, the iron center would formally correspond to Fe(0) (d^8). Altogether, the theoretical and spectroscopic data available for **744** indicated the presence of a strongly π-accepting Fischer-type carbyne ligand which stabilizes a low-valent Fe(0) center, instead of a high-valent Fe(IV) center. The authors pointed out that the DFT analysis suggested the further possibility of the complex featuring an Fe(−II) (d^{10}) center, which cannot be completely excluded when considering the metal and carbyne character of the occupied orbitals.[143] Carbyne complex **744** is reminiscent of $[\{\mathrm{K(Et_2O)}\}_2\{\mathrm{Cp^*Co{\equiv}CNAr^{Tripp2}}\}]$ (**117**), which was obtained by Figueroa and co-workers by reduction of an isocyanide complex (see Scheme 12, section 2.2.1).[137] Further examples of related chemistry are discussed in section 3.3.

Peters and co-workers also investigated the behavior of anionic silatrane complexes of the 4d and 5d metals from groups 8 and 9.[490−492] Reduction of the ruthenium or osmium M(I) metalloradicals $[(\mathrm{P}^{i\mathrm{Pr}}{}_{3}{}^{\mathrm{Si}})\mathrm{M(N_2)}]$ [M = Ru (**745**), Os (**746**); $\mathrm{P^R}{}_3{}^{\mathrm{Si}}$ = $[\mathrm{Si}(o\text{-}\mathrm{C_6H_4P}i\mathrm{Pr_2})_3]^-$ (**730**)] was shown to be feasible by cyclic voltammetry (Ru$^{\mathrm{I/0}}$ redox pair at −2.14 V and Os$^{\mathrm{I/0}}$ −1.94 V, vs Fc/Fc$^+$) and achieved on a preparative scale by treatment with $\mathrm{KC_8}$ (Scheme 90).[490] The resulting complexes $[\mathrm{K(thf)}_x][(\mathrm{P}^{i\mathrm{Pr}}{}_{3}{}^{\mathrm{Si}})\mathrm{M(N_2)}]$ [M = Ru (**747**), Os (**748**)] are competent catalysts for the $\mathrm{N_2}$-to-$\mathrm{NH_3}$ conversion reaction (see section 3.2).[491]

In a similar vein, the group 9 complexes $[\mathrm{K(thf)_3}][(\mathrm{P}^{i\mathrm{Pr}}{}_{3}{}^{\mathrm{Si}})\mathrm{M}]$ [M = Rh (**749**), Ir (**750**); Scheme 90] were isolated by reduction of the dinitrogen complexes $[(\mathrm{P}^{i\mathrm{Pr}}{}_{3}{}^{\mathrm{Si}})\mathrm{M(N_2)}]$ [M = Rh (**751**), Ir (**752**)].[431,492,493] The structural characterization, pulse EPR studies, and theoretical calculations indicate that in **749** and **750** the metal centers bind the silicon atom of the silatrane ligand via 2c-3e σ bonds ("half-bonds"). The electronic structure of these zerovalent complexes is defined by primarily metal-based SOMOs, stabilized by strong TM $4d_{z2}$ or $5d_{z2}$−$3p_z$ orbital mixing, which places substantial spin density on the silicon atom and destabilizes the antibonding transition-metal-silyl σ^*-orbitals. Furthermore, **749** and **750** exhibit significant metalloradical character, as shown by EPR spectroscopy and supported by DFT calculations. This was additionally corroborated by H atom abstraction reactions, which generated the M(I)-hydride complexes $[\mathrm{K(thf)_3}][(\mathrm{P}^{i\mathrm{Pr}}{}_{3}{}^{\mathrm{Si}})\mathrm{MH}]$ [M = Rh (**753**), Ir (**754**); Scheme 90].

Scheme 90. Synthesis of Silatrane Complexes of the Group 8 and 9 Second- and Third-Row Transition Metals[490−492]

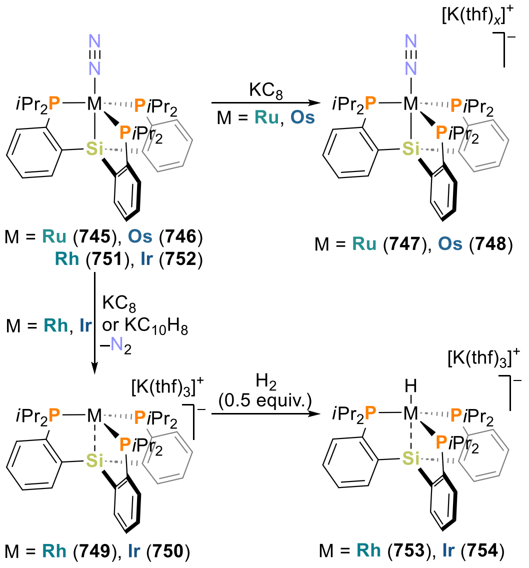

On related chemistry, Filippou and co-workers reported in 2018 that two-electron reduction of $[\mathrm{Tp'Mo(CO)_2(PMe_3)Cl}]$ (**755**, Tp′ = κ^3-N,N′,N″-hydridotris(3,5-dimethylpyrazolyl)-borate) with 2 equiv of sodium naphthalenide affords the metalate complex $\mathrm{Na[Tp'Mo(CO)_2(PMe_3)]}$ (**756**, Scheme 91).[494] **756** reacted with the NHC-stabilized Si(II) reagent $\mathrm{SiBr_2(SIDipp)}$ (SIDipp = $\mathrm{C[N(C_6H_3\text{-}2,6\text{-}}i\mathrm{Pr_2)CH_2]_2}$) to yield

Scheme 91. Reactivity of Metalate Na[Tp′Mo(CO)$_2$(PMe$_3$)] (756) with SiBr$_2$(SIDipp), and Subsequent Reduction of the Obtained Product to Yield a Dianionic 1,3-Dimetalla-2-silaallene[494]

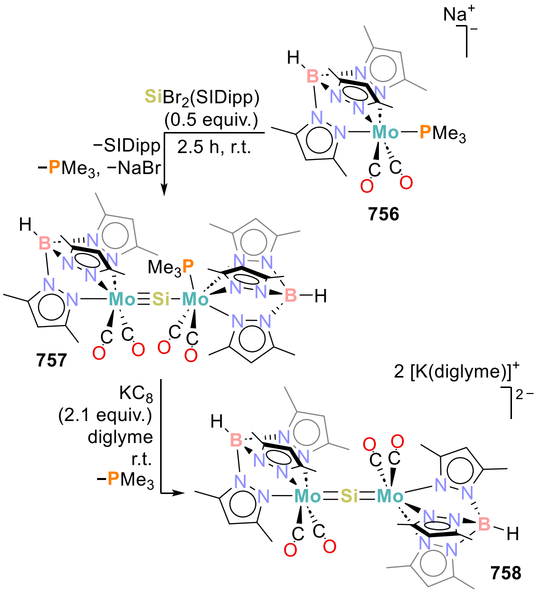

the metallasilylidyne complex $[Tp'(CO)_2Mo{\equiv}Si{-}Mo(CO)_2(PMe_3)Tp']$ (**757**). Cyclic voltammetry studies on **757** revealed an irreversible reduction event (−1.907 V vs Fc/Fc^+), prompting the authors to investigate its chemical reduction. Two-electron reduction of **757** by KC_8 (2.1 equiv) with concomitant PMe_3 elimination led to the 1,3-dimetalla-2-silaallene dianionic complex $[Tp'(CO)_2Mo{=}Si{=}Mo(CO)_2Tp']^{2-}$ (**758**, Scheme 91), isolated as the $[K(diglyme)]^+$ salt. Crystallographic characterization showed that dianion **758** features two cumulated double bonds to a linearly coordinated Si atom. The Si atom sits on a crystallographic inversion center, with the two 15 VE $Tp'(CO)_2Mo$ fragments in *antiperiplanar* conformation. IR spectroscopic analysis revealed intense absorption bands at 1765 and 1696 cm^{-1}, considerably low wavenumbers, suggesting strong π-backbonding from the electron rich metal centers to the terminal carbonyl ligands. Quantum chemical calculations support the 1,3-dimetalla-2-silaallene description given for **758**.

2.3.3.3. Metallalumatranes and Related Analogues.

Metallalumatranes featuring a dative M → Al bond were unreported until 2011, when Lu and co-workers described the first examples with zerovalent iron, cobalt, and nickel.[433,434] This type of molecule is structurally similar to the aforementioned metallaboratranes by Peters.[141,428] In these compounds, the transition metal atom acts as a Lewis base, donating electron density to a Lewis acidic aluminum atom. Deprotonation of the heptadentate ligand $N[o\text{-}(HNCH_2PiPr_2)C_6H_4]_3$ (**759**, see Scheme 92) followed by addition of $AlCl_3$ yields the metalloligand AltraPhos (alumatrane-phosphine), which has three pendant phosphine groups.[495]

Reactions of AltraPhos (Scheme 92 top) with $FeBr_2$ or $CoBr_2$ and KC_8, or with the readily available Ni(0) precursor $[Ni(cod)_2]$ (**240**, Scheme 92 middle, M = Al), afforded $[(N_2)MAl\{N[o\text{-}(NCH_2PiPr_2)C_6H_4]_3\}]$ {M = Fe [**760** (N_2)], Co [**761** (N_2)]} or $[NiAl\{N[o\text{-}(NCH_2PiPr_2)C_6H_4]_3\}]$ (**762**), respectively. End-on coordination of the dinitrogen ligand in **760** and **761** was determined by FT-IR spectroscopy ($\nu_{N\equiv N}$ = 2010 and 2081 cm^{-1}, respectively; see Table 2).

Crystallographic analysis of **760**−**762** confirmed the existence of the M → Al bond and, for **760** and **761**, the coordination of the dinitrogen ligand. However, for the iron complex, both the end-on coordinated compound, **760** (N_2), and a N_2-bridged diiron complex, $[\{\mathbf{760}\}_2(\mu\text{-}N_2)]$, were identified. The observation of both species suggests the existence of an equilibrium between them and shows that the N_2 ligand is labile. Furthermore, a slightly elongated N−N bond distance [1.107(4) Å vs d_{NN} = 1.0975 Å in free $N_2(g)$] implies the bridging N_2 ligand is partially activated. The measured M−Al bond lengths indicate that the strength of the metal−metal interaction decreases in the order Ni−Al (2.450(1) Å) > Co−Al (2.6202(9) Å) > Fe−Al (2.809(2) Å). Cyclic voltammetry studies (measured vs $[FeCp_2]^{0/+}$) showed single reversible reductions at −0.95 and −2.08 V for **760** (N_2) and **761** (N_2), respectively, assigned to the formal M^{-I}/M^0 couples, with the cobalt center being easier to reduce than the iron one, according to the difference in their redox potentials (1.12 V). The nickel analogue **762** showed a reversible oxidation event at −0.74 V, assigned to the Ni^0/Ni^I redox couple.

Scheme 92. Synthesis of (Hetero)metallic Complexes Featuring the Heptadentate Ligand $N[o\text{-}(HNCH_2PiPr_2)C_6H_4]3$ or Its Related Metalloligands $M\{N[o\text{-}(NCH_2PiPr_2)C_6H_4]_3\}$ (M = Al, Ga, In)[433,435,436]

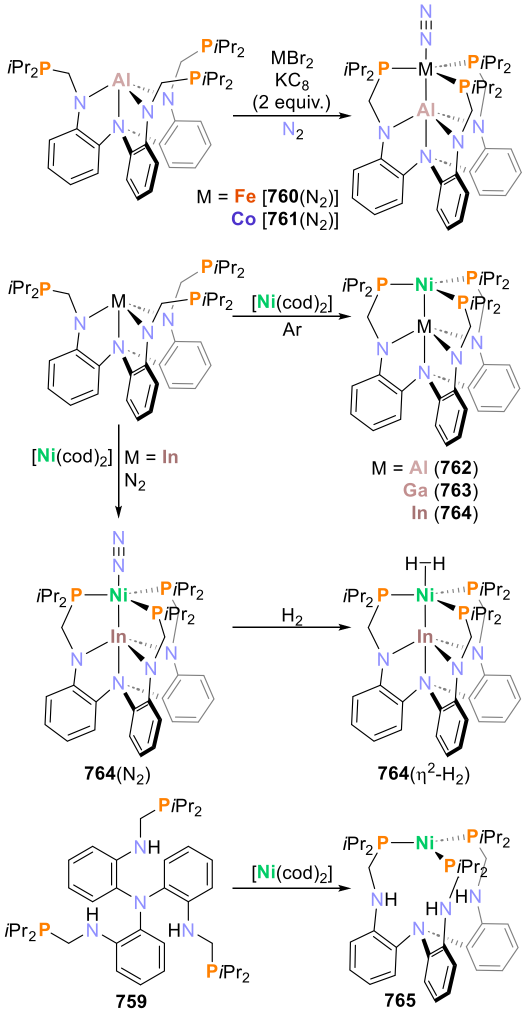

Lu and co-workers also reported the synthesis of the heterodinuclear complexes **763** and **764** (Scheme 92 middle, M = Ga, In)[436] and of the mononuclear nickel complex $[Ni\{N[o\text{-}(HNCH_2PiPr_2)C_6H_4]_3\}]$ (**765**, Scheme 92 bottom).[437] The metalloligands $M\{N[o\text{-}(NCH_2PiPr_2)C_6H_4]_3\}$ (M = Ga, In) and the complexes $[NiM\{N[o\text{-}(NCH_2PiPr_2)C_6H_4]_3\}]$ [M = Ga (**763**), In (**764**)] were synthesized by extension of the protocol used for the preparation of both AltraPhos and **762**.[433] Complexes **762**−**764** constitute a family of compounds with systematic tuning of the electronic environment of the Ni(0) center.[436] The different electronic environments created by the group 13 M(III) centers are evidenced by the downfield shift in the ^{31}P NMR resonance corresponding to the Ni-coordinated phosphine moieties [$\delta(C_6D_6)$ = 30.8 (**765**), 31.3 (**762**), 38.3 (**763**), 45 (**764**) ppm]. For the indium(III) derivative, **764**, the synthesis must be carried out under an argon atmosphere since, under N_2, the dinitrogen coordinated species **764** (N_2) is obtained (Scheme 92 middle). The dinitrogen ligand remains invariably coordinated even under prolonged vacuum but suffers ligand exchange after treatment with H_2 to generate the stable dihydrogen compound **764** (η^2-H_2) (Scheme 92 middle), which does not lose dihydrogen under vacuum. An interesting behavior was observed for the rest of the Ni(0) complexes upon exposure to either N_2 or H_2. While neither **765** nor **762** form N_2 or H_2-adducts, complex **763** is able to form the dihydrogen complex **763** (η^2-H_2). The analysis of HD coupling constants and T_1 relaxation time measurements performed by ^{1}H NMR spectroscopy suggest that **763** (η^2-H_2) and **764** (η^2-H_2) are genuine H_2 complexes with intact H−H bonds. H−D distances of 0.87 and 0.91 Å, respectively, were deduced from the H−D couplings, compared to 0.74 Å in free H_2. Unlike **764** (η^2-H_2), **763** (η^2-H_2) loses H_2 under vacuum, reverting to the parent compound **763**.

Crystallographic characterization and NMR spectroscopic data of **762**, **763**, and **764** indicate stronger Ni → M(III) dative bonds moving down the series M = Al, Ga, In, inversely related to their ionic radii. The Ni center thus becomes more electron-deficient for the larger M(III) ions in the metalloligand. Structural data also revealed that, as more electron density is withdrawn from the Ni center, the metal is forced higher above the plane of the three P atoms, becoming more accessible to bind small molecules such as N_2 or H_2.[436] The use of complexes **762**−**765** as catalyst precursors in the hydrogenation of olefins is discussed in section 3.1.4 (*vide infra*).

The adducts [NiM{N[*o*-(NCH_2PiPr_2)C_6H_4]$_3$}] [M = Al (**762**), Ga (**763**)], bearing zerovalent nickel centers,[433,436] each feature a reverse dative Ni(0) → M bond. Cyclic voltammetry (CV) of these compounds returned strongly negative potentials, with a reversible one-electron transfer process observed at −2.82 and −2.48 V vs $[FeCp_2]^{0/+}$ for **762** and **763**, respectively. Neither the mononuclear nickel complex **765** nor the free metalloligands M{N[*o*-(NCH_2PiPr_2)C_6H_4]$_3$} (M = Al, Ga) exhibited redox processes near those potentials, indicating that the electron transfer observed by CV was a function of the Ni−M moiety.

Consequently, the isolation of heterobimetallic metalates [NiM{N[*o*-(NCH_2PiPr_2)C_6H_4]$_3$}]$^-$ [M = Al (**766**), Ga (**767**), Scheme 93] resulting from the reduction of the neutral species **762** and **763** with KC_8 was reported in 2018.[81] The molecular and electronic structures of these anions were elucidated by X-ray crystallography, EPR spectroscopy, and quantum chemical calculations. The crystallographic investigations revealed that the Ni−Al bond in **766** contracts by 0.06 Å in comparison with **762**, indicating a strengthened interaction between the metal atoms.

Scheme 93. Synthesis of Formal Nickelate(−I) Complexes Supported by Group 13 Metalloligands, and Their Proposed Resonance Structures[81]

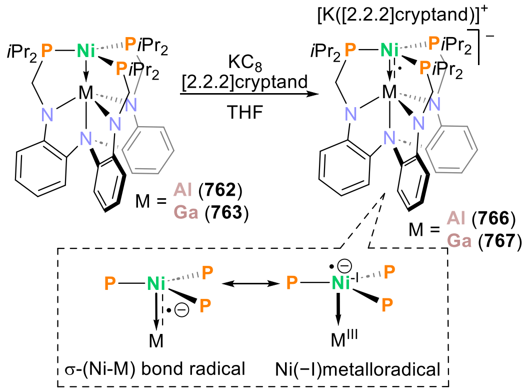

The EPR spectroscopic studies revealed substantial hyperfine couplings to the ^{27}Al, ^{69}Ga, and ^{71}Ga nuclei of 7.6, 37.0, and 47 mT, respectively. Based on the experimental and theoretical data, three limiting resonance structures were conceived: two featuring metal-centered metalloradicals [Ni(0)-M(II) or Ni(−I)-M(III)] and one intermediate structure where the additional electron injected into the complex upon reduction is shared between the Ni and M atoms. However, considering the changes observed in the bonds around the Ni center, the strength of the Ni−M dative bond, and the spin density distribution (as predicted via ^{31}P-hyperfine coupling and theoretical calculations), the contribution of a Ni(0)-M(II) resonance structure was ruled out, thus leaving the structures shown in Scheme 93 as the most probable. Taken collectively, the analysis (X-ray diffraction, EPR, and theoretical calculations) supports the proposal of a strongly reduced formal Ni(−I) character on the transition metal center of complexes **766** and **767**, with an unusual three-electron σ-bonding interaction.[81]

2.3.3.4. Metalates with Bonds between First-Row Transition Metals. Heterobimetallic complexes with bonds between first-row transition metals (TM) were also synthesized by the group of C. Lu, who has obtained different TM-based metalloligands from the heptadentate ligand **759**.[435,437,496−498] For instance, the complex [Cr{N[*o*-(NCH_2PiPr_2)C_6H_4]$_3$} (**768**) served as platform for the synthesis of a series of first-row M−Cr heterobimetallic compounds [MCr{N[*o*-(NCH_2PiPr_2)C_6H_4]$_3$}] [M = Mn (**769**), Fe (**770**), Co (**771**), Ni (**772**); Figure 15] for which a systematic tuning of the metal−chromium bonds was observed.[435,437]

The syntheses of **769**−**772** are largely analogous to those used for compounds **760**−**762** (Scheme 92). Crystallographic characterization showed increasing M−Cr bond distances and with decreasing formal bond order from 5 to 1 in the series from **769** (M = Mn) to **772** (M = Ni). Compound **769** has an ultrashort metal−metal bond distance of 1.8192(9) Å, associated with the presence of a quintuple bond. An inverse correlation was observed for the Cr−N distance, which decreased progressively from **769** to **772**. Multiple one-electron transfer processes were identified by cyclic voltammetry for these complexes. Theoretical calculations indicated an increasing polarization of the M−Cr bonds from **769** to **772**.[435]

Similar to the reactions that gave **766** and **767**,[81] chemical reduction of **770** with KC_8 (1 equiv, 94a) proceeds with formation of the anionic complex [FeCr{N[*o*-(NCH_2PiPr_2)-C_6H_4]$_3$}]$^-$ (**773**), isolated as the [K([18]crown-6)]$^+$ or the [K([2.2.2]cryptand)]$^+$ salt.[437] Crystallographic analysis of **773** revealed a slight elongation of the Fe−Cr bond length [d_{FeCr} (**770**) = 1.944 vs d_{FeCr} (**773**) = 1.974 Å] after reduction. Cr−N_{axial} distance is also elongated (Δd = 0.06 Å), while the Cr−P bonds are shortened (Δd = 0.02 Å) with respect to the neutral complex. Although such observations are consistent with the more reduced state of **773**, they indicate that the one-electron reduction is localized primarily at the chromium center, unlike in the cases of **766** and **767**. Hence, the authors assigned the tentative oxidation states Fe°Cr^{II} for the metal centers in **773**, and corroborated their assignment via DFT calculations and ^{57}Fe Mössbauer spectroscopy.[437]

Similarly, the titanium metalloligand [Ti{N[*o*-(NCH_2PiPr_2)-C_6H_4]$_3$}] (**774**) and the iron−titanium compound [FeTi{N[*o*-(NCH_2PiPr_2)C_6H_4]$_3$}] (**775**) were described by the same group, and their redox behavior studied to yield the series [FeTi{N[*o*-(NCH_2PiPr_2)C_6H_4]$_3$}]^n [*n* = 1+ (**776**), 0 (**775**), 1− (**777**)].[497,498] Reduction of complex **775** with KC_8

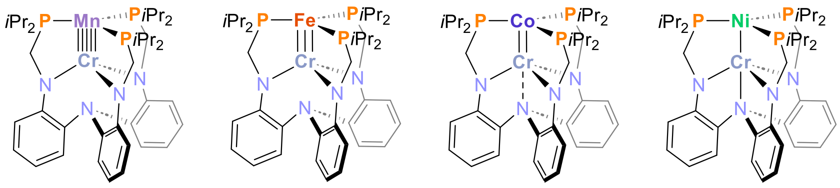

Bond lengths (Å):

	769	770	771	772
M-Cr =	1.820	1.944	2.140	2.411
Cr-N =	2.370	2.284	2.221	2.086

Figure 15. First-row heterobimetallic complexes featuring the metalloligand Cr{N[*o*-(NCH$_2$P*i*Pr$_2$)C$_6$H$_4$]$_3$} (**768**). Metal–metal and Cr–N distances to the apical N atom (N_{ap}) are shown for comparison. Average values for two crystallographically independent molecules are given for compounds Fe (**770**) and Co (**771**).[435]

Scheme 94. Chemical Reduction of Heterobimetallic Iron Complexes Featuring Metalloligands Based on First-Row Transition Metals[437,497]

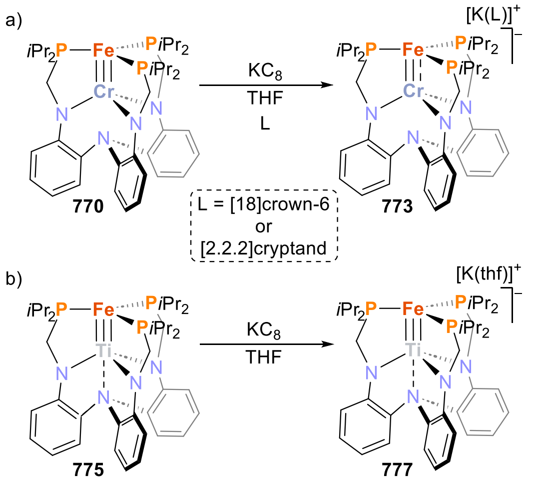

afforded the diamagnetic compound [K(thf)$_3$][FeTi{N[*o*-(NCH$_2$P*i*Pr$_2$)C$_6$H$_4$]$_3$}] (**777**, Scheme 94b). Analysis of the molecular orbital situation indicated an increased contribution of the titanium center in the Fe–Ti π-bonding MOs of **777**, while in the rest of the series, this contribution is rather limited. In addition, with the successive reduction events, the Fe–Ti bond length decreases substantially (d_{FeTi}(**776**) = 2.1613(10) Å, d_{FeTi}(**775**) = 2.0545(7) Å, d_{FeTi}(**777**) = 1.9494(6) Å). This contraction was attributed to a better energy match between the Fe and Ti 3d orbitals, which increases the Ti character in the σ- and π-symmetric MOs and results from the accumulation of negative charge at the Fe center. The metal centers in **775** and **777** are stabilized by both increased π-backbonding interaction to the phosphine groups and increased covalent π-bonding between the Fe centers and the Ti support, which delocalizes some of the excessive electron density from Fe to Ti.

Considering this, the authors proposed that the electronic structures of **776** and **775** are best described as containing a Ti(IV) support, and Fe(0) or Fe(−I) centers, respectively. In turn, the polarized Fe≡Ti bond in **777** presents spectroscopic features which would suggest the presence of an Fe(−II) center. Collectively, the theoretical and spectroscopic evidence indicates that the reductions leading to each member of the series [FeTi{N[*o*-(NCH$_2$P*i*Pr$_2$)C$_6$H$_4$]$_3$}]$^{+/0/-}$, from **776** to **775** to **777**, are iron-based. This contrasts with the analogous FeCr complex **773**, for which the chromium support metal was assigned as the center of reduction.[437]

3. METALATES IN SMALL-MOLECULE ACTIVATION AND CATALYSIS

The activation of small molecules is of great interest to contemporary inorganic chemistry due to their enduring relevance in important industrial processes such as catalysis and energy conversion. While the term "small molecules" might apply to a broad spectrum of chemical compounds, we wish to focus on the contributions studying the activation of H_2, N_2, CO_2, P_4, and some related model species.

As discussed in section 2.2.4, numerous alkene or arene metalates have been reported.[248,378,388,443,499,500] The reactivity studies performed on these complexes have proven their remarkable potential toward the formation of other coordination compounds and the activation of inert chemical bonds. Therefore, low-valent/highly reduced species seem particularly suited as effective tools to perform the catalytic transformation of small molecules.[501] Indeed, there has been steadily growing interest around small molecule activation promoted by transition metal anions in recent years. In this work, we will only highlight the contributions in which low-valent metalates mediate the transformation of small molecules or models for small molecules. However, in recent years, their participation as catalysts or catalytic intermediates in many other interesting reactions, such as cross-couplings (refs 419, 449−451, 457−460, 502−505) olefin isomerization,[316,321] functionalization of dienes,[20] carbonylation of heterocycles,[506] oligomerization of isocyanides,[507] or C–H bond activation and functionalization[24,508] has been widely documented.

3.1. Hydrogen Activation, Catalytic Hydrofunctionalization, and Dehydrogenation

Hydrogenation catalysis has been of keen interest to organometallic chemists for decades, and the attention this type of reaction receives is ever-growing as it is a versatile tool in, for example, the synthesis of numerous reduced organic compounds[509] through either classic or transfer hydrogenation reactions.[510] Likewise, other hydrofunctionalization reactions and catalytic dehydrogenations[511] can be useful to produce not only organic compounds and polymers, among others, but also hydrogen. Accounts on the advances in catalytic hydrogenation promoted by low-valent transition metals are available elsewhere. For instance, in 2015, Chirik reviewed the use of iron and cobalt complexes bearing redox-active ligands as catalysts in the hydrogenation of alkenes.[396] However, to the best of our knowledge, the chemistry of metalates in hydrogenation reactions has yet to be comprehensively reviewed.

3.1.1. Arene/Alkene Metalate Catalyzed Hydrogenation.

Iron,[378,499] cobalt,[248,388,443,499] and nickel[500] arene- and alkene-metalates have been used as precatalysts for hydrogenation,[248,443,499,500] transfer hydrogenation,[388] and hydrofunctionalization[378] reactions of a variety of unsaturated substrates. From these studies, it has become evident that metalates hold great potential to perform this type of reductive reaction. The reducing power of anionic complexes makes them particularly suitable for the activation of molecular hydrogen and, consequently, for hydrogenation reactions.

The use of bis(anthracene)metalates(−I) [M = Fe (**52**); Co (**14**)] as catalysts for hydrogenation reactions was reported for the first time in 2014.[499] These quasi-“naked” anionic metal species are stabilized by labile anthracene ligands which allow for a rapid exchange in the presence of a large excess of other *π*-acid ligands, i.e. unsaturated substrates such as olefins, ketones, etc. The hydrogenation of *α*-, *β*-, and ring-substituted styrenes (see Scheme 95a) was achieved under mild conditions (1 mol % catalyst, 20 °C, 2 bar H_2, toluene), while other linear- and cyclic alkenes (terminal, internal, and di- and trisubstituted) required a higher catalyst loading, as well as higher pressure and temperature (5 mol %, 10 bar H_2, 60 °C, toluene). In general, cobaltate **14** resulted in a significantly more active catalyst than the more oxidation-prone ferrate **52**, which efficiently hydrogenated only unbiased styrenes and 1-alkenes. This behavior might be due to the tendency of **52** to form the anthracene radical anion in the presence of strong donors in ligand exchange reactions, as previously demonstrated (see Scheme 21b, above).[181] In any case, both anthracenemetalates work essentially under ligand-free conditions and require no activation procedures or treatments, returning only minimal amounts of polymeric material as byproducts in reactions with styrenes and alkenes as substrates. Cobaltate complex **14** is also active in the hydrogenation of other unsaturated substrates, such as alkynes, aromatic and aliphatic ketones, and imines (10 bar H_2, 60 °C, Scheme 95a).

Scheme 95. Arene/Alkene Metalate-Catalyzed Hydrogenation of C═X Moieties (X = C, N, O) by Wolf, Jacobi von Wangelin, and Co-workers[248,499,500]

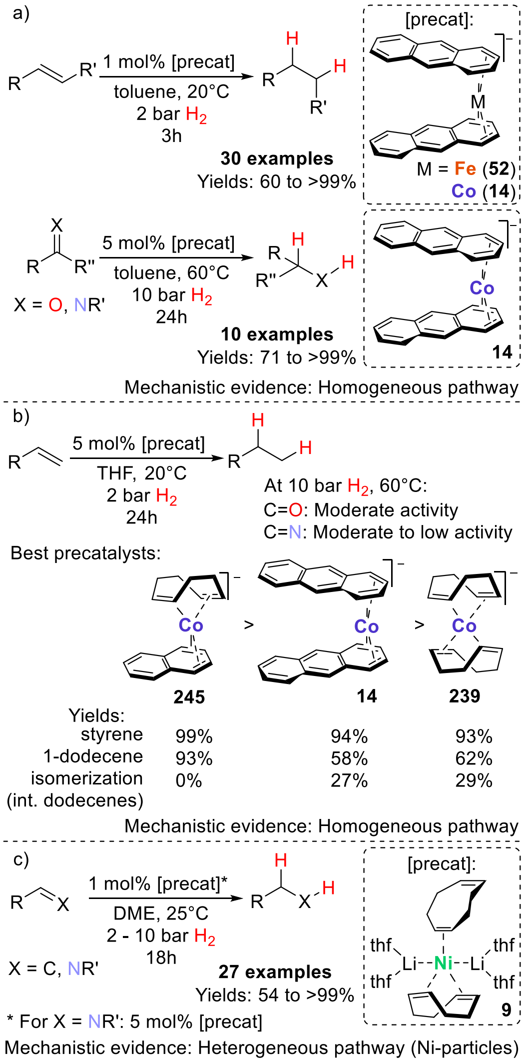

Based on monitoring studies and poisoning experiments (Hg; dibenzo[*a*,*e*]cyclooctatetraene, dct), it was proposed that the hydrogenation of olefins is homogeneous and proceeds by initial substitution of the anthracene ligands by the *π*-acceptor substrates. Rapid exchange of anthracene by styrene was identified by ^{1}H NMR spectroscopy. However, no reaction was observed between cobaltate precursor **14** and H_2 in absence of the substrate. Thus, it was proposed that H_2 activation occurred via oxidative addition at the cobalt-alkene species [Co(−I) → Co(I)], followed by insertion of the coordinated alkene into a Co−H bond to generate an alkylcobalt(I) hydride. The presence of *π*-acceptors (olefins, arenes) in excess in the reaction medium appear to stabilize the catalytically active species in the cycle. For the hydrogenation of carbonyl moieties, it was also postulated that the initiation of the cycle occurred at cobaltate **14**, with a cobalt(I) active species or metallic cobalt particles operating after the first turnover, at elevated temperature and H_2 pressure.[499]

Other alkene metalates, the heteroleptic cobaltate [Co(η^4-$C_{10}H_8$)(η^4-cod)]$^-$ (**245**), the classic [Co(η^4-cod)$_2$]$^-$ (**239**), and cobaltates [Co(η^4-cod)(η^2-styrene)$_2$]$^-$ (**265**), [Co(η^4-dct)(η^4-cod)]$^-$ (**266**), and [Co(η^4-dct)$_2$]$^-$ (**267**) (see Scheme 32a, above), were evaluated as precatalysts for hydrogenation of alkenes (see Scheme 95b).[248] The bis(anthracene)-metalates(−I) [M = Fe (**52**); Co (**14**)] were re-evaluated alongside these, due to their greater solubility in THF rather than toluene, which had been used in the previous catalytic experiments.[499] For the sake of comparison, ferrates [Cp^{R}Fe-(η^4-naphthalene)]$^-$ [Cp^R = Cp* (**201**), Cp (**202**)] were also tested, in parallel reactions for all of the precatalysts, under identical reaction conditions (5 mol % catalyst, 20 °C, 2 bar H_2, THF, 24 h), using styrene and 1-dodecene as model substrates. In general, and consistent with previous observations for catalyst **52**,[499] the ferrates showed lower activity in the hydrogenation reactions than the cobaltates. The homoleptic bis(η^4-dct)cobaltate **267** was completely inactive under the studied conditions, confirming the role of dct as a catalyst poison for homogeneous low-valent mononuclear species, as previously postulated in the case of the bis-(anthracene)metalate(−I)-catalyzed reactions.[499]

It is believed that the strong coordination of the dct ligand inhibits the ligand exchange process with the substrates. The polyarene cobaltates proved the most active precursors for both model substrates, with the heteroleptic complex **245** being the most efficient (Scheme 95b), in terms of both activity and selectivity (lower isomerization to internal alkenes for 1-dodecene). An extension of the substrate scope to include polar substrates (ketones and imines) revealed that harsher reaction conditions (10 bar H_2, 60 °C) are required for precatalyst **14** to perform efficiently in the hydrogenation of ketones and imines. Precatalysts **245** and **239** resulted in moderately efficient catalysis for the hydrogenation of dibenzylketone, but for *N*-benzylideneaniline were essentially inactive.[248]

Extensive mechanistic studies (NMR spectroscopy, ESI−mass spectrometry, and poisoning experiments) of the alkene hydrogenation reactions support a homogeneous pathway initiated by coordination of the substrate to the metal center, in a facile redox-neutral π-ligand exchange process, prior to H_2-activation.[499] For the reactions catalyzed by either **245** or **239**, mechanistic studies at the NMR scale revealed that the addition of styrene (20 equiv) to solutions of each complex resulted in the clean formation of complex **265** in both cases. Application of a H_2 atmosphere to the reaction mixtures rapidly led to complete hydrogenation of the coordinated styrene to ethylbenzene. However, hydrogenation of **265** in the absence of additional substrate led to immediate color-change to form a black solution, due to full consumption of the stabilizing π-ligand. Analogous hydrogenation of **265** in the presence of an excess of naphthalene resulted in the formation of its precursor, **245**, the most efficient among the studied complexes (see Scheme 32a). Such reconstitution of the catalyst was referred to by the authors as a release−catch mechanism (Scheme 96), which occurs after the complete hydrogenation of the reactive alkenes. Hence, **265** can be effectively assigned as a potential intermediate of styrene hydrogenations by cobaltate precatalysts. A species analogous to **265**, namely $[Co(\eta^4\text{-}C_{14}H_{10})(\eta^2\text{-styrene})_2]^-$ (**778**), was also observed through an ESI-MS analysis of a solution of **14** treated with styrene (20 equiv; see Figure 16, precatalyst formation). An equivalent experiment using 1-dodecene instead similarly afforded an analogue of **778**.[248] The observation of the 18-valence-electron bis(alkene) complexes, analogous to **265**, in the different reaction mixtures obtained from the cobaltates used as precatalysts strongly supports the ligand exchange mechanism originally postulated by the authors (Figure 16). These are, presumably, the resting states that serve as a reservoir for the catalytically active cobalt species in each case. It was thus speculated that the H_2 activation occurs after loss of an alkene ligand from such resting states, with concomitant formation of an unsaturated and reactive 16 e^- monoalkene-cobalt species.[248]

Scheme 96. Release−Catch Mechanism Proposed as Part of the Reaction Pathway in the Hydrogenation of Alkenes by Labile Cobaltates[248]

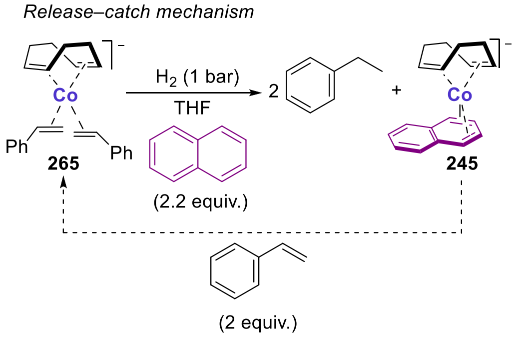

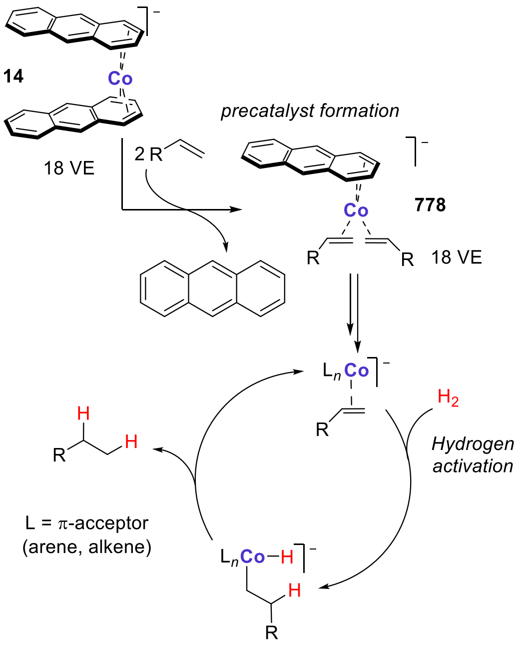

Figure 16. Activation of arene metalate precatalysts for hydrogenation reactions by π-ligand exchange with alkenes.[248,499]

The mechanism for the bis(anthracene)metalate-based hydrogenation catalysts was also examined by DFT calculations.[512] For both catalysts, **14** and **52**, the general steps of the mechanistic proposal were calculated to be similar. Initially, one substrate molecule displaces one anthracene ligand, and one hydrogen molecule coordinates. Then, oxidative addition of the hydrogen molecule yields a M(I)-dihydride species, followed by migratory insertion to give the M(I)-alkyl (or M(I)-alkoxide) intermediate. In the alkene hydrogenation cycle, an anthracene molecule recoordinates the metal center, promoting the reductive elimination of the alkane product (C−H bond formation) and regenerating the catalyst. The results of the calculations suggest that, before the oxidative addition step, there is an equilibrium between the closed-shell singlet state of **14** and the open-shell diradical Co(0) intermediates, whereas oxidative addition of the hydrogen molecule generates a more stable Co(I)-dihydride species. Hence, this system involves a Co(−I)/Co(0)/Co(I) catalytic cycle, and species both in singlet and triplet states (non-adiabatic reaction with spin crossing). Similarly, it was proposed that two different spin states (doublet and quartet) and three different oxidation states [Fe(−I)/Fe(0)/Fe(I)] are involved in the Fe(−I)-catalyzed alkene hydrogenation reaction. The rate-determining step is the insertion of the alkene substrate into the Co(I)−H bond, overcoming an energy barrier of ∼22.0 $kcal mol^{-1}$. For the Fe(−I)-catalyzed reaction, the migratory insertion of the substrate into a M−H bond is also the rate-determining step, but the process is associated with a higher energy barrier of 25.4 $kcal mol^{-1}$.

The higher barrier was attributed to the lower stability of its reactive low-spin metal-dihydride intermediate $[M(\text{anthracene})(H)_2(\text{alkene})]^-$ [ΔG = 19.0 (M = Fe) vs 13.6 (M = Co) $kcal mol^{-1}$]. Moreover, a comparison of the Mulliken charges of the M(−I) catalysts and the $M(H_2)$ intermediates indicated that the formation of the key low-spin oxidative-addition Fe(I)-dihydride intermediate is disfavored, which might explain its lower reactivity. Flexible coordination modes of the acidic ligands (e.g., anthracene decoordination/recoordination) involved in the catalysis favor the key elementary steps in the cycle. Similar theoretical observations were made for the ketone hydrogenation system, although it should be noted that the hydrogenation reactions are likely by a heterotopic catalyst (i.e., metallic nanoparticles of Fe and Co, respectively, *vide supra*).

Highly reduced nickel complexes are rare, and not many examples exist regarding their use in activation of small molecules. Wolf and Jacobi von Wangelin described that the long-known nickelate(−II) $[Li_2(thf)_4\{Ni(\eta^2\text{-cod})(\eta^4\text{-cod})\}]$ (**9**) enables the heterogeneous hydrogenation of C═X moieties (X = C, N, O) in olefins, imines, and enoates under mild conditions (Scheme 95c).[500] Precatalyst **9** was previously synthesized by Jonas and co-workers,[65] and only recently characterized by crystallographic analysis.[504] Unlike the bis(anthracene)metalates(−I) [M = Fe (**52**); Co (**14**)], which performed poorly for sterically hindered tri/tetra-substituted olefins,[248,499] **9** is an efficient precatalyst in the hydrogenation of hindered olefins. Using the same catalyst loading [1 mol % catalyst, 25 °C, 5 bar H_2, 15 h, 1,2-dimethoxyethane (DME)], the performance of the nickelate complex **9** in the hydrogenation of either triphenylethylene or 1-phenyl-1-cyclohexene was also significantly better than that of the related oxidized compound $[Ni(\eta^4\text{-cod})_2]$ (**240**). Nonetheless, complex **9** does not catalyze the hydrogenation of polyaromatic compounds such as anthracene or naphthalene, or heterocycles such as quinolines. Compared to precatalysts **14** or **52**, the active nickel species generated from **9** can hydrogenate sterically hindered tri/tetra-substituted olefins at lower H_2 pressures and temperature, while being compatible with several functional groups (OH, esters, halides). Different behavior was also observed in the monitoring of the reaction progress for selected substrates (1-octene, 2-octene, and α-methylstyrene) at lower pressures (1.9 bar H_2), for which considerable induction periods and sigmoidal behaviors were observed. These might indicate slow catalyst formation and nucleation processes to form heterogeneous species during the reaction. This proposal was strongly supported by poisoning experiments with Hg, dct, benzonitrile and naphthalene, which indicated that the operating active species was heterotopic. Analysis of the formed species through transmission electron microscopy (TEM) revealed the presence of particles 10−15 nm and larger in diameter. For reducible olefins (e.g., triphenylethylene), spectroscopic analysis and cyclic voltammetry suggested the formation of the triphenylethylene-dianion, indicating a possible electron-transfer initiated mechanism. The mechanistic experiments performed support the postulate that nickel nanoparticles are responsible for the catalytic activity observed, while the formation of the catalyst might be substrate dependent.[500]

3.1.2. Hydrogenation Catalysts Containing Redox-Active Ligands.

Redox-active (noninnocent) ligands have attracted considerable interest as stabilizing scaffolds for cobalt hydrogenation catalysts, and have been the focus point of recent studies.[379,443] Fe(II)-BIAN precatalysts were evaluated for the hydrogenation of olefins (including tri- and tetrasubstituted susbtrates).[379] The tetrahedral complex $[(^{Dipp}BIAN)FeCl_2]$ (**779**), analogous to $[(^{Dipp}BIAN)FeBr_2]$ (**536**),[378] was the precatalyst of choice for the hydrogenation of the alkene substrates, and was found to catalyze the reaction only after activation with a strong reductant. Carrying out catalytic tests with a system consisting of *in situ* treatment of **779** with *n*BuLi (3 equiv), the selected olefinic substrates studied in this preliminary evaluation were hydrogenated in excellent yields (Scheme 97a).

Scheme 97. Hydrogenation of C═X Bonds Mediated by Reduced "(BIAN)M" (M = Fe, Co) Catalytic Systems[379,443]

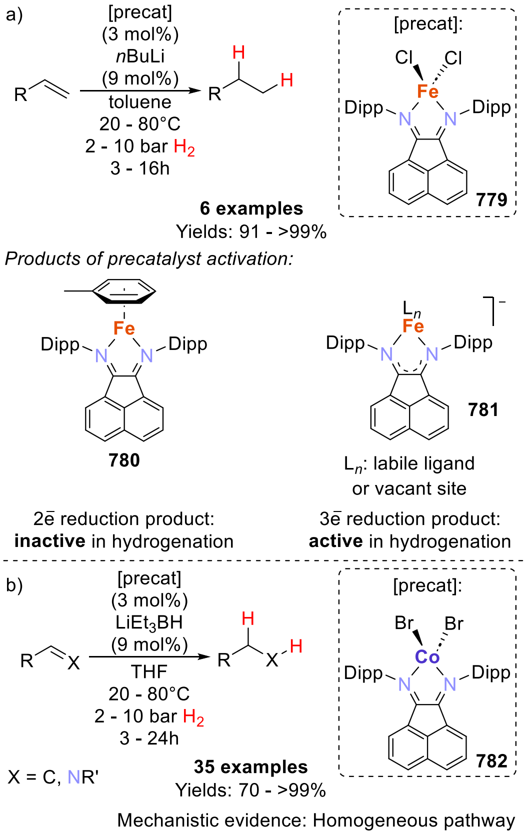

Nonetheless, the authors tried to identify the formed species by reproducing the activation reaction on a preparative scale. This led to the isolation of two main complexes after extraction, in a 70:30 ratio: the previously reported complex $[(^{Dipp}BIAN)Fe(\eta^6\text{-}C_7H_8)]$ (**780**)[377] and a species whose structure could not be fully identified (**781**, see Scheme 97a for a representation of the products). Complex **780** is the product of formal two-electron reduction of **779**, whereas the minor species **781** was proposed to be a low-valent compound formed by three-electron reduction. It was suggested that the low-valent complex **781** might feature either a radical anion or a dianionic BIAN ligand. **781** reproduced the catalytic activity of the *in situ* generated system, while **780** proved inactive in the hydrogenation of α-methylstyrene (1.9 bar H_2, 20 °C, 3 h).

The use of BIAN-stabilized cobaltate complexes[374] as catalysts allowed for the hydrogenation of sterically hindered trisubstituted alkenes, imines, and quinolines under mild conditions (2−10 bar H_2, 20−80 °C).[443] The simple catalytic system is formed from the stable precursor $[(^{Dipp}BIAN)CoBr_2]$ (**782**) and $LiEt_3BH$ as cocatalyst (Scheme 97b). The reduction of the Co^{II} catalyst precursor in the presence of olefins proved beneficial for the overall catalytic activity, probably due to their coordination to, and consequent stabilization of, the low-valent species. Under standard conditions, turnover frequencies (TOF) of 780 h^{-1} were achieved for the hydrogenation of α-methylstyrene. Synthetic, kinetic, and spectroscopic experiments provided further details on the reaction mechanism and support a homogeneous pathway involving homotopic cobaltate catalysts, probably stabilized by alkene/hydrido ligands. For instance, Hg poisoning experiments had minimal effect on the reaction rate, while addition of $P(OMe)_3$ resulted in the partial or complete inhibition of the catalytic activity even when substoichiometric amounts (0.3 mol %) of the poisoning agent were used.

Furthermore, when complex **782** was treated with $LiEt_3BH$ (3 equiv), and the crude catalyst mixture was analyzed using LIFDI–MS (liquid injection field desorption–mass spectrometry), the low-valent dimeric species $[(^{Dipp}BIAN)Co]_2$ was identified. The authors surmised that such a dimeric species might be indicative of the participation of a monomeric "$(^{Dipp}BIAN)Co$" fragment in the catalysis. Carrying out the reductive dehalogenation of **782** in the presence and absence of arenes/olefins yielded three different reduced species (Scheme 98) providing further evidence of the redox noninnocence of the BIAN ligand. Reactions of **782** with $LiEt_3BH$ (3 equiv) in THF with 1,5-cod present, in benzene, or in Et_2O, afforded the cobaltate $[Li(thf)_{3.5}\{(^{Dipp}BIAN)Co(cod)\}]$ (**783**), the neutral complex $[(^{Dipp}BIAN)Co(\eta^6\text{-}C_6H_6)]$ (**784**), or the dinuclear hydridocobaltate $[Li(thf)_3(L)\{(^{Dipp}BIAN)Co\}_2(\mu\text{-}H)_3]$ (**785**, L = Et_2O, thf), respectively. According to the bond distances determined by X-ray diffraction analysis, complex **784** features the radical anion state of the BIAN ligand [C–C bond length = 1.433(2) Å; average C–N bond length = 1.3235 Å]. Additional characterization (EPR spectroscopy, magnetic moment, LIFDI–MS, and cyclic voltammetry) revealed that **784** contains a high-spin Co(I) center and thus is accurately described as $[(BIAN^-)Co^I(\eta^6\text{-}C_6H_6)]$. Compound **785** also bears the radical anion state of the BIAN ligand according to the structural parameters [C–N bond lengths = 1.333(3)–1.349(3) Å; C–C bond lengths = 1.412(3)–1.419(3)Å], which are in good agreement with the theoretical predictions.[443]

Scheme 98. Cobalt Complexes Isolated from the Reactivity Studies of $[(^{Dipp}BIAN)CoBr_2]$ (782) with $LiEt_3BH$ in the Presence/Absence of Olefins/Arenes[443]

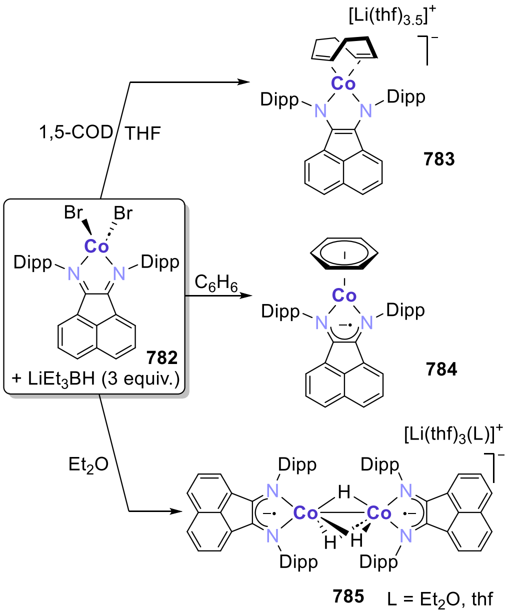

It was revealed that the counterion plays a significant role on the catalytic activity of the precatalysts. While the potassium salt **540** resulted in complete inactivity, the lithium analogue **783** catalyzed the reaction, although less effectively than the *in situ* combination of **782** and $LiEt_3BH$. Addition of Lewis acids improved the activity of **783**. The η^6-benzene complex **784** was also completely inactive, while the dinuclear hydridocobaltate anion **785** had a high activity and was considered a catalytically competent off-cycle intermediate.[443]

Roşca and co-workers found that phosphine α-iminopyridine (PNN)-based Fe–N_2 complexes activate molecular hydrogen via metal–ligand cooperation (MLC) to afford an anionic Fe(0)-hydride complex.[513] The group reported that the highly reactive anionic dinitrogen compound $K[(PNN)Fe(N_2)]$ (**786**, Scheme 99) shows divergent behavior in the presence and absence of molecular hydrogen. Compound **786** is obtained by reduction of the dinuclear iron dinitrogen complex $[\{(PNN)Fe(N_2)\}_2(\mu\text{-}N_2)]$ (**787**) with $KN(SiMe_3)_2$ under N_2 in the presence of a crown ether or cryptand at low temperatures (<−30 °C, Scheme 99), and features a dearomatized pyridine core with a deprotonated benzylic position (radical anionic ligand). Above this temperature and in the absence of H_2, **786** undergoes ligand-assisted disproportionation to afford two new paramagnetic species, [K(chelate)][**788**] and [K(chelate)][**789**] (chelate = [2.2.2]-cryptand or [18]crown-6; see Scheme 99, top). The formation of these two species was explained by an intermolecular hydrogen atom transfer from the methyl substituent on the α-carbon atom of the imino group to the vinylic carbon atom adjacent to the PtBu$_2$ moiety of another complex. Compound

Scheme 99. Divergent Behavior of $K[(PNN)Fe(N_2)]$ (786) in the Presence and in Absence of Molecular Hydrogen, and Formation of an Anionic Fe(0)-Hydride Complex[513]

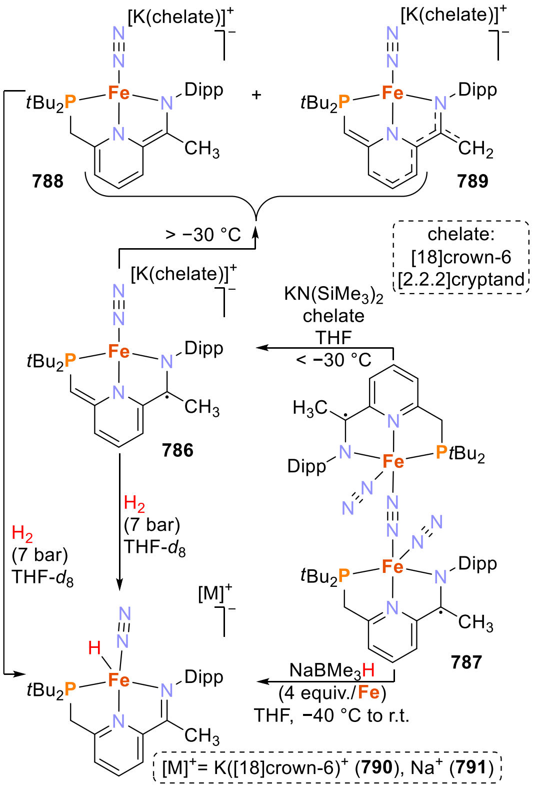

788 corresponds to the one-electron reduction product of the dinuclear complex **787** which can be independently synthesized by reduction of **787** with KC_8 in the presence of a chelating agent. FT-IR stretching bands for the dinitrogen ligand in **788** show that this complex is a highly reduced product with increased metal-to-ligand backbonding [ν_{NN}(**788**) = 1927 or 1912 cm^{-1} for the [K([2.2.2]cryptand)]$^+$ or [K([18]crown-6)]$^+$ adducts, respectively, vs ν_{NN}(**787**) = 2039 and 2059 cm^{-1}]. Compound **789** is a conjugation-stabilized complex. The relative ease of C−H bond cleavage in the α-imine methyl group (calculated BDFE = 48.7 kcalmol^{-1}) and subsequent proton coupled electron transfer (PCET) to stabilize the negative charge through ligand-based reduction was proposed as the driving force for the formation of **788** and **789**.

Upon treatment of the anionic complex **786** with dihydrogen (7 bar, 16 h), a color change from brown to green was observed, and a diamagnetic species M[(PNN)-FeH(N_2)] [M = K([18]crown-6) (**790**)] with a phosphorus-coupled hydride resonance in the ^{1}H NMR (δ_H = −22 ppm, J_{HP} = 63 Hz) formed. In the hydride complex, the pyridine ring of the PNN ligand is rearomatized, with the ligand oxidized to its neutral form. The formation of **790** was attributed to a ligand-assisted dihydrogen splitting reaction, where the driving force is the rearomatization of the chelating ligand. The MLC was confirmed by the reaction of **786** with D_2, upon which not only was a deuteride complex observed, but also deuteration in the benzylic position of the phosphino arm of the ligand. The mixture of disproportionation products **788** and **789** react with dihydrogen under the same conditions to afford hydride **790**. However, when **788** was exposed to D_2, no incorporation of deuterium on the α-positions of the ligand was observed, suggesting a different mechanism of activation for the dihydrogen molecule. In this case, a bimolecular (homolytic) metal-based dihydrogen splitting occurred.

The anionic hydride complex can be more conveniently accessed (as the sodium salt **791**) upon reaction of the dinuclear complex **787** with an excess of $NaBMe_3H$ (4 equiv per Fe center). Reaction of either the dinuclear complex **787** or the anionic species **786** with carbon monoxide afforded the dicarbonyl compounds [(PNN)Fe(CO)$_2$]$^{0/-}$ [**792** (neutral), **793** (anionic)]. The anionic complex features a dearomatized pyridine core and exhibits contrasting behavior compared with the dinitrogen analogue **786**. **793** is stable at room temperature and in solution (1 week) without undergoing PCET reactivity, probably because of the nonradical nature of the chelate, and does not react with H_2, up to pressures of 10 bar. The contrasting behavior of the described complexes highlights the regulating role that the PNN ligand plays on the reactivity of its compounds.[513]

3.1.3. Pincer-Supported Manganates in Hydrogenation Catalysis.

Kempe and co-workers described an efficient and chemoselective Mn(I)-mediated system for the hydrogenation of imines to amines and sought insight into its mechanistic and kinetic minutiae. Potassium manganate species were found to play mechanistically crucial roles in imine hydrogenation reactions using complex [BrMn(CO)$_2$-(PN^{triazine}P)] (**794**, PN^{triazine}P = 2,6-bis(P*i*Pr$_2$NH)-4-Ph-triazine) as the precatalyst.[442] The reduction of aldimines and ketimines (over 30 examples; conditions: 20 bar H_2, 50 °C, 4 h, see Scheme 100) was achieved using a low catalyst loading (0.4 mol %) for most substrates. The system tolerates imines with challenging and sensitive functional groups (olefins, ketones, nitriles, nitro, aryl iodo substituents, benzyl ether). For the model substrate N-benzylideneaniline (Ph-N=CH-Ph) and other selected examples, the reaction could be conducted on a multigram scale, with yields of at least 90%.

Scheme 100. Hydrogenation of Imines Catalyzed by [BrMn(CO)$_2$(PN^{triazine}P)] (794)[442]

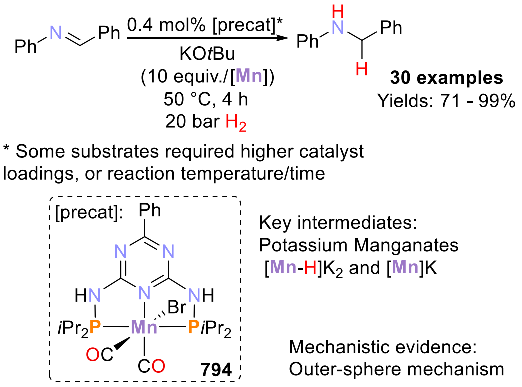

Mechanistic investigations included studies on the role of the base in the activation of the catalyst, determination of the order of the reaction components, stoichiometric tests to gain insights into the reaction pathway, and a Hammett study. Stoichiometric tests on the NMR scale were carried out using the previously described hydride complex [HMn(CO)$_2$-(PN^{triazine}P)] (**795**) since this complex was known to form from the reaction between **794**, KO*t*Bu (1 equiv), and H_2.[514] The reaction of **795** with 1 or 2 equiv of KO*t*Bu gave the products of single and double deprotonation of the NH motifs in the ligand backbone, [Mn−H]HK (**796**, [Mn−H] = [HMn(CO)$_2$(PN^{triazine}P)]) and [Mn−H]K$_2$ (**797**), were identified. No further deprotonation was observed upon addition of excess base (10 equiv). Reproducing these reactions in the presence of substrate (equimolar ratio) revealed that for substoichiometric amounts of base, no hydride transfer occurred. By contrast, the reaction is significantly accelerated when 2 equiv of KO*t*Bu are used. Therefore, the doubly deprotonated potassium manganate species **797** was identified as the catalytically active species in this system (Scheme 101).

In the bimetallic complex **797**, the potassium cations are coordinated to the anionic nitrogen atoms in the ligand backbone, and to the triazine cavity. The inactivity of the neutral and singly deprotonated complexes (**795** and **796**, respectively) contrasts with the efficiency of the doubly deprotonated compound **797**, suggesting that the hydride transfer might be favored by the anionic nature of the manganese species, resulting from the two negatively charged nitrogen atoms. Because of these charged atoms, conjugated with the triazine motif, the hydride ligand is more electron-rich. Further investigations into the catalytic cycle indicated that catalyst precursor **794** is activated by an excess KO*t*Bu in the presence of H_2, to produce the doubly deprotonated species **797** (Scheme 101). After hydride transfer to the imine substrate, the amine product and species [Mn]K (**798**, Scheme 101) are formed. The latter compound reacts with H_2 and KO*t*Bu to regenerate the catalytically active species, **797**.

X-ray crystallographic studies showed that compound **798** crystallizes as a coordination polymer, in which the potassium cation binds both the triazine cavity and a negatively charged nitrogen atom, additionally linking another unit of the

Scheme 101. Mechanistic Cycle Proposed for the Hydrogenation of Imines, Involving Potassium Manganate Intermediates[442]

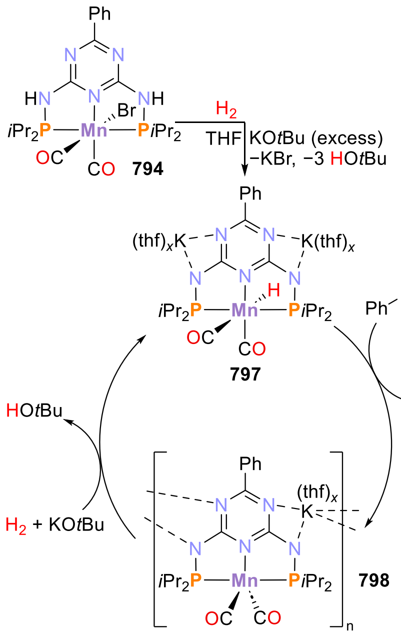

Scheme 102. Catalytic Hydrogenation of CO_2 to Formate Enabled by Low-Valent Manganate Species[517]

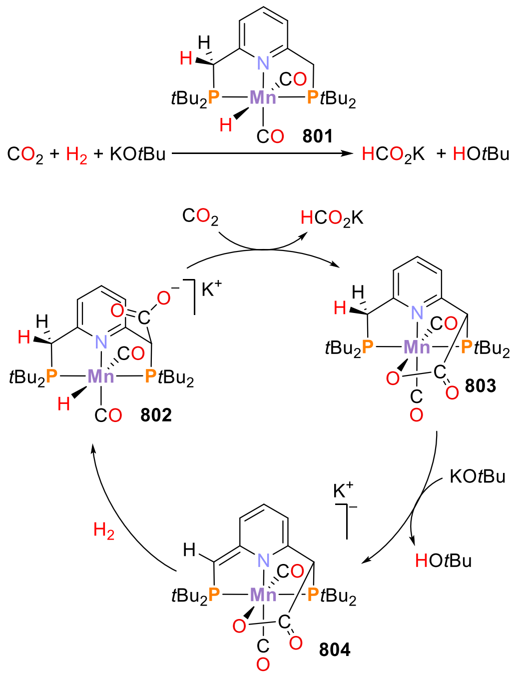

complex. The authors attributed the exceptional stability of the bimetallic catalyst to the cavity provided by the triazine motif. The influence of the reaction components on the rate of reaction was also investigated. The reaction rate has a first order dependence on the concentration of imine substrate and on the bimetallic hydride complex [Mn−H]K_2 (**797**) but is independent of the concentration of base. Therefore, the process corresponds to a global second order reaction. The hydride transfer is a well-defined reaction, probably via an outer-sphere mechanism since no observable manganese amide complex was identified. The dihydrogen molecule is activated by the bimetallic dicarbonylmanganate **798** to regenerate **797**. In conclusion, both manganate species are essential in the performance of the described catalytic imine hydrogenation system.[442]

Liu and co-workers reported that a related polymeric manganate hydride complex bearing a PNP pincer ligand, $[Li\{HMn(CO)_2(PNP)\}]_n$ [**799**, PNP = $N(CH_2CH_2PPh_2)_2$] also served as an active catalyst in hydrogenation reactions.[515] Synthesized by deprotonation of the neutral precursor $[HMn(CO)_2(PN^{H}P)\}]$ [**800**, $PN^{H}P$ = $NH(CH_2CH_2PPh_2)_2$] by $LiCH_2SiMe_3$ under 20 bar of H_2, 10 mol % of the lithium manganate hydrogenated a series of aldimines and ketimines; conditions: 40 bar H_2, 140 °C, 16 h. Notably, **800** was much less effective under the same conditions.

It is noteworthy that carbonyl manganate anions related to **797** and **799** have been proposed as steady state species and catalyst intermediates in chemoselective electrochemical hydrogenations of aldehydes and ketones.[516]

In related work, Shaouma and co-workers presented the catalytic hydrogenation of CO_2 to formate using the PNP-pincer complex **801** (see Scheme 102).[517] Deprotonation of **801** gives a reactive hydride species $[(*PNP)MnH]^-$, which binds CO_2 with its ligand backbone to generate the species $[(CO_2{-}PNP)MnH]$ (**802**). This complex is capable of eliminating formate with binding of further CO_2 to give **803**. Following a second ligand deprotonation, yielding **804**, addition of H_2 regenerates the hydride complex **802**. This work shows how metal−ligand cooperativity in anionic manganese pincer complexes enables an effective mechanism for CO_2 hydrogenation, which circumvents the classic insertion step into the metal hydride bond. Ligand deprotonation is crucial to boost the hydridcity of the complex.

These studies illustrate the significant potential of bifunctional alkali metal manganate catalysts for hydrogenation reactions.

3.1.4. Bimetallic Transition-Metal Magnesium Catalysts.

In 2022, Maron and Xu described the activation of the dihydrogen molecule at the heterotrimetallic complex $[\{(^{Ar}nacnac)Mg\}_2Ni(C_2H_4)_2]$ (**705**, *vide supra*, section 2.3.2).[479] Reaction of **705** with H_2 (r.t. for 24 h or 60 °C for 2 h) allowed the isolation of the diamagnetic compound $[\{(^{Ar}nacnac)Mg\}_2Ni(\mu\text{-}H)_4]$ (**805**, Scheme 103), along with free ethane (detected by ^1H NMR spectroscopy). X-ray diffraction analysis of **805** showed that the core of the trimetallic (Mg−Ni−Mg) complex is slightly bent, with the four hydride ligands approximately in the same plane.

Scheme 103. Activation of Dihydrogen at the Heterotrimetallic Complex $[\{(^{Ar}nacnac)Mg\}_2Ni(C_2H_4)_2]$ (705)[479]

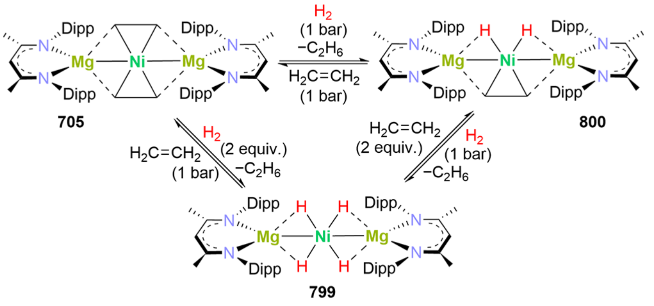

The hydrides present weak interactions with the magnesium centers (on average, d_{MgH} = 2.03 Å). This evidence, along with characterization by ^{1}H NMR spectroscopy indicating the presence of hydride ligands ($\delta = -13.47$ ppm) and XPS measurements consistent with a Ni(II) center in **805** as in **705**, suggest that the activation of H_2 likely involves a cooperative heterometallic Ni/Mg mechanism, instead of oxidative addition to the Ni center. By exposing **805** to an ethylene atmosphere, the nickelaspiropentane complex **705** was reobtained. Additionally, evidence of the stepwise conversion of **705** into **805** was obtained from the reaction of **805** with a stoichiometric amount of ethylene (2 equiv), yielding the mixed-ligand complex $[\{(^{\mathrm{Ar}}\mathrm{nacnac})\mathrm{Mg}\}_2\mathrm{Ni}(\mathrm{C}_2\mathrm{H}_4)(\mu\text{-H})_2]$ (**806**, Scheme 103). Compound **806** is an isolable intermediate in the transformation of **705** and H_2 (r.t.) to **805**. Altogether, the experimental evidence and theoretical calculations supported a cooperative Mg/Ni dihydrogen activation mechanism in which the transition metal center does not suffer oxidation.[479]

Using 1 to 5 mol % of **705** as a precatalyst, under 1 bar of H_2 and at room temperature, **705** efficiently catalyzed the hydrogenation of a variety of unsaturated substrates (aliphatic and aromatic olefins, silyl enol ethers, enamines, imines, quinolines, arenes and alkynes; 16 examples in total, see Scheme 104). Most olefinic substrates were hydrogenated in quantitative yield using a catalyst loading of 1 mol %, except for *p*-fluoro styrene, the silyl enol ether 1-phenyl-1-trimethylsiloxyethylene, and the enamine 1-pyrrolidinocyclohexene, which required a higher catalyst loading (5 mol %). The hydrogenation of the silyl enol ether was also evaluated using the nickel(0) and nickel(II) complexes $[\mathrm{Ni(cod)}_2]$ (**240**) and $(\mathrm{Ph}_3\mathrm{P})_2\mathrm{NiCl}_2$ (**807**) under the same reaction conditions. Whereas the trimetallic nickelaspiropentane complex **705** gave quantitative conversion of the substrate to its hydrogenated product, the Ni(0) species **240** returned a maximum of 16% yield after a prolonged reaction time (24 h). No product was detected using the Ni(II)-phosphine complex **807**. These results stress the importance of the presence of the Z-type Mg-metalloligands at the transition metal and support their involvement in the cooperative activation of the dihydrogen molecule as key in the efficiency of **705** as a precatalyst in hydrogenation reactions.[479] Additionally, the system constitutes a rare example of nickel-catalyzed hydrogenation of imines, yielding over 90% of the corresponding amine products using a catalyst loading of 5 mol %. Notably, the complex is capable of hydrogenating more challenging substrates in high yields under mild conditions (room temperature and 1 bar H_2) using a higher catalyst loading. In the case of arene substrates, higher temperatures (80 °C) were necessary to achieve comparable yields of hydrogenated products.[479]

Scheme 104. Hydrogenation of Unsaturated Substrates Catalyzed by $[\{(^{\mathrm{Ar}}\mathrm{nacnac})\mathrm{Mg}\}_2\mathrm{Ni}(\mathrm{C}_2\mathrm{H}_4)_2]$ (705)[479]

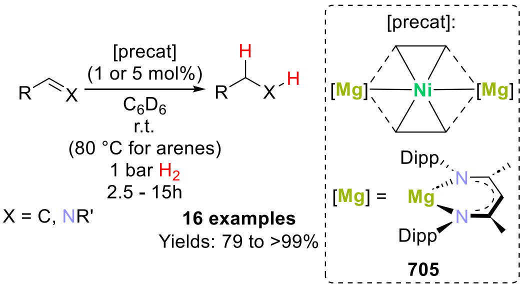

Mechanism (DFT): bimetallic Mg/Ni cooperation

In 2019, Chen and Zeng described a simple system based on chromium or cobalt salts, diimine or carbene ligands, and MeMgBr, which mediates the hydrogenation of polycyclic aromatic hydrocarbons (PAHs).[18,518] While the precatalysts are salts in common oxidation states [M(II), M(III); M = Cr, Co], the theoretical mechanistic modeling (DFT) revealed that low-valent anionic intermediates participate during the reaction given the presence of MeMgBr. Using the continuous variations method (Job's plots), the authors determined that the reactive species in the hydrogenation, for either metal, has a 1:1 metal-to-ligand stoichiometry. For the Cr-mediated reaction, according to DFT studies, oxidative addition of H_2 to diimine Cr(0) or Cr(I) intermediates would be thermodynamically unfavorable. Accessible pathways were calculated for a transmetalation process from MeMgBr to the Cr center, in which hydrogenolysis of the resulting methyl-Cr complex produces an active monohydride metalate with loss of methane (Scheme 105). Theoretical analysis of the cobalt complex revealed a similar activation process in the NHC-Co system (Scheme 105). Moreover, the calculations indicated that for both Cr and Co, energetically low-lying intermediates are found only in the case of the M(0) species for the second hydrogenolysis, occurring upon coordination of the PAHs substrate (specifically anthracene). Consequently, in both cases, zerovalent anionic monohydrides, formed via hydrogenolysis, were invoked as the active species for the hydrogenation of PAHs.[518]

Scheme 105. Formation via Hydrogenolysis of Active Monohydride M(0) (M = Cr or Co) Intermediates Involved in the Hydrogenation of PAHs[518]

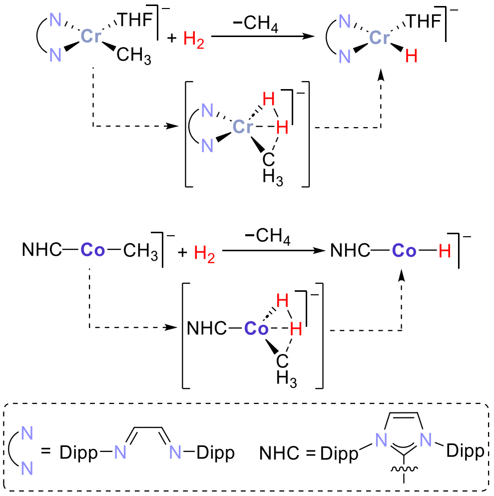

3.1.5. Hydrogen Activation and Hydrogenation Catalysis with Metallatranes and Related Complexes.

Dihydrogen complexes have been postulated as intermediates preceding H_2 activation at transition metals, initiating the process through side-on coordination of the H_2 molecule.[519−521] Peters and Lu have contributed to this field by using 3d metal complexes featuring chelating metalloligands, reporting examples of hydride transfer reactions as well as catalytic hydrogenations.[436,521−527] For instance, these two groups independently reported hydride transfer reactions from cobalt- and nickel-dihydrogen complexes, respectively, supported by boratrane ligand scaffolds.[522,523] The anionic dihydrogen complex $[(P_3^B)Co(\eta^2\text{-}H_2)]^-$ (**808**, P_3^B = tris[2-(diisopropylphosphino)phenyl]borane; as $[M(thf)_n]^+$ salt, M = Na, K)[528,529] was obtained by reduction of the Co(I) compound $[(P_3^B)CoBr]$ (**809**) with strong reductants ($NaC_{10}H_8$ or K). **808** acts as a strong hydride donor, slowly reacting with the poor hydride acceptor BEt_3 under a hydrogen atmosphere to generate the corresponding Et_3BH^- salt in high yields (86% in 20 h) and the mixed-hydride complex $[(P_3^B)CoH(\eta^2\text{-}H_2)]$ (**810**, Scheme 106a).[522] This behavior shows that the thermodynamic hydricity of **808** almost equates that of main group hydrogen donors or other strong hydridic transition metal complexes. Although the behavior was kinetically reproducible, the experimental evidence could not unequivocally support either of the possible reaction pathways for the hydride transfer, i.e., direct hydride transfer or formation of a dihydride intermediate. Theoretical calculations pointed toward the dihydride intermediate, $[(P_3^B)Co(H)_2]^-$, as the lower energy transition state, favorable by 4.8 kcal mol^{-1}.[522]

Scheme 106. Cobalt- and Nickel-Dihydrogen Complexes Supported by Boratrane Ligands, Reported by the Peters and Lu Groups[522,523]

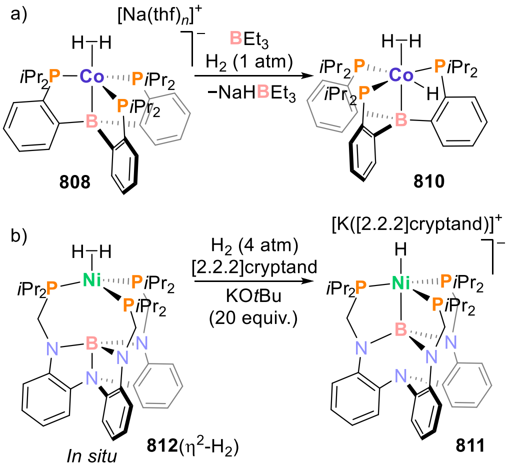

Later, the Lu group described a similar behavior at an anionic Ni(0) hydride complex, featuring a related double-decker boron metalloligand.[523] Complex $[HNiB\{N[o\text{-}(NCH_2PiPr_2)C_6H_4]_3\}]^-$ (**811**), obtained from the *in situ* generated dihydrogen adduct $[(\eta^2\text{-}H_2)NiB\{N[o\text{-}(NCH_2PiPr_2)C_6H_4]_3\}]$ [**812**(η^2-H_2)] in the presence of [2.2.2]cryptand and base (Scheme 106b), acts as an extraordinarily strong hydride donor, also capable of reacting with BEt_3 via complete hydride transfer within minutes. Contrasting with the behavior observed for the cobalt-dihydrogen complex **808**,[522] the experimental and theoretical evidence suggests that hydride transfer from **811** is considerably more favorable than H atom transfer. Furthermore, this study suggested that the ease of deprotonating dihydrogen ligands is more dependent on the stability of the resulting hydride complex, than on the binding energy or degree of activation of the coordinated dihydrogen molecule.

Considering the propensity of $[NiM\{N[o\text{-}(NCH_2PiPr_2)C_6H_4]_3\}]$ (M = Ga (**763**), In (**764**), Scheme 92, section 2.3.3.3, *vide supra*) to bind dihydrogen,[521] these were used as precatalysts in olefin hydrogenation (Scheme 107a).[436] The hydrogenation of styrene was efficiently catalyzed by complex **763** under mild conditions (>99% yield, TOF = 2.4 h^{-1}, 5 mol % precatalyst, 1 atm H_2, r.t.), while **764** performed poorly. Neither the monometallic compound **765** nor the metallalumatrane **762** exhibited activity. Precatalyst **763** performed better for terminal unhindered olefins (e.g., 1-octene, 1-hexene) than for internal olefins, and it was inactive for the hydrogenation of alkynes or aldehydes. **764** mediated hydrogenation much slower for all the olefins—for styrene, hydrogenation was 24-times slower using **764** instead of **763**. In the presence of H_2, **764** primarily promoted their isomerization, while in its absence only traces of isomerized substrates were detected. Although no catalytic cycle was explicitly proposed, key mechanistic insights were obtained. Mercury poisoning tests suggested that a homogeneous species is responsible for the catalysis. Furthermore, since **764** promotes olefin isomerization only in the presence of H_2, it was proposed that the same mechanistic pathway might be operating for both precatalysts, albeit much slower for **764**. Labeling studies carried out under catalytic conditions with complex **763** and D_2 showed incorporation of deuterium atoms in every position of the double bond, which indicates a reversibility on the insertion of the olefin substrate, made possible via β-H elimination. The differing reactivity between $[NiGa\{N[o\text{-}(NCH_2PiPr_2)C_6H_4]_3\}]$ (**763**) and $[NiIn\{N[o\text{-}(NCH_2PiPr_2)C_6H_4]_3\}]$ (**764**) was preliminarily attributed to a lower relative rate of reductive elimination of the hydrogenated product for **764** with respect to **763**, rendering β-H elimination a competitive pathway and leading to the isomerization products. It was proposed that isolable dihydrogen complex **764**(η^2-H_2) might be the resting state, with further activation of H_2 acting as the rate-determining step in the catalytic reaction mediated by **764**. At low temperatures, **763**(η^2-H_2) was also proposed as the resting state, while at room temperature, **763**(η^2-H_2) reversibly

Scheme 107. Hydrogenation of (a) Olefins and (b) CO_2 Catalyzed by $[NiGa\{N[o\text{-}(NCH_2PiPr_2)C_6H_4]_3\}]$ (763)[436,524]

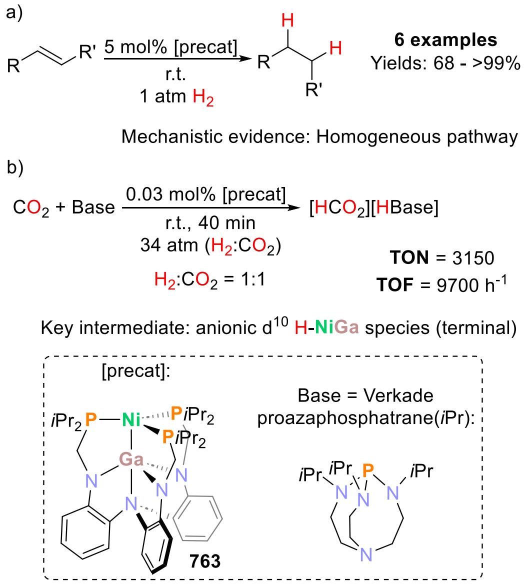

coordinates the substrate in a fast equilibrium. Furthermore, in the hydrogenation of styrene, a normal primary kinetic isotope effect of 1.7 was measured, suggesting that the cleavage of the H−H bond might be involved in the rate-determining step.[436]

Compound **763** also showed remarkable activity in the direct hydrogenation of CO_2 to formate at ambient temperature, in the presence of a Verkade proazaphosphatrane base (Scheme 107b).[524] High turnover numbers (TON = 3150) and frequencies (initial TOF = 9700 h^{-1}), as well as excellent yields were obtained. Base-assisted heterolytic cleavage of H_2 occurred at the Ni(0) complex **763**(η^2-H_2) thanks to the cooperative interaction between the transition metal and the Lewis acidic Ga(III) center from the stabilizing metalloligand, which acts as a σ-acceptor. The significant effect exerted by the metalloligand was ascribed to a strong inverse *trans* influence of the Ga Lewis acid. This becomes evident by comparison of the catalytic tests using complexes **765** or **763**. The former complex is practically inactive for the hydrogenation of CO_2 under the studied conditions. Unlike **763**, **765** does not bind H_2,[436] indicating this coordination is a crucial step in the catalysis. Likewise, the *in situ* combination of **765** with $GaCl_3$ did not afford the product, proving that the metalloligand framework in the precatalyst, with the intact Ni−Ga interaction, is necessary for the performance of the catalyst. The necessity of a strong base was confirmed, by contrasting the reactivity of the Verkade base with weaker bases such as NEt_3, for which no appreciable activity was observed.

Two key catalytic intermediates were identified for the hydrogenation reaction promoted by **763**: the anionic Ni(0) hydride $[HNiGa\{N[o\text{-}(NCH_2PiPr_2)C_6H_4]_3\}]^-$ (**813**) and the anionic formate adduct $[(HCO_2)NiGa\{N[o\text{-}(NCH_2PiPr_2)C_6H_4]_3\}]^-$ (**814**). Both intermediates were observed by NMR spectroscopy, independently prepared, and structurally characterized as bis(triphenylphosphine)iminium (PPN) salts. **813** was obtained by deprotonation of **763** with *n*-BuLi, while **814** is formed after exposure of **813** to an atmosphere of CO_2. By contrast, the Ni(0) complex **763** does not bind CO_2 even at higher pressures (34 atm). ^{31}P NMR spectroscopic screening of the reaction indicated that the predominant species after the catalysis is the formate adduct **814**, suggesting no appreciable decomposition of the catalyst. In addition to characterization by physical and spectroscopic methods, DFT calculations support the formation of a terminal hydride complex, which is more stable than a bridged Ni(μ-H)Ga intermediate. The thermodynamic hydricity of **813** indicates that it is a strong hydride donor ($\Delta G°_{H-} \approx 31$ kcalmol^{-1}), the strongest reported for nickel at this time, and among the strongest of any 3d metal complex (note that the aforementioned Ni(0) hydride **811** has an even lower thermodynamic hydricity, $\Delta G°_{H-} \approx 21{,}4 \pm 1.0$ kcal mol^{-1}).[523] A mechanism for the hydrogenation of CO_2 to formate was postulated using this heterobimetallic system (see Figure 17), in which complex **763** initially coordinates H_2, to form the nonclassical dihydrogen species **763**(η^2-H_2). Subsequent deprotonation generates the anionic terminal hydride **813**. Hydride transfer to CO_2 produces complex **814**, which, after release of the formate product, regenerates catalyst **763** (Figure 17).[524]

Lu and Gagliardi gathered further mechanistic details on the hydrogenation of CO_2 catalyzed by **763** and similar complexes, compiled in a follow-up study.[525] A key insight from this work is that the deprotonation of the coordinated dihydrogen ligand in **763**(η^2-H_2) not only depends on the basicity but, more strongly, on the steric hindrance of the base, while the hydride transfer from **813** to the CO_2 molecules occurs via an outer-sphere mechanism. The dependence on the base strength is reduced once enough formate has been formed, according to energy barrier calculations. Formate then has a cocatalytic role in the reaction and acts as a proton shuttle between **763**(η^2-H_2) and the Verkade base (see Figure 17). These observations might indicate that the overall rate-determining step is the formate-assisted hydride transfer to CO_2, rather than the deprotonation of the coordinated η^2-H_2 ligand as originally proposed.

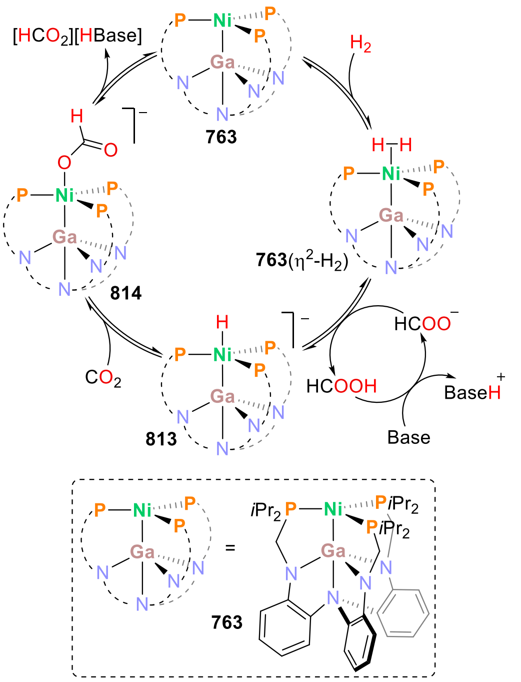

Figure 17. General catalytic cycle for the hydrogenation of CO_2 to formate mediated by $[NiGa\{N[o\text{-}(NCH_2PiPr_2)C_6H_4]_3\}]$ (**763**).[524]

The study was extended to similar heterobimetallic complexes, in two different series: M_1−M_2 complexes (M_1 = Fe, Co, Pd, or Pt and M_2 = Al or Ga) and Ni−M_2 (M_2 = Fe, Co, Al, Ga, or In). For these, it was found that the free energy of activation for the hydride transfer to CO_2 is linearly dependent on the thermodynamic hydricity of the metal hydride. The calculations also indicate that the formate release step should be favored for various combinations of metals in the heterobimetallic complexes: CoAl, CoGa, NiAl, and NiGa. The authors found that, theoretically, the best catalysts for the hydrogenation of CO_2 in these series should be the NiGa (as in **763**) and CoGa combinations. Moreover, it was proposed that further improvement of the performance of catalyst **763** might be achieved by reducing steric hindrance on the phosphine motifs of the heptadentate ligand and on the base. This might not only facilitate the deprotonation on the dihydrogen complex but could also allow the use of weaker or cheaper bases.[525]

In further studies, Lu and co-workers observed moderate hydrogen activation at $Co^{-I}(\eta^2\text{-}H_2)$ scaffolds featuring the Lewis acidic group 13 metalloligands.[526] The highly reduced cobaltates $[Co(\eta^2\text{-}H_2)M\{N[o\text{-}(NCH_2PiPr_2)C_6H_4]_3\}]^-$ {M = Al [**815**(η^2-H_2)], Ga [**816**(η^2-H_2)], In [**817**(η^2-H_2)]} were obtained by treating the corresponding metalloligands with $CoBr_2$ and $LiEt_3BH$ at low temperatures under argon (see Scheme 108).

Scheme 108. Synthesis of $[Li(thf)_n][Co(\eta^2\text{-}H_2)M\{N[o\text{-}(NCH_2PiPr_2)C_6H_4]_3\}]$ [$\mathbf{815}(\eta^2\text{-}H_2)$–$\mathbf{817}(\eta^2\text{-}H_2)$] Cobaltates by Lu and Co-workers[526]

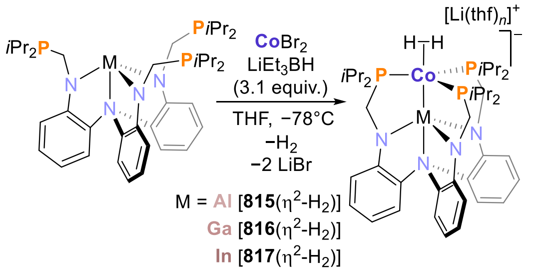

The supporting group 13 ions exert an inverse *trans*-influence, which induces side-on H_2 coordination and fine-tunes its degree of activation in these rare d^{10} dihydrogen adducts. Consistent with the low-valent, formally negative oxidation state, the compounds are diamagnetic. $T_{1\,\text{min}}$ relaxation times and J_{HD} measurements performed on the broad hydridic signals observed by ^{1}H NMR spectroscopy (δ = −7.0, −7.7, and −7.7 ppm for M = Al, Ga, In, respectively) correlate well with the assignment of the H_2 motif as a nonclassical dihydrogen ligand ($T_{1\,\text{min}}$ = 26, 27, and 29 ms, respectively) and with the fast H/D scrambling observed at ambient temperature. The d_{HH} bond distances obtained from these NMR experiments [0.96(1) (Al), 0.98(3) (Ga), 1.00(1) (In) Å] are longer than those previously obtained for the Ni analogues $\mathbf{763}(\eta^2\text{-}H_2)$ and $\mathbf{764}(\eta^2\text{-}H_2)$ [0.87 (Ga), 0.91 (In) Å)], for which short $T_{1\,\text{min}}$ relaxation times of ≤16 and 23 ms were measured.[436] The isoelectronic Ni(0) complexes, however, do not scramble H_2/D_2. Altogether, these observations indicate greater degree of activation for the dihydrogen ligand in the cobaltates compared to the Ni compounds, possibly due to the greater π-basicity of Co relative to Ni or the formally negative oxidation state of the Co center.

To gain insight into the nature of the H_2 ligand, DFT calculations were performed considering the possible hydridic species, namely the nonclassical hydride $[Co(\eta^2\text{-}H_2)ML]^-$, the terminal dihydride $[Co(H)_2ML]^-$, or the bridging/terminal dihydride $[H\text{–}Co(\mu\text{-}H)ML]^-$ (L = $N[o\text{-}(NCH_2PiPr_2)\text{-}C_6H_4]_3$), as in those reported for similar Ni-boratrane species.[530,531] The dihydrogen-Co complexes were energetically more favorable than the species featuring terminal dihydrides by only a small energy difference. The authors suggested that such a small energy difference might indicate facile H_2 cleavage at the Co(−I) center, in agreement with the fast H/D scrambling observed in the NMR experiments.[526]

The influence of the group 13 center on the reactivity of the heterobimetallic cobaltates is clearly illustrated by their performance as precatalysts for CO_2 hydrogenation.[527] The group of Lu observed preliminarily that, upon exposure to a mixture of H_2/CO_2 (1:1; 1.8 atm), complexes $\mathbf{815}(\eta^2\text{-}H_2)$ and $\mathbf{816}(\eta^2\text{-}H_2)$ produced formate and another cobalt-containing species. For comparison, the related compounds $[(N_2)CoM\{N[o\text{-}(NCH_2PiPr_2)C_6H_4]_3\}]^-$ {M = Al [$\mathbf{815}(N_2)$], Ga [$\mathbf{816}(N_2)$], In [$\mathbf{817}(N_2)$]} were prepared. Considering the ease of preparation of the end-on dinitrogen adducts and the good yields of the synthetic protocol used, further in-depth catalytic and mechanistic studies were performed with complexes $\mathbf{815}(N_2)$–$\mathbf{817}(N_2)$. The synthesis of $\mathbf{815}(N_2)$–$\mathbf{817}(N_2)$ is conducted as a one-pot reaction, by stirring the corresponding metalloligand (M = Al, Ga, In) with $CoCl_2$ (THF as solvent), followed by Na/Hg (3.1 equiv) and [PPN][tetrakis(3,5-bis(trifluoromethyl)phenyl)borate]. Upon exposure to a hydrogen atmosphere (1.8 atm), $\mathbf{815}(N_2)$–$\mathbf{817}(N_2)$ transform rapidly into the dihydrogen adducts $\mathbf{815}(\eta^2\text{-}H_2)$–$\mathbf{817}(\eta^2\text{-}H_2)$, confirming that $\mathbf{815}(N_2)$–$\mathbf{817}(N_2)$ could be suitable precursors in the hydrogenation reactions. Consequently, $\mathbf{815}(N_2)$–$\mathbf{817}(N_2)$ were tested as precatalysts for the hydrogenation of CO_2 (Scheme 109, top) under the optimized conditions established for the Ni(0)Ga system [Catalyst loading: 0.031 mol %, Base: Verkade proazaphosphatrane (stoichiometric), CO_2/H_2 = 1:1, 34 atm, room temperature; Scheme 107b, *vide supra*].[524] In these tests, $\mathbf{817}(N_2)$ was completely inactive, while $\mathbf{815}(N_2)$ and $\mathbf{816}(N_2)$ catalyzed the hydrogenation of CO_2, affording moderate to high yields of formate (59% and 97%, respectively) and initial turnover frequencies of 1500 and 11000 h^{-1} (see Scheme 109, bottom). For the most active complex $\mathbf{816}(N_2)$, the catalyst loading could be lowered as far as 0.004 mol %, achieving a remarkable 6-fold increase in turnover number from 3100 (for a catalyst loading of 0.031 mol %) to 19000.

Scheme 109. Hydrogenation of CO_2 Catalyzed by Group 13 Metalloligand-Stabilized Cobaltates[527]

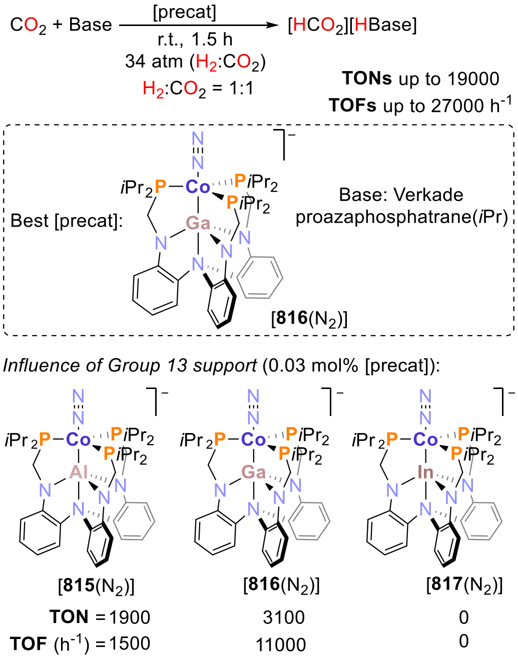

Model reactions were performed to understand the behavior of the catalytic system. The reversible coordination of the dihydrogen ligand to the cobalt center was, for example, found to be mechanistically relevant. By replacing the atmosphere of the reaction vessel from H_2 to N_2, the dihydrogen adducts transform back into the dinitrogen complexes (Scheme 110, top).

As previously observed, exposure of $\mathbf{816}(N_2)$ to a CO_2/H_2 (1:1, 1.8 atm) mixture afforded formate, along with a new cobalt species identified as the mixed-hydride Co(I) complex $[(\eta^2\text{-}H_2)HCoGa\{N[o\text{-}(NCH_2PiPr_2)C_6H_4]_3\}]$ [$\mathbf{818}(\eta^2\text{-}H_2)$]. Under vacuum, $\mathbf{818}(\eta^2\text{-}H_2)$ releases H_2, forming $[HCoGa\{N[o\text{-}(NCH_2PiPr_2)C_6H_4]_3\}]$ (**818**). Similar behavior was observed for the aluminum derivative $\mathbf{815}(N_2)$, yielding the analogous compounds $\mathbf{819}(\eta^2\text{-}H_2)$ and **819**. Both Co(I)Ga hydrides, $\mathbf{818}(\eta^2\text{-}H_2)$ and **818**, as well as the Co(I)Al analogue

Scheme 110. Synthesis of Mechanistically Relevant Intermediates in the Hydrogenation of CO_2 by Group 13 Metalloligand-Stabilized Cobaltates[527]

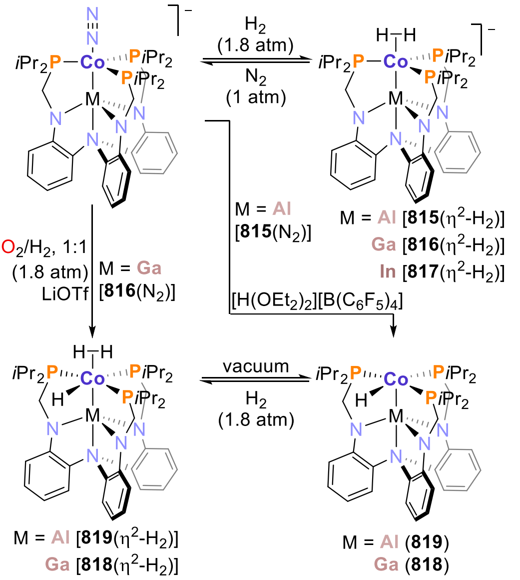

819, were independently synthesized (Scheme 110). Spectroscopic characterization of **818**(η^2-H_2) and **819**(η^2-H_2) not only revealed the lability of the dihydrogen ligand but also the reversibility of its formation under hydrogen atmosphere/vacuum. The different oxidation states of the metal center in the dihydrogen complexes substantially affect the approximate d_{HH} bond distances of the coordinated η^2-H_2 ligand inferred from NMR experiments ($T_{1\ min}$ relaxation times): 0.96 or 0.98 Å in the anionic Co(−I) complexes **815**(η^2-H_2) and **816**(η^2-H_2), respectively (*vide supra*) vs 0.85 or 0.86 Å in the dihydrogen-hydride species **819**(η^2-H_2) and **818**(η^2-H_2).[527]

NMR experiments provided further mechanistic details on the Co−Ga system. These indicated that different resting states operate, depending on the base used. Using the strong Verkade base, complex **816**(η^2-H_2) was identified as the resting state, while for weaker bases it was found to be the dihydrogen-hydride species **818**(η^2-H_2). These observations are reflected in the rate-determining step for the reaction. In the first case, hydride transfer from **816**(η^2-H_2) to CO_2 is rate-limiting, while for the weak base system this becomes the deprotonation of **818**(η^2-H_2).

DFT calculations gave additional insights and support an unusual Co(−I)/Co(I) redox reaction for the H_2-activation step (see Figure 18), in which a dihydride complex is formed. **816**(η^2-H_2) thus acts as a masked Co(I) dihydride, sufficiently hydridic (according to the thermodynamic considerations and DFT calculations) to transfer to CO_2. Another crucial conclusion from the theoretical studies is that the release of formate is assisted by the anionic charge on the formate adduct (Figure 18, species **820**). The deprotonation of **818**(η^2-H_2) to regenerate the catalytically active species **816**(η^2-H_2) is initially promoted by the presence of the strong Verkade base, and then sustained by formate acting as a proton shuttle, as previously observed for the Ni−Ga analogous catalyst **763**.[525] DFT calculations also support mechanistic proposals different from that portrayed in Figure 18, albeit ones which would involve an overall four-electron redox cycle, involving Co(III) intermediates.[527]

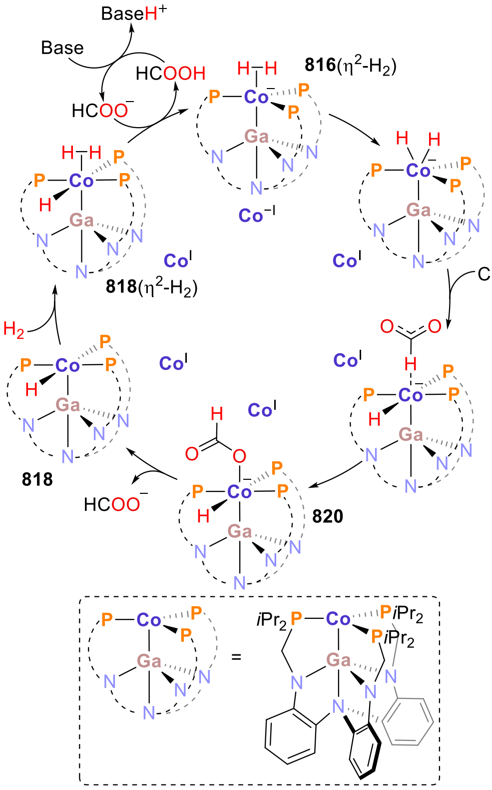

Figure 18. One of the mechanistic proposals for the hydrogenation of CO_2 to formate mediated by **816**(N_2).[527]

3.1.6. Polysilane Hydrogenation Catalyzed by Ni(0) Hydride Complexes.

Hydrogen can also be used to cleave chemical bonds via hydrogenolysis.[532] Trincado and Grützmacher showed that the Ni(I) complexes [Ni(TFA)(trop$_2$NR)] [trop$_2$NR, R = H (**821**), Me (**822**); trop = 5Hdibenzo[*a*,*d*]cyclohepten-5-yl; TFA = trifluoroacetate] react with different hydrogen sources under basic conditions (Me_2NHBH_3 (DMAB)/KO*t*Bu or $LiAlH_4$ or H_2/KO*t*Bu) to afford the Ni(0) compounds M[NiH(trop$_2$NR)] [M = K, R = H (**823**); M = Li, R = Me (**824**)] or K[(trop$_2$NR)Ni(μ-H)Ni(trop$_2$NR)] [R = H (**825**), Me (**826**)] (Scheme 111a). Compound **826** reacted with Ph_2SiH_2 to give [Ni(trop$_2$NMe)(η^2-HSiHPh$_2$)] (**827**). The latter species reacted with a base (K[Me_2NBH_3]) to afford the anionic silyl complex [Ni(SiHPh$_2$)(trop$_2$NMe)]$^-$ (**828**).

Complexes **824**−**826** were evaluated as catalyst precursors for the hydrogenolysis of polysilanes. The catalytic hydrogenolysis of the oligosilanes H(SiPh$_2$)$_n$H using the anionic complexes **824**−**826** (0.03 equiv K[Me_2NBH_3], r.t., 1 bar H_2) quantitatively affords the monomer SiH_2Ph_2. The Ni(I) compound **822** was also a competent catalyst for this reaction, albeit affording lower yields of product (79%, see Scheme 111b). In addition, the authors demonstrated that the trifluoroacetate complex **822** transforms into the dinuclear compound **826** in the presence of molecular hydrogen and a base. In general, the hydrogenolysis of different polysilanes (5 examples, Scheme 111b) returned good-to-excellent yields of product and could be scaled up (for methylated silanes) affording over 80% isolated yield of Me_2SiH_2. Catalyst poisoning tests with Hg or PPh_3 indicated that a homogeneous system might be operative. DFT calculations suggested that the

Scheme 111. Anionic Ni(0)-Hydride Complexes Featuring the Amino-bis(olefin) Ligands $trop_2NR$ and Their Use as Catalysts for the Hydrogenolysis of Polysilanes[532]

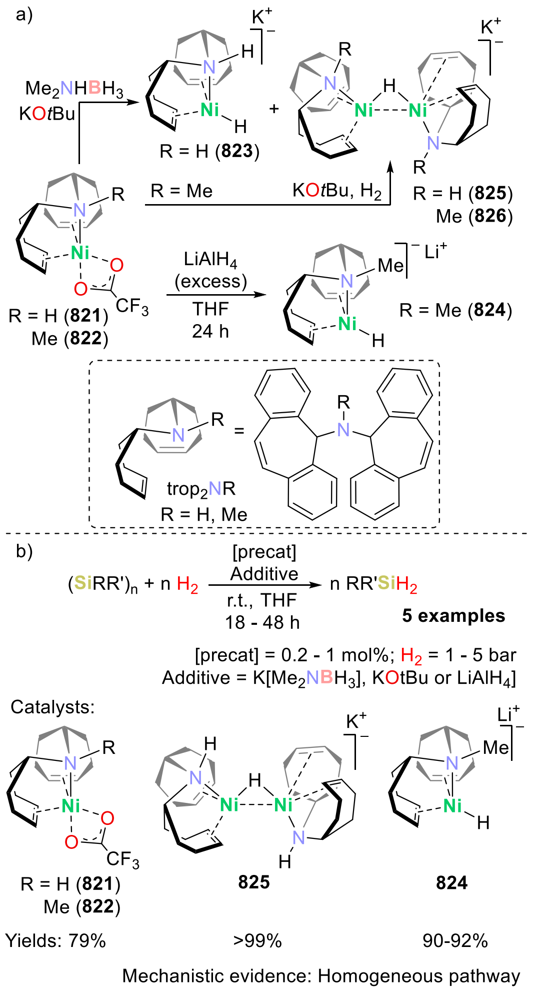

Ni(0)-hydride anion, in which one olefin of the $trop_2NR$ ligand has decoordinated, serves as a catalytic intermediate.

The presence of an electron-rich metal center able to promote both σ-bond metathesis and oxidative addition reactions and the double hemilabile ligand creating a vacant site appear to be key features responsible for the high catalytic activity of the anionic d^{10}-$[Ni(SiHPh_2)(trop_2NR)]^-$ (R = H, Me; X = H, SiR_3) complexes.

3.1.7. Transfer Hydrogenation, Hydroboration, and Hydrosilylation.

In addition to the activation of molecular hydrogen, transfer hydrogenation[388] and other hydrofunctionalization[378,533] reactions mediated by metalate complexes have been studied. For instance, Xu, Cui, and co-workers reported a system for the efficient hydrosilylation of carbonyl compounds catalyzed by the ferrate complex $[(\eta^5\text{-Cp})Fe(CO)_2]^-$, as the potassium or $[NEt_4]^+$ salts (K[**2**] or $[NEt_4]$[**2**]).[14,533] An initial screening of the reaction conditions revealed that both K[**2**] and the more soluble $[NEt_4]$[**2**] facilitate the hydrosilylation of acetophenone (catalyst loading = 0.5 mol %) with $PhSiH_3$ as reductant (Scheme 112). No difference in activity was observed between both catalysts, suggesting that the cation does not play a significant role in this system, beyond improving the solubility of the complex.

In the case of the aromatic ketones/aldehydes (10 examples, Scheme 112), all three Si−H bonds of $PhSiH_3$ participate in the reaction, converting 3 equiv of substrate. For aliphatic substrates, the product corresponds to the doubly substituted bis(alkoxy)silane (9 examples, Scheme 112). The catalyst tolerates a wide range of functional groups, and the system is chemoselective. Quantitative conversions were achieved under the optimized reaction conditions [neat, 0.5 mol % catalyst, room temperature]. At catalyst loadings as low as 0.02 mol %, catalyst $[NEt_4]$[**2**] converted 82% of acetophenone in 10 min, a TOF of 24540 h^{-1}. Furthermore, the system could be scaled up to 100 mmol of substrate without a loss in efficiency. In search of mechanistic information, $[NEt_4]$[**2**] was individually treated with acetophenone or $PhSiH_3$. However, no reaction was observed under the reaction conditions used. Nonetheless, the authors suggested that a possible reaction pathway might involve the oxidative addition of the hydrosilane to ferrate **2**, to yield a highly reactive iron hydride intermediate as a catalytically active species. No further mechanistic evidence was provided.[533]

Scheme 112. Hydrosilylation of Ketones and Aldehydes Catalyzed by $[(\eta^5\text{-Cp})Fe(CO)_2]^-$[533]

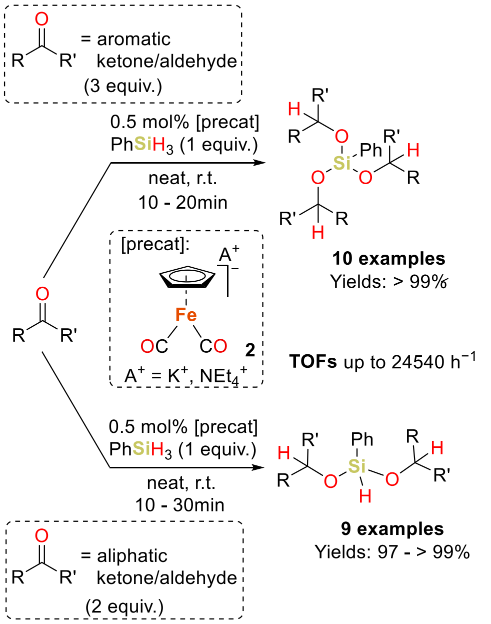

Jacobi von Wangelin and Wolf reported an efficient system for the dehydrogenation of a variety of amine-boranes and the transfer hydrogenation of challenging olefins, imines and N-heteroarenes.[388] Previous studies had found that the precursors $[M(\eta^4\text{-}C_{14}H_{10})_2]^-$ [M = Fe (**52**); Co (**14**)] and $[Co(\eta^4\text{-cod})_2]^-$ (**239**) performed poorly for the hydrogenation of trisubstituted alkenes and for the dehydrogenation of amine-boranes.[248,499] In search for more efficient precatalysts, the group turned to the complexes $[K(thf)_n\{Co(^{Ar}BIAN)(\eta^4\text{-cod})\}]$ (**540**: *n* = 1.5, Ar = Dipp; **541**: *n* = 1, Ar = Mes; see Scheme 65 for the synthetic procedure), which incorporate the redox-active ^{Ar}BIAN ligand (section 2.2.10.1, *vide supra*). These highly reduced cobaltate anions served as precatalysts for the dehydrogenation of ammonia borane (NH_3BH_3, AB) and related amine-boranes under mild conditions. Complex **540** promoted the dehydrogenation of dimethylamine-borane (Me_2NHBH_3, DMAB), yielding a mixture of polyaminoborane, borazine and polyborazine. The mixture of products indicated that the system released more than one equivalent of H_2 from the amine-borane. The evidence gathered from reaction monitoring and poisoning experiments indicated that the catalytic species might be homotopic. Additionally, the authors found that **540** effectively catalyzes the transfer hydrogenation of olefins, imines, and quinolines using NH_3BH_3 as a dihydrogen surrogate (Scheme 113a). The mass balance indicated that up to 2 equiv of H_2 could be transferred from AB.[388]

Scheme 113. Transfer Hydrogenation, Hydrogenation, and Hydroboration Reactions Catalyzed by the Highly Reduced Complexes [K(thf)$_n${Co(^{Ar}BIAN)(η^4-cod)}] (540/541)[388] and [K([18]crown-6)(thf)$_{0.5}$][(^{Dipp}BIAN)Fe(η^4-cod)] (537)[378]

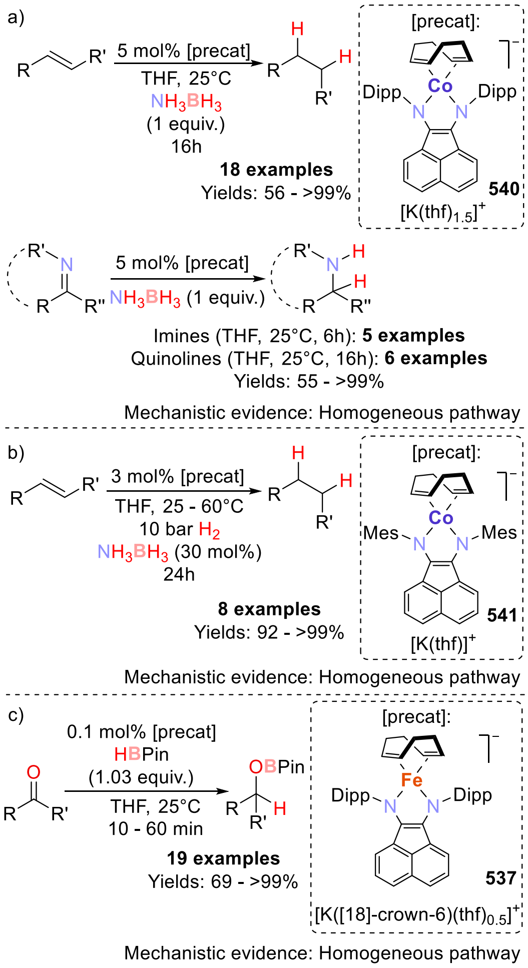

Mechanistic studies and poisoning tests (Hg test or addition of $P(OMe)_3$ or dct) suggest that the reaction occurs via a homogeneous catalyst. Moreover, the experiments revealed that in the transfer hydrogenation the rate-determining step probably involves a proton transfer from the amine-borane. Given the second-order rate law obtained with respect to cobalt, these experiments also suggest that a species composed of more than one cobalt atom is operative. Good conversions were observed for the hydrogenation of alkenes from AB using complex **541** as a precatalyst (Scheme 113b). In this case, challenging trisubstituted olefins were transformed via a different mixed protocol, involving activation of the catalyst **541** by AB (used as an additive), with subsequent hydrogenation using molecular hydrogen (10 bar).[388]

Wolf and co-workers, furthermore, reported an efficient iron-catalyzed hydroboration of ketones, using low-valent complexes featuring the redox-active ligand BIAN as precatalysts.[378] Cyclic voltammetry showed high reduction potentials for complexes [(^{Dipp}BIAN)Fe(L)]$^-$ (L = η^4-cod, bis(norbornyl), ^{Dipp}BIAN, **537**–**539**; see Scheme 64 above), which were therefore anticipated to be good candidates to perform reductive transformations. In fact, under mild conditions [0.1 mol % catalyst load, small excess HBpin (1.03 equiv), 25 °C, THF, 10 min], both **537** and **538** returned quantitative conversions (>99%) of the model substrate acetophenone, though the homoleptic complex **539** afforded only moderate yields of product (67%). This result was attributed to the lack of vacant coordination sites in the precatalyst **539**.

Investigations of the scope of the system (19 examples, see Scheme 113) were carried out under the optimized conditions using complex [(^{Dipp}BIAN)Fe(η^4-cod)]$^-$ (**537**), finding that the system efficiently transforms substituted acetophenones, with either electron-donating or electron-withdrawing groups. Sterically demanding substrates were also reduced, requiring only longer reaction times. Furthermore, the system was selective for halogenated acetophenones (no observable dehalogenation), and for *α*,*β*-unsaturated substrates (no reduction of C=C bonds). Monitoring of the model reaction (hydroboration of acetophenone) using *in situ* IR spectroscopy revealed full consumption of the substrate in only 30 s with a catalyst loading of 0.05 mol %, corresponding to a turnover frequency of 220 000 h^{-1}. Further mechanistic experiments included a poisoning test using mercury, where no inhibition was observed, and individual reactions between complex **537** and the substrate or HBpin. While the reaction of **537** with HBpin did not lead to new signals in the ^{11}B NMR spectrum, addition of acetophenone to **537** gave an immediate color change, along with disappearance of the $\nu_{C=O}$ stretching band of acetophenone from the IR spectrum. Thus, it was concluded that **537** acts as a precatalyst in this system.[378]

The nickel(0) complexes [(κ^2-*C*,*N*-^{Ar}NHCPyO)Ni(cod)]$^-$ by Kennedy and co-workers bearing bidentate NHC–pyridone ligands (Scheme 50, section 2.2.7, *vide supra*) catalyze the hydroboration of styrene by HBpin (Scheme 114).[326] Complexes **412**–**414** proved to be competent precatalysts, affording quantitative conversion of the olefin with >70%

Scheme 114. Hydroboration of Styrene Catalyzed by Nickel(0) Complexes [(κ^2-*C*,*N*-^{Ar}NHCPyO)Ni(cod)]$^-$ Bearing Bidentate NHC–Pyridone Ligands[326]

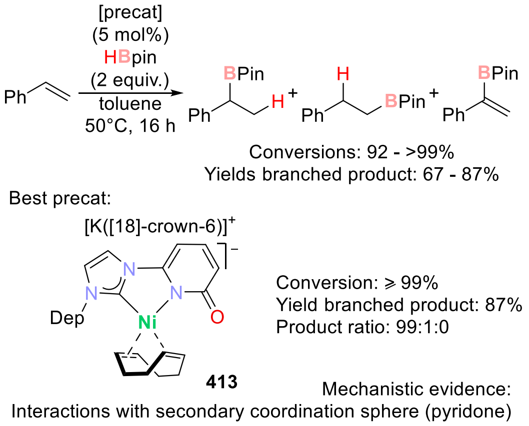

selectivity toward the branched product with 5 mol % catalyst loading at slightly elevated temperatures (50 °C) in toluene. Under the same conditions, the tricoordinate complex $[(\kappa^2\text{-}C,N\text{-}^{Dipp}NHCPyO)Ni(\eta^2\text{-}MeCN)]^-$ (**417**) was also an efficient catalyst, yielding 70% of the branched product. Only negligible amounts of the dehydroboration product were detected.

Using catalyst $[(\kappa^2\text{-}C,N\text{-}^{Mes}NHCPyO)Ni(cod)]^-$ (**412**), efficient hydroboration was reported for *trans-β*-methylstyrene (80% yield branched product), while for *α*-methylstyrene the reaction gave poor results in terms of yield and selectivity (16% yield, branched:linear = 58:42) probably due to increased steric hindrance at the benzylic position of the substrate.

For comparison, the hydroboration of styrene was carried out using the analogous neutral Ni(0) compound $[(\kappa^2\text{-}C,N\text{-}^{Mes}NHCPy)Ni(cod)]$ (**829**), featuring an unsymmetrical NHC-pyridine ligand. Complex **829** converted styrene much less efficiently (60%, 3% yield of branched product) and selectively (branched:linear:dehydroboration product ratio = 31:46:23) than **412**. The superior catalytic properties of the NHC-pyridone complexes likely result from Lewis acid−base interactions between HBpin and the pyridone O atom.[326]

3.1.8. Dehydrogenation/Dehydrogenative Coupling of (Alkyl)amine−Boranes.

Grützmacher and Lichtenberg reported the use of the low-valent Fe(I)-trop$_2$dae complexes [M(solv)$_n${Fe(trop$_2$dae)}] [M = Li, solv = Et$_2$O, n = 2 (**586**); M = Na, solv = thf, *n* = 3 (**587**), see section 2.2.10.4] as precatalysts in the dehydrogenation of dimethylamine-borane (Me_2NHBH_3, DMAB).[383] Compound **587** does not react with H_2 in nonpolar solvents (1.5 bar, *T* = 25 °C), but dehydrogenates DMAB efficiently at room temperature (>99% conversion, 5 mol % precat, 4 h, open system; see Scheme 115a). Under the same conditions, **586** showed only moderate activity (35%, 4 h). The marked difference in performance of both catalysts indicates a strong influence of the contact ion pair. This was evidenced by performing catalytic tests in the presence of additives such as [15]crown-5 or [(nBu)$_4$N]Br which decreased the reaction rate, suggesting an important role of ion-pairing in the mechanism. Other mechanistic experiments, such as selective poisoning of the catalyst (0.2 equiv of PPh_3 or 0.1 equiv of $P(OMe)_3$) or analysis of small aliquots of reaction solutions by scanning electron microscopy (SEM), support a homogeneous mechanism for the dehydrogenation reactions, although no mechanistic proposal was reported. Complex **587** also catalyzes the dehydrogenative alcoholysis of silanes to produce oligo/poly(silyl ethers) from polyols and silanes in an efficient manner, under mild conditions (3 mol % precatalyst, room temperature).[383]

Similarly, an efficient dehydrogenative coupling (dehydrogenative polymerization) of (alkyl)amine−boranes was reported by the same group.[382] The complexes [Fe(trop$_2$dad)(L)] [L = thf (**582**), MeCN (**583**)] were tested as precatalysts for the dehydrogenative polymerization of methylamine−borane (MAB) using a catalyst loading of 5 mol % (toluene, 23 °C, open system; Scheme 115b). Both catalysts show remarkable activity in the dehydrogenative coupling of MAB, giving full conversion after a reaction time of 8.5 min, evidenced by the release of 1 equiv of H_2. Analysis of the polymeric material obtained (poly-MAB, analyzed by mass spectrometry) indicated that it consisted of at least 22 repeating units. A turnover frequency (TOF) of 5.1×10^{-2} s^{-1} was reported, reflecting the high activity of the catalytic system. A short induction period was observed for the reactions catalyzed by either of the complexes, thus suggesting that these are acting as precatalysts. Mechanistic tests, such as varying the solvent and poisoning experiments, indicate that a homogeneous catalytic regime might operate. Good conversions (5 mol % of precatalyst **582**, 23 °C, open system; see Scheme 115b) were also reported for the dehydrogenative polymerization of ammonia-borane $H_3N{\cdot}BH_3$ (AB) or the cyclodimerization of dimethylamine−borane (DMAB), although the excellent activity observed in the conversion of MAB was not matched. The complexes [{Na(thf)$_3$[Fe(trop$_2$dad)]}] (**579**) and [Na(thf)$_3${Fe(trop$_2$dae)}] (**587**) were also evaluated as potential catalysts for dehydrogenative polymerization reactions, with the former being only moderately active, and the latter species being inactive.[382]

Scheme 115. Catalytic Dehydrogenation/Dehydrogenative Coupling of (Alkyl)amine−Boranes Promoted by Fe(I)-dad Complexes[382,383]

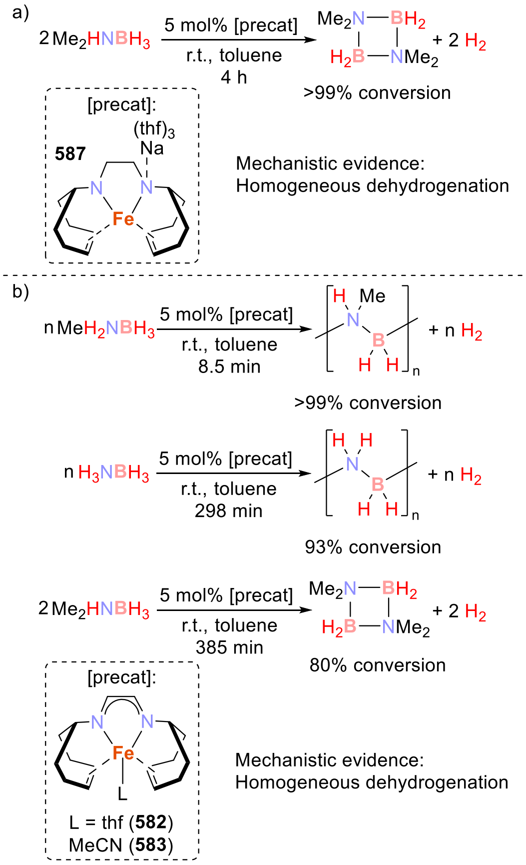

3.2. Nitrogen Activation and Functionalization

Nitrogen fixation by transition metal complexes is currently.[27−29,534−545] Coordination of N_2 to one or several low-oxidation state metal centers is typically required for subsequent NN bond cleavage and conversion of N_2 into ammonia (NH_3) or other nitrogen compounds. Due to their electron-rich nature, low-valent transition metalate complexes are capable of strongly activating N_2 and mediating subsequent transformations of the N_2 ligand.

3.2.1. General Comments on N_2 Activation by Metalate Complexes.

The complexes M[$(N_2)Co(PMe_3)_3$], [M = Li (**830**), Na (**831**), K (**832**)], (Et$_2$O)RMg[$(N_2)Co(PMe_3)_3$] (**833**, R = CH_3, $CH_2CH(CH_3)_2$, $C(CH_3)_3$, C_6H_5)

and $Me_2Al[(N_2)Co(PMe_3)_3]$ (**834**) reported by Klein and Huttner represent early examples of metalates containing dinitrogen ligands.[545,546] In the solid state, the potassium salt $K[Co(N_2)(PMe_3)_3]$ (**832**) features an end-on coordinated N_2 ligand and forms a hexamer through additional interactions of N_2 with the potassium cations, while the magnesium and aluminum compounds have dimeric N_2-bridged structures.[545] Furthermore, the protonation of coordinated dinitrogen ligands at electron-rich ferrates and cobaltates was described as early as 1983. Reactions of compounds $M[(N_2)Co(PPh_3)_3]$ (**830**−**832**), $[Mg(thf)_4][(N_2)FeEt(PPh_3)_2]_2$ (**835**), or $[Mg(thf)_4][(N_2)Co(PPh_3)_3]_2$ (**836**) with H_2SO_4 afforded small amounts of hydrazine and ammonia (0.11 mol −0.31 mol *per* mol of TM).[547] A more recent example showed that coordinated dinitrogen ligands at the complexes $[MgCl(thf)_2][\{PhB(CH_2P\textit{i}Pr_2)_3\}Fe(N_2)]$ (**837**) or $[Mg(thf)_4][\{PhB(CH_2P\textit{i}Pr_2)_3\}Co(N_2)]_2$ (**838**) react with electrophiles to produce diazenido complexes.[548]

The degree of N≡N bond activation in transition metal complexes can be readily identified through the $\nu_{N\equiv N}$ band observed by FT-IR spectroscopy. Selected $\nu_{N\equiv N}$ stretching frequencies can be found in Table 2. For example, it is possible to observe similarities between the stretching frequencies for the free N_2 (g) molecule,[549] and that for $Fe(N_2)(CO)_2(CNAr^{Tripp2})_2$ (**69**)[149] or $(N_2)Co(SiMe_3)(CNAr^{Mes2})_3$ (**98**)[127] in which the dinitrogen ligands exhibit a low degree of activation ($\nu_{N\equiv N}$ approximates to the value of free N_2 (g); see Table 2). By contrast, changes in the degree of activation of a coordinated N_2 ligand become evident by comparing the stretching frequencies of the neutral complex $[(^{Ad}P^{Pym}DI)Fe(N_2)]$ (**551**), and that of its reduced analogue $[Na([18]crown\text{-}6)(thf)_2][(^{Ad}P^{Pym}DI)Fe(N_2)]$ (**558**),[393] or the series of neutral, anionic and dianionic complexes $[(P_3^{\,B})Fe(N_2)]^{0/1-/2-}$ (0: **719**, 1−: **720**, 2−: **723**; see Table 2).[141,486] The increase in backbonding from the more electron-rich metal center causes a shift in the $\nu_{N\equiv N}$ band to lower values, and indicates a higher degree of activation.[393]

3.2.2. N_2 Activation and Functionalization at Transition Metal-Phosphine Complexes.

In 2019, Zhang and Xi reported that low valent anionic species with highly activated dinitrogen ligands were obtained upon reduction of neutral mononuclear chromium or dinuclear chromium-dinitrogen complexes featuring multisubstituted cyclopentadienyl-phosphine ligands.[555] Reduction of either the mononuclear Cr(II) precursor $[\{\textit{o}\text{-}(C_6H_4PCy_2)C_5Et_4\}CrCl]$ (**839**) or the dinuclear Cr(I) complex $[\{\textit{o}\text{-}(C_6H_4PCy_2)C_5Et_4\}Cr(N_2)]_2(\mu\text{-}N_2)$ (**840**) by alkali metals allowed isolation of the anionic Cr(0) compounds $[M([2.2.2]cryptand)][\{\textit{o}\text{-}(C_6H_4PCy_2)C_5Et_4\}Cr(N_2)_2]$ [M = K (**841**), Rb (**842**), Cs (**843**); see Scheme 116]. These diamagnetic complexes have similar features in the solid state, with the main difference being that the alkali metal cations coordinate one or four N atoms in **842** or **843**, respectively, whereas in the potassium metalate **841** no interaction was observed. The molecular structures show Cr−N bond lengths in the range of single bonds (1.820 to 1.834 Å) and slightly activated N_2 ligands (d_{NN} = 1.132 to 1.151 Å; $\nu_{N\equiv N}$ = 1822 to 1907 cm^{-1}).

Scheme 116. Synthesis of Anionic Cr(0)-Dinitrogen Complexes and N_2-Functionalization to Generate a Chromium Hydrazido Compound[555]

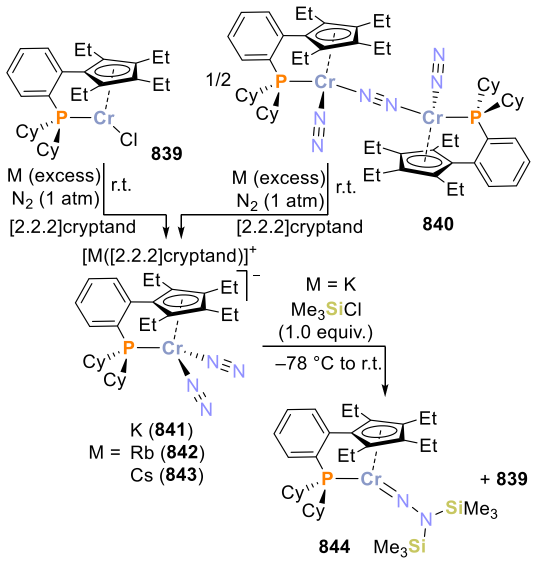

Preliminary N_2 functionalization tests were performed on **841** with acids $[HBAr^F_4{\cdot}2Et_2O$, (LutH)X (X = Cl, OTf; Lut = 2,6-lutidine)] or with Me_3SiCl. In the protonation reactions, the authors detected small amounts of ammonia or hydrazine (∼5% based on N atoms). In turn, the silylation of **841** with Me_3SiCl (1 equiv) generated the bis(silyl)hydrazido complex $[\{\textit{o}\text{-}(C_6H_4PCy_2)C_5Et_4\}Cr{=}NN(SiMe_3)_2]$ (**844**) along with the Cr(II) species **839**. The monosilylated product was not observed. The structural differences observed by crystallographic analysis of **844** compared to **841** evidence the formation of a hydrazido motif: the Cr−N distance is in the range of a M−N double bond (1.680 Å) while the N−N distance is much longer than in the anionic complex (1.372 Å). Since hydrazido complexes have been proposed as intermediates in the catalytic reduction of N_2, the authors evaluated the performance of the series of synthesized complexes in the silylation of N_2 to $N(SiMe_3)_3$. The most active precatalyst was the neutral complex $[\{\textit{o}\text{-}(C_6H_4P\textit{i}Pr_2)C_5Et_4\}CrCl]$ (**845**), an analogue of **839**, which afforded 26 equiv of amine product per Cr (2000 equiv Me_3SiCl, 2000 equiv K as reductant).[555]

Nitrogen functionalization has been achieved at cobalt complexes with chelating phosphine ligands.[556,557] In 2019, Miller and Long described Co(−I)-dinitrogen complexes featuring two examples of the triphos family of tripodal ligands, specifically N-triphos and C-triphos.[556] Two-electron reduction of the Co(I) precursors [(triphos)CoCl] [triphos = $N(CH_2PPh_2)_3$ (**846**), $MeC(CH_2PPh_2)_3$ (**847**)] with Mg powder in THF under a nitrogen atmosphere afforded the Co(−I) complexes $[Mg(thf)_4][\{E(CH_2PPh_2)_3\}Co(N_2)]_2$ [E = N (**848**), MeC (**849**); see Scheme 117, top], analogous to the aforementioned $[Mg(thf)_4][(N_2)Co(PPh_3)_3]_2$ (**836**) or $[Mg(thf)_4][\{PhB(CH_2P\textit{i}Pr_2)_3\}Co(N_2)]_2$ (**838**), among others.[547,548,558]

848 and **849** coordinate dinitrogen between the cobalt centers and the stabilizing Mg^{2+} cation in an end-on bridging fashion. The ligands show a significant degree of activation, as evidenced by the FT-IR data [$\nu_{N\equiv N}$(**848**) = 1878 cm^{-1}; $\nu_{N\equiv N}$(**849**) = 1872 cm^{-1}] and the elongated N−N bond distances in the molecular structure of **848** (1.157(6) and 1.156(7) Å). Metathesis of the counterion with alkali metal cations in both cases yielded the corresponding ion-paired mononuclear complexes $[\{E(CH_2PPh_2)_3\}Co(\mu\text{-}N_2)M]$ [E = N (**850**), MeC (**851**); M = Li(thf)$_x$, Na(thf)$_x$, K(thf)$_x$, K([18]crown-6); Scheme 117]. Additionally, **848** and **849** reacted with Me_3SiCl (2.5 equiv) in THF, affording products

Scheme 117. N_2 Activation and Functionalization at (Triphos)Co(−I)-Dinitrogen Complexes[556]

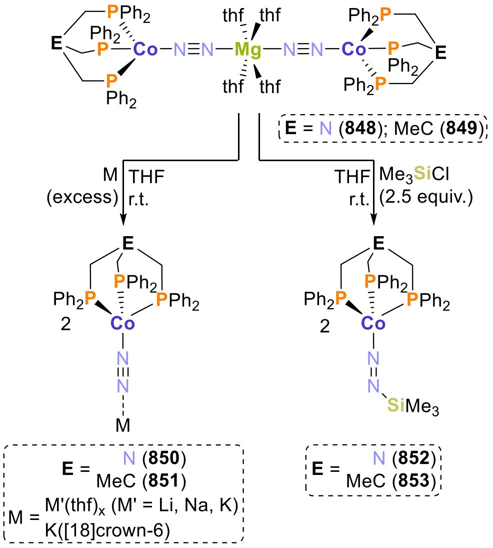

identified as the silyldiazenido derivatives $[\{E(CH_2PPh_2)_3\}Co(NNSiMe_3)]$ [E = N (**852**), MeC (**853**); Scheme 117], on the basis of the lower frequency NN stretching bands [ν_{NN}(**852**) = 1678 cm^{-1}; ν_{NN}(**853**) = 1672 cm^{-1}] and ^{29}Si NMR spectroscopic characterization.[556]

In 2021, another contribution reported that dinitrogen coordinates to Co(−I) centers supported by phosphine ligands, specifically the chelating diphosphine 1,2-bis(dicyclohexylphosphino)ethane (dcpe).[557] Reduction of the Co(II) complex [(dcpe)CoCl(N−P)] [**854**, N−P = (3,5-Me_2-C_6H_3)NP*i*Pr_2] by an excess of alkali metal (Na, K or Cs) under a nitrogen atmosphere gave the anionic compounds [M(solv)][(dcpe)Co(N_2)$_2$] [M = Na (**855**), K (**856**), Cs (**857**); Scheme 118]. Compounds **855**−**857** were also accessed via sequential reduction of the Co(II) precursor, first with KC_8 to afford a Co(I) intermediate **858**, which was further reduced with alkali metals under a nitrogen atmosphere (3 equiv, Scheme 118).

Crystallographic characterization of **855**−**857** confirmed the coordination of two N_2 molecules to the cobalt center, in a rare example of cobalt complexes with more than one dinitrogen ligand. In all cases, the N−N bond lengths are longer and the IR stretching bands are shifted to lower frequencies (e.g., for **856**, dNN = 1.128(3)−1.150(3) Å, $\nu_{N\equiv N}$ = 1837 and 1931 cm^{-1}) than those in the free N_2 molecule, indicating significant activation. Treating **855**−**857** with [2.2.2]cryptand afforded the $[M([2.2.2]cryptand)]^+$ analogues, [M([2.2.2]cryptand)][(dcpe)Co(N_2)$_2$] [M = Na (**859**), K (**860**)] and [(dcpe)Co(N_2)$_2$ Cs([2.2.2]cryptand)] (**861**). In the Cs compound, the counterion is coordinated to both dinitrogen ligands. Compared to **855**−**857**, the encapsulation of the cation by [2.2.2]cryptand causes a decrease in the degree of activation of the N_2 units. Silylation of **856** with *i*Pr_3SiCl (1.5 equiv) resulted in the diazenido complex [{(dcpe)Co(NNSi*i*Pr_3)}$_2$(μ-N_2)] (**862**), which was crystallographically characterized. In the diazenido complex, the N−N bond distances of the functionalized motifs are in the range of typical N═N double bonds [1.2080(18) Å - 1.2051(17) Å]. FT-IR spectroscopy further supported the reduction of the dinitrogen ligands to diazenido units (ν_{NN} = 1696 cm^{-1}). Quantum chemical calculations revealed that **862** has an open-shell singlet ground state, and that the silyldiazenido fragment and the cobalt center exhibit delocalization due to a combination of σ-donation from N to the Co center and π-backbonding back to the diazenido moiety.

Scheme 118. Synthesis of (Diphosphine)Co(−I)-Dinitrogen Complexes and Silylation of Coordinated N_2-Ligands Yielding Diazenido Motifs[557]

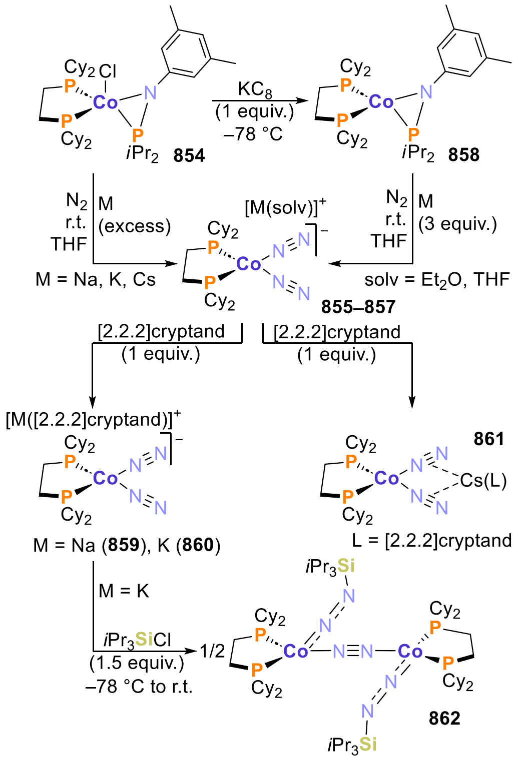

The Schneider group has studied N_2 splitting at pincer (PNP) rhenium complexes (PNP^- = N(CH_2CH_2P-*t*Bu_2)$_2$$^-$).[28,559,560] In 2014, the group established that the reductive transformation of dinitrogen by the Re(III) precursor [$ReCl_2$(PNP)] (**863**) to the Re(V) nitride complex [Re(N)Cl(PNP)] (**864**) occurs through an intermediate N_2-bridged dinuclear complex, [{(PNP)ClRe}$_2$(N_2)] (**865**), as supported by DFT calculations.[560] The group subsequently revisited and expanded this mechanistic proposal, including additional structural, spectroscopic, electrochemical, and kinetic data which pointed toward the participation of an anionic Re(I) species as an intermediate. Compound **865** was isolated and characterized, and was found to feature a moderately activated bridging N_2 ligand.[559] Electrochemical and computational investigations indicated that **863** coordinates the N_2 ligand and undergoes two-electron reduction to generate an anionic Re(I) complex, $[ReCl(N_2)(PNP)]^-$ (**866**). This undergoes comproportionation with further **863** to give the bridged N_2-complex **865**, with concomitant chloride loss. Furthermore, computational calculations indicate that prior to the Re(I)/Re(III) comproportionation process, no significant N_2 activation occurs. In the electrochemically driven reaction, the formation of the bridged complex **865** is irreversible.

3.2.3. N_2 Activation and Functionalization by N-Heterocyclic Carbene Complexes.

Very recently, Wei, Xi, and co-workers described the functionalization of N_2 at a low-valent anionic chromium complex featuring NHC and Cp* ligands.[561] The bis(dinitrogen) compound [K([2.2.2]-cryptand)][Cp*Cr(I*i*Pr$_2$Me$_2$)(N$_2$)$_2$] (**867**, I*i*Pr$_2$Me$_2$ = 1,3-diisopropyl-4,5-dimethylimidazol-2-yldene) formed either directly, by reaction between the Cr(II) precursor [Cp*CrCl(I*i*Pr$_2$Me$_2$)] (**868**) with KC$_8$ (3 equiv) in the presence of [2.2.2]cryptand, or by stepwise reduction of **868** (1.2 equiv KC$_8$), forming the dinuclear compound [{Cp*Cr(I*i*Pr$_2$Me$_2$)}(*μ*-N$_2$){Cp*Cr(I*i*Pr$_2$Me$_2$)(N$_2$)}] (**869**), which is further reduced (3 equiv KC$_8$) to yield **867**. Anionic **867** features significantly activated dinitrogen ligands (ν_{NN} = 1760 and 1846 cm^{-1}; d_{NN} = 1.153(2) Å and 1.1425(19) Å) according to spectroscopic and crystallographic characterization. To functionalize the N$_2$ ligand, the reactivity of *in situ* generated **867** was evaluated. Different products were obtained depending on the bulkiness of the silyl reagent used in the silylation of **867**. Whereas reaction between **867** and *i*Pr$_3$SiCl (1.1 equiv) led to the formation of the chromium diazenido complex [Cp*Cr(I*i*Pr$_2$Me$_2$)(NNSi*i*Pr$_3$)] (**870**; Scheme 119), the use of the less bulky reagent Me$_3$SiCl afforded the chromium side-on η^2-hydrazido species [Cp*Cr(I*i*Pr$_2$Me$_2$)(η^2-Me$_3$SiNNSiMe$_3$)] (**871**) as the major product, along with the Cr(II) complex **868**. Crystallographic characterization of the diazenido and hydrazido derivatives confirmed the significant reduction of the N−N bond order to values in the range of typical double (d_{NN} = 1.243(2) Å) or single (d_{NN} = 1.4671(15) Å) bonds, respectively.

Scheme 119. N$_2$ Functionalization at the Anionic Chromium Complex [Cp*Cr(I*i*Pr$_2$Me$_2$)(N$_2$)$_2$]$^-$ (867)[561]

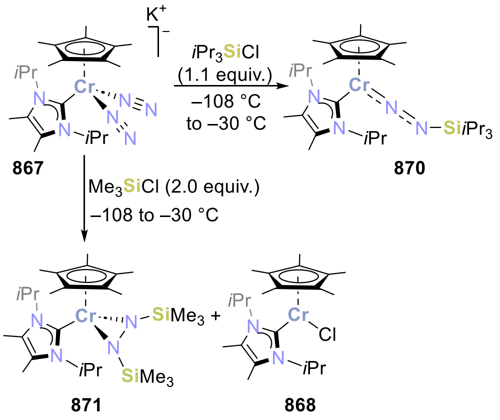

867−**871** were evaluated as catalysts in the silylation of N$_2$ to produce N(SiMe$_3$)$_3$, finding that the complexes were active, producing 2.0 to 5.9 equiv of the silylated amine in 24 h (1000 equiv KC$_8$, 1000 equiv Me$_3$SiCl). Remarkably, the authors anticipated a nucleophilic character for complex **871**, confirmed by reaction with unsaturated substrates such as CO$_2$ and *t*BuNCO. In the first case, two molecules of CO$_2$ inserted into the N−Si and Cr−N bonds of the coordinated hydrazido unit, yielding a new *N*,*O*-chelating hydrazido-chromium complex, [Cp*Cr(I*i*Pr$_2$Me$_2$){κ^2-*N*,*O*-OC(Me$_3$Si)NNC(O)OSiMe$_3$}] (**872**). Similarly, reaction with *t*BuNCO yielded the analogous product of insertion [Cp*Cr(I*i*Pr$_2$Me$_2$){κ^2-*N*,*O*-OC(NtBu)N(SiMe$_3$)N}] (**873**). Both compounds were crystallographically characterized.[561]

The potential of metalates to mediate N$_2$ functionalization reactions is illustrated in recent work by Peters and co-workers, in which the syntheses of complexes [K([18]crown-6){(N$_2$)Fe(CAAC)$_2$}] (**392**)[79] and [(P$_3^B$)Fe(N$_2$)]$^-$ (**720**)[141] were reported (see sections 2.2.7 and 2.3.3.1, respectively). According to the FT-IR data, both complexes feature significantly activated dinitrogen ligands (see Table 2). The functionalization of these species with silyl chlorides was then achieved.[79,428] By treating the carbene complex **392** with trimethylsilyl chloride (Me$_3$SiCl; see Scheme 120a) a rapid color change, accompanied by the appearance of a broad band in the FT-IR spectrum ($\nu_{N\equiv N}$ = 1675 cm^{-1}), were suggestive of functionalization of the N$_2$ molecule. However, the complex that presumably resulted, [(CAAC)$_2$Fe(N═NSiMe$_3$)] (**874**), decomposed rapidly to [Fe(CAAC)$_2$] (**385**). The use of a bulkier chloro-silane reagent, triethylsilyl chloride, gave access to the diazenido compound [(CAAC)$_2$Fe(N═NSiEt$_3$)] (**875**, $\nu_{N\equiv N}$ = 1690 cm^{-1}). Peters and co-workers furthermore showed that systems reactive toward silylation at the *β*-nitrogen of Fe−N$_2$ complexes might be susceptible to efficient reductive protonation.[141,430,562] Therefore, the anionic complex **392**, the related neutral compound [Fe(CAAC)$_2$] (**385**) and its cationic precursor [Fe(CAAC)$_2$]BAr$^F_4$ (**390**, see Scheme 46a, above) were tested as catalysts for nitrogen fixation.

Scheme 120. (a) Silylation of the Coordinated N$_2$-Ligand in Complex [K([18]crown-6){(N$_2$)Fe(CAAC)$_2$}] (392) and (b) Low-Temperature Nitrogen Fixation Using (CAAC)$_2$Fe Complexes as Catalysts[79]

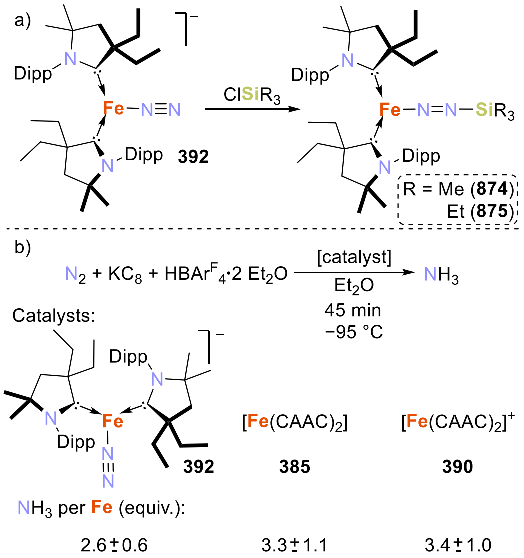

At room temperature, **385** is unable to coordinate N$_2$ and performed poorly in the presence of excess KC$_8$ and HBAr$^F_4$·2Et$_2$O in diethyl ether. Conducting the reaction at −95 °C, however, afforded 3.3 equiv of NH$_3$ per equivalent of iron (see Scheme 120b). A similar performance was reported for the cationic compound **390** and slightly lower yields were obtained with the anionic precursor **392**, under the same conditions. Even at temperatures as low as −78 °C, the performance of the catalyst was rather poor. Compound **385** was also evaluated as a catalyst in N$_2$ silylation, in the presence of a large excess of both KC$_8$ and trimethylsilyl chloride (600 equiv of each), leading to the formation of 24.4 ± 2.7 equiv of N(SiMe$_3$)$_3$.[79]

Deng and co-workers reported NHC-stabilized cobalt-dinitrogen complexes, and their functionalization to yield coordinated diazene compounds.[550] Reduction of the cobalt(I) complex [(ICy)$_3$CoCl] (**876**, ICy = 1,3-dicyclohexylimidazol-

2-ylidene) by KC_8 under a N_2 atmosphere afforded the Co(0)−N_2 complex [$(ICy)_3Co(N_2)$] (**877**), featuring an end-on dinitrogen ligand (Scheme 121a). The low energy N−N stretching frequencies observed ($\nu_{N\equiv N}$ = 1917 cm^{-1}, in KBr) indicate a moderate activation of the N_2 unit. Further reduction of **877** with alkali metals (AM = K, Rb, Cs; 1.2 equiv) yielded the series of bis(dinitrogen)cobalt(−I) complexes [$AM(ICy)_2Co(N_2)_2$] (AM = K[**878**], Rb[**879**], Cs[**880**]; Scheme 121a), obtained as 1D-coordination polymers. Treatment of K[**878**] with [18]crown-6 afforded [$K([18]crown\text{-}6)(ICy)_2Co(N_2)_2$] (K([18]crown-6)[**878**]), in which the $[K([18]crown\text{-}6)]^+$ cation coordinates one of the N_2 ligands. DFT calculations indicated that the dinitrogen ligands at the formally d^{10} Co(−I) center engage in substantial π-backbonding into the N_2 π* orbital, as reflected by the significantly red-shifted IR stretching vibration ($\nu_{N\equiv N}$ = 1807 cm^{-1}, in KBr). The Co(−I) complexes **878**−**880** reacted with anhydrous acids (triflic acid or HCl, −78 °C, Et_2O) to yield hydrazine (23−31% yields per cobalt atom) and trace amounts of ammonia. By contrast, analogous reaction with the neutral complex **877** gave only traces of hydrazine product. Attempts to isolate the intermediates in the protonation reactions were unsuccessful. Nonetheless, by treating K[**878**] with chlorosilanes (R_3SiCl), the cobalt diazene complexes [$(ICy)_2Co(\eta^2\text{-}R_3SiNNSiR_3)$] [R = Me (**881**), Et (**882**), Scheme 121a] were formed.

Scheme 121. (a) NHC-Stabilized Cobalt-Dinitrogen Complexes or Their Functionalized Products and (b) Catalytic Silylation of N_2 by Low-Valent Cobalt[550]

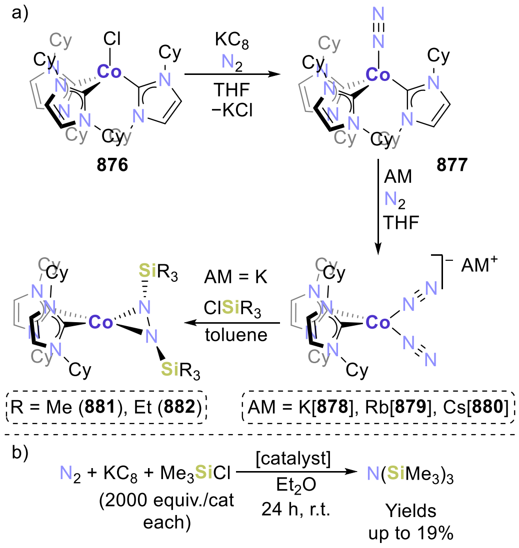

Catalysts:	TON
[$(ICy)_3Co(N_2)$]	125
[$K(ICy)_2Co(N_2)_2$]	107
[$(K[18]crown\text{-}6)(ICy)_2Co(N_2)_2$]	118
[$(ICy)_2Co(\eta^2\text{-}Me_3SiNNSiMe_3)_2$]	109
[$(ICy)_2Co(\eta^2\text{-}Et_3SiNNSiEt_3)_2$]	121

The solution magnetic moments of species **881** or **882** (approximately 3.0 μB) agree well with reported examples of low-spin cobalt(II)−NHC compounds. These observations are also consistent with the EPR characterization, which exhibits signals typical of low-spin square planar Co(II) complexes. The N−N distances of the dianionic diazene $\eta^2\text{-}R_3SiNNSiR_3$ ligands indicate the presence of single bonds (**881**: 1.450(4) Å; **882**: 1.457(3) Å). Compounds **876**−**882** afforded comparable yields of the silylated product $N(SiMe_3)_3$ (15−19%, relative to Me_3SiCl) in the silylation of dinitrogen under the following conditions (Scheme 121b): N_2 (1 atm), KC_8 (2000 equiv relative to catalyst) and Me_3SiCl (2000 equiv relative to catalyst), at room temperature. These yields correspond to TONs between 107 and 125. The catalytic activity of complexes **881** and **882** is particularly noteworthy, since diazene species have frequently been proposed as key intermediates in the alternating N_2 reduction pathway.[563−565] Independent reactivity tests with complex **881** provided further insights on this matter: While **881** failed to react with either further reductant (KC_8) or Me_3SiCl at room temperature, the presence of both reagents in excess amounts produces $N(SiMe_3)_3$ in 85% yield. Therefore, the diazene complex **881** was proposed to be a possible intermediate in the catalytic silylation of N_2 by the NHC-stabilized cobalt complexes.

3.2.4. N_2 Activation and Functionalization by Amido and β-Diketiminate Metalates.

Schley, Tonks, and co-workers reported that the reduction of [$Ti\{N(SiMe_3)_2\}_3$] (**883**) by KC_8 in toluene affords the mixed-valent inverse sandwich complex [$K(toluene)$][$\{N(SiMe_3)_2\}_2Ti(\mu\text{-}C_7H_8)Ti\{N(SiMe_3)_2\}_2$] (**884**, Scheme 122).[566] This complex had previously been incorrectly identified as [$Li(tmeda)_2$][$Ti\{N(SiMe_3)_2\}_2(\mu,\eta^2{:}\eta^2\text{-}N_2)$]$_2$ (**885**) featuring two bridging side-on N_2 ligands.[567] The significant elongation of the C−C bonds (1.436(4)−1.449(4) Å) in the bridging toluene unit in **884** indicates that it corresponds to a $C_7H_8^{2-}$. The metric parameters and the solution magnetic moment (1.67 μB, overall S = 1/2) suggested that **884** is a mixed-valent Ti(II)/Ti(III) complex.

Scheme 122. Reassessment of the N_2 Activation by Low-Valent Ti-Amide Complexes: Evidence of the Formation of an Inverse Sandwich Complex Instead of a Bridged Side-on Dinitrogen Adduct[566]

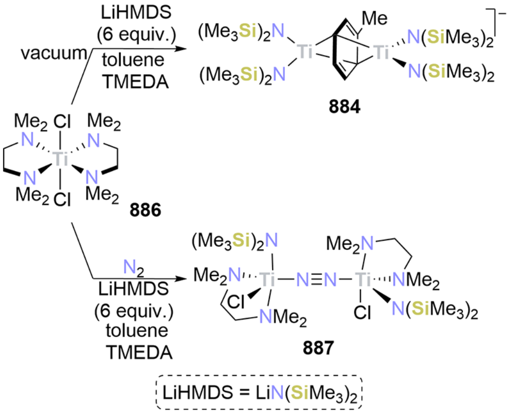

Theoretical modeling (DFT) revealed that a structure with an inverse sandwich arrangement is in better agreement with the data of **885** than a dinitrogen bridged compound. Attempts to synthesize the latter complex again from $(tmeda)_2TiCl_2$ (**886**) under the originally reported conditions led only to the formation of **884** and the end-on dinitrogen bridging compound [$(tmeda)Ti\{N(SiMe_3)_2\}_2Cl$]$_2$($\mu$-$N_2$) (**887**, Scheme 122), also described in the previous work.[566,567] In addition, Schley and Tonks examined the reduction of Ti(III) complexes under nitrogen, and could identify different Ti(IV)-nitride products.

Holland and co-workers have made remarkable contributions to nitrogen fixation chemistry through investigations into the use of low-coordinate iron and cobalt compounds.[551,552,568−574] Among these are the dinuclear complexes AM$_2$[(nacnac)M(NN)M(nacnac)] [M = Fe, nacnac = CH[C(Me)N(2,6-iPr$_2$C$_6$H$_3$)]$_2$, AM = Na (**888**), K (**889**) Rb (**890**), Cs (**891**) or nacnac = CH[C(tBu)N(2,6-iPr$_2$C$_6$H$_3$)]$_2$, AM = K (**892**); M = Co, nacnac = CH[C(tBu)N(2,6-iPr$_2$C$_6$H$_3$)]$_2$, AM = Na (**893**), K (**894**)], featuring dinitrogen ligands with NN bond orders of two as evidenced by the N−N bond lengths and stretching frequencies (Scheme 123 shows the potassium ferrates and the sodium and potassium cobaltates).[552,569,570,574]

Scheme 123. Dinuclear (a) Iron, (b) Cobalt, or Nickel Anionic Complexes Featuring Significantly Activated Bridging Dinitrogen Ligands[552,569,570,575]

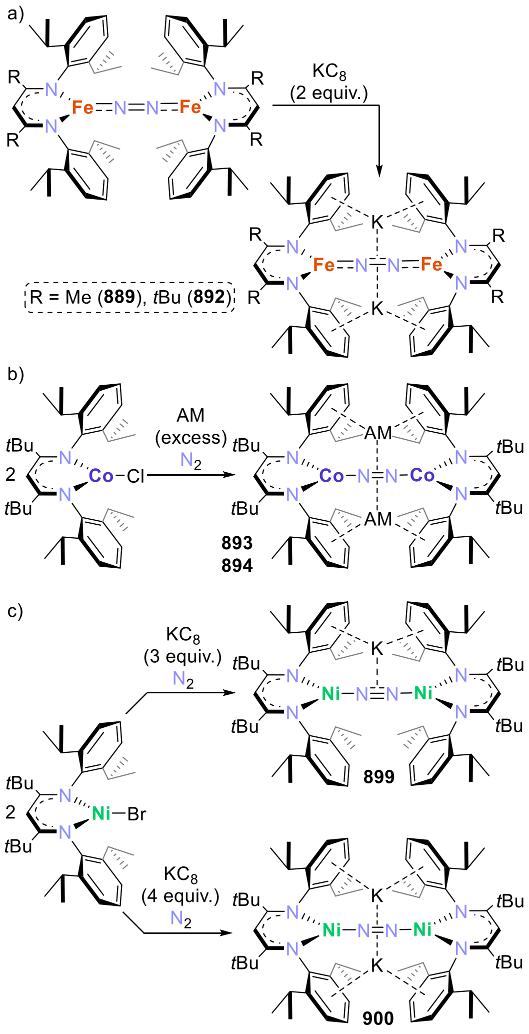

Complex	N-N bond distances (Å)
K$_2$[(^{Me}nacnac)Fe(NN)Fe(nacnac^{Me})]	1.215(6)
K$_2$[(^{tBu}nacnac)Fe(NN)Fe(nacnac^{tBu})]	1.233(6)
Na$_2$[(nacnac)Co(NN)Co(nacnac)]	1.211(3)
K$_2$[(nacnac)Co(NN)Co(nacnac)]	1.220(2)
K[(nacnac)Ni(NN)Ni(nacnac)]	1.143(8)
K$_2$[(nacnac)Ni(NN)Ni(nacnac)]	1.185(8)

The greatest weakening of the dinitrogen ligands was observed for the iron complex **892** ($\nu_{N\equiv N}$ = 1589 cm^{-1}) and for the cobalt compound **894** ($\nu_{N\equiv N}$ = 1599 cm^{-1}).[552,569] The solid-state geometry of the iron complexes **888**−**892** was affected by the nature of the alkali metal cation. Rotation about the FeNNFe core was observed, with greater rotation of the β-diketiminate ligand backbones with respect to one another accommodating increasing size of the counterion. The extent of N$_2$ activation was largely unaffected by these structural changes, and computational studies showed this was due to orbital mixing enabling similar backbonding into the π* orbitals of N$_2$ regardless of the orientation of the ligands.[574]

Remarkably, the reduction of the Fe(II) complex [(^{Me3}nacnac)Fe(μ-Cl)]$_2$] (**895**) by potassium under a nitrogen atmosphere afforded a tetrairon bis(nitride) complex [(^{Me3}nacnac)$_3$Fe$_3$(N)$_2$K$_2$(Cl)$_2$Fe(nacnac^{Me3})] (**896**, ^{Me3}nacnac = MeC[C(tBu)N(2,6-iPr$_2$C$_6$H$_3$)]$_2$). **896** features an Fe$_3$N$_2$ core, in which three iron atoms cooperate with the potassium cations to fully cleave the N−N triple bond, promoting a six-electron reduction of dinitrogen. Based on the combined characterization data, the tetrairon complex was reported to be composed of two Fe^{2+} and two Fe^{3+} centers.[551] The reactivity of **896** is significantly influenced by pairing interactions with the alkali metal counterions, as demonstrated, upon addition of [18]crown-6, by the formation of a mixed-valent Fe(II)/Fe(III) anionic triiron complex derived from the aforementioned Fe$_3$N$_2$ core.[568] In this species, new N−H and Fe−C bonds are formed after intramolecular C−H bond activation.

The authors proposed that the ability to form and break bonds in such a compound can be regarded as an “alkali control” strategy, in which reactions of N$_2$-derived nitrides (e.g., N−C bond formation) can be promoted. This very interesting reactivity, however, involves compounds of iron in its most common oxidation states, and therefore, will not be further discussed herein. For details, we refer the reader to the original literature.[551,568]

Limberg and co-workers described the dinuclear Ni(I) compound [(nacnac)Ni(NN)Ni(nacnac)] (**897**, nacnac = CH[C(tBu)N(2,6-iPr$_2$C$_6$H$_3$)]$_2$) which similarly coordinates dinitrogen in a bridging end-on fashion.[575] The dinitrogen ligand is weakly activated, evidenced by the stretching vibration in the FT-IR spectrum ($\nu_{N\equiv N}$ = 2164 cm^{-1}). Compound **897** can be generated *in situ* by reduction of [(nacnac)NiBr] (**898**) with KC$_8$, and further reduced to yield the singly and doubly reduced complexes K[(nacnac)Ni(NN)-Ni(nacnac)] (**899**) and K$_2$[(nacnac)Ni(NN)Ni(nacnac)] (**900**, see Scheme 123c). The two single-electron reduction events further activated the dinitrogen ligands, as indicated by their elongated N−N bond distances (Scheme 123, bottom). DFT calculations predicted that, for both **899** and **900**, these reduction events affected the bridging N$_2$ ligand instead of the β-diketiminato units or the metal centers. Given the significantly elongated NN bond, the N$_2$ unit in **900** has a diazene character.

In another example of the role of the cation in the nature of the isolated metalate complex, Holland and co-workers described additional iron and cobalt complexes featuring linear M−NN−Mg−NN−M cores (M = Fe, Co).[576] Reduction of precursors [(^{tBu}nacnac)FeCl] (**901**), [(^{Me}nacnac)Fe(μ-Br)]$_2$ (**902**), or [(^{tBu}nacnac)Co(thf)] (**903**) by activated Rieke magnesium in THF afforded complexes [Mg(thf)$_4$]-[(^{R}nacnac)M(μ-N$_2$)]$_2$ [M = Fe, R = tBu (**904**), M = Fe, R = Me (**905**), M = Co, R = tBu (**906**)]. These compounds share similar structural features in the central core with the (triphos)cobalt complexes $[Mg(thf)_4][\{E(CH_2PPh_2)_3\}Co(N_2)]_2$ [E = N (**848**), MeC (**849**)], described above.[556] The iron complexes **904** and **905** are metastable, and could only be characterized in solution. A comparison of the stretching frequencies of **904**−**906** [$\nu_{N\equiv N}$(**904**) = 1808 cm^{-1}, $\nu_{N\equiv N}$(**905**) = 1818 cm^{-1}, $\nu_{N\equiv N}$(**906**) = 1868 cm^{-1}) with those of the dinuclear complexes **892** ($\nu_{N\equiv N}$ = 1589 cm^{-1}) and **894** ($\nu_{N\equiv N}$ = 1599 cm^{-1}) evidence the striking difference between both types of compounds: While in all the complexes the dinitrogen ligands are significantly activated, N≡N weakening in the potassium metalates **892** and **894** is substantially more acute than in the trinuclear M−NN−Mg−NN−M compounds **904**−**906**, which contain formally zerovalent transition metal centers. This effect was attributed to the different interaction established between the dinitrogen ligands and the cations, since in **892** and **894** the counterions bind the N_2 motifs in a side-on fashion, whereas in **904**−**906** these units are coordinated between the transition metal and magnesium cation in a bridging end-on mode.[576]

Later, Holland reported that an iron-based system composed of the diketiminato-iron(II) bromide complex, $[(^{Dipp}nacnac)Fe(\mu\text{-}Br)]_2$ (**907**, ^{Dipp}nacnac = CH[C(Me)N(2,6-iPr$_2$C$_6$H$_3$)]$_2$), sodium, a crown ether, and trimethylsilyl bromide promotes the coupling of N_2 and unactivated arenes at low temperature, to afford aniline derivatives.[572] The efficiency of the system relies on the ability of the catalyst to both coordinate the arene and dinitrogen and on the coordinated N_2 motif to undergo partial silylation. The proposed mechanism consists of a sequential activation of the arene substrate, functionalization of N_2 and migration of the aryl ligand to the functionalized N_2-ligand.

In initial studies, **907** was converted to the Fe(I) species $[(^{Dipp}nacnac)Fe\cdot benzene]$ (**908**), which was reduced further by either KC$_8$ or Na in the presence of a crown ether ([18]crown-6 or [15]crown-5) to afford the Fe(0) complex $[K([18]crown\text{-}6][(^{Dipp}nacnac)Fe(\eta^4\text{-}C_6H_6)]$ (K[**909**]) and the benzene C−H activation product $[Na([15]crown\text{-}5][(^{Dipp}nacnac)Fe(Ph)(H)]$ (Na[**910**]), respectively. Further studies revealed that the Fe(0) and Fe(II) species **909** and **910** are in an equilibrium in THF. In turn, Na[**910**] formally loses the hydride ligand as H·, affording the three-coordinate complex $[Na([15]crown\text{-}5][(^{Dipp}nacnac)Fe(Ph)]$ (Na[**911**]), which served as platform to explore N_2 binding. Under a nitrogen atmosphere at low temperature, **911** coordinates N_2 to afford $[(^{Dipp}nacnac)Fe(N_2)(Ph)]^-$ (**912**, Scheme 124, top). Silylation of the coordinated N_2 ligand by Me$_3$SiBr (2 equiv) at low temperature produced the arylhydrazido complex $[(^{Dipp}nacnac)FeN(Ph)N(SiMe_3)_2]^-$ (**913**), in which migration of the phenyl ligand to the functionalized dinitrogen unit has occurred. Performing the silylation of **912** with the bulkier iPr$_3$SiOTf, afforded the singly silylated product $[(^{Dipp}nacnac)Fe(Ph)\{NN(Si\,iPr_3)\}]^-$ (**914**) and the Fe(II) complex $[(^{Dipp}nacnac)Fe(Ph)]$ (**915**). **914** appears to be an initial stage in the silylation of N_2 before migration of the phenyl ligand. Addition of an excess of the silylation reagent and reductant to **913** or **914** afforded the aniline derivative (Scheme 124, top). The presence of a large excess of bromide from Me$_3$SiBr then promotes the regeneration of **907**. Based on these insights, a synthetic cycle for the coupling of N_2 and arenes at iron was developed.[572]

To ensure that all reactions are compatible, the iron(II) complex **907** was treated with Na (30 equiv/Fe), benzene (20 equiv), and [15]crown-5 (5 equiv) at room temperature, followed by cooling the solution to −108 °C, and adding Me$_3$SiBr (6 equiv). This protocol produced C$_6$H$_5$N(SiMe$_3$)$_2$ in 24% yield per iron atom. Slight modification enabled the development of a cyclic procedure in which the addition of the reagents is performed at the proper temperature for either C−H activation or nitrogen binding and silylation. After addition of Me$_3$SiBr, the solution is allowed to warm to room temperature to regenerate **911**, evidenced by a color change. Further cooling−silylation−warming cycles, with addition of 2 equiv of Me$_3$SiBr in each cycle, provided the formation of the aniline derivatives in higher cumulative yields, although the yield of N(SiMe$_3$)$_3$ increases with each cycle, and the yield of the aniline derivative attenuates. Scheme 124 (bottom) shows the product distribution in the coupling of three arene substrates with N_2 after 5 cycles of Me$_3$SiBr addition (2 equiv/cycle).

Scheme 124. Binding of N_2 to the Fe(I) Species $[Na([15]crown\text{-}5][(^{Dipp}nacnac)Fe(Ph)]$ (Na[911]) and Functionalization of Coordinated N_2 (Top) And Product Distribution in the Iron-Mediated Coupling of Arenes with N_2 (Bottom)[a][572]

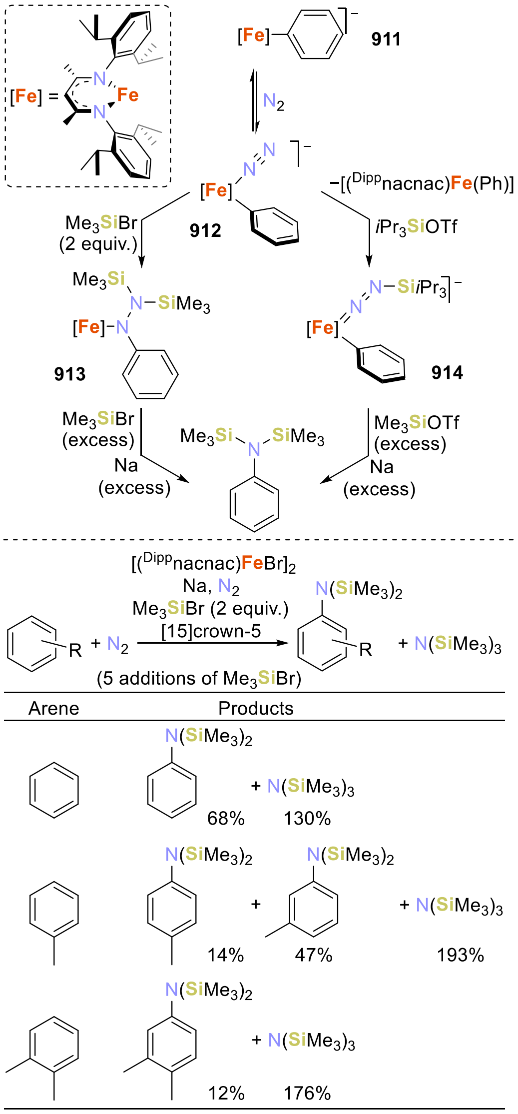

[a] Yields shown are relative to iron atom.

The proposed reaction mechanism for the transformation of arenes and dinitrogen to anilines can be represented by the simplified cycle depicted in Figure 19. Reduction of the Fe(II) complex **907** in the presence of the arene substrate produces the (arene)Fe(0) species **909**, which undergoes C−H activation to form the hydride species **910**. Hydride loss under reducing conditions, and N_2 binding at low temperature, affords the Fe(I) complex **912**, in which the N_2 unit is silylated to afford the (arylhydrazido)Fe(II) complex **913**. At this point, the mixture is allowed to warm to room temperature, after which further silylation under reducing conditions yields the amine products and an Fe(II) species which, upon warming to room temperature, reduces and coordinates the arene to form **909**, thereby closing the cycle. This remarkable strategy could pave the way for the development of future catalytic systems for the coupling of hydrocarbons and N_2.

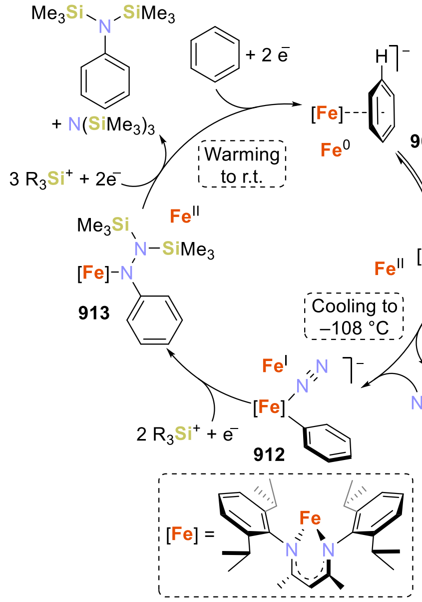

Figure 19. Cyclic pathway for the coupling of of N_2 and unactivated arenes, including key isolated intermediates.[572]

Further mechanistic details on this transformation have recently been reported.[573] In the previous study,[572] the exact pathway through which reduction, silylation, and migration occurred could not be completely described. With the aid of synthetic, structural, magnetic, spectroscopic, kinetic, and computational studies, the authors have now elucidated additional key steps, reporting a high-valent iron(IV) disilylhydrazido(2−) complex, an intermediate in the silylation of **912** to afford the (arylhydrazido)Fe(II) complex **913** (Figure 19).

Scheme 125. Synthesis of an Iron(IV) Disilylhydrazido(2−) Intermediate from the Anionic Fe(I) Complex 912[573]

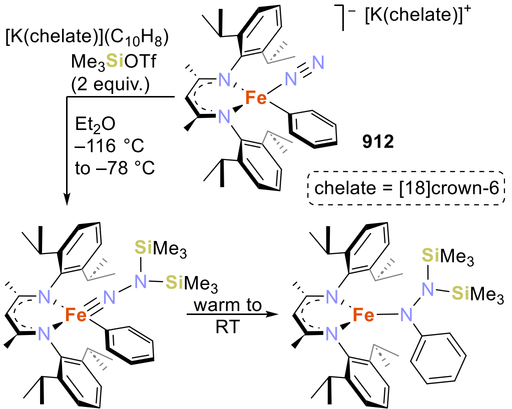

912

916 **913**

The transient Fe(IV) species $[(^{\mathrm{Dipp}}\mathrm{nacnac})\mathrm{Fe(Ph)}\{\mathrm{NN(SiMe_3)_2}\}]$ (**916**, Scheme 125) was isolated from the reaction of the Fe(I) complex **912** with Me_3SiOTf (2 equiv) at −116 °C, extracting the product at −78 °C and crystallizing it at −35 °C. The low temperature handling of this compound was necessary, due to its thermal instability. Upon warming to room temperature, the product of aryl migration, **913**, was obtained. In an attempt to further stabilize the product, the group turned to the bulkier xylyl substituent, synthesizing the analogue to the Fe(I) complex **911**, $[(^{\mathrm{Dipp}}\mathrm{nacnac})\mathrm{Fe(Xyl)}]^-$ (**917**, Xyl = 2,6-$Me_2C_6H_3$), which coordinates N_2 to give $[(^{\mathrm{Dipp}}\mathrm{nacnac})\mathrm{Fe(N_2)(Xyl)}]^-$ (**918**). Treatment of the latter compound with Me_3SiOTf (2 equiv) and K([18]crown-6)($C_{10}H_8$) afforded the product of aryl migration $[(^{\mathrm{Dipp}}\mathrm{nacnac})\mathrm{FeN(Xyl)N(SiMe_3)_2}]^-$ (**919**), analogous to **913**, which was crystallographically characterized. The corresponding intermediate of this transformation, the iron(IV) disilylhydrazido(2−) with a xylyl substituent, was not isolated but could be spectroscopically identified at low temperature. Kinetics of the aryl migration in these complexes and additional computational investigations of the mechanism of N−C bond formation from the high-valent Fe(IV) intermediate were also reported. For further details, we refer the reader to the original literature.[573]

3.2.5. N_2 Binding and Activation at Biomimetic Metalate Species.

Holland and co-workers have reported N_2 binding by sulfur-supported iron(0) metalates, acting as facsimiles of the FeMo cofactor (FeMoco), a sulfur-rich iron−molybdenum site for N_2 reduction in nitrogenase enzymes.[577,578] Initial reduction of the high-spin iron(II) precursor [LFe(thf)$_2$] [**920**, L = {1,3-(2-S-3-Ar-6-F-C_6H_2)$_2$-(C_6H_4)}; Ar = 2,4,6-triisopropylphenyl] by stoichiometric KC_8 yielded the corresponding iron(I) complex K[LFe] (**921**, Scheme 126).[577] EPR spectroscopy and a solution magnetic moment of 2.1 μ_B indicated a low = spin ($S = 1/2$) iron(I) center in **921**, while the crystal structure showed η^6-bonding to the central arene ring of the ligand.

Further reduction by an additional equivalent of KC_8 under a nitrogen atmosphere, followed by addition of [18]crown-6, resulted in the dark red iron(0) complex [K{[18]crown-6}]$_2$[LFeN$_2$] (**922**). XRD analysis confirmed that N_2 was bound as a terminal ligand and featured only η^2-coordination to the arene. IR spectroscopy revealed an N−N stretching frequency of 1880 cm^{-1}. This strong activation was attributed to the powerful electron-donating abilities of the thiolate groups, enabling significant backbonding from the iron center into the N_2 π^* orbitals. Despite this strong Fe−N_2 interaction, the N_2 ligand remained labile, undergoing exchange with $^{15}N_2$ at −70 °C in the solid state, and samples of **922** kept at ambient temperature for a few hours no longer exhibited N_2 vibrations. SQUID magnetometry suggested the complex featured an unusual high-spin ($S = 1$) iron(0) center, observations corroborated by DFT calculations performed on a truncated model of **922**.

To examine whether Fe−S bond dissociation could provide a coordination site for N_2 binding, as hypothesized for FeMoco, the tris(thiolate) complex K[LFe(SAr′)] (**923**) was

Scheme 126. Nitrogen Activation by Sulfur-Supported Iron Complexes by Holland and Co-workers[577,578]

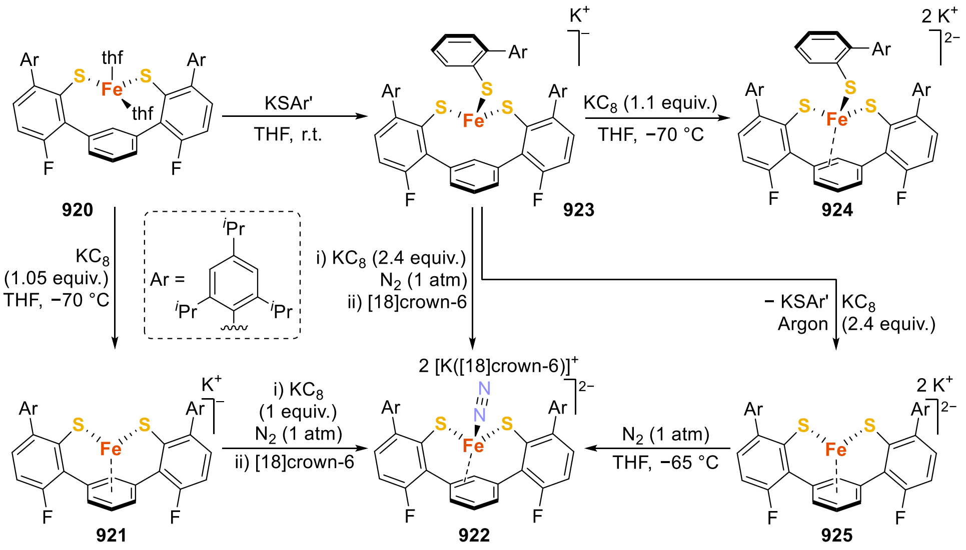

synthesized by reaction of precursor **920** with KSAr′ [Ar′ = −2-(Ar)-C_6H_4] (Scheme 126). The unsaturated, three-coordinate **923** was supported by reversible binding of a molecule of THF at low temperature. Reduction by 2.4 equiv of KC_8 under nitrogen yielded **922**, with production of free thiolate, confirming that Fe−S cleavage could facilitate N_2 binding to the low-valent iron sulfide complex.

The mechanistic details of these processes were expanded on in a subsequent report.[578] Reduction of **923** with stoichiometric KC_8 yields the corresponding iron(I) complex K_2[LFe(SAr′)] (**924**, Scheme 126), demonstrating that the Fe−S linkage remained intact at this level of reduction. Though crystallization attempts were unsuccessful, a combination of experimental evidence (Mössbauer, EPR, and EXAFS spectroscopy) and calculations indicated a high-spin (S = 3/2) iron(I) tris(thiolate) complex, with η^2-coordination to the arene. The complex exhibited limited thermal stability. While maintaining **924** at −70 °C, no loss of thiolate was observed by Mössbauer spectroscopy within 40 min. Upon warming to room temperature, however, features consistent with the presence of **921** were observed within 20 min.

In contrast to the intact Fe−S linkage retained in **924**, reduction of **923** by 2.4 equiv of KC_8 under argon resulted in the iron(0) complex K_2[LFe] (**925**), with loss of KSAr′. Thus, loss of the thiolate is triggered by reduction and does not occur only in the presence of N_2. Complex **925** could also be prepared directly from precursor **920** using excess KC_8.

In the solid-state, **925** was found to be structurally similar to **921**, with η^6-bonding to the central arene, albeit with longer Fe−S/Fe−C bond lengths consistent with a more reduced iron center. Thermal instability limited characterization of **925** beyond Mössbauer spectroscopy, which alongside DFT calculations was taken to indicate a high-spin (S = 1) iron(0) center. Exposure of **925** to N_2 resulted in the formation of **922**, as observed by Mössbauer spectroscopy. The change from η^6- to η^2-bonding to the central arene led the authors to suggest that N_2 binding competes with binding to the arene, a hypothesis supported by DFT calculations that indicated π-backbonding between the iron center and both ligands.

Mössbauer spectra of samples of **923** treated by 3.6 equiv of KC_8 under N_2 indicated the formation of a new, highly unstable species which was speculated to be a formal iron(−I) species, $K_3[LFeN_2]$ (**926**). Though not substantially characterized, treatment of **926** with BHT or H_2O produced substoichiometric amounts of ammonia and hydrazine. While attempts to catalytically perform N_2 reduction were unsuccessful, treatment of **923** with KC_8 and acid (50 equiv each) afforded substoichiometric amounts of NH_3, up to 0.41 equiv of NH_3 per Fe center using BHT as the proton source.

Hydride species have been invoked as possible intermediates in the intimate nitrogen fixation mechanism at FeMoco. A bridging hydride form of this cofactor was proposed, based on spectroscopic data.[579] Considering that transient hydride ligands bridging two or more iron centers might facilitate N_2 binding at an iron site of FeMoco, Peters and co-workers reported a series of diiron complexes with bridging hydride ligands. These included an anionic mixed valent Fe(II)/Fe(I) species which exhibited an impressive affinity toward N_2 binding.[580] The synthesis of the dinuclear complexes was enabled by the use of a bulky hexadentate ligand, $[SiP_2O]H_2$, reminiscent of the previously described siltrane scaffolds reported by the same group (section 2.3.3.2, *vide supra*).[142,143,431,432,490−492] The reaction of ligand $[SiP_2O]H_2$ (Scheme 127) with $FeBr_2$ (2 equiv) and sodium amalgam under a N_2 atmosphere afforded the bridging hydride complex

Scheme 127. Formation of a Mixed-Valent $Fe_2(\mu\text{-H})_2$ Anionic Species[580]

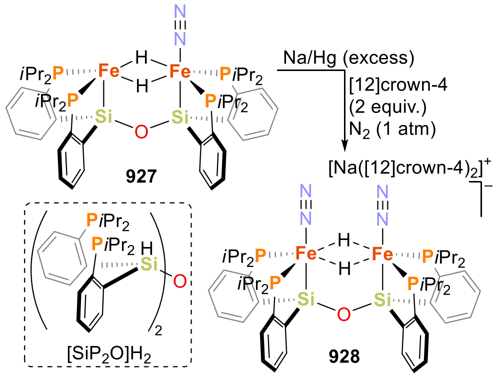

$[\{SiP_2O\}Fe_2(\mu\text{-}H)_2(N_2)]$ (**927**). Further reaction of **927** with sodium amalgam under a nitrogen atmosphere in the presence of a sequestering agent afforded the anionic complex $[Na([12]crown\text{-}4)_2][\{SiP_2O\}Fe_2(\mu\text{-}H)_2(N_2)_2]$ (**928**, see Scheme 127).

Solution magnetometry measurements indicated that **928** is an $S = 1/2$ species ($\mu_{eff} = 1.7\ \mu B$), whereas two coupled $\nu_{N\equiv N}$ vibrations (2023 and 1979 cm^{-1}) were observed by infrared spectroscopy. At room temperature, the N_2 ligands in **927** and **928** are not labile, as demonstrated by spectroscopic analysis after multiple freeze−pump−thaw cycles. The authors also proved that **927** coordinates another molecule of N_2 at −80 °C to afford the bis(dinitrogen) species $[\{SiP_2O\}Fe_2(\mu\text{-}H)_2(N_2)_2]$ (**929**), according to IR spectroscopy. However, the second N_2 ligand is easily lost in solution upon warming to room temperature, affording **927** again. Cyclic voltammetry and UV−vis measurements confirmed that the neutral bis(N_2) species is predominant in solution at low temperature, and exhibits a reversible reduction event (−2.04 V), assigned to the formation of the anionic complex **928**. Therefore, the chemical reduction of **927** is coupled to the coordination of the second N_2 molecule to form **928**. The authors attributed this observation to a much stronger binding affinity of N_2 (10^6-fold enhancement) to the reduced $Fe_2(\mu\text{-}H)_2$ core, according to a large equilibrium binding constant and thermodynamic data obtained through electrochemical analysis. Moreover, the electrochemical data suggests that **929** is an intermediate in the reduction of **927** to **928**, and that N_2 coordination precedes the electron transfer process. Both **927** and **928** reacted with acid and a reductant ($HBAr^F{}_4/KC_8$, 48 equiv each, −78 °C Et_2O), to give N_2 to NH_3 production in comparable amounts (1.4 ± 0.5 equiv NH_3 for **927**, 1.1 ± 0.2 equiv NH_3 for **928**), demonstrating the potential of these complexes as nitrogenase models.[580]

3.2.6. N_2 Activation and Functionalization by Metallatrane Metalates.

As described in section 2.3.3, Peters and co-workers developed metalates featuring a family of Sacconi-type P_3^E tetradentate ligands (Figure 20) (refs 141, 142, 428−430, 432, 553, 562, 581, and 582). Using this platform, the Peters group has extensively contributed to the field of nitrogen activation and functionalization.[27,583]

For instance, the reactivity of iron-coordinated dinitrogen ligands toward silyl halide reagents was evaluated.[428] By treating the *in situ* generated species $[(P_3^B)Fe(N_2)]^-$ (**720**) with trimethylsilyl chloride, the silyldiazenido complex $[(P_3^B)Fe(N{=}NSiMe_3)]$ (**930**) was obtained (Scheme 128), comparable to compound **874** (see Scheme 120a).[79] Further reduction of **930** with sodium amalgam afforded $[Na(thf)][(P_3^B)Fe(NNSiMe_3)]$ (**931**). Compound **931** can also be accessed by direct reduction of the Fe(I) precursor $[(P_3^B)FeBr]$ (**718**) in the presence of an excess of Me_3SiCl (Scheme 128, upper left).

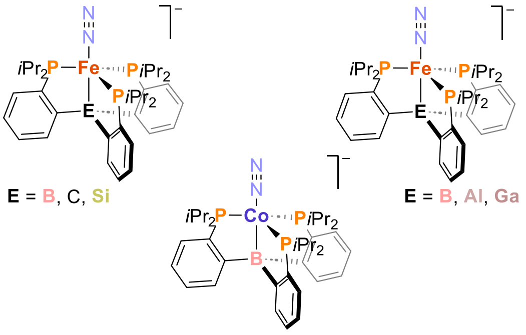

Figure 20. Anionic iron and cobalt complexes featuring P_3^E (E = B, C, Al, Si, Ga) tetradentate ligand scaffolds, of relevance in nitrogen activation, developed by Peters and co-workers.

Scheme 128. Reactivity of N_2 Bound Iron Metallaboratranes toward Silyl Chlorides by Peters and Co-workers[428]

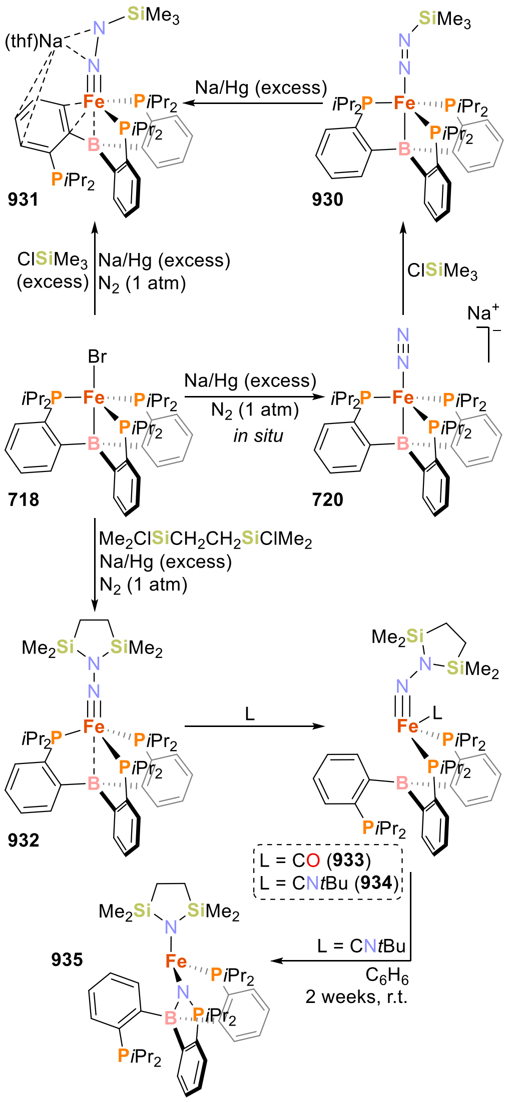

As with complexes **719**−**722** (*vide supra*), the P_3^B ligand acts as a flexible scaffold to stabilize different electronic environments,[141] adjusting Fe−B distance [d_{FeB}(**720**) = 2.293 Å vs d_{FeB}(**930**) = 2.435 Å vs d_{FeB}(**931**) = 2.319 Å] or the geometry at the metal center. This was further demonstrated by the reaction of **718** with sodium amalgam (excess) under nitrogen in the presence of 1,2-bis(chlorodimethylsilyl)ethane, which led to the disilylation of the bound N_2 ligand (Scheme 128, down left). The disilylhydrazido(2−) motif in the product **932** is coordinated to the metal center through an Fe≡N triple bond. A comparison of the Fe−N and N−N bond distances for complexes **720**, **930**−**932**′ (optimized structure of **932** described by the simplified model, **932**′, in which the *i*Pr groups were substituted by Me; see Figure 21) clearly illustrates the changes that occur at the dinitrogen ligand:

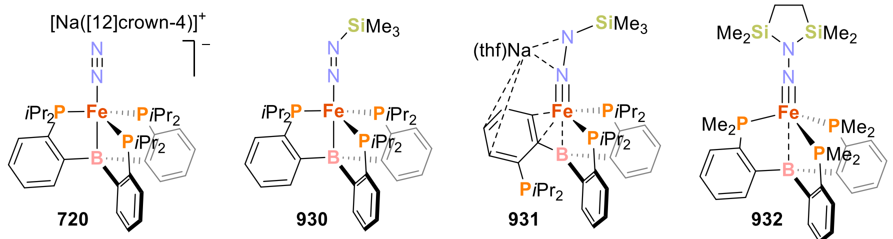

Bond lengths (Å):

	720	930	931	932
Fe-N =	1.776	1.696	1.673	1.629*
N-N =	1.149	1.225	1.260	1.349*

Figure 21. Fe−N and N−N bond distances in complexes **720**, **930**−**932**′ (* From geometry optimization at the B3LYP/6-31G(d) level).[428]

upon functionalization, the Fe−N bond distances shorten as the N−N lengths elongate.

Further treatment of **932** with donor ligands such as CO or *t*BuNC led to substitution of one of the phosphine arms of the P_3^B framework, yielding the Fe≡N compounds **933** (L = CO) and **934** (L = *t*BuNC) (Scheme 128). In solution, the isocyanide derivative **934** slowly decomposed to generate a phosphoraniminato/disilylamido iron(II) complex, **935**, resulting from N−N bond cleavage (Scheme 128, bottom).[428] The related anionic compound $[(P_3^C)Fe(N_2)]^-$ (**936**) also reacted with trimethylsilyl chloride to generate the diamagnetic diazenido complex $[(P_3^C)Fe(N_2SiMe_3)]$ (**937**), similar to **930**.[562]

The reactivity exhibited by the (P_3^B)Fe systems served as a basis to investigate the catalytic conversion of N_2 into NH_3.[430] At−78 °C, the addition of excess acid ($HBAr^F_4$) to the highly reduced compound $[Na([12]crown\text{-}4)_2][(P_3^B)Fe(N_2)]$ (**720**) afforded a mixture of compounds in which the main species identified were the ammonia complex $[(P_3^B)Fe(NH_3)]^+$ (**938**) (30−35% of the total Fe) and the unsaturated compound $[(P_3^B)Fe]^+$ (**725**, 40−45% of the total Fe). Reduction of such a mixture regenerated **720**. This behavior indicated that a cyclic protonation, followed by reduction, was possible in the frame of a nitrogen fixation system. After evaluating a variety of reductants and acids (e.g., $HBAr^F_4/KC_8$ or $[Ph_2NH_2]OTf/Cp^*_2Co$), the authors found that, under a nitrogen atmosphere, the sequential addition of an excess of $HBAr^F_4$ (48 equiv) to **720** followed by reductant (KC_8, 58 equiv, −78 °C, Et_2O) affords 7.0 equiv of NH_3 per Fe center (on average; see Scheme 129). A similar catalytic run using the cationic complex $[(P_3^B)Fe]BAr^F_4$ (**725**) yielded 6.2 equiv of NH_3 per Fe center. Other iron salts and molecular species were also evaluated, at best yielding only substoichiometric conversion of N_2 to NH_3. The terminally bonded species **938**, $[(P_3^B)Fe(N_2H_4)]^+$ (**939**), and $[(P_3^B)Fe(NH_2)]$ (**940**) were identified as potential intermediates.[429] Nevertheless, the authors did not exclude the possible involvement of species of higher nuclearity or, for example, iron nitride species in the catalytic pathway.[430]

Scheme 129. Catalytic Conversion of N_2 into NH_3 at Low-Valent (P_3^B)Fe Complexes[429,430]

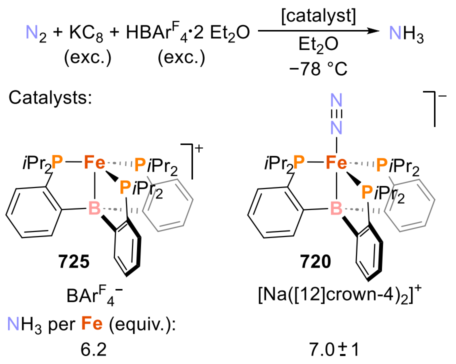

Scheme 130. Protonation of the Dinitrogen Ligand in the Anionic Compounds $[(P_3^B)Fe(N_2)]^-$ (720) and $[(P^{iPr}_3{}^{Si})Fe(N_2)]^-$ (738)[581,582]

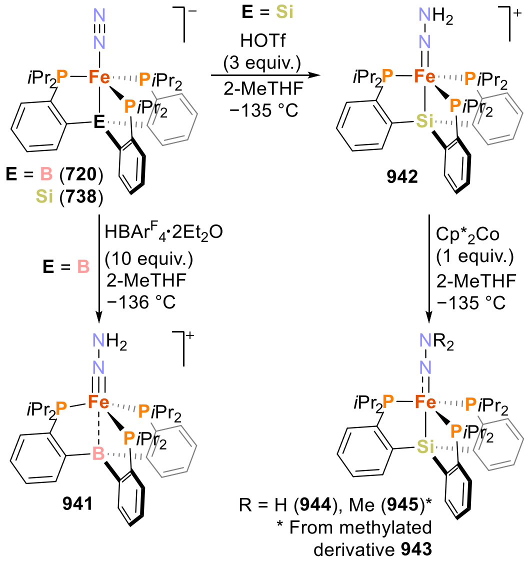

Protonation of the compounds $[(P_3^B)Fe(N_2)]^-$ (**720**) and $[(P^{iPr}_3{}^{Si})Fe(N_2)]^-$ (**738**) afforded the doubly protonated products $[(P_3^B)Fe{\equiv}N{-}NH_2]^+$ (**941**)[581] and $[(P^{iPr}_3{}^{Si})Fe{=}NNH_2]^+$ (**942**),[582] respectively, which were studied as potential intermediates in the iron-catalyzed reduction of dinitrogen (Scheme 130). The unstable hydrazido(2−) product $[(P_3^B)Fe{\equiv}N{-}NH_2]^+$ (**941**)[581] is reminiscent of compound **932**, featuring a disilylhydrazido(2−) motif (Scheme 128, *vide supra*).[428] Species **941** was detected after addition of an excess of acid ($HBAr^F_4$·$2Et_2O$, 10 equiv) to **720** at −136 °C in the absence of an exogenous reductant, and characterized by a combined experimental (EPR, ENDOR, EXAFS, ^{57}Fe Mössbauer spectroscopy) and theoretical analysis. The characterization strongly supports the presence of the Fe−N triple bond and the double protonation at the distal nitrogen atom. This indicates that the protonation occurs via a "Chatt-type" pathway. Compound **941**, however, was characterized in conditions (10 equiv $HBAr^F_4$, −136 °C, 2-MeTHF) that differ considerably from the catalytic nitrogen fixation system described in Scheme 129 (HBAr$^F_4$, KC$_8$, −78 °C, Et$_2$O).

To determine whether **941** could be detected in mixtures emulating the studied catalytic system (without exogenous reductant), EPR spectra of two solutions of **720**, at −136 °C in 2-MeTHF and at −78 °C in Et$_2$O, were recorded after addition of acid. Signals attributed to **941** were observed in both mixtures. Upon warming (−40 °C), **941** transforms into different species, including the ammonia-coordinated complex $[(P_3^B)Fe(NH_3)]^+$ (**938**), even in the absence of a reductant.[429] This suggests that a double protonation of the distal nitrogen atom, to produce **941** or a related species, is viable and likely involved in the catalytic nitrogen fixation promoted by $[(P_3^B)Fe(N_2)]^-$ (**720**).[581] Theoretical calculations (DFT) on the mechanism of protonation of **720** indicated that, although the protonation of the anionic complex can occur via many possible reaction pathways, the favored path seems to involve a triple proton transfer to the distal nitrogen atom, forming one ammonia molecule and an iron nitrido complex.[584]

Despite the evidence of the possible role of **941**, due to its instability, it was not possible to perform crystallographic analysis or further reactivity studies on this complex. Thus, the isostructural compound $[(P^{iPr}{}_3{}^{Si})Fe{=}NNH_2]^+$ (**942**), formed by protonation of $[(P^{iPr}{}_3{}^{Si})Fe(N_2)]^-$ (**738**) at −135 °C, was crystallographically characterized.[582] The more stable methylated complex $[(P^{iPr}{}_3{}^{Si})Fe{=}NNMe_2]^+$ (**943**) was formed by the reaction of **738** with MeOTf. Moreover, the transformation of **942** to NH$_3$ via an Fe-NH$_2$NH$_2$$^+$ intermediate was demonstrated. One-electron reduction of the cationic complexes afforded the neutral compounds $[(P^{iPr}{}_3{}^{Si})Fe{=}NNR_2]$ [R = H (**944**), Me (**945**)]. Thawing of solutions containing both **942** and **944** resulted in disproportionation to generate $[(P^{iPr}{}_3{}^{Si})Fe\text{-}NH_2NH_2]^+$ (**946**), along with the neutral $[(P^{iPr}{}_3{}^{Si})Fe(N_2)]$ (**947**) and the ammonia complex $[(P^{iPr}{}_3{}^{Si})Fe(NH_3)]^+$ (**948**), consistent with previous observations of liberation of ammonia from **942**.[142,432] These mechanistically relevant observations indicate that the protonation of a coordinated N$_2$ ligand in these systems can proceed via a distal intermediate that undergoes reduction/disproportionation to afford intermediates such as **946**, which eventually serves as a source of NH$_3$ by late-stage N−N cleavage.[582]

Increasing the amount of acid and reductant in the reaction catalyzed by $[(P_3^B)Fe(N_2)]^-$ (**720**; Scheme 129) led to a substantial increase in the quantity of ammonia produced.[585,586] The formation of up to 64 equiv of ammonia per Fe center was observed by increasing the amount of HBAr$^F_4$ and KC$_8$ to 1500 and 1800 equiv, respectively. Under the same conditions, the analogous complexes $[K(Et_2O)_{0.5}]$-$[(P_3^C)Fe(N_2)]$ (**936**) and $[Na([12]crown\text{-}4)_2][(P^{iPr}{}_3{}^{Si})Fe(N_2)]$ (**738**) afforded 47 and 4.4 equiv of ammonia, respectively (per Fe equiv).[586] Moreover, using the increased amounts of acid and reductant, and by subjecting the reaction to mercury lamp irradiation, the efficiency of the catalysis by **720** was further increased, generating up to 94 equiv of ammonia (88.1 ± 8.0 equiv NH$_3$/Fe equiv).[585] The related complex $[(C^{Si}P^{Ph}{}_3)Fe(N_2)]^-$ (**949**, $C^{Si}P^{Ph}{}_3$ = $(Ph_2PCH_2SiMe_2)_3CH$) yielded only insignificant amounts of NH$_3$ upon treatment with acid and reductant ($[H(Et_2O)_2]$-$[BAr^F_4]$ and KC$_8$).[562,587]

The role of the hydride/borohydride complex $[(P_3^B)(\mu\text{-}H)Fe(N_2)(H)]$ (**950**), in the catalytic N$_2$-to-NH$_3$ system by $[(P_3^B)Fe(N_2)]^-$ (**720**),[430,588] was also investigated in detail.[586] **950** can be synthetically converted to the anionic complex **720** upon reaction with HBAr$^F_4$ and KC$_8$, and is a competent catalyst in the reduction of N$_2$. Mechanistic evidence suggests that compound **950** is an off-cycle resting state of the overall catalysis, and that it can be converted to the catalytically active **720**, reentering the catalytic cycle.[586] Moreover, NMR monitoring of a reaction performed under photolytic conditions with the hydride/borohydride complex $[(P_3^B)(\mu\text{-}H)Fe(N_2)(H)]$ (**950**, −78 °C) led to the identification of the neutral $[(P_3^B)Fe(N_2)]$ (**719**) and the hydrido complex $[(P_3^B)(\mu\text{-}H)Fe(H_2)(H)]$ (**951**). This observation was attributed to a transformation involving reductive elimination of H$_2$ from **950** affording **719**, which might regenerate **720** under irradiation.[585]

Peters and co-workers proved that protonation of a highly reduced Fe−N$_2$ complex leads to the formation of a neutral Fe(NNH$_2$) hydrazido(2−) intermediate, which can be protonated in turn to promote the heterolytic cleavage of the N−N bond, forming an iron nitride species and releasing ammonia.[486] The protonation of the 18-valence-electron dianionic complex $[(P_3^B)Fe(N_2)]^{2-}$ (**723**), freshly prepared *in situ* from the anionic **720**, was studied (Scheme 131).

Scheme 131. Sequential Protonation of the Dianionic Complex $[(P_3^B)Fe(N_2)]^{2-}$ (723) Leading to a Terminal Fe(IV) Nitride and Ammonia[486]

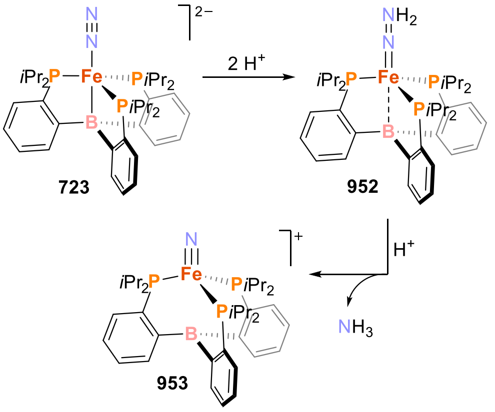

Compound **723** reacted with an excess of either triflic acid or HBAr$^F_4$ in supercooled 2-MeTHF (91−137 K) within 15 min to afford the neutral hydrazido compound $[(P_3^B)Fe{=}N{=}NH_2]$ (**952**, $S = 0$), according to ^{57}Fe Mössbauer spectroscopy. Reactions of **723** with either acid for prolonged periods of time afforded another product, in approximately 50% yield (HOTf), displaying the characteristic parameters of Fe(IV) nitrides in C_3 symmetry in the ^{57}Fe Mössbauer spectrum. The latter product was assigned to be complex $[(P_3^B)Fe{\equiv}N]^+$ (**953**, Scheme 131). It was proposed that the formation of the Fe(IV)-nitride from **723** proceeds by rapid protonation at low temperature, to yield the hydrazido complex **952** via a diazenido $[(P_3^B)Fe(N_2H)]^-$ species. Further protonation of **952**, via an unobserved transient hydrazidium cationic species $[(P_3^B)Fe(NNH_3)]^+$, resulted in heterolytic N−N bond rupture leading to the nitride complex **953** with release of ammonia. In a larger-scale experiment, protonation of complex **723** with HOTf in supercooled 2-MeTHF afforded NH$_3$ in 36.0(5)% isolated yield.

Moreover, the authors proved that it is possible to double the isolated yield to 73(17)% by the sequential reaction of **723** with HOTf and Cp*$_2$Co in supercooled 2-MeTHF. Therefore, the simultaneous use of the two reductants, KC_8 and Cp^*_2Co, can drive the catalytic N_2 fixation in this system. However, the dianionic complex **723** is only accessible by treatment with the stronger reductant KC_8, since Cp^*_2Co alone is only sufficiently strong to produce $[(P_3^B)Fe(N_2)]^-$ (**720**).[589]

From complex **723** to the nitride compound **953**, a range of six formal oxidation states of iron are observed, from Fe(−II) (d^{10}) to Fe(IV) (d^4). It should be noted that the assignment of these formal oxidation states may not account for the effect of the Z-type ligand (Fe-to-B σ-backbonding) or the additional metal-to-phosphine π-backbonding.[486] In fact, the experimental and calculated pre-edge transitions in the XANES spectrum of the dianionic complex **723** indicate that its physical oxidation state must involve a d^n configuration of $n < 10$. Therefore, the $(P_3^B)Fe$ unit donates electron density into the covalent Fe−B/P backbonding interactions, modulating the oxidation state of the metal center until the electrons are transferred to the N−N moiety upon protonation.

The electronic structure of the series of complexes $[(P_3^B)Fe(N_2)]^n$ [n = 0 (**719**), 1− (**720**), 2− (**723**)] was investigated using DFT calculations by Vyas, Grover and coworkers.[590] The theoretical study examined model systems of the complexes, featuring a simplified ligand (tris-[(dimethylphosphino)phenyl]borane, $P_3^{B'}$). The variation in the oxidation states of the iron center was attributed to the flexible coordination environment provided by the P_3^B ligand. The Fe−B interaction can, therefore, function as a reservoir of electron density to support and modulate the various oxidation states. These changes were found to be crucial in the system of nitrogen activation. Moreover, calculated optimized structures of the complexes indicated that complex $[(P_3^B)Fe(N_2)]^{2-}$ (**723**) corresponds to the species of lowest energy. As reduction of the iron center takes place, the calculated Fe−B bond distances elongate in the series of complexes $[(P_3^B)Fe(N_2)]^n$ (n = 0: 2.280 Å, n = 1−: 2.345 Å, and n = 2−: 2.369 Å), and the Fe−N bond distances shorten (n = 0: 1.973 Å, n = 1−: 1.807 Å, and n = 2−: 1.779 Å), due to increased π-backbonding from the metal center to the dinitrogen ligand. The HOMO−LUMO gap was found to be of 4.43, 3.59 and 2.76 eV for the series $[(P_3^B)Fe(N_2)]^n$ (n = 0, 1−, 2−), respectively, indicating that the dianionic complex $[(P_3^B)Fe(N_2)]^{2-}$ (**723**) will be the more reactive species. Consequently, the theoretical analysis of the bonding situation corroborates the experimental evidence, suggesting that the nitrogen activation process is more viable at the more reduced iron center.

A comparison of $(P_3^E)Fe$ (E = B, C, Si) revealed that the (P_3^B)-supported system is the most catalytically active for the N_2-to-NH_3 reaction in the presence of external proton and electron sources under all the conditions evaluated.[430,432,562,585,586] To further investigate this matter, a structure-to-function study was carried out aiming to determine the effect of the apical Lewis acidic atom, including additional dinitrogen−iron compounds featuring the tetradentate P_3^E ligands (E = B, Al, Ga).[591] Similar to the synthesis of $[(P_3^B)Fe(N_2)]^n$ [n = 0 (**719**), 1− (**720**)] (Scheme 86, *vide supra*), the series of complexes $[(P_3^E)Fe(N_2)]^n$ [$P_3^E = P_3^{Al}$: n = 0 (**954**), 1− (**955**) or $P_3^E = P_3^{Ga}$: n = 0 (**956**), 1− (**957**)] was obtained. Their bonding is best described as featuring a dative Fe→E(III) interaction, with a comparable degree of activation of the coordinated N_2 ligands in each set of complexes, $[(P_3^E)Fe(N_2)]$ or $[(P_3^E)Fe(N_2)]^-$. Their electronic structures and the flexibility of the Fe−E bonds are also similar, and the anionic complexes feature Fe(−I) centers as a result of iron-based reduction events. Therefore, the anionic complexes **955** and **957** were also tested for the catalytic N_2-to-NH_3 reaction under previously optimized conditions, using excess $HBAr^F_4$/KC_8 or $[Ph_2NH_2]OTf/Cp^*_2Co$ (−78 °C, Et_2O). Using the combination $HBAr^F_4/KC_8$, the catalysts **955** and **957** afforded only 2.5 ± 0.1 (17 ± 1% yield NH_3/H^+) and 2.7 ± 0.2 (17 ± 1% yield NH_3/H^+) equivalents of NH_3 per Fe center, respectively. With the combination $[Ph_2NH_2]OTf/Cp^*_2Co$, the efficiency of the reaction improved (**955**: 4.1 ± 0.9 equiv of NH_3 per Fe; **957**: 3.6 ± 0.3 equiv of NH_3 per Fe). Nonetheless, none of these systems was as efficient as the one catalyzed by $[(P_3^B)Fe(N_2)]^-$ (**720**). Individual monitoring of the reactions between the anionic complexes **955** and **957** and lower stoichiometries of acid and reductant (10 and 12 equiv, respectively) indicated that the catalysts are rather robust under these conditions and, consequently, their significantly lower activity in the reduction of N_2 cannot be attributed to decomposition. Complexes **955** and **957** were found to be more selective toward the hydrogen evolution reaction, and might be susceptible to the formation of hydride species similar to $[(P_3^B)(\mu\text{-}H)Fe(N_2)(H)]$ (**950**), explaining the lower efficiency of the catalysis.

Related $(P_3^B)Co$ complexes are also active in nitrogen fixation.[553] Reduction of the cobalt compound $[(P_3^B)Co(N_2)]$ (**958**)[528] with sodium naphthalenide ($NaC_{10}H_8$), followed by addition of [12]crown-4, afforded the diamagnetic anionic complex $[Na([12]crown\text{-}4)_2][(P_3^B)Co(N_2)]$ (**959**, Scheme 132a). The dinitrogen ligand becomes significantly more activated upon reduction, as evidenced by the red-shift in the stretching vibrations in the FT-IR spectrum [$\nu_{N\equiv N}$(**958**) = 2089 cm^{-1} vs $\nu_{N\equiv N}$(**959**) = 1978 cm^{-1}, see Table 2].[528,553] Treatment of **959** with an excess of $HBAr^F_4/KC_8$ (48 equiv $HBAr^F_4$, 58 equiv KC_8, −78 °C, Et_2O) generates 2.4 ± 0.3 equiv of NH_3/Co (Scheme 132b). The analogous iron complex $[(P_3^B)Fe(N_2)]^-$ (**720**) is more active than the cobalt

Scheme 132. (a) Synthesis of the Anionic Complex $[(P_3^B)Co(N_2)]^-$ (959) and (b) N_2-to-NH_3 Conversion Mediated by Anionic Iron or Cobalt Complexes[430,553]

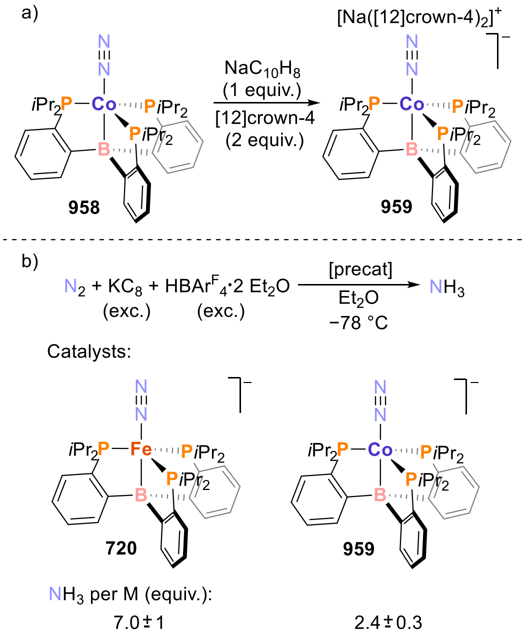

analogue by a 3-fold ratio (Scheme 132b).[430] In the absence of either acid or reductant, no formation of NH_3 was observed. Various neutral cobalt complexes were evaluated for this reaction under the same conditions, yielding substoichiometric amounts of ammonia in the best case. Apart from complex **959**, only the oxidized product $[(P_3^B)Co]BAr^F_4$ (**960**) mediated the N_2-to-NH_3 conversion in superstoichiometric yields (1.6 ± 0.2 equiv of NH_3/Co), albeit less effectively than **959**.

The divergent activity of the $(P_3^B)Fe$ and $(P_3^B)Co$ complexes were rationalized by performing a structure-to-function analysis. While *a priori* the degree of activation of the dinitrogen ligand at the metal center seems to correlate well with the better performance of the iron complex in the reaction [$\nu_{N\equiv N}$(**720**) = 1905 cm^{-1} vs $\nu_{N\equiv N}$(**959**) = 1978 cm^{-1}], other complexes with an apparent higher degree of activation (e.g., $[Na([12]crown\text{-}4)_2][(P^{iPr}{}_3{}^{Si})Fe(N_2)]$ (**738**), $\nu_{N\equiv N}$ = 1920 cm^{-1})[432] gave lower N_2-to-NH_3 conversion (0.8 ± 0.4 equiv/Fe). Instead, the flexibility of the M−E bond *trans* to the M−N_2 moiety seems to be a crucial factor in explaining why certain complexes appear to be particularly active N_2 reduction catalysts. Moreover, the results seem to indicate that the anionic charge in metalate complexes results in a higher basicity of the N_2 ligand, which, together with the flexibility of the M−E bond, favors the production of ammonia from N_2.[553]

In related work, Lu and co-workers showed that reduction of the complexes $[(N_2)MAl\{N[o\text{-}(NCH_2PiPr_2)C_6H_4]_3\}]$ {M = Fe [**760**(N_2)], Co [**761**(N_2)]} (see section 2.3.3.3) with KC_8 affords anionic complexes $[K(L)][(N_2)MAl\{N[o\text{-}(NCH_2PiPr_2)C_6H_4]_3\}]$ (M = Fe, L = [18]crown-6 [**961**(N_2)]; M = Co, L = [2.2.2]cryptand [**962**(N_2)], Scheme 133a).[433,434] In the solid state, the iron complex **760**(N_2) is in equilibrium between the end-on species and a N_2-bridged dimer [{**760**}$_2$(μ-N_2)] (*vide supra*). For the latter, the bridging N_2 ligand was activated to some extent, as reflected by the slightly elongated N−N bond distance [1.107(4) Å].[433,434] Reduction of the zerovalent complexes **760**(N_2) and **761**(N_2) further activates the coordinated dinitrogen ligand in **961**(N_2) and **962**(N_2), formally in the negative oxidation state M(−I).[434]

Scheme 133. (a) Chemical Reduction of $[(N_2)MAl\{N[o\text{-}(NCH_2PiPr_2)C_6H_4]_3\}]$ {M = Fe [760(N_2)], Co [761(N_2)]} and (b) Functionalization of Coordinated N_2 at the Fe(−I) Complex 961(N_2)

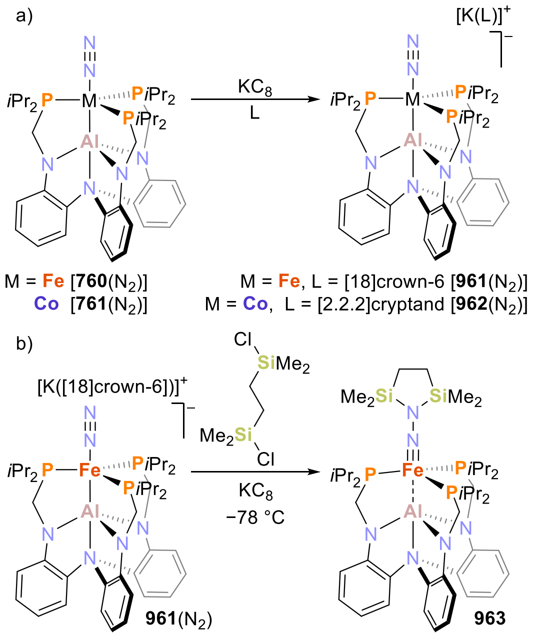

An alternative preparation of these complexes consists of treating $FeBr_2$ or $CoBr_2$, with metalloligand AltraPhos and 3 equiv of KC_8, as opposed to the 2 equiv used for the synthesis of the zerovalent compounds (see Scheme 92, above). FT-IR characterization revealed, after reduction, a decrease in the $\nu_{N\equiv N}$ stretching frequencies (on average 85 cm^{-1}, see Table 2). In accordance with this, the d_{NN} bond distances measured for both complexes [d_{NN}(**961**) = 1.135(4) Å vs d_{NN}(**962**) = 1.116(8) Å] are longer in the anionic complexes (*cf.* d[{**760**}$_2$(μ-N_2)] = 1.107(4) Å vs d_{NN} = 1.0975 Å in free N_2). Further evidence of the higher degree of activation of the N_2 ligand at Fe(−I) was obtained by reactions of **961**(N_2) or **962**(N_2) with 1,2-bis(chlorodimethylsilyl)ethane. At room temperature, **962**(N_2) furnished the neutral **761**(N_2), while the reaction at −78 °C resulted in an intractable mixture. By contrast, the reaction of **961**(N_2) with 1,2-bis(chlorodimethylsilyl)ethane afforded a disilylhydrazido(2−) complex $[\{N_2(SiMe_2CH_2)_2\}FeAl\{N[o\text{-}(NCH_2PiPr_2)C_6H_4]_3\}]$ (**963**, Scheme 133b) (c.f. complex **932**, Scheme 128b).[428]

The same group described a bimetallic iron−tin complex which catalyzes the conversion of N_2 into NH_3.[592] One- and two-electron reductions of the previously reported Fe(II) complex $[BrFeSn\{N[o\text{-}(NCH_2PiPr_2)C_6H_4]_3\}]$[593] (**964**) by either 1.1 or 2.2 equiv of KC_8 under a nitrogen atmosphere afforded the neutral, $[(N_2)FeSn\{N[o\text{-}(NCH_2PiPr_2)C_6H_4]_3\}]$ (**965**) and doubly reduced complex $[\{(thf)_3K\}(N_2)FeSn\{N[o\text{-}(NCH_2PiPr_2)C_6H_4]_3\}]$ (**966**), respectively. The increased electron density in **966** with respect to **965** is reflected by the red-shift of the stretching bands of their dinitrogen ligands (1944 cm^{-1} for [K([2.2.2]cryptand)][**966**] vs 2011 cm^{-1} for **965**).

The valency of complexes **964**−**966** was described using an adapted Feltham−Enemark notation,[489] given that assigning individual oxidation states for both metals can be complicated by the presence of an intermetal covalent bond. Therefore, **964**, **965**, and **966** were assigned electronic configurations of $\{FeSn\}^8$, $\{FeSn\}^9$, and $\{FeSn\}^{10}$, respectively. The reaction of **966** with a slight excess of Me_3SiCl allowed isolation and structural characterization of the diazenido complex $[(Me_3SiN_2)FeSn\{N[o\text{-}(NCH_2PiPr_2)C_6H_4]_3\}]$ (**967**, Scheme 134a). A comparison of the Fe−N and N−N bond lengths for the triad of complexes **965**−**967** shows progressive elongation of the N−N bonds (1.112(2) Å in **965**, 1.143(6) Å in **966**, 1.182(3) Å in **967**) and contraction of the Fe−N bonds (1.7933(14) Å in **965**, 1.762(5) Å in **966**, 1.686(2) Å in **967**). The structural analysis of **967** indicates that the Me_3SiN_2 unit is between the two possible resonance forms for a diazenido ligand: bent diazenido and diazenium ligand.

It remained unclear, after analysis by ^{57}Fe Mössbauer spectroscopy, whether the electron configuration of **967** should be described as an $\{FeSn\}^{10}$ unit engaged in π-backbonding with a silyldiazenium(1+) ligand or as an $\{FeSn\}^8$ unit acting as π-donor to a diazenido(2−) ligand. Quantum chemical calculations (DFT) indicated a strong correlation between the charge on the Sn center (atom trans to the N_2 unit) and both the polarization of the N_2 unit and the charge on the distal N atom.

Scheme 134. N_2 Functionalization and Catalytic N_2 to NH_3 Reduction at Iron−Tin Complexes[592]

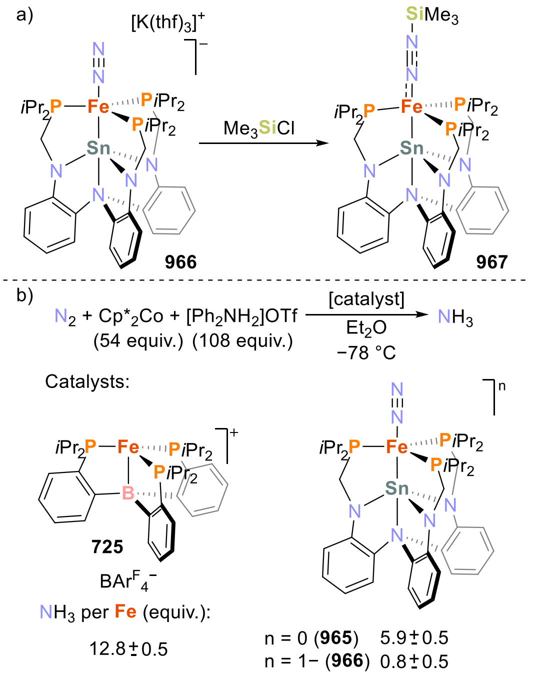

Complexes **965**−**967** were evaluated in the catalytic N_2 to NH_3 reduction reaction, using $[Ph_2NH_2]OTf$ (108 equiv) as the acid and Cp^*_2Co (54 equiv) as a reductant (1 atm N_2, Et_2O, −78 °C, 3 h). Under these conditions (see Scheme 134b), while the neutral complex **965** generated 5.9(5) turnovers of NH_3 (33% yield), its catalytic performance did not match that of Peters' cationic complex $[(P_3^B)Fe]BAr^F_4$ (**725**),[429] which afforded 12.8 turnovers of NH_3 (72% yield). The anionic complex **966** afforded only substoichiometric amounts of NH_3 (0.8(5) turnovers of NH_3, 5% yield) as a precatalyst, attributed to its low solubility in Et_2O. The diazenido complex **967** matched the catalytic performance of **965** (4.6(2) turnovers of NH_3, 26% yield), within the experimental error. **967** was also tested as catalyst in the silylation of N_2 with Me_3SiCl and KC_8, given that diazenido complexes have been proposed as intermediates in such reactions. However, only 1.2 equiv of $N(SiMe_3)_3$ were afforded under the studied conditions.

Similarly, a series of anionic cobalt-dinitrogen complexes $[(N_2)CoV\{N[o\text{-}(NCH_2PiPr_2)C_6H_4]_3\}]^-$ [**968**(N_2)], $(N_2)CoCr\{N[o\text{-}(NCH_2PiPr_2)C_6H_4]_3\}]^-$ [**969**(N_2)] and $[(N_2)Co_2\{N[o\text{-}(NCH_2PiPr_2)C_6H_4]_3\}]^-$ [**970**(N_2)], featuring V, Cr, or Co-based metalloligands were later reported.[496,498,554,594] Figure 22 shows the structures of these heterobimetallic cobalt complexes, and the N−N bond distances obtained from crystallographic analyses. The dinitrogen molecule is slightly less activated in the dicobalt and CoAl complexes, **970**(N_2) and **962**(N_2), than in the analogues **968**(N_2) and **969**(N_2). These distances are consistent with the values observed for the N_2 stretching vibration by infrared spectroscopy (see Table 2) and, in general, indicate weakly activated N_2 units.[434,496,554] Furthermore, across this series of heterobimetallic cobalt complexes DFT calculations indicated that the N_2 π^* molecular orbitals are energetically inaccessible, which is consistent both with the crystallographic parameters and the trends in the FT-IR spectra. In addition, the theoretical analysis indicated that the electronic structures of the anionic CoV, CoCr (and the hypothetical CoTi species, which was not isolated) are approximately similar to that of the CoAl complex $[(N_2)CoAl\{N[o\text{-}(NCH_2PiPr_2)C_6H_4]_3\}]^-$ [**962**(N_2), Scheme 133a, *vide supra*],[434] i.e., d^{10} Co(−I) centers bound to M(III) supporting metals.[496] In contrast, complex **970**(N_2), featuring a late transition metal support, consists of a Co(0) center binding to a Co(II) atom.[554]

The dicobalt complex $[(N_2)Co_2\{N[o\text{-}(NCH_2PiPr_2)\text{-}C_6H_4]_3\}]^-$ [**970**(N_2)] is stable under vacuum.[554] Consequently, this complex and its neutral analogue $[(N_2)Co_2\{N[o\text{-}(NCH_2PiPr_2)C_6H_4]_3\}]$ (**971**) were evaluated in the catalytic silylation of N_2. Using **971** as a precatalyst (0.05 mol %) in the presence of a large excess of Me_3SiCl and KC_8 under an atmosphere of N_2 (r.t., 12 h, THF), $N(SiMe_3)_3$ was obtained in 30% yield, with a TON of 195 ± 25 (Scheme 135). The anionic complex **970**(N_2) was equally efficient (27% yield, TON = 178 ± 37), on average. The performance of other cobalt species such as $[\mathbf{761}(N_2)]$[433] was comparatively poor.

Only the mixture of $CoCl_2$ (2 equiv) with the heptadentate ligand $N[o\text{-}(HNCH_2PiPr_2)C_6H_4]_3$ reproduced the catalytic activity of **971**/**970** (N_2) (25% yield, TON = 172 ± 16). Catalyst performance was practically unaffected by the presence of additives such as PMe_3 or *t*BuNC. This, among other mechanistic tests, indicated that a homogeneous species was responsible for the catalysis. According to the proposed mechanism, the reaction occurs only at the Co(0) atom. Nonetheless, DFT calculations revealed that the Co−Co interaction is weakened substantially upon coordination of the N_2 molecule and broken during the subsequent silylation step. Importantly, the Co(0)−Co(II) interaction reforms with the release of trisilylhydrazide. The hemilabile nature of the metal−metal interaction thus appears to be a critical factor influencing the catalysis.

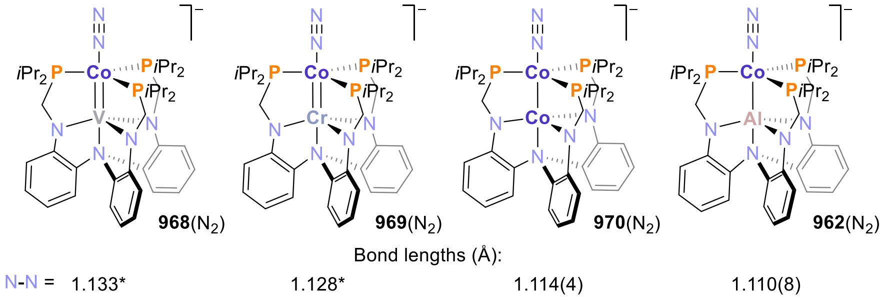

Figure 22. Heterobimetallic cobalt complexes featuring V, Cr, Co, and Al metalloligands, $M\{N[o\text{-}(NCH_2PiPr_2)C_6H_4]_3\}$. N−N bond distances are shown for comparison. *Average values for two crystallographically independent molecules.[434,496,554]

Scheme 135. Catalytic Silylation of N_2 Using Complexes $[(N_2)Co_2\{N[o\text{-}(NCH_2P\mathit{i}Pr_2)C_6H_4]_3\}]^{0/-}$[554]

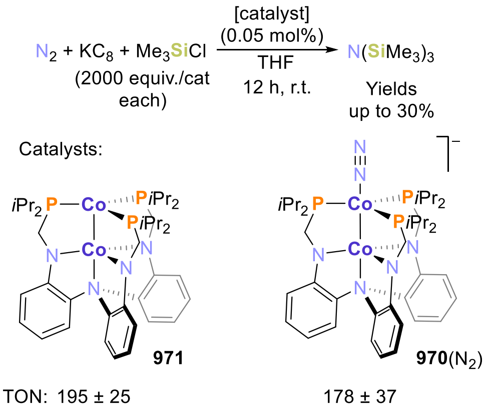

Very recently, Fang, Cui, and co-workers reported a series of Co(−I)−N_2 complexes supported by rare-earth metals via Co→RE (RE = rare-earth metal) interactions, and their activity in catalytic silylation of N_2.[595] Reduction of the Co(I) complexes $[\{N[CH_2-o\text{-}(NCH_2PPh_2)C_6H_4]_3\}RECoI]$ [RE = Sc (**972**), Lu (**973**), Yb (**974**), Y (**975**), Gd (**976**)] with $KHBEt_3$ (3 equiv) in the presence of crown ether afforded the anionic dinitrogen adducts $[K([18]crown\text{-}6)(THF)_x][\{N\text{-}[CH_2-o\text{-}(NCH_2PPh_2)C_6H_4]_3\}RECo(N_2)]$ [RE = Sc (**977**), Lu (**978**), Yb (**979**), Y (**980**), Gd (**981**); see Scheme 136a]. The analogous Co(I) and Co(−I) complexes lacking a supporting rare-earth metal center, $[\{N[CH_2-o\text{-}(NHCH_2PPh_2)C_6H_4]_3\}CoI]$ (**982**) and $[Na([12]crown\text{-}4)_2]\text{-}[\{N[CH_2-o\text{-}(NHCH_2PPh_2)C_6H_4]_3\}Co(N_2)]$ (**983**), were also synthesized (Scheme 136a).

The characterization of the C_3-symmetric complexes **977**−**981** and computational calculations support Co→RE dative bonds in all cases, as well as weakly activated dinitrogen ligands ($\nu_{N\equiv N}$ = 2044−2026 cm^{-1}). This might be the result of an interplay between a reduced Lewis acidity of the supporting RE(III) metal and the less electron-donating diphenyl phosphine groups, compared to the alkyl substituted phosphines in Lu's heptadentate ligand.[434,496,554] Nonetheless, a correlation between the degree of activation of the dinitrogen ligand and the p*K*a values of the aqueous $[RE(OH_2)_6]^{3+}$ ions showed that more Lewis acidic RE(III) ions in the ligand are associated with less activated N_2 ligands in the Co(−I)−N_2 complexes. Accordingly, **981**, stabilized by the least Lewis acidic Gd(III) ion, induced the strongest activation of the coordinated N_2 unit. The marked effect exerted by the RE(III) supporting metal is also evident upon comparison of the $\nu_{N\equiv N}$ stretching bands of **977**−**981** with that of the unsupported complex **983**, which features a more activated N_2 ligand ($\nu_{N\equiv N}$ = 1969 cm^{-1}).

The anionic complexes **977**−**981**, as well as the mononuclear Co(I) compound **982**, were tested in the catalytic silylation of N_2 in the presence of KC_8 and Me_3SiCl (THF, 25 °C, 4 days; Scheme 136b). All the complexes were active for this reaction, with the CoLu compound **978** exhibiting the best catalytic performance within the tested compounds (24% yield, TON = 16). Moreover, the supporting RE(III) ions were found to be crucial to promoting catalytic turnovers: whereas complexes **977**−**981** catalyzed the reaction with TONs in the range of 3 to 16, and yields of $N(SiMe_3)_3$ up to 24%, the unsupported Co(I) complex **982** performed poorly under the same conditions, affording only 2% yield of product, with a TON of 1.3. The anionic compound **983** was not tested due to its instability in solution. Therefore, the authors proposed that the supporting RE(III) ions play an additional role in the stabilization of the highly reduced Co(−I) centers, and possibly in other catalytically relevant intermediates, as well as in maintaining the geometry and rigidity of the species involved in the catalysis.[595]

Scheme 136. (a) Synthesis of Co(−I)-RE(III) and Unsupported Co(−I) N_2-Adducts and (b) Catalytic Silylation of N_2 Using the Synthesized Complexes[595]

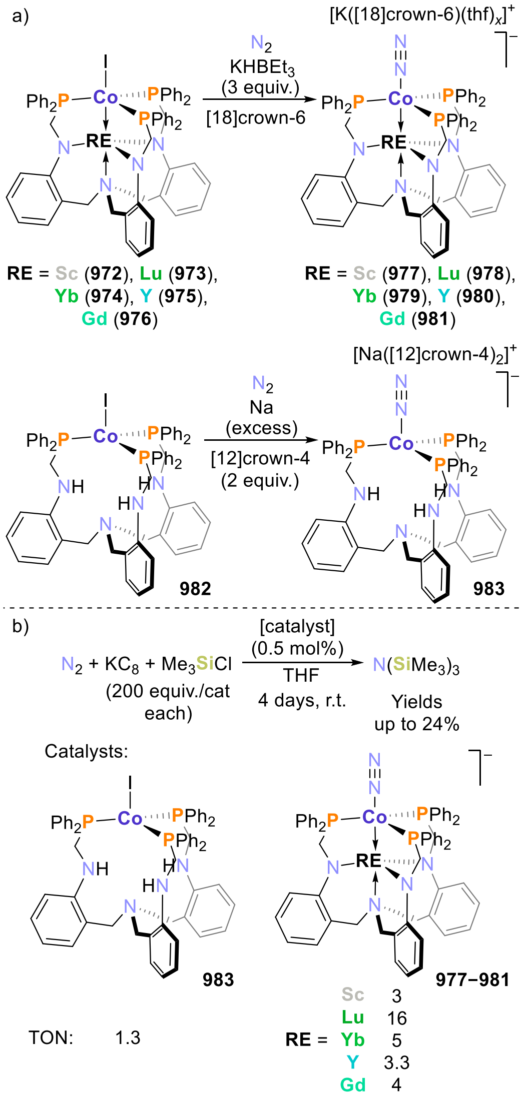

Peters and co-workers demonstrated that the isostructural ruthenium and osmium silatrane complexes $[K(thf)_x][(P^{iPr}{}_3{}^{Si})\text{-}M(N_2)]$ [M = Ru (**747**), Os (**748**); section 2.3.3.2, *vide supra*] are competent catalysts for the N_2-to-NH_3 conversion (Scheme 137).[491] FT-IR characterization of **747** and **748** revealed that these compounds feature significantly activated N_2 ligands [$\nu_{N\equiv N}$(**747**) = 1960 cm^{-1}, $\nu_{N\equiv N}$(**748**) = 1931 cm^{-1}]. Consequently, N_2-to-NH_3 conversion was studied under conditions similar to those used with related iron systems such as $[(P^{iPr}{}_3{}^{Si})Fe(N_2)]^-$ (**738**) or $[(P_3{}^B)Fe(N_2)]^-$ (**720**) (46 equiv $HBAr^F{}_4$, 50 equiv KC_8, 1 atm, −78 °C, Et_2O).[430,432] Using complexes **747** and **748** the reaction

Scheme 137. (a) N_2-to-NH_3 Conversion Reactions by Group 8 M-Silatrane Complexes and (b) Protonation Reactions of $[(P^{iPr}{}_3{}^{Si})Os(N_2)]^-$ (748)[491]

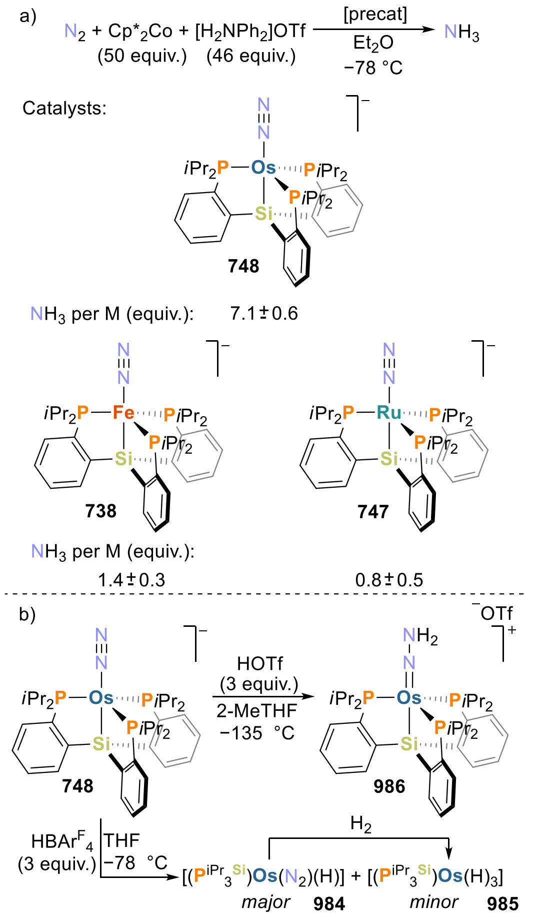

afforded 4.3 ± 0.3 equiv and 1.6 ± 0.3 equiv of NH_3 per metal complex, respectively.

With the milder reagents $[H_2NPh_2]OTf$ (46 equiv) as the acid source and $Cp^*{}_2Co$ (50 equiv) as the reductant in Et_2O at −78 °C, the ruthenium complex **747** or the iron analogue **738** afforded only substoichiometric or stoichiometric amounts of ammonia, respectively, while the osmium complex **748** afforded 7.1 ± 0.6 equiv of NH_3 per osmium center (Scheme 137a). Increasing the amount of acid and reductant in the reaction catalyzed by $[(P^{iPr}{}_3{}^{Si})Os(N_2)]^-$ (**748**) to 1500 equiv of $[H_2NPh_2]OTf$ and 1800 equiv of $Cp^*{}_2Co$, respectively, led to a yield of 120 ± 11 equiv of NH_3 per Os.

The reaction of **748** with $HBAr^F{}_4$ at −78 °C afforded a mixture of the osmium hydrides $[(P^{iPr}{}_3{}^{Si})Os(N_2)(H)]$ (**984**) and $[(P^{iPr}{}_3{}^{Si})Os(H)_3]$ (**985**, Scheme 137b). These two hydride compounds were independently synthesized and reacted with acid and reductant under the N_2-to-NH_3 conditions ($HBAr^F{}_4$ or $[H_2NPh_2]OTf$, 46 equiv; KC_8 or $Cp^*{}_2Co$, 50 equiv; 1 atm, −78 °C, Et_2O) without appreciable formation of ammonia. Further mechanistic tests also indicated that hydrides **984** and **985** form during the catalysis and are catalytically inactive states. In turn, reaction between **748** and HOTf (3 equiv) in thawing 2-MeTHF (−135 °C) generated the hydrazido(2−) complex $[(P^{iPr}{}_3{}^{Si})Os{=}NNH_2]OTf$ (**986**), which was structurally authenticated. Treatment of **986** with 46 equiv of $[H_2NPh_2]OTf$ and 50 equiv of $Cp^*{}_2Co$ at low temperature afforded 2.6 equiv of ammonia per osmium center, illustrating that it facilitates the generation of ammonia in this system and is a viable intermediate in the N_2-to-NH_3 conversion. Notably, while the analogous iron- or ruthenium-based systems require stronger reductants to drive the reduction of N_2, the osmium system operates with the milder $Cp^*{}_2Co$, but only at low temperature.

3.3. Activation of CO and CO_2

Carbon monoxide and carbon dioxide are fundamentally important molecules in industry and nature. While carbon monoxide is widely used as a C1-feedstock in industry,[157,596] CO_2 is an inert and thermodynamically stable molecule. Nevertheless, the chemical valorization of CO_2 is attracting enormous interest due to its role as a greenhouse gas.[597,598] It has long been known that the nucleophilic character of transition metalate complexes can be harnessed in such processes. In a pioneering study published in 1988, Focchi investigated the reaction of $K[V(C_6H_6)_2]$ (**987**) with CO and CO_2.[73] In both cases, a range of C_1 and C_2 products were detected, including HCO_3^-, $HCOO^-$, $HC_2O_4^{2-}$, $C_2O_4^{2-}$, and minor amounts of $HOCH_2COO^-$. CO, H_2, and C_2H_2 were not detected in the headspace of the reactions. By contrast, Corella and Cooper observed the addition of CO_2 to coordinated benzene upon reaction of CO_2 with $[Cr(\eta^4\text{-}C_6H_6)(CO)_3]^{2-}$ (**988**), resulting in the formation of substituted cyclohexadienyl complexes.[599] Furthermore, the reductive disproportionation of CO_2 into carbonate and carbon monoxide by dianionic carbonyl metalates based on vanadium, group 6 metals (Cr, Mo, W) and group 8 metals (Fe, Ru, Os) is well-documented.[600,601]

3.3.1. CO Activation by Ferrates, Cobaltates, and Molybdates.

CO and CO_2 activation by metalates has increasingly gained interest in recent years, including some catalytic applications. The carbonylation of tertiary amines using low-valent iron catalysts was described in 2019.[602] The series of low valent carbonyl-iron complexes $K_2[Fe(CO)_4]$ (K_2[**1**]), $Fe(CO)_5$ (**18**), $[Fe_3(CO)_{12}]$ (**22**) and $[(\eta^5\text{-}Cp)Fe(CO)_2]_2$ (**651**) were evaluated in the catalysis. The carbonylation of C−N bonds in tertiary amines was initially studied using the following conditions: *N*,*N*-dimethylaniline as the model substrate, 6 mol % catalyst loading, 55 bar of CO and MeI as a promoter (0.8 equiv) at 200 °C for 15 h in acetonitrile. Under these conditions, the selective carbonylation of one N−Me bond was achieved in moderate yields (40−72%) using the neutral complexes **18**, **22**, or **651** as catalysts. By comparison, the iron metalate K_2[**1**] afforded quantitative yields of the product *N*-methylacetanilide. To achieve comparable yields with catalyst **18** or **651**, the reaction time had to be extended to 60 h. At lower pressures (8 bar), a decrease in the catalytic activity was observed for all the catalysts (17−58% yield), though the carbonylferrate K_2[**1**] still exhibited the highest activity (58% yield). Therefore, K_2[**1**] was specifically examined in further catalytic screening (Scheme 138). To overcome the loss of activity observed with the lower pressure of CO, the use of Lewis acids additives was evaluated. Upon addition of either $Sc(OTf)_3$ or $Nd(OTf)_3$ (60 mol %), the carbonylation by ferrate K_2[**1**] led to quantitative generation of *N*-methylacetanilide under 8 bar of CO. The reaction scope was found to extend to methylamine substrates with electron withdrawing or electron donating groups, as well as ethylamine substrates (10 examples in total). Yields varied substantially across the range of substrates (28 to 99%).

Scheme 138. Carbonylation of Tertiary Amines Catalyzed by a Low-Valent Ferrate, $K_2[Fe(CO)_4]$ (K_2[1])[602]

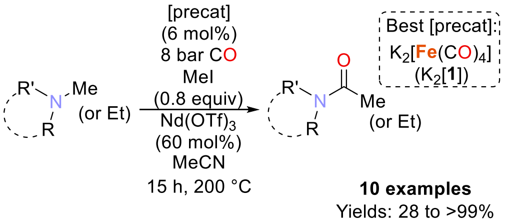

As mentioned above (section 2.3.3.2), the iron-carbyne complex $[(P^{iPr}{}_3{}^{Si})Fe{\equiv}C\text{-}OSiMe_3]$ (**744**, Scheme 89, *vide supra*) was obtained from the the anionic carbonylferrate $[(P^{iPr}{}_3{}^{Si})Fe\{CONa(thf)_3\}]$ (**741**) and a silyl electrophile.[143] In a similar vein, the Peters group reported the reduction of carbonyl ligands at related examples of anionic iron and cobalt complexes.[603−605] Reduction of the dicarbonyliron complex $[(PhP_2{}^B)Fe(CO)_2]$ [**989**, $PhP_2{}^B$ = PhB(*o*-$iPr_2PC_6H_4)_2$] with potassium in the presence of benzo[15]crown-5 affords ferrates in two distinct oxidation states: the monoanionic compound $[K(benzo[15]crown\text{-}5)_2][(PhP_2{}^B)Fe(CO)_2]$ (**990**) was obtained with one equivalent of potassium, whereas an excess of reducing agent gave the complex $[K(benzo[15]\text{-}crown\text{-}5)_2]_2[(PhP_2{}^B)Fe(CO)_2]$ (**991**, see Scheme 139).[603]

Scheme 139. Reduction of an Iron-Dicarbonyl Complex in the Absence and in the Presence of a Silyl Electrophile: Synthesis of a CO-Derived Iron Dicarbyne[603]

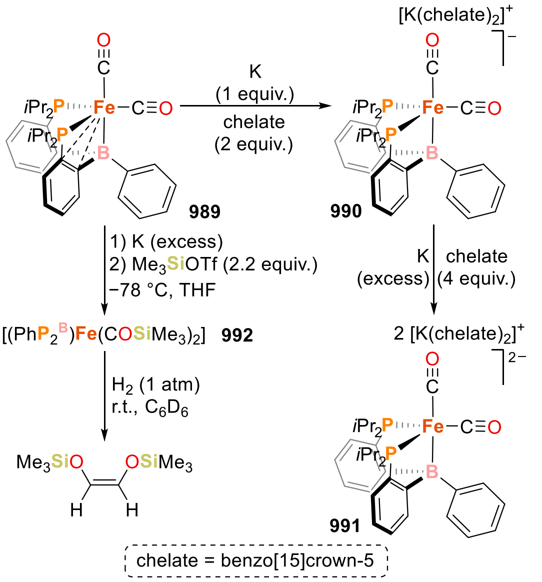

The increase in electron density at the metal atom is reflected by the significant red-shift of the stretching bands for the carbonyl ligands in **989**−**991** [ν_{CO}(**989**) = 1908 cm^{-1}, ν_{CO}(**990**) = 1857 cm^{-1}, ν_{CO}(**991**) = 1738 cm^{-1}]. The low energy C−O stretch of **991** indicated that the functionalization of the CO ligands should be feasible. In line with this, the reduction of the dicarbonyl compound **989** by potassium in the presence of trimethylsilyl triflate (Me_3SiOTf) afforded the silylated product $[(PhP_2{}^B)Fe(COSiMe_3)_2]$ (**992**, Scheme 139), which can be described as a double terminal iron-carbyne complex. The characterization data of **992** (X-ray diffraction, NMR, and ^{57}Fe Mössbauer spectra) point to extensive Fe−C multiple bonding and an additional C−B interaction in one of the carbyne units. Based on an analysis of the structural parameters and DFT calculations on a simplified model complex $(Me_3P)_2Fe(COSiH_3)_2$, the first three resonance forms shown in Figure 23 (from left to right) should be more representative of the bonding situation of **992** than the one in the right. In addition, compound **992** reacted with H_2 (1 atm, r.t.) via hydrogenative C−C coupling to afford the olefin *Z*-$Me_3SiOCH{=}CHOSiMe_3$, a functionalized CO-derived product (Scheme 139).

The previously reported carbonyl complex $[(P_3{}^B)Fe(CO)]$ (**721**)[141] reacts with H_2 to afford the bridged-hydride species $[(P_3{}^B)(\mu\text{-}H)Fe(H)(CO)$ (**993**).[588,604] Complex **993** undergoes two-electron reduction to afford the dianionic hydridocarbonyl compound **994** featuring a significantly activated CO ligand (ν_{CO} = 1575 cm^{-1}; see Scheme 140). Compound **994** is protonated with traces of water to afford an unstable anionic trihydride complex $[K(thf)_n][(P_3{}^B)(\mu\text{-}H)Fe(H)_2(CO)]$ (**995**), which loses a molecule of hydrogen to yield the hydrocarbonylferrate $[K(thf)_n][(P_3{}^B)FeH(CO)]$ (**996**). Moreover, the dianionic ferrate **994** is silylated at the oxygen atom upon reaction with Me_3SiOTf (>2 equiv) to afford $[(P_3{}^B)Fe\text{-}CH_2OSiMe_3]$ (**997**, Scheme 140). In complex **997** the hydride ligands have migrated to the carbonyl carbon atom. While **997** reacts with different Brønsted acids to yield the bridged hydride **993**, the functionalized $-CH_2OSiMe_3$ fragment is released as CH_3OSiMe_3 or $PhSiH_2CH_2OSiMe_3$ in the presence of hydrogen (hydrogenolysis) or silanes, respectively (Scheme 140, bottom). The functionalization reaction of the CO thus results in a net 4-electron reduction of a carbonyl ligand.[604]

A trisphosphine supported carbonylcobaltate complex can also be O-functionalized to afford a carbyne motif.[605] The cobalt complex $[(P_2{}^P)CoBr(CO)]$ (**998**, $P_2{}^P$ = PhP(*o*-$iPr_2PC_6H_4)_2$) undergoes reduction by sodium to yield the Co(−I) compounds $[NaL_n][(P_2{}^P)Co(CO)]$ [L_n = $(solv)_x$ (**999**), ([12]crown-4)$_2$ (**1000**); Scheme 141]. The carbonyl ligands in the reduced complexes present a high degree of activation, according to the stretching vibrations [ν_{CO}(**999**) = 1731 cm^{-1}; ν_{CO}(**1000**) = 1752 cm^{-1}]. Treatment of **999** with silyl electrophiles ($R_2R'SiOTf$) afforded the carbyne complexes $[(P_2{}^P)Co{\equiv}C\text{-}OSiR_2R']$ [R = R′ = *i*Pr (**1001**), R = Ph, R′ = *t*Bu (**1002**)] in a high yield. These species were identified as terminal carbyne complexes via structural characterization of

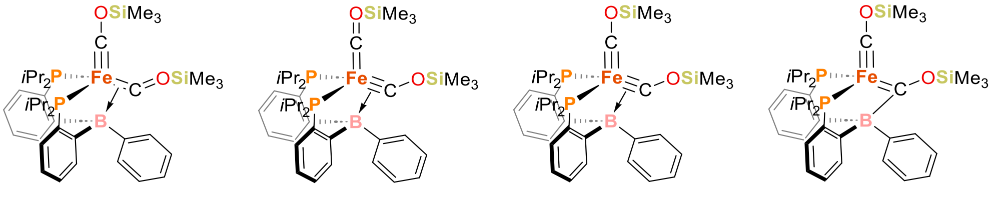

Figure 23. Relevant resonance structures of the iron dicarbyne complex $[(PhP_2{}^B)Fe(COSiMe_3)_2]$ (**992**).

Scheme 140. Formation of Hydrido(carbonyl)Iron Complexes and Reduction of an Iron-Bound Carbonyl Ligand Followed by Release of the CO-Functionalized Product[588,604]

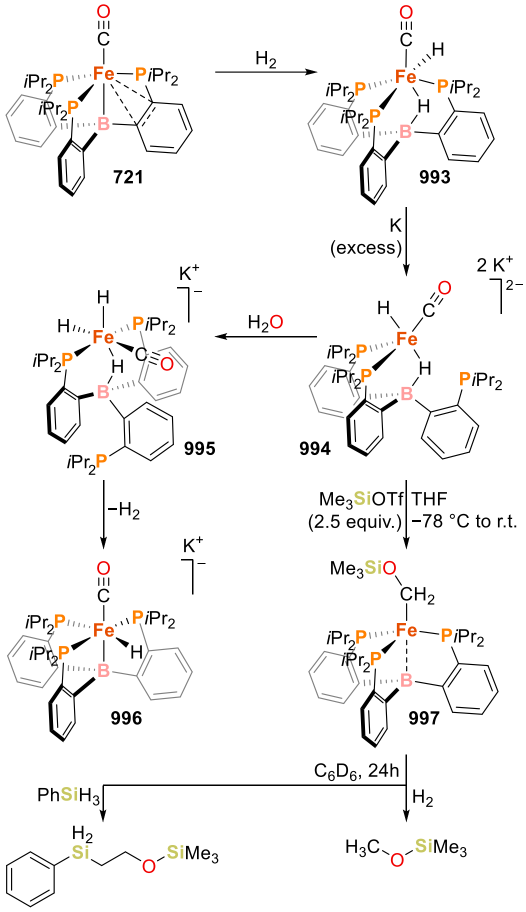

Scheme 141. Synthesis of a $(P_2^P)Co(-I)$-Carbonyl Complex and Its O-Functionalization to Afford Terminal Carbyne Compounds[605]

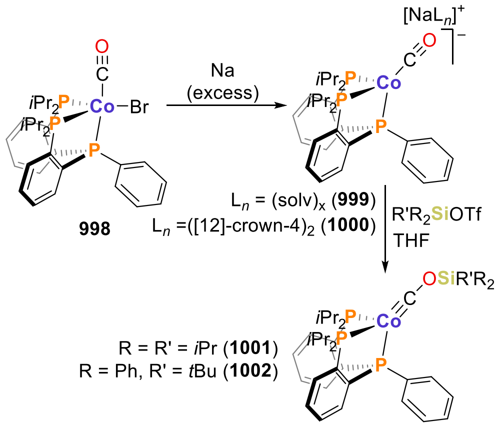

the *t*BuPh$_2$ derivative **1002**, which features a significantly shortened Co−C bond (1.640(4) Å) and an elongated C−O distance (1.260(5) Å).

In 2016, Agapie and Buss described a remarkable transformation taking place at a molybdenum complex bearing a terphenyl−diphosphine ligand (tpdp = 1,4-bis(2-(diisopropylphosphino)phenyl)benzene).[606] The formally zerovalent complex [Mo(tpdp)(CO)$_2$] (**1003**) undergoes four-electron deoxygenative reductive coupling of carbon monoxide in the presence of four equivalents of an appropriate electrophile (E^+, ECl = *i*Pr$_3$SiCl or Me$_3$SiCl) under a nitrogen atmosphere to afford the molybdenum dinitrogen compound [Mo(tpdp)N$_2$] (**1004**), along with products EOC≡CE and E$_2$O resulting from rearrangement and functionalization of the carbonyl ligands (Scheme 142). This transformation is enabled by the architecture of the ligand scaffold, which allows both the formation of a highly anionic overall complex and the adoption of different coordination modes, stabilizing the several intermediates involved in the reaction pathway. In this context, the authors identified and characterized the anionic species [K$_2$(thf)$_3$][Mo(tpdp)(CO)$_2$] (**1005**) and [K$_3$(thf)$_{2.5}$][Mo(tpdp)(CO)$_2$] (**1006**), formally containing Mo(−II) (**1005**) and Mo(−III) (**1006**) metal centers, upon reducing the neutral precursor **1003** with two equivalents or an excess of KC$_8$, respectively. In the solid state, both **1005** and **1006** are potassium-ion-bridged polynuclear clusters, where the cations interact with one phosphine arm, the oxygen atoms of the carbonyl donors, and the ligand *π*-systems.

Scheme 142. Deoxygenative CO-Upgrade at a Molecularly Defined Mo-tpdp Scaffold: The tpdp Motif Allows for the Storage of Two (1005) or Three (1006) Redox Equivalents, Therefore Activating the Coordinated CO[606]

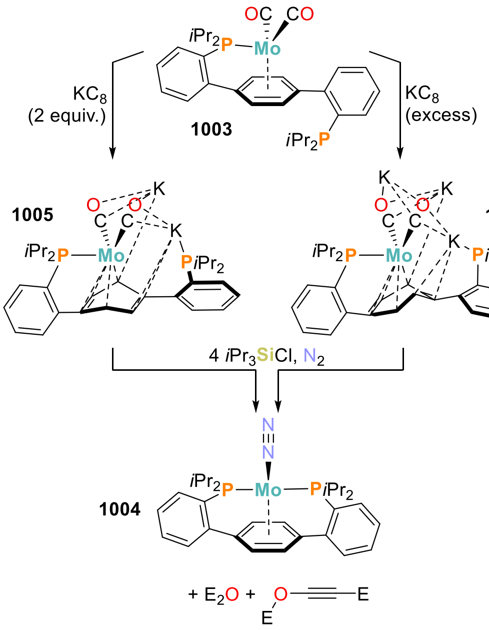

The molybdenum-arene hapticity changes from η^6-coordination in **1003** to either η^4-coordination in compound **1005** or η^3-coordination in **1006**, causing significant distortion from planarity in the central arene. For this motif, the C−C bond metrics are indicative of a considerable delocalization of anionic charge into the terphenyl moiety and the adoption of a partial cyclohexyldienyl dianion character. In this extreme case, **1005** can be described as a Mo(0) anion and **1006** as a Mo(−I) species. Across the reduction series [Mo(tpdp)(CO)$_2$]$^{n-}$ (n = 0, 1, 2), the X-ray data also reveal the elongation of C−O and contraction of Mo−CO bond lengths, consistent with the attenuation of the observed CO stretching frequencies in the IR spectra and the significantly deshielded ^{13}CO resonances visible by $^{13}C\{^1H\}$ NMR spectroscopy.

Altogether, the experimental evidence points to strongly activated CO ligands, susceptible to electrophilic attack as demonstrated with $\mathrm{R_3SiCl}$ reagents (R = Me, *i*Pr). In fact, **1005** and **1006** react with four equivalents of $i\mathrm{Pr_3SiCl}$ to yield the CO functionalized product $i\mathrm{Pr_3SiOC{\equiv}CSi}i\mathrm{Pr_3}$ and compound **1003** in 50% and 75% yields, respectively. This scenario suggested a redox imbalance, where **1005** or **1006** also acted as sacrificial reductants. Addition of $\mathrm{KC_{10}H_8}$ and $i\mathrm{Pr_3SiCl}$ to the mixture of **1006** and $i\mathrm{Pr_3SiCl}$ led to almost quantitative formation of **1004**, along with products $i\mathrm{Pr_3SiOC{\equiv}CSi}i\mathrm{Pr_3}$ and $i\mathrm{Pr_3SiOSi}i\mathrm{Pr_3}$, with no apparent formation of **1003**.

The same authors presented a detailed mechanistic study for this intricate reaction sequence, establishing the elementary reaction steps involved in the CO cleavage and coupling at a single molybdenum site.[607] These works rationalize the design principles for CO activation at monometallic complexes. In connection with the reductive catenation of C1 oxygenates, Agapie reported the anionic carbide K[Mo(tpdp)(C)(CO)] (**1007**), which is an open-shell species.[608]

Within the remarkable chemistry of the Mo-tpdp system, in 2018 the Agapie group also discovered that the low-valent anionic nitride complex M[Mo(tpdp)(N)] (**1008**, M = Na, K) undergoes *N*-atom transfer upon addition of CO, affording a cyanate anion and a mixture of neutral carbonyl complexes $[\mathrm{Mo(tpdp)(CO)}_n]$ [*n* = 1 (**1009**) or 3 (**1010**); Scheme 143].[609] Two-electron reduction of the Mo(IV) precursor [Mo(tpdp)(N)(OTf)] (**1011**) yielded the nitride compound **1008**. Characterization by multinuclear NMR spectroscopy and X-ray diffraction indicated the presence of a terminal nitride ligand, an η^6 Mo−arene binding mode to the central aromatic ring of the ligand scaffold, and one dissociated phosphine arm of the terphenyl chelate. For K[**1008**] a tetrameric $\mathrm{N_4K_4}$ cubane arrangement was observed in the solid-state molecular structure, which precluded Mo−Mo bonding (Mo−Mo distance is ca. 6.5 Å). As seen with $[\mathrm{K_2(thf)_3}][\mathrm{Mo(tpdp)(CO)_2}]$ (**1005**) and $[\mathrm{K_3(thf)_{2.5}}][\mathrm{Mo(tpdp)(CO)_2}]$ (**1006**),[606] the potassium cation interacts with the π-system in the ligand scaffold and with the nitride unit.

Scheme 143. Synthesis of a Reduced Anionic (Nitride) molybdenum Complex and N⁻ Group Transfer Reactivity[609]

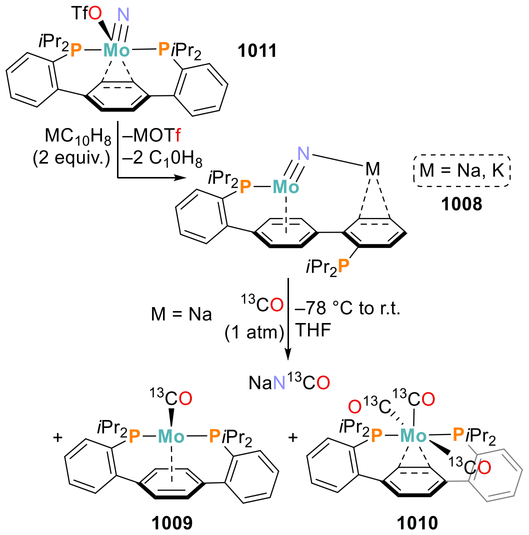

The electronic structure of the anion **1008** was investigated by DFT, revealing the important role of the flexible terphenyl diphosphine ligand in stabilizing this unusual terminal nitrido complex with high formal *d* electron count. The hemilability of tpdp allows for variable binding modes that prevent the population of antibonding orbitals with respect to the Mo−N interaction. DFT calculations also indicated that the lone pair on the nitride is relatively high in energy (HOMO−2), making it nucleophilic, in agreement with the experimental observation of its carbonylation in solution under an atmosphere of CO. This work provides a useful strategy for promoting productive group transfer reactivity in stable early transition-metal nitrides. Recently, Mazzanti, Maron, and Agapie showed that the nitride ligand in Na[**1008**] is partially transferred to the uranium(III) precursor $[\mathrm{U(OSi}t\mathrm{Bu_3)_3(thf)_2}]$ (**1012**), affording the first example of a transition metal-capped uranium nitride $\mathrm{Na}[\mathrm{U(OSi}t\mathrm{Bu_3)_3}(\mu\text{-N})\mathrm{Mo(tpdp)}]$ (**1013**).[610] The experimental and computational data point to an *N*-transfer accompanied by a two-electron transfer from uranium to molybdenum, formally resulting in the nitride triply bonded to U(V) and singly bonded to Mo(0). The isolated compound **1013** displays a U−Mo interaction in the solid state.

3.3.2. $\mathrm{CO_2}$ Activation by Metalates Containing Sc, Mn, Fe, Co, and Ni.

Reactions of $\mathrm{CO_2}$ with $[\mathrm{K([18]crown\text{-}6)}][\mathrm{Sc\{N(SiMe_3)_2\}_3}]$ (**419**, Scheme 51, *vide supra*) afford mixtures of the oxalate complex, $\{\mathrm{K_2([18]crown\text{-}6)_3}\}\{[\{(\mathrm{Me_3Si})_2\mathrm{N}\}_3\mathrm{Sc}]_2(\mu\text{-}\mathrm{C_2O_4}\text{-}\kappa^1\mathrm{O}{:}\kappa^1\mathrm{O}'')\}$ (**1014**), and a $\mathrm{CO_2}^-$ radical anion complex, $[\{(\mathrm{Me_3Si})_2\mathrm{N}\}_3\mathrm{Sc}(\mu\text{-OCO-}\kappa^1\mathrm{O}{:}\kappa^1\mathrm{O}')\mathrm{K([18]crown\text{-}6)}]_n$ (**1015**, Scheme 144).[328] Complex **1015** is similar to $[\mathrm{K_2([18]crown\text{-}6)_2}]\{[(\mu\text{-}\mathrm{CO_2})(\{(\mathrm{Me_3Si})_2\mathrm{N}\})_3\mathrm{Y}(\mu\text{-}\mathrm{CO_2})]\}$ (**1016**), which was previously obtained from the reaction of $[\mathrm{Y\{N(SiMe_3)_2\}_3}]/\mathrm{K}$ with $\mathrm{CO_2}$ in the presence of [18]crown-6.[611]

Scheme 144. $\mathrm{CO_2}$ Activation by Scandate(II) Amide Complex 419

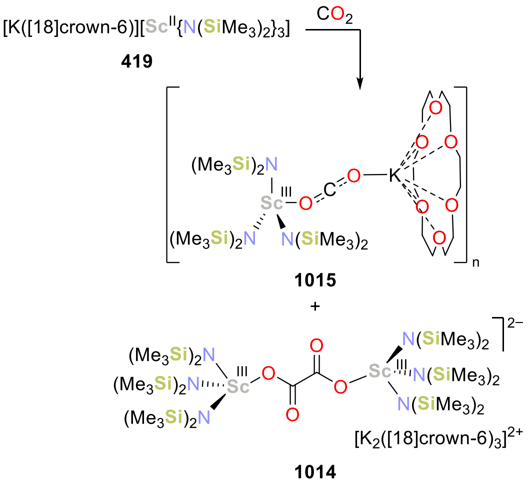

Manganese complexes are useful alternatives to the rhenium analogues for the electrochemical reduction of $\mathrm{CO_2}$.[612−615] In studies on the electrochemical reduction of $\mathrm{CO_2}$ to CO using manganese catalysts, Kubiak and co-workers identified several anionic species as key intermediates. The system formed by catalyst *fac*-$[\mathrm{MnBr}(t\mathrm{bpy})(\mathrm{CO})_3]$ (**1017**, *t*bpy = 4,4′−di−*tert*−butyl−2,2′−bipyridine) in a Brønsted acid (2,2,2-trifluoroethanol, TFE, 1.4 M) is selective for the production of CO from $\mathrm{CO_2}$ with TOF of 340 $\mathrm{s^{-1}}$.[612] In this system, three distinct manganese species were detected, in different oxidation states. The first corresponds to catalyst **1017**, which undergoes one-electron reduction with loss of the bromide ligand to afford a Mn−Mn dimer, [Mn(*t*bpy)$(CO)_3$]$_2$ (**1018**). Further reduction leads to an anionic complex, [Mn(*t*bpy)$(CO)_3$]$^-$ (**1019**), which was identified as the catalytically active species.

The structure of the anionic complex was confirmed through X-ray crystallography, facilitated by direct synthesis of [K([18]crown-6)][**1019**] by reduction of **1017** with KC_8. The complex features a manganese center in a pentacoordinate environment with a partially reduced bipyridine ligand. Moreover, substantial metal-to-ligand backbonding to the carbonyl units is evidenced by the low energy CO stretching frequencies observed by infrared spectroelectrochemistry [IR-SEC, ν_{CO} = 1907 and 1807 cm^{-1}]. These findings indicate that the behavior of the manganese catalyst is comparable to that of previously studied rhenium systems,[173,616−618] which have shown remarkable activity in the electrochemical reduction of CO_2.

To circumvent the problem of the dimerization of the one-electron reduction product, the same group developed a related manganese complex featuring a bulkier bipyridine ligand, 6,6′-dimesityl-2,2′-bipyridine (mesbpy).[613] Like in the previous case, the catalyst *fac*-[MnBr(mesbpy)$(CO)_3$] (**1020**) is electrochemically reduced to produce a singly and a doubly reduced species, [Mn(mesbpy)$(CO)_3$] (**1021**) and [Mn(mesbpy)$(CO)_3$]$^-$ (**1022**) respectively. The formation of both species occurs at approximately the same potential. By contrast to the *t*bpy-based system, the neutral species **1021** does not dimerize owing to the steric protection provided by the bulky ligand. The reduced compounds, **1021** and **1022** were synthesized by reaction with KC_8 and characterized in the solid state [ν_{CO} = 1917 and 1815 cm^{-1}]. The anionic species **1022** binds CO_2, yielding a Mn(I)-COOH intermediate in the presence of H$^+$, which requires further reduction to initiate the catalytic production of CO. The high selectivity and improved catalytic activity for CO_2 reduction in the presence of elevated concentrations of acid were partly explained by the non-innocence of the bpy ligand: the electron density on the bpy ligand favors the charge transfer to CO_2 through both σ and π interactions. Furthermore, a 10-fold increase in the reaction rate was achieved by the addition of Mg^{2+} cations as a Lewis acid instead of TFE.[614] The resulting intermediate is capped by a Mg^{2+} cation, weakening a C−O bond in the coordinated CO_2 unit. Upon addition of a second CO_2 molecule the activated C−O bond is broken and CO_3^{2-} is released as $MgCO_3$. This generates a cationic Mn(I)-tetracarbonyl species, electrochemical reduction of which releases CO and regenerates **1022**.

In the search of a similar system featuring redox-inactive ligands, the mixed carbonyl-isocyanide complexes BrMn$(CO)_3$(CNAr^{Dipp2})$_2$ (**40**) and [Mn(thf)$(CO)_2$(CNAr^{Dipp2})$_3$]OTf (**1023**) were investigated by Kubiak, Figueroa, and coworkers.[615] While the analysis of the electronic structure of the bipyridine-based systems could be complicated by redox events at the ligand, the electronic description of the mixed-ligand complexes **40** and **1023** is comparably straightforward (*vide supra*, section 2.2.3.1).[123,124] The pentacoordinate anionic intermediate [Mn$(CO)_3$(CNAr^{Dipp2})$_2$]$^-$ (**39**) is a stable analogue of the homoleptic carbonyl complex [Mn$(CO)_5$]$^-$ (**37**), and the redox chemistry of these mixed-ligand complexes occurs at the metal center. The electrochemical behavior of **40** (and that of the analogous Cl$^-$ and I$^-$ complexes) toward CO_2 was consistent with the reactivity observed for the anionic compound **39** with CO_2. Stoichiometric reaction between **39** and CO_2 afforded the zerovalent compound [Mn$(CO)_3$(CNAr^{Dipp2})$_2$] (**49**, Scheme 3, section 2.2.3.1, *vide supra*), dimers $Mn_2(CO)_7$(CNAr^{Dipp2})$_3$ (**1024**) and $Mn_2(CO)_8$(CNAr^{Dipp2})$_2$ (**1025**, see Scheme 145a), free isocyanide ligand and unreacted **39**. Nonetheless, by using a 1:10 ratio of **39**:CO_2, complete consumption of **39** with formation of CO_3^{2-} and dimers **1024** and **1025** was observed. Therefore, metalate **39** (2 equiv) promoted the reductive disproportionation of CO_2.

Scheme 145. (a) Structures of Dimers $Mn_2(CO)_7$(CNAr^{Dipp2})$_3$ (1024) and $Mn_2(CO)_8$(CNAr^{Dipp2})$_2$ (1025) and (b) Proposed Mechanism of Reductive Disproportionation of CO_2 Promoted by Metalate Na[Mn$(CO)_3$(CNAr^{Dipp2})$_2$] (39)[615]

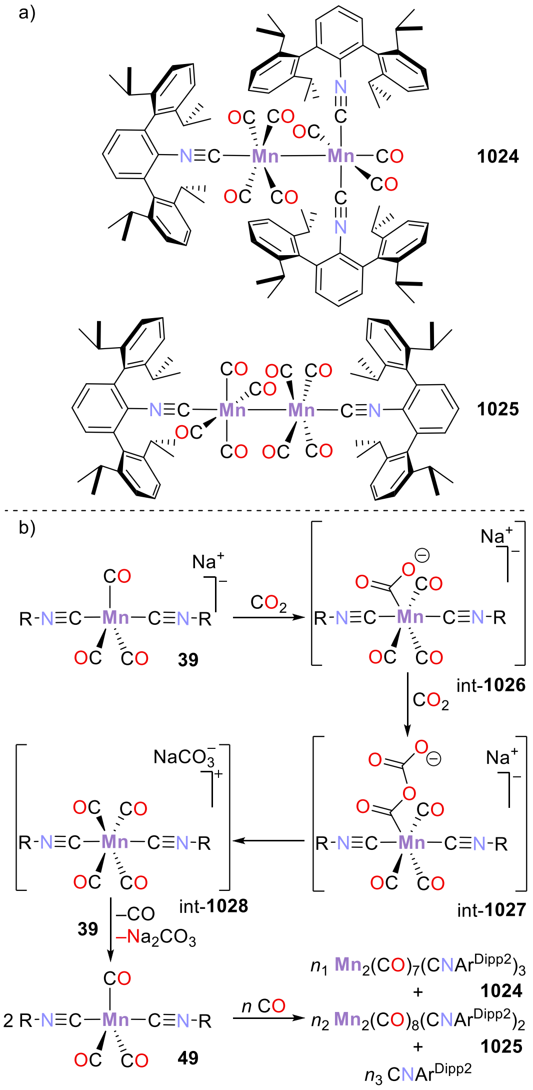

A mechanism for the transformation of CO_2 to CO and CO_3^{2-} by metalate **39** was described (Scheme 145b). According to this proposal, complex **39** reacts with CO_2 to form a metallocarboxylate intermediate, Na[Mn$(CO_2)$$(CO)_3$(CNAr^{Dipp2})$_2$] (int-**1026**), which conducts a nucleophilic attack on another molecule of CO_2, forming a bound

−CO(O)CO$_2$ ligand at the Mn center (int-**1027**). Int-**1027** decomposes into CO$_3^{2-}$, generating a cationic tetracarbonyl complex, [Mn(CO)$_4$(CNAr^{Dipp2})$_2$]$^+$ (int-**1028**). This species is reduced, affording the zerovalent compound **49** with release of CO. In an independent reaction between compound **49** and CO, the rapid formation of the dimers **1024** and **1025** was identified. Therefore, **49** was proposed to act as a trap for the CO formed in the reductive disproportionation of CO$_2$. Due to this generation of various off-cycle species, the system cannot engage in catalytic turnover.

In another example of this reactivity, the bulky tetraisocyanide dianion Na$_2$[Fe(CNAr^{Mes2})$_4$] (**51**; Scheme 4, *vide supra*)[125] activates CO$_2$ to produce CO and carbonate (CO$_3^{2-}$), via reductive disproportionation.[619] Treatment of a solution of metalate **51** with 1 atm of CO$_2$ yielded a new diamagnetic species. Crystallographic analysis revealed it to be the carbonyl complex Fe(CO)(CNAr^{Mes2})$_4$ (**1029**, Scheme 146). The reactivity toward CO$_2$ parallels that of the carbonyl dianion complex Na$_2$[Fe(CO)$_4$] (Na$_2$[**1**]), which affords Fe(CO)$_5$ (**18**).[600,601] Moreover. the five-coordinate complex **1029** is isostructural with the previously described dinitrogen complex Fe(N$_2$)(CNAr^{Mes2})$_4$ (**61**, Scheme 5, *vide supra*).[125]

Scheme 146. Reactivity of the Dianionic Complex Na$_2$[Fe(CNAr^{Mes2})$_4$] (51) toward CO$_2$[619]

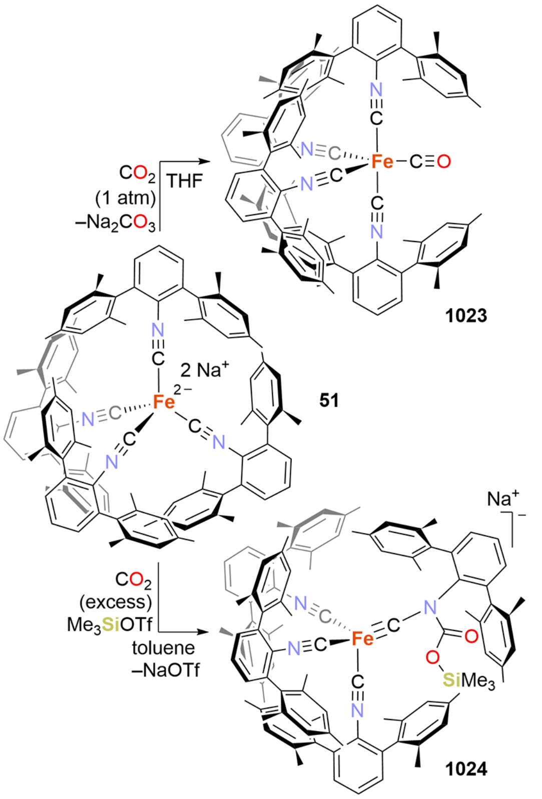

By treating **51** with CO$_2$ in the presence of silyl triflates (R$_n$Me$_{3-n}$SiOTf), a silylated CO$_2$ adduct was obtained, Na[Fe≡CN{(Ar^{Mes2})(C(O)OSiMe$_3$)}(CNAr^{Mes2})$_3$] (**1030**, for Me$_3$SiOTf, see Scheme 146), which presents as a contact-ion pair. X-ray crystallography indicated that this four-coordinate product is a terminal iron carbyne compound (Fe−C = 1.658(10) Å), in which the C$_{Carbyne}$ atom is substituted by an aryl carbamate group. This product is the formal result of silylative trapping of a molecule of CO$_2$. The −C(O)OSiR$_3$ group directly binds to an isocyano nitrogen atom, prior to electronic rearrangement. DFT calculations performed on a truncated model of the carbyne complex reproduced the experimental structure. Furthermore, the formation of the carbyne product seems in response to the bulk of the silyl triflate reagent: while treatment with PhMe$_2$SiOTf also exclusively afforded the carbyne-carbamate Na[Fe≡CN{(Ar^{Mes2})(C(O)OSiMe$_2$Ph)}(CNAr^{Mes2})$_3$] (**1031**), the reaction with the more bulky Ph$_2$MeSiOTf led to the corresponding product Na[Fe≡CN{(Ar^{Mes2})(C(O)-OSiMePh$_2$)}(CNAr^{Mes2})$_3$] (**1032**) in only 10% yield, along with significant amounts of the carbonyl compound **1029**. This disparity was attributed to changes in the steric profile of the silane, making it kinetically inefficient to trap the CO$_2$ adduct of **51**. In the absence of the silane, the CO$_2$ adduct engages in a traditional mechanism of reductive disproportionation, thereby producing the carbonyl complex **1029**.

As previously mentioned (section 2.2.6.1), Müller, Wolf and co-workers reported an anionic iron complex featuring a pyridyl-phosphinine motif, namely [K([18]crown-6)][Cp*Fe-(L)] [**323**, L = 2-(2′-pyridyl)-4,6-diphenylphosphinine], which exists as two isomeric forms in solution depending on the coordination mode adopted by the ligand: **323-*π*** and **323-*σ*** (*vide supra*).[276] Given the coordinative flexibility and non-innocence of the ligand in **323-*π*** and **323-*σ***, the reactivity of this species (in solution) toward CO$_2$ was investigated. An immediate color change was observed, accompanied by the replacement of the resonances of **323-*π*** and **323-*σ*** by two new resonances in the ^{31}P{^{1}H} NMR spectrum (δ = 97.0 and 116.0 ppm), suggesting that both isomers had reacted with CO$_2$. Fractional crystallization allowed the structural characterization of both species.

Isomer **323-*σ*** reacted with CO$_2$ to generate complex **1033** (Scheme 147), in which one C═O bond is fully cleaved at room temperature. The cleavage of the CO$_2$ molecule thereby generated an Fe-CO species and a P−O moiety at the *σ*-coordinated bidentate ligand. The continued coordination of the bidentate ligand to the metal center was attributed to electronic flexibility of the phosphinine moiety. The *π*-coordinated isomer, **323-*π***, reacted with CO$_2$ to give complex **1034** (Scheme 147) the product of addition of an intact CO$_2$

Scheme 147. Activation of CO$_2$ by the Anionic Species [K([18]crown-6)][Cp*Fe(L)] (323)[276a]

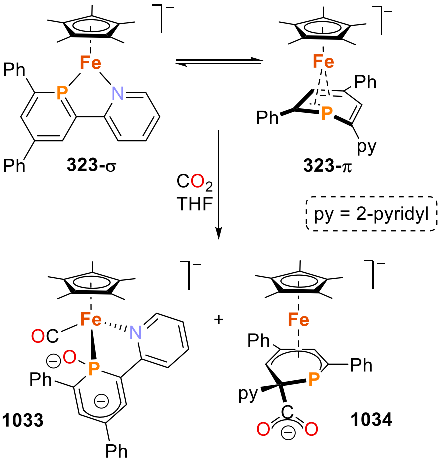

[a] The anionic species are stabilized by [K([18]crown-6)]$^+$ cations.

molecule to a carbon atom of the phosphinine unit. The resulting ligand can be described as a carboxylate-substituted phosphacyclohexadienyl motif, which coordinates the metal center in an η^5-fashion. The carboxylate unit in the ligand is κ^2-coordinated to the potassium cation (not shown in Scheme 147). For the reaction of both isomers with CO_2, DFT calculations indicated that only small energy barriers must be overcome to reach the products of activation (**323-*σ*** → **1033** = 3.5 kcalmol^{-1}; **323-*π*** → **1034** = 5.5 kcalmol^{-1}). In both cases, these barriers are considerably lower than that for the isomerization between **323-*σ*** and **323-*π*** (27.0 kcalmol^{-1}, *vide supra*).[276]

The highly reduced Mabiq complex Na(OEt$_2$)[Fe(Mabiq)] (**1035**, Mabiq = 2−4:6−8-bis(3,3,4,4-tetramethyldihydropyrrolo)-10−15-(2,2′-biquinazolino)-[15]-1,3,5,8,10,14-hexaene1,3,7,9,11,14-N$_6$) developed by Hess and co-workers is a noteworthy precatalytic intermediate in the selective electrocatalytic reduction of CO_2 to CO.[620] Detailed spectroscopic and computational studies indicate that the complex features an intermediate spin Fe(II) center coupled to a ligand biradical, resulting in a *S* = 1 spin state for the complex. Since the metal atom does not feature a "low-valent" metal center, we would like to refer the reader to the original literature for further details on the promising catalytic properties and intricate reaction mechanism as well as the closely related Co-Mabiq catalysts.[621]

As described in section 3.1, remarkable heterobimetallic catalysts for CO_2 hydrogenation were developed by Lu and co-workers based on metalates involving group 13 elements and Ni and Co.[524−527] The reactivity of the nickelates [NiM{N[*o*-(NCH$_2$P*i*Pr$_2$)C$_6$H$_4$]$_3$}]$^-$ [M = Al (**766**), Ga (**767**)] toward carbon dioxide was also studied.[81,622] These complexes reacted with CO_2 (1 atm) within minutes, forming K_2CO_3 and a 1:1 mixture of the corresponding neutral compound [NiM{N[*o*-(NCH$_2$P*i*Pr$_2$)C$_6$H$_4$]$_3$}] [M = Al (**762**), Ga (**763**)] and carbonyl complex [(CO)NiM{N[*o*-(NCH$_2$P*i*Pr$_2$)C$_6$H$_4$]$_3$}] [M = Al (**1036**), Ga (**1037**); see Scheme 148]. The presence of carbonyl ligands was evidenced by infrared spectroscopy [ν_{CO}(**1036**) = 1953 cm^{-1}; ν_{CO}(**1037**) 1962 cm^{-1}]. These observations suggested that the CO_2 molecule underwent two-electron reduction, promoted by the anionic complex [NiM{N[*o*-(NCH$_2$P*i*Pr$_2$)C$_6$H$_4$]$_3$}]$^-$ (2 equiv), to generate CO_3^{2-} and CO, with the latter being trapped by the corresponding neutral compound [NiM{N[*o*-(NCH$_2$P*i*Pr$_2$)C$_6$H$_4$]$_3$}] to afford **1036** or **1037**.

Scheme 148. Reactivity of the Heterobimetallic Nickelates [NiM{N[*o*-(NCH$_2$PiPr$_2$)C$_6$H$_4$]$_3$}]$^-$ [M = Al (766), Ga (767)] toward Carbon Dioxide[622]

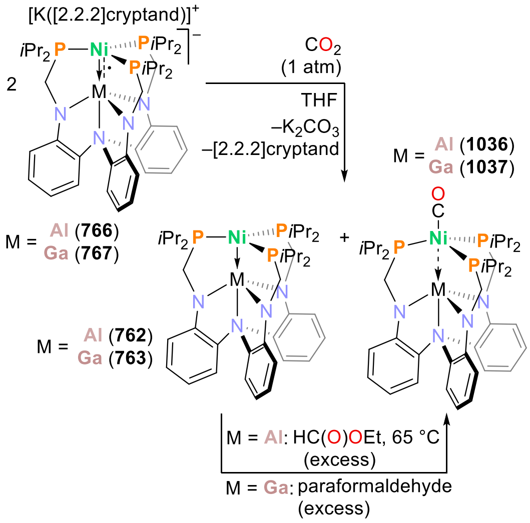

Complexes **1036** and **1037** were independently synthesized by treating the neutral compounds **762** or **763** with ethyl formate and paraformaldehyde, respectively (Scheme 148). In the proposed mechanism for the reductive disproportionation of CO_2 to carbonate and carbon monoxide, the anionic complexes **766**/**767** react with CO_2 to produce a Ni^I-metallacarboxylate, which is further reduced by another equivalent of **766**/**767**, affording a formally dianionic nickel diolate. Insertion of a second molecule of CO_2 produces a Ni intermediate with a di-CO_2 arrangement (Ni−C(OK)−O−C(O)-OK), which decomposes into CO_3^{2-} and a bound CO unit in **1036**/**1037**. The stability of the carbonyl compounds unfortunately hampers a possible turnover via CO release.

Inspired by the structure of the C-cluster of the Ni carbon monoxide dehydrogenase (CODH), Lu and co-workers developed a related family of nickel−iron heterobimetallic compounds, including reduced species that engage in the reductive disproportionation of CO_2 to carbonate and carbon monoxide.[623] The NiFe complex [NiFe{N[*o*-(NCH$_2$P*i*Pr$_2$)-C$_6$H$_4$]$_3$}] (**1038**) reacted with KC_8 to afford the reduced complex [K(thf)$_3$NiFe{N[*o*-(NCH$_2$P*i*Pr$_2$)C$_6$H$_4$]$_3$}] (K[**1039**], Scheme 149a). Crystallographic analysis revealed the formation of a contact ion pair by interaction of the K(thf)$_3^+$ unit with two phenyl rings from the ligand. An analogue with a noninteracting cation was obtained by performing the reduction in the presence of the phosphazenium cation, [P(NMeCy)$_4$]$^+$, which afforded [P(NMeCy)$_4$][NiFe{N[*o*-(NCH$_2$P*i*Pr$_2$)C$_6$H$_4$]$_3$}] ([P(NMeCy)$_4$][**1039**]).

The carbonyl derivatives of both the neutral and the reduced species [(CO)NiFe{N[*o*-(NCH$_2$P*i*Pr$_2$)C$_6$H$_4$]$_3$}]^n [*n* = 0 (**1040**), 1− (**1041**), Scheme 149a] were also synthesized by direct treatment of either **1038** or **1039** with CO, contrasting with the analogous treatment of **762** or **763** which afforded intractable mixtures.[622] Furthermore, addition of LiHBEt$_3$ to complex **1040** also yields the anionic carbonyl complex. The reduced nature of the anionic complex is reflected in the FT-IR spectrum [ν_{CO}(**1040**) = 1954 cm^{-1}; ν_{CO}(**1041**) 1930 cm^{-1}]. Crystallographic, spectroscopic (NMR, EPR, UV−vis, ^{57}Fe Mössbauer) and DFT analyses indicated that the nickel center is zerovalent, with the reduction events exclusively affecting the iron center in the supporting ligand, Fe(III)→Fe(II). The Ni^{0}Fe^{II} anionic species **1039** reductively disproportionates CO_2 into carbonate and metal-bound CO as shown in Scheme 149b. A CO_2-bound species, proposed to be an intermediate, was identified through electrochemical investigations. The neutral complex **1038** did not behave similarly toward CO_2.

3.4. Activation of White Phosphorus

3.4.1. General Remarks on White Phosphorus Activation.

The reports on the activation and functionalization of P_4 by transition metal complexes, including examples by metalates, have been extensively reviewed.[151,624−626] Thus, this review will focus only on the most recent and relevant contributions to this area that have been reported since the year 2020 and which were therefore not covered by the aforementioned review. Prior examples will be discussed in a generalized manner for context.

Scheme 149. (a) Bioinspired Heterobimetallic Nickel−Iron Complexes and (b) Their Reactivity toward Reductive Disproportionation of CO_2[623]

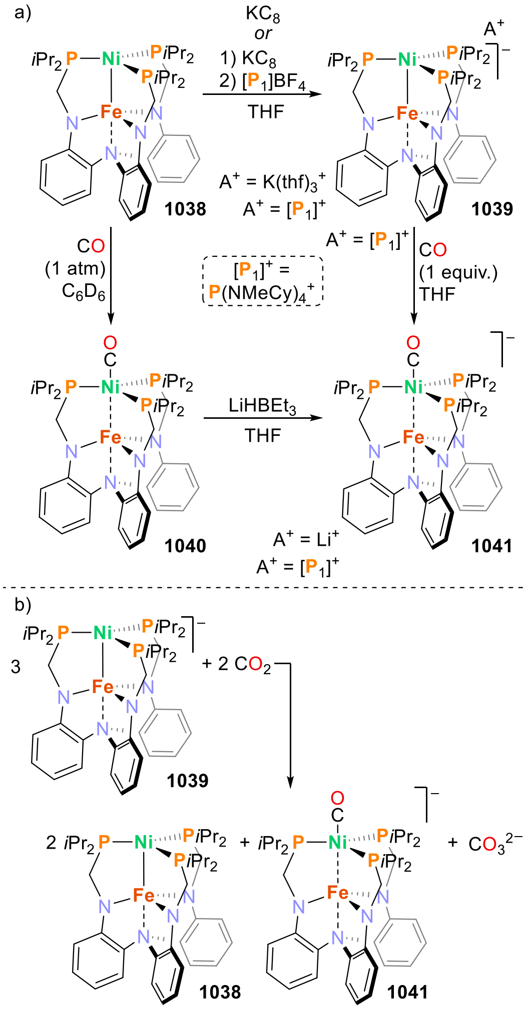

One early landmark example is the decaphosphatitanocene compound $[K([18]crown\text{-}6)]_2[Ti(\eta^5\text{-}cyclo\text{-}P_5)_2]$ (**1042**, Scheme 150) reported by Ellis and co-workers.[627] This complex, which was the first example of an entirely inorganic, "carbon-free" all-phosphorus metallocene, was obtained by treatment of a highly reactive naphthalenetitanate(−II) (**150**, generated *in situ* by reduction of $TiCl_4(thf)_2$ with potassium naphthalenide[628]) with P_4 (2.5 equiv). The resulting metallocene has a formally zerovalent titanium center.

Scheme 150. Synthesis of the Carbon-Free Sandwich Complex $[(cyclo\text{-}P_5)_2Ti]^{2-}$ (1042) by Ellis and Coworkers[627]

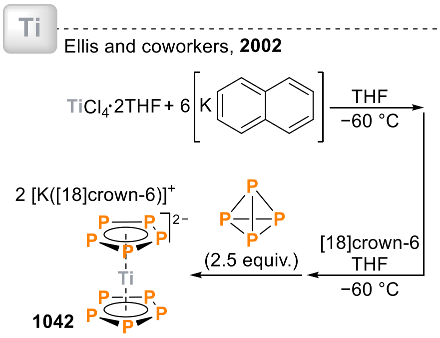

Considering the variety of polyphosphorus ligands obtained by interaction of the P_4 tetrahedron with transition metals, a useful way to organize the contributions in this area is by the degree of degradation or aggregation at the metal center. Examples of the reactivity of white phosphorus with metalloradicals are beyond the scope of the present article. However, these have been reviewed elsewhere.[151,624]

3.4.2. P_4 Activation by Ferrates.

Examples of products of activation of P_4 at low-valent iron metalates are summarized in Figure 24. These results show that reduced P_2, P_4, and P_7 fragments are accessible from the P_4 molecule and low-valent ferrate complexes.

A recent example of the generation of a reduced P_4 ligand was published by Lammertsma and co-workers, who isolated the complexes $Li[Cp^*Fe(CO)_2(\eta^1\text{-}P_4\cdot BAr_3)]$ (**1043**, Figure

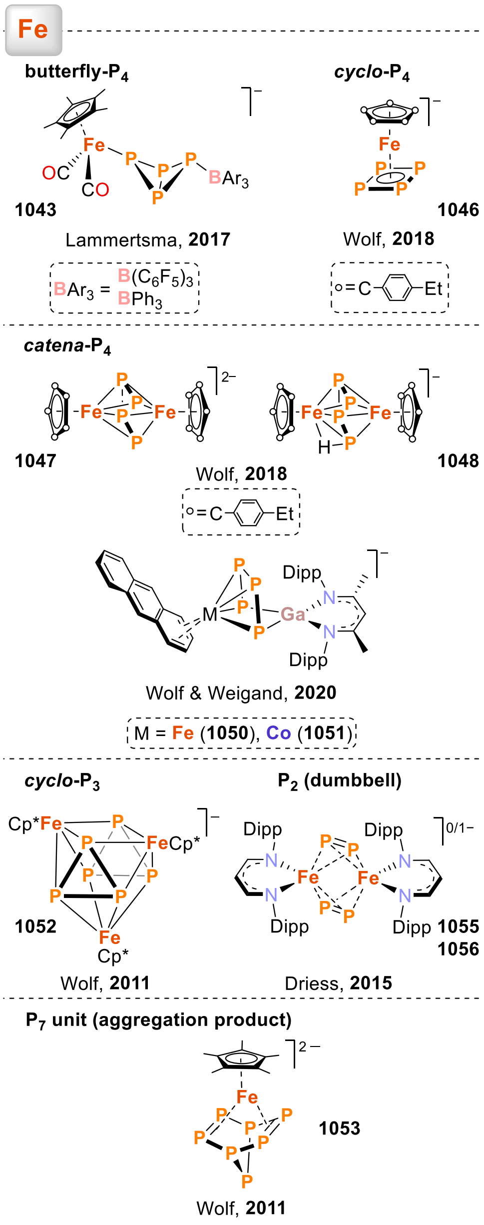

Figure 24. Products of activation of P_4 (degradation) at low-valent iron complexes/ferrates.

24)[629] by reaction of the nucleophilic iron metalate, Li[Cp*Fe(CO)$_2$] (**1044**) with white phosphorus in the presence of Lewis acids (BAr$_3$; Ar = C$_6$F$_5$, Ph). The outcome of the reaction resembles that of P$_4$ with other organic or p-block element-based nucleophiles.[630] A bicyclo[1.1.0]tetraphosphabutanide anion with a “butterfly” structure is obtained, which has been trapped by the Lewis acid, generating a metalphosphido-borane interaction. **1043** can be protonated at its nucleophilic P site, with loss of the borane, to yield metal-substituted η^1-P$_4$H ligands, though these decompose within 24 h.

Wolf and co-workers reported the formation of a tetraphosphacyclobutadiene (P$_4^{2-}$) ligand, as well as P$_4$ chains coordinated to iron centers.[631] Reduction of [Cp^{R}Fe(μ-Br)]$_2$ (**1045**, Cp^R = C$_5$(C$_6$H$_4$-4-Et)$_5$) with potassium naphtalenide (KC$_{10}$H$_8$, 4 equiv), followed by addition of P$_4$ (2 equiv), afforded the *cyclo*-P$_4$ compound [{Cp^{R}Fe(η^4-*cyclo*-P$_4$)}]$^-$ (**1046**, Figure 24). In the solid state, this anion forms a contact ion pair with the [K([18]crown-6)]$^+$ cation. DFT calculations performed on a truncated model confirmed that, in **1046**, an iron center in a d^6 configuration is coordinated to a delocalized planar *cyclo*-P$_4$ unit. By contrast, reduction of **1045** with an excess of sodium amalgam in the presence of P$_4$ yielded the highly air sensitive catenated species [Na$_2$(thf)$_5$-{(Cp^{R}Fe)$_2$(μ,$\eta^{4:4}$-P$_4$)}] (**1047**, Figure 24). While **1047** is readily protonated by Et$_3$N·HCl, [H(Et$_2$O)$_2$][BAr$^F{}_4$], or trace amounts of water, even simple dissolution of the complex in THF slowly results in decomposition to give the protonated ferrate [Na(thf)$_3${(Cp^{R}Fe)$_2$(μ,$\eta^{4:4}$-P$_4$)(H)}] (**1048**, Figure 24). Reactions of **1047** with suitable electrophiles, such as an excess of Me$_3$SiCl, resulted in the functionalization of P$_4$ chains with release of the functionalized polyphosphido fragments from the metal center (mixture of P$_7$(SiMe$_3$)$_3$, P(SiMe$_3$)$_3$, and PH(SiMe$_3$)$_2$ in a 10:1:1 ratio).

Heterobimetallic complexes with highly reduced P$_4$ ligands, derived from iron and cobalt metalates, were reported in 2020 by Wolf, Weigand and co-workers.[632] The metalates [M(η^4-C$_{14}$H$_{10}$)$_2$]$^-$ [M = Fe (**52**); Co (**14**)] reacted with the gallium tetraphosphido species [(nacnac)Ga(κ^2-P$_4$)] (**1049**, nacnac = CH[CMeN(2,6-*i*Pr$_2$C$_6$H$_3$)]$_2$), which contains an activated (butterfly) P$_4$ unit.[633] The strategy afforded the heterobimetallic complexes [(η^4-C$_{14}$H$_{10}$)M(μ−κ^4:κ^2-P$_4$)Ga(nacnac)]$^-$ [M = Fe (**1050**), Co (**1051**); Figure 24]. These compounds contain a bridging *catena*-P$_4$ ligand in which the transition metal centers are coordinated to the four phosphorus atoms, and the gallium center only coordinates the two terminal P atoms of the open chain. The reaction of cobaltate **14** with an excess of **1049** did not result in the substitution of both anthracene ligands, affording only **1051**.

Notably, an early, related example of reaction between a ferrate complex and white phosphorus was reported for the heteroleptic metalate [K([18]crown-6){Cp*Fe(η^4-C$_{10}$H$_8$)}] (**201**).[218] By treating **201** with white phosphorus, a metal-mediated fragmentation-reaggregation of the P$_4$ tetrahedron occurs, and two major products are isolated after fractional crystallization: the anionic cluster [K([18]crown-6)(thf)$_2$]-[(Cp*Fe)$_3$(P$_3$)$_2$] (**1052**, Figure 24) and the mononuclear complex [{K([18]crown-6)}$_2$(Cp*FeP$_7$)] (**1053**, Figure 24). Compound **1053** is the product of aggregation of white phosphorus, and showcases a P$_7$ norbornadiene-like framework, whereas in cluster **1052** the fragmentation of P$_4$ leads to two *cyclo*-P$_3$ scaffolds binding three Cp*Fe units.

A related contribution by Driess and co-workers reported the fragmentation of P$_4$ at a low-valent β-diketiminato-iron(I) complex, [(nacnac)Fe·toluene] (**1054**, nacnac = CH[CHN-(2,6-*i*Pr$_2$C$_6$H$_3$)]$_2$).[634] The selective cleavage of the P$_4$ tetrahedron at **1054** afforded the neutral iron(III) compound [{(nacnac)Fe}$_2$(μ_2:η^2,η^2-P$_2$)$_2$] (**1055**, see Figure 24), bearing two bridging dumbbell P$_2^{2-}$ ligands. Reduction of **1055** by metallic potassium afforded the rare mixed-valence iron(II,III) anion [{(nacnac)Fe}$_2$(μ_2:η^2,η^2-P$_2$)$_2$]$^-$ (**1056**), isostructural with **1055**. DFT calculations along with Mössbauer spectroscopic studies support a delocalized mixed-valent configuration for the iron centers.[634]

3.4.3. P$_4$ Activation Mediated by Cobaltates.

A summary of the products of P$_4$ activation at low-valent cobalt complexes, reported up to late 2020,[151,624−626] is illustrated in Figure 25. Several examples involve the use of diimine/diketimine ligand scaffolds.[385,387,635] For instance, both the highly reduced cobaltate [K(OEt$_2$)$_2${Co($^{\mathrm{Dipp}}$BIAN)(η^4-1,5-cod)}] (**540**) and the analogous complex [K([18]crown-6)(thf)$_{1.5}$][Co(PHDI)(η^4-1,5-cod)] (**542**; Scheme 65, above) were suitable platforms to activate white phosphorus. These complexes reduced P$_4$ to *cyclo*-P$_4$ moieties with different oxidation states.[385,387] **540** reacted with P$_4$ to yield the dianionic complex [{($^{\mathrm{Dipp}}$BIAN)Co}$_2$(μ-η^4:η^4-P$_4$)]$^{2-}$ (**1057**).[385] X-ray diffraction analysis on **1057** revealed that the P$_4$ unit in this complex is best described as a superposition of two mesomeric structures consisting of two P$_2^{2-}$ dumbbell units and a P$_4^{4-}$ motif. Oxidation of compound **1057** by [Cp$_2$Fe]BAr$^F{}_4$ resulted in monoanionic and neutral tetraphosphido complexes to complete the series [{($^{\mathrm{Dipp}}$BIAN)Co}$_2$(μ-η^4:η^4-P$_4$)]$^{n-}$ [n = 2 (**1057**), n = 1 (**1058**), n = 0 (**1059**); Figure 25 shows only the dianionic species **1057**], which feature

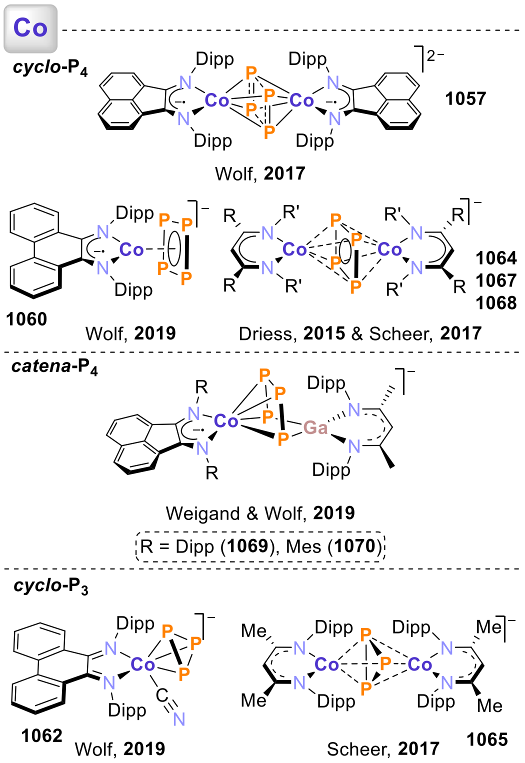

Figure 25. Complexes obtained by activation of white phosphorus at low-valent cobalt compounds.

either cyclic P_4^{4-} units or open-chain P_4^{4-} ligands. Thus, the oxidation process, and the strength of the interaction with the potassium counterion, impact the structure rather than the oxidation state of the polyphosphorus ligand. The presence of the redox-active BIAN ligand appears crucial to achieve a high degree of reduction of the P_4 units.

By contrast, P_4 activation by the cobaltate **542** results in a mononuclear complex $[(\mathrm{PHDI})\mathrm{Co}(\eta^4\text{-}P_4)]^-$ (**1060**, Figure 25).[387] Structural authentication for complex **1060** and metric parameters of the P_4 ligand were obtained through the adduct $[\mathrm{K}([18]\mathrm{crown\text{-}6})][(\mathrm{PHDI})\mathrm{Co}(\mu^2{:}\eta^1,\eta^4\text{-}P_4)\mathrm{W(CO)}_5]$ (**1061**). The almost perfectly square *cyclo*-P_4^{2-} unit observed in the molecular structure is best described as featuring six delocalized π-electrons. The bond lengths of the motif lie between the values expected for P−P single and P═P double bonds (av. 2.147(7) Å). Selective functionalization of the *cyclo*-P_4 ring in complex **1060** with diorganochlorophosphanes resulted in the quantitative formation of the corresponding neutral ring-expansion η^4-*cyclo*-P_5R_2 products. The latter species react with cyanide salts (2 equiv) to fragment the *cyclo*-P_5R_2 into P_3 and P_2 units, namely the anionic (*cyclo*-P_3)cobaltate complex $[(\mathrm{PHDI})\mathrm{Co(CN)}(cyclo\text{-}P_3)]^-$ (**1062**, Figure 25) and a series of 1-cyanodiphosphan-1-ide anions.

A similar planar *cyclo*-P_4 unit and a *cyclo*-P_3 complex were obtained by activation of P_4 at the formal dicobalt(0) complex $[\mathrm{K}_2\{(\mathrm{nacnac})\mathrm{Co}\}_2(\mu_2{:}\eta^1,\eta^1\text{-}N_2)]$ (**1063**, nacnac = $\mathrm{CH[CMeN(2,6\text{-}Me_2C_6H_3)]_2}$).[635] The products were the monoanionic compounds $[\{(\mathrm{nacnac})\mathrm{Co}\}_2(\mu_2{:}\eta^4,\eta^4\text{-}P_4)]^-$ (**1064**) and $[\{(\mathrm{nacnac})\mathrm{Co}\}_2(\mu_2{:}\eta^3,\eta^3\text{-}P_3)]^-$ (**1065**). Extrusion of a P atom from the P_4 ligand of **1064** leads to the constitution of the *cyclo*-P_3 motif observed in **1065**. **1064** can also be accessed by reduction of its neutral congener, $[\{(\mathrm{nacnac})\mathrm{Co}\}_2(\mu_2{:}\eta^4,\eta^4\text{-}P_4)]$ (**1066**), prepared from a suitable Co(I) precursor. Analogously, thermally induced extrusion of a P atom from **1066** yields the neutral congener of **1065**. Magnetic measurements (Evans method and SQUID) indicated that **1064** is a mixed-valent $\mathrm{Co^I{-}Co^{II}}$ species, while in **1065** the *cyclo*-P_3^{3-} unit bridges two Co(II) centers.[635] Driess and co-workers described the synthesis of further examples of cobalt complexes featuring *cyclo*-P_4^{2-} motifs, similar to **1064**. The two-step procedure first involves the activation of P_4 at Co(I) precursors featuring related diketimine ligands (nacnac = $\mathrm{CH[CHN(2,6\text{-}}i\mathrm{Pr_2C_6H_3)]_2}$ or $\mathrm{CH[CMeN(2,6\text{-}Et_2C_6H_3)]_2}$), to generate analogous dinuclear cobalt compounds with a neutral tetraphosphacyclobutadiene bridging ligand. The latter species were then reduced by $\mathrm{KC_8}$ to afford $[\{(\mathrm{nacnac})\mathrm{Co}\}_2(\mu_2{:}\eta^4,\eta^4\text{-}P_4)]^-$ (**1067**/**1068**).[636] Figure 25 shows the generic structure of complexes **1064**, **1067** and **1068** and the structure of compound **1065**.

The complexes $[\mathrm{K(OEt_2)}\{\mathrm{Co}(^{\mathrm{Ar}}\mathrm{BIAN})(\eta^4\text{-}1,5\text{-cod})\}]$ [$^{\mathrm{Ar}}$BIAN = $^{\mathrm{Dipp}}$BIAN (**540**), $^{\mathrm{Mes}}$BIAN (**541**)] were treated with $[(\mathrm{nacnac})\mathrm{Ga}(\kappa^2\text{-}P_4)]$ (**1049**) by a synthetic protocol similar to that which yielded $[(\eta^4\text{-}C_{14}H_{10})\mathrm{M}(\mu\text{-}\eta^4{:}\kappa^2\text{-}P_4)\mathrm{Ga(nacnac)}]^-$ [M = Fe (**1050**), Co (**1051**); Figure 25, *vide supra*].[386,632] This procedure afforded the heterodinuclear cobalt−gallium compounds $[\mathrm{K(dme)_2}\{(^{\mathrm{Ar}}\mathrm{BIAN})\mathrm{Co}(\mu\text{-}\eta^4{:}\kappa^2\text{-}P_4)\mathrm{Ga(nacnac)}\}]$ [$^{\mathrm{Ar}}$BIAN = $^{\mathrm{Dipp}}$BIAN (**1069**), $^{\mathrm{Mes}}$BIAN (bis(mesitylimino)acenaphthenediimine) (**1070**)], featuring *catena*-P_4 ligands. Reactivity studies performed on **1070** showed that these complexes can be functionalized with alkylchlorophosphanes ($R_n\mathrm{PCl}_{3-n}$) to afford polyphosphorus *cyclo*-P_5R_2 compounds. In the case of the dialkylchlorophosphanes $R_2\mathrm{PCl}_2$ (R = *i*Pr, Cy, and *t*Bu) the functionalization is accompanied by release of the Ga(nacnac) fragment.

Since late 2020,[151,427,477,624−626] further reports on the activation of P_4 by low-valent cobalt complexes have appeared. As previously mentioned, Hey-Hawkins, Wolf, and co-workers, described the reactions of the bis(phosphide)carborane complex $[\mathrm{K}([18]\mathrm{crown\text{-}6})(\mathrm{thf})][\mathrm{Co}\{1,2\text{-}(\mathrm{PMes})_2\mathrm{C_2B_{10}H_{10}}\}(\eta^4\text{-cod})]$ (*rac*-**330**) with cyclohexyl isocyanide (Cy-N≡C) and *tert*-butylphosphaalkyne (*t*Bu-C≡P), which afford the 16 VE bis(isocyanide) and diphosphacyclobutadiene complexes *rac*-**333** and *rac*-**334**, via ligand substitution (Scheme 42; section 2.2.6.2, *vide supra*).[134] The reactivity of *rac*-**330** toward white phosphorus was also evaluated. Depending on the *rac*-**330**:P_4 ratio used, two distinct products were obtained (Scheme 151). A 1:1 reaction afforded complex $[\mathrm{K}([18]\mathrm{crown\text{-}6})][meso\text{-}\mathbf{1071}]$ (Scheme 151), resulting from the fragmentation of the P_4 tetrahedron into P_3 and P_1 motifs.[134] This behavior contrasts, for example, with the formation of *cyclo*-P_4 rings at the similar anionic species $[\mathrm{Co}(^{\mathrm{Dipp}}\mathrm{BIAN})(\eta^4\text{-}1,5\text{-cod})]^-$ (**540**) or $[\mathrm{Co(PHDI)}(\eta^4\text{-}1,5\text{-cod})]^-$ (**542**), bearing nitrogen-chelates.[385,387]

Scheme 151. White Phosphorus Activation at Complex $[\mathrm{K}([18]\mathrm{crown\text{-}6})(\mathrm{thf})][\mathrm{Co}\{1,2\text{-}(\mathrm{PMes})_2\mathrm{C_2B_{10}H_{10}}\}(\eta^4\text{-cod})]$ (*rac*-330; Cations Are Omitted for Clarity)[134]

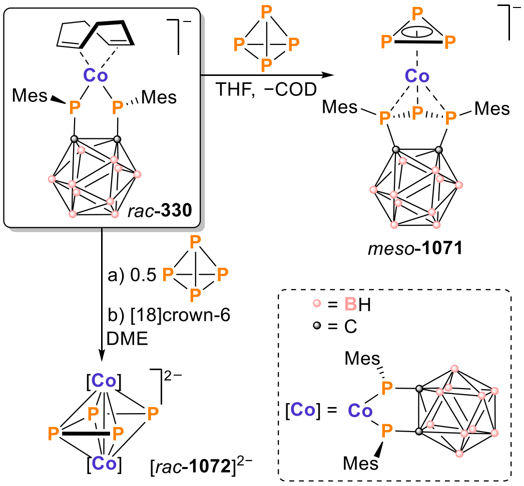

The Co(I) complex $[meso\text{-}\mathbf{1071}]^-$ is a 18 VE species containing a *cyclo*-P_3 and a η^3-triphospholanido ligand, probably resulting from intramolecular abstraction of a P^+ fragment by the nucleophilic phosphanido moieties. Theoretical calculations provided a detailed explanation on the coordination and inner-sphere fragmentation of the P_4 molecule at *rac*-**330**, and support the proposed abstraction by the phosphanido ligand. In contrast, by using a 2:1 *rac*-**330**:P_4 ratio and adding [18]crown-6, the reaction product is a bimetallic complex, $[\mathrm{K}([18]\mathrm{crown\text{-}6})]_2[rac\text{-}\mathbf{1072}]$ (Scheme 151), bearing a bridging *catena*-P_4 ligand, $\mu{-}\eta^4{:}\eta^4\text{-}P_4^{2-}$, i.e., a cis-1,3-tetraphosphabutadienediide motif. The short intermetallic distance (2.651(1) Å) indicates the presence of a Co−Co single bond. BS-DFT calculations revealed that $[rac\text{-}\mathbf{1072}]^{2-}$ contains two low-spin $3d^7$ Co(II) atoms, which are antiferromagnetically coupled via one of the terminal P atoms of the P_4^{2-} chain. By means of time-resolved $^{31}\mathrm{P}\{^1\mathrm{H}\}$ NMR spectroscopic monitoring, it was established that $[rac\text{-}\mathbf{1072}]^{2-}$ results from the reaction of $[meso\text{-}\mathbf{1071}]^-$ with a

https://doi.org/10.1021/acs.chemrev.3c00121
Chem. Rev. 2024, 124, 1323−1463

second equivalent of the bis(phosphanido)cobaltate *rac*-**330**.[134]

Wolf and co-workers studied the activation of P_4 by a heteroleptic magnesium cobaltate sandwich complex.[427] Treatment of [(^{Dep}nacnac)MgCo($P_2C_2tBu_2$)(η^4-cod)] (**688**, *vide supra*) with white phosphorus (P_4) in toluene (75 °C, 18 h) led to the formation of the *cyclo*-P_4 sandwich complex [(^{Dep}nacnac)MgCo(*cyclo*-P_4)($P_2C_2tBu_2$)]$_2$ (**1073**, Scheme 152) via substitution of the 1,5-cyclooctadiene ligand.

Scheme 152. Synthesis of a Cyclo-P_4 Heteroleptic Sandwich Complex from a Magnesium Cobaltate[427]

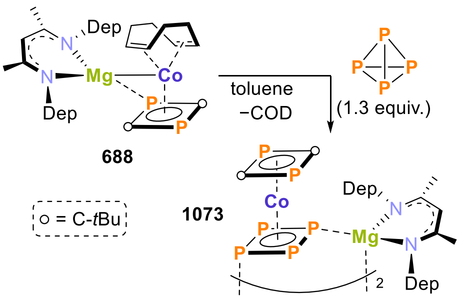

The solid-state structure shows that each magnesium moiety is coordinatively saturated by binding to a P atom of each *cyclo*-P_4 unit, with no interaction between the magnesium and cobalt centers. Two of the P−P bond lengths of the *cyclo*-P_4 unit are slightly longer (P1−P2/P1−P4 distances, 2.2083(5)/2.2184(5) Å, respectively) than the other two (P3−P2/P3−P4 2.1641(5)/2.1740(5) Å, respectively). The *cyclo*-P_4 ligand is similar to the other examples reported with metals such as iron or cobalt.[151] However, the phosphorus rich compound **1073** represents the first example of an anionic cobaltate sandwich compound featuring a *cyclo*-P_4 ligand, according to the authors.[427]

Heavy tetraphospholide anions formed at heterometallic cobaltates were later reported by the same group.[477] These were obtained when the complexes [Ar^{Dipp2}TtCo($P_2C_2tBu_2$)(η^4-cod)] [Tt = Ge (**693**), Sn (**694**), Pb (**695**)] and Sn[Co($P_2C_2tBu_2$)(η^4-cod)]$_2$ (**696**) (Scheme 82, *vide supra*) reacted with white phosphorus. While reaction between the germanium derivative and white phosphorus was unsuccessful even upon heating, analogous treatment of the tin compounds **694** or **696** with P_4 afforded the triple decker compound [($P_2C_2tBu_2$)$_2$Co$_2$(μ,η^5:η^5-SnP_4)] (**1074**, Scheme 153) in each case. Using **696** proved to be more efficient, yielding **1074** in a more selective manner. Likewise, **695** reacted with P_4 to the corresponding lead complex [($P_2C_2tBu_2$)$_2$Co$_2$(μ,η^5:η^5-PbP_4)] (**1075**). The latter can also be accessed in a one-pot reaction between the magnesium cobaltate **688**, Pb(acac)$_2$ and P_4. However, the product in this case is obtained with (^{Dep}nacnac)Mg(acac) (**1076**) as a contaminant.

In both cases, the triple decker complexes feature a planar *cyclo*-TtP_4 middle deck, as evidenced through the X-ray characterization. The lead derivative, though, resulted unstable at room temperature, depositing metallic lead, and forming a different triple decker compound, namely the *cyclo*-P_4 complex [($P_2C_2tBu_2$)$_2$Co$_2$(μ,η^4:η^4-P_4)] (**1077**). The combined structural and calculated data indicate that the heavy tetraphospholide anions TtP_4^{2-}, analogous to the known *cyclo*-P_5 ligand P_5^-, possess a planar structure with almost identical P−P bond lengths, and therefore are aromatic. According to IBO analyses on the TtP_4^{2-} ring (TPSS D3BJ/def2-SVP level) the delocalized π-system involves the Tt, P1/P3, P2/P4 centers, and its interaction with the transition metal atoms corresponds to a typical π-coordination.[477]

Scheme 153. Formation of Heavy Tetraphospholide Anions by Reaction of Heterometallic Cobaltates with White Phosphorus[477]

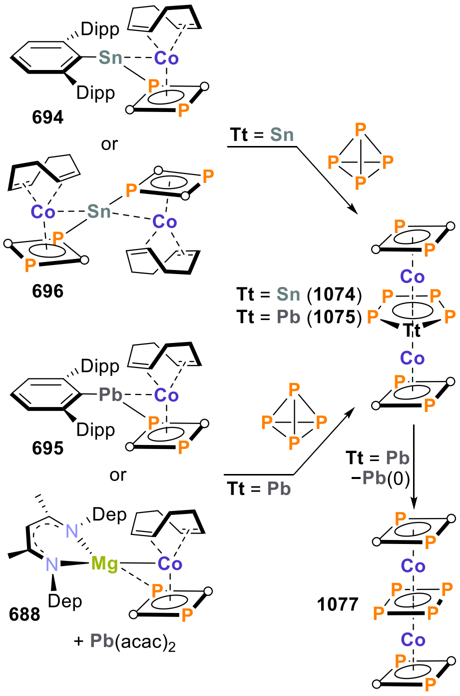

3.4.4. P_4 Activation by Molybdenum and Tungsten Complexes.

Anionic polyphosphido complexes based on 4d/5d metals have also been described. For instance, Figueroa and co-workers described the synthesis of low-valent Mo-isocyanide complexes featuring η^4-end-deck *cyclo*-P_4 ligands (Figure 26).[151,637,638] The neutral compounds (η^4-*cyclo*-P_4)MoI$_2$(CO)(CNAr^{Dipp2})$_2$ [**1078**, Dipp = 2,6-(iPr)$_2$C$_6$H$_3$]

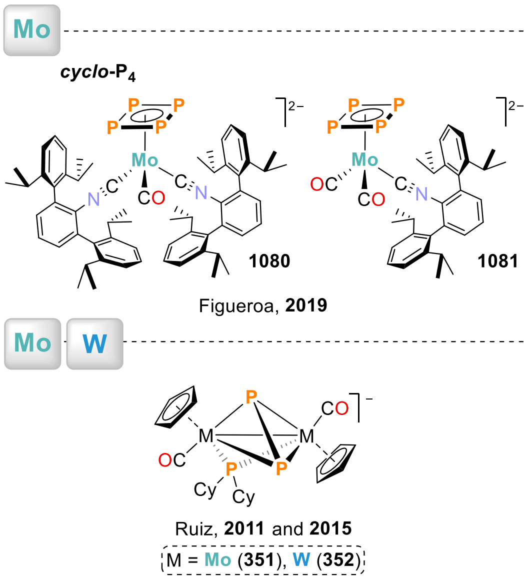

Figure 26. 4d and 5d metalates featuring polyphosphido ligands.

Scheme 154. Synthesis of Homoleptic 1,3-Diphosphacyclobutadiene Sandwich Complexes (Top) And Follow-up Chemistry to Yield Either Substituted 1,3-Diphosphacyclobutadiene Ligands (Middle and Bottom Right) or 1,3-Diphosphacyclobutene Derivatives (Bottom Left-Center)[210,211a]

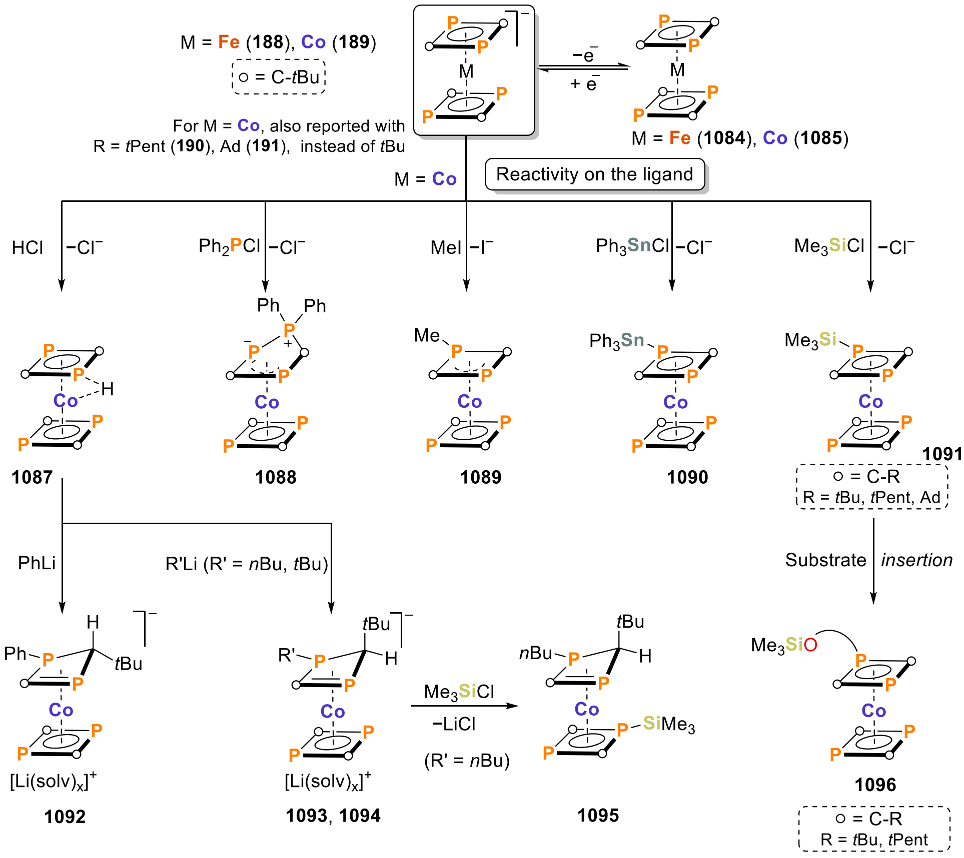

[a]O-based substrate = ethers, epoxides, lactones, aldehydes, ketones, isocyanates.

and $(\eta^4$-*cyclo*-$P_4)Mo(CO)_2(CNAr^{Dipp2})_2$ (**1079**) were obtained by activation of the P_4 at isocyanide-Mo precursors.[638] These complexes bear the six π-electron [*cyclo*-$P_4]^{2-}$ dianion ligand. To further investigate the nature of the aromatic [*cyclo*-$P_4]^{2-}$ ligand, the bonding situation of the complexes and the influence of the formal oxidation state of the metal on the ligand, the reduction of the complexes **1078** and **1079** was studied. The Mo(IV) (d^2) compound **1078** was treated with an excess KC_8, followed by addition of dibenzo[18]crown-6, to give the low-valent complex $\{K_2$(dibenzo[18]crown-6)$\}[(\eta^4$-*cyclo*-$P_4)Mo(CO)(CNAr^{Dipp2})_2]$ (K_2[**1080**]) after four-electron reduction. The collective characterization data (^{31}P NMR, FT-IR, X-ray diffraction) suggested that the *cyclo*-P_4 ligand remained unaltered after reduction and indicated that the three-legged piano stool complex has a highly reduced metal center, forming a contact ion pair between the Mo-anion and potassium cations.

Similar reduction of complex **1079** with KC_8 (excess) afforded a mixture of complex **1080** and the dicarbonyl compound $K_2[(\eta^4$-*cyclo*-$P_4)Mo(CO)_2(CNAr^{Dipp2})]$ (**1081**). Upon reduction, compound **1079** loses either one CO ligand to afford complex **1080** or one isocyanide ligand yielding **1081**. By treating **1080** with CO (1 atm), the complex was fully converted to **1081**. Again, the *cyclo*-P_4 motif in **1081** has a common electronic structure with **1080** or the parent compounds **1078** and **1079**, according to the metric parameters. Furthermore, the increased electron density in **1081** is also evidenced, as it was for **1080**. The experimental data and computational calculations support the formulation of both complexes as including aromatic [*cyclo*-$P_4]^{2-}$ dianions bound to zerovalent metal fragments.[637]

As mentioned in section 2.2.6.4, Ruiz and co-workers reported that the triply bonded anions $[M_2(\eta^5\text{-}Cp)_2(\mu\text{-}PCy_2)(\mu\text{-}CO)_2]^-$ [M = Mo (**358**), W (**359**); *vide supra*] activate white phosphorus under mild conditions to afford the anionic diphosphorus complexes $[M_2Cp_2(\mu\text{-}PCy_2)(CO)_2(\mu\text{-}\kappa^2{:}\kappa^2\text{-}P_2)]^-$ [M = Mo (**351**), W (**352**), see Figure 26).[304,639] The molybdenum analogue features a Mo_2P_2 tetrahedral core with the P_2 unit bridging the two metal centers. The tungsten analogue could not be isolated due to its extreme air-sensitivity, but indirect structural proof was obtained through characterization of the methylated derivative $[W_2Cp_2(\mu\text{-}PCy_2)(CO)_2(\mu\text{-}\kappa^2{:}\kappa^2\text{-}P_2Me)]$ (**354**).

3.5. Reactions of Transition Metalates with Unsaturated Organophosphorus Compounds

3.5.1. Metalate-Mediated Phosphaalkyne Oligomerization.

The metal-mediated cyclodimerization of phosphaalkynes constitutes a useful route to access π-coordinated diphosphacyclobutadiene ligands.[640] Early examples of the application of this strategy include the synthesis of complexes $[Cp^RM(P_2C_2tBu_2)]$ (**1082**, M = Co, Rh, Ir; Cp^R = Cp, Cp*), featuring η^4-coordinated 1,3-diphosphacyclobutadiene ligands,[641−643] some Ti(0), Mo(0) and Fe(0) species,[644−649] and the first example of a homoleptic bis(1,3-diphosphacyclobutadiene) complex, the neutral $[Ni(P_2C_2tBu_2)_2]$

Scheme 155. Chemistry of the Anionic Complexes $[Co(\eta^4\text{-}P_2C_2R_2)_2]^-$ (189−191) toward Coinage Metals: Assembly of Oligonuclear Complexes through σ-Coordination[212,654−656]

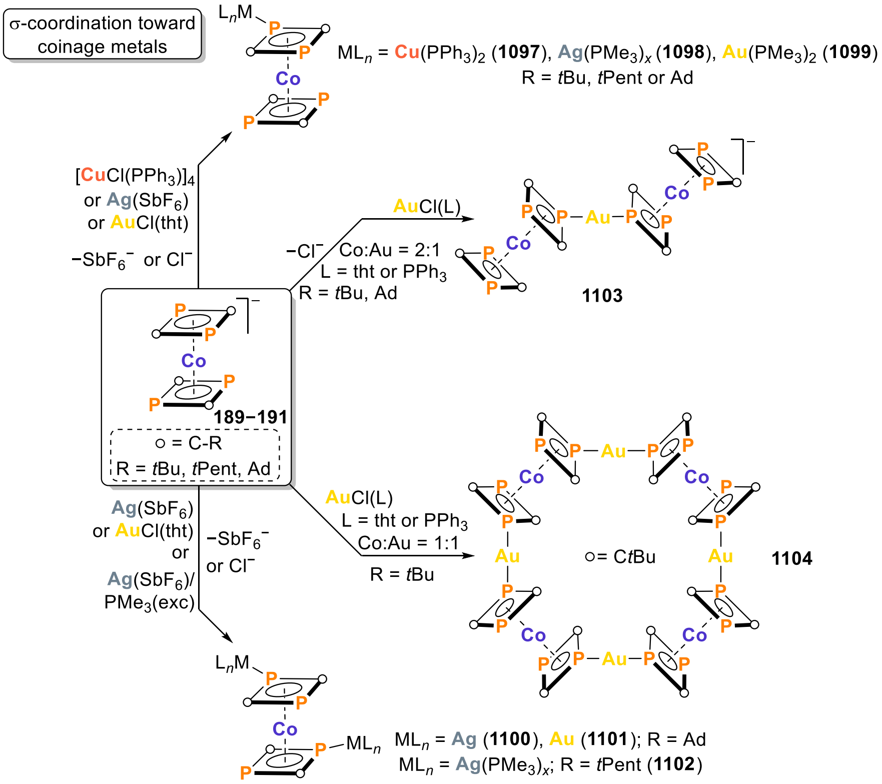

(1083).[650,651] The steric hindrance on the carbon atom of the parent phosphaalkyne determines whether the 1,2- or 1,3-diphosphacyclobutadiene ligand is obtained, with bulky substituents kinetically favoring the 1,3-isomer.[640]

In this context, Wolf and co-workers examined the reactions of phosphaalkynes RC≡P (R = tBu, Ad, tPent) with the labile bis(anthracene)metalate(−I) [M = Fe (**52**); Co (**14**)] complexes.[87,210,211] The homoleptic diphosphacyclobutadiene complexes $[M(\eta^4\text{-}P_2C_2R_2)_2]^-$ [M = Fe, R = tBu (**188**), M = Co, R = tBu (**189**), tPent (**190**), Ad (**191**); Scheme 22, *vide supra*] were isolated, characterized, and their reactivity extensively evaluated (Scheme 154).[87,210,211] As in the case of the parent metalates $[M(\eta^4\text{-}C_{14}H_{10})_2]^-$ [M = Fe (**52**); Co (**14**)], the iron compound **188** is more prone to oxidation than the cobalt analogue **189**.[475] Cyclic voltammetry studies revealed that upon oxidation of the anionic complexes, the neutral species $[M(P_2C_2tBu_2)_2]$ [M = Fe (**1084**), Co (**1085**)] can be obtained, and the process is reversible. The M(0) compounds were isolated by oxidation of the anionic complexes with ferrocenium hexafluorophosphate, $[Cp_2Fe]PF_6$ (Scheme 154).[213,475] **1084** is a phosphorus analogue of the elusive sandwich bis(η^4-cyclobutadiene)iron(0). According to calculations carried out for the simplified diamagnetic 18-electron dianion $[Fe(P_2C_2Me_2)_2]^{2-}$ (**1086′**), further reduction of complex **188** is theoretically viable.[211] Nonetheless, all attempts to further reduce **188** to form the dianion $[Fe(P_2C_2tBu_2)_2]^{2-}$ (**1086**) were unsuccessful. The latter species was not observed by cyclic voltammetry, nor could it be prepared by using strong reducing agents such as potassium graphite or potassium naphthalenide.

3.5.2. Reactivity of Diphosphacyclobutadiene Cobaltates and Ferrates.

Further reactivity studies on the chemistry of **189** afforded a range of functionalized complexes and demonstrated its ability to act as a versatile building block for phosphaorganometallic species. For instance, reaction with electrophiles (see Scheme 154, center) allows for the functionalization of the ligand through one of its phosphorus atoms. Using this methodology, the cobalt hydride complex $[Co(P_2C_2tBu_2)_2H]$ (**1087**) and the ring-expansion product $[Co(P_3C_2tBu_2Ph_2)(P_2C_2tBu_2)]$ (**1088**) were obtained.[210] Compound **189** reacted with MeI, ClSnPh$_3$ or Me$_3$SiCl to afford the corresponding P-substituted ligands, thus forming the neutral complexes $[Co(P_2C_2tBu_2R)(P_2C_2tBu_2)]$ [R = Me (**1089**), SnPh$_3$ (**1090**), SiMe$_3$ (**1091**)]. The hydride complex **1087** reacts with lithium organyls (R′Li, R′ = Ph, nBu, tBu) to generate rare 1,3-diphosphacyclobutene complexes [R′ = Ph (**1092**), nBu (**1093**), tBu (**1094**); Scheme 154, bottom left-center]. Reaction of the anionic complex **1093** with Me$_3$SiCl led to the quantitative formation of $[Co(\eta^3\text{-}P_2C_2tBu_2HnBu)(\eta^4\text{-}P_2C_2tBu_2SiMe_3)]$ (**1095**), in which both P_2C_2 rings have been functionalized.[652] In addition, oxygen-containing substrates (ethers, epoxides, lactones, aldehydes, ketones or isocyanates) insert into the Si−P bond of the silyl-derivative **1091**, thereby generating new P−O bonds (**1096**, Scheme 154, bottom right).[653]

The phosphorus atom on the diphosphacyclobutadiene ligands of **189**−**191** can further coordinate other metal centers, acting as metalloligands, to obtain oligonuclear complexes. This type of chemistry is of significance in catalysis and supramolecular chemistry. When the homoleptic complexes **189**−**191** were treated with metal salts from groups 8−11, different types of interactions were identified.[212,654−656] The expected σ-coordination of metal cations from group 11 (M = Cu, Ag, Au) to the cobaltates **189**−**191** as metalloligands (Scheme 155, top), afforded the series of neutral dinuclear compounds $[Co(\eta^4\text{-}P_2C_2R_2ML_n)(\eta^4\text{-}P_2C_2R_2)]$ [R = tBu, tPent,

Scheme 156. Reactivity of 189 and 191 toward Metal Precursors from Groups 8−10

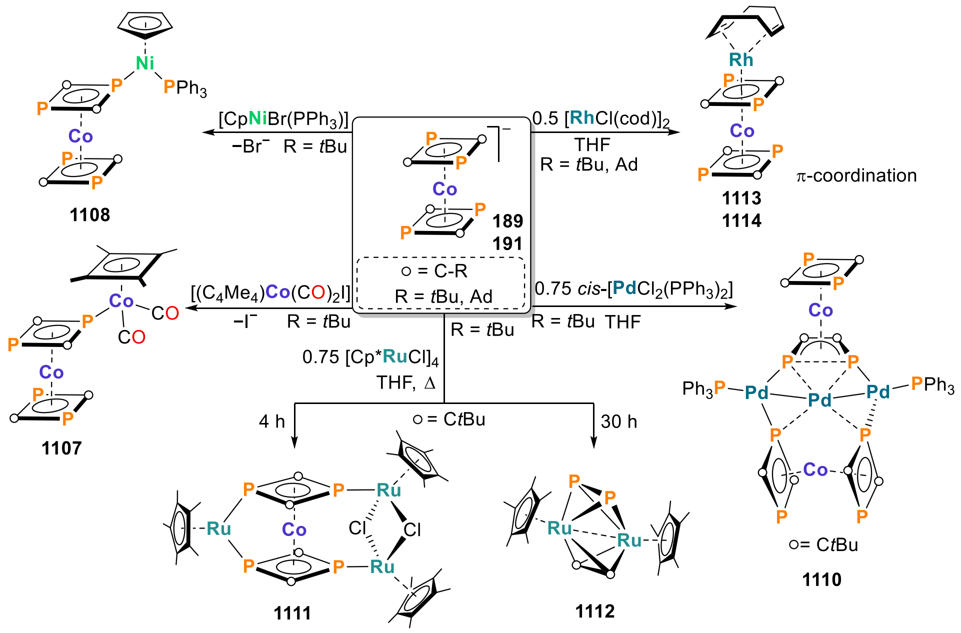

Ad; ML$_n$ = Cu(PPh$_3$)$_2$ (**1097**), Ag(PMe$_3$)$_x$ (**1098**), Au(PMe$_3$)$_2$ (**1099**)].[654,655]

Furthermore, the phosphorus atom of the diphosphacyclobutadiene units of **190** or **191** served as a platform for the synthesis of $[M\{Co(\eta^4\text{-}P_2C_2Ad_2)_2\}]_x$ [M = Ag (**1100**); M = Au (**1101**)], which exist as coordination polymers in the solid state, and of the trinuclear complexes $[Co\{\eta^4\text{-}P_2C_2tPent_2[Ag(PMe_3)_x]\}_2]$ (**1102**) or $[Au\{Co(\eta^4\text{-}P_2C_2R_2)_2\}_2]^-$ [R = *t*Bu, Ad (**1103**)], shown in Scheme 155. This type of complex showcases phosphorus atoms of at least one of the diphosphacyclobutadiene ligands σ-bonded to coinage metals, or connecting two sandwich motifs as in **1103**.[212] It was thereby demonstrated that the coordination of the phosphaorganometallic ligand can occur through more than one of its phosphorus atoms.[654,655] Being able to functionalize multiple phosphorus atoms on **189** was also crucial in the self-assembly of the unprecedented octanuclear molecular square $[Au\{Co(\eta^4\text{-}P_2C_2tBu_2)_2\}]_4$ (**1104**, Scheme 155), an example of a metallosupramolecular compound which can be obtained from different gold precursors in the presence of 4 equiv of anion **189**.[656]

The flexidentate coordination behavior of **189** or **191** was demonstrated with group 8−10 metals (Scheme 156).[476,657] Coordination studies showed that the diphosphacyclobutadiene moiety of **189** also acts as a σ-donor ligand toward the cobalt(I) or nickel(II) complexes $(C_4Me_4)CoI(CO)_2$ (**1105**) or CpNiBr(PPh$_3$) (**1106**) to afford $[Co(\eta^4\text{-}P_2C_2tBu_2ML_n)(\eta^4\text{-}P_2C_2R_2)]$ [ML$_n$ = $(C_4Me_4)Co(CO)_2$ (**1107**)] and $[Co(\eta^4\text{-}P_2C_2tBu_2ML_n)(\eta^4\text{-}P_2C_2R_2)]$ [ML$_n$ = CpNi(PPh$_3$) (**1108**) (Scheme 156, left).[657] The latter two complexes are analogous to the coinage metal derivatives **1097**−**1099** mentioned above.[654,655] However, whereas simple σ-coordination of a P atom occurs in any of these cases, cobaltates **189** or **191** engage in rearrangement, insertion and fragmentation reactions toward other transition metal complexes, thereby creating new oligonuclear compounds with unprecedented structures.[476]

In section 2.3.2, the formation of diphosphanickelacyclopentadiene ligands via insertion of Ni fragments into intact 1,3-diphosphacyclobutadiene moieties was discussed (*vide supra*). Complex **189** and the heteroleptic sandwich complex **688** behave similarly toward Ni fragments, yielding the aforementioned diphospha-nickelacyclopentadiene motifs (Scheme 81b, *vide supra*). Compounds **689** and **692** constitute, to the best of our knowledge, the sole examples of such insertion into diphosphacyclobutadiene ligands.[427,476]

Likewise, upon reaction of **189** with the palladium(II) precursor *cis*-[PdCl$_2$(PPh$_3$)$_2$] (**1109**), the diphosphacyclobutadiene ligand of one molecule of cobaltate **189** is transformed to generate compound $[Pd_3(PPh_3)_2\{Co(\eta^4\text{-}1,3\text{-}P_2C_2tBu_2)_2\}_2]$ (**1110**, Scheme 156, bottom right). The resulting motif constitutes a rare 1,4-diphospha-2-butene ligand, proposed to have formed by isomerization of a 1,3-diphosphabutadiene unit to the 1,2-isomer, followed by activation of the resulting P−P bond at the central palladium center. This P−P bond is weakened, as observed from the crystallographic metric parameters of **1110** (P−P = 2.401(1) Å). Compound **1110** is a pentanuclear complex, with a chain of three palladium atoms. The central palladium atom completes its coordination environment with the phosphorus atoms of the isomerized diphosphacyclobutadiene unit, and with a chelating molecule of cobaltate **189** (Scheme 156).

Compound **189** also behaves as a chelate toward ruthenium, as identified by reaction with the halide cluster, [Cp*RuCl]$_4$ (**230**, Scheme 156, bottom). The product is the tetranuclear complex **1111**, in which every phosphorus atom in the homoleptic cobaltate is coordinated to ruthenium centers through σ-bonds. This coordination mode necessitates adoption of an eclipsed conformation by the diphosphacyclobutadiene sandwich compound. Prolonged reaction of the cobaltate **189** with the ruthenium cluster **230** caused the $P_2C_2tBu_2$ ligand to fragment, in a process possibly involving the chelating tetranuclear complex **1111**, to generate the dinuclear ruthenium-"P_2C_2" species **1112**. Finally, reactions of the Rh(I) dimer [RhCl(cod)]$_2$ (**401**) with cobaltate **189** or **191**, demonstrated π-coordination of the 1,3-$P_2C_2tBu_2$ unit. The products, complexes $[Rh(cod)\{Co(P_2C_2R_2)_2\}]$ [R = *t*Bu (**1113**), Ad (**1114**); Scheme 156, upper right), present bridging $\mu,\eta^4{:}\eta^4$ diphosphacyclobutadiene ligands. The reactivity of the π-bound complexes toward additional phosphaalkyne substrate suggested that the synthesis of a genuine triple-decker complex might be feasible in the case of the adamantyl derivative.[476]

3.5.3. Reactivity of Di-*tert*-butyldiphosphatetrahedrane toward Metalates.

Diphosphacyclobutadiene complexes were also obtained from reactions of a phosphaalkyne dimer, di-*tert*-butyldiphosphatetrahedrane, $(t\mathrm{BuCP})_2$ (**1115**) with various metalates.[658] Compound **1115**, reported by Wolf and co-workers in 2019, was obtained by nickel catalyzed dimerization of the corresponding phosphaalkyne monomer.[659] The reactivity of the diphosphatetrahedrane toward $[\mathrm{Fe}(\eta^4\text{-}\mathrm{C}_{14}\mathrm{H}_{10})_2]^-$ (**52**, the $[\mathrm{K}([18]\mathrm{crown}\text{-}6)]^+$ salt), cobaltate $[\mathrm{Co}(\eta^4\text{-cod})_2]^-$ (**239**),[7] or complexes $[(^{\mathrm{Dipp}}\mathrm{BIAN})\mathrm{M}(\eta^4\text{-cod})]^-$ [M = Fe (**537**), Co (**540**)] was investigated (Scheme 157). The reaction between **52** and **1115** afforded the heteroleptic compound $[\mathrm{K}([18]\mathrm{crown}\text{-}6)][\mathrm{Fe}(1,2\text{-}t\mathrm{Bu}_2\mathrm{C}_2\mathrm{P}_2)(\eta^4\text{-}\mathrm{C}_{14}\mathrm{H}_{10})]$ (**1116**), featuring a rare 1,2-diphosphacyclobutadiene ligand (Scheme 157a). Similar treatment of **239** with $(t\mathrm{BuCP})_2$ furnished, instead, a mixture of compounds, of which the major product was characterized as the homoleptic 1,2-diphosphacyclobutadiene-containing complex $[\mathrm{K}([18]\mathrm{crown}\text{-}6)(1,4\text{-dioxane})_4][\mathrm{Co}(1,2\text{-}t\mathrm{Bu}_2\mathrm{C}_2\mathrm{P}_2)_2]$ (**1117**) and the minor species corresponds to the known 1,3-isomer $[\mathrm{Co}(1,3\text{-}\mathrm{P}_2\mathrm{C}_2t\mathrm{Bu}_2)_2]^-$ (**189**, see Scheme 157b).[210] The observed reactivity indicates that the diphosphatetrahedrane $(t\mathrm{BuCP})_2$ serves as a precursor to the rare 1,2-$t\mathrm{Bu}_2\mathrm{C}_2\mathrm{P}_2$ ligand, as opposed to the 1,3-isomer which generally results from head-to-tail cyclodimerization of the parent phosphaalkyne $t\mathrm{BuC{\equiv}P}$.

Scheme 157. Reactivity of Di-*tert*-butyldiphosphatetrahedrane toward Different Metalates[658,659]

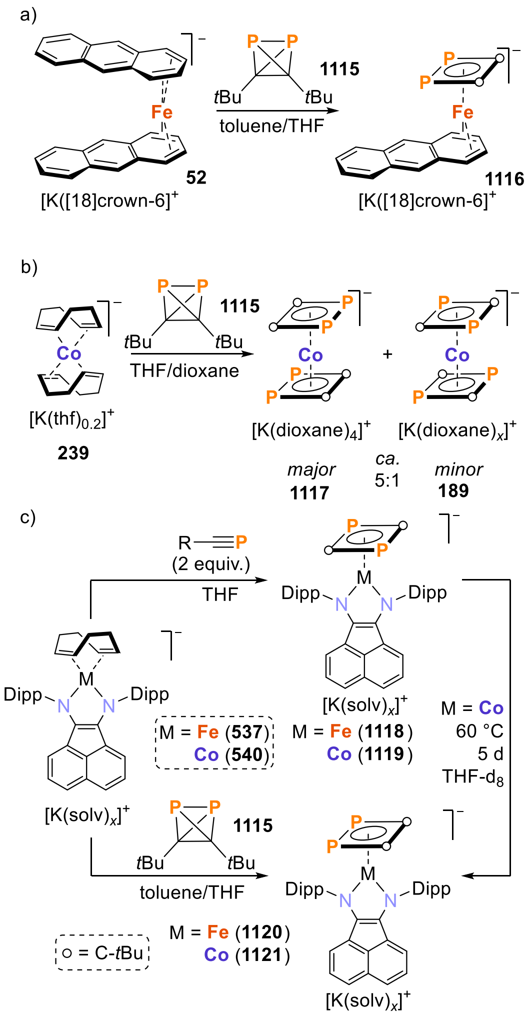

The 1,2-diphosphacyclobutadiene ligands are, therefore, the result of P−C bond cleavage in the $\mathrm{C}_2\mathrm{P}_2$ tetrahedron of **1115**. To confirm this hypothesis, the diiminometalates $[(^{\mathrm{Dipp}}\mathrm{BIAN})\mathrm{M}(\eta^4\text{-cod})]^-$ [M = Fe (**537**), Co (**540**)] were independently treated with $t\mathrm{BuC{\equiv}P}$ (2 equiv) or with **1115** (1 equiv) (see Scheme 157c). As in the case of the homoleptic alkene/arene metalates, the interaction between $[(^{\mathrm{Dipp}}\mathrm{BIAN})\mathrm{M}(\eta^4\text{-cod})]^-$ and $t\mathrm{BuC{\equiv}P}$ yielded the terminal 1,3-diphosphacyclobutadiene complexes $[(^{\mathrm{Dipp}}\mathrm{BIAN})\mathrm{M}(1,3\text{-}\mathrm{P}_2\mathrm{C}_2t\mathrm{Bu}_2)]^-$ [M = Fe (**1118**), Co (**1119**)], while reactions of the metalates with the diphosphatetrahedrane molecule generated the 1,2-isomers $[(^{\mathrm{Dipp}}\mathrm{BIAN})\mathrm{M}(1,2\text{-}t\mathrm{Bu}_2\mathrm{C}_2\mathrm{P}_2)]^-$ [M = Fe (**1120**), Co (**1121**)]. After prolonged heating (60 °C, THF-d_8, 5 d), compound **1119** isomerizes to **1121**. Comparative reactivity studies were performed on the BIAN cobaltate complexes, to gain insights into the reactivity of these isomeric ligands.[658]

Clear differences were observed after reaction with electrophiles: While treatment of the 1,3-isomer **1119** with HCl, $\mathrm{Me}_3\mathrm{SiCl}$ or $\mathrm{Cy}_2\mathrm{PCl}$ afforded mainly the dimeric compound $[(^{\mathrm{Dipp}}\mathrm{BIAN})\mathrm{Co}(\mu\text{-Cl})]_2$ (**1122**), compound **1121** reacted with these electrophiles to yield a bridged 1,2-diphosphacyclobutadiene dinuclear complex, $[\{(^{\mathrm{Dipp}}\mathrm{BIAN})\mathrm{Co}\}_2(\mu,\eta^4{:}\eta^4\text{-}1,2\text{-}\mathrm{P}_2\mathrm{C}_2t\mathrm{Bu}_2)]$ (**1123**, see Scheme 158, top). Furthermore, it was also possible to obtain a product of ring expansion from **1121** and $\mathrm{Cy}_2\mathrm{PCl}$ (Scheme 158, bottom), which led to the isolation of the neutral $[(^{\mathrm{Dipp}}\mathrm{BIAN})\mathrm{Co}(\eta^4\text{-}\mathrm{P}_3\mathrm{C}_2t\mathrm{Bu}_2\mathrm{Cy}_2)]$ (**1124**) and confirms the synthetic utility of the 1,2-diphosphacyclobutadiene moiety. In the case of the 1,3-isomer **1119**, analogous treatment with $\mathrm{Cy}_2\mathrm{PCl}$ resulted in an unselective reaction. For all the BIAN-containing metalates, the characterization data indicate the presence of dianionic

Scheme 158. Initial Reactivity Studies of a Coordinated 1,2-Diphosphacyclobutadiene Ligand[658]

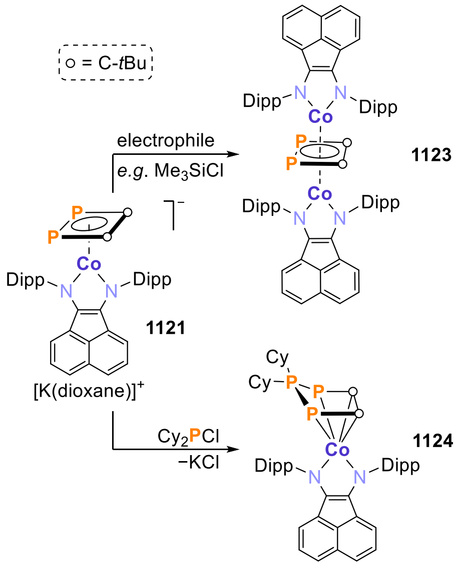

$BIAN^{2-}$ ligands, with bonding best described as between the two possible extreme electronic cases: neutral π-accepting P_2C_2tBu$_2$ ligands with low-spin M(I) centers, or dianionic π-donating P_2C_2tBu$_2$ ligands at low-spin M(III) centers.[658]

4. SUMMARY AND OUTLOOK

The chemistry of low-valent transition metalates has developed tremendously over the last one and a half decades. Previously, metalates stabilized by carbonyl, alkene and arene ligands were principally known, while research efforts focused on the synthesis, characterization, and only basic reactivity of new types of metalates. Early work in the area revealed the high synthetic utility of carbonylate anions as nucleophiles in organic chemistry and as synthons for the preparation of oligonuclear transition metal carbonyl compounds. Furthermore, it was shown that alkene and arene metalates containing labile alkene or arene ligands may serve as powerful "sources of transition metal anions" (J. E. Ellis), which enable the synthesis of a large variety of low oxidation-state transition metal complexes. This pioneering work laid the foundation for recent advances in metalate chemistry, by intimating that the high reactivity of these complexes could be applied in a broader spectrum of synthesis, and even catalysis.

To date, the chemistry of the transition metal carbonylate anions continues to fascinate as the field is revisited with more sophisticated spectroscopic and structural techniques, enabling the remaining "gaps" in the field to be closed—as exemplified by Korber's characterization of the tricarbonyl nickelate $[Ni(CO)_3]^{2-}$ (**26**). Likewise, the development of bulky isocyanide ligands by Figueroa has enabled the isolation of complexes with unique coordination environments and unusual reactivities (as demonstrated, for example, by the recent characterization of the fluoroborylene-iron complex **67** and the P_2-iron complex **73**).

In comparison with the well-established carbonyl and isocyanide complexes, alkene and polyarene ligands in metalates are usually much more labile. As a result, alkene and arene metalates are potent reagents—by serving as precursors, a wide range of organometallic complexes have become accessible. In addition, metalates acting as sources of metal atoms to generate unique heterobimetallic clusters have opened another highly important avenue of investigation in the field (e.g., compounds **236**, **237**, and **242**).

While the synthesis of alkene, arene and carbonyl metalates is relatively well-explored, metalates with sophisticated new architectures have been prepared by introducing carbon-, nitrogen- and phosphorus-based ligands. The variety of metalates stabilized by carbenes, phosphines, amides, and imines is simply astonishing. Indeed, much of the recent progress in the field is due to advances in ligand design, which offers precise control over the coordination and electronic properties of the metal atom. This has also provided ligand scaffolds which, through their flexibility, can adapt to support metal centers as they engage in further reactivity, illustrated by the varying hapticity of phosphinine ligands in complexes **308**, **309**, and **311–316**. The development of sophisticated metalates stabilized by tailored ligands translates into ever more successful applications in small molecule activation and catalysis. For instance, the P_3^B ligand, featured in complexes **718–728**, has been demonstrated to continue its stabilization of an iron center as it undergoes a series of oxidation state changes enforced by activation of small molecules, by altering its coordination mode. In addition, interesting molecular properties which offer specialized applications, such as magnetic anisotropy, can be incorporated into new complexes.

The significant influence of ion-pairing effects on the stability and reactivity of metalates was largely neglected until recently. However, there are a growing number of examples showing that the countercation (usually an alkali or alkaline earth metal cation) substantially influences their reactivity and catalytic properties. In particular, ion-pairing interactions are crucial for stabilizing highly charged metalate anions and enable unusual coordination geometries (e.g., in the hydride complexes **706–716**).

Furthermore, the interaction of transition metal atoms with Lewis acidic p-block elements (e.g., Al and Ga) and the synthesis of bimetallic transition metalates are successful recent strategies for tuning the electronic properties and the reactivity of metalate anions. A range of binuclear metalate anions has been developed by the groups of Peters and Lu, which are very effective in N_2 functionalization and CO_2 reduction chemistry.

Indeed, the development of reactive low-oxidation state metalate anions that efficiently and selectively transform small inorganic molecules such as H_2, CO, CO_2, N_2, and P_4 is arguably the most striking advance in the field. Prior to the period covered in this review, the potential of metalates in these areas had largely been overlooked. Moreover, the importance of metalate anions as key catalytic intermediates has become increasingly clear, and the number of catalytic transformations in which they are implicated has grown rapidly. Catalytic applications include cross-couplings, isomerizations, hydrogenations and dehydrogenations as well as CO_2 and N_2 reductions. The electron-rich nature of transition metalates is a key asset for the success of these applications.

Considering the impressive depth and the large variety of the metalate chemistry, it seems a reasonable assessment that the field is approaching maturity. Nevertheless, further exciting developments can be expected building on the results described in this review.

What is next for the field?

Although "it is very difficult to predict—especially the future" (Niels Bohr), we wish to conclude this article with a short outlook highlighting some possible future developments in the area:

1) **Synthesis of metalates.** While their molecular design has become increasingly sophisticated, the synthetic routes employed have remained limited to classical approaches (see Figure 1 in section 1), most commonly the reduction of suitable precursor compounds with a strong reducing reagent such as KC_8. New innovative synthesis techniques (e.g., ball milling) might enable more selective reactions and give access to previously unknown metalate species. The continued improvement of experimental and theoretical characterization techniques will also provide greater understanding of the fundamental nature of new classes of metalates, as they emerge.

2) **Small molecule activation.** The ability of highly reduced metalate complexes to mediate challenging transformations of unreactive molecules will continue to be of prime interest. Increasingly sophisticated ligand design should enable more effective and selective transformations.

3) **Homogeneous catalysis.** The potential of low-valent metalates in homogeneous catalysis is increasingly being

realized. In particular, metalates have much potential in reductive catalysis, e.g. in hydrogenations and (as the reverse reaction) dehydrogenations. Surprisingly, to the best of our knowledge there are no applications of metalate anions in asymmetric catalysis; this is likely an area of interest in the future. Reported insights into the mechanistic minutiae surrounding metalate-mediated transformations will also permit greater rational design in the synthesis of metalate complexes intended to act as effective precatalysts.

4) **Ion-pairing effects and metal−metal bonding.** Recent studies have revealed the crucial influence of ion-pairing on the reactivity of metalate anions. In the future, the interaction of metalates with Lewis acidic metal cations should be studied in more detail to delineate the characteristics of ion-pairing in such species. Using these interactions, the reactivity of metalates can be tuned, which will have an impact on the development of catalytic processes.

5) **Synthesis of new metal clusters and inorganic materials.** The use of metalates as metal atom sources for metal clusters and heterometallic materials is still in its infancy. However, this strategy will become increasingly important in the future and might eventually be used to introduce transition metal atoms into molecular materials. Furthermore, some low-coordinate metalates show very interesting magnetic properties, e.g., magnetic anisotropy and slow magnetic relaxation, which are naturally essential for the design of magnetic materials.

So far, the chemistry of low-valent transition metalates has mainly been of fundamental academic interest. However, considering the plethora of significant developments described in this review, it seems very likely that many new applications of metalate anions will appear in diverse contexts. It is the aim of this review to enlighten and inspire future researchers to develop new applications of these fascinating and often highly reactive species. Based on the impressive, rapid advancement of the field over the last 15 years, the future of transition metalate chemistry looks very bright!

AUTHOR INFORMATION

Corresponding Authors

Vanessa R. Landaeta − *University of Regensburg, Institute of Inorganic Chemistry, 93040 Regensburg, Germany;* Present Address: Istituto di Chimica dei Composti Organometallici, Consiglio Nazionale delle Ricerche (ICCOM-CNR). Via Madonna del Piano 10, 50019 Sesto Fiorentino (Italy); orcid.org/0000-0002-8009-7337; Email: Vanessa.Landaeta@ur.de

Robert Wolf − *University of Regensburg, Institute of Inorganic Chemistry, 93040 Regensburg, Germany;* orcid.org/0000-0003-4066-6483; Email: robert.wolf@ur.de

Author

Thomas M. Horsley Downie − *University of Regensburg, Institute of Inorganic Chemistry, 93040 Regensburg, Germany;* orcid.org/0000-0001-5027-450X

Complete contact information is available at:
https://pubs.acs.org/10.1021/acs.chemrev.3c00121

Author Contributions

V.R.L. and R.W. developed the concept. V.R.L. gathered the data and wrote the original draft. R.W. conceived and supervised the project and acquired funding. T.M.H.D. edited and revised the draft. All authors have given approval to the final version of the manuscript. CRediT: **Vanessa R. Landaeta** conceptualization, data curation, writing-original draft, writing-review & editing; **Thomas M. Horsley Downie** writing-review & editing; **Robert Wolf** conceptualization, funding acquisition, supervision, writing-review & editing.

Notes

The authors declare no competing financial interest.

Biographies

Vanessa R. Landaeta graduated in chemistry from Universidad Simón Bolívar, Caracas (Venezuela) and received her doctoral degree from the Instituto Venezolano de Investigaciones Científicas (IVIC). After postdoctoral Marie Curie research training in the Consiglio Nazionale delle Ricerche (Italy), she started her independent research career at Universidad Simón Bolívar, where she subsequently became full professor. After a period as guest researcher with AntonioTogni (ETH Zurich, Switzerland), she joined the Wolf group in Regensburg from 2020 to 2023 as a postdoctoral researcher. Currently, she is a researcher at the Istituto di Chimica dei Composti Organometallici (ICCOM-CNR) in Florence, Italy. Her research interests include inorganic/organometallic chemistry, ligand design, and homogeneous catalysis.

Thomas M. Horsley Downie received his MChem (Hons) in Chemistry from Newcastle University (UK) in 2017. Undertaking his PhD at the University of Bath (UK) under the supervision of Dr. David Liptrot, he completed his thesis in 2021 on the chemistry of copper(I) complexes with main group functionalities. Since 2022, he has conducted postdoctoral research in the group of Prof. Robert Wolf at the University of Regensburg (Germany), developing methods for the functionalization of white phosphorus. His research interests include main group chemistry, small molecule activation, and organometallic synthesis and catalysis.

Robert Wolf started his research career at the University of Cambridge, UK, under the guidance of Dominic S. Wright. He was awarded a PhD from Leipzig University for work in phosphorus chemistry supervised by Evamarie Hey-Hawkins. After postdoctoral research with Philip P. Power (UC Davis, USA) and Koop Lammertsma (VU Amsterdam, The Netherlands), he started his independent career at University of Münster (mentor: Werner Uhl). He became Professor of Inorganic Chemistry at the University of Regensburg in 2011, where he was recently promoted to a chair. His research interests lie at the crossroads of low-oxidation state transition metal chemistry, homogeneous (photo)catalysis, and phosphorus chemistry.

ACKNOWLEDGMENTS

We thank Rafael E. Rodríguez-Lugo and Gábor Balász (both University of Regensburg, Germany) for their invaluable support in the preparation of this manuscript. Joshua S. Figueroa (UC San Diego, USA), C. Gunnar Werncke (University of Marburg, Germany), and the anomymous referees are thanked for their numerous helpful comments. R.W. gratefully acknowledges financial support by the European Research Council (ERC CoG 772299) and the Deutsche Forschungsgemeinschaft (DFG, RTG IonPairs in *Re-*

Action project 426795949, and WO1496/9-2) for research activities in transition metalate chemistry.

DEDICATION

This paper is dedicated to John E. Ellis (University of Minnesota, USA), a pioneer in transition metalate chemistry, on the occasion of his retirement.

ABBREVIATIONS

AB = ammonia borane (NH_3BH_3)
acac = acetylacetonate
Ad = adamantyl
AE = alkaline earth
AltraPhos = $Al[N\{o\text{-}(NCH_2P\mathit{i}Pr_2)C_6H_4\}_3]$
AM = alkali metal
anthr = anthracene
Ar = aryl
Ar^{DArF2} = 2,6-bis[3,5-bis(trifluoromethyl)phenyl]-4-fluorophenyl
Ar^{Dipp2} = 2,6-bis(2,6-diisopropylphenyl)phenyl
Ar^{Mes2} = 2,6-bis(2,4,6-trimethylphenyl)phenyl
Ar^{Tripp2} = 2,4,6-tris(2,6-diisopropylphenyl)phenyl
$BAr^F{}_4$ = tetrakis[(3,5-bis(trifluoromethyl)phenyl]borate
Bcat = boronic acid catechol ester
bda = benzylideneacetone
BDFE = bond dissociation free energy
^{Dipp}BIAN = 1,2-bis(2,6-diisopropylphenylimino)-acenaphthene
^{Mes}BIAN = 1,2-bis(2,4,6-dimethylphenylimino)-acenaphthene
BINC = (bis(2-isocyanophenyl)phenylphosphonate)
bp = benzophenone
bpa = bis(2-picolyl)amine
^{Dipp}BPDI = $2,6\text{-}(2,6\text{-}\mathit{i}Pr_2{-}C_6H_3N{=}CPh)_2C_5H_3N$
bpy = 2,2′-bipyridine
BS-DFT = broken symmetry DFT
BTMSA = bis(trimethylsilyl)acetylene
CAAC = cyclic(alkyl)(amino)carbene
CASSCF = complete active space self-consistent field
CHD = cyclohexadiene
CKphos = 1-((3aR,8aR)-2,2-dimethyl-4,4,8,8-tetrakis-(perfluorophenyl)tetrahydro-[1,3]dioxolo[4,5-*e*] [1,3,2]-dioxaphosphepin-6-yl)pyrrolidine
$CNAr_3NC$ = 2,2′′-diisocyano-3,5,3′′,5′′-tetramethyl-1,1′:3′,1′′-terphenyl
cod = 1,5-cyclooctadiene
CODH = carbon monoxide dehydrogenase
Cp = cyclopentadienyl
Cp* = pentamethylcyclopentadienyl
Cp‴ = $\eta^5\text{-}C_5H_2\text{-}1,2,4\text{-}\mathit{t}Bu_3$
CP MAS NMR = cross-polarization magic angle spinning NMR
[2.2.2]cryptand = $N(CH_2CH_2OCH_2CH_2OCH_2CH_2)_3N$
CV = cyclic voltammetry
Cy = cyclohexyl
dach = 1,2-diaminocyclohexane
dad = 1,4-diazabutadiene
dae = 1,2-diaminoethylene
dap = 1,3-diaminopropane
DBU = 1,8-diazabicyclo [5.4.0] undec-7-ene
dct = dibenzo[*a*,*e*]cyclooctatetraene
Dep = (2,6-diethyl)phenyl
DFT = density functional theory
DHC = dehydrocoupling
Dipp = (2,6-diisopropyl)phenyl
DMAB = dimethylaminoborane (Me_2NHBH_3)
DMAP = *p*-dimethylaminopyridine
^{Dipp2}dmdad = *N*,*N*′-bis(2,6-diisopropylphenyl)butane-2,3-diimine
dme = dimethoxyethane
dmf = dimethylformamide
dmpe = 1,2-bis(dimethylphosphino)ethane
dppe = 1,2-bis(diphenylphosphino)ethane
dvtms = divinyltetramethyldisiloxane
en = ethylenediamine
ENDOR = electron nuclear double resonance
EPR = electron paramagnetic resonance
ESI = electrospray ionization
Et = ethyl
EXAFS = extended X-ray absorption fine structure
EXSY = exchange spectroscopy
Fc = ferrocene
FT-IR = Fourier-transform infrared
HAT = hydrogen atom transfer
HBpin = pinacolborane
HERFD-XANES = high-energy-resolution fluorescence-detected XANES
HMPA = hexamethylphosphoramide
HOMO = highest-occupied molecular orbital
IBO = intrinsic bond orbital
ICy = 1,3-dicyclohexylimidazol-2-ylidene
$IMAr^{Mes2}$ = 5-(Ar^{Mes2}-imino)furanone
IMes = 1,3-bis(2,4,6-trimethylphenyl)imidazol-2-ylidene
ipa = iminopropenamide
IPr = 1,3-bis(2,6-diisopropylphenyl)imidazol-2-ylidene
*i*Pr = isopropyl
IR-SEC = infrared spectroelectrochemistry
L^{Dipp} = 1,3-bis(2,6-diisopropylphenyl)imidazol-2-ylidene
LIFDI-MS = liquid injection field desorption mass spectrometry
Me = methyl
Me_2dad = 1,4-dimethyl-diazabuta-1,3-diene, 2-MeTHF, 2-methyltetrahydrofuran
Mes = mesityl (1,3,5-trimethylphenyl)
mesbpy = 6,6′-dimesityl-2,2′-bipyridine
MesIm = 1-mesitylimidazol-2-ylidene
MLC = metal−ligand cooperation
MO = molecular orbital
MS = mass spectrometry
nacnac = $CH[C(\mathit{t}Bu)N(2,6\text{-}\mathit{i}Pr_2C_6H_3)]_2$
^{Ar}nacnac = $CH(ArNCMe)_2$
^{Dipp}nacnac = $HC\{C(Me)N(2,6\text{-}C_6H_3\mathit{i}Pr_2)\}_2$
^{Me3}nacnac = $MeC[C(\mathit{t}Bu)N(2,6\text{-}\mathit{i}Pr_2C_6H_3)]_2$
nbd = norbornadiene
NBO = natural bond orbital
*n*Bu = *n*-butyl
NHC = *N*-heterocylic carbene
NMP = *N*-methylpyrrolidone
NMR = nuclear magnetic resonance
NON = 4,5-bis(2,6-diisopropylanilido)-2,7-di-*tert*-butyl-9,9-dimethylxanthene
OTf = triflate; trifluoromethanesulfonate
$P_2{}^P$ = $PhP(o\text{-}\mathit{i}Pr_2PC_6H_4)_2$
$P_3{}^B$ = tris[2-(diisopropylphosphino)phenyl]borane
$P_3{}^C$ = tris[2-(diisopropylphosphino)phenyl]methyl

$P^{iPr}{}_{3}{}^{Si}$ = tris[2-(diisopropylphosphino)phenyl]silyl
$P^{Ph}{}_{3}{}^{Si}$ = tris[2-(diphenylphosphino)phenyl]silyl
PCP = 2,6-(CH_2PtBu_2)$_2$-1-yl-C_6H_3
PDI = pyridine-diimine
Ph = phenyl
$PhP_2{}^{B}$ = PhB(*o*-*i*Pr$_2$PC_6H_4)$_2$
PHDI = bis(2,6-diisopropylphenyl)phenanthrene-9,10-diimine)
PMDETA = *N*,*N*,*N*′,*N*″,*N*″-pentamethyldiethylenetriamine
PN^{triazine}P = 2,6-bis(P*i*Pr$_2$NH)-4-Ph-triazine
py = pyridyl
QTAIM = quantum theory of atoms in molecules
R* = 2,4,6-*t*Bu$_3$-C_6H_2
r.t. = room temperature
SEM = scanning electron microscopy
SOMO = singly occupied molecular orbital
*t*bpy = 4,4′-di-*tert*-butyl-2,2′-bipyridine
*t*Bu = *tert*-butyl
*t*BuIm = 1-*tert*-butylimidazol-2-ylidene
TEM = transmission electron microscopy
TFA = trifluoroacetate
TFE = 2,2,2-trifluoroethanol
thf = tetrahydrofuran
TM = transition metal
TMEDA = 1,2-bis(dimethylamino)ethane
tol = tolyl
TolNCNTol = di(*p*-tolyl)carbodiimide
*t*Pent = *tert*-pentyl
tpdp = 1,4-bis(2-(diisopropylphosphino)phenyl)benzene
TPP = 2,4,6-triphenylphosphinine
tpy = 2,2’:6′,2”-terpyridine
trop = 5H-dibenzo[*a*,*d*]cyclohepten-5-yl
trop$_2$NH = bis(5Hdibenzo[*a*,*d*]cyclohepten-5-yl)amine
Tt = tetrel
VE = valence electron
VtCXES = valence-to-core X-ray emission spectroscopy
XANES = X-ray absorption near-edge structure spectroscopy
XPS = X-ray photoelectron spectroscopy
Xyl = xylyl (2,6-dimethylphenyl)

REFERENCES

(1) Ellis, J. E. Metal Carbonyl Anions: From $[Fe(CO)_4]^{2-}$ to $[Hf(CO)_6]^{2-}$ and Beyond. *Organometallics* **2003**, *22*, 3322−3338.

(2) Ellis, J. E. Adventures with Substances Containing Metals in Negative Oxidation States. *Inorg. Chem.* **2006**, *45*, 3167−3186.

(3) Ellis, J. E. The Chatt Reaction: Conventional Routes to Homoleptic Arenemetalates of d-Block Elements. *Dalton Trans.* **2019**, *48*, 9538−9563.

(4) Wilke, G. Neues über cyclische Butadien-Oligomere. *Angew. Chem.* **1960**, *72*, 581−582.

(5) Bogdanović, B.; Kröner, M.; Wilke, G. Übergangsmetallkomplexe, I. Olefin-Komplexe des Nickels(0). *Justus Liebigs Ann. Chem.* **1966**, *699*, 1−23.

(6) Fischer, K.; Jonas, K.; Wilke, G. Tris(ethylene)nickel(0). *Angew. Chem., Int. Ed. Engl.* **1973**, *12*, 565−566.

(7) Jonas, K.; Mynott, R.; Krüger, C.; Sekutowski, J. C.; Tsay, Y.-H. Bis(*η*-1,5-cyclooctadiene)cobaltlithium. *Angew. Chem., Int. Ed. Engl.* **1976**, *15*, 767−768.

(8) Jonas, K.; Schieferstein, L.; Krüger, C.; Tsay, Y.-H. Tetrakis(ethylene)irondilithium and Bis(η^4-1,5-cyclooctadiene)irondilithium. *Angew. Chem., Int. Ed. Engl.* **1979**, *18*, 550−551.

(9) Jonas, K. New findings in the arene chemistry of the 3d transition metals. *Pure Appl. Chem.* **1990**, *62*, 1169−1174.

(10) Werncke, C. G. *Very Low Oxidation States in Organometallic Chemistry*, In Comprehensive Organometallic Chemistry IV; Parkin, G., Meyer, K., O'Hare, D. B., Eds.; Elsevier: Oxford, 2022, 61−108.

(11) Ouellette, E. T.; Magdalenski, J. S.; Bergman, R. G.; Arnold, J. Applications of Low-Valent Transition Metalates: Development of a Reactive Noncarbonyl Rhenium(I) Anion. *Acc. Chem. Res.* **2022**, *55*, 783−793.

(12) Collman, J. P.; Finke, R. G.; Cawse, J. N.; Brauman, J. I. Oxidative-Addition Reactions of the $Na_2Fe(CO)_4$ Supernucleophile. *J. Am. Chem. Soc.* **1977**, *99*, 2515−2526.

(13) Bock, P. L.; Boschetto, D. J.; Rasmussen, J. R.; Demers, J. P.; Whitesides, G. M. Stereochemistry of Reactions at Carbon-Transition Metal *σ* Bonds. $(CH_3)_3CCHDCHDFe(CO)_2C_5H_5$. *J. Am. Chem. Soc.* **1974**, *96*, 2814−2825.

(14) Theys, R. D.; Dudley, M. E.; Hossain, M. M. Recent Chemistry of the η^5-Cyclopentadienyl Dicarbonyl Iron Anion. *Coord. Chem. Rev.* **2009**, *253*, 180−234.

(15) Karen, P. Oxidation State, A Long-Standing Issue! *Angew. Chem., Int. Ed.* **2015**, *54*, 4716−4726.

(16) Chan, W. T. K.; Wong, W.-T. A Brief Introduction to Transition Metals in Unusual Oxidation States. *Polyhedron* **2013**, *52*, 43−61.

(17) Fortier, S.; Gomez-Torres, A. Redox Chemistry of Discrete Low-Valent Titanium Complexes and Low-Valent Titanium Synthons. *Chem. Commun.* **2021**, *57*, 10292−10316.

(18) Cong, X.; Zeng, X. Mechanistic Diversity of Low-Valent Chromium Catalysis: Cross-Coupling and Hydrofunctionalization. *Acc. Chem. Res.* **2021**, *54*, 2014−2026.

(19) Fürstner, A. Iron Catalysis in Organic Synthesis: A Critical Assessment of What It Takes To Make This Base Metal a Multitasking Champion. *ACS Cent. Sci.* **2016**, *2*, 778−789.

(20) McNeill, E.; Ritter, T. 1,4-Functionalization of 1,3-Dienes With Low-Valent Iron Catalysts. *Acc. Chem. Res.* **2015**, *48*, 2330−2343.

(21) Gómez-Suárez, A.; Nelson, D. J.; Nolan, S. P. Metallate Complexes of the Late Transition Metals: Organometallic Chemistry and Catalysis. In *Advances in Organometallic Chemistry*; Pérez, P. J., Ed.; Academic Press, 2018; Vol. *69*, pp 283−327.

(22) Werncke, C. G Synthesis, Properties, and Reactivity of Linear Open-Shell 3d-Metal(I) Complexes. In Encyclopedia of Inorganic and Bioinorganic Chemistry. 2023, Scott, R. A., Eds.; Wiley-VCH: Weinheim, 1−30.

(23) Magnoux, C.; Mills, D. P. Metallocene Anions: From Electrochemical Curiosities to Isolable Complexes. *Eur. J. Inorg. Chem.* **2022**, No. e202101063.

(24) Gao, K.; Yoshikai, N. Low-Valent Cobalt Catalysis: New Opportunities for C-H Functionalization. *Acc. Chem. Res.* **2014**, *47*, 1208−1219.

(25) Bera, S. S.; Szostak, M. Cobalt-N-Heterocyclic Carbene Complexes in Catalysis. *ACS Catal.* **2022**, *12*, 3111−3137.

(26) Cai, Y.; Jiang, S.; Dong, L.; Xu, X. Synthesis and Reactivity of Heterometallic Complexes Containing Mg- or Zn-Metalloligands. *Dalton Trans.* **2022**, *51*, 3817−3827.

(27) Chalkley, M. J.; Drover, M. W.; Peters, J. C. Catalytic N_2-to-NH_3(or -N_2H_4) Conversion by Well-Defined Molecular Coordination Complexes. *Chem. Rev.* **2020**, *120*, 5582−5636.

(28) Forrest, S. J. K.; Schluschaß, B.; Yuzik-Klimova, E. Y.; Schneider, S. Nitrogen Fixation via Splitting into Nitrido Complexes. *Chem. Rev.* **2021**, *121*, 6522−6587.

(29) Kim, S.; Loose, F.; Chirik, P. J. Beyond Ammonia: Nitrogen-Element Bond Forming Reactions with Coordinated Dinitrogen. *Chem. Rev.* **2020**, *120*, 5637−5681.

(30) Weber, J. E.; Bhutto, S. M.; Genoux, A. T.-Y.; Holland, P. L. Dinitrogen Binding and Functionalization. In *Comprehensive Organometallic Chemistry IV*; Parkin, G., Meyer, K., O'Hare, D. B., Eds.; Elsevier: Oxford, 2022; pp 521−554.

(31) Holland, P. L. Electronic Structure and Reactivity of Three-Coordinate Iron Complexes. *Acc. Chem. Res.* **2008**, *41*, 905−914.

(32) Cammarota, R. C.; Clouston, L. J.; Lu, C. C. Leveraging Molecular Metal-Support Interactions for H_2 and N_2 Activation. *Coord. Chem. Rev.* **2017**, *334*, 100−111.

(33) Pyykkö, P. Dirac-Fock One-Centre Calculations Part 8. The $^1\Sigma$ States of ScH, YH, LaH, AcH, TmH, LuH and LrH. *Phys. Scr.* **1979**, *20*, 647.

(34) Kaupp, M. The Role of Radial Nodes of Atomic Orbitals for Chemical Bonding and the Periodic Table. *J. Comput. Chem.* **2007**, *28*, 320−325.

(35) Korobkov, I.; Gambarotta, S.; Yap, G. P. A. The First Thorium Arene Complex: A Divalent Synthon. *Angew. Chem., Int. Ed.* **2003**, *42*, 814−818.

(36) Langeslay, R. R.; Fieser, M. E.; Ziller, J. W.; Furche, F.; Evans, W. J. Synthesis, Structure, and Reactivity of Crystalline Molecular Complexes of the $\{[C_5H_3(SiMe_3)_2]_3Th\}^{1-}$ Anion Containing Thorium in the Formal + 2 Oxidation State. *Chem. Sci.* **2015**, *6*, 517−521.

(37) Barluzzi, L.; Giblin, S. R.; Mansikkamäki, A.; Layfield, R. A. Identification of Oxidation State +1 in a Molecular Uranium Complex. *J. Am. Chem. Soc.* **2022**, *144*, 18229−18233.

(38) Murillo, J.; Bhowmick, R.; Harriman, K. L. M.; Gomez-Torres, A.; Wright, J.; Meulenberg, R. W.; Miró, P.; Metta-Magaña, A.; Murugesu, M.; Vlaisavljevich, B.; et al. Actinide Arene-Metalates: Ion Pairing Effects on the Electronic Structure of Unsupported Uranium-Arenide Sandwich Complexes. *Chem. Sci.* **2021**, *12*, 13360−13372.

(39) Murillo, J.; Bhowmick, R.; Harriman, K. L. M.; Gomez-Torres, A.; Wright, J.; Miro, P.; Metta-Magana, A. J. J.; Murugesu, M.; Vlaisavljevich, B.; Fortier, S. Actinide Arene-Metalates: 2. A Neutral Uranium Bis(Anthracenide) Sandwich Complex and Elucidation of Its Electronic Structure. *Chem. Commun.* **2022**, *58*, 9112−9115.

(40) Kelly, R. P.; Maron, L.; Scopelliti, R.; Mazzanti, M. Reduction of a Cerium(III) Siloxide Complex To Afford a Quadruple-Decker Arene-Bridged Cerium(II) Sandwich. *Angew. Chem., Int. Ed.* **2017**, *56*, 15663−15666.

(41) Moore, W. N. G.; Ziller, J. W.; Evans, W. J. Optimizing Alkali Metal (M) and Chelate (L) Combinations for the Synthesis and Stability of $[M(L)][(C_5H_4SiMe_3)_3Y]$ Yttrium(II) Complexes. *Organometallics* **2021**, *40*, 3170−3176.

(42) Willauer, A. R.; Fadaei-Tirani, F.; Zivkovic, I.; Sienkiewicz, A.; Mazzanti, M. Structure and Reactivity of Polynuclear Divalent Lanthanide Disiloxanediolate Complexes. *Inorg. Chem.* **2022**, *61*, 7436−7447.

(43) Kelly, R. P.; Toniolo, D.; Tirani, F. F.; Maron, L.; Mazzanti, M. A Tetranuclear Samarium(II) Inverse Sandwich from Direct Reduction of Toluene by a Samarium(II) Siloxide. *Chem. Commun.* **2018**, *54*, 10268−10271.

(44) Angadol, M. A.; Woen, D. H.; Windorff, C. J.; Ziller, J. W.; Evans, W. J. *tert*-Butyl(cyclopentadienyl) Ligands Will Stabilize Nontraditional +2 Rare-Earth Metal Ions. *Organometallics* **2019**, *38*, 1151−1158.

(45) Moehring, S. A.; Evans, W. J. Evaluating Electron Transfer Reactivity of Rare-Earth Metal(II) Complexes Using EPR Spectroscopy. *Organometallics* **2020**, *39*, 1187−1194.

(46) Moehring, S. A.; Miehlich, M.; Hoerger, C. J.; Meyer, K.; Ziller, J. W.; Evans, W. J. A Room-Temperature Stable Y(II) Aryloxide: Using Steric Saturation to Kinetically Stabilize Y(II) Complexes. *Inorg. Chem.* **2020**, *59*, 3207−3214.

(47) Moehring, S. A.; Evans, W. J. Evaluating Electron-Transfer Reactivity of Complexes of Actinides in + 2 and + 3 Oxidation States by Using EPR Spectroscopy. *Chem. Eur. J.* **2020**, *26*, 1530−1534.

(48) Jenkins, T. F.; Bekoe, S.; Ziller, J. W.; Furche, F.; Evans, W. J. Synthesis of a Heteroleptic Pentamethylcyclopentadienyl Yttrium(II) Complex, $[K(2.2.2\text{-Cryptand})]\{(C_5Me_5)_2Y^{II}[N(SiMe_3)_2]\}$, and Its C-H Bond Activated Y(III) Derivative. *Organometallics* **2021**, *40*, 3917−3925.

(49) Zhai, D. D.; Du, H. Z.; Zhang, X. Y.; Liu, Y. F.; Guan, B. T. Potassium Yttrium Ate Complexes: Synergistic Effect Enabled Reversible H_2 Activation and Catalytic Hydrogenation. *ACS Catal.* **2019**, *9*, 8766−8771.

(50) Gao, Y.; Pink, M.; Smith, J. M. Alkali Metal Ions Dictate the Structure and Reactivity of an Iron(II) Imido Complex. *J. Am. Chem. Soc.* **2022**, *144*, 1786−1794.

(51) Grubel, K.; Brennessel, W. W.; Mercado, B. Q.; Holland, P. L. Alkali Metal Control over N−N Cleavage in Iron Complexes. *J. Am. Chem. Soc.* **2014**, *136*, 16807−16816.

(52) Broere, D. L. J.; Mercado, B. Q.; Bill, E.; Lancaster, K. M.; Sproules, S.; Holland, P. L. Alkali Cation Effects on Redox-Active Formazanate Ligands in Iron Chemistry. *Inorg. Chem.* **2018**, *57*, 9580−9591.

(53) Bauer, J.; Braunschweig, H.; Dewhurst, R. D. Metal-Only Lewis Pairs with Transition Metal Lewis Bases. *Chem. Rev.* **2012**, *112*, 4329−4346.

(54) Hicks, J.; Vasko, P.; Goicoechea, J. M.; Aldridge, S. The Aluminyl Anion: A New Generation of Aluminium Nucleophile. *Angew. Chem., Int. Ed.* **2021**, *60*, 1702−1713.

(55) Coles, M. P.; Evans, M. J. The Emerging Chemistry of the Aluminyl Anion. *Chem. Commun.* **2023**, *59*, 503−519.

(56) Keil, P. M.; Soyemi, A.; Weisser, K.; Szilvási, T.; Limberg, C.; Hadlington, T. J. Cationic Tetrylene-Iron(0) Complexes: Access Points for Cooperative, Reversible Bond Activation and Open-Shell Iron(−I)-Ferrato-Tetrylenes. *Angew. Chem., Int. Ed.* **2023**, *62*, No. e202218141.

(57) Krogman, J. P.; Gallagher, J. R.; Zhang, G.; Hock, A. S.; Miller, J. T.; Thomas, C. M. Assignment of the Oxidation States of Zr and Co in a Highly Reactive Heterobimetallic Zr/Co Complex Using X-Ray Absorption Spectroscopy (XANES). *Dalton Trans.* **2014**, *43*, 13852−13857.

(58) Krogman, J. P.; Bezpalko, M. W.; Foxman, B. M.; Thomas, C. M. Multi-Electron Redox Processes at a Zr(IV) Center Facilitated by an Appended Redox-Active Cobalt-Containing Metalloligand. *Dalton Trans.* **2016**, *45*, 11182−11190.

(59) Auer, M.; Zwettler, K.; Eichele, K.; Schubert, H.; Sindlinger, C. P.; Wesemann, L. Synthesis of Cobalt-Tin and -Lead Tetrylidynes—Reactivity Study of the Triple Bond. *Angew. Chem., Int. Ed.* **2023**, *62*, No. e202305951.

(60) Widemann, M.; Eichele, K.; Schubert, H.; Sindlinger, C. P.; Klenner, S.; Pöttgen, R.; Wesemann, L. Synthesis and Hydrogenation of Heavy Homologues of Rhodium Carbynes: $[(Me_3P)_2(Ph_3P)\text{-}Rh{\equiv}E\text{-}Ar^*]$ (E = Sn, Pb). *Angew. Chem., Int. Ed.* **2021**, *60*, 5882−5889.

(61) Mankad, N. P. Diverse Bimetallic Mechanisms Emerging from Transition Metal Lewis Acid/Base Pairs: Development of Co-Catalysis with Metal Carbenes and Metal Carbonyl Anions. *Chem. Commun.* **2018**, *54*, 1291−1302.

(62) Hieber, W.; Leutert, F. Äthylendiamin-substituierte Eisencarboyle und eine neue Bildungsweise von Eisencarbonylwasserstoff (XI. Mitteil. über metallcarbonyle). *Ber. Dtsch. Chem. Ges.* **1931**, *64*, 2832−2839.

(63) Leach, P. A.; Geib, S. J.; Corella, J. A.; Warnock, G. F.; Cooper, N. J. Synthesis and Structural Characterization of $[Co\{CN(2,6\text{-}C_6H_3Me_2)\}_4]^-$, the First Transition Metal Isonitrilate. *J. Am. Chem. Soc.* **1994**, *116*, 8566−8574.

(64) Warnock, G. F.; Cooper, N. J. The First Transition-Metal Isonitrilate: Synthesis and Characterization of $K[Co(2,6\text{-}Me_2C_6H_3NC)_4]$. *Organometallics* **1989**, *8*, 1826−1827.

(65) Jonas, K. Dilithium-Nickel-Olefin Complexes. Novel Bimetal Complexes Containing a Transition Metal and a Main Group Metal. *Angew. Chem., Int. Ed. Engl.* **1975**, *14*, 752−753.

(66) Bandy, J. A.; Berry, A.; Green, M. L. H.; Perutz, R. N.; Prout, K.; Verpeaux, J.-N. Synthesis of Anionic Sandwich Compounds: $[Ti(\eta\text{-}C_6H_5R)_2]^-$ and the Crystal Structure of $[K(18\text{-Crown-6})(\mu\text{-}H)Mo(\eta\text{-}C_5H_5)_2]$. *J. Chem. Soc., Chem. Commun.* **1984**, 729−731.

(67) Blackburn, D. W.; Britton, D.; Ellis, J. E. A New Approach to Bis(arene)titanium(0) and -titanium(−I) Complexes; Structure of Bis(arene)titanates(1−). *Angew. Chem., Int. Ed. Engl.* **1992**, *31*, 1495−1498.

(68) Jonas, K.; Häselhoff, C.-C.; Goddard, R.; Krüger, C. Manganese(II)cyclopentadienide and Cyclopentadienylmanganese-

(biphenyl) as Starting Materials for the Synthesis of Carbonyl Free Organomanganese Complexes. *Inorg. Chim. Acta* **1992**, *198–200*, 533–541.

(69) Aresta, M.; Nobile, C. F.; Rossi, M.; Sacco, A. Dinitrogen Complexes of Cobalt(0) and Cobalt(−I). *J. Chem. Soc. D Chem. Commun.* **1971**, *0*, 781.

(70) Brennessel, W. W.; Young, V. G., Jr.; Ellis, J. E. Bis(1,2,3,4-η^4-anthracene)cobaltate(1−). *Angew. Chem., Int. Ed.* **2002**, *41*, 1211–1215.

(71) Jonas, K.; Schieferstein, L. Simple Route to Li- or Zn-Metalated η^5-Cyclopentadienyliron-Olefin Complexes. *Angew. Chem., Int. Ed. Engl.* **1979**, *18*, 549–550.

(72) Jonas, K.; Klusmann, P.; Goddard, R. PentamethylcycIopentadienylbis(ethen)eisen - Ein 17e-Halbsandwichkomplex mit leicht verdrängbaren Ethenliganden. *Z. Naturforsch. B* **1995**, *50b*, 394–404.

(73) Fochi, G. Bis-Arene-Vanadium Anions as Reducing Agents towards Carbon Dioxide and Monoxide. *J. Organomet. Chem.* **1988**, *350*, C1–C3.

(74) Drance, M. J.; Sears, J. D.; Mrse, A. M.; Moore, C. E.; Rheingold, A. L.; Neidig, M. L.; Figueroa, J. S. Terminal Coordination of Diatomic Boron Monofluoride to Iron. *Science* **2019**, *363*, 1203–1205.

(75) Till, M.; Kelly, J. A.; Ziegler, C. G. P.; Wolf, R.; Guo, T.; Ringenberg, M. R.; Lutsker, E.; Reiser, O. Synthesis and Characterization of Bidentate Isonitrile Iron Complexes. *Organometallics* **2021**, *40*, 1042–1052.

(76) Hickey, A. K.; Lee, W. T.; Chen, C. H.; Pink, M.; Smith, J. M. A Bidentate Carbene Ligand Stabilizes a Low-Coordinate Iron(0) Carbonyl Complex. *Organometallics* **2016**, *35*, 3069–3073.

(77) Hickey, A. K.; Chen, C. H.; Pink, M.; Smith, J. M. Low-Valent Iron Carbonyl Complexes with a Tripodal Carbene Ligand. *Organometallics* **2015**, *34*, 4560–4566.

(78) Ung, G.; Rittle, J.; Soleilhavoup, M.; Bertrand, G.; Peters, J. C. Two-Coordinate Fe^0 and Co^0 Complexes Supported by Cyclic (Alkyl)(amino)carbenes. *Angew. Chem., Int. Ed.* **2014**, *53*, 8427–8431.

(79) Ung, G.; Peters, J. C. Low-Temperature N_2 Binding to Two-Coordinate L_2Fe^0 Enables Reductive Trapping of $L_2FeN_2^-$ and NH_3 Generation. *Angew. Chem., Int. Ed.* **2015**, *54*, 532–535.

(80) Wang, Q.; Manzano, R. A.; Tinnermann, H.; Sung, S.; Leforestier, B.; Krämer, T.; Young, R. D. Access to and Reactivity of Fe^0, Fe^{-I}, Fe^I, and Fe^{II} $PC_{carbene}P$ Pincer Complexes. *Angew. Chem., Int. Ed.* **2021**, *60*, 18168–18177.

(81) Vollmer, M. V.; Xie, J.; Cammarota, R. C.; Young, V. G.; Bill, E.; Gagliardi, L.; Lu, C. C. Formal Nickelate(−I) Complexes Supported by Group 13 Ions. *Angew. Chem., Int. Ed.* **2018**, *57*, 7815–7819.

(82) Cavaillé, A.; Saffon-Merceron, N.; Nebra, N.; Fustier-Boutignon, M.; Mézailles, N. Synthesis and Reactivity of an End-Deck Cyclo-P_4 Iron Complex. *Angew. Chem., Int. Ed.* **2018**, *57*, 1874–1878.

(83) Reingold, J. A.; Virkaitis, K. L.; Carpenter, G. B.; Sun, S.; Sweigart, D. A.; Czech, P. T.; Overly, K. R. Chemical and Electrochemical Reduction of Polyarene Manganese Tricarbonyl Cations: Hapticity Changes and Generation of Syn- and Anti-Facial Bimetallic η^4,η^6-Naphthalene Complexes. *J. Am. Chem. Soc.* **2005**, *127*, 11146–11158.

(84) Jonas, K.; Rüsseler, W.; Angermund, K.; Krüger, C. Benzene as Bridging Ligand in Main Group Metal-Transition Metal-Arene Complexes. *Angew. Chem., Int. Ed. Engl.* **1986**, *25*, 927–928.

(85) Chatt, J.; Watson, H. R. Complexes of Zerovalent Vanadium, Chromium, Molybdenum and Tungsten with a Ditertiary Phosphine. *Nature* **1961**, *189*, 1003–1004.

(86) Chatt, J.; Watson, H. R. 491. Complexes of Zerovalent Transition Metals with the Ditertiary Phosphine, $Me_2P\cdot CH_2\cdot CH_2\cdot PMe_2$. *J. Chem. Soc.* **1962**, *0*, 2545–2549.

(87) Brennessel, W. W.; Ellis, J. E. Naphthalene and Anthracene Cobaltates(1−): Useful Storable Sources of an Atomic Cobalt Anion. *Inorg. Chem.* **2012**, *51*, 9076–9094.

(88) Housecroft, C. E.; Sharpe, A. G. Organometallic Compounds of d-Block Elements. In*Inorganic Chemistry*; Pearson: Harlow, England, 2012; pp 887–889.

(89) Lin, J. T.; Hagen, G. P.; Ellis, J. E. Highly Reduced Organometallics. 9. Synthesis and Characterization of the Tetrasodium Tetracarbonylmetalates(4−) of Chromium, Molybdenum, and Tungsten, $Na_4M(CO)_4$: Their Reactions with Weak Acids To Generate $H_2M_2(CO)_8{}^{2-}$ (M = Cr, Mo, and W). *J. Am. Chem. Soc.* **1983**, *105*, 2296–2303.

(90) Carpenter, A. E.; Mokhtarzadeh, C. C.; Ripatti, D. S.; Havrylyuk, I.; Kamezawa, R.; Moore, C. E.; Rheingold, A. L.; Figueroa, J. S. Comparative Measure of the Electronic Influence of Highly Substituted Aryl Isocyanides. *Inorg. Chem.* **2015**, *54*, 2936–2944.

(91) Weber, L. Homoleptic Isocyanide Metalates. *Angew. Chem., Int. Ed.* **1998**, *37*, 1515–1517.

(92) Gruden, M.; Zlatar, M. What Is the Nature of Bonding in $[Fe(CO)_3(NO)]^-$ and $[Fe(CO)_4]^{2-}$? *Theor. Chem. Acc.* **2020**, *139*, 126.

(93) Klein, J. E. M. N.; Miehlich, B.; Holzwarth, M. S.; Bauer, M.; Milek, M.; Khusniyarov, M. M.; Knizia, G.; Werner, H.-J.; Plietker, B. The Electronic Ground State of $[Fe(CO)_3(NO)]^-$: A Spectroscopic and Theoretical Study. *Angew. Chem., Int. Ed.* **2014**, *53*, 1790–1794.

(94) Clarkson, L. M.; Clegg, W.; Hockless, D. C. R.; Norman, N. C. Structure of a Thallium(I) Transition-Metal Carbonyl Salt Tl[Fe(CO)$_3$(NO)]. *Acta Crystallogr. Sect. C* **1992**, *48*, 236–239.

(95) Pannell, K. H.; Chen, Y. S.; Belknap, K.; Wu, C. C.; Bernal, I.; Creswick, M. W.; Huang, H. N. Structure and Reactivity of $M^+[Fe(CO)_3(NO)]^-$. *Inorg. Chem.* **1983**, *22*, 418–427.

(96) Burkhardt, L.; Vukadinovic, Y.; Nowakowski, M.; Kalinko, A.; Rudolph, J.; Carlsson, P. A.; Jacob, C. R.; Bauer, M. Electronic Structure of the Hieber Anion $[Fe(CO)_3(NO)]^-$ Revisited by X-Ray Emission and Absorption Spectroscopy. *Inorg. Chem.* **2020**, *59*, 3551–3561.

(97) Plietker, B.; Dieskau, A. The Reincarnation of the Hieber Anion $[Fe(CO)_3(NO)]^-$ - a New Venue in Nucleophilic Metal Catalysis. *Eur. J. Org. Chem.* **2009**, *2009*, 775–787.

(98) Klein, J. E. M. N.; Holzwarth, M. S.; Hohloch, S.; Sarkar, B.; Plietker, B. Redox-Active Triazolium-Derived Ligands in Nucleophilic Fe-Catalysis - Reactivity Profile and Development of a Regioselective O-Allylation. *Eur. J. Org. Chem.* **2013**, *2013*, 6310–6316.

(99) Magens, S.; Plietker, B. Fe-Catalyzed Thioesterification of Carboxylic Esters. *Chem. Eur. J.* **2011**, *17*, 8807–8809.

(100) Dieskau, A. P.; Begouin, J.-M.; Plietker, B. $Bu_4N[Fe(CO)_3(NO)]^-$ Catalyzed Hydrosilylation of Aldehydes and Ketones. *Eur. J. Org. Chem.* **2011**, *2011*, 5291–5296.

(101) Holzwarth, M. S.; Alt, I.; Plietker, B. Catalytic Activation of Diazo Compounds Using Electron-Rich, Defined Iron Complexes for Carbene-Transfer Reactions. *Angew. Chem., Int. Ed.* **2012**, *51*, 5351–5354.

(102) Chi, C.; Wang, J.-Q.; Hu, H.-S.; Zhang, Y.-Y.; Li, W.-L.; Meng, L.; Luo, M.; Zhou, M.; Li, J. Quadruple Bonding between Iron and Boron in the $BFe(CO)_3^-$ Complex. *Nat. Commun.* **2019**, *10*, 4713.

(103) Wang, J.-Q.; Chi, C.; Lu, J.-B.; Meng, L.; Luo, M.; Hu, H.-S.; Zhou, M.; Li, J. Triple Bonds between Iron and Heavier Group-14 Elements in the $AFe(CO)_3^-$ Complexes (A = Ge, Sn, and Pb). *Chem. Commun.* **2019**, *55*, 5685–5688.

(104) Wang, J.-Q.; Chi, C.; Hu, H.-S.; Li, X.; Luo, M.; Li, J.; Zhou, M. Multiple Bonding Between Group 3 Metals and $Fe(CO)_3^-$. *Angew. Chem., Int. Ed.* **2020**, *59*, 2344–2348.

(105) Pyykkö, P.; Riedel, S.; Patzschke, M. Triple-Bond Covalent Radii. *Chem. Eur. J.* **2005**, *11*, 3511–3520.

(106) Jin, X.; Wang, G.; Zhou, M. Mg(I)-Fe(−II) and Mg(0)-Mg(I) Covalent Bonding in the $Mg_nFe(CO)_4^-$ (n = 1, 2) Anion Complexes: An Infrared Photodissociation Spectroscopic and Theoretical Study. *Phys. Chem. Chem. Phys.* **2023**, *25*, 7697–7703.

(107) Jin, X.; Zhou, Y.; Wang, G.; Zhou, M. Mg-Fe Bonding in the MgFe(CO)$_n{}^+$ (n = 4−9) Cation Complexes: An Infrared Photodissociation Spectroscopic and Theoretical Study. *J. Phys. Chem. A* **2023**, *127*, 4483−4491.

(108) Faraonov, M. A.; Kuzmin, A. V.; Khasanov, S. S.; Shestakov, A. F.; Otsuka, A.; Yamochi, H.; Kitagawa, H.; Konarev, D. V. Negatively Charged Iron-Bridged Fullerene Dimer $\{Fe(CO)_2\text{-}\mu_2\text{-}\eta^2,\eta^2\text{-}C_{60}\}_2{}^{2-}$. *Inorg. Chem.* **2022**, *61*, 20144−20149.

(109) Konarev, D. V.; Khasanov, S. S.; Shestakov, A. F.; Ishikawa, M.; Otsuka, A.; Yamochi, H.; Saito, G.; Lyubovskaya, R. N. Spin Crossover in Anionic Cobalt-Bridged Fullerene $(Bu_4N^+)\{Co(Ph_3P)\}_2(\mu_2\text{-}Cl^-)(\mu_2\text{-}\eta^2,\eta^2\text{-}C_{60})_2$ Dimers. *J. Am. Chem. Soc.* **2016**, *138*, 16592−16595.

(110) Chi, C.; Pan, S.; Meng, L.; Luo, M.; Zhao, L.; Zhou, M.; Frenking, G. Alkali Metal Covalent Bonding in Nickel Carbonyl Complexes ENi(CO)$_3{}^-$. *Angew. Chem., Int. Ed.* **2019**, *58*, 1732−1738.

(111) Lorenz, C.; Kaas, M.; Korber, N. $[A([18]\text{Crown-6})]_2[Ni(CO)_3]\cdot 8NH_3$ (*A* = K, Rb) - An Ammoniate with a Trigonal Planar $[Ni(CO)_3]^{2-}$ Anion. *Z. Anorg. Allg. Chem.* **2018**, *644*, 1678−1680.

(112) Behrens, H.; Lohöfer, F. Zur Kenntnis der Chemie der Metallcarbonyle in flüssigem Ammoniak, VII. Über Dihydrogen-Hexacarbonyl-Diniccolat(−I), 1. Teil. *Chem. Ber.* **1961**, *94*, 1391−1402.

(113) Pacchioni, G.; Fantucci, P.; Valenti, V. The Electronic Structure of Carbonyl Metal Clusters: I. An INDO Investigation of Mono-, Di- and Trinuclear Nickel Complexes. *J. Organomet. Chem.* **1982**, *224*, 89−105.

(114) Kaim, W. "Guilty" Verdict—Evidence for the Noninnocence of Cyanide. *Angew. Chem., Int. Ed.* **2011**, *50*, 10498−10500.

(115) Jach, F.; Wagner, F. R.; Amber, Z. H.; Rüsing, M.; Hunger, J.; Prots, Y.; Kaiser, M.; Bobnar, M.; Jesche, A.; Eng, L. M.; et al. Tricyanidoferrates(−IV) and Ruthenates(−IV) with Non-Innocent Cyanido Ligands. *Angew. Chem., Int. Ed.* **2021**, *60*, 15879−15885.

(116) Jach, F.; Block, T.; Prots, Y.; Schmidt, M.; Bobnar, M.; Pöttgen, R.; Ruck, M.; Höhn, P. Non-Innocent Cyanido Ligands: Tetracyanidoferrate(−II) as Carbonyl Copycat. *Dalton Trans.* **2022**, *51*, 7811−7816.

(117) Höhn, P.; Jach, F.; Karabiyik, B.; Prots, Y.; Agrestini, S.; Wagner, F. R.; Ruck, M.; Tjeng, L. H.; Kniep, R. $Sr_3[Co(CN)_3]$ and $Ba_3[Co(CN)_3]$: Crystal Structure, Chemical Bonding, and Conceptional Considerations of Highly Reduced Metalates. *Angew. Chem., Int. Ed.* **2011**, *50*, 9361−9364.

(118) Jach, F.; Höhn, P.; Prots, Y.; Ruck, M. Synthesis and Crystal Structure of the Electron-Rich Cyano-Rhodate $Ba_3[Rh(CN)_3]$. *Z. Anorg. Allg. Chem.* **2015**, *641*, 998−1001.

(119) Jach, F.; Höhn, P.; Senyshyn, A.; Ruck, M.; Kniep, R. Synthesis and Crystal Structure of the Highly Reduced -Metalate $Ba_3[Ir(CN)_3]$. *Z. Anorg. Allg. Chem.* **2012**, *638*, 1959−1961.

(120) Dunbar, K. R.; Heintz, R. A. Chemistry of Transition Metal Cyanide Compounds: Modern Perspectives. In *Progress in Inorganic Chemistry*; Wiley; 1996; pp 283−391.

(121) Ellis, J. E.; Barger, P. T.; Winzenburg, M. L.; Warnock, G. F. Highly Reduced Organometallics XXVII. Synthesis, Isolation and Characterization of Trisodium Tricarbonylcobaltate(3−), and Initial Studies on Its Derivative Chemistry. *J. Organomet. Chem.* **1990**, *383*, 521−530.

(122) Chen, Z.; Deng, Y.; Bian, J.; Li, L.; Xu, G. A Density Functional Theory Study on Boundary of "Superreduced" Transition Metal Carbonyl Anions $[M(CO)_n]^{Z-}$(M = Cr, N = 5, 4, 3, Z = 2, 4, 6; M = Mn, N = 5, 4, 3, Z = 1, 3, 5; M = Fe, N = 4, 3, 2, Z = 2, 4, 6; M = Co, N = 4, 3, 2, Z = 1, 3, 5). *J. Mol. Struct. THEOCHEM* **1998**, *434*, 155−161.

(123) Stewart, M. A.; Moore, C. E.; Ditri, T. B.; Labios, L. A.; Rheingold, A. L.; Figueroa, J. S. Electrophilic Functionalization of Well-Behaved Manganese Monoanions Supported by *m*-Terphenyl Isocyanides. *Chem. Commun.* **2011**, *47*, 406−408.

(124) Agnew, D. W.; Moore, C. E.; Rheingold, A. L.; Figueroa, J. S. Kinetic Destabilization of Metal-Metal Single Bonds: Isolation of a Pentacoordinate Manganese(0) Monoradical. *Angew. Chem., Int. Ed.* **2015**, *54*, 12673−12677.

(125) Mokhtarzadeh, C. C.; Margulieux, G. W.; Carpenter, A. E.; Weidemann, N.; Moore, C. E.; Rheingold, A. L.; Figueroa, J. S. Synthesis and Protonation of an Encumbered Iron Tetraisocyanide Dianion. *Inorg. Chem.* **2015**, *54*, 5579−5587.

(126) Margulieux, G. W.; Weidemann, N.; Lacy, D. C.; Moore, C. E.; Rheingold, A. L.; Figueroa, J. S. Isocyano Analogues of $[Co(CO)_4]^n$: A Tetraisocyanide of Cobalt Isolated in Three States of Charge. *J. Am. Chem. Soc.* **2010**, *132*, 5033−5035.

(127) Carpenter, A. E.; Margulieux, G. W.; Millard, M. D.; Moore, C. E.; Weidemann, N.; Rheingold, A. L.; Figueroa, J. S. Zwitterionic Stabilization of a Reactive Cobalt Tris-Isocyanide Monoanion by Cation Coordination. *Angew. Chem., Int. Ed.* **2012**, *51*, 9412−9416.

(128) Drance, M. J.; Mokhtarzadeh, C. C.; Melaimi, M.; Agnew, D. W.; Moore, C. E.; Rheingold, A. L.; Figueroa, J. S. Controlled Expansion of a Strong-Field Iron Nitride Cluster: Multi-Site Ligand Substitution as a Strategy for Activating Interstitial Nitride Nucleophilicity. *Angew. Chem., Int. Ed.* **2018**, *57*, 13057−13061.

(129) Fox, B. J.; Sun, Q. Y.; DiPasquale, A. G.; Fox, A. R.; Rheingold, A. L.; Figueroa, J. S. Solution Behavior and Structural Properties of Cu(I) Complexes Featuring *m*-Terphenyl Isocyanides. *Inorg. Chem.* **2008**, *47*, 9010−9020.

(130) Ditri, T. B.; Fox, B. J.; Moore, C. E.; Rheingold, A. L.; Figueroa, J. S. Effective Control of Ligation and Geometric Isomerism: Direct Comparison of Steric Properties Associated with Bis-Mesityl and Bis-Diisopropylphenyl m-Terphenyl Isocyanides. *Inorg. Chem.* **2009**, *48*, 8362−8375.

(131) Utz, T. L.; Leach, P. A.; Geib, S. J.; Cooper, N. J. Synthesis, Derivatization, and Structural Characterization of $[Mn(CNC_6H_3Me_2\text{-}2,6)_5]^-$, a Five-Coordinate Isonitrilate Complex Containing Mn-I. *Chem. Commun.* **1997**, 847−848.

(132) Utz, T. L.; Leach, P. A.; Geib, S. J.; Cooper, N. J. Formation of the 1,4-Diazabutadien-2-Yl Complex $[Mn(CNPh^*)_4\{C({=}NPh^*)C(CH_3){=}N(Ph^*)\}]$ through Methylation of a Manganese(-I) Isonitrilate. *Organometallics* **1997**, *16*, 4109−4114.

(133) Brennessel, W. W.; Ellis, J. E. $[Fe(CNXyl)_4]^{2-}$: An Isolable and Structurally Characterized Homoleptic Isocyanidemetalate Dianion. *Angew. Chem., Int. Ed.* **2007**, *46*, 598−600.

(134) Coburger, P.; Leitl, J.; Scott, D. J.; Hierlmeier, G.; Shenderovich, I. G.; Hey-Hawkins, E.; Wolf, R. Synthesis of a Carborane-Substituted Bis(phosphanido) Cobaltate(I), Ligand Substitution, and Unusual P_4 Fragmentation. *Chem. Sci.* **2021**, *12*, 11225−11235.

(135) Carpenter, A. E.; Chan, C.; Rheingold, A. L.; Figueroa, J. S. A Well-Defined Isocyano Analogue of HCo(CO)$_4$. 2: Relative Brønsted Acidity as a Function of Isocyanide Ligation. *Organometallics* **2016**, *35*, 2319−2326.

(136) Mokhtarzadeh, C. C.; Carpenter, A. E.; Spence, D. P.; Melaimi, M.; Agnew, D. W.; Weidemann, N.; Moore, C. E.; Rheingold, A. L.; Figueroa, J. S. Geometric and Electronic Structure Analysis of the Three-Membered Electron-Transfer Series $[(\mu\text{-}CNR)_2[CpCo]_2]^n$ (n = 0, 1−, 2−) and Its Relevance to the Classical Bridging-Carbonyl System. *Organometallics* **2017**, *36*, 2126−2140.

(137) Mokhtarzadeh, C. C.; Moore, C. E.; Rheingold, A. L.; Figueroa, J. S. A Highly-Reduced Cobalt Terminal Carbyne: Divergent Metal- and α-Carbon-Centered Reactivity. *J. Am. Chem. Soc.* **2018**, *140*, 8100−8104.

(138) Tondreau, A. M.; Milsmann, C.; Lobkovsky, E.; Chirik, P. J. Oxidation and Reduction of Bis(imino)pyridine Iron Dicarbonyl Complexes. *Inorg. Chem.* **2011**, *50*, 9888−9895.

(139) Blake, M. P.; Kaltsoyannis, N.; Mountford, P. Heterobimetallic Complexes Containing Ca-Fe or Yb-Fe Bonds: Synthesis and Molecular and Electronic Structures of $[M\{CpFe(CO)_2\}_2(THF)_3]_2$ (M = Ca or Yb). *J. Am. Chem. Soc.* **2011**, *133*, 15358−15361.

(140) Blake, M. P.; Kaltsoyannis, N.; Mountford, P. Synthesis and Reactions of β-Diketiminate-Supported Complexes with Mg-Fe or Yb-Fe Bonds. *Chem. Commun.* **2013**, *49*, 3315−3317.

(141) Moret, M.-E.; Peters, J. C. Terminal Iron Dinitrogen and Iron Imide Complexes Supported by a Tris(phosphino)borane Ligand. *Angew. Chem., Int. Ed.* **2011**, *50*, 2063−2067.

(142) Mankad, N. P.; Whited, M. T.; Peters, J. C. Terminal Fe^I-N_2 and Fe^{II}···H-C Interactions Supported by Tris(phosphino)silyl Ligands. *Angew. Chem., Int. Ed.* **2007**, *46*, 5768−5771.

(143) Lee, Y.; Peters, J. C. Silylation of Iron-Bound Carbon Monoxide Affords a Terminal Fe Carbyne. *J. Am. Chem. Soc.* **2011**, *133*, 4438−4446.

(144) Brennessel, W. W.; Kucera, B. E.; Young Jr, V. G.; Ellis, J. E. Crystal Structures and Spectroscopic Characterization of $MBr_2(CNXyl)_n$ (M = Fe and Co, n = 4; M = Ni, n = 2; Xyl = 2,6-Dimethylphenyl), and of Formally Zero-Valent Iron as a Cocrystal of $Fe(CNXyl)_5$ and $Fe_2(CNXyl)_9$. *Acta Crystallogr. Sect. C* **2019**, *75*, 1118−1127.

(145) Pomeroy, R. K.; Vancea, L.; Calhoun, H. P.; Graham, W. A. G. Stereochemically Nonrigid Six-Coordinate Metal Carbonyl Complexes. 3. The Series cis-$Fe(CO)_4(SnR_3)_2$ (R = Methyl, Ethyl, Propyl, Butyl, Phenyl, Chloro) and the X-Ray Structure of Tetracarbonylbis-(triphenylstannyl)iron(II). *Inorg. Chem.* **1977**, *16*, 1508−1514.

(146) Poliakoff, M.; Turner, J. J. Infrared Spectra and Photochemistry of the Complex Pentacarbonyliron in Solid Matrices at 4 and 20 K: Evidence for Formation of the Complex Tetracarbonyliron. *J. Chem. Soc., Dalton Trans.* **1973**, 1351−1357.

(147) Poliakoff, M.; Turner, J. J. Structure and Reactions of Matrix-Isolated Tetracarbonyliron(0). *J. Chem. Soc., Dalton Trans.* **1974**, 2276−2285.

(148) Zhou, M.; Andrews, L.; Bauschlicher, C. W. Spectroscopic and Theoretical Investigations of Vibrational Frequencies in Binary Unsaturated Transition-Metal Carbonyl Cations, Neutrals, and Anions. *Chem. Rev.* **2001**, *101*, 1931−1962.

(149) Drance, M. J.; Wang, S.; Gembicky, M.; Rheingold, A. L.; Figueroa, J. S. Probing for Four-Coordinate Zerovalent Iron in a π-Acidic Ligand Field: A Functional Source of FeL_4 Enabled by Labile Dinitrogen Binding. *Organometallics* **2020**, *39*, 3394−3402.

(150) Wang, S.; Sears, J. D.; Moore, C. E.; Rheingold, A. L.; Neidig, M. L.; Figueroa, J. S. Side-on Coordination of Diphosphorus to a Mononuclear Iron Center. *Science* **2022**, *375*, 1393−1397.

(151) Giusti, L.; Landaeta, V. R.; Vanni, M.; Kelly, J. A.; Wolf, R.; Caporali, M. Coordination Chemistry of Elemental Phosphorus. *Coord. Chem. Rev.* **2021**, *441*, 213927.

(152) Chin, H. B.; Smith, M. B.; Wilson, R. D.; Bau, R. Variations in Molecular Geometry along the Isoelectronic Series Octacarbonyldicobalt, Octacarbonyl Cobalt Ferrate 1-, and Octacarbonyl Diferrate (2−). *J. Am. Chem. Soc.* **1974**, *96*, 5285−5287.

(153) Brunet, J.-J.; Neibecker, D.; Shyam Srivastava, R. The Reaction of $[PPN][HFe(CO)_4]$ with Styrene in THF: An Unexpected and Facile Synthesis of $[PPN]_2[Fe_2(CO)_8]$. *J. Organomet. Chem.* **1993**, *461*, 169−172.

(154) Neumüller, B.; Petz, W. Reaction of $Fe_2(CO)_9$ with Lithium: Preparation and Structures of Compounds with Strong Ion Pairing. *Organometallics* **2001**, *20*, 163−170.

(155) Carpenter, A. E.; Rheingold, A. L.; Figueroa, J. S. A Well-Defined Isocyano Analogue of $HCo(CO)_4$. 1: Synthesis, Decomposition, and Catalytic 1,1-Hydrogenation of Isocyanides. *Organometallics* **2016**, *35*, 2309−2318.

(156) Hapke, M.; Hilt, G. Introduction to Cobalt Chemistry and Catalysis. In *Cobalt catalysis in organic synthesis: Methods and reactions*; Hapke, M., Hilt, G., Eds.; Wiley-VCH Verlag GmbH & Co., 2020; pp 1−23.

(157) Hartwig, J. Catalytic Carbonylation. In *Organotransition Metal Chemistry: From Bonding to Catalysis*; University Science Books: Sausalito, CA, 2010; pp 745−824.

(158) Carpenter, A. E.; Moore, C. E.; Rheingold, A. L.; Figueroa, J. S. A Well-Defined Isocyano Analogue of $HCo(CO)_4$. 3: Hydride Migration to Olefins, H-Atom Transfer and Reactivity toward Protic Sources. *Organometallics* **2021**, *40*, 968−978.

(159) Ruff, J. K. Chemistry of the Dinuclear Carbonyl Anions. II. Mixed-Metal Derivatives. *Inorg. Chem.* **1968**, *7*, 1818−1821.

(160) Chan, C.; Carpenter, A. E.; Gembicky, M.; Moore, C. E.; Rheingold, A. L.; Figueroa, J. S. Associative Ligand Exchange and Substrate Activation Reactions by a Zero-Valent Cobalt Tetraisocyanide Complex. *Organometallics* **2019**, *38*, 1436−1444.

(161) Carpenter, A. E.; Wen, I.; Moore, C. E.; Rheingold, A. L.; Figueroa, J. S. $[1,1\text{-}Co_2(CO)_6(CNAr_{Mes})_2]$: A Structural Mimic of the Elusive D_{2d} Isomer of $[Co_2(CO)_8]$. *Chem. Eur. J.* **2013**, *19*, 10452−10457.

(162) Mokhtarzadeh, C. C.; Rheingold, A. L.; Figueroa, J. S. Dinitrogen Binding, P_4-Activation and Aza-Büchner Ring Expansions Mediated by an Isocyano Analogue of the CpCo(CO) Fragment. *Dalton Trans.* **2016**, *45*, 14561−14569.

(163) Connelly, N. G.; Raven, S. J.; Geiger, W. E.; Lane, G. A.; Rieger, P. H. Stabilization of Anion Radicals by the Pentaphenylcyclopentadienyl Ligand. Evidence for Symmetrical Metal-C_5R_5 Bonding in $[(\eta\text{-}C_5Ph_5)M(CO)_2]^-$ (M = Co, Rh). *J. Am. Chem. Soc.* **1986**, *108*, 6219−6224.

(164) Schore, N. E.; Ilenda, C. S.; Bergman, R. G. Chemical and Electrochemical Reduction of η^5-Cyclopentadienyldicarbonylcobalt-(I) and η^5-Cyclopentadienyl(triphenylphosphine)carbonylcobalt(I). Synthesis, Crystal and Molecular Structure, and Chemistry of Sodium and Bis(triphenylphosphine)iminium Bis(η^5-cyclopentadienyl)di-μ-carbonyl-dicobaltate, a Binuclear Cobalt Radical Anion. *J. Am. Chem. Soc.* **1977**, *99*, 1781−1787.

(165) Barybin, M. V.; Brennessel, W. W.; Kucera, B. E.; Minyaev, M. E.; Sussman, V. J.; Young, V. G.; Ellis, J. E. Homoleptic Isocyanidemetalates of 4d- and 5d-Transition Metals: $[Nb(CNXyl)_6]^-$, $[Ta(CNXyl)_6]^-$, and Derivatives Thereof. *J. Am. Chem. Soc.* **2007**, *129*, 1141−1150.

(166) Brennessel, W. W.; Romanenkov, A.; Young Jr, V. G.; Ellis, J. E. Tantalum Isocyanide Complexes: $TaI(CNDipp)_6$ (Dipp is 2,6-Diisopropylphenyl) and Ionic $[Ta(CNDipp)_7][Ta(CNDipp)_6]$, a Formal Disproportionation Product of the 17-Electron Ta^0 Metalloradical $Ta(CNDipp)_6$. *Acta Crystallogr. Sect. C* **2019**, *75*, 135−140.

(167) Chakarawet, K.; Davis-Gilbert, Z. W.; Harstad, S. R.; Young Jr, V. G.; Long, J. R.; Ellis, J. E. $Ta(CNDipp)_6$: An Isocyanide Analogue of Hexacarbonyltantalum(0). *Angew. Chem., Int. Ed.* **2017**, *56*, 10577−10581.

(168) Salsi, F.; Neville, M.; Drance, M.; Hagenbach, A.; Chan, C.; Figueroa, J. S.; Abram, U. A Closed-Shell Monomeric Rhenium(1−) Anion Provided by *m*-Terphenyl Isocyanide Ligation. *Chem. Commun.* **2020**, *56*, 7009−7012.

(169) Salsi, F.; Neville, M.; Drance, M.; Hagenbach, A.; Figueroa, J. S.; Abram, U. $\{M^I(CO)X(CNAr^{DArF2})_4\}$ (DArf = 3,5-$(CF_3)_2C_6H_3$; M = Re and Tc; X = Br and Cl) Complexes: Convenient Platforms for the Synthesis of Low-Valent Rhenium and Technetium Compounds. *Organometallics* **2021**, *40*, 1336−1343.

(170) Barybin, M. V.; Young, V. G.; Ellis, J. E. First Homoleptic Isocyanides of Niobium and Tantalum. *J. Am. Chem. Soc.* **1999**, *121*, 9237−9238.

(171) Dewey, C. G.; Ellis, J. E.; Fjare, K. L.; Pfahl, K. M.; Warnock, G. F. P. A Facile Atmospheric Pressure Synthesis of the Hexacarbonylmetalate Ions, $M(CO)_6$, of Niobium and Tantalum. *Organometallics* **1983**, *2*, 388−391.

(172) Ellis, J. E.; Warnock, G. F.; Barybin, M. V.; Pomije, M. K. New PF_3 and Carbonyl Chemistry of Tantalum. *Chem. Eur. J.* **1995**, *1*, 521−527.

(173) Smieja, J. M.; Kubiak, C. P. Re(bipy-tBu)$(CO)_3$Cl-Improved Catalytic Activity for Reduction of Carbon Dioxide: IR-Spectroelectrochemical and Mechanistic Studies. *Inorg. Chem.* **2010**, *49*, 9283−9289.

(174) Benson, E. E.; Kubiak, C. P. Structural Investigations into the Deactivation Pathway of the CO_2 Reduction Electrocatalyst Re(bpy)-$(CO)_3$Cl. *Chem. Commun.* **2012**, *48*, 7374−7376.

(175) Benson, E. E.; Sampson, M. D.; Grice, K. A.; Smieja, J. M.; Froehlich, J. D.; Friebel, D.; Keith, J. A.; Carter, E. A.; Nilsson, A.; Kubiak, C. P. The Electronic States of Rhenium Bipyridyl Electrocatalysts for CO_2 Reduction as Revealed by X-Ray Absorption

Spectroscopy and Computational Quantum Chemistry. *Angew. Chem., Int. Ed.* **2013**, *52*, 4841−4844.

(176) Barnett, B. R.; Rheingold, A. L.; Figueroa, J. S. Monomeric Chini-Type Triplatinum Clusters Featuring Dianionic and Radical-Anionic π*-Systems. *Angew. Chem., Int. Ed.* **2016**, *55*, 9253−9258.

(177) Neville, M. L.; Chan, C.; Barnett, B. R.; Hernandez, R. E.; Moore, C. E.; Figueroa, J. S. Three-Coordinate Monoanions of Rhodium(1−) and Iridium(1−): Isolable Examples of Coordinatively-Unsaturated Metalate Anions. *Polyhedron* **2023**, *243*, 116565.

(178) García-Vivó, D.; Ramos, A.; Ruiz, M. A. Cyclopentadienyl and Related Complexes of the Group 6 Elements Having Metal-Metal Triple Bonds: Synthesis, Structure, Bonding and Reactivity. *Coord. Chem. Rev.* **2013**, *257*, 2143−2191.

(179) Jang, M.; Ellis, J. E. Tris(η^4-naphthalene)zirconate(2−). *Angew. Chem., Int. Ed. Engl.* **1994**, *33*, 1973−1975.

(180) Brennessel, W. W.; Ellis, J. E.; Pomije, M. K.; Sussman, V. J.; Urnezius, E.; Young, V. G. Tris(η^4-naphthalene)- and Tris(1−4-η^4-anthracene)Tantalate(1−): First Homoleptic Arene Complexes of Anionic Tantalum. *J. Am. Chem. Soc.* **2002**, *124*, 10258−10259.

(181) Brennessel, W. W.; Jilek, R. E.; Ellis, J. E. Bis(1,2,3,4-η^4-anthracene)ferrate(1−): A Paramagnetic Homoleptic Polyarene Transition-Metal Anion. *Angew. Chem., Int. Ed.* **2007**, *46*, 6132−6136.

(182) Jilek, R. E.; Jang, M.; Smolensky, E. D.; Britton, J. D.; Ellis, J. E. Structurally Distinct Homoleptic Anthracene Complexes, $[\mathrm{M}(\mathrm{C}_{14}\mathrm{H}_{10})_3]^{2-}$, M = Titanium, Zirconium, Hafnium: Tris(arene) Complexes for a Triad of Transition Metals. *Angew. Chem., Int. Ed.* **2008**, *47*, 8692−8695.

(183) Kucera, B. E.; Jilek, R. E.; Brennessel, W. W.; Ellis, J. E. Bis(pyrene)metal Complexes of Vanadium, Niobium and Titanium: Isolable Homoleptic Pyrene Complexes of Transition Metals. *Acta Crystallogr. Sect. C Struct. Chem.* **2014**, *70*, 749−753.

(184) Kucera, B. E.; Young, V. G.; Brennessel, W. W.; Ellis, J. E. Syntheses and Crystal Structures of New Naphthalene- and Anthracene-Vanadate Salts and an Unprecedented Dimetallabis(anthracene) Sandwich Complex: $[\mathrm{Na}(\mathrm{tetrahydrofuran})_3]$-$[\mathrm{V}_2(\mathrm{anthracene})_2]$. *Acta Crystallogr. Sect. C Struct. Chem.* **2022**, *78*, 148−163.

(185) Huang, W.; Khan, S. I.; Diaconescu, P. L. Scandium Arene Inverted-Sandwich Complexes Supported by a Ferrocene Diamide Ligand. *J. Am. Chem. Soc.* **2011**, *133*, 10410−10413.

(186) Ghana, P.; Hoffmann, A.; Spaniol, T. P.; Okuda, J. Reduced Arene Complexes of Scandium. *Chem. Eur. J.* **2020**, *26*, 10290−10296.

(187) Ghana, P.; Spaniol, T. P.; Okuda, J. Scandium Reduced Arene Complex: Protonation and Reaction with Azobenzene. *Chem. Asian. J.* **2021**, *16*, 3170−3178.

(188) Ghana, P.; Schrader, S.; Rajeshkumar, T.; Spaniol, T. P.; Englert, U.; Maron, L.; Okuda, J. Reduced Arene Complexes of Hafnium Supported by a Triamidoamine Ligand. *Angew. Chem., Int. Ed.* **2021**, *60*, 14179−14187.

(189) Nakanishi, Y.; Ishida, Y.; Kawaguchi, H. Synthesis and Reactions of a Zirconium Naphthalene Complex Bearing a Tetraanionic C-Capped Triaryloxide Ligand. *Dalton Trans.* **2016**, *45*, 15879−15885.

(190) Nakanishi, Y.; Ishida, Y.; Kawaguchi, H. An Anionic η^2-Naphthalene Complex of Titanium Supported by a Tripodal $[\mathrm{O}_3\mathrm{C}]$ Ligand and Its Reactions with Dinitrogen, Anthracene and THF. *Dalton Trans.* **2018**, *47*, 6903−6907.

(191) Huang, W.; Diaconescu, P. L. P_4 activation by Group 3 Metal Arene Complexes. *Chem. Commun.* **2012**, *48*, 2216−2218.

(192) Huang, W.; Diaconescu, P. L. Aromatic C-F Bond Activation by Rare-Earth-Metal Complexes. *Organometallics* **2017**, *36*, 89−96.

(193) Brosmer, J. L.; Huang, W.; Diaconescu, P. L. Reduction of Diphenylacetylene Mediated by Rare-Earth Ferrocene Diamide Complexes. *Organometallics* **2017**, *36*, 4644−4648.

(194) Nikiforov, G. B.; Crewdson, P.; Gambarotta, S.; Korobkov, I.; Budzelaar, P. H. M. Reduction of Titanium Supported by a σ-/π-Bonded Tripyrrole Ligand: Ligand C-N Bond Cleavage and Coordination of Olefin and Arene with an Inverse Sandwich Structure. *Organometallics* **2007**, *26*, 48−55.

(195) Ilango, S.; Vidjayacoumar, B.; Gambarotta, S.; Gorelsky, S. I. Low-Valent Vanadium Complexes of a Pyrrolide-Based Ligand. Electronic Structure of a Dimeric V(I) Complex with a Short and Weak Metal-Metal Bond. *Inorg. Chem.* **2008**, *47*, 3265−3273.

(196) Pomije, M. K.; Kurth, C. J.; Ellis, J. E.; Barybin, M. V. First Conventional Syntheses and Isolation of Bis(naphthalene)metal(0) Complexes. Structural Characterization of $\mathrm{V}(\eta^6\text{-}\mathrm{C}_{10}\mathrm{H}_8)_2$. *Organometallics* **1997**, *16*, 3582−3587.

(197) Labrum, N. S.; Losovyj, Y.; Caulton, K. G. A New Access Route to Dimetal Sandwich Complexes, Including a Radical Anion. *Chem. Commun.* **2018**, *54*, 12397−12399.

(198) Bradley, D. C.; Hursthouse, M. B.; Newing, C. W.; Welch, A. J. Square Planar and Tetrahedral Chromium(II) Complexes; Crystal Structure Determinations. *J. Chem. Soc., Chem. Commun.* **1972**, 567−568.

(199) König, S. N.; Schneider, D.; Maichle-Mössmer, C.; Day, B. M.; Layfield, R. A.; Anwander, R. Divalent Transition Metal Silylamide Ate Complexes. *Eur. J. Inorg. Chem.* **2014**, *2014*, 4302−4309.

(200) Elschenbroich, C.; Möckel, R. Bis(η^6-naphthalene)chromium(0). *Angew. Chem., Int. Ed. Engl.* **1977**, *16*, 870−871.

(201) Kündig, E. P.; Timms, P. L. Metal Atom Preparation and Ligand Displacement Reactions of Bisnaphthalenechromium and Related Compounds. *J. Chem. Soc. Chem. Commun.* **1977**, *0* (24), 912−913.

(202) Brennessel, W. W.; Ellis, J. E. (18-Crown-6)potassium [(1,2,5,6-η)-cycloocta-1,5-diene][(1,2,3,4-η)-naphthalene]ferrate(−I). *Acta Crystallogr. Sect. E* **2012**, *68*, m1230−m1231.

(203) Tanaka, N.; Sato, Y. Univalent Tris(2,2′-bipyridine)ferrate Anion in Acetonitrile. *Inorg. Nucl. Chem. Lett.* **1966**, *2*, 359−362.

(204) Hall, F. S.; Reynolds, W. L. Preparation of an Iron(0) Complex with 2,2′-Bipyridine. *Inorg. Chem.* **1966**, *5*, 931−932.

(205) Mahon, C.; Reynolds, W. L. Preparation of Sodium Tris(2,2’-bipyridine)ferrate(−I). *Inorg. Chem.* **1967**, *6*, 1927−1928.

(206) Herzog, S.; Präkel, H. Über die Entladung des $[\mathrm{FeDipy}_3]^{2+}$-Kations zum Tris-2,2′-Dipyridyl-Eisen $[\mathrm{FeDipy}_3]$. *Z. Chem.* **1965**, *5*, 469−470.

(207) Brennessel, W. W.; Ellis, J. E. Homoleptic 2,2’-Bipyridine Metalates(−I) of Iron and Cobalt, One Cocrystallized with an Anthracene Radical Anion and the other with Neutral Anthracene. *Acta Crystallogr. Sect. C* **2014**, *70*, 828−832.

(208) England, J.; Scarborough, C. C.; Weyhermüller, T.; Sproules, S.; Wieghardt, K. Electronic Structures of the Electron Transfer Series $[\mathrm{M}(\mathrm{bpy})_3]^n$, $[\mathrm{M}(\mathrm{tpy})_2]^n$, and $[\mathrm{Fe}(^t\mathrm{bpy})_3]^n$ (M = Fe, Ru; n = 3+, 2+, 1+, 0, 1−): A Mössbauer Spectroscopic and DFT Study. *Eur. J. Inorg. Chem.* **2012**, *2012*, 4605−4621.

(209) Brennessel, W. W.; Ellis, J. E. Crystal Structures of Two Novel Iron Isocyanides from the Reaction of 2,6-Dimethylphenyl Isocyanide, CNXyl, with Bis(anthracene)Ferrate(−1). *Acta Crystallogr. Sect. E* **2022**, *78*, 60−65.

(210) Wolf, R.; Ehlers, A. W.; Slootweg, J. C.; Lutz, M.; Gudat, D.; Hunger, M.; Spek, A. L.; Lammertsma, K. The Homoleptic Sandwich Anion $[\mathrm{Co}(\mathrm{P}_2\mathrm{C}_2t\mathrm{Bu}_2)_2]^-$: A Versatile Building Block for Phosphaorganometallic Chemistry. *Angew. Chem., Int. Ed.* **2008**, *47*, 4584−4587.

(211) Wolf, R.; Slootweg, J. C.; Ehlers, A. W.; Hartl, F.; de Bruin, B.; Lutz, M.; Spek, A. L.; Lammertsma, K. A Phosphorus Analogue of Bis(η^4-Cyclobutadiene)Iron(0). *Angew. Chem., Int. Ed.* **2009**, *48*, 3104−3107.

(212) Malberg, J.; Wiegand, T.; Eckert, H.; Bodensteiner, M.; Wolf, R. Gold(I) and Silver(I) Complexes of Diphosphacyclobutadiene Cobaltate Sandwich Anions. *Chem. Eur. J.* **2013**, *19*, 2356−2369.

(213) Wolf, R.; Ghavtadze, N.; Weber, K.; Schnöckelborg, E.-M.; de Bruin, B.; Ehlers, A. W.; Lammertsma, K. P—C Dichotomy: Divergent Iron(−I)-Mediated Alkyne and Phosphaalkyne Cyclooligomerisations. *Dalton Trans.* **2010**, *39*, 1453−1456.

(214) Fürstner, A.; Martin, R.; Majima, K. Cycloisomerization of Enynes Catalyzed by Iron(0)-Ate Complexes. *J. Am. Chem. Soc.* **2005**, *127*, 12236−12237.

(215) Fürstner, A.; Majima, K.; Martín, R.; Krause, H.; Kattnig, E.; Goddard, R.; Lehmann, C. W. A Cheap Metal for a "Noble" Task: Preparative and Mechanistic Aspects of Cycloisomerization and Cycloaddition Reactions Catalyzed by Low-Valent Iron Complexes. *J. Am. Chem. Soc.* **2008**, *130*, 1992−2004.

(216) Fürstner, A.; Martin, R.; Krause, H.; Seidel, G.; Goddard, R.; Lehmann, C. W. Preparation, Structure, and Reactivity of Nonstabilized Organoiron Compounds. Implications for Iron-Catalyzed Cross Coupling Reactions. *J. Am. Chem. Soc.* **2008**, *130*, 8773−8787.

(217) Wolf, R.; Schnöckelborg, E.-M. A Reactive Iron Napthalene Complex Provides Convenient Access to the "Cp*Fe$^-$" Synthon (Cp*=C$_5$Me$_5$). *Chem. Commun.* **2010**, *46*, 2832−2834.

(218) Schnöckelborg, E.-M.; Weigand, J. J.; Wolf, R. Synthesis of Anionic Iron Polyphosphides by Reaction of White Phosphorus with "Cp*Fe$^-$. *Angew. Chem., Int. Ed.* **2011**, *50*, 6657−6660.

(219) Schnöckelborg, E. M.; Khusniyarov, M. M.; de Bruin, B.; Hartl, F.; Langer, T.; Eul, M.; Schulz, S.; Pöttgen, R.; Wolf, R. Unraveling the Electronic Structures of Low-Valent Naphthalene and Anthracene Iron Complexes: X-Ray, Spectroscopic, and Density Functional Theory Studies. *Inorg. Chem.* **2012**, *51*, 6719−6730.

(220) Rezaei Rad, B.; Herrmann, D.; Lescop, C.; Wolf, R. A Tetradentate Metalloligand: Synthesis and Coordination Behaviour of a 2-Pyridyl-Substituted Cyclobutadiene Iron Complex. *Dalton Trans.* **2014**, *43*, 4247−4250.

(221) Wiegel, A.-K.; Rad, B. R.; Herrmann, D.; Wolf, R. Synthesis and Characterization of Tetra(pyridyl)cyclobutadiene Iron Complexes [Cp*Fe(C$_4$py$_4$)]$^{-}$ (Py = 3-Pyridyl and 4-Pyridyl, Cp* = C$_5$Me$_5$). *Z. Anorg. Allg. Chem.* **2015**, *641*, 2065−2070.

(222) Henne, F. D.; Schnöckelborg, E. M.; Feldmann, K. O.; Grunenberg, J.; Wolf, R.; Weigand, J. J. Observation of a Chloride-Bridged P-P Bond in the Phosphorus Cation [L(Cl)P(μ-Cl)P(Cl)L]$^+$ (L = NHC). *Organometallics* **2013**, *32*, 6674−6680.

(223) Schnöckelborg, E.-M.; Hartl, F.; Langer, T.; Pöttgen, R.; Wolf, R. Redox-Active, Dinuclear Sandwich Compounds [Cp*Fe(μ-L)-FeCp*] (L = Naphthalene and Anthracene). *Eur. J. Inorg. Chem.* **2012**, *2012*, 1632−1638.

(224) Hatanaka, T.; Ohki, Y.; Kamachi, T.; Nakayama, T.; Yoshizawa, K.; Katada, M.; Tatsumi, K. Naphthalene and Anthracene Complexes Sandwiched by Two {(Cp*)FeI} Fragments: Strong Electronic Coupling between the FeI Centers. *Chem. Asian. J.* **2012**, *7*, 1231−1242.

(225) Lacoste, M.; Varret, F.; Toupet, L.; Astruc, D. Organodiiron "Electron Reservoir" Complexes Containing A Polyaromatic Ligand: Syntheses, Stabilization, Delocalized Mixed Valences, And Intramolecular Coupling. *J. Am. Chem. Soc.* **1987**, *109*, 6504−6506.

(226) Rabaâ, H.; Lacoste, M.; Delville-Desbois, M. H.; Ruiz, J.; Gloaguen, B.; Ardoin, N.; Astruc, D.; Le Beuze, A.; Saillard, J. Y.; Linares, J.; et al. Electronic Interplay between Two Iron Centers across Polyaromatic Ligands: Syntheses, Redox Chemistry, and Electronic Structures of the Electron-Reservoir 36- to 38-Electron Complexes [(FeCp*)$_2$(μ_2-η^{12}-Polyaromatic)]$^{q+}$ (q = 0−2) Including Mixed Valences And. *Organometallics* **1995**, *14*, 5078−5092.

(227) Malberg, J.; Lupton, E.; Schnöckelborg, E. M.; de Bruin, B.; Sutter, J.; Meyer, K.; Hartl, F.; Wolf, R. Synthesis and Electronic Structure of Dissymmetrical, Naphthalene-Bridged Sandwich Complexes [Cp′Fe(μ-C$_{10}$H$_8$)MCp*]^x (x = 0, + 1; M = Fe, Ru; Cp′ = η^5-C$_5$H$_2$-1,2,4-tBu$_3$; Cp* = η^5-C$_5$Me$_5$). *Organometallics* **2013**, *32*, 6040−6052.

(228) Inoue, H.; Nagao, Y.; Haruki, E. A Phenyl-Lithium Activated Fe$_4$S$_4$ Cluster as a Hydride Transfer Agent in the Hydrogenation of Carbonyl Compounds. *J. Chem. Soc., Chem. Commun.* **1985**, 501−502.

(229) Inoue, H.; Suzuki, M. Catalytic Function of the Phenyl-Lithium-Treated Fe$_4$S$_4$Cl$_4$$^{2-}$ Cluster in the Hydrogenation of Cis- and Trans-Stilbenes. *J. Chem. Soc., Chem. Commun.* **1980**, 817−818.

(230) Zhurkin, F. E.; Wodrich, M. D.; Hu, X. A Monometallic Iron(I) Organoferrate. *Organometallics* **2017**, *36*, 499−501.

(231) Wilson, R. J.; Hastreiter, F.; Reiter, K.; Büschelberger, P.; Wolf, R.; Gschwind, R. M.; Weigend, F.; Dehnen, S. [Co@Sn$_6$Sb$_6$]$^{3-}$: An Off-Center Endohedral 12-Vertex Cluster. *Angew. Chem., Int. Ed.* **2018**, *57*, 15359−15363.

(232) Hoidn, C. M.; Rödl, C.; McCrea-Hendrick, M. L.; Block, T.; Pöttgen, R.; Ehlers, A. W.; Power, P. P.; Wolf, R. Synthesis of a Cyclic Co$_2$Sn$_2$ Cluster Using a Co$^-$ Synthon. *J. Am. Chem. Soc.* **2018**, *140*, 13195−13199.

(233) Brennessel, W. W.; Young Jr, V. G.; Ellis, J. E. Towards Homoleptic Naphthalenemetalates of the Later Transition Metals: Isolation and Characterization of Naphthalenecobaltates(1−). *Angew. Chem., Int. Ed.* **2006**, *45*, 7268−7271.

(234) Jonas, K.; Krüger, C. Alkali Metal-Transition Metal π-Complexes. *Angew. Chem., Int. Ed. Engl.* **1980**, *19*, 520−537.

(235) Brennessel, W. W.; Ellis, J. E. (2.2.2-Cryptand)potassium Tetrakis(η^2-ethylene)cobaltate(−I). *Acta Crystallogr. Sect. E Struct. Reports Online* **2012**, *68*, 1257−1258.

(236) Kruck, T.; Lang, W.; Engelmann, A. Synthesis of Tetrakis(trifluorophosphine)cobalt Hydride and Hexakis(trifluorophosphine)tungsten(0). *Angew. Chem., Int. Ed. Engl.* **1965**, *4*, 148−149.

(237) Highsmith, R. E.; Bergerud, J. R.; MacDiarmid, A. G. Reaction of the Protonic Acids, HCo(PF$_3$)$_4$ and HCo(CO)$_4$, with NN-Dimethyl(trimethylsilyl)amine to Form Silylammonium Compounds. *J. Chem. Soc. D Chem. Commun.* **1971**, 48−49.

(238) Kruck, T.; Lang, W.; Derner, N.; Stadler, M. Über Metalltrifluorphosphin-Komplexe, XXIII. Darstellung und Reaktionen der Tetrakis(trifluorphosphin)-Metallhydride von Kobalt, Rhodium und Iridium. *Chem. Ber.* **1968**, *101*, 3816−3826.

(239) Ibers, J. A.; Frenz, B. A. Structure of Hydridotetrakis(trifluorophosphine)cobalt(I), CoH(PF$_3$)$_4$. *Inorg. Chem.* **1970**, *9*, 2403−2408.

(240) Muetterties, E. L.; Hirsekorn, F. J. Chemistry of the Transition Metal-Hydrogen Bond. II. HCo[P(OR)$_3$]$_4$. *J. Am. Chem. Soc.* **1974**, *96*, 7920−7926.

(241) Muetterties, E. L.; Hirsekorn, F. J. A New Organometallic Reagent, KCo[P(OR)$_3$]$_4$. *J. Chem. Soc., Chem. Commun.* **1973**, 683b−684.

(242) Dhar, S. K.; Kurcz, W. E. Polarographic Evidence of the Formation of a Uni-Negative Bipyridyl Complex of Cobalt in Dimethylformamide. *J. Electroanal. Chem. Interface Electrochem.* **1974**, *53*, 325−328.

(243) Brennessel, W. W.; Ellis, J. E. (2.2.2-Cryptand)potassium Tetracarbonylcobaltate(−I). *Acta Crystallogr. Sect. E Struct. Reports Online* **2014**, *70*, 180.

(244) Klein, H.-F.; Ellrich, K.; Lamac, S.; Lull, G.; Zsolnai, L.; Huttner, G. Anthracen- und Phenanthren-Cobalt-Verbindungen mit Trimethylphosphan-Liganden. *Z. Naturforsch. B* **1985**, *40B*, 1377−1382.

(245) Hammer, R.; Klein, H.-F. The Tetrakis(trimethylphosphine)-cobalt Anion. *Z. Naturforsch. B* **1977**, *32B*, 138−143.

(246) Döring, M.; Uhlig, E.; Taldbach, T. Zur Reaktion von [Li(TMED)$_2$][Co(COD)$_2$] mit π-Akzeptorliganden. *Z. Anorg. Allg. Chem.* **1991**, *600*, 163−167.

(247) Brennessel, W. W.; Ellis, J. E. ([2.2.2]Cryptand-κ^6O) potassium (η^4-Cyclooctadiene)bis(η^2-pyrene)cobaltate(1−) Pentane Hemisolvate. *Acta Crystallogr. Sect. E* **2012**, *68*, m1013−m1014.

(248) Büschelberger, P.; Gärtner, D.; Reyes-Rodriguez, E.; Kreyenschmidt, F.; Koszinowski, K.; Jacobi von Wangelin, A.; Wolf, R. Alkene Metalates as Hydrogenation Catalysts. *Chem. Eur. J.* **2017**, *23*, 3139−3151.

(249) Sussman, V. J.; Ellis, J. E. From Storable Sources of Atomic Nb$^-$ and Ta$^-$ Ions to Isolable Anionic Tris(1,3-butadiene)Metal Complexes: [M(η^4-C$_4$H$_6$)$_3$]$^-$, M = Nb, Ta. *Angew. Chem., Int. Ed.* **2008**, *47*, 484−489.

(250) Sussman, V. J.; Ellis, J. E. A Total Loss of Innocence: Double Ortho-Metallation of Bis(triphenylphosphano)iminium Cation, [N-(PPh$_3$)$_2$]$^+$, by Tris(η-naphthalene)tantalate(1−). *Chem. Commun.* **2008**, No. 43, 5642−5644.

(251) Morse, P. M.; Shelby, Q. D.; Do Kim, Y.; Girolami, G. S. Ethylene Complexes of the Early Transition Metals: Crystal

Structures of $[\mathrm{HfEt_4(C_2H_4)^{2-}}]$ and the Negative-Oxidation-State Species $[\mathrm{TaHEt(C_2H_4)_3{}^{3-}}]$ and $[\mathrm{WH(C_2H_4)_4{}^{3-}}]$. *Organometallics* **2008**, *27*, 984−993.

(252) Holloway, J. D. L.; Bowden, W. L.; Geiger, W. E. Unusual Electron-Transfer Processes Involving Electron-Rich and Electron-Deficient Metallocenes. *J. Am. Chem. Soc.* **1977**, *99*, 7089−7090.

(253) Holloway, J. D. L.; Geiger, W. E. Electron-Transfer Reactions of Metallocenes. Influence of Metal Oxidation State on Structure and Reactivity. *J. Am. Chem. Soc.* **1979**, *101*, 2038−2044.

(254) Bard, A. J.; Garcia, E.; Kukharenko, S.; Strelets, V. V. Electrochemistry of Metallocenes at Very Negative and Very Positive Potentials. Electrogeneration of 17-Electron $\mathrm{Cp_2Co^{2+}}$, $\mathrm{Cp_2Co^{2-}}$, and $\mathrm{Cp_2Ni^{2-}}$ Species. *Inorg. Chem.* **1993**, *32*, 3528−3531.

(255) Robbins, J. L.; Edelstein, N. M.; Cooper, S. R.; Smart, J. C. Syntheses and Electronic Structures of Decamethylmanganocenes. *J. Am. Chem. Soc.* **1979**, *101*, 3853−3857.

(256) Gubin, S. P.; Smirnova, S. A.; Denisovich, L. I. Redox Properties of Cyclopentadienylmetal Compounds II. Cobaltocene, Nickelocene and Related Compounds. *J. Organomet. Chem.* **1971**, *30*, 257−265.

(257) Mugnier, Y.; Moise, C.; Tirouflet, J.; Laviron, E. Reduction electrochimique du ferrocene. *J. Organomet. Chem.* **1980**, *186*, C49−C52.

(258) Geiger, W. E. Electroreduction of Cobaltocene. Evidence for a Metallocene Anion. *J. Am. Chem. Soc.* **1974**, *96*, 2632−2634.

(259) Ito, N.; Saji, T.; Aoyagui, S. Electrochemical Formation of Stable Ferrocene Anion and the Formal Rate Constant of the $\mathrm{Ferrocene^{0/-}}$ Electrode. *J. Organomet. Chem.* **1983**, *247*, 301−305.

(260) Hung-Low, F.; Bradley, C. A. Synthesis of a Bis(Indenyl) Co(I) Anion: A Reactive Source of a 14 Electron Indenyl Co(I) Equivalent. *Inorg. Chem.* **2013**, *52*, 2446−2457.

(261) Hung-Low, F.; Bradley, C. A. Indenyl Ligands as Supports for Reactive, Low-Valent Cobalt(I) Fragments. *Organometallics* **2011**, *30*, 2636−2639.

(262) Malischewski, M.; Seppelt, K. Structural Characterization of Potassium Salts of the Decamethylmanganocene Anion $\mathrm{Cp^*{}_2Mn^-}$. *Dalton Trans.* **2019**, *48*, 17078−17082.

(263) Goodwin, C. A. P.; Giansiracusa, M. J.; Greer, S. M.; Nicholas, H. M.; Evans, P.; Vonci, M.; Hill, S.; Chilton, N. F.; Mills, D. P. Isolation and Electronic Structures of Derivatized Manganocene, Ferrocene and Cobaltocene Anions. *Nat. Chem.* **2021**, *13*, 243−248.

(264) Walawalkar, M. G.; Pandey, P.; Murugavel, R. The Redox Journey of Iconic Ferrocene: Ferrocenium Dications and Ferrocenate Anions. *Angew. Chem., Int. Ed.* **2021**, *60*, 12632−12635.

(265) Astruc, D. Why Is Ferrocene so Exceptional? *Eur. J. Inorg. Chem.* **2017**, *2017*, 6−29.

(266) Smart, J. C.; Robbins, J. L. A Low Spin Manganocene and Its Novel Anionic Derivative. Synthesis and Characterization of Decamethylmanganocene Complexes. *J. Am. Chem. Soc.* **1978**, *100*, 3936−3937.

(267) Freyberg, D. P.; Robbins, J. L.; Raymond, K. N.; Smart, J. C. Crystal and Molecular Structures of Decamethylmanganocene and Decamethylferrocene. Static Jahn-Teller Distortion in a Metallocene. *J. Am. Chem. Soc.* **1979**, *101*, 892−897.

(268) Tresp, D. S.; Neugebauer, H.; Grimme, S.; Hansen, A.; Prokopchuk, D. E. Electronic Effects of Aminoindenyl Ligands Coordinated to Manganese: Structures and Properties of a $\mathrm{Mn^0}$ Metalloradical and Bimetallic $\mathrm{Mn^{-I}/Mn^{I}}$ Adduct. *Organometallics* **2022**, *41*, 3055−3063.

(269) Lee, S.; Lovelace, S. R.; Cooper, N. J. Two-Electron and One-Electron Reduction of the Indenyl Complex $[\mathrm{Mn}(\eta^5\text{-}\mathrm{C_9H_7})(\mathrm{CO})_3]$ and Reversible Counterion-Controlled Comproportionation of $[\mathrm{Mn}(\eta^5\text{-}\mathrm{C_9H_7})(\mathrm{CO})_3]$ and $[\mathrm{Mn}(\eta^3\text{-}\mathrm{C_9H_7})(\mathrm{CO})_3]^{2-}$ To Give $[\mathrm{Mn}(\eta^5\text{-}\mathrm{C_9H_7})(\mathrm{CO})_3]^-$. *Organometallics* **1995**, *14*, 1974−1982.

(270) Saito, M.; Matsunaga, N.; Hamada, J.; Furukawa, S.; Tada, T.; Herber, R. H. Anionic Stannaferrocene and Its Unique Electronic State. *Chem. Lett.* **2019**, *48*, 163−165.

(271) Rosa, P.; Mézailles, N.; Ricard, L.; Mathey, F.; Le Floch, P. Dianionic Homoleptic Biphosphinine Complexes of Group 4 Metals. *Angew. Chem., Int. Ed.* **2000**, *39*, 1823−1826.

(272) Rosa, P.; Mézailles, N.; Ricard, L.; Mathey, F.; Le Floch, P.; Jean, Y. Dianionic Iron and Ruthenium(2−) Biphosphinine Complexes: A Formal $\mathrm{d^{10}}$ Ruthenium Complex with a Square Planar Geometry. *Angew. Chem., Int. Ed.* **2001**, *40*, 1251−1253.

(273) Mézailles, N.; Rosa, P.; Ricard, L.; Mathey, F.; Floch, P. Le. Biphosphinine Rhodium and Cobalt(−1) Complexes. *Organometallics* **2000**, *19*, 2941−2943.

(274) Hartl, F.; Mahabiersing, T.; Le Floch, P.; Mathey, F.; Ricard, L.; Rosa, P.; Záliš, S. Electronic Properties of 4,4′,5,5′-Tetramethyl-2,2′-Biphosphinine (tmbp) in the Redox Series Fac-$[\mathrm{Mn(Br)(Co)_3(tmbp)}]$, $[\mathrm{Mn(Co)_3(tmbp)}]_2$, and $[\mathrm{Mn(Co)_3(tmbp)}]^-$: Crystallographic, Spectroelectrochemical, and DFT Computational Study. *Inorg. Chem.* **2003**, *42*, 4442−4455.

(275) Rezaei Rad, B.; Chakraborty, U.; Mühldorf, B.; Sklorz, J. A. W.; Bodensteiner, M.; Müller, C.; Wolf, R. Synthesis, Structure, and Reactivity of Pentamethylcyclopentadienyl 2,4,6-Triphenylphosphinine Iron Complexes. *Organometallics* **2015**, *34*, 622−635.

(276) Leitl, J.; Marquardt, M.; Coburger, P.; Scott, D. J.; Streitferdt, V.; Gschwind, R. M.; Müller, C.; Wolf, R. Facile C═O Bond Splitting of Carbon Dioxide Induced by Metal-Ligand Cooperativity in a Phosphinine Iron(0) Complex. *Angew. Chem., Int. Ed.* **2019**, *58*, 15407−15411.

(277) Coles, N. T.; Abels, A. S.; Leitl, J.; Wolf, R.; Grützmacher, H.; Müller, C. Phosphinine-Based Ligands: Recent Developments in Coordination Chemistry and Applications. *Coord. Chem. Rev.* **2021**, *433*, 213729.

(278) Hoidn, C. M.; Wolf, R. Reaction of a 2,4,6-Triphenylphosphinine Ferrate Anion with Electrophiles: A New Route to Phosphacyclohexadienyl Complexes. *Dalton Trans.* **2016**, *45*, 8875−8884.

(279) Nief, F.; Fischer, J. Ligand Exchange Reaction of Ferrocene with 2,4,6-Triphenylphosphabenzene. Synthesis and Structural Study of Isomeric (η^5-Phosphacyclohexadienyl) (η^5-Cyclopentadienyl) Iron (II) Complexes Containing a η^5-Phosphadienyl Unit. *Organometallics* **1986**, *5*, 877−883.

(280) Kurtz, D. A.; Zhang, J.; Sookezian, A.; Kallick, J.; Hill, M. G.; Hunter, B. M. A Cobalt Phosphine Complex in Five Oxidation States. *Inorg. Chem.* **2021**, *60*, 17445−17449.

(281) Berners-Price, S. J.; Colquhoun, L. A.; Healy, P. C.; Byriel, K. A.; Hanna, J. V. Copper(I) and Gold(I) Complexes with Cis-Bis(Diphenylphosphino)Ethylene. Crystal Structures and ^{31}P Cross-Polarization Magic Angle Spinning Nuclear Magnetic Resonance Studies. *J. Chem. Soc., Dalton Trans.* **1992**, 3357−3363.

(282) Coburger, P.; Demeshko, S.; Rödl, C.; Hey-Hawkins, E.; Wolf, R. Oxidative P-P Bond Addition to Cobalt(−I): Formation of a Low-Spin Cobalt(III) Phosphanido Complex. *Angew. Chem., Int. Ed.* **2017**, *56*, 15871−15875.

(283) Kreienbrink, A.; Sárosi, M. B.; Rys, E. G.; Lönnecke, P.; Hey-Hawkins, E. Carbaborane-Substituted 1,2-Diphosphetanes. *Angew. Chem., Int. Ed.* **2011**, *50*, 4701−4703.

(284) Kreienbrink, A.; Lönnecke, P.; Findeisen, M.; Hey-Hawkins, E. Endocyclic P-P Bond Cleavage in Carbaborane-Substituted 1,2-Diphosphetane: A New Route to Secondary Phosphinocarbaboranes. *Chem. Commun.* **2012**, *48*, 9385−9387.

(285) Kreienbrink, A.; Heinicke, S.; Duong Pham, T. T.; Frank, R.; Lönnecke, P.; Hey-Hawkins, E. Carbaborane-Substituted 1,2,3-Triphospholanes and 1-Aza-2,5-Diphospholane: New Synthetic Approaches. *Chem. Eur. J.* **2014**, *20*, 1434−1439.

(286) Dalton, D. M.; Rappé, A. K.; Rovis, T. Perfluorinated Taddol Phosphoramidite as an L,Z-Ligand on Rh(I) and Co(−I): Evidence for Bidentate Coordination via Metal-$\mathrm{C_6F_5}$ Interaction. *Chem. Sci.* **2013**, *4*, 2062−2070.

(287) Brammer, L.; Mareque Rivas, J. C.; Spilling, C. D. An Intramolecular N-H···Co Hydrogen Bond and a Structure Correlation Study of the Pathway for Protonation of the $\mathrm{Co(CO)_3L^-}$ Anion (L = CO, $\mathrm{PR_3}$). *J. Organomet. Chem.* **2000**, *609*, 36−43.

(288) Brammer, L.; Mareque Rivas, J. C.; Zhao, D. Unexpectedly Lengthened N-H···Co Hydrogen Bonds? *Inorg. Chem.* **1998**, *37*, 5512−5518.

(289) Brammer, L.; McCann, M. C.; Bullock, R. M.; McMullen, R.; Sherwood, P. $Et_3NH^+Co(CO)_4^-$: Hydrogen-Bonded Adduct or Simple Ion Pair? Single-Crystal Neutron Diffraction Study at 15 K. *Organometallics* **1992**, *11*, 2339−2341.

(290) Amatore, C.; Jutand, A. Anionic Pd(0) and Pd(II) Intermediates in Palladium-Catalyzed Heck and Cross-Coupling Reactions. *Acc. Chem. Res.* **2000**, *33*, 314−321.

(291) Kolter, M.; Böck, K.; Karaghiosoff, K.; Koszinowski, K. Anionic Palladium(0) and Palladium(II) Ate Complexes. *Angew. Chem., Int. Ed.* **2017**, *56*, 13244−13248.

(292) Kolter, M.; Koszinowski, K. Second Comes First: Switching Elementary Steps in Palladium-Catalyzed Cross-Coupling Reactions. *Chem. Eur. J.* **2020**, *26*, 12212−12218.

(293) Luo, J.; Theron, R.; Sewell, L. J.; Hooper, T. N.; Weller, A. S.; Oliver, A. G.; McIndoe, J. S. Rhodium-Catalyzed Selective Partial Hydrogenation of Alkynes. *Organometallics* **2015**, *34*, 3021−3028.

(294) Janusson, E.; Zijlstra, H. S.; Nguyen, P. P. T.; MacGillivray, L.; Martelino, J.; McIndoe, J. S. Real-Time Analysis of $Pd_2(dba)_3$ Activation by Phosphine Ligands. *Chem. Commun.* **2017**, *53*, 854−856.

(295) Váňa, J.; Terencio, T.; Petrović, V.; Tischler, O.; Novák, Z.; Roithová, J. Palladium-Catalyzed C−H Activation: Mass Spectrometric Approach to Reaction Kinetics in Solution. *Organometallics* **2017**, *36*, 2072−2080.

(296) Schwartsburd, L.; Cohen, R.; Konstantinovski, L.; Milstein, D. A Pincer-Type Anionic Platinum(0) Complex. *Angew. Chem., Int. Ed.* **2008**, *47*, 3603−3606.

(297) Alonso, M.; García, M. E.; Ruiz, M. A.; Hamidov, H.; Jeffery, J. C. Chemistry of the Phosphinidene Oxide Ligand. *J. Am. Chem. Soc.* **2004**, *126*, 13610−13611.

(298) Alonso, M.; Alvarez, M. A.; García, M. E.; Ruiz, M. A.; Hamidov, H.; Jeffery, J. C. Oxidation Reactions of the Phosphinidene Oxide Ligand. *J. Am. Chem. Soc.* **2005**, *127*, 15012−15013.

(299) Alonso, M.; Alvarez, M. A.; García, M. E.; García-Vivó, D.; Ruiz, M. A. Chemistry of the Oxophosphinidene Ligand. 1. Electronic Structure of the Anionic Complexes $[MCp\{P(O)R^*\}(CO)_2]^-$ (M = Mo, W; R* = 2,4,6-$C_6H_2{}^tBu_3$) and Their Reactions with H^+ and C-Based Electrophiles. *Inorg. Chem.* **2010**, *49*, 8962−8976.

(300) Alonso, M.; Alvarez, M. A.; García, M. E.; Ruiz, M. A.; Hamidov, H.; Jeffery, J. C. Chemistry of the Oxophosphinidene Ligand. 2. Reactivity of the Anionic Complexes $[MCp\{P(O)R^*\}(CO)_2]^-$ (M = Mo, W; R* = 2,4,6-$C_6H_2{}^tBu_3$) toward Electrophiles Based on Elements Different from Carbon. *Inorg. Chem.* **2010**, *49*, 11595−11605.

(301) Alonso, M.; Alvarez, M. A.; García, M. E.; García-Vivó, D.; Ruiz, M. A. Nucleophilic Behaviour of Dioxo- and Thiooxophosphorane Complexes $[MoCp(CO)_2\{E,P\text{-}EP(O)(2,4,6\text{-}C_6H_2{}^tBu_3)\}]^-$ (E = O, S). *Dalton Trans.* **2014**, *43*, 16074−16083.

(302) Alvarez, M. A.; García, M. E.; Ruiz, M. A.; Toyos, A.; Vega, M. F. Low-Temperature N-O Bond Cleavage and Reversible N—P Bond Formation Processes in the Reactions of the Unsaturated Anions $[M_2(\eta^5\text{-}C_5H_5)_2(\mu\text{-}PCy_2)(\mu\text{-}CO)_2]^-$ (M = Mo, W) with the Nitrosyl Complex $[Re(\eta^5\text{-}C_5H_4Me)(CO)_2(NO)]^+$. *Inorg. Chem.* **2013**, *52*, 3942−3952.

(303) Alvarez, M. A.; García, M. E.; García-Vivó, D.; Ruiz, M. A.; Vega, M. F. Hydride, Gold(I) and Related Derivatives of the Unsaturated Ditungsten Anion $[W_2Cp_2(\mu\text{-}PCy_2)(\mu\text{-}CO)_2]^-$. *Dalton Trans.* **2014**, *43*, 16044−16055.

(304) Alvarez, M. A.; García, M. E.; García-Vivó, D.; Ruiz, M. A.; Vega, M. F. Reactions of the Unsaturated Ditungsten Anion $[W_2Cp_2(\mu\text{-}PCy_2)(\mu\text{-}CO)_2]^-$ with C- and P-Based Electrophiles. *Organometallics* **2015**, *34*, 870−878.

(305) Alvarez, M. A.; Casado-Ruano, M.; García, M. E.; García-Vivó, D.; Ruiz, M. A. Structural and Chemical Effects of the $PtBu_2$ Bridge at Unsaturated Dimolybdenum Complexes Having Hydride and Hydrocarbyl Ligands. *Inorg. Chem.* **2017**, *56*, 11336−11351.

(306) Alvarez, M. A.; García, M. E.; García-Vivó, D.; Huergo, E.; Ruiz, M. A. Hydride, Alkyl and Carbyne Derivatives of the Unsaturated Heterometallic Anion $[MoWCp_2(\mu\text{-}PCy_2)(\mu\text{-}CO)_2]^-$. *J. Organomet. Chem.* **2019**, *893*, 61−71.

(307) Alvarez, M. A.; García, M. E.; García-Vivó, D.; Ruiz, M. A.; Toyos, A. The Doubly-Bonded Ditungsten Anion $[W_2Cp_2(\mu\text{-}PPh_2)(NO)_2]^-$: An Entry to the Chemistry of Unsaturated Nitrosyl Complexes. *Dalton Trans.* **2016**, *45*, 13300−13303.

(308) Alvarez, M. A.; García, M. E.; García-Vivó, D.; Huergo, E.; Ruiz, M. A. Synthesis of the Unsaturated $[MMoCp(\mu\text{-}PR_2)(CO)_5]^-$ Anions (M = Mn, R = Ph; M = Re, R = Cy): Versatile Precursors of Heterometallic Complexes. *Eur. J. Inorg. Chem.* **2017**, *2017*, 1280−1283.

(309) Alvarez, M. A.; García-Vivó, D.; Huergo, E.; Ruiz, M. A. Trapping of an Heterometallic Unsaturated Hydride: Structure and Properties of the Ammonia Complex $[MoMnCp(\mu\text{-}H)(\mu\text{-}PPh_2)(CO)_5(NH_3)]$. *Inorganics* **2018**, *6*, 125.

(310) Alvarez, M. A.; García, M. E.; García-Vivó, D.; Huergo, E.; Ruiz, M. A. Acceptor Behavior and E-H Bond Activation Processes of the Unsaturated Heterometallic Anion $[MoReCp(\mu\text{-}PCy_2)(CO)_5]^-$(Mo═Re). *Organometallics* **2018**, *37*, 3425−3436.

(311) Alvarez, M. A.; García, M. E.; García-Vivó, D.; Rueda, M. T.; Ruiz, M. A.; Toyos, A.; Vega, M. F. Terminal vs. Bridging Coordination of CO and NO Ligands after Decarbonylation of $[W_2Cp_2(\mu\text{-}PR_2)(CO)_3(NO)]$ Complexes (R = Ph, Cy). An Experimental and Computational Study. *Dalton Trans.* **2017**, *46*, 10440−10451.

(312) Alvarez, M. A.; García, M. E.; García-Vivó, D.; Ruiz, M. A.; Toyos, A. E-H Bond Activation and Insertion Processes in the Reactions of the Unsaturated Hydride $[W_2Cp_2(\mu\text{-}H)(\mu\text{-}PPh_2)(NO)_2]$. *Inorg. Chem.* **2018**, *57*, 2228−2241.

(313) Alvarez, M. A.; García, M. E.; García-Vivó, D.; Ramos, A.; Ruiz, M. A.; Toyos, A. N-O Bond Activation and Cleavage Reactions of the Nitrosyl-Bridged Complexes $[M_2Cp_2(\mu\text{-}PCy_2)(\mu\text{-}NO)(NO)_2]$ (M = Mo, W). *Inorg. Chem.* **2018**, *57*, 15314−15329.

(314) Alvarez, M. A.; García, M. E.; García-Vivó, D.; Guerra, A. M.; Ruiz, M. A.; Falvello, L. R. Chemistry of a Nitrosyl Ligand κ:η-Bridging a Ditungsten Center: Rearrangement and N-O Bond Cleavage Reactions. *Inorg. Chem.* **2022**, *61*, 14929−14933.

(315) Hickey, A. K.; Lutz, S. A.; Chen, C.-H.; Smith, J. M. Two-State Reactivity in C-H Activation by a Four-Coordinate Iron(0) Complex. *Chem. Commun.* **2017**, *53*, 1245−1248.

(316) Lutz, S. A.; Hickey, A. K.; Gao, Y.; Chen, C. H.; Smith, J. M. Two-State Reactivity in Iron-Catalyzed Alkene Isomerization Confers σ-Base Resistance. *J. Am. Chem. Soc.* **2020**, *142*, 15527−15535.

(317) Massad, I.; Marek, I. Alkene Isomerization through Allylmetals as a Strategic Tool in Stereoselective Synthesis. *ACS Catal.* **2020**, *10*, 5793−5804.

(318) Biswas, S. Mechanistic Understanding of Transition-Metal-Catalyzed Olefin Isomerization: Metal-Hydride Insertion-Elimination vs. π-Allyl Pathways. *Comments Inorg. Chem.* **2015**, *35*, 300−330.

(319) Back, O.; Henry-Ellinger, M.; Martin, C. D.; Martin, D.; Bertrand, G. ^{31}P NMR Chemical Shifts of Carbene-Phosphinidene Adducts as an Indicator of the π-Accepting Properties of Carbenes. *Angew. Chem., Int. Ed.* **2013**, *52*, 2939−2943.

(320) Roy, S.; Mondal, K. C.; Roesky, H. W. Cyclic Alkyl(Amino) Carbene Stabilized Complexes with Low Coordinate Metals of Enduring Nature. *Acc. Chem. Res.* **2016**, *49*, 357−369.

(321) Garhwal, S.; Kaushansky, A.; Fridman, N.; de Ruiter, G. Part per Million Levels of an Anionic Iron Hydride Complex Catalyzes Selective Alkene Isomerization via Two-State Reactivity. *Chem. Catal.* **2021**, *1*, 631−647.

(322) Garhwal, S.; Kaushansky, A.; Fridman, N.; Shimon, L. J. W.; de Ruiter, G. Facile H/D Exchange at (Hetero)Aromatic Hydrocarbons Catalyzed by a Stable Trans-Dihydride *n*-Heterocyclic Carbene (NHC) Iron Complex. *J. Am. Chem. Soc.* **2020**, *142*, 17131−17139.

(323) Garhwal, S.; Fridman, N.; De Ruiter, G. Z-Selective Alkyne Functionalization Catalyzed by a Trans-Dihydride N-Heterocyclic

Carbene (NHC) Iron Complex. *Inorg. Chem.* **2020**, *59*, 13817−13821.

(324) Wang, P.; Cheng, J.; Wang, D.; Yang, C.; Leng, X.; Deng, L. Cobalt(−I)- and Rhodium(−I)-Mediated Dearylation of N-Aryl N-Heterocyclic Carbene Ligands. *Organometallics* **2020**, *39*, 2871−2877.

(325) Varela-Izquierdo, V.; López, J. A.; de Bruin, B.; Tejel, C.; Ciriano, M. A. Three-Coordinate Rhodium Complexes in Low Oxidation States. *Chem. Eur. J.* **2020**, *26*, 3270−3274.

(326) Afandiyeva, M.; Kadam, A. A.; Wu, X.; Brennessel, W. W.; Kennedy, C. R. Synthesis, Structure, and Hydroboration Reactivity of Anionic Nickel(0) Complexes Supported by Bidentate NHC-Pyridone Ligands. *Organometallics* **2022**, *41*, 3014−3023.

(327) Woen, D. H.; Chen, G. P.; Ziller, J. W.; Boyle, T. J.; Furche, F.; Evans, W. J. End-On Bridging Dinitrogen Complex of Scandium. *J. Am. Chem. Soc.* **2017**, *139*, 14861−14864.

(328) Woen, D. H.; Chen, G. P.; Ziller, J. W.; Boyle, T. J.; Furche, F.; Evans, W. J. Solution Synthesis, Structure, and CO_2 Reduction Reactivity of a Scandium(II) Complex, $\{Sc[N(SiMe_3)_2]_3\}^-$. *Angew. Chem., Int. Ed.* **2017**, *56*, 2050−2053.

(329) Zadrozny, J. M.; Xiao, D. J.; Atanasov, M.; Long, G. J.; Grandjean, F.; Neese, F.; Long, J. R. Magnetic Blocking in a Linear Iron(I) Complex. *Nat. Chem.* **2013**, *5*, 577−581.

(330) Zadrozny, J. M.; Xiao, D. J.; Long, J. R.; Atanasov, M.; Neese, F.; Grandjean, F.; Long, G. J. Mössbauer Spectroscopy as a Probe of Magnetization Dynamics in the Linear Iron(I) and Iron(II) Complexes $[Fe(C(SiMe_3)_3)_2]^{1-/0}$. *Inorg. Chem.* **2013**, *52*, 13123−13131.

(331) Cai, I. C.; Lipschutz, M. I.; Tilley, T. D. A Bis(amido) Ligand Set That Supports Two-Coordinate Chromium in the +1, +2, and +3 Oxidation States. *Chem. Commun.* **2014**, *50*, 13062−13065.

(332) Werncke, C. G.; Suturina, E.; Bunting, P. C.; Vendier, L.; Long, J. R.; Atanasov, M.; Neese, F.; Sabo-Etienne, S.; Bontemps, S. Homoleptic Two-Coordinate Silylamido Complexes of Chromium(I), Manganese(I), and Cobalt(I). *Chem. Eur. J.* **2016**, *22*, 1668−1674.

(333) Werncke, C. G.; Bunting, P. C.; Duhayon, C.; Long, J. R.; Bontemps, S.; Sabo-Etienne, S. Two-Coordinate Iron(I) Complex $[Fe\{N(SiMe_3)_2\}_2]^-$: Synthesis, Properties, and Redox Activity. *Angew. Chem., Int. Ed.* **2015**, *54*, 245−248.

(334) Weller, R.; Müller, I.; Duhayon, C.; Sabo-Etienne, S.; Bontemps, S.; Werncke, C. G. Quasilinear 3d-Metal(I) Complexes $[KM(N(Dipp)SiR_3)_2]$ (M = Cr-Co) - Structural Diversity, Solution State Behaviour and Reactivity. *Dalton Trans.* **2021**, *50*, 4890−4903.

(335) Lin, C. Y.; Fettinger, J. C.; Grandjean, F.; Long, G. J.; Power, P. P. Synthesis, Structure, and Magnetic and Electrochemical Properties of Quasi-Linear and Linear Iron(I), Cobalt(I), and Nickel(I) Amido Complexes. *Inorg. Chem.* **2014**, *53*, 9400−9406.

(336) Lipschutz, M. I.; Yang, X.; Chatterjee, R.; Tilley, T. D. A Structurally Rigid Bis(amido) Ligand Framework in Low-Coordinate Ni(I), Ni(II), and Ni(III) Analogues Provides Access to a Ni(III) Methyl Complex via Oxidative Addition. *J. Am. Chem. Soc.* **2013**, *135*, 15298−15301.

(337) Lipschutz, M. I.; Chantarojsiri, T.; Dong, Y.; Tilley, T. D. Synthesis, Characterization, and Alkyne Trimerization Catalysis of a Heteroleptic Two-Coordinate Fe^I Complex. *J. Am. Chem. Soc.* **2015**, *137*, 6366−6372.

(338) Reckziegel, A.; Battistella, B.; Schmidt, A.; Werncke, C. G. Intricate Road to Linear Anionic Nickel(I) Hexamethyldisilazanide $[Ni(N(SiMe_3)_2)_2]^-$. *Inorg. Chem.* **2022**, *61*, 7794−7803.

(339) Werncke, C. G.; Gómez, A. G. Synthesis, Properties, and Reactivity of Linear Open-Shell 3d-Metal(I) Complexes. *Encyclopedia of Inorganic and Bioinorganic Chemistry* **2022**, 1−30.

(340) Lin, C. Y.; Guo, J. D.; Fettinger, J. C.; Nagase, S.; Grandjean, F.; Long, G. J.; Chilton, N. F.; Power, P. P. Dispersion Force Stabilized Two-Coordinate Transition Metal-Amido Complexes of the -N(SiMe$_3$)Dipp (Dipp = C_6H_3-2,6-Pr^i_2) Ligand: Structural, Spectroscopic, Magnetic, and Computational Studies. *Inorg. Chem.* **2013**, *52*, 13584−13593.

(341) Power, P. P. Stable Two-Coordinate, Open-Shell (d^1-d^9) Transition Metal Complexes. *Chem. Rev.* **2012**, *112*, 3482−3507.

(342) Lipschutz, M. I.; Tilley, T. D. Synthesis and Reactivity of a Conveniently Prepared Two-Coordinate Bis(amido) Nickel(II) Complex. *Chem. Commun.* **2012**, *48*, 7146−7148.

(343) Zadrozny, J. M.; Atanasov, M.; Bryan, A. M.; Lin, C.-Y.; Rekken, B. D.; Power, P. P.; Neese, F.; Long, J. R. Slow Magnetization Dynamics in a Series of Two-Coordinate Iron(II) Complexes. *Chem. Sci.* **2013**, *4*, 125−138.

(344) Yang, J.; Tilley, T. D. Efficient Hydrosilylation of Carbonyl Compounds with the Simple Amide Catalyst $[Fe\{N(SiMe_3)_2\}_2]$. *Angew. Chem., Int. Ed.* **2010**, *49*, 10186−10188.

(345) Weller, R.; Völlinger, L.; Werncke, C. G. On the Synthesis and Reduction of Trigonal Halido Bis(Silylamido) Metalates of Chromium to Cobalt. *Eur. J. Inorg. Chem.* **2021**, *2021*, 4383−4392.

(346) Müller, I.; Schneider, C.; Pietzonka, C.; Kraus, F.; Werncke, C. G. Reduction of 2,2′-Bipyridine by Quasi-Linear 3d-Metal(I) Silylamides—A Structural and Spectroscopic Study. *Inorganics* **2019**, *7*, 117.

(347) Irwin, M.; Jenkins, R. K.; Denning, M. S.; Krämer, T.; Grandjean, F.; Long, G. J.; Herchel, R.; McGrady, J. E.; Goicoechea, J. M. Experimental and Computational Study of the Structural and Electronic Properties of Fe^{II}(2,2′-bipyridine)(Mes)$_2$ and $[Fe^{II}(2,2'\text{-bipyridine})(Mes)_2]^-$, a Complex Containing a 2,2′-Bipyridyl Radical Anion. *Inorg. Chem.* **2010**, *49*, 6160−6171.

(348) Irwin, M.; Krämer, T.; McGrady, J. E.; Goicoechea, J. M. On the Structural and Electronic Properties of $[Zn_2(4,4'\text{-bipyridine})(Mes)_4]^{n-}$ (n = 0−2), a Homologous Series of Bimetallic Complexes Bridged by Neutral, Anionic, and Dianionic 4,4’-Bipyridine. *Inorg. Chem.* **2011**, *50*, 5006−5014.

(349) Scarborough, C. C.; Sproules, S.; Weyhermüller, T.; DeBeer, S.; Wieghardt, K. Electronic and Molecular Structures of the Members of the Electron Transfer Series $[Cr(^t\text{bpy})_3]^n$ (n = 3+, 2+, 1+, 0): An X-Ray Absorption Spectroscopic and Density Functional Theoretical Study. *Inorg. Chem.* **2011**, *50*, 12446−12462.

(350) Bowman, A. C.; Sproules, S.; Wieghardt, K. Electronic Structures of the $[V(^t\text{bpy})_3]^z$ (z = 3+, 2+, 0, 1-) Electron Transfer Series. *Inorg. Chem.* **2012**, *51*, 3707−3717.

(351) Bowman, A. C.; England, J.; Sproules, S.; Weyhermüller, T.; Wieghardt, K. Electronic Structures of Homoleptic [Tris(2,2’-bipyridine)M]^n Complexes of the Early Transition Metals (M = Sc, Y, Ti, Zr, Hf, V, Nb, Ta; N = 1+, 0, 1-, 2-, 3-): An Experimental and Density Functional Theoretical Study. *Inorg. Chem.* **2013**, *52*, 2242−2256.

(352) Wang, M.; England, J.; Weyhermüller, T.; Wieghardt, K. Electronic Structures of “Low-Valent” Neutral Complexes $[NiL_2]^0$ (S = 0; L = bpy, phen, tpy) - An Experimental and DFT Computational Study. *Eur. J. Inorg. Chem.* **2015**, *2015*, 1511−1523.

(353) Müller, I.; Munz, D.; Werncke, C. G. Reactions of Alkynes with Quasi-Linear 3d Metal(I) Silylamides of Chromium to Cobalt: A Comparative Study. *Inorg. Chem.* **2020**, *59*, 9521−9537.

(354) Sieg, G.; Pessemesse, Q.; Reith, S.; Yelin, S.; Limberg, C.; Munz, D.; Werncke, C. G. Cobalt and Iron Stabilized Ketyl, Ketiminyl and Aldiminyl Radical Anions. *Chem. Eur. J.* **2021**, *27*, 16760−16767.

(355) Nikiforov, G. B.; Vidyaratne, I.; Gambarotta, S.; Korobkov, I. Titanium-Promoted Dinitrogen Cleavage, Partial Hydrogenation, and Silylation. *Angew. Chem., Int. Ed.* **2009**, *48*, 7415−7419.

(356) Vidyaratne, I.; Crewdson, P.; Lefebvre, E.; Gambarotta, S. Dinitrogen Coordination and Cleavage Promoted by a Vanadium Complex of a σ,π,σ-Donor Ligand. *Inorg. Chem.* **2007**, *46*, 8836−8842.

(357) Gómez-Torres, A.; Mavragani, N.; Metta-Magaña, A.; Murugesu, M.; Fortier, S. Molecular Capacitors: Accessible 6- and 8-Electron Redox Chemistry from Dimeric “Ti(I)” and “Ti(0)” Synthons Supported by Imidazolin-2-Iminato Ligands. *Inorg. Chem.* **2022**, *61*, 16856−16873.

(358) Sorsche, D.; Miehlich, M. E.; Searles, K.; Gouget, G.; Zolnhofer, E. M.; Fortier, S.; Chen, C. H.; Gau, M.; Carroll, P. J.; Murray, C. B.; et al. Unusual Dinitrogen Binding and Electron Storage in Dinuclear Iron Complexes. *J. Am. Chem. Soc.* **2020**, *142*, 8147−8159.

(359) Lichtenberg, C.; Garcia Rubio, I.; Viciu, L.; Adelhardt, M.; Meyer, K.; Jeschke, G.; Grützmacher, H. A Low-Valent Iron Imido Heterocubane Cluster: Reversible Electron Transfer and Catalysis of Selective C−C Couplings. *Angew. Chem., Int. Ed.* **2015**, *54*, 13012−13017.

(360) Tejel, C.; Ciriano, M. A.; Del Río, M. P.; Van Den Bruele, F. J.; Hetterscheid, D. G. H.; Spithas, N. T.; de Bruin, B. Deprotonation Induced Ligand-to-Metal Electron Transfer: Synthesis of a Mixed-Valence Rh(−I,I) Dinuclear Compound and Its Reaction with Dioxygen. *J. Am. Chem. Soc.* **2008**, *130*, 5844−5845.

(361) Maire, P.; Sreekanth, A.; Büttner, T.; Harmer, J.; Gromov, I.; Rüegger, H.; Breher, F.; Schweiger, A.; Grützmacher, H. Synthesis of a Rhodaazacyclopropane and Characterization of Its Radical Cation by EPR Spectroscopy. *Angew. Chem., Int. Ed.* **2006**, *45*, 3265−3269.

(362) Tejel, C.; Ciriano, M. A.; del Río, M. P.; Hetterscheid, D. G. H.; Tsichlis i Spithas, N.; Smits, J. M. M.; de Bruin, B. Ligand Oxidation of a Deprotonated Bis(Picolyl)Amine Ir^I(Cod) Complex. *Chem. Eur. J.* **2008**, *14*, 10932−10936.

(363) Tejel, C.; del Río, M. P.; Ciriano, M. A.; Reijerse, E. J.; Hartl, F.; Záliš, S.; Hetterscheid, D. G. H.; Tsichlis i Spithas, N.; de Bruin, B. Ligand-Centred Reactivity of Bis(Picolyl)Amine Iridium: Sequential Deprotonation, Oxidation and Oxygenation of a "Non-Innocent" Ligand. *Chem. Eur. J.* **2009**, *15*, 11878−11889.

(364) Tejel, C.; Del Río, M. P.; Asensio, L.; Van Den Bruele, F. J.; Ciriano, M. A.; Tsichlis I Spithas, N.; Hetterscheid, D. G. H.; de Bruin, B. Cooperative Double Deprotonation of Bis(2-picolyl)amine Leading to Unexpected Bimetallic Mixed Valence (M^{-I}, M^I) Rhodium and Iridium Complexes. *Inorg. Chem.* **2011**, *50*, 7524−7534.

(365) Paul, N. D.; Krämer, T.; McGrady, J. E.; Goswami, S. Dioxygen Activation by Mixed-Valent Dirhodium Complexes of Redox Non-Innocent Azoaromatic Ligands. *Chem. Commun.* **2010**, *46*, 7124−7126.

(366) Chiang, K. P.; Scarborough, C. C.; Horitani, M.; Lees, N. S.; Ding, K.; Dugan, T. R.; Brennessel, W. W.; Bill, E.; Hoffman, B. M.; Holland, P. L. Characterization of the Fe−H Bond in a Three-Coordinate Terminal Hydride Complex of Iron(I). *Angew. Chem., Int. Ed.* **2012**, *51*, 3658−3662.

(367) Rodriguez, M. M.; Stubbert, B. D.; Scarborough, C. C.; Brennessel, W. W.; Bill, E.; Holland, P. L. Isolation and Characterization of Stable Iron(I) Sulfide Complexes. *Angew. Chem., Int. Ed.* **2012**, *51*, 8247−8250.

(368) Lohrey, T. D.; Maron, L.; Bergman, R. G.; Arnold, J. Heterotetrametallic Re-Zn-Zn-Re Complex Generated by an Anionic Rhenium(I) *β*-Diketiminate. *J. Am. Chem. Soc.* **2019**, *141*, 800−804.

(369) Lohrey, T. D.; Rao, G.; Britt, R. D.; Bergman, R. G.; Arnold, J. H_2 Activation and Direct Access to Terminal Nitride and cyclo-P_3 Complexes by an Acceptor-Free Rhenium(II) *β*-Diketiminate. *Inorg. Chem.* **2019**, *58*, 13492−13501.

(370) Ouellette, E. T.; Magdalenski, J. S.; Bergman, R. G.; Arnold, J. Heterobimetallic-Mediated Dinitrogen Functionalization: N-C Bond Formation at Rhenium-Group 9 Diazenido Complexes. *Inorg. Chem.* **2022**, *61*, 16064−16071.

(371) Lohrey, T. D.; Bergman, R. G.; Arnold, J. Controlling Dinitrogen Functionalization at Rhenium through Alkali Metal Ion Pairing. *Dalton Trans.* **2019**, *48*, 17936−17944.

(372) Ouellette, E. T.; Carpentier, A.; Joseph Brackbill, I.; Lohrey, T. D.; Douair, I.; Maron, L.; Bergman, R. G.; Arnold, J. *σ* or *π*? Bonding Interactions in a Series of Rhenium Metallotetrylenes. *Dalton Trans.* **2021**, *50*, 2083−2092.

(373) Zhang, R.; Wang, Y.; Zhao, Y.; Redshaw, C.; Fedushkin, I. L.; Wu, B.; Yang, X.-J. Main-Group Metal Complexes of *α*-Diimine Ligands: Structure, Bonding and Reactivity. *Dalton Trans.* **2021**, *50*, 13634−13650.

(374) Bernauer, J.; Pölker, J.; Jacobi von Wangelin, A. Redox-Active BIAN-Based Diimine Ligands in Metal-Catalyzed Small Molecule Syntheses. *ChemCatChem.* **2022**, *14*, No. e202101182.

(375) Blanchard, S.; Derat, E.; Desage-El Murr, M.; Fensterbank, L.; Malacria, M.; Mouriès-Mansuy, V. Non-Innocent Ligands: New Opportunities in Iron Catalysis. *Eur. J. Inorg. Chem.* **2012**, *2012*, 376−389.

(376) Chacon-Teran, M. A.; Findlater, M. Redox-Active BIAN-Based Iron Complexes in Catalysis. *Eur. J. Inorg. Chem.* **2022**, *30*, e202200363.

(377) Wekesa, F. S.; Arias-Ugarte, R.; Kong, L.; Sumner, Z.; McGovern, G. P.; Findlater, M. Iron-Catalyzed Hydrosilylation of Aldehydes and Ketones under Solvent-Free Conditions. *Organometallics* **2015**, *34*, 5051−5056.

(378) Maier, T. M.; Gawron, M.; Coburger, P.; Bodensteiner, M.; Wolf, R.; van Leest, N. P.; de Bruin, B.; Demeshko, S.; Meyer, F. Low-Valence Anionic *α*-Diimine Iron Complexes: Synthesis, Characterization, and Catalytic Hydroboration Studies. *Inorg. Chem.* **2020**, *59*, 16035−16052.

(379) Villa, M.; Miesel, D.; Hildebrandt, A.; Ragaini, F.; Schaarschmidt, D.; Jacobi von Wangelin, A. Synthesis and Catalysis of Redox-Active Bis(Imino)Acenaphthene (BIAN) Iron Complexes. *ChemCatChem.* **2017**, *9*, 3203−3209.

(380) Larson, P. J.; Wekesa, F. S.; Singh, A.; Smith, C. R.; Rajput, A.; McGovern, G. P.; Unruh, D. K.; Cozzolino, A. F.; Findlater, M. Synthesis, Characterization, Electrochemical Properties and Theoretical Calculations of (BIAN) Iron Complexes. *Polyhedron* **2019**, *159*, 365−374.

(381) Lichtenberg, C.; Viciu, L.; Vogt, M.; Rodríguez-Lugo, R. E.; Adelhardt, M.; Sutter, J.; Khusniyarov, M. M.; Meyer, K.; de Bruin, B.; Bill, E.; et al. Low-Valent Iron: An Fe(I) Ate Compound as a Building Block for a Linear Trinuclear Fe Cluster. *Chem. Commun.* **2015**, *51*, 13890−13893.

(382) Lichtenberg, C.; Adelhardt, M.; Gianetti, T. L.; Meyer, K.; de Bruin, B.; Grützmacher, H. Low-Valent Iron Mono-Diazadiene Compounds: Electronic Structure and Catalytic Application. *ACS Catal.* **2015**, *5*, 6230−6240.

(383) Lichtenberg, C.; Viciu, L.; Adelhardt, M.; Sutter, J.; Meyer, K.; de Bruin, B.; Grützmacher, H. Low-Valent Iron(I) Amido Olefin Complexes as Promotors for Dehydrogenation Reactions. *Angew. Chem., Int. Ed.* **2015**, *54*, 5766−5771.

(384) Fedushkin, I. L.; Skatova, A. A.; Chudakova, V. A.; Fukin, G. K. Four-Step Reduction of dpp-Bian with Sodium Metal: Crystal Structures of the Sodium Salts of the Mono-, Di-, Tri- and Tetraanions of dpp-Bian. *Angew. Chem., Int. Ed.* **2003**, *42*, 3294−3298.

(385) Pelties, S.; Maier, T.; Herrmann, D.; de Bruin, B.; Rebreyend, C.; Gärtner, S.; Shenderovich, I. G.; Wolf, R. Selective P_4 Activation by a Highly Reduced Cobaltate: Synthesis of Dicobalt Tetraphosphido Complexes. *Chem. Eur. J.* **2017**, *23*, 6094−6102.

(386) Ziegler, C. G. P.; Maier, T. M.; Pelties, S.; Taube, C.; Hennersdorf, F.; Ehlers, A. W.; Weigand, J. J.; Wolf, R. Construction of Alkyl-Substituted Pentaphosphido Ligands in the Coordination Sphere of Cobalt. *Chem. Sci.* **2019**, *10*, 1302−1308.

(387) Hoidn, C. M.; Maier, T. M.; Trabitsch, K.; Weigand, J. J.; Wolf, R. [3+2] Fragmentation of a Pentaphosphido Ligand by Cyanide. *Angew. Chem., Int. Ed.* **2019**, *58*, 18931−18936.

(388) Maier, T. M.; Sandl, S.; Shenderovich, I. G.; Jacobi von Wangelin, A.; Weigand, J. J.; Wolf, R. Amine-Borane Dehydrogenation and Transfer Hydrogenation Catalyzed by *α*-Diimine Cobaltates. *Chem. Eur. J.* **2019**, *25*, 238−245.

(389) Wang, X.; Zhao, Y.; Gong, S.; Liu, B.; Li, Q.-S.; Su, J.-H.; Wu, B.; Yang, X.-J. Mono- and Dinuclear Heteroleptic Cobalt Complexes with *α*-Diimine and Polyarene Ligands. *Chem. Eur. J.* **2015**, *21*, 13302−13310.

(390) Sgro, M. J.; Stephan, D. W. Synthesis and Exchange Reactions of Ni-Dimine-COD, Acetylene and Olefin Complexes. *Dalton Trans.* **2010**, *39*, 5786−5794.

(391) Maier, T. M.; Coburger, P.; van Leest, N. P.; Hey-Hawkins, E.; Wolf, R. Direct Synthesis of an Anionic 13-Vertex Closo-Cobaltacarborane Cluster. *Dalton Trans.* **2019**, *48*, 15772−15777.

(392) Regenauer, N. I.; Jänner, S.; Wadepohl, H.; Roşca, D.-A. A Redox-Active Heterobimetallic N-Heterocyclic Carbene Based on a

Bis(imino)pyrazine Ligand Scaffold. *Angew. Chem., Int. Ed.* **2020**, *59*, 19320−19328.

(393) Doll, J. S.; Regenauer, N. I.; Bothe, V. P.; Wadepohl, H.; Roşca, D. A. Redox Activity of Iron Diazine-Diimine Carbonyl and Dinitrogen Complexes: A Comparative Study of the Influence of the Heterocyclic Ring. *Inorg. Chem.* **2022**, *61*, 520−532.

(394) Bart, S. C.; Lobkovsky, E.; Chirik, P. J. Preparation and Molecular and Electronic Structures of Iron(0) Dinitrogen and Silane Complexes and Their Application to Catalytic Hydrogenation and Hydrosilation. *J. Am. Chem. Soc.* **2004**, *126*, 13794−13807.

(395) Römelt, C.; Weyhermüller, T.; Wieghardt, K. Structural Characteristics of Redox-Active Pyridine-1,6-Diimine Complexes: Electronic Structures and Ligand Oxidation Levels. *Coord. Chem. Rev.* **2019**, *380*, 287−317.

(396) Chirik, P. J. Iron- and Cobalt-Catalyzed Alkene Hydrogenation: Catalysis with Both Redox-Active and Strong Field Ligands. *Acc. Chem. Res.* **2015**, *48*, 1687−1695.

(397) Russell, S. K.; Bowman, A. C.; Lobkovsky, E.; Wieghardt, K.; Chirik, P. J. Synthesis and Electronic Structure of Reduced Bis(imino)pyridine Manganese Compounds. *Eur. J. Inorg. Chem.* **2012**, *2012*, 535−545.

(398) Bowman, A. C.; Milsmann, C.; Bill, E.; Lobkovsky, E.; Weyhermüller, T.; Wieghardt, K.; Chirik, P. J. Reduced N-Alkyl Substituted Bis(imino)Pyridine Cobalt Complexes: Molecular and Electronic Structures for Compounds Varying by Three Oxidation States. *Inorg. Chem.* **2010**, *49*, 6110−6123.

(399) Bowman, A. C.; Milsmann, C.; Hojilla Atienza, C. C.; Lobkovsky, E.; Wieghardt, K.; Chirik, P. J. Synthesis and Molecular and Electronic Structures of Reduced Bis(imino)pyridine Cobalt Dinitrogen Complexes: Ligand versus Metal Reduction. *J. Am. Chem. Soc.* **2010**, *132*, 1676−1684.

(400) Tondreau, A. M.; Milsmann, C.; Patrick, A. D.; Hoyt, H. M.; Lobkovsky, E.; Wieghardt, K.; Chirik, P. J. Synthesis and Electronic Structure of Cationic, Neutral, and Anionic Bis(imino)pyridine Iron Alkyl Complexes: Evaluation of Redox Activity in Single-Component Ethylene Polymerization Catalysts. *J. Am. Chem. Soc.* **2010**, *132*, 15046−15049.

(401) Fernández, I.; Trovitch, R. J.; Lobkovsky, E.; Chirik, P. J. Synthesis of Bis(imino)pyridine Iron Di- and Monoalkyl Complexes: Stability Differences between $FeCH_2SiMe_3$ and $FeCH_2CMe_3$ Derivatives. *Organometallics* **2008**, *27*, 109−118.

(402) Tondreau, A. M.; Stieber, S. C. E.; Milsmann, C.; Lobkovsky, E.; Weyhermüller, T.; Semproni, S. P.; Chirik, P. J. Oxidation and Reduction of Bis(imino)pyridine Iron Dinitrogen Complexes: Evidence for Formation of a Chelate Trianion. *Inorg. Chem.* **2013**, *52*, 635−646.

(403) Scott, J.; Gambarotta, S.; Korobkov, I.; Budzelaar, P. H. M. Reduction of (Diiminopyridine)iron: Evidence for a Noncationic Polymerization Pathway? *Organometallics* **2005**, *24*, 6298−6300.

(404) Doll, J. S.; Eichelmann, R.; Hertwig, L. E.; Bender, T.; Kohler, V. J.; Bill, E.; Wadepohl, H.; Roşca, D. A. Iron-Catalyzed Trimerization of Terminal Alkynes Enabled by Pyrimidinediimine Ligands: A Regioselective Method for the Synthesis of 1,3,5-Substituted Arenes. *ACS Catal.* **2021**, *11*, 5593−5600.

(405) Scott, J.; Vidyaratne, I.; Korobkov, I.; Gambarotta, S.; Budzelaar, P. H. M. Multiple Pathways for Dinitrogen Activation during the Reduction of an Fe Bis(iminepyridine) Complex. *Inorg. Chem.* **2008**, *47*, 896−911.

(406) Herzog, S.; Taube, R. Neutralkomplexe Des 2,2′-Dipyridyls Teil I Darstellung und Eigenschaften. *Z. Chem.* **1962**, *2*, 208−214.

(407) Behrens, H.; Meyer, K. Über neue Darstellungsweisen von Nickel(0)-Komplexen aus Nickelocen. *Z. Naturforsch. B* **1966**, *21*, 489−490.

(408) Khusniyarov, M. M.; Weyhermüller, T.; Bill, E.; Wieghardt, K. Tuning the Oxidation Level, the Spin State, and the Degree of Electron Delocalization in Homo- And Heteroleptic Bis(α-Diimine) Iron Complexes. *J. Am. Chem. Soc.* **2009**, *131*, 1208−1221.

(409) Rodríguez-Lugo, R. E.; Trincado, M.; Vogt, M.; Tewes, F.; Santiso-Quinones, G.; Grützmacher, H. A Homogeneous Transition Metal Complex for Clean Hydrogen Production from Methanol-Water Mixtures. *Nat. Chem.* **2013**, *5*, 342−347.

(410) Sinha, V.; Trincado, M.; Grützmacher, H.; de Bruin, B. DFT Provides Insight into the Additive-Free Conversion of Aqueous Methanol to Dihydrogen Catalyzed by [Ru(trop$_2$dad)]: Importance of the (Electronic) Flexibility of the Diazadiene Moiety. *J. Am. Chem. Soc.* **2018**, *140*, 13103−13114.

(411) Govindarajan, N.; Sinha, V.; Trincado, M.; Grützmacher, H.; Meijer, E. J.; de Bruin, B. An In-Depth Mechanistic Study of Ru-Catalysed Aqueous Methanol Dehydrogenation and Prospects for Future Catalyst Design. *ChemCatChem.* **2020**, *12*, 2610−2621.

(412) de Zwart, F. J.; Sinha, V.; Trincado, M.; Grützmacher, H.; de Bruin, B. Computational Mechanistic Studies of Ruthenium Catalysed Methanol Dehydrogenation. *Dalton Trans.* **2022**, *51*, 3019−3026.

(413) Prokopchuk, D. E.; Lough, A. J.; Rodríguez-Lugo, R. E.; Morris, R. H.; Grützmacher, H. Insights into Metal-Ligand Hydrogen Transfer: A Square-Planar Ruthenate Complex Supported by a Tetradentate Amino-Amido-Diolefin Ligand. *Chem. Commun.* **2016**, *52*, 6138−6141.

(414) Casas, F.; Trincado, M.; Rodríguez-Lugo, R.; Baneerje, D.; Grützmacher, H. A Diaminopropane Diolefin Ru(0) Complex Catalyzes Hydrogenation and Dehydrogenation Reactions. *ChemCatChem.* **2019**, *11*, 5241−5251.

(415) Trincado, M.; Sinha, V.; Rodríguez-Lugo, R. E.; Pribanic, B.; de Bruin, B.; Grützmacher, H. Homogeneously Catalysed Conversion of Aqueous Formaldehyde to H_2 and Carbonate. *Nat. Commun.* **2017**, *8*, 14990.

(416) Yang, X.; Gianetti, T. L.; Wörle, M. D.; van Leest, N. P.; de Bruin, B.; Grützmacher, H. A Low-Valent Dinuclear Ruthenium Diazadiene Complex Catalyzes the Oxidation of Dihydrogen and Reversible Hydrogenation of Quinones. *Chem. Sci.* **2019**, *10*, 1117−1125.

(417) Bösken, J.; Rodríguez-Lugo, R. E.; Nappen, S.; Trincado, M.; Grützmacher, H. Reduction of Nitrous Oxide by Light Alcohols Catalysed by a Low-Valent Ruthenium Diazadiene Complex. *Chem. Eur. J.* **2023**, *29*, No. e202203632.

(418) Borys, A. M.; Hevia, E. The Anionic Pathway in the Nickel-Catalysed Cross-Coupling of Aryl Ethers. *Angew. Chem., Int. Ed.* **2021**, *60*, 24659−24667.

(419) Somerville, R. J.; Borys, A. M.; Perez-Jimenez, M.; Nova, A.; Balcells, D.; Malaspina, L. A.; Grabowsky, S.; Carmona, E.; Hevia, E.; Campos, J. Unmasking the Constitution and Bonding of the Proposed Lithium Nickelate "$Li_3NiPh_3(solv)_3$": Revealing the Hidden C_6H_4 Ligand. *Chem. Sci.* **2022**, *13*, 5268−5276.

(420) Borys, A. M.; Malaspina, L. A.; Grabowsky, S.; Hevia, E. Towards Hexagonal Planar Nickel: A Dispersion-Stabilised Tri-Lithium Nickelate. *Angew. Chem., Int. Ed.* **2022**, *61*, No. e202209797.

(421) Blake, M. P.; Kaltsoyannis, N.; Mountford, P. Probing the Limits of Alkaline Earth-Transition Metal Bonding: An Experimental and Computational Study. *J. Am. Chem. Soc.* **2015**, *137*, 12352−12368.

(422) Green, R.; Walker, A. C.; Blake, M. P.; Mountford, P. Synthesis, Characterisation and Structural Studies of Amidinate and Guanidinate Alkaline Earth-Transition Metal Bonded Complexes. *Polyhedron* **2016**, *116*, 64−75.

(423) Garçon, M.; Bakewell, C.; White, A. J. P.; Crimmin, M. R. Unravelling Nucleophilic Aromatic Substitution Pathways with Bimetallic Nucleophiles. *Chem. Commun.* **2019**, *55*, 1805−1808.

(424) Garçon, M.; Bakewell, C.; Sackman, G. A.; White, A. J. P.; Cooper, R. I.; Edwards, A. J.; Crimmin, M. R. A Hexagonal Planar Transition-Metal Complex. *Nature* **2019**, *574*, 390−393.

(425) Garçon, M.; Phanopoulos, A.; Sackman, G. A.; Richardson, C.; White, A. J. P.; Cooper, R. I.; Edwards, A. J.; Crimmin, M. R. The Continuum Between Hexagonal Planar and Trigonal Planar Geometries. *Angew. Chem., Int. Ed.* **2022**, *61*, No. e202211948.

(426) Garçon, M.; Phanopoulos, A.; White, A. J. P.; Crimmin, M. R. Reversible Dihydrogen Activation and Catalytic H/D Exchange with Group 10 Heterometallic Complexes. *Angew. Chem., Int. Ed.* **2023**, *62*, No. e202213001.

(427) Kelly, J. A.; Gramüller, J.; Gschwind, R. M.; Wolf, R. Low-Oxidation State Cobalt-Magnesium Complexes: Ion-Pairing and Reactivity. *Dalton Trans.* **2021**, *50*, 13985−13992.

(428) Moret, M. E.; Peters, J. C. N_2 Functionalization at Iron Metallaboratranes. *J. Am. Chem. Soc.* **2011**, *133*, 18118−18121.

(429) Anderson, J. S.; Moret, M. E.; Peters, J. C. Conversion of Fe-NH_2 to Fe-N_2 with Release of NH_3. *J. Am. Chem. Soc.* **2013**, *135*, 534−537.

(430) Anderson, J. S.; Rittle, J.; Peters, J. C. Catalytic Conversion of Nitrogen to Ammonia by an Iron Model Complex. *Nature* **2013**, *501*, 84−87.

(431) Whited, M. T.; Mankad, N. P.; Lee, Y.; Oblad, P. F.; Peters, J. C. Dinitrogen Complexes Supported by Tris(phosphino)silyl Ligands. *Inorg. Chem.* **2009**, *48*, 2507−2517.

(432) Lee, Y.; Mankad, N. P.; Peters, J. C. Triggering N_2 Uptake via Redox-Induced Expulsion of Coordinated NH_3 and N_2 Silylation at Trigonal Bipyramidal Iron. *Nat. Chem.* **2010**, *2*, 558−565.

(433) Rudd, P. A.; Liu, S.; Gagliardi, L.; Young, V. G.; Lu, C. C. Metal-Alane Adducts with Zero-Valent Nickel, Cobalt, and Iron. *J. Am. Chem. Soc.* **2011**, *133*, 20724−20727.

(434) Rudd, P. A.; Planas, N.; Bill, E.; Gagliardi, L.; Lu, C. C. Dinitrogen Activation at Iron and Cobalt Metallalumatranes. *Eur. J. Inorg. Chem.* **2013**, *2013*, 3898−3906.

(435) Clouston, L. J.; Siedschlag, R. B.; Rudd, P. A.; Planas, N.; Hu, S.; Miller, A. D.; Gagliardi, L.; Lu, C. C. Systematic Variation of Metal-Metal Bond Order in Metal-Chromium Complexes. *J. Am. Chem. Soc.* **2013**, *135*, 13142−13148.

(436) Cammarota, R. C.; Lu, C. C. Tuning Nickel with Lewis Acidic Group 13 Metalloligands for Catalytic Olefin Hydrogenation. *J. Am. Chem. Soc.* **2015**, *137*, 12486−12489.

(437) Rudd, P. A.; Liu, S.; Planas, N.; Bill, E.; Gagliardi, L.; Lu, C. C. Multiple Metal-Metal Bonds in Iron-Chromium Complexes. *Angew. Chem., Int. Ed.* **2013**, *52*, 4449−4452.

(438) Sandl, S.; Jacobi von Wangelin, A. The Role of Organoferrates in Iron-Catalyzed Cross-Couplings. *Angew. Chem., Int. Ed.* **2020**, *59*, 5434−5437.

(439) Yamada, S. Cation-π Interactions in Organic Synthesis. *Chem. Rev.* **2018**, *118*, 11353−11432.

(440) Kennedy, C. R.; Lin, S.; Jacobsen, E. N. The Cation-π Interaction in Small-Molecule Catalysis. *Angew. Chem., Int. Ed.* **2016**, *55*, 12596−12624.

(441) Mahmudov, K. T.; Gurbanov, A. V.; Guseinov, F. I.; Guedes da Silva, M. F. C. Noncovalent Interactions in Metal Complex Catalysis. *Coord. Chem. Rev.* **2019**, *387*, 32−46.

(442) Freitag, F.; Irrgang, T.; Kempe, R. Mechanistic Studies of Hydride Transfer to Imines from a Highly Active and Chemoselective Manganate Catalyst. *J. Am. Chem. Soc.* **2019**, *141*, 11677−11685.

(443) Sandl, S.; Maier, T. M.; Van Leest, N. P.; Kröncke, S.; Chakraborty, U.; Demeshko, S.; Koszinowski, K.; de Bruin, B.; Meyer, F.; Bodensteiner, M.; et al. Cobalt-Catalyzed Hydrogenations via Olefin Cobaltate and Hydride Intermediates. *ACS Catal.* **2019**, *9*, 7596−7606.

(444) Bogdanović, B.; Schwickardi, M. Transition Metal Catalyzed Preparation of Grignard Compounds. *Angew. Chem., Int. Ed.* **2000**, *39*, 4610−4612.

(445) Scheiper, B.; Bonnekessel, M.; Krause, H.; Fürstner, A. Selective Iron-Catalyzed Cross-Coupling Reactions of Grignard Reagents with Enol Triflates, Acid Chlorides, and Dichloroarenes. *J. Org. Chem.* **2004**, *69*, 3943−3949.

(446) Fürstner, A.; Leitner, A.; Méndez, M.; Krause, H. Iron-Catalyzed Cross-Coupling Reactions. *J. Am. Chem. Soc.* **2002**, *124*, 13856−13863.

(447) Martin, R.; Fürstner, A. Cross-Coupling of Alkyl Halides with Aryl Grignard Reagents Catalyzed by a Low-Valent Iron Complex. *Angew. Chem., Int. Ed.* **2004**, *43*, 3955−3957.

(448) Fürstner, A.; Leitner, A. Iron-Catalyzed Cross-Coupling Reactions of Alkyl-Grignard Reagents with Aryl Chlorides, Tosylates, and Triflates. *Angew. Chem., Int. Ed.* **2002**, *41*, 609−612.

(449) Weber, K.; Schnöckelborg, E.-M.; Wolf, R. Catalytic Properties of Low Oxidation State Iron Complexes in Cross-Coupling Reactions: Anthracene Iron(−I) Complexes as Competent Catalysts. *ChemCatChem.* **2011**, *3*, 1572−1577.

(450) Casitas, A.; Krause, H.; Lutz, S.; Goddard, R.; Bill, E.; Fürstner, A. Ligand Exchange on and Allylic C-H Activation by Iron(0) Fragments: π-Complexes, Allyliron Species, and Metallacycles. *Organometallics* **2018**, *37*, 729−739.

(451) Bedford, R. B. How Low Does Iron Go? Chasing the Active Species in Fe-Catalyzed Cross-Coupling Reactions. *Acc. Chem. Res.* **2015**, *48*, 1485−1493.

(452) Carter, E.; Murphy, D. M. The Role of Low Valent Transition Metal Complexes in Homogeneous Catalysis: An EPR Investigation. *Top. Catal.* **2015**, *58*, 759−768.

(453) Bedford, R. B.; Brenner, P. B.; Carter, E.; Cogswell, P. M.; Haddow, M. F.; Harvey, J. N.; Murphy, D. M.; Nunn, J.; Woodall, C. H. TMEDA in Iron-Catalyzed Kumada Coupling: Amine Adduct versus Homoleptic "Ate" Complex Formation. *Angew. Chem., Int. Ed.* **2014**, *53*, 1804−1808.

(454) Muñoz III, S. B.; Daifuku, S. L.; Sears, J. D.; Baker, T. M.; Carpenter, S. H.; Brennessel, W. W.; Neidig, M. L. The N-Methylpyrrolidone (NMP) Effect in Iron-Catalyzed Cross-Coupling with Simple Ferric Salts and MeMgBr. *Angew. Chem., Int. Ed.* **2018**, *57*, 6496−6500.

(455) Felkin, H.; Knowles, P. J.; Meunier, B.; Mitschler, A.; Ricard, L.; Weiss, R. Preparation and Crystal Structure of π-Cyclopentadienyl-1,2-Bis(diphenylphosphino)ethaneironmagnesium Bromide Tris(tetrahydrofuran), a Transition-Metal Grignard Reagent. *J. Chem. Soc., Chem. Commun.* **1974**, 44.

(456) Muñoz, S. B.; Daifuku, S. L.; Brennessel, W. W.; Neidig, M. L. Isolation, Characterization, and Reactivity of $Fe_8Me_{12}^-$: Kochi's S = 1/2 Species in Iron-Catalyzed Cross-Couplings with MeMgBr and Ferric Salts. *J. Am. Chem. Soc.* **2016**, *138*, 7492−7495.

(457) Parchomyk, T.; Koszinowski, K. Ate Complexes in Iron-Catalyzed Cross-Coupling Reactions. *Chem. Eur. J.* **2016**, *22*, 15609−15613.

(458) Parchomyk, T.; Koszinowski, K. Solution and Gas-Phase Reactivity of $Me_{12}Fe_8^-$ and Related Cluster Ions. *Chem. Eur. J.* **2017**, *23*, 3213−3219.

(459) Parchomyk, T.; Demeshko, S.; Meyer, F.; Koszinowski, K. Oxidation States, Stability, and Reactivity of Organoferrate Complexes. *J. Am. Chem. Soc.* **2018**, *140*, 9709−9720.

(460) Borys, A. M.; Hevia, E. Mechanisms of the Nickel-Catalysed Hydrogenolysis and Cross-Coupling of Aryl Ethers. *Synthesis* **2022**, *54*, 2976−2990.

(461) Borys, A. M.; Hevia, E. New Frontiers in Alkali-Metal Nickelates. *Chimia* **2023**, *77*, 242.

(462) Taube, R.; Stransky, N.; Höboldt, W. σ-Organokomplexe mit einer niederen Oxydationsstufe des Zentralatoms: Lithium-trisphenylniccolat(0)-3-Tetrahydrofuran. *Z. Chem.* **1979**, *19*, 412−413.

(463) Taube, R. New Results in the Coordination Chemistry of σ-Bonded Carbanionic Ligands. *Pure Appl. Chem.* **1983**, *55*, 165−176.

(464) Taube, R.; Steinborn, D.; Drevs, H.; Chuong, P. N.; Stransky, N.; Langlotz, J. Redoxstabilität in Der σ-Organoübergangsmetallchemie. *Z. Chem.* **1988**, *28*, 381−396.

(465) Hope, H.; Power, P. P. Isolation and Crystal Structures of the Halide-Free and Halide-Rich Phenyllithium Etherate Complexes $[(PhLi{\cdot}Et_2O)_4]$ and $[(PhLi{\cdot}Et_2O)_3{\cdot}LiBr]$. *J. Am. Chem. Soc.* **1983**, *105*, 5320−5324.

(466) Liptrot, D. J.; Power, P. P. London Dispersion Forces in Sterically Crowded Inorganic and Organometallic Molecules. *Nat. Rev. Chem.* **2017**, *1*, 4.

(467) Green, S. P.; Jones, C.; Stasch, A. Stable Magnesium(I) Compounds with Mg-Mg Bonds. *Science* **2007**, *318*, 1754−1757.

(468) Bonyhady, S. J.; Green, S. P.; Jones, C.; Nembenna, S.; Stasch, A. A Dimeric Magnesium(I) Compound as a Facile Two-Center/Two-Electron Reductant. *Angew. Chem., Int. Ed.* **2009**, *48*, 2973−2977.

(469) Jones, C. Dimeric Magnesium(I) β-Diketiminates: A New Class of Quasi-Universal Reducing Agent. *Nat. Rev. Chem.* **2017**, *1*, 59.

(470) Green, M. L. H.; Moser, G. A.; Packer, I.; Petit, F.; Forder, R. A.; Prout, K. Inorgano-Grignard Reagents. Reactions and Crystal Structure of Bis-μ-[bis-(η-cyclopentadienyl)hydridomolybdenum]-bis{di-μ-bromo-[cyclohexylmagnesium (diethyl ether)magnesium]}; a Cyclic Compound Containing Covalent $MoMg_2$ Systems. *J. Chem. Soc., Chem. Commun.* **1974**, 839−840.

(471) Jonas, K.; Koepe, G.; Krüger, C. Heterometallic Dinuclear Complexes by Ethene Displacement with Grignard Compounds or Diorganomagnesium Compounds. *Angew. Chem., Int. Ed. Engl.* **1986**, *25*, 923−925.

(472) Hicks, J.; Hoyer, C. E.; Moubaraki, B.; Manni, G. L.; Carter, E.; Murphy, D. M.; Murray, K. S.; Gagliardi, L.; Jones, C. A Two-Coordinate Manganese(0) Complex with an Unsupported Mn-Mg Bond: Allowing Access to Low Coordinate Homo- and Hetero-bimetallic Compounds. *J. Am. Chem. Soc.* **2014**, *136*, 5283−5286.

(473) Birchall, C.; Moxey, G. J.; McMaster, J.; Blake, A. J.; Lewis, W.; Kays, D. L. A Monomeric, Heterobimetallic Complex with an Unsupported Mg-Fe Bond. *Inorg. Chim. Acta* **2017**, *458*, 97−100.

(474) Ekkert, O.; White, A. J. P.; Toms, H.; Crimmin, M. R. Addition of Aluminium, Zinc and Magnesium Hydrides to Rhodium-(III). *Chem. Sci.* **2015**, *6*, 5617−5622.

(475) Wolf, R.; Ehlers, A. W.; Khusniyarov, M. M.; Hartl, F.; Debruin, B.; Long, G. J.; Grandjean, F.; Schappacher, F. M.; Pöttgen, R.; Slootweg, J. C.; et al. Homoleptic Diphosphacyclobutadiene Complexes $[M(\eta^4\text{-}P_2C_2R_2)_2]^{x-}$ (M = Fe, Co; x = 0, 1). *Chem. Eur. J.* **2010**, *16*, 14322−14334.

(476) Rödl, C.; Wolf, R. Flexidentate Coordination Behavior and Chemical Non-Innocence of a Bis(1,3-diphosphacyclobutadiene) Sandwich Anion. *Chem. Eur. J.* **2019**, *25*, 8332−8343.

(477) Kelly, J. A.; Streitferdt, V.; Dimitrova, M.; Gschwind, R. M.; Berger, R. J. F.; Wolf, R. Transition-Metal-Stabilized Heavy Tetraphospholide Anions. *J. Am. Chem. Soc.* **2022**, *144*, 20434−20441.

(478) Huang, J.; Zheng, X.; Del Rosal, I.; Zhao, B.; Maron, L.; Xu, X. Nickel(0)-Induced β-H Elimination of Magnesium Alkyls: Formation and Reactivity of Heterometallic Hydrides. *Inorg. Chem.* **2020**, *59*, 13473−13480.

(479) Cai, Y.; Jiang, S.; Rajeshkumar, T.; Maron, L.; Xu, X. A Planar Nickelaspiropentane Complex with Magnesium-Based Metalloligands: Synthesis, Structure, and Synergistic Dihydrogen Activation. *J. Am. Chem. Soc.* **2022**, *144*, 16647−16655.

(480) Chen, M.; Jiang, S.; Maron, L.; Xu, X. Transition Metal-Induced Dehydrogenative Coupling of Zinc Hydrides. *Dalton Trans.* **2019**, *48*, 1931−1935.

(481) Shoshani, M. M.; Liu, J.; Johnson, S. A. Mechanistic Insight into H/D Exchange by a Pentanuclear Ni-H Cluster and Synthesis and Characterization of Structural Analogues of Potential Intermediates. *Organometallics* **2018**, *37*, 116−126.

(482) Bontemps, S.; Bouhadir, G.; Dyer, P. W.; Miqueu, K.; Bourissou, D. Quasi-Thermoneutral P → B Interactions within Di- and Tri-Phosphine Boranes. *Inorg. Chem.* **2007**, *46*, 5149−5151.

(483) Bontemps, S.; Bouhadir, G.; Gu, W.; Mercy, M.; Chen, C.-H.; Foxman, B. M.; Maron, L.; Ozerov, O. V.; Bourissou, D. Metallaboratranes Derived from a Triphosphanyl-Borane: Intrinsic C_3 Symmetry Supported by a Z-Type Ligand. *Angew. Chem., Int. Ed.* **2008**, *47*, 1481−1484.

(484) Sircoglou, M.; Bontemps, S.; Bouhadir, G.; Saffon, N.; Miqueu, K.; Gu, W.; Mercy, M.; Chen, C. H.; Foxman, B. M.; Maron, L.; et al. Group 10 and 11 Metal Boratranes (Ni, Pd, Pt, CuCl, AgCl, AuCl, and Au^+) Derived from a Triphosphine-Borane. *J. Am. Chem. Soc.* **2008**, *130*, 16729−16738.

(485) Braunschweig, H.; Dewhurst, R. D. Transition Metals as Lewis Bases: "Z-Type" Boron Ligands and Metal-to-Boron Dative Bonding. *Dalton Trans.* **2011**, *40*, 549−558.

(486) Thompson, N. B.; Green, M. T.; Peters, J. C. Nitrogen Fixation via a Terminal Fe(IV) Nitride. *J. Am. Chem. Soc.* **2017**, *139*, 15312−15315.

(487) Chalkley, M. J.; Peters, J. C. A Triad of Highly Reduced, Linear Iron Nitrosyl Complexes: $\{FeNO\}^{8-10}$. *Angew. Chem., Int. Ed.* **2016**, *55*, 11995−11998.

(488) Dong, H. T.; Chalkley, M. J.; Oyala, P. H.; Zhao, J.; Alp, E. E.; Hu, M. Y.; Peters, J. C.; Lehnert, N. Exploring the Limits of Dative Boratrane Bonding: Iron as a Strong Lewis Base in Low-Valent Non-Heme Iron-Nitrosyl Complexes. *Inorg. Chem.* **2020**, *59*, 14967−14982.

(489) Enemark, J. H.; Feltham, R. D. Principles of Structure, Bonding, and Reactivity for Metal Nitrosyl Complexes. *Coord. Chem. Rev.* **1974**, *13*, 339−406.

(490) Takaoka, A.; Gerber, L. C. H.; Peters, J. C. Access to Well-Defined Ruthenium(I) and Osmium(I) Metalloradicals. *Angew. Chem. Int. Ed.* **2010**, *49*, 4088−4091.

(491) Fajardo, J.; Peters, J. C. Catalytic Nitrogen-to-Ammonia Conversion by Osmium and Ruthenium Complexes. *J. Am. Chem. Soc.* **2017**, *139*, 16105−16108.

(492) Nance, P. J.; Thompson, N. B.; Oyala, P. H.; Peters, J. C. Zerovalent Rhodium and Iridium Silatranes Featuring Two-Center, Three-Electron Polar σ Bonds. *Angew. Chem., Int. Ed.* **2019**, *58*, 6220−6224.

(493) Takaoka, A.; Peters, J. C. A Homologous Series of Cobalt, Rhodium, and Iridium Metalloradicals. *Inorg. Chem.* **2012**, *51*, 16−18.

(494) Ghana, P.; Arz, M. I.; Chakraborty, U.; Schnakenburg, G.; Filippou, A. C. Linearly Two-Coordinated Silicon: Transition Metal Complexes with the Functional Groups M≡Si - M and M═Si═M. *J. Am. Chem. Soc.* **2018**, *140*, 7187−7198.

(495) Su, W.; Kim, Y.; Ellern, A.; Guzei, I. A.; Verkade, J. G. Facile Synthesis of Monomeric Alumatranes. *J. Am. Chem. Soc.* **2006**, *128*, 13727−13735.

(496) Clouston, L. J.; Bernales, V.; Carlson, R. K.; Gagliardi, L.; Lu, C. C. Bimetallic Cobalt-Dinitrogen Complexes: Impact of the Supporting Metal on N_2 Activation. *Inorg. Chem.* **2015**, *54*, 9263−9270.

(497) Moore, J. T.; Chatterjee, S.; Tarrago, M.; Clouston, L. J.; Sproules, S.; Bill, E.; Bernales, V.; Gagliardi, L.; Ye, S.; Lancaster, K. M.; et al. Enhanced Fe-Centered Redox Flexibility in Fe-Ti Heterobimetallic Complexes. *Inorg. Chem.* **2019**, *58*, 6199−6214.

(498) Eisenhart, R. J.; Clouston, L. J.; Lu, C. C. Configuring Bonds between First-Row Transition Metals. *Acc. Chem. Res.* **2015**, *48*, 2885−2894.

(499) Gärtner, D.; Welther, A.; Rad, B. R.; Wolf, R.; Jacobi von Wangelin, A. Heteroatom-Free Arene-Cobalt and Arene-Iron Catalysts for Hydrogenations. *Angew. Chem., Int. Ed.* **2014**, *53*, 3722−3726.

(500) Maier, T. M.; Sandl, S.; Melzl, P.; Zweck, J.; Jacobi von Wangelin, A.; Wolf, R. Heterogeneous Olefin Hydrogenation Enabled by a Highly-Reduced Nickel(−II) Catalyst Precursor. *Chem. Eur. J.* **2020**, *26*, 6113−6117.

(501) Beaumier, E. P.; Pearce, A. J.; See, X. Y.; Tonks, I. A. Modern Applications of Low-Valent Early Transition Metals in Synthesis and Catalysis. *Nat. Rev. Chem.* **2019**, *3*, 15−34.

(502) Erdelmeier, I.; Won, J.; Park, S.; Decker, J.; Bülow, G.; Baik, M.-H.; Gais, H.-J. Nickel-Catalyzed Anionic Cross-Coupling Reaction of Lithium Sulfonimidoyl Alkylidene Carbenoids With Organo-lithiums. *Chem. Eur. J.* **2020**, *26*, 2914−2926.

(503) Gülak, S.; Stepanek, O.; Malberg, J.; Rad, B. R.; Kotora, M.; Wolf, R.; Jacobi von Wangelin, A. Highly Chemoselective Cobalt-Catalyzed Biaryl Coupling Reactions. *Chem. Sci.* **2013**, *4*, 776−784.

(504) Nattmann, L.; Lutz, S.; Ortsack, P.; Goddard, R.; Cornella, J. A Highly Reduced Ni-Li-Olefin Complex for Catalytic Kumada-Corriu Cross-Couplings. *J. Am. Chem. Soc.* **2018**, *140*, 13628−13633.

(505) Kreyenschmidt, F.; Koszinowski, K. Low-Valent Ate Complexes Formed in Cobalt-Catalyzed Cross-Coupling Reactions with 1,3-Dienes as Additives. *Chem. Eur. J.* **2018**, *24*, 1168−1177.

(506) Church, T. L.; Getzler, Y. D. Y. L.; Byrne, C. M.; Coates, G. W. Carbonylation of Heterocycles by Homogeneous Catalysts. *Chem. Commun.* **2007**, 657−674.

(507) Hasegawa, S.; Ishida, Y.; Kawaguchi, H. Systematic Reductive Oligomerization of Isocyanides with a Vanadium(II) Complex. *Chem. Commun.* **2021**, *57*, 8296−8299.

(508) Oliveira, J. C. A.; Dhawa, U.; Ackermann, L. Insights into the Mechanism of Low-Valent Cobalt-Catalyzed C−H Activation. *ACS Catal.* **2021**, *11*, 1505−1515.

(509) Cabré, A.; Verdaguer, X.; Riera, A. Recent Advances in the Enantioselective Synthesis of Chiral Amines via Transition Metal-Catalyzed Asymmetric Hydrogenation. *Chem. Rev.* **2022**, *122*, 269−339.

(510) Li, Y. Y.; Yu, S. L.; Shen, W. Y.; Gao, J. X. Iron-, Cobalt-, and Nickel-Catalyzed Asymmetric Transfer Hydrogenation and Asymmetric Hydrogenation of Ketones. *Acc. Chem. Res.* **2015**, *48*, 2587−2598.

(511) Kumar, A.; Daw, P.; Milstein, D. Homogeneous Catalysis for Sustainable Energy: Hydrogen and Methanol Economies, Fuels from Biomass, and Related Topics. *Chem. Rev.* **2022**, *122*, 385−441.

(512) Wu, S. B.; Zhang, T.; Chung, L. W.; Wu, Y. D. A Missing Piece of the Mechanism in Metal-Catalyzed Hydrogenation: Co(−I)/Co(0)/Co(+I) Catalytic Cycle for Co(−I)-Catalyzed Hydrogenation. *Org. Lett.* **2019**, *21*, 360−364.

(513) Regenauer, N. I.; Wadepohl, H.; Roşca, D. A. Metal-Ligand Cooperativity in Iron Dinitrogen Complexes: Proton-Coupled Electron Transfer Disproportionation and an Anionic Fe(0)N_2 Hydride. *Inorg. Chem.* **2022**, *61*, 7426−7435.

(514) Kallmeier, F.; Dudziec, B.; Irrgang, T.; Kempe, R. Manganese-Catalyzed Sustainable Synthesis of Pyrroles from Alcohols and Amino Alcohols. *Angew. Chem., Int. Ed.* **2017**, *56*, 7261−7265.

(515) Wang, Y.; Liu, S.; Yang, H.; Li, H.; Lan, Y.; Liu, Q. Structure, Reactivity and Catalytic Properties of Manganese-Hydride Amidate Complexes. *Nat. Chem.* **2022**, *14*, 1233−1241.

(516) Fokin, I.; Siewert, I. Chemoselective Electrochemical Hydrogenation of Ketones and Aldehydes with a Well-Defined Base-Metal Catalyst. *Chem. Eur. J.* **2020**, *26*, 14137−14143.

(517) Schlenker, K.; Christensen, E. G.; Zhanserkeev, A. A.; McDonald, G. R.; Yang, E. L.; Lutz, K. T.; Steele, R. P.; VanderLinden, R. T.; Saouma, C. T. Role of Ligand-Bound CO_2 in the Hydrogenation of CO_2 to Formate with a (PNP)Mn Catalyst. *ACS Catal.* **2021**, *11*, 8358−8369.

(518) Han, B.; Ma, P.; Cong, X.; Chen, H.; Zeng, X. Chromium- and Cobalt-Catalyzed, Regiocontrolled Hydrogenation of Polycyclic Aromatic Hydrocarbons: A Combined Experimental and Theoretical Study. *J. Am. Chem. Soc.* **2019**, *141*, 9018−9026.

(519) Hartwig, J. F. Oxidative Addition of Nonpolar Reagents. In *Organotransition Metal Chemistry: From Bonding to Catalysis*; University Science Books: Sausalito, CA, 2010; pp 266−269.

(520) Crabtree, R. H. Dihydrogen Complexation. *Chem. Rev.* **2016**, *116*, 8750−8769.

(521) Cammarota, R. C.; Xie, J.; Burgess, S. A.; Vollmer, M. V.; Vogiatzis, K. D.; Ye, J.; Linehan, J. C.; Appel, A. M.; Hoffmann, C.; Wang, X.; et al. Thermodynamic and Kinetic Studies of H_2 and N_2 Binding to Bimetallic Nickel-Group 13 Complexes and Neutron Structure of a Ni(η^2-H_2) Adduct. *Chem. Sci.* **2019**, *10*, 7029−7042.

(522) Deegan, M. M.; Hannoun, K. I.; Peters, J. C. Dihydrogen Adduct (Co-H_2) Complexes Displaying H-Atom and Hydride Transfer. *Angew. Chem., Int. Ed.* **2020**, *59*, 22631−22637.

(523) Prat, J. R.; Cammarota, R. C.; Graziano, B. J.; Moore, J. T.; Lu, C. C. Toggling the Z-Type Interaction off-on in Nickel-Boron Dihydrogen and Anionic Hydride Complexes. *Chem. Commun.* **2022**, *58*, 8798−8801.

(524) Cammarota, R. C.; Vollmer, M. V.; Xie, J.; Ye, J.; Linehan, J. C.; Burgess, S. A.; Appel, A. M.; Gagliardi, L.; Lu, C. C. A Bimetallic Nickel-Gallium Complex Catalyzes CO_2 Hydrogenation via the Intermediacy of an Anionic d^{10} Nickel Hydride. *J. Am. Chem. Soc.* **2017**, *139*, 14244−14250.

(525) Ye, J.; Cammarota, R. C.; Xie, J.; Vollmer, M. V.; Truhlar, D. G.; Cramer, C. J.; Lu, C. C.; Gagliardi, L. Rationalizing the Reactivity of Bimetallic Molecular Catalysts for CO_2 Hydrogenation. *ACS Catal.* **2018**, *8*, 4955−4968.

(526) Vollmer, M. V.; Xie, J.; Lu, C. C. Stable Dihydrogen Complexes of Cobalt(−I) Suggest an Inverse Trans-Influence of Lewis Acidic Group 13 Metalloligands. *J. Am. Chem. Soc.* **2017**, *139*, 6570−6573.

(527) Vollmer, M. V.; Ye, J.; Linehan, J. C.; Graziano, B. J.; Preston, A.; Wiedner, E. S.; Lu, C. C. Cobalt-Group 13 Complexes Catalyze CO_2 Hydrogenation via a Co(−I)/Co(I) Redox Cycle. *ACS Catal.* **2020**, *10*, 2459−2470.

(528) Suess, D. L. M.; Tsay, C.; Peters, J. C. Dihydrogen Binding to Isostructural S = 1/2 and S = 0 Cobalt Complexes. *J. Am. Chem. Soc.* **2012**, *134*, 14158−14164.

(529) Gunderson, W. A.; Suess, D. L. M.; Fong, H.; Wang, X.; Hoffmann, C. M.; Cutsail, G. E.; Peters, J. C.; Hoffman, B. M. Free H_2 Rotation vs Jahn-Teller Constraints in the Nonclassical Trigonal (TPB)Co-H_2 Complex. *J. Am. Chem. Soc.* **2014**, *136*, 14998−15009.

(530) Harman, W. H.; Peters, J. C. Reversible H_2 Addition across a Nickel-Borane Unit as a Promising Strategy for Catalysis. *J. Am. Chem. Soc.* **2012**, *134*, 5080−5082.

(531) Harman, W. H.; Lin, T.-P.; Peters, J. C. A d^{10} Ni-(H_2) Adduct as an Intermediate in H-H Oxidative Addition across a Ni-B Bond. *Angew. Chem., Int. Ed.* **2014**, *53*, 1081−1086.

(532) Pribanic, B.; Trincado, M.; Eiler, F.; Vogt, M.; Comas-Vives, A.; Grützmacher, H. Hydrogenolysis of Polysilanes Catalyzed by Low-Valent Nickel Complexes. *Angew. Chem., Int. Ed.* **2020**, *59*, 15603−15609.

(533) Lou, K.; Zhou, Q.; Wang, Q.; Fan, X.; Xu, X.; Cui, C. CpFe$(CO)_2$ Anion-Catalyzed Highly Efficient Hydrosilylation of Ketones and Aldehydes. *Dalton Trans.* **2021**, *50*, 11016−11020.

(534) Singh, D.; Buratto, W. R.; Torres, J. F.; Murray, L. J. Activation of Dinitrogen by Polynuclear Metal Complexes. *Chem. Rev.* **2020**, *120*, 5517−5581.

(535) Bhutto, S. M.; Holland, P. L. Dinitrogen Activation and Functionalization Using β-Diketiminate Iron Complexes. *Eur. J. Inorg. Chem.* **2019**, *2019*, 1861−1869.

(536) Kendall, A. J.; Mock, M. T. Dinitrogen Activation and Functionalization with Chromium. *Eur. J. Inorg. Chem.* **2020**, *2020*, 1358−1375.

(537) Piascik, A. D.; Ashley, A. E. Group 8 Transition Metal-Dinitrogen Complexes. *Transition Metal-Dinitrogen Complexes*. Nishibayashi, Y., Ed.; Wiley-VCH: 2019, 285−335

(538) Lu, C. C.; Prinslow, S. D. Group 9 Transition Metal-Dinitrogen Complexes. *Transition Metal-Dinitrogen Complexes*. Nishibayashi, Y., Ed.; Wiley-VCH: 2019, 337−402

(539) Stucke, N.; Flöser, B. M.; Weyrich, T.; Tuczek, F. Nitrogen Fixation Catalyzed by Transition Metal Complexes: Recent Developments. *Eur. J. Inorg. Chem.* **2018**, *2018*, 1337−1355.

(540) Nishibayashi, Y. Development of Catalytic Nitrogen Fixation Using Transition Metal-Dinitrogen Complexes under Mild Reaction Conditions. *Dalton Trans.* **2018**, *47*, 11290−11297.

(541) Lv, Z.-J.; Wei, J.; Zhang, W.-X.; Chen, P.; Deng, D.; Shi, Z.-J.; Xi, Z. Direct Transformation of Dinitrogen: Synthesis of N-Containing Organic Compounds via N-C Bond Formation. *Natl. Sci. Rev.* **2020**, *7*, 1564−1583.

(542) Tanabe, Y.; Nishibayashi, Y. Recent Advances in Catalytic Nitrogen Fixation Using Transition Metal-Dinitrogen Complexes under Mild Reaction Conditions. *Coord. Chem. Rev.* **2022**, *472*, 214783.

(543) Tanabe, Y.; Nishibayashi, Y. Recent Advances in Catalytic Silylation of Dinitrogen Using Transition Metal Complexes. *Coord. Chem. Rev.* **2019**, *389*, 73−93.

(544) Nishibayashi, Y. Recent Progress in Transition-Metal-Catalyzed Reduction of Molecular Dinitrogen under Ambient Reaction Conditions. *Inorg. Chem.* **2015**, *54*, 9234−9247.

(545) Hammer, R.; Klein, H.-F.; Friedrich, P.; Huttner, G. Hexameric $KN_2Co[P(CH_3)_3]_3$—A Novel Potassium-Dinitrogen Cluster. *Angew. Chem., Int. Ed. Engl.* **1977**, *16*, 485−486.

(546) Klein, H. F.; Koenig, H.; Koppert, S.; Ellrich, K.; Riede, J. Cobalt Diazenides of Main-Group I-III Metals: X-Ray Structure of a Grignard Compound Containing (Dinitrogen)(trimethylphosphane)-cobaltate Anions. *Organometallics* **1987**, *6*, 1341−1345.

(547) Yamamoto, A.; Miura, Y.; Ito, T.; Chen, H. L.; Iri, K.; Ozawa, F.; Miki, K.; Kasai, N.; Sei, T.; Tanaka, N. Preparation, X-Ray Molecular Structure Determination, and Chemical Properties of Dinitrogen-Coordinated Cobalt Complexes Containing Triphenylphosphine Ligands and Alkali Metal or Magnesium. Protonation of the Coordinated Dinitrogen to Ammonia and Hydrazin. *Organometallics* **1983**, *2*, 1429−1436.

(548) Betley, T. A.; Peters, J. C. Dinitrogen Chemistry from Trigonally Coordinated Iron and Cobalt Platforms. *J. Am. Chem. Soc.* **2003**, *125*, 10782−10783.

(549) MacKay, B. A.; Fryzuk, M. D. Dinitrogen Coordination Chemistry: On the Biomimetic Borderlands. *Chem. Rev.* **2004**, *104*, 385−401.

(550) Gao, Y.; Li, G.; Deng, L. Bis(dinitrogen)cobalt(−1) Complexes with NHC Ligation: Synthesis, Characterization, and Their Dinitrogen Functionalization Reactions Affording Side-on Bound Diazene Complexes. *J. Am. Chem. Soc.* **2018**, *140*, 2239−2250.

(551) Rodriguez, M. M.; Bill, E.; Brennessel, W. W.; Holland, P. L. N_2 Reduction and Hydrogenation to Ammonia by a Molecular Iron-Potassium Complex. *Science* **2011**, *334*, 780−783.

(552) Ding, K.; Pierpont, A. W.; Brennessel, W. W.; Lukat-Rodgers, G.; Rodgers, K. R.; Cundari, T. R.; Bill, E.; Holland, P. L. Cobalt-Dinitrogen Complexes with Weakened N-N Bonds. *J. Am. Chem. Soc.* **2009**, *131*, 9471−9472.

(553) Del Castillo, T. J.; Thompson, N. B.; Suess, D. L. M.; Ung, G.; Peters, J. C. Evaluating Molecular Cobalt Complexes for the Conversion of N_2 to NH_3. *Inorg. Chem.* **2015**, *54*, 9256−9262.

(554) Siedschlag, R. B.; Bernales, V.; Vogiatzis, K. D.; Planas, N.; Clouston, L. J.; Bill, E.; Gagliardi, L.; Lu, C. C. Catalytic Silylation of Dinitrogen with a Dicobalt Complex. *J. Am. Chem. Soc.* **2015**, *137*, 4638−4641.

(555) Yin, J.; Li, J.; Wang, G. X.; Yin, Z. B.; Zhang, W. X.; Xi, Z. Dinitrogen Functionalization Affording Chromium Hydrazido Complex. *J. Am. Chem. Soc.* **2019**, *141*, 4241−4247.

(556) Apps, S. L.; Miller, P. W.; Long, N. J. Cobalt(−I) Triphos Dinitrogen Complexes: Activation and Silyl-Functionalisation of N_2. *Chem. Commun.* **2019**, *55*, 6579−6582.

(557) Zhong, M.; Cui, X.; Wu, B.; Wang, G.-X.; Zhang, W.-X.; Wei, J.; Zhao, L.; Xi, Z. Dinitrogen Functionalization Affording Structurally Well-Defined Cobalt Diazenido Complexes. *CCS Chem.* **2022**, *4*, 532−539.

(558) Hammer, R.; Klein, H.-F.; Schubert, U.; Frank, A.; Huttner, G. A Novel Hetero-Bimetallic Dinitrogen Complex. *Angew. Chem., Int. Ed. Engl.* **1976**, *15*, 612−613.

(559) Lindley, B. M.; Van Alten, R. S.; Finger, M.; Schendzielorz, F.; Würtele, C.; Miller, A. J. M.; Siewert, I.; Schneider, S. Mechanism of Chemical and Electrochemical N_2 Splitting by a Rhenium Pincer Complex. *J. Am. Chem. Soc.* **2018**, *140*, 7922−7935.

(560) Klopsch, I.; Finger, M.; Würtele, C.; Milde, B.; Werz, D. B.; Schneider, S. Dinitrogen Splitting and Functionalization in the Coordination Sphere of Rhenium. *J. Am. Chem. Soc.* **2014**, *136*, 6881−6883.

(561) Yin, Z. B.; Wu, B.; Wang, G. X.; Wei, J.; Xi, Z. Dinitrogen Functionalization Affording Chromium Diazenido and Side-on H_2-Hydrazido Complexes. *J. Am. Chem. Soc.* **2023**, *145*, 7065−7070.

(562) Creutz, S. E.; Peters, J. C. Catalytic Reduction of N_2 to NH_3 by an Fe-N_2 Complex Featuring a C-Atom Anchor. *J. Am. Chem. Soc.* **2014**, *136*, 1105−1115.

(563) Djurdjevic, I.; Einsle, O.; Decamps, L. Nitrogenase Cofactor: Inspiration for Model Chemistry. *Chem. Asian. J.* **2017**, *12*, 1447−1455.

(564) Köthe, C.; Limberg, C. Late Metal Scaffolds That Activate Both, Dinitrogen and Reduced Dinitrogen Species N_xH_y. *Z. Anorg. Allg. Chem.* **2015**, *641*, 18−30.

(565) Barney, B. M.; McClead, J.; Lukoyanov, D.; Laryukhin, M.; Yang, T. C.; Dean, D. R.; Hoffman, B. M.; Seefeldt, L. C. Diazene (HN = NH) is a Substrate for Nitrogenase: Insights into the Pathway of N_2 Reduction. *Biochemistry* **2007**, *46*, 6784−6794.

(566) Huh, D. N.; Koby, R. F.; Stuart, Z. E.; Dunscomb, R. J.; Schley, N. D.; Tonks, I. A. Reassessment of N_2 Activation by Low-Valent Ti-Amide Complexes: A Remarkable Side-on Bridged Bis-N_2 Adduct Is Actually an Arene Adduct. *Chem. Sci.* **2022**, *13*, 13330−13337.

(567) Duchateau, R.; Gambarotta, S.; Beydoun, N.; Bensimon, C. Side-On versus End-On Coordination of Dinitrogen to Titanium (II) and Mixed-Valence Titanium(I)/Titanium(II) Amido Complexes. *J. Am. Chem. Soc.* **1991**, *113*, 8986−8988.

(568) MacLeod, K. C.; Menges, F. S.; McWilliams, S. F.; Craig, S. M.; Mercado, B. Q.; Johnson, M. A.; Holland, P. L. Alkali-Controlled C−H Cleavage or N-C Bond Formation by N_2-Derived Iron Nitrides and Imides. *J. Am. Chem. Soc.* **2016**, *138*, 11185−11191.

(569) Smith, J. M.; Lachicotte, R. J.; Pittard, K. A.; Cundari, T. R.; Lukat-Rodgers, G.; Rodgers, K. R.; Holland, P. L. Stepwise Reduction of Dinitrogen Bond Order by a Low-Coordinate Iron Complex. *J. Am. Chem. Soc.* **2001**, *123*, 9222−9223.

(570) Smith, J. M.; Sadique, A. R.; Cundari, T. R.; Rodgers, K. R.; Lukat-Rodgers, G.; Lachicotte, R. J.; Flaschenriem, C. J.; Vela, J.; Holland, P. L. Studies of Low-Coordinate Iron Dinitrogen Complexes. *J. Am. Chem. Soc.* **2006**, *128*, 756−769.

(571) McWilliams, S. F.; Holland, P. L. Dinitrogen Binding and Cleavage by Multinuclear Iron Complexes. *Acc. Chem. Res.* **2015**, *48*, 2059−2065.

(572) McWilliams, S. F.; Broere, D. L. J.; Halliday, C. J. V; Bhutto, S. M.; Mercado, B. Q.; Holland, P. L. Coupling Dinitrogen and Hydrocarbons through Aryl Migration. *Nature* **2020**, *584*, 221−226.

(573) Bhutto, S. M.; Hooper, R. X.; Mercado, B. Q.; Holland, P. L. Mechanism of Nitrogen-Carbon Bond Formation from Iron(IV) Disilylhydrazido Intermediates during N_2 Reduction. *J. Am. Chem. Soc.* **2023**, *145*, 4626−4637.

(574) McWilliams, S. F.; Rodgers, K. R.; Lukat-Rodgers, G.; Mercado, B. Q.; Grubel, K.; Holland, P. L. Alkali Metal Variation and Twisting of the FeNNFe Core in Bridging Diiron Dinitrogen Complexes. *Inorg. Chem.* **2016**, *55*, 2960−2968.

(575) Pfirrmann, S.; Limberg, C.; Herwig, C.; Stößer, R.; Ziemer, B. A Dinuclear Nickel(I) Dinitrogen Complex and Its Reduction in Single-Electron Steps. *Angew. Chem., Int. Ed.* **2009**, *48*, 3357−3361.

(576) Dugan, T. R.; MacLeod, K. C.; Brennessel, W. W.; Holland, P. L. Cobalt-Magnesium and Iron-Magnesium Complexes with Weakened Dinitrogen Bridges. *Eur. J. Inorg. Chem.* **2013**, 3891−3897.

(577) Čorić, I.; Mercado, B. Q.; Bill, E.; Vinyard, D. J.; Holland, P. L. Binding of Dinitrogen to an Iron-Sulfur-Carbon Site. *Nature* **2015**, *526*, 96−99.

(578) Speelman, A. L.; Čorić, I.; Van Stappen, C.; Debeer, S.; Mercado, B. Q.; Holland, P. L. Nitrogenase-Relevant Reactivity of a Synthetic Iron-Sulfur-Carbon Site. *J. Am. Chem. Soc.* **2019**, *141*, 13148−13157.

(579) Igarashi, R. Y.; Laryukhin, M.; Dos Santos, P. C.; Lee, H. I.; Dean, D. R.; Seefeldt, L. C.; Hoffman, B. M. Trapping H^- Bound to the Nitrogenase FeMo-Cofactor Active Site during H_2 Evolution: Characterization by ENDOR Spectroscopy. *J. Am. Chem. Soc.* **2005**, *127*, 6231−6241.

(580) Rittle, J.; McCrory, C. C. L.; Peters, J. C. A 10^6-Fold Enhancement in N_2-Binding Affinity of an $Fe_2(\mu\text{-}H)_2$ core upon Reduction to a Mixed-Valence $Fe^{II}Fe^{I}$ state. *J. Am. Chem. Soc.* **2014**, *136*, 13853−13862.

(581) Anderson, J. S.; Cutsail, G. E.; Rittle, J.; Connor, B. A.; Gunderson, W. A.; Zhang, L.; Hoffman, B. M.; Peters, J. C. Characterization of an Fe≡N-NH_2 Intermediate Relevant to Catalytic N_2 Reduction to NH_3. *J. Am. Chem. Soc.* **2015**, *137*, 7803−7809.

(582) Rittle, J.; Peters, J. C. An Fe-N_2 Complex That Generates Hydrazine and Ammonia via Fe═NNH_2: Demonstrating a Hybrid Distal-to-Alternating Pathway for N_2 Reduction. *J. Am. Chem. Soc.* **2016**, *138*, 4243−4248.

(583) Garrido-Barros, P.; Derosa, J.; Chalkley, M. J.; Peters, J. C. Tandem Electrocatalytic N_2 Fixation via Proton-Coupled Electron Transfer. *Nature* **2022**, *609*, 71−76.

(584) Kaczmarek, M. A.; Malhotra, A.; Balan, G. A.; Timmins, A.; de Visser, S. P. Nitrogen Reduction to Ammonia on a Biomimetic Mononuclear Iron Centre: Insights into the Nitrogenase Enzyme. *Chem. Eur. J.* **2018**, *24*, 5293−5302.

(585) Buscagan, T. M.; Oyala, P. H.; Peters, J. C. N_2-to-NH_3 Conversion by a Triphos-Iron Catalyst and Enhanced Turnover under Photolysis. *Angew. Chem., Int. Ed.* **2017**, *56*, 6921−6926.

(586) Del Castillo, T. J.; Thompson, N. B.; Peters, J. C. A Synthetic Single-Site Fe Nitrogenase: High Turnover, Freeze-Quench ^{57}Fe Mössbauer Data, and a Hydride Resting State. *J. Am. Chem. Soc.* **2016**, *138*, 5341−5350.

(587) Rittle, J.; Peters, J. C. Fe-N_2/CO Complexes That Model a Possible Role for the Interstitial C Atom of FeMo-Cofactor (FeMoco). *Proc. Natl. Acad. Sci. U. S. A.* **2013**, *110*, 15898−15903.

(588) Fong, H.; Moret, M. E.; Lee, Y.; Peters, J. C. Heterolytic H_2 Cleavage and Catalytic Hydrogenation by an Iron Metallaboratrane. *Organometallics* **2013**, *32*, 3053−3062.

(589) Chalkley, M. J.; Del Castillo, T. J.; Matson, B. D.; Roddy, J. P.; Peters, J. C. Catalytic N_2-to-NH_3 Conversion by Fe at Lower Driving Force: A Proposed Role for Metallocene-Mediated PCET. *ACS Cent. Sci.* **2017**, *3*, 217−223.

(590) Vyas, N.; Kumar, A.; Ojha, A. K.; Grover, A. Electronic Structure of Iron Dinitrogen Complex $[(TPB)FeN_2]^{2-/1-/0}$: Correlation to Mössbauer Parameters. *RSC Adv.* **2020**, *10*, 7948−7955.

(591) Fajardo, J.; Peters, J. C. Tripodal P_3^XFe-N_2 Complexes (X = B, Al, Ga): Effect of the Apical Atom on Bonding, Electronic Structure, and Catalytic N_2-to-NH_3 Conversion. *Inorg. Chem.* **2021**, *60*, 1220−1227.

(592) Dorantes, M. J.; Moore, J. T.; Bill, E.; Mienert, B.; Lu, C. C. Bimetallic Iron-Tin Catalyst for N_2 to NH_3 and a Silyldiazenido Model Intermediate. *Chem. Commun.* **2020**, *56*, 11030−11033.

(593) Coste, S. C.; Vlaisavljevich, B.; Freedman, D. E. Magnetic Anisotropy from Main-Group Elements: Halides versus Group 14 Elements. *Inorg. Chem.* **2017**, *56*, 8195−8202.

(594) Clouston, L. J.; Bernales, V.; Cammarota, R. C.; Carlson, R. K.; Bill, E.; Gagliardi, L.; Lu, C. C. Heterobimetallic Complexes That Bond Vanadium to Iron, Cobalt, and Nickel. *Inorg. Chem.* **2015**, *54*, 11669−11679.

(595) Zhang, Y.; Pan, X.; Xu, M.; Xiong, C.; Hong, D.; Fang, H.; Cui, P. Dinitrogen Complexes of Cobalt(−I) Supported by Rare-Earth Metal-Based Metalloligands. *Inorg. Chem.* **2023**, *62*, 3836−3846.

(596) Peng, J.-B.; Geng, H.-Q.; Wu, X.-F. The Chemistry of CO: Carbonylation. *Chem.* **2019**, *5*, 526−552.

(597) Sang, R.; Hu, Y.; Razzaq, R.; Mollaert, G.; Atia, H.; Bentrup, U.; Sharif, M.; Neumann, H.; Junge, H.; Jackstell, R.; et al. A Practical Concept for Catalytic Carbonylations Using Carbon Dioxide. *Nat. Commun.* **2022**, *13*, 4432.

(598) Artz, J.; Müller, T. E.; Thenert, K.; Kleinekorte, J.; Meys, R.; Sternberg, A.; Bardow, A.; Leitner, W. Sustainable Conversion of Carbon Dioxide: An Integrated Review of Catalysis and Life Cycle Assessment. *Chem. Rev.* **2018**, *118*, 434−504.

(599) Corella, J. A.; Cooper, N. J. Metal-Mediated Addition of Carbon Dioxide to the Activated Benzene in $[Cr(\eta^4\text{-}C_6H_6)(CO)_3]^{2-}$. *J. Am. Chem. Soc.* **1990**, *112*, 2832−2834.

(600) Maher, J. M.; Cooper, N. J. Reduction of CO_2 to CO by Transition-Metal Dianions. *J. Am. Chem. Soc.* **1980**, *102*, 7604−7606.

(601) Lee, G. R.; Maher, J. M.; Cooper, N. J. Reductive Disproportionation of Carbon Dioxide by Dianionic Carbonylmetalates of the Transition Metals. *J. Am. Chem. Soc.* **1987**, *109*, 2956−2962.

(602) Nasr Allah, T.; Savourey, S.; Berthet, J.-C.; Nicolas, E.; Cantat, T. Carbonylation of C—N Bonds in Tertiary Amines Catalyzed by Low-Valent Iron Catalysts. *Angew. Chem., Int. Ed.* **2019**, *58*, 10884−10887.

(603) Suess, D. L. M.; Peters, J. C. A CO-Derived Iron Dicarbyne That Releases Olefin upon Hydrogenation. *J. Am. Chem. Soc.* **2013**, *135*, 12580−12583.

(604) Deegan, M. M.; Peters, J. C. CO Reduction to CH_3OSiMe_3: Electrophile-Promoted Hydride Migration at a Single Fe Site. *J. Am. Chem. Soc.* **2017**, *139*, 2561−2564.

(605) Deegan, M. M.; Peters, J. C. O-Functionalization of a Cobalt Carbonyl Generates a Terminal Cobalt Carbyne. *Chem. Commun.* **2019**, *55*, 9531−9534.

(606) Buss, J. A.; Agapie, T. Four-Electron Deoxygenative Reductive Coupling of Carbon Monoxide at a Single Metal Site. *Nature* **2016**, *529*, 72−75.

(607) Buss, J. A.; Agapie, T. Mechanism of Molybdenum-Mediated Carbon Monoxide Deoxygenation and Coupling: Mono- and Dicarbyne Complexes Precede C-O Bond Cleavage and C-C Bond Formation. *J. Am. Chem. Soc.* **2016**, *138*, 16466−16477.

(608) Bailey, G. A.; Buss, J. A.; Oyala, P. H.; Agapie, T. Terminal, Open-Shell Mo Carbide and Carbyne Complexes: Spin Delocalization and Ligand Noninnocence. *J. Am. Chem. Soc.* **2021**, *143*, 13091−13102.

(609) Buss, J. A.; Cheng, C.; Agapie, T. A Low-Valent Molybdenum Nitride Complex: Reduction Promotes Carbonylation Chemistry. *Angew. Chem., Int. Ed.* **2018**, *57*, 9670−9674.

(610) Barluzzi, L.; Jori, N.; He, T.; Rajeshkumar, T.; Scopelliti, R.; Maron, L.; Oyala, P.; Agapie, T.; Mazzanti, M. Heterometallic Uranium/Molybdenum Nitride Synthesis via Partial N-Atom Transfer. *Chem. Commun.* **2022**, *58*, 4655−4658.

(611) Fang, M.; Farnaby, J. H.; Ziller, J. W.; Bates, J. E.; Furche, F.; Evans, W. J. Isolation of $(CO)^{1-}$ and $(CO_2)^{1-}$ Radical Complexes of Rare Earths via $Ln(NR_2)_3$/K Reduction and $[K_2(18\text{-Crown-}6)_2]^{2+}$ Oligomerization. *J. Am. Chem. Soc.* **2012**, *134*, 6064−6067.

(612) Smieja, J. M.; Sampson, M. D.; Grice, K. A.; Benson, E. E.; Froehlich, J. D.; Kubiak, C. P. Manganese as a Substitute for Rhenium in CO_2 Reduction Catalysts: The Importance of Acids. *Inorg. Chem.* **2013**, *52*, 2484−2491.

(613) Sampson, M. D.; Nguyen, A. D.; Grice, K. A.; Moore, C. E.; Rheingold, A. L.; Kubiak, C. P. Manganese Catalysts with Bulky Bipyridine Ligands for the Electrocatalytic Reduction of Carbon Dioxide: Eliminating Dimerization and Altering Catalysis. *J. Am. Chem. Soc.* **2014**, *136*, 5460−5471.

(614) Sampson, M. D.; Kubiak, C. P. Manganese Electrocatalysts with Bulky Bipyridine Ligands: Utilizing Lewis Acids to Promote Carbon Dioxide Reduction at Low Overpotentials. *J. Am. Chem. Soc.* **2016**, *138*, 1386−1393.

(615) Agnew, D. W.; Sampson, M. D.; Moore, C. E.; Rheingold, A. L.; Kubiak, C. P.; Figueroa, J. S. Electrochemical Properties and CO_2-Reduction Ability of *m*-Terphenyl Isocyanide Supported Manganese Tricarbonyl Complexes. *Inorg. Chem.* **2016**, *55*, 12400−12408.

(616) Kumar, B.; Smieja, J. M.; Kubiak, C. P. Photoreduction of CO_2 on p-Type Silicon Using Re(bipy-Bu^t)$(CO)_3$Cl: Photovoltages Exceeding 600 mV for the Selective Reduction of CO_2 to CO. *J. Phys. Chem. C* **2010**, *114*, 14220−14223.

(617) Smieja, J. M.; Benson, E. E.; Kumar, B.; Grice, K. A.; Seu, C. S.; Miller, A. J. M.; Mayer, J. M.; Kubiak, C. P. Kinetic and Structural Studies, Origins of Selectivity, and Interfacial Charge Transfer in the Artificial Photosynthesis of CO. *Proc. Natl. Acad. Sci. U. S. A.* **2012**, *109*, 15646−15650.

(618) Kumar, B.; Smieja, J. M.; Sasayama, A. F.; Kubiak, C. P. Tunable, Light-Assisted Co-Generation of CO and H_2 from CO_2 and H_2O by Re(bipy-tbu)$(CO)_3$Cl and p-Si in Non-Aqueous Medium. *Chem. Commun.* **2012**, *48*, 272−274.

(619) Mokhtarzadeh, C. C.; Moore, C. E.; Rheingold, A. L.; Figueroa, J. S. Terminal Iron Carbyne Complexes Derived from Arrested CO_2 Reductive Disproportionation. *Angew. Chem., Int. Ed.* **2017**, *56*, 10894−10899.

(620) Rickmeyer, K.; Niederegger, L.; Keilwerth, M.; Hess, C. R. Multifaceted Role of the Noninnocent Mabiq Ligand in Promoting Selective Reduction of CO_2 to CO. *ACS Catal.* **2022**, *12*, 3046−3057.

(621) Tok, G. C.; Reiter, S.; Freiberg, A. T. S.; Reinschlüssel, L.; Gasteiger, H. A.; de Vivie-Riedle, R.; Hess, C. R. H_2 Evolution from Electrocatalysts with Redox-Active Ligands: Mechanistic Insights from Theory and Experiment Vis-à-Vis Co-Mabiq. *Inorg. Chem.* **2021**, *60*, 13888−13902.

(622) Vollmer, M. V.; Cammarota, R. C.; Lu, C. C. Reductive Disproportionation of CO_2 Mediated by Bimetallic Nickelate(−I)/Group 13 Complexes. *Eur. J. Inorg. Chem.* **2019**, *2019*, 2140−2145.

(623) Prat, J. R.; Gaggioli, C. A.; Cammarota, R. C.; Bill, E.; Gagliardi, L.; Lu, C. C. Bioinspired Nickel Complexes Supported by an Iron Metalloligand. *Inorg. Chem.* **2020**, *59*, 14251−14262.

(624) Hoidn, C. M.; Scott, D. J.; Wolf, R. Transition-Metal-Mediated Functionalization of White Phosphorus. *Chem. Eur. J.* **2021**, *27*, 1886−1902.

(625) Caporali, M.; Gonsalvi, L.; Rossin, A.; Peruzzini, M. P_4 Activation by Late-Transition Metal Complexes. *Chem. Rev.* **2010**, *110*, 4178−4235.

(626) Cossairt, B. M.; Piro, N. A.; Cummins, C. C. Early-Transition-Metal-Mediated Activation and Transformation of White Phosphorus. *Chem. Rev.* **2010**, *110*, 4164−4177.

(627) Urnezius, E.; Brennessel, W. W.; Cramer, C. J.; Ellis, J. E.; Schleyer, P. von Ragué A Carbon-Free Sandwich Complex $[(P_5)_2Ti]^{2-}$. *Science* **2002**, *295*, 832−834.

(628) Ellis, J. E.; Blackburn, D. W.; Yuen, P.; Jang, M. Highly Reduced Organometallics. 35. Synthesis and Chemistry of the First Isolable Bis(naphthalene)titanium Complexes. Structural Characterization of $[Ti(\eta^4\text{-}C_{10}H_8)_2(SnMe_3)_2]^{2-}$. *J. Am. Chem. Soc.* **1993**, *115*, 11616−11617.

(629) Borger, J. E.; Jongkind, M. K.; Ehlers, A. W.; Lutz, M.; Slootweg, J. C.; Lammertsma, K. Metalate-Mediated Functionalization of P_4 by Trapping Anionic $[Cp^*Fe(CO)_2(\eta^1\text{-}P_4)]^-$ with Lewis Acids. *ChemistryOpen* **2017**, *6*, 350−353.

(630) Borger, J. E.; Ehlers, A. W.; Slootweg, J. C.; Lammertsma, K. Functionalization of P_4 through Direct P—C Bond Formation. *Chem. Eur. J.* **2017**, *23*, 11738−11746.

(631) Chakraborty, U.; Leitl, J.; Mühldorf, B.; Bodensteiner, M.; Pelties, S.; Wolf, R. Mono- and Dinuclear Tetraphosphabutadiene Ferrate Anions. *Dalton Trans.* **2018**, *47*, 3693−3697.

(632) Ziegler, C. G. P.; Hennersdorf, F.; Weigand, J. J.; Wolf, R. Iron-Gallium and Cobalt-Gallium Tetraphosphido Complexes. *Z. Anorg. Allg. Chem.* **2020**, *646*, 552−557.

(633) Prabusankar, G.; Doddi, A.; Gemel, C.; Winter, M.; Fischer, R. A. P-P Bond Activation of P_4 Tetrahedron by Group 13 Carbenoid and Its Bis Molybdenum Pentacarbonyl Adduct. *Inorg. Chem.* **2010**, *49*, 7976−7980.

(634) Yao, S.; Szilvási, T.; Lindenmaier, N.; Xiong, Y.; Inoue, S.; Adelhardt, M.; Sutter, J.; Meyer, K.; Driess, M. Reductive Cleavage of P_4 by Iron(I) Centres: Synthesis and Structural Characterisation of $Fe_2(P_2)_2$ Complexes with Two Bridging P_2^{2-} Ligands. *Chem. Commun.* **2015**, *51*, 6153−6156.

(635) Spitzer, F.; Graßl, C.; Balázs, G.; Mädl, E.; Keilwerth, M.; Zolnhofer, E. M.; Meyer, K.; Scheer, M. Nacnac-Cobalt-Mediated P_4 Transformations. *Chem. Eur. J.* **2017**, *23*, 2716−2721.

(636) Yao, S.; Lindenmaier, N.; Xiong, Y.; Inoue, S.; Szilvási, T.; Adelhardt, M.; Sutter, J.; Meyer, K.; Driess, M. A Neutral Tetraphosphacyclobutadiene Ligand in Cobalt(I) Complexes. *Angew. Chem., Int. Ed.* **2015**, *54*, 1250−1254.

(637) Mandla, K. A.; Neville, M. L.; Moore, C. E.; Rheingold, A. L.; Figueroa, J. S. Dianionic Mononuclear cyclo-P_4 Complexes of Zero-Valent Molybdenum: Coordination of the cyclo-P_4 Dianion in the Absence of Intramolecular Charge Transfer. *Angew. Chem., Int. Ed.* **2019**, *58*, 15329−15333.

(638) Mandla, K. A.; Moore, C. E.; Rheingold, A. L.; Figueroa, J. S. Photolytic Reductive Elimination of White Phosphorus from a Mononuclear cyclo-P_4 Transition Metal Complex. *Angew. Chem., Int. Ed.* **2019**, *58*, 1779−1783.

(639) Alvarez, M. A.; García, M. E.; García-Vivó, D.; Ramos, A.; Ruiz, M. A. Mild P_4 Activation to Give an Anionic Diphosphorus Complex with a Dual Binding Ability at a Single P Site. *Inorg. Chem.* **2011**, *50*, 2064−2066.

(640) Chirila, A.; Wolf, R.; Chris Slootweg, J.; Lammertsma, K. Main Group and Transition Metal-Mediated Phosphaalkyne Oligomerizations. *Coord. Chem. Rev.* **2014**, *270−271*, 57−74.

(641) Hitchcock, P. B.; Maah, M. J.; Nixon, J. F. First Example of Cyclodimerisation of a Phospha-Alkyne to a 1,3-Diphosphacyclobutadiene. Syntheses of Complexes of the Type $[M(\eta^5\text{-}C_5R_5)\{\eta^4\text{-}(Bu^tCP)_2\}]$ R = H or Me; M = Co, Rh, or Ir): Crystal and Molecular Structure of η^5-Pentamethylcyclopentadienyl-2,4-di-t-butyl-1,3-diphosphacyclobutadienecobalt(I), $[Co(\eta^5\text{-}C_5Me_5)\{\eta^4\text{-}(Bu^tCP)_2\}]$. *J. Chem. Soc., Chem. Commun.* **1986**, 737−738.

(642) Binger, P.; Milczarek, R.; Mynott, R.; Regitz, M.; Rösch, W. 1,3-Diphosphacyclobutadienecobalt(I) Complexes from Phosphaalkynes. *Angew. Chem., Int. Ed. Engl.* **1986**, *25*, 644−645.

(643) Binger, P.; Milczarek, R.; Mynott, R.; Krüger, C.; Tsay, Y.-H.; Raabe, E.; Regitz, M. λ^3-1,3-Diphosphacyclobutadiene-Cobalt Complexes by Cyclodimerization of λ^3-Phosphaalkynes. *Chem. Ber.* **1988**, *121*, 637−645.

(644) Driess, M.; Hu, D.; Pritzkow, H.; Schäufele, H.; Zenneck, U.; Regitz, M.; Rösch, W. Reaktive π-Komplexe der elektronenreichen Übergangsmetalle, IV. Cyclisierungsreaktionen von t-Butylphosphaacetylen an π-Areneisen-Komplexen. *J. Organomet. Chem.* **1987**, *334*, C35−C38.

(645) Binger, P.; Biedenbach, B.; Schneider, R.; Regitz, M. Phosphaalkyne Cyclodimerization Using Iron Complexes. *Synthesis* **1989**, *1989*, 960−961.

(646) Böhm, D.; Knoch, F.; Kummer, S.; Schmidt, U.; Zenneck, U. 2,4-Di-*tert*-butyl-1λ^3,3λ^3-diphosphinines: Targeted Synthesis at Iron(0) Centers and Oxidative Release. *Angew. Chem., Int. Ed. Engl.* **1995**, *34*, 198−201.

(647) Binger, P.; Glaser, G.; Albus, S.; Krüger, C. (η^8-Cyclooctatetraene)(η^4-1,2- and -1,3-diphosphacyclobutadiene)-titanium: Preparation, Structure, and Reactivity. *Chem. Ber.* **1995**, *128*, 1261−1265.

(648) Brauers, G.; Green, M.; Jones, C.; Nixon, J. F. Synthesis of a Mononuclear η^2(4e)-Bonded Phosphaalkyne Complex, Transformation into an η^4-1,3-Diphosphacyclobutadiene Complex. *J. Chem. Soc., Chem. Commun.* **1995**, 1125−1126.

(649) Scheer, M.; Krug, J. Zur Reaktion von *tert*-Butyl-Phosphaalkin mit Molybdänkomplexen. *Z. Anorg. Allg. Chem.* **1998**, *624*, 399−405.

(650) Wettling, T.; Wolmershäuser, G.; Binger, P.; Regitz, M. Bis(2,4-di-t-butyl-η^4-1,3-diphosphacyclobutadiene)nickel. *J. Chem. Soc. Chem. Commun.* **1990**, No. 21, 1541−1543.

(651) Himmel, D.; Seitz, M.; Scheer, M. Beiträge Zum Reaktionsverhalten von Phosphaalkinen gegenüber Übergangsmetallkomplexen — Synthese und Kristallstrukturanalyse von $[(Ph_3P)_2Pt(\eta^2\text{-}PCMes)]$, $[M(CO)_3(\eta^4\text{-}P_2C_2Mes_2)]$ (M = Fe, Ru), $[Cp^*Mo(CO)Cl(\eta^4\text{-}P_2C_2{}^tBu_2)]$ Und $[K(tol)_2]_2[Mn(CO)_4\{Mn(CO)_3(\eta^4\text{-}P_2C_2{}^tBu)\}_2]_2$. *Z. Anorg. Allg. Chem.* **2004**, *630*, 1220−1228.

(652) Rödl, C.; Schwedtmann, K.; Weigand, J. J.; Wolf, R. 1,3-Diphosphacyclobutene Cobalt Complexes. *Chem. Eur. J.* **2019**, *25*, 6180−6188.

(653) Rödl, C.; Malberg, J. B.; Wolf, R. Functionalization of 1,3-Diphosphacyclobutadiene Cobalt Complexes via Si-P Bond Insertion. *Z. Naturforsch. B* **2018**, *73*, 895−909.

(654) Wiegand, T.; Eckert, H.; Grimme, S.; Malberg, J.; Wolf, R. Solid State NMR Studies and Chemical Shift Calculations of a Gold(I) Complex with a Diphosphacyclobutadiene Cobaltate Sandwich Anion. *Solid State Nucl. Magn. Reson.* **2013**, *53*, 13−19.

(655) Malberg, J.; Wiegand, T.; Eckert, H.; Bodensteiner, M.; Wolf, R. Copper(I) and Silver(I) Complexes of 1,3-Diphosphacyclobutadiene Sandwich Anions: Synthesis, Crystal Structures, and Solution and Solid-State NMR Spectroscopic Characterization. *Eur. J. Inorg. Chem.* **2014**, *2014*, 1638−1651.

(656) Malberg, J.; Bodensteiner, M.; Paul, D.; Wiegand, T.; Eckert, H.; Wolf, R. Preparation of an Organometallic Molecular Square by

Self-Assembly of Phosphorus-Containing Building Blocks. *Angew. Chem., Int. Ed.* **2014**, *53*, 2771−2775.

(657) Rödl, C.; Wolf, R. Cobalt(I) and Nickel(II) Complexes of Bis(1,3-diphosphacyclobutadiene) Sandwich Anions. *Eur. J. Inorg. Chem.* **2016**, *2016*, 736−742.

(658) Hierlmeier, G.; Coburger, P.; Scott, D. J.; Maier, T. M.; Pelties, S.; Wolf, R.; Pividori, D. M.; Meyer, K.; van Leest, N. P.; de Bruin, B. Di-*tert*-Butyldiphosphatetrahedrane as a Source of 1,2-Diphosphacyclobutadiene Ligands. *Chem. Eur. J.* **2021**, *27*, 14936−14946.

(659) Hierlmeier, G.; Coburger, P.; Bodensteiner, M.; Wolf, R. Di-*tert*-butyldiphosphatetrahedrane: Catalytic Synthesis of the Elusive Phosphaalkyne Dimer. *Angew. Chem., Int. Ed.* **2019**, *58*, 16918−16922.

(660) Tiefenthaler, S. M.; Kleemiss, F.; Korber, N. [A([18]Crown-6)]$_2$[Pt(CO)$_3$] · 10 NH$_3$ (A=K, Rb) − A Crystal Structure Containing the Long Postulated [Pt(CO)$_3$]$^{2-}$. *Z. Anorg. Allg. Chem.* **2022**, *648*, e202100378.

(661) Tiefenthaler, S. M.; Korber, N. [K([2.2.2]-Crypt)]K[Pt$_3$(μ^2-CO)$_3$(PPh$_3$)$_3$] · 3NH$_3$ − A New Chini-Type Platinum Carbonyl Complex. *Z. Anorg. Allg. Chem.* **2023**, *649*, No. e202200286.

(662) Moore, J. T.; Dorantes, M. J.; Pengmei, Z.; Schwartz, T. M.; Schaffner, J.; Apps, S. L.; Gaggioli, C. A.; Das, U.; Gagliardi, L.; Blank, D. A.; Lu, C. C. Light-Driven Hydrodefluorination of Electron-Rich Aryl Fluorides by an Anionic Rhodium-Gallium Photoredox Catalyst. *Angew. Chem. Int. Ed.* **2022**, *61*, No. e202205575.

(663) Moore, J. T.; Lu, C. C. Catalytic Hydrogenolysis of Aryl C−F Bonds Using a Bimetallic Rhodium−Indium Complex. *J. Am. Chem. Soc.* **2020**, *142*, 11641−11646.

(664) Wang, Z.-C.; Qiao, L.; Sun, Z.-M.; Scheer, M. Inorganic Ferrocene Analogue [Fe(P$_4$)$_2$]$^{2-}$. *J. Am. Chem. Soc.* **2022**, *144*, 6698−6702.

(665) Young, V. G.; Brennessel, W. W.; Ellis, J. E. Crystal Structure and Synthesis of the Bis(anthracene)dicuprate Dianion as the Dipotassium Salt, [K(tetrahydrofuran)$_2$]$_2$[{Cu(9,10-η^2-anthracene)}$_2$], the First Anionic Arene Complex of Copper. *Acta Cryst C* **2023**, *79*, 456−463.

NOTE ADDED IN PROOF

The following relevant literature came to our attention after the manuscript was accepted. Korber and co-workers reported the crystallographic characterization of [*A*([18]crown-6]$_2$[Pt(CO)$_3$] · 10 NH$_3$ (**1125**), representing the first mononuclear platinum carbonylate, and the Chini type cluster [K([2.2.2]-cryptand)]K[Pt$_3$(μ^2-CO)$_3$(PPh$_3$)$_3$] · 3NH$_3$ (**1126**, *A* = K, Rb, [18]crown-6).[660,661] The compounds were serendipitously obtained as single crystals from reaction mixtures of the Zintl phase K$_6$Rb$_6$Ge$_{17}$ with Pt(CO)$_2$(PPh$_3$)$_2$, [18]crown-6 and [2.2.2]-cryptand in liquid ammonia. The trigonal planar carbonyl platinate dianion observed in **1125** is analogous to the [Ni(CO)$_3$]$^{2-}$ anion in compound **26** (section 2.2.1.). The structure of **1126** displays a monomeric Chini-type dianion [Pt$_3$(μ^2-CO)$_3$(PPh$_3$)$_3$]$^{2-}$ containing terminally coordinated triphenylphosphine ligands on each Pt atom. It was speculated that the stabilizing effect of liquid ammonia towards negatively charged species might be a crucial factor for the formation of **1126**. In work related to the chemistry described in section 3.1.5, Lu and co-workers reported the utilization of a bimetallic RhGa photoredox catalyst [RhGa{N[*o*-(NCH$_2$P*i*Pr$_2$)-C$_6$H$_4$]$_3$}]$^-$ (**1127**) in the catalytic hydrogenolysis of C−F bonds driven by violet (395 nm) LED light.[662] An analogous RhAl complex proved to be less active. However, it is important to note that RhIn complex [RhIn{N[*o*-(NCH$_2$P*i*Pr$_2$)C$_6$H$_4$]$_3$}]$^-$ (**1128**), the heavier congener of **1127**, catalyzes similar hydrodefluorination reactions under thermal conditions (1 atm H$_2$ pressure and 70−90 °C).[663] A purely inorganic sandwich complex [Fe(*cyclo*-P$_4$)$_2$]$^{2-}$ (**1129**) was recently reported by Sun and co-workers. This complex is related to the decaphosphatitanocene dianion **1042** described in section 3.4.[664] Finally, a recent report by Ellis and co-workers on the preparation and crystallographic characterization of the remarkable complex [K(thf)$_2$]$_2$[{Cu(9,10-η^2-C$_{14}$H$_{10}$)}$_2$] (**1130**, C$_{14}$H$_{10}$ = anthracene) is noteworthy.[665] Compound **1130** is the first anionic arene complex of copper. In the solid state, the complex forms a dinuclear ion-contact structure with the copper atoms bound in a nearly linear fashion to the 9,10-carbons of the central ring of anthracene. The [K(thf)$_2$]$^+$ cations form a sandwich type arrangement with the exo-arene rings.